ARTICLE IN PRESS Available online http://jopr.mpob.gov.my/category/article-in-press/

Journal of Oil Palm Research

Vol. 35 (4) • December 2023



REVIEW ARTICLE

- A Review of Non-destructive Ripeness Detection Techniques for Oil Palm Fresh Fruit Bunches
- Prospects and State-of-the-art in Production of Bio-based Succinic Acid from Oil Palm Trunk



eISSN 2811-4701

MPOB

JOURNAL OF OIL PALM RESEARCH (formerly known as ELAEIS)

JOURNAL OF OIL PALM RESEARCH (JOPR), an international refereed journal, carries full-length original research papers, short communications and scientific review papers on various aspects of oil palm and palm oil and other palms. JOPR is published four times per year, *i.e.* March, June, September and December.

© Malaysian Palm Oil Board (MPOB), 2023

All rights reserved. No part of this publication may be reproduced in any form or by any means without the written permission of MPOB.

Impact Factor:
1.3
data from *2022 Journal Citation Report*® Science Edition
– A Clarivate Analytics product.

For more information on advertisement for the JOPR, please write to:

Editor-in-Chief
Journal of Oil Palm Research
Malaysian Palm Oil Board
6 Persiaran Institusi, Bandar Baru Bangi
43000 Kajang, Selangor, Malaysia

Tel: *603-8769 4400*
E-mail: *jopr.admin@mpob.gov.my*
Website: *jopr.mpob.gov.my*

DISCLAIMER
Views of writers expressed in this publication are not necessarily endorsed by or represent the views of MPOB.

MPOB Press
Malaysian Palm Oil Board
6 Persiaran Institusi, Bandar Baru Bangi
43000 Kajang, Selangor, Malaysia
Tel: +603-8769 4400 | Fax: +603-8925 9446
E-mail: *jopr.admin@mpob.gov.my*

JOURNAL OF OIL PALM RESEARCH

Vol. 35(4) December 2023

CONTENTS

REVIEW ARTICLES

543 A Review of Non-Destructive Ripeness Detection Techniques for Oil Palm Fresh Fruit Bunches
Mohamed Yasser Mohamed Mansour; Katrina D. Dambul and Choo Kan Yeep

555 Prospects and State-of-the-art in Production of Bio-based Succinic Acid from Oil Palm Trunk
Nurul Adela Bukhari; Soh Kheang Loh; Abdullah Amru Indera Luthfi; Abu Bakar Nasrin and Peer Mohamed Abdul

RESEARCH ARTICLES

582 Phenotypic Variability of Elaeis Oleifera Germplasm Revealed By Principal Component and Cluster Analyses
Zulkifli Yaakub; Marhalil Marjuni; Suzana Mustaffa; Wan Nor Salmiah Tun Mohd Salim; Fatin Mohd Nasir; Norziha Abdullah; Mohd Din Amiruddin; Rajanaidu Nookiah; Ahmad Kushairi Din and Meilina Ong-Abdullah

596 Metabarcoding in Diet Assessment of Adult Parasitoid Species, Dolichogenidea metesae (Hymenoptera: Braconidae) Towards Its Conservation and Management in the Oil Palm Plantation
Fuat Salbi; Aqilah Sakinah Badrulisham; Nur Azura Adam; Izfa Riza Hazmi and Salmah Yaakop

607 Dynamics of Sucrose Phosphate Synthase and Fructose Bisphosphate Synthase in Oil Palms Fertilised with Low Nitrogen [$(NH_2)_2CO$] Dose with NPPT-NBPT Coating in Red-yellow Podzolic Soil
Eka Tarwaca Susila Putra; Benito Heru Purwanto; Eko Hanudin and Taufan Alam

616 Geostatitical Assessment of Heavy Metals and Nutrients Availability in Soil of Oil Palm Plantation Affected by Bauxite Mining
Mazidah Zulkifli; Nur Shuhada Muhamad Tajudin; Mohd Fuad Miskon; Fikriah Faudzi and Nurul Mayzaitul Azwa Jamaludin

626 Molecular Screening of Basal Stem Rot Resistance Genes in Oil Palm
Mohd Amin Ab-Halim; Rozana Rosli; Eng Ti Leslie Low; Zeti-Azura Mohamed-Hussein and Rajinder Singh

639 Thermal Analysis and Non-Isothermal Thermogravimetric Kinetics Analysis Using Coats–redfern Method of a Torrefied Empty Fruit Bunches
Mohamad Azri Sukiran; Peter Adeniyi Alaba; Abu Bakar Nasrin; Astimar Abdul Aziz and Soh Kheang Loh

653 A Structural Design of a Passive Wearable Exoskeleton to Assist Oil Palm Harvesting Operation
Muhammad Fuad Mohamad; Sharence Nai Sowati; Hazlina Selamat; Aizreena Azaman and Hazreen H. Harith

668 Optimisation of FAME Production from Waste Cooking Palm Oil with KOH Catalyst Supported on Palm Kernel Shells Ash (PKSA) using Response Surface Methodology (RSM)
Hussanai Sukkathanyawat and Kittisak Wichianwat

682 Economical Study of Bio-Based Polybutylene Succinate Production from Oil Palm Biomass
Rohani Arpa; Abdullah Amru Indera Luthfi; Nurul Adela Bukhari; Jian Ping Tan; Safa Senan Mahmod and Muhammad Zulhaziman Mat Salleh

694 Characteristics of Sunflower Wax, Carnauba Wax and Beeswax in Palm Superolein Blended Oil
Norazura Aila Mohd Hassim; Sivaruby Kanagaratnam; Saw Mei Huey; Nur Haqim Ismail; Rafidah Abd. Hamid; Muhammad Hanif Miskandar and Noor-Soffalina Sofian-Seng

713 Linear Kinetics Modelling and Thermodynamics Study of Supercritical CO_2-Derived Oil Extracts from Fruit Palm Peels
Usman Bello; Nurul Aini Amran; Sharifah Samsuri and Muhammad Syafiq Hazwan Ruslan

725 Synthesis and Physicochemical Properties of Estolide Ester and Amide Made from Used Cooking Oil as Bio-lubricant
Seng Soi Hoong; Mohd Zan Arniza; Nek Mat Din Nik Siti Mariam; Abu Hassan Noor Armylisas; Sook Wah Tang; Tuan Ismail Tuan Noor Maznee and Shoot Kian Yeong

SHORT COMMUNICATION

738 Chemical Profiling of Palm Oil and other Selected Plant Oils by Proton Nuclear Magnetic Resonance Combined with Chemometrics
Noor Idayu Tahir; Asiah Nabihan Ishak; Teh Seok Sin; Abrizah Othman and Umi Salamah Ramli

Cover picture:
1. Ripe oil palm fresh fruit bunch (FFB).
2. Oil palm trunk as a promising feedstock for succinic acid production.

EDITORIAL BOARD

(1 January 2022 – 31 December 2023)

Datuk Dr. Ahmad Parveez Ghulam Kadir
Malaysia (Editor-in-Chief)

Dr. Carl Traeholt
Malaysia

Prof. Dr. Matthias Finkbenier
Germany

Dr. Julie Flood
United Kingdom

Prof. Dr. Dirk Prufer
Germany

Prof. Dr. Douglas G Hayes
USA

Prof. Fredolin Tangang
Malaysia

Prof. Dr. Norzulani Khalid
Malaysia

Prof. Dr. Ir. Azmi Yahya
Malaysia

PUBLICATION COMMITTEE

CHAIRPERSON
Datuk Dr. Ahmad Parveez Ghulam Kadir

SECRETARY
Dr. Anita Taib

COMMITTEE MEMBERS
Dr. Zainab Idris
Dr. Ramle Moslim
Dr. Sivaruby Kanagaratnam
Dr. Astimar Abdul Aziz
Dr. Mohamad Arif Abd Manaf
Dr. Meilina Ong Abdullah
Dr. Aki @ Zaki Aman
Dr. Zafarizal Aldrin Azizul Hasan
Ruba'ah Masri
Johari Minal
Mohd Saufi Awang
Iptisam Abdul Wahab

Journal of Oil Palm Research Vol. 35 (4) December 2023 p. 543-554
DOI: https://doi.org/10.21894/jopr.2022.0063

A REVIEW OF NON-DESTRUCTIVE RIPENESS CLASSIFICATION TECHNIQUES FOR OIL PALM FRESH FRUIT BUNCHES

MOHAMED YASSER MOHAMED AHMED MANSOUR[1]; KATRINA D. DAMBUL[1]* and CHOO KAN YEEP[1]

ABSTRACT

Grading of oil palm fresh fruit bunches (FFB) is commonly conducted using visual inspection by trained workers who inspect the oil palm FFB according to the colour and the number of the loose fruits on the ground. However, this method is labour intensive and time consuming. In addition, the workers may misclassify the fruit's ripeness due to the height of the tree, miscounting the loose fruits, unclear vision of the bunches on the tree and lighting conditions. Unripe or overripe bunches result in a less efficient palm oil refining process, low palm oil quality and profit losses. Non-destructive techniques can offer better solutions for ripeness classifications with higher accuracy. The techniques are field and lab spectroscopy, computer vision, hyperspectral imaging, laser-light backscattering imaging and fruit battery sensor. Spectroscopy, hyperspectral imaging and laser-light backscattering imaging techniques need to be deployed with a special set up which may not be suitable for real-time ripeness classification. Computer vision, using image processing techniques and machine learning algorithms allow real-time in situ *ripeness classification via mobile devices. This article aims to review the feasibility of each method to allow real-time* in situ *ripeness classification of the oil palm fruit bunches with high accuracy.*

Keywords: computer vision, hyperspectral imaging, laser-light backscattering imaging, ripeness classification, spectroscopy.

Received: 12 November 2021**; Accepted:** 3 August 2022**; Published online:** 28 September 2022.

INTRODUCTION

The Malaysian oil palm industry is one of the key contributors to Malaysia's gross domestic product (GDP). According to the 2021 Malaysia's Selected Agricultural Indicators publication, oil palm was the main contributor to the agriculture sector with RM36.9 billion (37.1%) and agriculture contributed 7.4% to Malaysia's GDP in 2020. Palm oil plantation in Malaysia has grown rapidly from 55 000 ha in 1960 to 6.17 million hectares in 2021 (MPOB 2021; Nambiappan *et al.*, 2018). Moreover, 85% of the global palm oil supply is shared between Malaysia and Indonesia (Goh *et al.*, 2016; Kushairi *et al.*, 2018). However, the unprecedented COVID-19 pandemic caused crude palm oil (CPO) production to drop by 3.6% to 19.14 million tonnes in 2020 and further declined to 18.11 million tonnes in 2021 (MPOB, 2021).

The oil palm's fresh fruit bunch (FFB) contains CPO which is derived from the flesh of the fruit, the mesocarp and palm kernel oil (PKO) from the kernel of the fruit (Basyuni *et al.*, 2017; Mba *et al.*, 2015). About 80% of palm oil is used in food products such as cooking oil, margarine, shortening and others and 20% is used in oleochemicals as in cosmetics, pharmaceutical, detergent and plastic products (Soh *et al.*, 2009). The CPO is mainly used for edible products while PKO is used in a wide range of applications in oleochemical industry (Denis, 2014; Sambanthamurthi, 2000).

The quality of the palm oil can be determined by the physical properties of the bunches (colour, shape or texture) or by its biochemical characteristics such as oil content (OC), which affects the oil extraction

[1] Faculty of Engineering, Multimedia University, Persiaran Multimedia, 63100 Cyberjaya, Selangor, Malaysia.

* *Corresponding author e-mail: katrina@mmu.edu.my*

rate (OER) and free fatty acids (FFAs), which are also known as acid value (AV) (Mat Sharif *et al.*, 2017). Oils with high FFAs content are usually low in quality and show higher losses during the palm oil refining process (Cornelius, 1966).

In oil palm estates, the common way of determining the ripeness of the palm oil fresh fruit bunches on the tree is by human vision where human graders inspect the bunches and classify them according to the colour and the number of loose fruits on the ground near the tree. This grading method is labour intensive, time-consuming and may lead to inaccurate classification of the fruit ripeness which may result in less efficient palm oil refining process, low quality palm oil and profit losses (Kairi *et al.*, 2020). In addition, current research on oil palm grading techniques only handles the grading of one type of oil palm fruit (either *nigrescens* or *virescens*) which makes its application limited and most of the research on non-destructive methods are only in the research stage and not being implemented in the actual plantation or being commercialised.

Non-destructive techniques for ripeness classification of FFBs are field and lab spectroscopy (Che Man *et al.*, 1999; Kasemsumran *et al.*, 2012; Makky and Soni, 2014), computer vision (Hussain *et al.*, 2019; Lecun *et al.*, 2015; Onoja *et al.*, 2019; Saleh and Liansitim, 2020), digital image processing (Choong *et al.*, 2006; Gibon *et al.*, 2009; Sunilkumar and Babu, 2013), hyperspectral analysis (Bensaeed *et al.*, 2014; Junkwon *et al.*, 2009), optical sensing (Utom *et al.*, 2018), inductive frequency technique (Harun *et al.*, 2013), laser-light backscattering imaging (Mohd Ali *et al.*, 2020) and fruit battery (Misron *et al.*, 2020a).

The first section of this review elaborates the characteristics of oil palm including its OC, FFAs, and deterioration of bleachability index (DOBI) and the next section reviews the current non-destructive techniques to grade oil palm FFB with the feasibility to be deployed as a real-time application in palm oil estates. This article also discusses the gap in finding an effective industrial solution replacing the common grading techniques using visual inspection by trained workers in the field.

OIL PALM

Species of oil palm include *Elaeis guineensis*, *Elaeis oleifera* and *Elaeis odora*. There are three types of oil palm fruit which are *dura, pisifera* and *tenera*, where *tenera* is a cross between *dura* and *pisifera* (Basyuni *et al.*, 2017). Based on the colour, there are two types of fruitlets which are *nigrescens* that change colour from black or dark purple in the unripe stage to dark red in the ripe stage whereas *virescens* changes colour from dark green to deep orange in the unripe and ripe stages respectively (Sunilkumar and Babu, 2013). In Malaysia, the oil palm is *E. guineensis* mainly from the *tenera* variety (Jaffar *et al.*, 2009).

The inner flesh of the fruit is called mesocarp where the CPO is extracted (Basyuni *et al.*, 2017). CPO is mainly made of glycerides while other non-glyceride components are found in small amounts (Basyuni *et al.*, 2017; Mba *et al.*, 2015). Non-glyceride components include FFAs, moisture, trace metals and impurities. Another parameter is carotene content. DOBI is a ratio between the content of carotenes and secondary oxidation products. DOBI acts as a good test for the quality of the CPO (Kushairi *et al.*, 2018). DOBI ranges from 2.99 to 3.24 for good oil quality. A high DOBI range indicates excellent quality oil (Cherie *et al.*, 2019). Chlorophyll and triacylglycerols highly affect the surface colour of the mesocarp. Triacylglycerols are the maximum accumulation of oil components which replace the chlorophyll in the mesocarp as the fruitlets ripen. Chlorophyll's role is to synthesise the carbohydrates in the fruitlet. In an unripe fruit, the chlorophyll level is high. As the fruit matures to ripeness, the chlorophyll level decreases and the triacylglycerols amount which has been synthesised increases at a high rate. The colour of the fruitlets is affected by this process and changes from black to purple. After the fruitlet ripens, the colour changes from orange to red (Harun *et al.*, 2013; Misron *et al.*, 2011).

Factors affecting the oil quality are OC, which affects the OER, and FFAs due to lipolysis or the action of water when there are glycerides present. FFAs should have a maximum concentration of 5% in CPO (Che Man *et al.*, 1999). Oils with high FFAs content (more than 5%) are normally of low quality and will cause high losses during the refining process (Cornelius, 1966; Gibon *et al.*, 2009). Other factor affecting OC is moisture.

GRADING TECHNIQUES

Due to the limitations of the human vision, visual inspection techniques may not be highly accurate. Thus, non-destructive techniques to classify the ripeness of the oil palm FFB have been proposed. These grading techniques of oil palm FFBs include spectroscopy, computer vision *e.g.*, digital image processing, hyperspectral imaging, laser-light backscattering and fruit battery sensor.

Spectroscopy

In infrared spectroscopy, the infrared spectrum is obtained when an infrared radiation is passed through a sample and the absorbed fraction of the

incident radiation at a specific energy is determined. The energy at which any peak in an absorption spectrum appears corresponds to the frequency of vibration as a part of a sample molecule (Stuart, 2005). Different stages of fruit ripeness will show peaks at different specific wavelengths.

In recent years, infrared spectroscopy has been used in the evaluation of fruit ripeness such as tomato (Lu *et al.*, 2017) and apple (Nturambirwe *et al.*, 2019). It is also proposed as a rapid and non-destructive technique in determining the ripeness of oil palm FFBs on-site (Makky and Soni, 2014) and other quality standards such as oil quality, FFAs and water content (Cherie *et al.*, 2019; Makky and Soni, 2014; Stuart, 2004). Since the colour of the surface of oil palm FFB changes continuously due to the presence of chlorophyll and carotenoid content, it is possible to determine the ripeness level of the FFBs by evaluating the biochemical changes as it is related to changes in colour (Makky and Soni, 2014). Chlorophyll levels are higher in unripe bunches. In ripe bunches, chlorophyll levels are lower with higher carotenoid levels (Bensaeed *et al.*, 2014; Harun *et al.*, 2013). Chlorophyll is known to absorb most blue and red light in the visible spectrum range with a wavelength range of approximately 400-650 nm and it reflects green light. Carotenoids have absorbance within the visible spectrum of 400 nm and 500 nm.

In near infrared (NIR) spectroscopy, the reflectance of the NIR spectral data is obtained using NIR spectrometers. In order to process and analyse the spectral data, chemometrics using statistical methods are used to develop a calibration model (Iqbal *et al.*, 2019). One of the commonly used statistical method for the calibration model is partial least square (PLS) regression, which works by finding the linear regression model and then comparing the predicted FFB characteristics with the characteristics measured by chemical analysis (Cherie *et al.*, 2019).

In 2014, Makky and Sony used a portable VIS/NIR spectrometer with the wavelength range from 400-1000 nm to determine the ripeness of FFBs. Similar research was done by Iqbal *et al.* (2019) and Cherie *et al.* (2019) to determine the quality standards of FFBs using a shortwave infrared (SWIR) with a wavelength ranging from 1000-2500 nm (for water and oil content). Cherie *et al.* (2019) added to their predictive model the ability to predict the optimum harvest window. Simultaneous determination of quality parameters of vegetable oil could also be done by SWIR in less than a minute (Cherie *et al.*, 2019; Iqbal *et al.*, 2019).

In 2014, Makky and Soni applied two statistical methods to develop calibration models which are a forward-stepwise method to establish multiple linear regressions and a combination between principal component analysis (PCA) with multilayer perceptron neural network (Makky and Soni, 2014). Cherie *et al.* (2019) and Iqbal *et al.* (2019) used the statistical method PLS to develop the models to determine the ripeness and certain attributes of the FFBs related to its quality. Iqbal *et al.* (2019) showed that the calibration model using PLS performed well to predict the water content (based on absorbance data at 1900-2000 nm to indicate the presence of water) but not the oil content (based on absorbance data at the wavelengths of 1400-1500 nm). Thus, Iqbal *et al.* (2019) concluded that NIR spectroscopy can potentially be used to predict ripeness of FFBs based on its water content. However, the limitation of this method is the model developed is localised and only applicable for the study samples from the same oil palm plantation (Iqbal *et al.*, 2019). Cherie *et al.* (2019) used both PCA and PLC models to determine the oil content of the FFB using data obtained from the SWIR spectroscopy (1000-2500 nm).

Yap *et al.* (2019) used NIR spectroscopy at the wavelength range of 400-2200 nm with artificial neural network (ANN) to predict the FFBs ripeness. The spectral data was used for training of ANN model. ANN models with different number of hidden neurons ranging from 1-10 hidden neurons were tested to develop the most accurate model. After testing, results showed that a model with six hidden neurons has the lowest mean squared error (RMSE) and achieved the best prediction accuracy (Yap *et al.*, 2019). A study by Kasemsumran *et al.* (2012) used two near infrared (NIR) spectrometers, which are the long wavelength region of 1100-2500 nm (Silalahi *et al.*, 2016) due to the existence of fatty acids (Kawano *et al.*, 1995) and the visible-short wavelength region of 665-955 nm due to the existence of carotenoids at 700 nm (Moh *et al.*, 1999) and water at 900 nm (Kawano *et al.*, 1995). Quantitative analysis was performed to develop an oil calibration tool from using the NIR spectrometer as well as predicting the oil content of the FFBs (Kasemsumran *et al.*, 2012). Albakri *et al.* (2018) demonstrated the effectiveness of diffuse reflectance spectroscopy where the spectral analysis showed significant peaks at approximately 580-680 nm. The two wavelengths' peaks are correlated with the presence of chlorophyll and carotenoids in each ripeness stage. The study of the changes in the spectral data proved the applicability of spectroscopy as an assessment method (Albakri *et al.*, 2018).

Dan *et al.* (2018) studied the use of Raman spectroscopy in assessing and classifying the oil palm FFB ripeness levels. In Raman spectroscopy, a laser will illuminate a sample where the light incident on the sample will interact with the sample molecules and causes light scattering. The frequency of the scattered light is different from the incident light and is called Raman scattering (Bumbrah and Sharma, 2016). Dan *et al.* (2018) showed that Raman

TABLE 1. SUMMARY OF SPECTROSCOPY TYPE

Spectroscopy type	Wavelength	Detected component
Infrared (Makky and Soni, 2014)	400-650 nm 400-500 nm	Chlorophyll Carotenoids
Shortwave infrared (Cherie *et al.*, 2019)	1 000-2 500 nm	Water and oil content
Near infrared (Iqbal *et al.*, 2019)	1 900-2 000 nm 1 400-1 500 nm	Water content Oil content
Near infrared (Kawano *et al.*, 1995; Silalahi *et al.* 2016)	1 100-2 500 nm	Fatty acids
Near infrared (Moh *et al.*, 1999)	700 nm	Carotenoids
Near infrared (Kawano *et al.*, 1995)	900 nm	Water
Diffuse reflectance (Albakri *et al.*, 2018)	580-680 nm	Chloropyll and carotenoids

intensity of the FFBs increased from unripe to ripe due to the presence of carotenoid compounds and the results obtained could also be used to develop an ANN model.

Based on the reviews done with a summary shown in *Table 1* and *Figure 1*, the use of lab and field spectroscopy in the classification of oil palm FFBs ripeness levels is feasible. The spectral data of each ripeness level will show peaks at specific wavelengths which will indicate the presence of chlorophyll or carotenes. However, it is not very practical for field usage as it requires lab equipment and expert personnel for operational purpose. In conclusion, there are several disadvantages of conventional spectroscopy such as requiring laboratory analysis and specific spectral measurements procedures, and the portable spectrometer is also not suitable for on-site handheld applications. The spectroscopy results may also not be accurate in the presence of surrounding light.

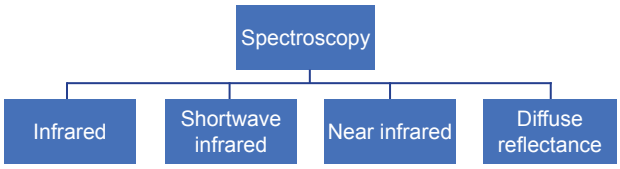


Figure 1. Summary of spectroscopy type used for the grading of oil palm FFBs.

Computer Vision

Computer vision is a scientific field in which information such as colour or brightness patterns can be extracted from digital images (Krishna, 2017; Prince, 2012). The extraction is done by analysing every pixel, grouping them and detecting edges which will eventually form the features which define every image (Bhardwaj *et al.*, 2019). Computer vision technique is being used in the agro-industrial field for automatic fruit harvesting and fruit scanning in supermarkets as well as in fruit sorting machines (Rachmawati *et al.*, 2017). One of the algorithms used in computer vision technique is convolution neural network (CNN). CNN is also used in deep learning algorithms. Deep learning is a class of machine learning which utilises many processing layers and this allowed improvements in speech recognition, object detection, visual object detection and other applications (Lecun *et al.*, 2015). CNN is one of the main deep learning architectures used for pattern recognition. CNN is designed to take advantage of the multiple array structure of the input image (Albawi *et al.*, 2018). CNN relies on the huge number of layers with a complex structure which allows it to process complex data. CNN is commonly used as a classifier to grade FFBs (Onoja *et al.*, 2019; Saleh and Liansitim, 2020).

In 2020, Saleh and Liansitim applied deep learning methods to develop an algorithm to classify FFBs of ripe and unripe classes based on their colour. CNN is used as a classifier of the ripeness of FFBs which identifies the colour feature of each class. The model reached 96% of training accuracy and 97% of validation accuracy (Saleh and Liansitim, 2020). Ibrahim *et al.* (2018) used a similar method of classifying oil palm fruits using CNN. They classified four ripeness classes and compared the results with hand-crafted features such as colour moments (accuracy of 67%), Fast Retina Key Point (FREAK) binary (accuracy of 71%) and Histogram of Oriented Gradient (HOG) texture (accuracy of 75%) with Support Vector Machine (SVM) as a classifier and with a pre-trained CNN model. Results of the hand-crafted feature with SVM shows the highest classification accuracy by HOG. AlexNet, a deep learning CNN developed to classify large dataset images (Krizhevsky *et al.*, 2017), was able to classify FFBs with 100% accuracy at a longer processing time and a CNN model consisting of a convolutional layer, a Rectified Linear unit (ReLu) layer, a pooling layer and followed by a fully connected layer (classification layer), showed the highest accuracy with significantly less processing time (Ibrahim *et al.*, 2018).

Wong *et al*. (2020) developed a computer vision algorithm with two functions to classify the ripeness of the oil palm fruit. The first function is to segment out the section of the image that contains the tree and the second function is to classify the ripeness of the oil palm fruit. The sliding method is used to separate the section of the palm tree. AlexNet is retrained on fully labelled dataset with different categories of oil palm fruit ripeness. The algorithm was able to show 85% accuracy on the test dataset (Wong *et al*., 2020).

Another application of the computer vision technique by Prasetyo *et al.* (2020) compared the performance of four deep learning models for detection and calculation of FFBs which are regional-based Convolutional Neural Network (R-CNN), Inception model V2 and V3 and ResNet (Prasetyo *et al*., 2020). Herman *et al.* (2020) proposed a model using a residual-based attention mechanism that could classify ripeness levels by recognising small detail differences between images. The highest accuracy achieved was 69% and this showed the effectiveness of the novel residual attention mechanism in recognising the small differences between different ripeness levels (Herman *et al*., 2020).

Computer vision technique has proven its efficiency in the application of ripeness classification with high accuracy compared to other techniques. This technique also allows the future improvement of real-time detecting and classifying FFBs on site. It allows human graders to correctly harvest the bunches at the optimum time with a user-friendly interface. It can be developed to be used on the mobile phone utilising onboard camera and this can offer a better solution for grading. Images captured with a regular phone camera which is normally in red-green-blue (RGB) format can be fed directly to the model for inference with no required pre-processing from the user. The drawback of this technique is that it requires time to find the right algorithm architecture and a big dataset for a high accuracy. With the advantage exceeding the drawbacks, computer vision techniques offer a viable solution for classifying the ripeness of oil palm FFBs. *Table 2* shows a summary of some of the computer vision techniques discussed in this section. It can be seen that different classification of ripeness levels have been investigated with a varying range of accuracy using different computer vision techniques.

Digital Image Processing

Digital image processing is a subset of computer vision. Digital image processing includes the digitalisation, histogram, segmentation, filtering, manipulation, wrapping and compression of images (Bezdek *et al*., 1999). Digital image processing technique uses a digital camera to capture the RGB images of the FFBs and extracts the colour feature of the RGB images using certain algorithms. As colour is an indication of oil palm ripeness (Shabdin *et al*., 2016), colour is analysed through colour analysis which extracts the RGB value from images which is unique for each ripeness class. Further processing can be done such as conversion to different colour space such as L*a*b, HIS and others (Azad *et al*., 2017).

Choong *et al.* (2006) studied the correlation between the OC of different maturity level of FFBs with its colour band. Digital image processing was utilised by using graphic mask operation and multi-plain histogram. The collected images are of ripeness levels of ripe, under ripe and over ripe. The results showed correlation between the oil content and the red colour band (Choong *et al*., 2006).

Jaffar *et al.* (2009) did similar research using computer assisted photogrammetric technique to correlate the colour of the oil palm fruit to its OC. The photogrammetric methodology includes five phases which are image acquisition, image pre-processing, image segmentation, digital number (DN) calculation and classification of the FFBs. The images were then processed to eliminate noise. Image segmentation

TABLE 2. SUMMARY OF COMPUTER VISION TECHNIQUES

Computer vision technique	Classification class	Accuracy
Convolution neural network (Saleh and Liansitim, 2020)	Ripe and unripe	96% (training)
Convolution neural network (Ibrahim *et al*., 2018)	Ripe, unripe, overripe and under-ripe	100% (AlexNet) 75% (HOG) 71% (FREAK)
Computer vision algorithm (Wong *et al*., 2020)	Ripe, unripe and under-ripe	85% (HSV)
Deep learning model (Herman *et al*., 2020)	Ripe, raw, less ripe, almost ripe, ripening, perfectly ripe and too ripe	69% (DenseNet Sigmoid) 69% (ResAtt DenseNet) 64% (DenseNet + SE Layer) 60% (AlexNet)

includes cropping the image, converting RGB to L*a*b colour space and segmenting the image using K-means. The average DN is calculated for the segmented and unsegmented images. The values for DN of the segmented images can be used to classify between ripe and unripe and the threshold value is 3.5 (Jaffar *et al*., 2009).

In 2013, Sunilkumar and Babu used models developed with RGB values as well as L*a*b values to classify the oil palm FFB. The colour values of the bunches were recorded using colorimeter of four ripeness classes. L* values range from 34.24 to 52.03, a* values range from -7.56 to 33.92 and b* values range from 3.09 to 49.54. RGB images of the bunches were captured using digital camera. The colour values for R range from 57.69 to 230.06, G values range from 39.41 to 114.74 and B values range 14.56 to 81.95. The L*a*b model has an accuracy of 89% in predicting the OC, which is higher than the RGB model which has an accuracy of 66% (Sunilkumar and Babu, 2013).

Hue, saturation, and intensity (HSI) colour models can also be used to correlate the ripeness of FFBs with the oil content. Tan *et al.* (2010) investigated a non-destructive technique to measure the colour of the fruits at different ripeness levels and correlated the collected colour data with the oil content. The images were captured using a digital colour camera with an infrared (IR) filtered tungsten halogen lamp. For each fruit bunch, images were taken from three different sides and the images were processed to compute the RGB values for hue histogram. Hue histogram is the average of each HSI data for each side of the FFB. The results initially showed a low correlation of r=0.7933 because some fruits had colour differences due to biological variation. When the FFBs had the same ripening patterns, the correlation between the OC and colour of the fruits improved to r=0.9519 (Tan *et al*., 2010). Shabdin *et al*. (2016) similarly used HSI model to classify ripe and unripe oil palm FFB. WEKA software was used to analyse the captured images. After converting the RGB values to HSI values using MATLAB, ANN was used as a classifier with an average accuracy of 70% (Shabdin *et al*., 2016).

Fadilah *et al.* (2012) developed an intelligent grading system. Multilayer perceptron (MLP) neural network was used as a classifier. MLP is one of the basic artificial neural network architectures and it consists of an input layer, a hidden layer and an output layer. To obtain the best MLP performance, several combinations of activation functions and output neurons were tested. Two methods were tested for classifying four ripeness levels. In the first method, ANN with full features was used as the MLP input. In the second method, PCA was used as a pre-processor to reduce the dimensionality. From the results, the first method showed 91.67% classification accuracy while the second method showed 93.33% classification accuracy (Fadilah *et al*., 2012). PCA successfully extracted the best features that could represent the data and feed it to the MLP instead of training the MLP with all the features which contain irrelevant data (Fadilah *et al*., 2012). In 2014, Fadilah and Mohamad-Saleh also used a similar methodology to develop an automated classification system. Two methods used to reduce the hue values were PCA and stepwise discriminant analysis (SDA). The results showed that using PCA with MLP gave the same results of 83.5% while SDA with MLP showed 94.0%. SDA was able to extract 12 features which best represent the data, compared with the 10 features extracted by PCA (Fadilah and Mohamad-Saleh, 2014).

An automated inspection machine has been developed by Makky *et al.* (2014) using machine vision. This research utilised the design of the inspection machine by Makky and Soni (2013). The machine aims to automatically inspect and determine the quality parameters of the oil palm from ripeness, OC and FFAs. Digital image processing model is utilised to assess the FFBs by transforming the RGB values to HSI which allows more data to be collected through the images (Gonzalez *et al*., 2009). The results proved the accuracy of the model to predict the ripeness, OC and FFAs (Makky *et al*., 2014).

A similar automated oil palm FFB inspection machine was developed by Alfatni *et al.* (2020) to classify the ripeness of the oil palm FFB. This work combined digital image processing with ANN with different regions of interest for comparison purposes. Statistical colour feature and colour histogram were used to collect the data for classification. Colour histogram model with ANN showed more reliable results and better classification accuracy compared to the statistical colour feature with an overall accuracy of 94% for an image size of 100 x 100 pixels (Alfatni *et al*., 2020).

Some of the methods used for digital image processing require specialised equipment that is not suitable to be deployed on site. Harvesters may not know how to operate the equipment and some of the photos also need special lighting for reliable classification. A simple experimental setup is required to ensure that it can be easily used by harvesters. *Figure 2* shows a summary of computer vision techniques used to grade the ripeness levels of oil palm FFBs. *Table 3* shows a summary of some digital image processing techniques discussed in this section.

Hyperspectral Imaging

Hyperspectral imaging is a combination of spectroscopy and imaging technique (Saaed *et al*., 2019). Hyperspectral image processing

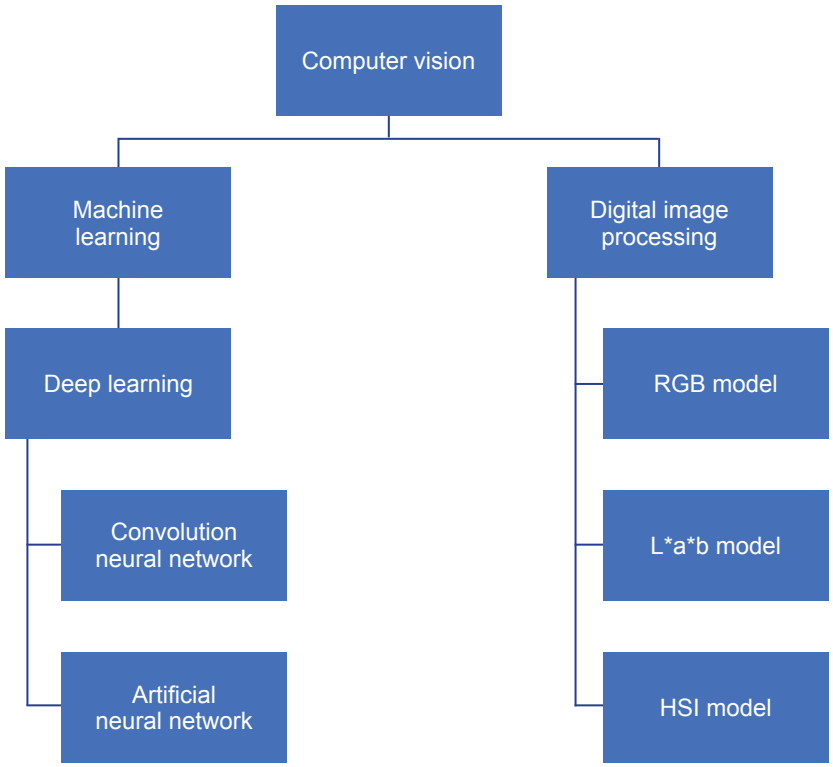


Figure 2. Summary of computer vision techniques used in grading oil palm FFBs.

TABLE 3. SUMMARY OF DIGITAL IMAGE PROCESSING TECHNIQUES

Digital image processing technique	Classification class	Results
Colour band (Choong *et al.*, 2006)	Ripe, under ripe and overripe	Correlation between oil content and red colour band
Photogrammetric (Jaafar *et al.*, 2009)	Ripe and unripe	Threshold value is 3.5
RGB and L*a*b (Sunikumar and Babu, 2013)	Ripe, unripe, under-ripe and overripe	89.00% (accuracy of L*a*b)
HSI model (Shabdin *et al.*, 2016)	Ripe and unripe	70.00% (accuracy of ANN)
Multilayer perceptron neural network (Fadilah *et al.*, 2012)	Ripe, unripe, under-ripe and overripe	93.33% (accuracy of ANN with PCA as reduced features) 91.67% (accuracy of ANN full features)
Automated inspection machine (M. Alfatni *et al.*, 2020)	Ripe, overripe and under- ripe	94.00% (accuracy of colour histogram model with ANN)

utilises computer algorithms to extract and manipulate the information from the vis-near infrared or near-infrared hyperspectral images for the purpose of classification, analysis and others. Typical hyperspectral image processing includes multiple phases which includes image acquisition, calibration, spectral processing, dimensionality reduction and classification (Park and Yoon, 2015). The hyperspectral camera measures the diffuse reflected light at a different wavelength from the surface of the object over a hundred contiguous narrow wavelengths (ElMasry and Sun, 2010). Chemical (such as OC and FFAs) and physical properties (such as shape, colour and texture) are analysed through the collected spectral data (Park and Yoon, 2015; Saaed *et al.*, 2019).

Junkwon *et al.* (2009) investigated the characteristics of oil palm FFB such as ripeness, OC and FFAs using hyperspectral imaging. Since the ripeness varies across the bunch, the data collected was from the whole bunch. The hyperspectral camera captures spectral images of wavelengths ranging from 400-1000 nm. Prediction models were developed based on the data collected. OC and FFA models showed coefficient of determination (R^2) 99.70% and 99.50% respectively. Ripeness was estimated using an average relative reflectance which showed an estimation rate of 97.92% (Junkwon *et al.*, 2009).

Bensaeed *et al.* (2014) detected the ripeness of oil palm fruits using hyperspectral imaging (HSI) at a wavelength range of 400-1000 nm. The study was conducted on three fruit types (*nigrescens*, *virescens* and *oleifera*). The collected data was used to train an ANN classification model according to different ripeness levels. Chlorophyll is present at approximately 675 nm while the ripeness of each category can be differentiated at wavelength 750-910 nm. The ANN classification model showed an accuracy of more than 95% for all the three fruit types (Bensaeed *et al.*, 2014).

Based on the reviews done on using hyperspectral imaging for ripeness classification of oil palm FFBs, it was found that hyperspectral imaging requires a specialised set up for the hyperspectral camera and a booth with uniform lighting for capturing the images as the surrounding light affects the performance of the imaging process. Thus, hyperspectral imaging is not suitable for handheld and on-site application due to its limitation with the set up and the need for expert personnel for operation.

Laser-light Backscattering Imaging

Recently, laser-light backscattering has been used in agriculture to detect the quality of fruits and vegetables (watermelon, bananas and potatoes) (Adebayo *et al.*,2016; Malaysia Department of Standards, 2007; Mohd Ali *et al.*, 2020; Mollazade *et al.*, 2012; Sunilkumar and Babu, 2013). Mohd Ali *et al.* (2020) studied the possibility of the combination of computer vision and laser-light backscattering imaging to measure the oil content of FFBs and detect the colour of three different ripeness levels. A charge coupled device (CCD) camera was used to capture the RGB images and backscattering images at different ripeness levels. The RGB and backscattering images were processed for optimal results. The results of the multivariate algorithm showed promising results of coefficient of determination (R^2) higher than 0.8 and an average classification accuracy of 85% (Mohd Ali *et al.*, 2020). Thus, laser-light backscattering imaging can potentially be used in the future for detecting the ripeness levels of oil palm FFBs.

Fruit Battery Sensor

Fruit battery is a sensor which consists of electrochemical cell. Two metal electrodes are inserted into the fruit to detect the chemical reaction that occurs in the fruit. The two chemical reaction processes are oxidation and reduction processes. Anode loses electrons during the oxidation process and cathode gains the electrons. This flow of electrons forms an electric current. Misron *et al.* (2020a) developed an oil palm fruit maturity sensor based on a battery sensor. The fruit battery is inserted on the fruit surface. The sensor is intended to be used by graders to sort the bunches before the milling process. The developed sensor was tested to measure the ripeness of four levels of ripeness. Each ripeness level generates a different voltage which is used for determining the maturity of each fruit. An average voltage of between 20 to 30 mV is considered ripe fruit while unripe fruits have an average voltage of 13 mV (Misron *et al.*, 2020a; 2020b). This sensor can potentially be used to detect the ripeness of the oil palm FFBs after it has been harvested, but not when it is still on the trees.

CONCLUSION

This article reviews and discusses non-destructive techniques to determine the ripeness of oil palm FFBs. The techniques discussed are spectroscopy, computer vision, digital image processing, hyperspectral imaging, laser-light backscattering imaging and fruit battery sensor. This review concluded that spectroscopy, hyperspectral imaging and laser-light backscattering need to be deployed with a specialised set up which is not suitable for real-time *in-situ* classification in the oil palm estate. Digital image processing technique requires special lighting conditions in lab and in the field. Computer vision technique does not require special lighting conditions as the image classification or object detection models are being trained on a variety of images of FFBs in different lighting conditions. Computer vision can also be implemented on mobile phones or a single board computer which is suitable for real-time on- site ripeness classification. Moreover, computer vision provides the feasibility of developing autonomous harvester as well as autonomous grading drone which can lead to huge advancement in the oil palm industry.

ACKNOWLEDGEMENT

The authors acknowledged that this work was funded and supported by the Ministry of Higher Education, Malaysia (MOHE-FRGS) with grant number FRGS/1/2019/TK04/MMU/03/7.

REFERENCES

Adebayo, S E; Hashim, N; Abdan, K and Hanafi, M (2016). Application and potential of backscattering imaging techniques in agricultural and food processing - A review. *J. Food Eng.*, *169*: 155-164.

Albakri, N; Abdullah, S; Supian, L S; Arsad, N; Zan, S D and Bakar, A A A (2018). Assessment of palm oil fruit bunch maturity based on diffuse reflectance spectroscopy technique. *IEEE 7th Int. Conf. Photonics (ICP 2018)*. Langkawi, Kedah. p. 1-3.

Albawi, S; Mohammed, T A and Al-Zawi, S (2018). Understanding of a convolutional neural network. *Proc. of 2017 International Conference on Engineering and Technology, ICET 2017*. Institute of Electrical and Electronics Engineers Inc. p. 1-6.

Alfatni, M S M; Mohamed Shariff, A R; Ben Saaed, O M; Albhbah, A M and Mustapha, A (2020). Colour feature extraction techniques for real time system of oil palm fresh fruit bunch maturity grading. *IOP Conf. Ser. Earth Environ. Sci.*, *540(1)*: 0-9.

Azad, M; Hasan, M and K M (2017). Color image processing in digital image. *Int. J. New Technol. Res.*, *3(3)*: 263334.

Basyuni, M; Amri, N; Putri, L A P; Syahputra, I and Arifiyanto, D (2017). Characteristics of fresh fruit bunch yield and the physicochemical qualities of palm oil during storage in North Sumatra, Indonesia. *Indones. J. Chem.*, *17(2)*: 182-190.

Bensaeed, O M; Shariff, A M; Mahmud, A B; Shafri, H and Alfatni, M (2014). Oil palm fruit grading using a hyperspectral device and machine learning algorithm. *IOP Conf. Ser. Earth Environ. Sci.*, *20(1)*: 012017.

Bezdek, J C; Keller, J; Krisnapuram, R and Pal, N R (1999). Image processing and computer vision - Fuzzy-models and algorithims for pattern recognition and image processing. *The Handbook of Fuzzy Sets Series (4)*. Springer, Boston, MA, USA. p. 547-678.

Bhardwaj, K K; Banyal, S and Sharma, D K (2019). Artificial intelligence based diagnostics, therapeutics and applications in biomedical engineering and bioinformatics. *Internet of Things in Biomedical Engineering.* Elsevier Inc., Amsterdam, Netherlands. p. 161-187.

Bumbrah, G S and Sharma, R M (2016). Raman spectroscopy-Basic principle, instrumentation and selected applications for the characterization of drugs of abuse. *Egypt. J. Forensic Sci.*, *6(3)*: 209-215.

Chalmers, J M; Edwards, H G M and Hargreaves, M D (2012). *Infrared and Raman Spectroscopy in Forensic Science.* John Wiley and Sons. Ltd, Chichester, UK. 648 pp.

Che Man, Y B; Moh, M H and Van De Voort, F R (1999). Determination of free fatty acids in crude palm oil and refined-bleached-deodorized palm olein using Fourier transform infrared spectroscopy. *J. Am. Oil Chem. Soc.*, *76(4)*: 485-490.

Cherie, D; Rini, R and Makky, M (2019). Determination of the optimum harvest window and quality attributes of oil palm fresh fruit bunch using non-destructive shortwave infrared spectroscopy. *Proc. of the 2nd International Conference on Biosciences and Medical Engineering (ICBME2019)*. Bali, Indonesia. p. 020034.

Choong, T S Y; Abbas, S; Shariff, A R; Halim, R; Ismail, M H S; Yunus, R; Ali, S and Ahmadun, F R (2006). Digital image processing of palm oil fruits. *Int. J. Food Eng.*, *2(2)*: 7-12.

Cornelius, J A (1966). Some technical aspects influencing the quality of palm kernels. *J. Sci. Food Agric.*, *17(2)*: 57-61.

Dan, S A M; Hashim, F H; Raj, T; Huddin, A B and Hussain, A (2018). Classification of oil palm fresh fruit bunches (FFB) using Raman spectroscopy. *Int. J. Eng. Technol.*, *7(4)*: 184-188.

Denis, J M (2014). The future of oil palm as a major global crop: Opportunities and challenges. *J. Oil Palm Res.*, *26(1)*: 1-24.

ElMasry, G and Sun, D W (2010). Principles of hyperspectral, imaging technology. *Hyperspectral Imaging for Food Quality Analysis and Control*. Elsevier. p. 3-43.

Fadilah, N and Mohamad-Saleh, J (2014). Color feature extraction of oil palm fresh fruit bunch image for ripeness classification. *13th Int. Conf. Appl. Comput. Appl. Comput. Sci.* p. 51-55.

Fadilah, N; Mohamad-Saleh, J; Halim, Z A; Ibrahim, H and Ali, S S S (2012). Intelligent color vision system for ripeness classification of oil palm fresh fruit bunch. *Sensors (Switzerland)*, *12(10)*: 14179-14195.

Gibon, V; Ayala, J V; Dijckmans, P; Maes, J and de Greyt, W D (2009). Future prospects for palm oil refining and modifications. *OCL - Ol. Corps Gras Lipides*, *16(4)*: 193-200.

Goh, K J; Wong, C K and Ng, P H C (2016). Oil palm. *Encycl. Appl. Plant Sci.*, *3(3)*: 382-390.

Gonzalez, R C; Woods, R E and Masters, B R (2009). Digital Image Processing. 3rd edition. *J. Biomed. Opt.*, *14(2)*: 029901.

Hanlan, J; Skoog, D A and West, D M (1973). *Principles of Instrumental Analysis.* Cengage Learning, Boston, USA. 1056 pp.

Harun, N H; Misron, N; Sidek, R M; Aris, I; Ahmad, D; Wakiwaka, H and Tashiro, K (2013). Investigations on a novel inductive concept frequency technique for the grading of oil palm fresh fruit bunches. *Sensors (Switzerland)*, *13(2)*: 2254-2266.

Herman, H; Susanto, A; Cenggoro, T W; Suharjito, S and Pardamean, B (2020). Oil palm fruit image ripeness classification with computer vision using deep learning and visual attention. *J. Telecommun. Electron. Comput. Eng.*, *12(2)*: 21-27.

Hussain, M; Bird, J J and Faria, D R (2019). A study on CNN transfer learning for image classification. *Advances in Intelligent Systems and Computing*. Springer, Germany. p. 191-202.

Ibrahim, Z; Sabri, N and Isa, D (2018). Palm oil fresh fruit bunch ripeness grading recognition using convolutional neural network. *J. Telecommun. Electron. Comput. Eng.*, *10(3-2)*: 109-113.

Iqbal, Z; Herodian, S and Widodo, S (2019). Development of partial least square (PLS) prediction model to measure the ripeness of oil palm fresh fruit bunch (FFB) by using NIR spectroscopy. *IOP Conf. Ser. Earth Environ. Sci.*, *347(1)*.

Jaffar, A; Jaafar, R; Jamil, N; Low, C Y and Abdullah, B (2009). Photogrammetric grading of oil palm fresh fruit bunches. *Int. J. Mech. Mechatronics Eng.*, *9(10)*: 18-24.

Junkwon, P; Takigawa, T; Okamoto, H; Hasegawa, H; Koike, M; Sakai, K; Siruntawineti, J; Chaeychomsri, W; Vanavichit, A; Tittinuchanon, P and Bahalayodhin, B (2009). Hyperspectral imaging for nondestructive determination of internal qualities for oil palm (*Elaeis guineensis* Jacq. var. *tenera*). *Agric. Inf. Res.*, *18(3)*: 130-141.

Kairi, M I; Baharudin, M S; Arnan, M Z; Rahman, A F; Abdu Hilmi, S M H S; Ngteni, R; Yunus, M F M and Asis, A J (2020). Possible changes in milling technology via industry 4.0. *Palm Oil Eng. Bull.*, *(134)*: 29-34.

Kasemsumran, S; Thanapase, W; Punsuvon, V and Ozaki, Y (2012). A feasibility study on non-destructive determination of oil content in palm fruits by visible-near infrared spectroscopy. *J. Near Infrared Spectrosc.*, *20(6)*: 687-694.

Kawano, S; Abe, H and Iwamoto, M (1995). Development of a calibration equation with temperature compensation for determining the brix value in intact peaches. *J. Near Infrared Spectrosc.*, *3(4)*: 211-218.

Kitchin, C R (2004). Introduction to spectroscopy. *Optical Astronomical Spectroscopy.* IOP Publishing Ltd. 288 pp.

Krishna, R (2017). Computer vision: Foundation and applications. *Ref. B.*, 213.

Krizhevsky, A; Sutskever, I and Hinton, G E (2017). ImageNet classification with deep convolutional neural networks. *Communications of the ACM*. Curran Associates Inc., Red Hook, NY, USA. p. 84-90.

Kushairi, A; Loh, S K; Azman, I; Hishamuddin, E; Ong-Abdullah, M; Izuddin, Z B M N; Razmah, G; Sundram, S and Parveez, G K A (2018). Oil palm economic performance in Malaysia and R&D progress in 2018. *J. Oil Palm Res.*, *30(2)*: 163-195.

Lecun, Y; Bengio, Y and Hinton, G (2015). Deep learning. *Nature*, *521(7553)*: 436-444.

Lu, H; Wang, F; Liu, X and Wu, Y (2017). Rapid assessment of tomato ripeness using visible/near-infrared spectroscopy and machine vision. *Food Anal. Methods*, *10(6)*: 1721-1726.

Makky, M and Soni, P (2013). Development of an automatic grading machine for oil palm fresh fruits bunches (FFBs) based on machine vision. *Comput. Electron. Agric.*, *93*: 129-139.

Makky, M and Soni, P (2014). *In situ* quality assessment of intact oil palm fresh fruit bunches using rapid portable non-contact and non-destructive approach. *J. Food Eng.*, *120(1)*: 248-259.

Makky, M; Soni, P and Salokhe, V M (2014). Automatic non-destructive quality inspection system for oil palm fruits. *Int. Agrophysics*, *28(3)*: 319-329.

Malaysia Department of Standards (2007). MS 814:2007 Palm Oil - Specification (Second Revision).

MPOB, Economics and Industry Development Division, (2022). Malaysia Palm Oil Board. https://bepi.mpob.gov.my/index.php/en/, accessed on 25 January 2022.

Mat Sharif, Z B; Mohd Taib, N B; Yusof, M S; Rahim, M Z; Mohd Tobi, A L and Othman, M S (2017). Study on handing process and quality degradation of oil palm fresh fruit bunches (FFB). *IOP Conf. Ser. Mater. Sci. Eng.*, *203(1)*.

Mba, O I; Dumont, M J and Ngadi, M (2015). Palm oil: Processing, characterization and utilization in the food industry - A review. *Food Biosci.*, *10*: 26-41.

Misron, N; Ying, L Q; Firdaus, R N; Abdullah, N; Mailah, N F and Wakiwaka, H (2011). Effect of inductive coil shape on sensing performance of linear displacement sensor using thin inductive coil and pattern guide. *Sensors*, *11(11)*: 10522-10533.

Misron, N; Azhar, N S K; Hamidon, M N; Aris, I; Tashiro, K and Nagata, H (2020a). Fruit battery with charging concept for oil palm maturity sensor. *Sensors*, *20(1)*: 226.

Misron, N; Azhar, N S K; Hamidon, M N; Aris, I; Tashiro, K and Nagata, H (2020b). Effect of charging parameter on fruit battery-based oil palm maturity sensor. *Micromachines*, *11(9)*: 806.

Moh, M H; Che Man, Y B; Badlishah, B S; Jinap, S; Saad, M S and Abdullah, W J W (1999). Quantitative analysis of palm carotene using Fourier transform infrared and near infrared spectroscopy. *J. Am. Oil Chem. Soc.*, *76(2)*: 249-254.

Mohd Ali, M; Hashim, N and Abdul Hamid, A S (2020). Combination of laser-light backscattering imaging and computer vision for rapid determination of oil palm fresh fruit bunches maturity. *Comput. Electron. Agric.*, *169 (November 2019)*: 105235.

Mollazade, K; Omid, M; Tab, F A and Mohtasebi, S S (2012). Principles and applications of light backscattering imaging in quality evaluation of agro-food products: A review. *Food Bioprocess Technol.*, *5(5)*: 1465-1485.

Nambiappan, B; Ismail, A; Hashim, N; Ismail, N; Shahari, D N; Idris, N A N; Omar, N; Salleh, K M; Hassan, N A M and Kushairi, A (2018). Malaysia: 100 years of resilient palm oil economic performance. *J. Oil Palm Res.*, *30(1)*: 13-25.

Nturambirwe, J F I; Nieuwoudt, H H; Perold, W J and Opara, U L (2019). Non-destructive measurement of internal quality of apple fruit by a contactless NIR spectrometer with genetic algorithm model optimization. *Sci. African*, *3*: e00051.

Onoja, E; Chandren, S; Abdul Razak, F I; Mahat, N A and Wahab, R A (2019). Oil palm (*Elaeis guineensis*) biomass in Malaysia: The present and future prospects. *Waste and Biomass Valorization*, *10(8)*: 2099-2117.

Park, B and Yoon, S C (2015). Real-time hyperspectral imaging for food safety. *Food Engineering Series*. Springer, Germany. p. 305-329.

Prasetyo, N A; Pranowo; Santoso, A J; Pranowo, and Santoso, A J (2020). Automatic detection and calculation of palm oil fresh fruit bunches using faster R-CNN. *Int. J. Appl. Sci. Eng.*, *17(2)*: 121-134.

Prince, S J D (2012). *Computer Vision*. Cambridge University Press, Cambridge. 598 pp.

Rachmawati, E; Supriana, I and Khodra, M L (2017). Toward a new approach in fruit recognition using hybrid RGBD features and fruit hierarchy property. *Int. Conf. Electr. Eng. Comput. Sci. Informatics*, *2017(1)*: 1-6.

Saaed, O M Ben; Alfatni, M S M; Rashid, A; Shariff, M; Hawedi, H S; Saaed, O M Ben; Alfatni, M S M; Rashid, A; Shariff, M and Hawedi, H S (2019). Modeling ripeness grading of palm oil fresh fruit bunches through image processing using artificial neural network. *Geo-SPMag°8 24th edition*. p. 19-38.

Saleh, A Y and Liansitim, E (2020). Palm oil classification using deep learning. *Sci. Inf. Technol. Lett.*, *1(1)*: 1-8.

Sambanthamurthi, R (2000). Chemistry and biochemistry of palm oil. *Prog. Lipid Res.*, *39(6)*: 507-558.

Shabdin, M K; Shariff, A R M; Johari, M N A; Saat, N K and Abbas, Z (2016). A study on the oil palm fresh fruit bunch (FFB) ripeness detection by using hue, saturation and intensity (HSI) approach. *IOP Conf. Ser. Earth Environ. Sci.*, *37(1)*: 012039.

Silalahi, D D; Reaño, C E; Lansigan, F P; Panopio, R G; Bantayan, N C; Davrieux, F; Caliman, J P; Yuana, Y Y and Sudarno (2016). Near infrared spectroscopy: A rapid and non-destructive technique to assess the ripeness of oil palm (*Elaeis guineensis* Jacq.) fresh fruit. *J. Near Infrared Spectrosc.*, *24(2)*: 179-190.

Soh, A C; Wong, C K; Ho, Y W and Choong, C W (2009). *Handbook of Plant Breeding: Oil Crops*. Callisto Reference, New York, USA. 298 pp.

Stuart, B H (2004). *Infrared Spectroscopy: Fundamentals and Application*. John Wiley and Sons, New Jersey, USA. 245 pp.

Sunilkumar, K and Babu, D S S (2013). Surface color based prediction of oil content in oil palm (*Elaeis guineensis* Jacq.) fresh fruit bunch. *African J. Agric. Res.*, *8(6)*: 564-569.

Tan, Y A; Low, K W; Lee, C K and Low, K S (2010). Imaging technique for quantification of oil palm fruit ripeness and oil content. *Eur. J. Lipid Sci. Technol.*, *112(8)*: 838-843.

Utom, S L; Mohamad, E J; Ameran, H L M; Kadir, H A; Muji, S Z M; Rahim, R A and Pusppanathan, J (2018). Non-destructive oil palm fresh fruit bunch (FFB) grading technique using optical sensor. *Int. J. Integr. Eng.*, *10(1)*: 35-39.

Wong, Z Y; Chew, W J and Phang, S K (2020). Computer vision algorithm development for classification of palm fruit ripeness. *AIP Conf. Proc.*, *2233(May)*: 030012.

Yap, X Y; Chia, K S; Rahman, H A and Teh, V (2019). A non-destructive oil palm fruit freshness prediction system with artificial neural network. *Int. J. Integr. Eng.*, *11(8)*: 159-163.

Journal of Oil Palm Research Vol. 35 (4) December 2023 p. 555-581
DOI: https://doi.org/10.21894/jopr.2023.0003

PROSPECTS AND STATE-OF-THE-ART IN PRODUCTION OF BIO-BASED SUCCINIC ACID FROM OIL PALM TRUNK

NURUL ADELA BUKHARI[1]*; SOH KHEANG LOH[1]; ABDULLAH AMRU INDERA LUTHFI[2]; ABU BAKAR NASRIN[1] and PEER MOHAMED ABDUL[2]

ABSTRACT

Bio-based chemicals possess enormous market potential in realising a circular economy. Industrially, succinic acid (SA) is an important precursor for the establishment of a sustainable biochemical industry. This article reviews the potential of oil palm trunk (OPT) for SA production, from bioconversion aspects such as biomass pretreatment, enzymatic saccharification, and fermentation, to technological advancement and process economics, assisted by Actinobacillus succinogenes*. For commercial SA exploitation, the focus should be on finding cheap biomass feedstock and optimising unit processes either for a partial or total displacement of expensive chemical paths during fermentation. OPT has been hailed as a viable candidate for the cost-effective production of SA, given its nutrient- and carbohydrate-rich sap and bagasse for improving the intended pretreatment and hydrolysis technologies. Type of operating modes, process configurations and fermentation factors concerning medium, substrate and culture have been identified as keys for advancing SA production from OPT in recent years. Lastly, the potential of OPT as part of a biorefinery feedstock for multiple bioconversion towards effective environmental management is designed to put forth the vision of a circular economy in the palm oil industry.*

Keywords: bioconversion, biomass pretreatment, biorefinery, oil palm biomass, succinic acid.

Received: 5 August 2022**; Accepted:** 21 November 2022**; Published online:** 31 January 2023.

INTRODUCTION

Bio-based materials and product value chains have been identified as the most resource-efficient pathway in creating a circular bioeconomy (Lokesh *et al*., 2018). It includes optimal utilisation of biological resources (residues, by-products and side streams) and their conversion into a variety of value-added products such as food, feed, bio-product, biochemical and bioenergy. The transition from an oil-based to a bio-based economy holds great potential in reducing fossil dependency, contributing to socio-economic growth, rural development, environmental benefits and technological advances (da Silva *et al*., 2020). Lignocellulosic plant-based materials are abundant and renewable as versatile resources that can be converted into a wide range of value-added products. The biochemical conversion methods of lignocellulosic biomass have been established as the most suitable for depolymerising its polysaccharides into sugars, which serve as platform molecules for further conversion into desired bio-products via microbial fermentation (Castro *et al*., 2017).

Succinic acid (SA), also called butanedioic acid, remains a promising bio-based platform chemical due to its versatility as a precursor to various commodities and speciality chemicals. SA or its derivatives can be used directly as a source of food additives, pharmaceuticals, surfactants, detergents, solvents, biodegradable plastics and fuels (Nghiem *et al*., 2017). It has been conventionally produced from petrochemical feedstock, *n*-butane, via catalytic hydrogenation of maleic anhydride.

[1] Malaysian Palm Oil Board,
6 Persiaran Institusi, Bandar Baru Bangi,
43000 Kajang, Selangor, Malaysia.

[2] Department of Chemical and Process Engineering,
Faculty of Engineering and Built Environment,
Universiti Kebangsaan Malaysia,
43600 UKM Bangi, Selangor, Malaysia.

* *Corresponding author e-mail: adela@mpob.gov.my*

Given an increase in worldwide environmental awareness associated with the petrochemical process, there has been a shift in world demand towards producing SA via microbial fermentation (Lee *et al*., 2022). However, bio-based SA production cost is unattractive and remains a tall order to compete with the giant petroleum-derived chemicals. Globally, much effort has been made to produce SA using *Actinobacillus succinogenes* from inexpensive and renewable feedstocks, including sugarcane bagasse, corn stover, corn fibre, carob pods (Lu *et al*., 2021), oil palm empty fruit bunch (OPEFB) (Khairil Anwar *et al*., 2021), oil palm frond (OPF), as well as oil palm trunk (OPT) (Luthfi *et al*., 2018).

Malaysia, one of the world's largest palm oil producers, has an oil palm planted area of 5.87 million hectares in 2020 (Parveez *et al*., 2021). Along with the production of crude palm oil, the Malaysian palm oil industry produces a huge amount of oil palm biomass from its plantations and milling activities. OPF, OPT and leaves can be obtained from oil palm plantations during the harvesting period and the rejuvenation of old plants, whereas other residues, such as OPEFB, are generated from palm oil mills (Yong *et al*., 2022). With its abundance, renewability, and low cost, OPT is a potential biomass for bioconversion. Only a small portion of the felled OPT is currently being used for plywood manufacturing and may be sold to interested parties, while the remainder is being shredded and mulched in the field to degrade naturally for nutrient recycling (Naidu *et al*., 2020). This conventional practice provides fertile grounds for the propagation of various pests and vermin, prompting the search for an alternative to exploit and tap the true potentials of underutilised OPT. The bioconversion of OPT into SA seems promising (Bukhari *et al*., 2021b) and could be a practical and profitable way to diversify its utilisation.

As biomass is a lignocellulosic material with varying degrees of recalcitrance, it is desirable to develop an efficient, low-cost, and environmental-friendly pretreatment method to facilitate biodegradation. Each pretreatment method has a different impact on all the subsequent bioconversion steps, in terms of sugar recovery, the toxicity of hydrolysates, enzymatic saccharification and fermentation (Castro *et al*., 2017). Many aspects of bioconversion must be considered for upscaling and commercialisation attempts, such as pretreatment process selection, cost-effectiveness (use of inexpensive and minimal chemicals), and route selection for efficient and easy-to-operate bioconversion. In addition, several problems have been encountered in SA production through microbial fermentation specifically by *A. succinogenes* such as substrate requirements, auxotrophy, inhibitory effect and low production rate. This article reviews the prospect of SA and analyses each steps in bioprocessing OPT for the production of SA by *A. succinogenes*, and provides an insight into its totality and practicality as a potential biomass feedstock for SA production in the future.

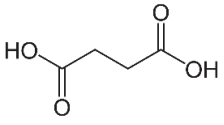
BACKGROUND AND PROPERTIES OF SUCCINIC ACID

In Europe, SA has historically been used as a general curative and natural antibiotic. Anecdotal evidence has suggested that it could promote neural system recovery, strengthen the immune system, compensate for energy drain in the body and brain, boost alertness, concentration and reflexes, and reduce stress (Vávra, 2009). Other traditional applications of SA include food additives, pharmaceutical intermediates, cosmetics, cement additives, detergents, plasticisers, toners and soldering fluxes (Nghiem *et al*., 2017). Before the emergence of fermentation technology for industrial production, SA was commercially manufactured from the by-product (C4 fractions) of naphtha, *i.e.*, a four-carbon compound (maleic acid or anhydride) via catalytic hydrogenation (*Figure 1*). However, due to price volatility and relatively high carbon footprints, the use of petroleum-based SA has been controversial. With growing public concern in recent years about overcoming this challenge, SA production has begun, driven by the desire to exploit renewable plant-based feedstock (Mancini *et al*., 2019).

Given its broad range of opportunities for various applications, SA has thus far been well-received as a versatile platform chemical. Its potential is reflected in the US Department of Energy's list as being one of the top 12 most promising value-added bio-based chemicals (Werpy and Petersen, 2004). Also known as butanedioic acid ($C_4H_6O_4$) or amber acid, SA is a four-carbon aliphatic dicarboxylic acid, with the two -COOH groups attaching to two different C atoms. It appears as an odourless and colourless crystalline solid. *Table 1* outlines its chemical structure and properties.

TABLE 1. PHYSICAL PROPERTIES OF SUCCINIC ACID

Properties	Value
IUPAC ID	Butanedioic acid
Formula	$C_4H_6O_4$
Molar mass (g mol^{-1})	118.09
Density (g cm^{-3})	1.56
Boiling point (°C)	235.00
Melting point (°C)	184.00
Specific gravity	1.56
pK_{a1}	4.21
pK_{a2}	5.64



Succinic acid
[CAS 110-15-6]

Source: Lin *et al*. (2005).

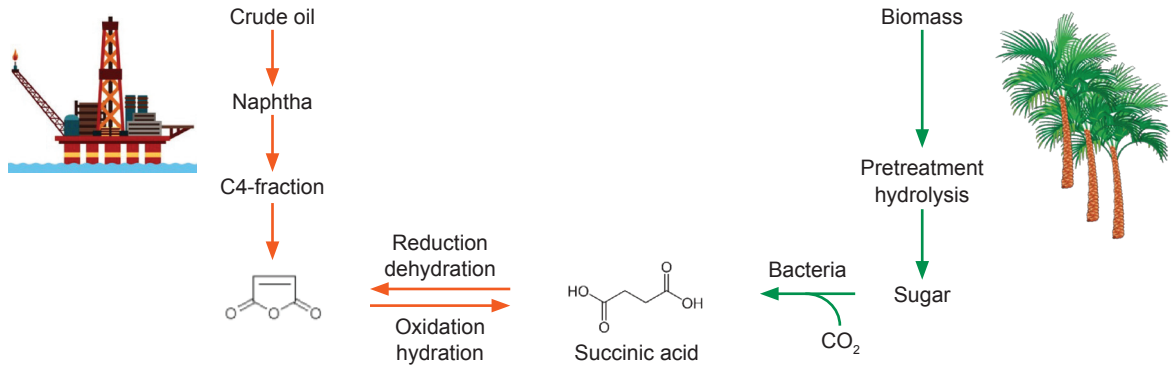


Figure 1. Production routes for succinic acid (adapted from Mancini et al.*, 2019).*

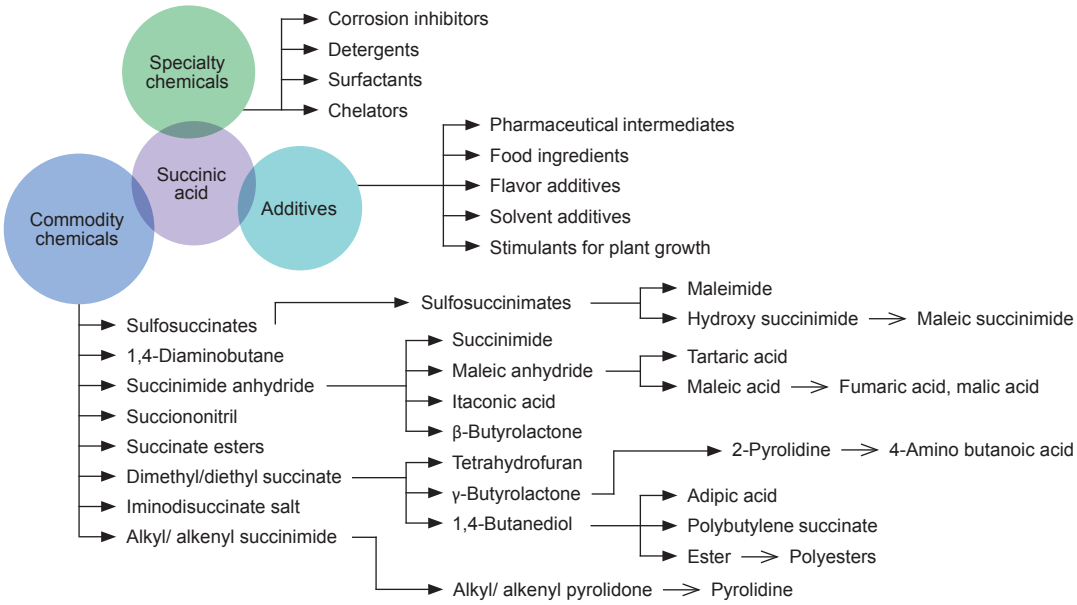


Figure 2. Various applications of succinic acid and its derivatives. Adapted from Akhtar et al.*, 2014.*

MARKET POTENTIAL AND APPLICATIONS OF SUCCINIC ACID

The commercial roles and fields of applications of SA and its derivatives are manifold (*Figure 2*). In detergency, SA is employed to produce additives, detergents, foaming agents and surfactants. In coating, it is applied as an ion chelator for pitting and anti-corrosion purposes. In agriculture, it has the role of a growth regulator for seed treatment and plant rooting (Cao *et al.*, 2013).

SA is used for various applications in the food industry. It acts as an acidity regulator, flavour-conditioning agent, bread-softening agent, flavour or oil micro-encapsulator and sweetener. Additionally, it improves the shelf life of food products, given its antimicrobial properties to inhibit the growth of bacteria, yeasts and moulds (Chimirri *et al.*, 2010). Generally considered safe by the United States Food and Drug Administration (Cao *et al.*, 2013), SA also offers utility potential in the pharmaceutical industry.

In cosmetic formulations, SA offers antioxidant properties and safety in manufacturing derivatives such as emollients, surfactants and emulsifiers (Palagina, 2017). Its high aqueous solubility favours its use as an effective alternative to salicylic acid as a preservative booster and therapeutic agent for anti-acne treatment (Wang *et al.*, 2014). SA has been reported to reduce the intensity of lipid peroxidation, potentially acting as an anti-pollution agent to improve product stability (Xiao *et al.*, 2012). Furthermore, it exhibits promising to energise and revitalise effects, given its role in enhancing mitochondrial activity in skin cells (Huffman *et al.*, 2014).

Recent applications involving SA lie in the polyester-polyurethane markets. Tetrahydrofuran (THF), γ-butylrolactone, and 1,4-butanediol (BDO) are some of the most popular chemicals deriving from SA (Nghiem *et al.*, 2017). THF is used widely as a solvent and feedstock for producing polytetramethylene ether glycol, which in turn is used as a precursor to making polyurethane

polymers. The most prominent role of SA in thermoplastic applications is the production of polybutylene succinate (PBS), a polyester derived from SA and BDO. The substantial demand for SA in PBS for food packaging is associated with non-toxicity, biodegradability and improved heat resistance (VMR, 2021). Moreover, BDO acts as a precursor to various speciality chemicals, which are used as solvents or raw materials in pharmaceuticals and agrochemicals (Cok *et al*., 2014).

In commercial terms, SA is priced at around USD5.9-9.0 kg^{-1} based on its purity. The estimated global SA market size in 2020 has been valued at USD147.42 million. With a compound annual growth rate of around 8.0% from 2021 to 2028, it is encouraging to anticipate a projected value of USD268.8 million by 2028 (VMR, 2021). During this forecast period, the adoption of SA as a promising alternative to adipic acid will be a key driver in the market for the production of polyurethane.

BIOCATALYSIS OF SUCCINIC ACID

As an intermediate of the tricarboxylic acid (TCA) cycle, SA represents a common metabolic end-product for many anaerobic microorganisms. While the choice of production host is diverse, the natural and native hosts being considered so far are capnophilic rumen microorganisms. On the other hand, non-natural production hosts are chosen based on their genetic accessibility, such as bacteria, yeast, fungi and recently microalgae (*Table 2*). The most commonly used strains include *A. succinogenes*, *Anaerobiospirillum succiniciproducens*, *Bacteroides fragilis*, *Corynebacterium crenatum*, *C. glutamicum*, *Mannheimia succiniciproducens*, *Escherichia coli*, *Saccharomyces cerevisiae* and *Yarrowia lipolytica* (Akhtar *et al*., 2014; Beauprez *et al*., 2010; Ong *et al*., 2019). Among these, *A. succinogenes* is reported as the most effective living reactor due to its capability to ferment a wide range of substrates (Guettler *et al*., 1999), including the four most abundant plant-based sugars, *i.e.*, glucose, fructose, xylose and arabinose.

Actinobacillus succinogenes as a Living Reactor

Originating from the *Pasteurellaceae* family, *Actinobacillus succinogenes* is a Gram-negative rod bacterium first isolated from the bovine rumen (Guettler *et al*., 1999). It is a facultative anaerobe with osmotolerant and pleomorphic properties. Its type strain is ATCC 55618. The complete genome of *A. succinogenes* 130Z was first publicly released via the GeneBank database in 2007, followed by detailed literature in 2010 (McKinlay *et al*., 2010). Several aspects of *A. succinogenes* as shown in *Table 3*, have been considered crucial for being one of the most promising SA-producing strains:

To produce succinate, *A. succinogenes* utilises the phosphoenolpyruvate (PEP) carboxylation pathway. *Figure 3* shows the carbon-flux distribution by *A. succinogenes* leading to the formation of succinate (alongside formate, acetate and ethanol). In this reductive TCA cycle, PEP is formed from the breakdown of glucose to serve as the branch point between the succinate-producing (C_4) pathway and the formate, acetate and ethanol-producing (C_3) pathway. These two reductive reactions allow for a balanced production of metabolites from PEP (Song and Lee, 2006).

Theoretically, 1.0 mol of SA can be produced from the fixation of 1.0 mol of CO_2 and 0.5 mol of glucose, alongside the need for 2.0 mol of NADH. Accordingly, a noteworthy obstacle in securing high succinate yields through the anaerobic pathway is NADH limitation. Therefore, the molar yield of succinate is limited to 1.0 mol per mol glucose, assuming that all the carbon flux undergoes exclusively the anaerobic fermentative pathway (Cheng *et al*., 2013; Vuoristo *et al*., 2016).

TABLE 2. BIOCATALYSTS INVESTIGATED FOR MICROBIAL CONVERSION OF SUCCINIC ACID

Type	Microorganism	Yield (g g^{-1})	References
Bacterium	*Actinobacillus succinogenes**,#, *Anaerobiospirillum succiniciproducens**,#, *Basfia succiniproducens**,#, *Bacteroides fragilis*#, *Mannheimia succiniciproducens**,#, *Enterococcus faecalis*, *Enterococcus flavescens*, *Escherichia coli*#, *Fibrobacter succinogenes*, *Clostridium thermosuccinogenes*, *Corynebacterium crenatum*#, *Corynebacterium glutamicum*#, *Klebsiella pneumoniae*, *Ruminococcus avefaciens*, *Ruminococcus champanellensis*, *Selenomonas ruminantium*	0.29 - 1.23	Guettler *et al*. (1999); Beauprez *et al*. (2010); Lee *et al*. (2002)
Yeast	*Saccharomyces cerevisiae*#, *Yarrowia lipolytica*#, *Candida brumptii*, *Candida catenulate*, *Candida zeylanoides*, *Pichia kudriavzevii*, *Penicillium simplicissimum*,	0.22 - 1.17	Kamzolova *et al*. (2009); Prabhu *et al*. (2020)
Fungus	*Aspergillus niger*, *Trichoderma reesei*, *Byssochlamys nivea*, *Paecilomyces varioti*, *Lentinus degener*, *Fusarium* spp., *Penicillium simplicissimum*, *Rhizophus* sp.	0.18 - 0.95	Alcantara *et al*. (2017); Bechthold *et al*. (2008)
Microalgae	*Micractinium* sp. IC-44	0.66	Sorokina *et al*. (2020)

Note: *- The most efficient producers; #- the most commonly used.

TABLE 3. FEATURES OF *Actinobacillus succinogenes* AS SUCCINIC ACID (SA) PRODUCER

Feature	References
Direct fermentation of water-extracted sugars	Carvalho *et al*. (2016)
Capability to use a broad range of carbon sources, including C5 and C6 sugars, disaccharides, and others (glucose, xylose, cellobiose, sucrose, fructose, maltose, lactose, mannose, arabinose, mannitol, and glycerol)	Pereira *et al*. (2018); Yang *et al*. (2020)
Performing scalable biorefinery streams	Bradfield *et al*. (2015)
Tolerance to high concentrations of glucose Tolerance to impurities in hydrolysates, such as furfural and hydroxymethylfurfural (HMF)	Song and Lee (2006) Diaz *et al*. (2018)
Resistance to high concentrations of SA	Guettler *et al*. (1999)
Favouring high CO_2 availability and reducing power	McKinlay *et al*. (2005); Schindler *et al*. (2014)
Fixation and consumption of CO_2	Van Der Werf *et al*. (1997)
Non-pathogenicity	McKinlay *et al*. (2010)
Ability to form biofilms	Mokwatlo *et al*. (2019)

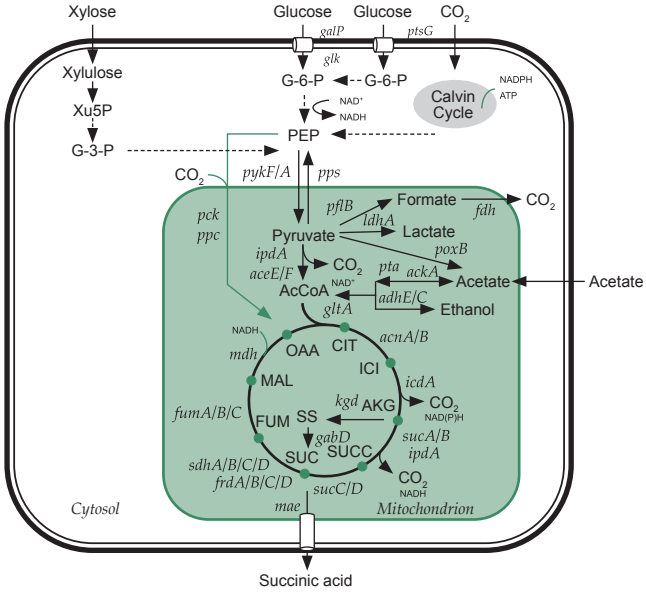


*Figure 3. Production pathways of succinic acid in prokaryotes (*e.g. A. succinogenes, M. succiniciproducens, E. coli, *and* C. glutamicum*). G-6-P: glucose-6-phosphate; G-3-P: glyceraldehyde-3-phosphate; PEP: phosphoenolpyruvate; CIT: citrate; ICI: isocitrate; AKG: α-oxoglutarate; SUCC: succinyl-CoA; SUC: succinate; FUM: fumarate; MAL: malate; and OAA: oxaloacetate (Dai* et al.*, 2020).*

In contrast to the practical application of engineered *E. coli* as a biocatalyst for SA production (Li *et al*., 2016), the metabolic engineering of *A. succinogenes* has been repressed by the lack of appropriate and complementing genetic tools (Dessie *et al*., 2018). Few attempts have thus been undertaken to develop different mutant strains of *A. succinogenes*. Zheng *et al*. (2013) adopted genome-shuffling techniques to improve SA production. However, it was difficult not only to achieve specific controllable traits caused by multiple randomly-occurring mutations but also to determine the exact mode of mutagenesis, with possible resultant irreversible genomic damage. Guarnieri *et al*. (2017) examined the knockout of enzymes involved in the pathways of by-product formation and the over-expression of enzymes in the reductive branch of the TCA cycle leading to SA production. Compared with the wild strain, the knockout mutants exhibited a delayed growth phase, slower sugar consumption, accumulation of unusual byproducts (*i.e.*, lactate), and lower SA production. As a whole, the metabolic engineering of *A. succinogenes* is still in an early incipient stage. Therefore, other perspectives for improving SA production warrant future investigations. These include a selection of efficient pretreatment, optimising fermentation conditions and simplifying overall process steps as strategies to achieve feasible SA processing.

Another challenge of using *A. succinogenes* is the requirement of expensive nitrogen sources such as yeast extract (YE) in fermenting SA. This is due to the presence of auxotrophic cells among the natural SA-producing strains isolated from the rumen, as

such cells rely on amino acids and vitamins readily available in a medium to function and replicate. Thus, complex media enriched with nutrients are necessitated to support the bacterial growth and biological activity of these strains (Beauprez *et al*., 2010). For fermentation using *A. succinogenes*, YE provides nutrients for bacterial growth and SA synthesis. Studies have reported the use of YE as high as 15-20 g L^{-1} in fermenting carob pod extracts (Carvalho *et al*., 2016), sugarcane molasses (Cao *et al*., 2018) and OPF hydrolysate (Luthfi *et al*., 2018). Unfortunately, the high costs of YE are impractical the for large-scale commercialisation of SA. Considerable effort has been devoted to reducing the costs by substituting YE with peanut meal, soybean meal, and cotton meal (Shen *et al*., 2015), corn steep liquor (Tan *et al*., 2016; Xi *et al*., 2013), Spent brewer's yeast hydrolysate (Jiang *et al*., 2010). However, there remain challenges for yield improvement as inferior SA yields have been reported, except for those mediums supplemented with additional biotin, vitamins and iron-containing compounds (Shen *et al*., 2016).

FEEDSTOCK FOR BIOCATALYSIS OF SUCCINIC ACID

Understanding the underlying mechanism of sugar uptake by the preferred biocatalyst is critical for determining low-cost alternative carbon sources as well as regulating metabolic pathways and fermentative processes for efficient SA production. *A. succinogenes* exhibits an excellent capability to metabolise a broad range of carbon sources due to its natural habitat (rumen of a ruminant), which is rich in various carbohydrate substrates (Dessie *et al*., 2018). In this context, the deployment of lignocellulosic biomass as feedstock for SA production has garnered global attention, considering their advantages - richness in carbohydrates, abundance, sustainability, and affordability. SA has been successfully produced from various lignocellulosic biomass (*Table 4*), such as sugarcane bagasse (Chen *et al*., 2021), corn fibre (Vallecilla-Yepez *et al*., 2021), blue agave (Corona-González *et al*., 2016), carob pod (Carvalho *et al*., 2016), Napier grass (Lee *et al*., 2022), citrus peel (Patsalou *et al*., 2017) and industrial hemp (Kuglarz and Grübel, 2018).

Lignocellulosic Oil Palm Biomass

Oil palm is regarded as the most economical and productive oil crop, accounting for approximately 77% of Malaysia's total agricultural land, *i.e.*, 5.9 million hectares in 2020 (Parveez *et al*., 2021). The Malaysian palm oil industry represents the largest contributor of lignocellulosic biomass, supplying more than 90% of the country's total biomass (Loh, 2017). Palm oil accounts for only 10% of the total dry matter of the mass harvested, with the remaining 90% made up of various biomass components (*Figure 4*). In terms of production, for each tonne of fresh fruit bunches (FFB) processed, approximately 225 kg of crude palm oil (CPO) is yielded. Besides, about 234 kg of OPEFB, 135 kg of mesocarp fibre (MF), 73 kg of palm kernel shell (PKS) and 67 kg of palm oil mill effluent (POME) are also generated. Furthermore, approximately 46 million tonnes of OPF and 22 million tonnes of OPT were estimated based on replanting and pruning activities in 2020. In terms of long-term soil management, more than 50% of OPF and OPT are allowed to decompose in the plantation sites (Loh, 2017).

As with other lignocellulosic biomass, oil palm biomass predominantly comprises three components, *i.e.*, cellulose, hemicellulose and lignin, alongside minor components such as starch, ash, extractives, water, minerals, silica and proteins (Eom *et al*., 2015b). Fibrous crystalline cellulose forms the core of the lignocellulosic complex, amorphous hemicellulose is found both between microfibrils and macrofibrils of cellulose, and lignin fills interfibrous areas and provides structural support to the lignocellulose matrices (Akhlisah *et al*., 2021).

Cellulose represents the major component of the cell wall of a plant. As a highly stable homopolymer, it consists of linear chains of D-glucose molecules linked by β-1,4-glycosidic bonds with a degree of polymerisation of up to 15 000 (Bajpai, 2016). The even distribution of hydroxides on both sides of its

TABLE 4. COMPOSTION OF LIGNOCELLULOSIC BIOMASS FOR SUCCINIC ACID PRODUCTION

Biomass	Composition (%)			References
	Cellulose	Hemicellulose	Lignin	
Sugarcane bagasse	41.00	24.00	24.00	Chen *et al*. (2021)
Corn fibre	21.00	27.50	0.80	Vallecilla-Yepez *et al*. (2021)
Blue agave	42.00	22.00	18.00	Corona-Gonzalez *et al*. (2016)
Napier grass	41.18	30.15	6.68	Sriariyanun *et al*. (2017)
Citrus peel	33.98	9.99	6.93	Rivas-Cantu *et al*. (2013)
Industrial hemp	40.10	16.00	14.80	Kuglarz and Grübel (2018)

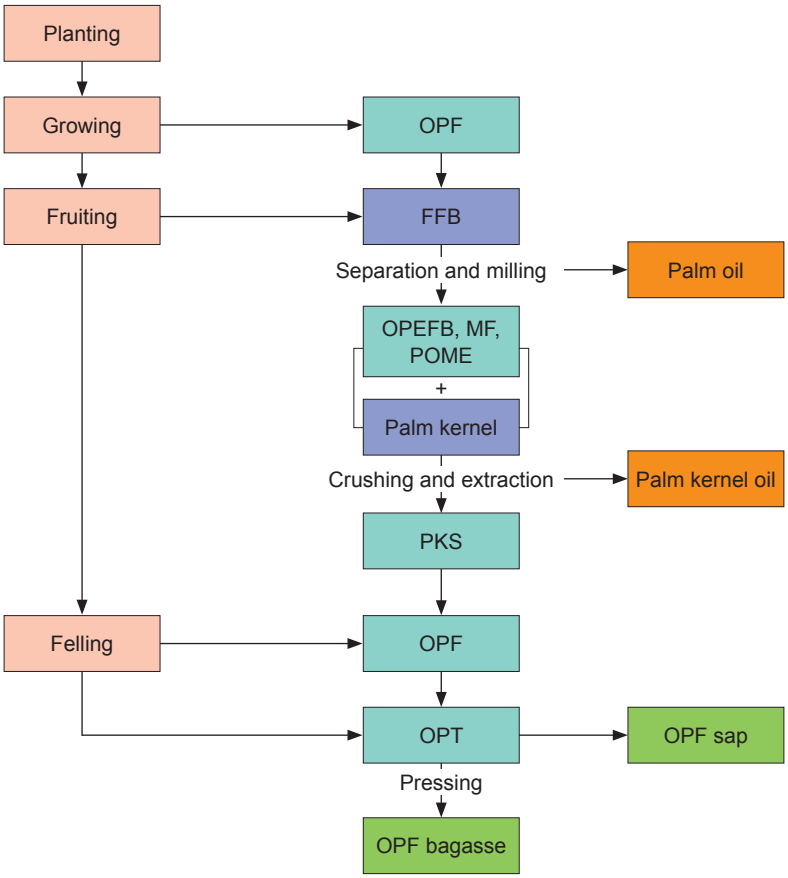


Figure 4. Biomass produced during the lifetime of an oil palm. Light blue: Biomass residues; yellow: commercialised products, green: biomass of this study. OPF - oil palm frond; FFB - fresh fruit bunch; OPEFB - oil palm empty fruit bunch; MF - mesocarp fibre; POME - palm oil mill effluent; PKS - palm kernel shell; OPT - oil palm trunk. Adapted from Dirkes et al.*, 2021.*

monomers allows for the formation of intra- and inter-molecular hydrogen bonds. Given such strong hydrogen bonding, cellulose is not only insoluble in most common solvents, including water, but also resistant to hydrolysis (Taherzadeh and Karimi, 2007a).

Hemicellulose, on the other hand, is a highly-branched polysaccharide. As a heteropolymer, it is structurally cross-linked with cellulose and lignin through hydrogen bonds with a degree of polymerisation of fewer than 200 (Asif, 2009). Hemicellulose is composed of a wide range of sugars including pentoses (such as xylose and arabinose) and hexoses (such as glucose, galactose, mannose, glucuronic acid, and galacturonic acid). Other deoxyhexose sugars such as rhamnose and fucose may also be found in trace amounts. The hydroxyl groups of these sugars are sometimes partially substituted with acetyl groups (Bajpai, 2016).

Lastly, lignin is the most abundant naturally occurring non-saccharide compound and a highly cross-linked aromatic heteropolymer distinctively different from other macromolecules of lignocellulosic biomass. Its predominant building unit, phenylpropane, comprises monolignols arranged in a three-dimensional (3D) amorphous structure. The most common monolignols, as precursors, are p-coumaryl (4-hydroxycinnamyl), coniferyl (3-methoxy-4-hydroxycinnamyl), and sinapyl (3,5-dimethoxy-4-hydroxycinnamyl) alcohols (Anwar *et al.*, 2014). These precursors are incorporated into the phenylpropane oligomers and labelled as p-hydroxyphenyl (H), guaiacyl (G), and syringyl (S) units, which collectively form the lignin structure (Fisher and Fong, 2014). It is noteworthy that lignin acts as a natural binding agent for both cellulose and hemicellulose in a 3D network, offering structural and mechanical support (Raud *et al.*, 2016). Hence, elevated lignin content is undesirable for bioprocessing as a much-reduced bioavailability of the substrate is to be anticipated due to the resistance of lignin to water and enzymes.

The amounts of carbohydrates and lignin depend on the type of biomass. Generally for oil palm biomass, the constituents are cellulose (44%-54%), hemicellulose (21%-34%), and lignin (10%-25%) (Akhlisah *et al.*, 2021; Diyanilla *et al.*, 2020; Loh, 2017). The high carbohydrate content of this type of biomass (>55%) offers very promising potential in bioconversion technologies (Ishak *et al.*, 2019; Pratiwi *et al.*, 2018).

Biomass of Focus in This Study - OPT

The economic lifespan of an oil palm tree ranges from 20 to 30 years, and the trees are usually replanted every 25 years to sustain oil productivity. Previously, the United Nations Environment Programme (UNEP, 2012) projected that about 128 296 ha of oil palms in Malaysia will be potential for OPT harvesting in the next decade. The distribution of potential areas for replanting is shown in *Figure 5*. In 2020, the availability of OPT was estimated to be 9.67 million tonnes (based on 75.5 t ha^{-1} of dry matter) from the total replanting area of 128 088 ha, covering Peninsular Malaysia (36%), Sabah (51%), and Sarawak (13%).

At present, OPT is mostly used as raw material in plywood manufacturing. The limited application has created a surplus, which is cut and shredded into pieces, spread on plantation sites and left to decompose for nutrient recycling. This conventional practice has been adopted since 1985 when open burning is prohibited entirely in Malaysia (Noor, 2003). Given the high lignin content and carbon to nitrogen (C:N) ratio (Loh *et al*., 2013), it may take approximately two years for the biomass to completely decompose (Murai *et al*., 2009), culminating in the rise of greenhouse gas (GHG) levels. Additionally, given the high sugar and moisture contents, the outer parts of OPT are susceptible to insect pests such as rhinoceros beetles, one of the most serious pests to oil palms, while the inner parts are attacked by white-rot fungi (Bahmani *et al*., 2016). It also serves as a carbon source for *Ganoderma* sp. to initiate basal stem rot infection, a major problem in the oil palm industry (Naidu *et al*., 2020). The presence of a large amount of OPT residue disrupts replanting and results in adverse effects on soil functioning and subsequent field maintenance (Uke *et al*., 2021). Under the zero-burning policy, disposal of OPT residue remains a challenge and thus, an urgent need for practical uses.

Given the lignocellulosic nature of OPT, there is a vast possibility that biomass can be harnessed for value-added products. Despite the various R&D options made available for adoption and applications, only a few products/technologies have reached either pilot or commercial stage, *e.g.*, plywood, lumber, flooring, microcrystalline cellulose (MCC), panel products (medium-density fibreboards, particle boards, and cement boards), and animal feed pellets and fuel pellets (Hoong *et al*., 2012; Nordin *et al*., 2004). Some of the inherit characteristics, such as high moisture and fibrous, would have hindered the application of OPT without pretreatment for wood-based industries (Dirkes *et al*., 2021). The prospects of OPT are huge considering now that R&D emphasises its conversion into sugar, chemical derivatives, bioethanol, bioplastic, pulp and paper and dietary supplements (Murata *et al*., 2013). OPT is a unique biomass feedstock for bioconversion. An understanding of its chemical composition is essential to fully tap the benefits.

Characteristics of sap pressed from OPT. The moisture content in OPT amounting to 74–80 wt.% of the whole trunk is indicative of a substantial amount of sap (juice) (Bukhari *et al*., 2019b). The sugar composition of pressed OPT sap has been analysed using high performance liquid chromatography (HPLC) (*Table 5*).

The amount of sugars in OPT sap varies between 40 and 141 g L^{-1}, with glucose being identified as the most dominant free sugar (*Table 5*). Sugar bioavailability differs within the trunk itself, thus, it is pertinent to determine which part of OPT should be valorised to extract the most sugars. For example, Lokesh *et al.* (2012) used the central section, Komonkiat and Cheirsilp (2013) combined

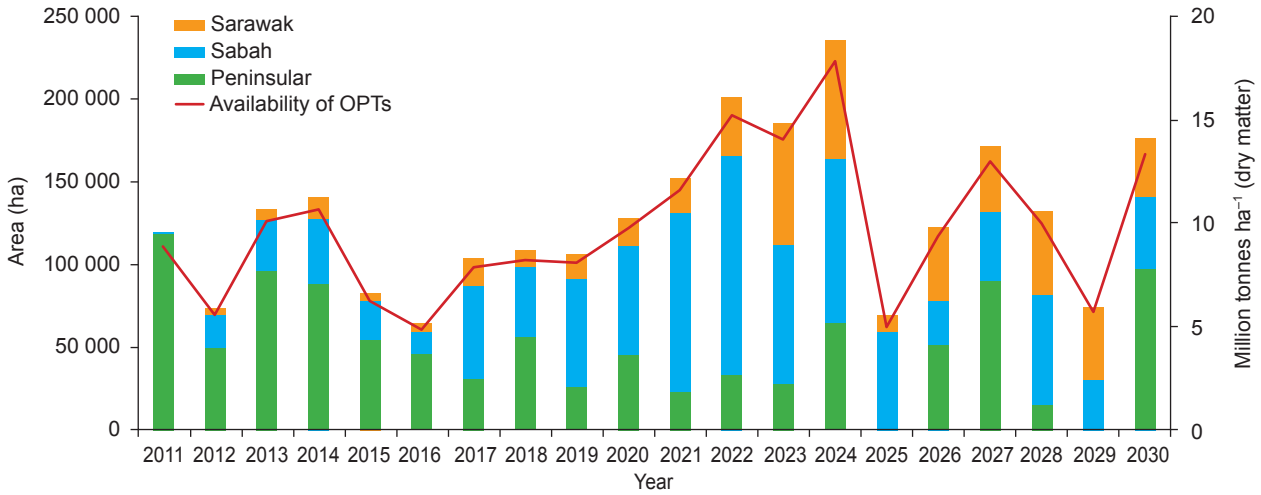


Figure 5. The potential dry weight of OPT deriving from the replanting sites. The area of a plantation site is estimated by subtracting the total area after 25 years from the total area of the subsequent year. Adapted from UNEP, 2012.

TABLE 5. COMPOSITION OF OIL PALM TRUNK SAP

Segmentation	Concentration of sugar (g L^{-1})					References
	Sucrose	Glucose	Fructose	Others*	Total	
Inner (central core)	33.28	16.01	1.55	4.58	55.42	Lokesh *et al*. (2012)
-	13.94	42.97	4.03	3.37	64.31	Norhazimah *et al.* (2013)
Combined whole	9.30	16.06	7.48	7.29	40.13	Komonkiat and Cheirsilp (2013)
Middle (7 cm disk)	31.90	67.40	38.50	3.50	141.30	Kunasundari *et al.* (2017)
Combined whole	10.10	26.73	5.89	n.d.	42.72	
Inner (top 2)	9.05	27.71	7.65	n.d.	44.41	
Inner (top 1)	14.81	33.12	4.07	n.d.	52.00	
Inner (bottom 2)	9.06	32.10	7.47	n.d.	48.63	
Inner (bottom 1)	9.16	28.87	4.19	n.d.	42.22	Bukhari *et al*. (2019b)
Middle (top 2)	10.24	18.67	8.02	n.d.	36.93	
Middle (top 1)	8.65	27.19	6.92	n.d.	42.76	
Middle (bottom 2)	8.70	20.61	4.95	n.d.	34.26	
Middle (bottom 1)	11.14	25.55	3.86	n.d.	40.55	

Note: n.d. - not determined; * - including galactose, maltose, xylose, arabinose and inositol.

all parts while Kunasundari *et al*. (2017) extracted a 7-cm disk from the middle of the trunk. Different heights and widths of the OPT were discovered to hold varying sugar compositions as well (Bukhari *et al*., 2019b) (*Table 5*). The sugar content increases from; 1) the outer to the inner zone, and 2) the lower to the upper of the OPT. The sap contains a higher sugar concentration in the inner zone (core area), where the parenchyma content is higher than in the outer area (Bukhari *et al*., 2019b). Regardless of the type of sugars, the OPT sap is undoubtedly rich in readily soluble fermentable sugars (mostly hexoses), which would be favoured by microorganisms and can be directly used as fermentative substrates.

Besides, OPT sap contains an abundance of free amino acids, vitamins, and macro- and micro-minerals. These are nutrients favourable for microbial fermentations (Bukhari *et al*., 2019b; Komonkiat and Cheirsilp, 2013; Kosugi *et al*., 2010). Various types of amino acids (*i.e.*, aspartic acid, lysine, arginine, glutamic acid, alanine, proline, methionine, *etc*.) and vitamins (*i.e.*, biotin, folic acid, cobalamin, niacin, pantothenic acid, pyridoxine, thiamine, *etc*.) are available in OPT sap (Bukhari *et al*., 2019b). As such, OPT sap can be considered an ideal feedstock for SA fermentation by *A. succinogenes*. Other bio-products that have been successfully biosynthesised from OPT sap are summarised in *Table 6*.

Unlike cellulosic woody or starchy materials, the use of pressed OPT sap is practically more economical, not only because no complex and expensive pretreatments are required, but also because it contains all the requisite sugars and nutrients for cell growth and product formation. In the biosynthesis of commodity chemicals, the cost of the substrate or the medium is a limiting and crucial factor for industrial-scale implementation. Cost-effective exploitation of OPT sap could help to revolutionise the bio-based industry. As calculated theoretically, approximately 123.2 t of sap could be attained from a ha of oil palm plantation; with a hypothetical sugar content of 4%, about 5 t of sugar could be produced (Dirkes *et al*., 2021). This represents nearly one-quarter of sugar beet yield (24 t sugar per ha), where cultivation is specific for sugar production (Hoffmann and Kenter, 2018). Accordingly, the sugary OPT sap offers viable potential for future implementation in the biotechnological fermentation of SA.

Characteristics of residual OPT bagasse. Alongside sap extraction, OPT bagasse (*i.e.*, fibre remaining after OPT pressing) likewise contains copious cellulosic materials that can be hydrolysed to produce monomeric sugars for subsequent fermentation (Bukhari *et al*., 2019a). Its high total structural carbohydrate content in the range of 57%-73% is ideal and favourable for microbial SA production (*Table 7*).

ESSENTIAL PROCESSES IN BIOCATALYSIS OF SA

Pretreatment of Lignocellulosic Materials

A notable barrier to recovering valuable materials from lignocellulosic bagasse is the degradation-resistant structure due to the presence of ester- and ether-based cross-linkages between the polysaccharides (cellulose and hemicellulose) and lignin. A pretreatment is therefore necessary to alter

TABLE 6. BIOTECHNOLOGICAL PRODUCTS PRODUCED FROM OPT SAP

Bio-product	Microorganism	Conditions	Titer ($g\ L^{-1}$)	Yield ($g\ g^{-1}$)	References
Ethanol	*Saccharomyces cerevisiae* ATCC 24860	30°C, pH 4.0 and 150 rpm for 24 hr	47.50	0.50	Adela and Loh (2015)
Ethanol	*Saccharomyces cerevisiae*	32°C, pH 6.0 and 170 rpm for 24 hr	-	0.55	Shahirah *et al*. (2015)
Ethanol	*Saccharomyces cerevisiae* CCT0762	30°C, pH 5.5 and 150 rpm for 24 hr	29.45	0.39	Mohd Zakria *et al*. (2017)
Ethanol	*Kluyveromyces marxianus* ATCC 46537	30°C, pH 5.5 and 150 rpm for 24 hr	29.61	0.39	
Butanol	*Clostridium acetobutylicum* DSM 1731	37°C, pH 6.0 and 120 rpm	7.29	0.36	Komonkiat and Cheirsilp (2013)
Butanol	*Clostridium beijerinckii* JCM 1390		2.29	0.22	
Lactic acid	*Bacillus coagulans* strain 191	55°C, pH 6.0 and 200 rpm	53.9	0.88	Kunasundari *et al*. (2017)
Polyhydroxyalkanoate	*Bacillus megaterium*	30°C, and 250 rpm for 16 hr	3.28	-	Lokesh *et al.* (2012)
Lipids	*Lipomyces starkeyi* NBRC 10381	30°C, pH 6.0 and 190 rpm for 96 hr	64.40	0.19	Juanssilfero *et al.* (2019)
Hydrogen	*Clostridium beijerinckii*	30°C, for 24 hr	1 973 mL L^{-1}		Noparat *et al.* (2012)

TABLE 7. COMPOSITION OF OIL PALM TRUNK FIBRE (BAGASSE)

Composition (%)				References
Cellulose	Hemicellulose	Total carbohydrates	Lignin	
38.85	23.84	62.69	20.36	Rattanaporn *et al*. (2018)
38.10	23.10	61.20	21.40	Noparat *et al*. (2017)
33.21	25.01	58.22	25.34	Pratiwi *et al*. (2018)
40.83	32.17	73.00	21.64	Tareen *et al*. (2021a)
33.90	31.90	65.80	n.d.	Ishak *et al*. (2019)
30.86	25.84	56.70	24.29	Bukhari *et al.* (2019a)

Note: n.d. - not determined.

such structural and compositional impediments to hydrolysis and subsequent degradation processes, to improve the digestibility and rate of enzymatic saccharification, and increase yields of targeted products (Luthfi *et al.*, 2017b). Pretreatment is the first step in bioconversion before saccharification. It overcomes biomass recalcitrance, which is caused by factors such as high lignin content, protection of cellulose by lignin, sheathing by hemicellulose, high cellulose crystallinity, degree of polymerisation, the low accessible surface area of cellulose and strong fibre strength (Akhlisah *et al.*, 2021). Pretreatment can be classified into four categories: Physical, physicochemical, chemical and biological (*Table 8*).

It is important to optimise the deployed pretreatment to match the chemical composition and internal structure of the corresponding biomass. Similarly, pretreatment should be prudently selected based on the targeted final products. In general, pretreatment aims to remove lignin, decrease cellulose crystallinity, increase accessible surface areas, and enhance the porosity of the materials, to facilitate subsequent enzymatic saccharification. Inefficient pretreatment leads to not only difficulties in hydrolysing or saccharifying the resultant residues by hydrolytic enzymes, but also the production of a considerable amount of toxic compounds that could possibly inhibit subsequent microbial fermentation. Therefore, pretreatment critically governs the economics of biomass conversion.

Typically, an effective pretreatment method must be able to produce a highly digestible cellulose material that can be easily hydrolysed at a low enzyme loading rate, minimise feedstock preparation and pre-processing prior to pretreatment, maximise recovery of all carbohydrates in usable forms, produce none or trace amounts of lignin-degrading products and other fermentation inhibitors and finally lower energy demand or allow reuse of energy. This will greatly enhance operational costs with low capital investment (Galbe and Zacchi, 2012; Shuai *et al.*, 2010).

TABLE 8. ADVANTAGES AND LIMITATIONS OF PRETREATMENT METHODS FOR OIL PALM TRUNK

Pretreatment method	Advantages	Limitations
Physical		
Mechanical/milling/ grinding	• Reduces cellulose crystallinity • Increases surface area	• High power and energy consumption
Physicochemical		
Steam explosion	• Causes lignin transformation • Partial hemicellulose solubilisation • Higher yield of glucose and hemicellulose in the two-step method • Industrially developed	• Generation of toxic compounds • Energy-intensive
Ammonia based (AFEX, ARP, SAA, LLA, LMAA, PAH)	• Increases accessible surface area • Low formation of inhibitors • Easy to recover and recycle	• Not efficient for raw materials with high lignin content • High cost of a large amount of ammonia • High energy required to maintain process temperature
CO_2 explosion	• Efficient removal of lignin • Increases accessible surface area • Cost-effective • Does not imply the generation of toxic compounds	• Does not affect lignin and hemicellulose • Very high-pressure requirements
Wet oxidation	• Efficient removal of lignin • Low formation of inhibitors • Minimises the energy demand (exothermic)	• High cost of oxygen and alkaline catalyst
Hydrothermal/LHW	• Cost-effective • Low formation of inhibitors	• High temperature demands high energy
Sulfite-based	• Depolymerising cellulose • Efficient removal of hemicellulose • Sulfonation of lignin	• High temperature demands high energy
Chemical		
Ozonolysis	• Selective lignin degradation • Does not imply the generation of toxic compounds • Operation at ambient temperature and pressure	• High cost due to a large amount of ozone needed
Organosolv	• Causes lignin and hemicellulose hydrolysis	• High cost • Requirement of solvent removal from the system
Alkaline	• Removal of lignin and hemicellulose, increase accessible surface area • Low formation of inhibitors	• Long residence time • Less lignin removal • Irrecoverable salts
Concentrated acid	• High glucose yield • Ambient temperatures	• High cost of acid and need to be recovered • Reactor corrosion problems • Formation of inhibitors
Diluted acid	• Fewer corrosion problems than concentrated acid • Solubilises hemicellulose • Alters lignin structure • Pre-hydrolysing cellulose	• Generation of degradation products • Requirement for neutralisation
Deep eutectic solvent	• Low formation of inhibitors • Dissolution of cellulose	• Pre-commercial
Ionic liquids	• Minimum degradation of desired products • Operation at low temperature	• Expensive • Requirement of washing before reuse
Biological		
Fungi, bacteria, archaea	• Degrades lignin and hemicellulose • Mild environmental conditions • Low capital cost • Low energy consumption	• Very low rate of hydrolysis • Loss of carbohydrates as consumedby the microbes • Contamination problems

Note: AFEX - ammonia fibre explosion/expansion; ARP - ammonia recycle percolation; SAA - soaking in aqueous ammonia; LLA - low-liquid ammonia; LMAA - low-moisture anhydrase ammonia; PAH - pressurised ammonium hydroxide; LHW - liquid hot water. Adapted from Alvira *et al*., 2010; Taherzadeh and Karimi, 2007b; Wang *et al*., 2009.

Exploration work on different pretreatment methods is somewhat limited for OPT (*Table 9*). Existing literature has highlighted physicochemical (hydrotreatment) (Eom *et al*., 2015a) and chemical pretreatment; including dilute acid (Noparat *et al*., 2015; Rattanaporn *et al*., 2018), sulfite (Noparat *et al*., 2017), and deep eutectic solvents (DES) (Zulkefli *et al*., 2017). Such pretreatments enhance the recovery and reveal the available fermentable sugars in OPT that could be referenced in SA production.

As outlined in *Table 9*, hydrothermal pretreatment or liquid hot water/autohydrolysis is one of the most promising among the low-cost pretreatment options, given the use of only water as the reaction medium at temperatures ranging from 160°C to 200°C. The identified optimum conditions in pre-treating OPT is 180°C for 30 min, which could yield the maximum amount of hemicellulosic sugars, with low concentrations of both furfural and HMF (Eom *et al*., 2015b). The hemicellulosic fractions in the prehydrolysates are essential to increase the initial concentration of fermentable sugars. Furthermore, the use of a mixture of cellulase, xylanase and cellobiase during hydrothermal pretreatment of a substrate could encourage the recovery of total sugars (Eom *et al*., 2015a; 2015b). A nearly twofold increase is possible for the direct application of pre-treated whole slurry as a substrate for enzymatic saccharification (sugars recovered: 43.5 g 100 g^{-1}), compared to washed pre-treated solids (sugars recovered: 23.3 g 100 g^{-1}) (*Table 9*).

Sulfite pretreatment of biomass feedstock (SPORL) consists of a short span of chemical treatment followed by mechanical size reduction (fiberisation). Active reagents include sulfite (SO_3^{-2}), bisulfite (HSO_3^{-1}), or their combination. A solution of sulfite salt (*e.g*., sodium, magnesium, ammonia, potassium or calcium) reacts first with the feedstock at temperatures ranging from 160°C-190°C and pH 2-4 for about 30 min. It is then fiberised with a disk mill to generate fibrous substrates for subsequent enzymatic saccharification and fermentation. SPORL produces readily-digestible substrates and ensures high recovery of hemicellulosic sugars with only a trace amount of fermentation inhibitors (Shuai *et al*., 2010). Furthermore, sulfonation increases the hydrophilicity of lignin, thus reducing the negative impacts on enzymatic saccharification. OPT pre-treated with SPORL allows >90% saccharification yields in 48 hr with a total fermentable sugar recovery of 62.5% (Noparat *et al*., 2017).

DESs, a potentially green alternative, have been used to pre-treat OPT. Given their similar properties with ionic liquids, DESs have attracted considerable interest for potential cost reduction in bioprocessing. DES composes of two or three charged components with high melting points (New *et al*., 2022). Interestingly, when combined, the components form a mixture with a depressed melting point, making it available as a liquid at ambient temperature (Zulkefli *et al*., 2017). Such a solvent can be easily prepared through atomic economic procedures. With its excellent compatibility and

TABLE 9. PRETREATMENT METHODS OF OIL PALM TRUNKS IN THE EXISTING LITERATURE

Pretreatment method	Conditions	Saccharification	Yield of sugar (g 100 g^{-1})		References
			Xylose	Glucose	
Hydrothermal	160°C -200°C, 30 min	Cellulase + xylanase + cellobiase	17.8	23.3	Eom *et al*. (2015b)
Hydrothermal	180°C, 30 min	Cellulase + xylanase	15.4	43.5	Eom *et al*. (2015a)
Sulphuric acid	3% H_2SO_4, 180°C, 40 min	Cellulase + β-glucosidase	-	80.0%*	Noparat *et al.* (2015)
SPORL	7% H_2SO_4 + 6% Na_2SO_3, 190°C, 30 min	Cellulase + β-glucosidase	26.5	22.4	Noparat *et al.* (2017)
Deep eutectic solvent	EAC: EG, 100°C, 48 hr	Cellulase + cellobiase	-	74%*	Zulkefli *et al.* (2017)
Oxalic acid (OA)	15% OA; 100°C, 60 min	Cellulase + cellobiase	-	14.4	Rattanaporn *et al.* (2018)
OA	1% OA; 120°C, 180 min	Cellulase	24.3	19.0	Bukhari *et al*. (2021b)
Alkaline hydrogen peroxide	30% H_2O_2, 70°C, 30 min	Cellulase	-	59.8%*	Tareen *et al*. (2020)
Steam explosion + alkaline	210°C, 4 min + 15% NaOH, 80°C, 90 min	Cellulase + β-glucosidase	-	88.5%*	Tareen *et al.* (2021a)

Note: SPORL - sulfite pretreatment to overcome recalcitrance of lignocellulose; EAC: EG - etylammonium chloride: ethylene glycol; * - cellulose-to-glucose conversion.

biodegradability, the presence of a DES ensures the stability of enzymatic activities over an extended period (Thi and Lee, 2019). Among the five DESs screened: choline chloride:glycerol (ChCl:Gly), choline chloride:ethylene glycol (ChCl:EG), choline chloride:urea (ChCl:U), ethylammonium chloride:glycerol (EAC:Gly) and ethylammonium chloride:ethylene glycol (EAC:EG), EAC:EG was found to be the most efficient in OPT pretreatment; having ability to dissolve 58% OPT upon heating at 100°C for 48 hr (Zulkefli *et al*., 2017).

More recently, alkaline hydrogen peroxide (AHP) has been optimised for OPT pretreatment with 3% H_2O_2 g g^{-1} of biomass at 70°C for 30 min optimum conditions. Up to 50% lignin can be removed, resulting in 46.2 g L^{-1} glucose with 59.8% enzymatic digestibility in 96 hr (Tareen *et al*., 2020). A more advanced OPT pretreatment under steam explosion conditions (210°C for 4 min) followed by alkaline extraction manages to yield more glucose (71.6 g L^{-1}). In optimising alkaline extraction, the Taguchi three-factor design was used to obtain the optimum conditions: 15% NaOH at 90°C for 60 min (Tareen *et al*., 2021b). Through this, the highest cellulose conversion of 88.5% can be afforded following 96-hr saccharification with combined enzymes (Tareen *et al*., 2021b).

Although many pretreatment methods are available, so far only a few are deemed feasible to be industrialised based on environmental and economic considerations (Akhtar *et al*., 2014). Its performance lies with the susceptibility of the glucosidic bonds between hemicellulose and cellulose to acid. Hydronium ions originated from acid catalysts that break the long cellulose and hemicellulose chains down into monomeric sugars (Lloyd and Wyman, 2005). Dilute acid pretreatment gives a high hemicellulose recovery in the liquid fraction while leaving most of the cellulose in the solid residues for subsequent enzymatic saccharification (Noparat *et al*., 2015). They suggested using 3% H_2SO_4 at 180°C for 40 min to achieve the highest glucose recovery with ~80% conversion yield. The operating conditions, including reaction time, temperature, and acid concentration are reportedly crucial to govern the treatment efficiency (Zhang *et al*., 2013). Due to the complexity of the lignocellulosic matrices, it is improbable for such pretreatment to break all polysaccharide-lignin linkages, and thus not all monomeric sugars are expected to be recovered.

Pretreatment with inorganic acids such as H_2SO_4 has been preferred due to their high catalytic performance and low costs, though disadvantageous in terms of equipment corrosion, low reaction selectivity, and formation of inhibitory by-products (Lee and Jeffries, 2011). To overcome these, organic acids have recently emerged as a more environmentally-sound alternative. Various organic acids have been investigated in pre-treating lignocellulosic biomass: Maleic acid for wheat straw (Barisik *et al*., 2016) and rice straw (Jung *et al*., 2015), oxalic acid for cassava stem (Sivamani and Baskar, 2018) and yellow poplar (Jeong and Lee, 2016). Citric acid, fumaric acid, and lactic acid have also been explored for biomass pretreatment (Sahu and Pramanik, 2018; Tang *et al*., 2018). To date, acetic acid, citric acid (Rattanaporn *et al*., 2018), maleic acid (Jung *et al*., 2014) and oxalic acid (Bukhari *et al*., 2021c) have been deployed in pre-treating OPT bagasse, given promising hydrolysates for subsequent fermentation. Reasonable operational conditions for OPT pretreatment, dilute (mild) acid concentration in particular, need to be enquired about to find the best possible route in OPT bioconversion.

Enzymatic Saccharification of Pre-treated Materials

Enzymatic saccharification is the subsequent step after the pretreatment of lignocellulosic biomass to yield fermentable sugars from mainly the released celluloses. Established as the most suitable hydrolysis method, the use of enzymes has demonstrated advantages over concentrated acid hydrolysis such as the relatively mild process conditions, high yields, and absence of corrosion (Duff and Murray, 1996). Enzymatic saccharification can also be performed to measure improvement in sugar conversion, which relates to pretreatment efficiency. In the saccharification of lignocellulosic biomass for the conversion of carbohydrates into sugars, three primary types of cellulases are responsible, as shown in *Table 10*.

TABLE 10. TYPES AND ACTION OF CELLULASES INVOLVED IN BIOMASS SACCHARIFICATION

Enzyme	EC number	Mode of action	References
Endoglucanases (EG, endo-1,4-β-D-glucanohydrolases)	EC 3.2.1.4	Attack regions of the internal amorphous sites amidst cellulose chains, generating oligosaccharides of various chain lengths	Kumar *et al.* (2008)
Exoglucanases (CBH, 1,4-β-D-glucan glucanohydrolases and 1-β-D-glucan cellobiohydrolases)	EC 3.2.1.91	Act on the reducing and non-reducing ends of cellulose chains, releasing either glucose (glucanohydrolases) or cellobiose (cellobiohydrolase) as the major products	Sun and Cheng (2002)
β-glucosidase (β-glucosidase glucohydrolases)	EC 3.2.1.21	Hydrolyse cellodextrin and cellobiose to glucose	Teugjas and Väljamäe (2013)

Commercial enzymatic cocktails contain diverse enzymes of undisclosed specifications (Kubicek and Kubicek, 2016). During saccharification, glycosidic linkages in hemicellulose molecules are broken, including random cleavages of internal bonds by endoxylanase (Maitan-Alfenas *et al*., 2015). Additionally, some ancillary enzymes could also attack hemicellulose such as glucuronidase, acetylesterase, β-xylosidase, glucomannanase, and gatactomannanase (Duff and Murray, 1996). In general, as cellulose is predominantly found in lignocellulosic biomass, glucose will be the most abundant hexose released in the hydrolysate after saccharification.

The cost of cellulases accounts for a substantial proportion of the total processing costs in the bioconversion of lignocellulosic materials. Cost-saving considerations must be put in place to provide the impetus to reducing enzymatic loadings and recovering used enzymes (Zabed *et al*., 2017). Potential enhancement and detailed mechanism of enzymatic saccharification remain a research focus, where R&D examples are copious in the literature. Endoxylanase for hydrolysing hemicellulose into monomeric sugars (mostly xylose) could be combined with cellulase to boost the hydrolytic performance (Luthfi *et al*., 2016). Additionally, supplementation of cellulase with a small amount of cellobiase (7:1 ratio) during enzymatic saccharification of pre-treated OPEFB was found to improve glucose production by 51%. In another comparative study, the yield of 31.4 g L^{-1} glucose from a combined enzymatic process was higher than that of 20.6 g L^{-1} from cellulase alone (Akhtar and Idris, 2017). Synergism between cellulase (CTec2®) and endoxylanase (HTec2®) has also been reported, as reflected by the optimum sugar yield of 54.2% g g^{-1} of raw OPF (Luthfi *et al*., 2018).

The use of additives such as surface-active agents (surfactants), proteins, and polymers represents another interesting approach to optimise enzymatic saccharification. The potential of such additives has been demonstrated for cost-effectiveness in enhancing cellulose conversion yield, decreasing enzyme loading and reducing hydrolysis time (Monschein *et al*., 2014). Two-pronged mechanisms have been evidenced by their action: The ability to adsorb to lignin, thus avoiding unspecific binding of enzymes to lignin, and modify the substrates, stabilise the enzymes plus improve enzymatic activities (Kristensen *et al*., 2007; Lin *et al*., 2017). However, only a few studies have hitherto investigated the effects of surfactants on the enzymatic saccharification of oil palm biomass. Zain *et al*. (2018) reported that an optimum loading of 1.31% (v v^{-1}) of Triton X-100 showed a conversion yield of 88% from the saccharified alkaline-pretreated OPF. Besides Triton X-100, Tween 80 at 0.25% (v v^{-1}) was found efficient, with a 23% higher yield in hydrolysing nitric acid-pre-treated OPEFB, compared to the control (Kamsani *et al*., 2018). The effect of surfactants could be potentially exploited to reduce saccharification time or enzyme loading, enabling a reduction in enzyme cost for lignocellulosic bioconversion. In future, the application of surfactants might become economically feasible, especially for high-solid loadings (Monschein *et al*., 2014).

Fermentation of Lignocellulosic Hydrolysates

Fermentation refers to microbial metabolism of simple sugars into targeted bio-products, in three different manners, *i.e.*, batch, fed-batch, and continuous mode. For the batch mode, a closed culture system is used, in which the fermentation medium is supplemented with essential ingredients to promote microbial growth and product formation. As the simplest mode, it requires only acids or bases to maintain the pH; no other complicated additives are needed (Zabed *et al*., 2017). The repeated-batch mode refers to the process in which an amount of fermented culture is removed from the system at specific intervals while the remaining portion is used as the inoculum for the next culture (Luthfi *et al*., 2017a). Under the fed-batch mode, the batch and continuous modes are combined for the targeted production. It represents a batch culture system into which substrates and other ingredients are fed, without any removal of the fermented broth (Zabed *et al*., 2017). Lastly, the continuous mode involves the sequential input of the necessary ingredients and the ongoing removal of products from the fermentation vessel. It is widely used in SA production, often contributing to productivity higher than the batch and fed-batch modes (Luthfi *et al*., 2018).

As with previously researched bioethanol production (Kassim *et al*., 2022), the bioconversion of lignocellulose into SA can also be performed through separate hydrolysis and fermentation (SHF), simultaneous saccharification and fermentation (SSF), simultaneous saccharification and co-fermentation (SSCF) and consolidated bioprocessing (CBP) (Lu *et al*., 2021). *Figure 6* presents the conventional steps in SA production. SHF includes two sequential steps, in which lignocellulose is first enzymatically hydrolysed, and the resultant sugars are then fermented into SA. Its notable advantage is that both steps can be performed (separately) under optimum temperatures, as enzymatic saccharification and microbial fermentation usually exhibit different thermal requirements (Devarapalli and Atiyeh, 2015).

Conversely, SSF integrates those two steps in the same bioreactor (as a one-step process). Compared with SHF, SSF demonstrates more advantages, not only in reducing the amounts of supplemented hydrolytic enzymes but also in increasing product yields. Moreover, enzymatic inhibition arising from

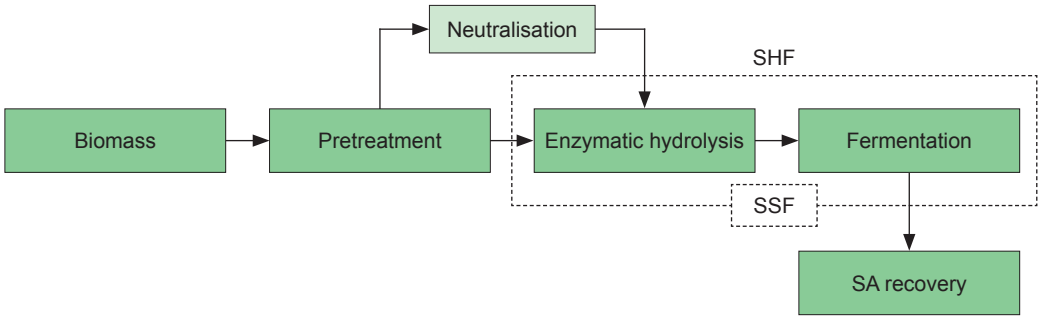


Figure 6. General schematic for succinic acid production from lignocellulosic biomass. Adapted from Lu et al.*, 2021.*

the resultant by-products can partly be addressed through SSF. Additionally, the combination of saccharification and fermentation in the same reactor incurs lower equipment costs (Valles *et al*., 2021). To optimise SA production, different fermentation strategies, modes and configurations have been examined. Additionally, factors affecting the fermentative performance, including carbon sources, nitrogen sources, pH regulators, and CO_2 availability have also been investigated (Putri *et al*., 2020).

TECHNOLOGICAL ADVANCEMENT AND PROCESS ECONOMICS

SA production has recently advanced greatly in fermentative technologies targeting high yield per unit of biomass. Attempts to improve process economics must take into consideration the various aspects of bioconversion in their entirety. For example, effective pretreatment is required to improve the enzymatic digestibility of biomass, which ultimately maximises the availability of fermentable sugars for conversion into SA. Against this background, *Table 11* lists current R&D endeavours mainly on the productivity of unit processes by optimising process parameters to gain economic feasibility.

Exploitation of Renewable Biomass and Selection of Operating Configurations

Investigations have been underway intending to search for new biomass substrates as a viable starting material for SA production. Carvalho *et al*. (2016) demonstrated for the first time that raw carob pods were efficient for SA production, with a favourable sugar yield recovery of 50% (w w^{-1}). A volumetric productivity of 1.67 g L^{-1} hr^{-1} and a yield of 0.39 g g^{-1} sugars were obtained via batch fermentation. Exploiting the metabolism of *A. succinogenes*, uncoupling cell growth from SA production, and deploying a fed-batch mode was implemented to boost the SA yield to 0.94 g g^{-1}, while maintaining by-products in trace amounts.

Chen *et al*. (2016) used sugarcane bagasse (SCB) hydrolysates as the carbon source, alongside their innovative application of the SCB residues as a cell-adsorption support. The SCB was pretreated with NaOH and H_2SO_4 to remove lignin before enzymatic saccharification, resulting in >90% lignin removal for the former with 0.25 M NaOH. Following this, the pretreated SCB was further hydrolysed by a multi-enzyme cocktail containing cellulase, xylanase, β-glucanase, and pectinase. The batch production of SA from 39.9 g L^{-1} of NaOH-pretreated SCB afforded a yield of 0.82 g g^{-1} and a productivity of 1.37 g L^{-1} hr^{-1}. Fed-batch was also employed to enhance the process with up to 70.8 g L^{-1} of SA and productivity of 1.42 g L^{-1} hr^{-1}. Additionally, the SCB residues were later used as a support for cell adsorption, demonstrating an improved SA productivity of 1.65 g L^{-1} hr^{-1} with good reusability in three batches of fermentation. In another study, SA production from sweet sorghum bagasse was reported for the first time (Lo *et al*., 2020). In this study, a low temperature (50°C) was employed to efficiently release cellulosic sugars after pretreatment with concentrated phosphoric acid; with 29.2 g L^{-1} released glucose to produce 17.8 g L^{-1} of SA, at a yield of 0.61 and a productivity of 0.98.

Salvachúa *et al*. (2016) examined the performance of *A. succinogenes* on xylose-enriched hydrolysates from dilute acid-pre-treated corn stover. The batch production of deacetylated hydrolysates led to 42.8 g L^{-1} of SA, at a yield of 0.74 g g^{-1} and a productivity of 1.27 g L^{-1} hr^{-1}. Besides, Shen *et al*. (2016) demonstrated that duckweed was a promising feedstock as its acid hydrolysis outperformed enzymatic saccharification and thermo-hydrolysis. To improve process economics, corn steep liquor powder was supplemented to replace yeast extract as a nitrogen source, with the resultant SA titer of 57.8 g L^{-1} in batch fermentation (Shen *et al*., 2016). Amongst the different configurations such as SHF, SSF, and semi-SSF evaluated, the use of viscosity-reducing enzymes in semi-SSF enhanced SA production to reach 75.46 g L^{-1}, at a yield of 0.83 g g^{-1} and productivity of 1.35 g L^{-1} hr^{-1} (Shen *et al*., 2018).

TABLE 11. RECENT R&D FOR OPTIMISING SUCCINIC ACID PRODUCTION BY *Actinobacillus succinogenes* FROM VARIOUS BIOMASSES (2016-2021)

Feedstock	Approach	Major focus	Fermentation kinetics			References
			P (g L^{-1})	*Q* (g L^{-1} hr^{-1})	*Y* (g g^{-1})	
Carob pods	SHF, batch	Optimisation of sugar extraction while minimising phenolic compounds	9.41	1.67	0.39	Carvalho *et al*. (2016)
	SHF, fed-batch	Reduction of by-products formation	18.97	1.32	0.94	
Sugarcane bagasse	SHF, batch	Optimisation of enzymes cocktails	39.90	1.37	0.82	Chen *et al*. (2016)
	SHF, fed-batch	Addition of 200 g L^{-1} condensed sugar	70.81	1.42	0.82	
	SHF, repeated batch	Utilisation of SCB residue as cell adsorption support	40.00	1.65	0.81	
Corn stover	SHF, batch	Fermentation of xylose from DA pretreatment	42.80	1.27	0.74	Salvachúa *et al*. (2016)
Duckweed	SHF, batch	Different pretreatments, CSL as nitrogen source	57.85	1.21	0.78	Shen *et al*. (2016)
	Semi-SSF, batch	Comparison of SHF, SSF and SSSF	75.46	1.35	0.83	Shen *et al*. (2018)
Sorghum bagasse	SHF, batch	Pretreatment using concentrated phosphoric acid at a mild temperature	17.80	0.98	0.61	Lo *et al*. (2020)
OPEFB	SSF, batch	Pretreatment using autoclave alkaline (AA)	20.90	0.44	0.29	Akhtar and Idris (2017)
	SSF, batch	Pretreatment using DA-microwave alkali	33.20	0.69	0.47	
	SSF, batch	Optimisation of SSF via RSM	42.90	0.89	0.61	Akhtar *et al*. (2020)
	SSF	Pretreatment using inorganic salt	38.85	0.54	0.39	Khairil Anwar *et al*. (2021)
	Semi-SSF		50.50	0.38	0.51	
OPF juice	SHF, batch	Effect of CO_2 in serum bottles and bioreactor scale	29.00	0.73	0.71	Tan *et al*. (2018)
OPF bagasse	SHF, batch	Pretreatment using alkaline and AA	36.6	0.61	0.71	Luthfi *et al*. (2016)
	SHF, repeated batch	Cells immobilisation on CSAC	44.10	1.30	0.90	Luthfi *et al*. (2017a)
	SHF, continuous, immobilisation	Cells immobilisation on CSAC	36.48	1.95	0.57	Luthfi *et al*. (2018)
	SHF, immobilisation	Cells immobilisation on clay pebbles	36.30	1.48	0.77	Luthfi *et al*. (2020)
OPT sap	SHF, batch	Optimisation of SHF	20.33	0.35	0.54	Bukhari *et al*. (2019b)
OPT bagasse	SHF, batch	Pretreatment using organic acid	17.50	0.36	0.44	Bukhari *et al*. (2021b)
OPT bagasse	SHF, batch	Optimisation of SHF condition, nutrient minimisation	21.10	0.35	0.58	Bukhari *et al*. (2021a)

Note: SHF - separate hydrolysis and fermentation; SSF - simultaneous saccharification and fermentation; OPEFB - oil palm empty fruit bunch; OPF - oil palm frond; OPT - oil palm trunk; SCB - sugarcane bagasse; DA - dilute acid; CSL - corn steep liquor; CSAC - coconut shell activated carbon; *P* - succinic acid concentration; *Q* - volumetric productivity; *Y* - succinic acid yield.

Progress for Succinic Acid Production from Oil Palm Biomasses

OPEFB has been investigated for SA production through two pretreatment methods, *i.e.*, dilute acid-microwave alkali (DA-MWA) and autoclave alkali (AA) (Akhtar and Idris, 2017). A higher SA titer of 33.3 g L^{-1} with 0.47 g g^{-1} yield representing a 59% improvement from DA-MWA was obtained compared with that of 20.9 g L^{-1} and 0.29 g g^{-1} from AA. DA-MWA was thus a better pretreatment method followed by SSF at 38°C, pH 6.5, and cellulase loading of 25 FPU g^{-1} OPEFB. The use of DA-MWA through microwave irradiation effectively disrupted the recalcitrant structure of OPEFB. DA-MWA outperformed AA in several aspects: Shorter

reaction time (20 min *vs.* 120 min), lower temperature (90°C *vs.* 121°C), and more effective lignin removal (73% *vs.* 40%) (Akhtar and Idris, 2017). The SA yield was further enhanced to 0.61 g g^{-1} at 36°C, pH 5, and cellulase loading of 38 FPU g^{-1} OPEFB under the optimised SHF operating conditions (Akhtar *et al.*, 2020).

Another pretreatment method using 15% (w v^{-1}) $Na_3PO_4.12H_2O$ and 5% (w v^{-1}) $ZnCl_2$ was deployed on OPEFB prior to *A. succinogenes* fermentation in a 16-L bioreactor (Khairil Anwar *et al*., 2021). Two different configurations were studied: SSF *vs.* semi-SSF. The hydrolysis reaction at 50°C was commenced first followed by fermentation at 37°C at the same reactor in semi-SSF, offering suitable conditions for microorganism survival. Higher SA concentration (50.5 *vs.* 38.9 g L^{-1}) and yield (0.51 *vs.* 0.39 g g^{-1}) were revealed in semi-SSF compared to that in SSF.

For SHF, its potential is undeniable as being commonly used for SA production (*Table 11*). Utilising OPF as the substrate, SA production could be further enhanced via this common configuration. The batch-mode production of AA-pretreated OPF produced 36.6 g L^{-1} of SA, with a yield of 0.71 g g^{-1} and a productivity of 0.61 g L^{-1} hr^{-1} (Luthfi *et al*., 2016). When *A. succinogenes* was immobilised on coconut shell activated carbon (CSAC), enhancement of SA production was reported by 23%, compared with that of free cells at 40.2 g L^{-1}. Repeated-batch fermentation using CSAC was performed for 5 cycles over 180 hr, achieving an average SA concentration of 44.1 g L^{-1}, yield of 0.87 g g^{-1}, and productivity of 1.34 g L^{-1} hr^{-1} in the bioreactor (Luthfi *et al*., 2017a). Fermentation in the continuous mode afforded enhanced productivity by 3-fold, reaching up to 1.95 g L^{-1} hr^{-1} (Luthfi *et al*., 2018). Besides, repeated-batch fermentation with clay pebbles for 5 cycles over 130 hr achieved an average SA concentration of 36.3 g L^{-1}, yield of 0.77 g g^{-1}, and productivity of 1.48 g L^{-1} hr^{-1}. The findings also demonstrated that immobilised cells are superior in reducing by-products formation which could be an interesting strategy to ease the subsequent downstream processing (Luthfi *et al*., 2020).

Tan *et al.* (2014) explored utilising OPF juice as a substrate for SA production by *A. succinogenes*. In this study, carbon dioxide (CO_2) was reported as another critical parameter in SA production through microbial anaplerotic reactions. High availability of CO_2 promotes the flux towards the C4 SA-producing pathway, since the fixation of CO_2 into the three-carbon PEP will be needed to form the four-carbon oxaloacetate. When the serum bottle fermentation of extracted OPF juice was supplemented with 400 mM of carbonate as a source of CO_2, the yield of SA rose from 0.47 to 0.71 g g^{-1} while its final titer was enhanced by 3.3-fold from 4.4 g L^{-1} to 19.1 g L^{-1}. In the bioreactor, the final titer of SA was found to have been affected by CO_2 sparging, in which 26.6 g L^{-1} of SA at a sparging rate of 0.1 vvm was improved to 30.7 g L^{-1} at 0.5 vvm. This finding was in line with the optimum sparging rate of CO_2 for achieving the highest CO_2 dissolved rate (Tan *et al*., 2018).

OPT as a Promising Feedstock for Succinic Acid Production

OPT is a highly nutrient-dense carbohydrate-based biomass that can be exploited as a cost-effective and renewable carbon source for bio-chemical industries. OPT contains a high level of structural carbohydrate (~60% of holocellulose) and is ideal for use as a feedstock in SA production. Moreover, it is one of the cheapest biomass which can be obtained at the cost of USD7-USD9 (RM30-RM40) per tonne.

An efficient OPT utilisation strategy can be achieved by separating the sap and fibrous residue (bagasse) using mechanical extraction in order to harness and access the maximum amount of sugars. The OPT sap contains ~5% (w v^{-1}) free sugars, such as sucrose, glucose and fructose, which is suitable for direct fermentation (Bukhari *et al*., 2019b). Being a carbon source supplier, OPT sap is advantageous as it also contains a high amount of nitrogen as well as a considerable amount of vitamins and amino acids which are suitable for microbial fermentation. Bukhari *et al*. (2019b) demonstrated for the first time that raw OPT sap was efficient as a sole substrate for SA production. A superior SA yield of 0.54 g g^{-1} was obtained in the medium without YE supplementation as compared to 0.50 g g^{-1} with YE. Hence, OPT fulfils the nutritional requirements of auxotrophic *A. succinogenes* 130Z to meet its physiological demands. Batch fermentation in a bioreactor using OPT sap without YE and minerals resulted in an SA yield of 0.52 g g^{-1}, which indicated an achievable cost reduction as a result of avoiding expensive nutrients. The use of OPT sap for bioconversion holds several economic advantages; operational without complex and expensive pretreatment, and relatively easy to handle during fermentation.

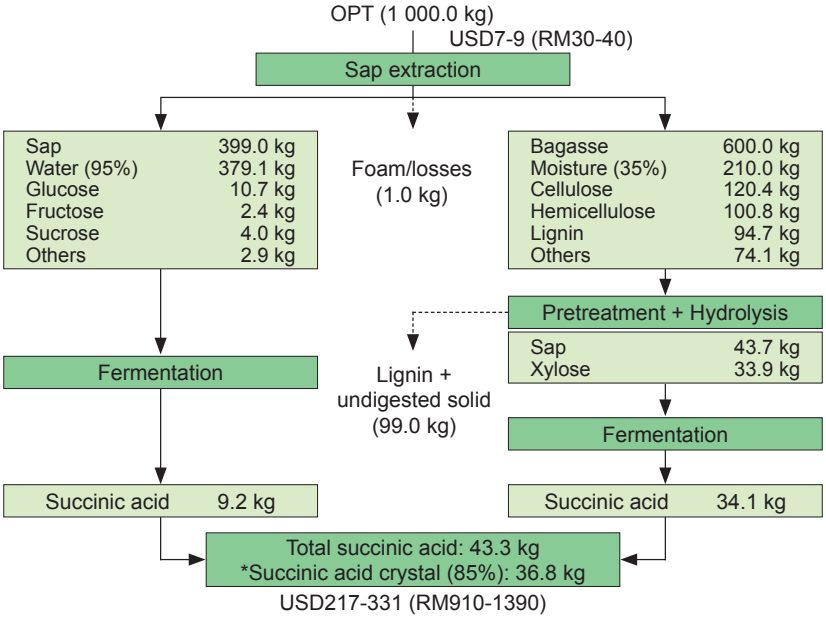
Bukhari *et al*. (2020) investigated the performance of organic acids (*i.e.*, citric acid, formic acid and oxalic acid) in pre-treating lignocellulosic OPT bagasse. Of these, oxalic acid at 5% (w v^{-1}) was the most effective in solubilising hemicellulose from OPT bagasse, producing a maximum xylose yield of 16.26 g 100 g^{-1} for 120 min. This yield was comparable to conventional pretreatment using dilute sulphuric acid. However, the SA fermentation by *A. succinogenes* was suppressed (SA yield of 0.13 g g^{-1}) at this concentration. Oxalic salts formed at the neutralisation step was the main inhibitor during fermentation. A much higher SA yield of 0.37 g g^{-1} was obtained while reducing the oxalic acid concentration to 1% (w v^{-1}) and prolonging the pretreatment time, for which an improved enzymatic

digestibility and fermentability satisfactorily achieved (Bukhari *et al*., 2021c). The results prove the potential of oxalic acid as an alternative to dilute sulphuric acid in biomass pretreatment, which warrants more attention to improve SA yield.

Two different routes have been exploited in SA production from OPT, considering that the microorganism employed has the capability to metabolise a wide range of sugars including glucose (C6) and xylose (C5) simultaneously into SA (Bukhari *et al*., 2021b). In terms of sugar yield, direct application of the whole slurry (Route 2) as substrate afforded a twofold increase compared to the washed pre-treated solid (Route 1). About 43.2 g 100 g^{-1} sugars were recovered from Route 2 in comparison to 22.1 g 100 g^{-1} from Route 1. Mass balance calculations demonstrated that 175.2 g of SA could be obtained from 1 kg of dry OPT bagasse using Route 2, which outperformed Route 1 at 152.6 g SA kg^{-1} OPT. The results showed that saccharification using the whole slurry was evidently more advantageous, given its practical ease of operation (*i.e.*, not requiring solid/liquid separation and washing) and cost-savings (*i.e.*, avoiding additional buffer solution for enzymatic reaction). This study proves that utilisation of both OPT streams for SA production can fully reap the benefit of *A. succinogenes* 130Z.

A cost-effective medium with minimum nutrient supplementation was developed to improve the process economics of SA production by *A. succinogenes* 130Z from OPT bagasse hydrolysate (Bukhari *et al*., 2021b). Different neutralising agents (NaOH, KOH and NH_4OH) were screened for pH adjustment to condition the acidic hydrolysates so as not to inhibit the subsequent biocatalytic activities. NaOH was found most promising and should be seriously considered in designing the bioprocess of SA from acid hydrolysates (Bukhari *et al*., 2021a). Next, different nitrogen sources and mineral salts were manipulated for cost reduction potential on SA fermentation (Bukhari *et al.*, 2021b). Clearly, YE was essential to be supplemented into acid hydrolysate to facilitate SA synthesis. Interestingly, one-third of the concentration of YE could be significantly reduced while the addition of mineral salts is unnecessary in fermenting OPT bagasse hydrolysate for SA production. As OPT bagasse hydrolysate has sufficient minerals to support SA fermentation, costly nutrients are entirely avoidable. Through this strategy, a batch fermentation of OPT bagasse hydrolysate in a bioreactor can result in SA yield of 0.58 g g^{-1}, which corresponds to 211 g of SA from 1 kg of dry OPT bagasse.

Efficient utilisation of OPT biomass is possible through the use of whole OPT, which allows for the maximum use of all available sugars (C5 and C6) for bioconversion into SA. Potentially, OPT sap might be the best source in terms of fermentation nutrients, for cost-effective microbial production. Overall, the total utilisation of OPT is able to produce 43.3 kg of SA from 1 t of OPT (*Figure 7*). Based on mass balance calculations, from 1 t of OPT, a SA production worthy of USD217-USD331 (RM910-RM1390) can be produced. OPT is currently sold at ~USD7-USD9 (RM30-RM40) t^{-1} of the trunk. The added value from OPT raw material to bio-based SA is approximately 30-fold. The findings could prevail and improve economies of scale in utilising OPT biomass as a potential feedstock for SA production.



Source: (Bukhari *et al*., 2019b; 2021a; 2021b)

Figure 7. Mass balance calculations for succinic acid production from 1 t of oil palm trunk (OPT).

CHALLENGES AND WAY FORWARD FOR SUCCINIC ACID PRODUCTION FROM OPT

Overall, the efficient exploitation of OPT to produce bio-based chemicals is able to minimise any environmental burden associated with, the disposal of the residues in particular. OPT serves as a cheap carbon source which would partially replace expensive pure sugar platforms in typical SA fermentation while improving the process economics. Some challenge of SA production from OPT is the inconsistency of feedstock supply and logistics issue; considering OPT is only available during replanting. In the current situation, the palm-plywood manufacturing industry has also generated a large quantity of OPT residues such as veneer waste, OPT end cuts and core logs, which are not utilised at all to benefit the industry. Hence, it is beneficial to explore the potential commercialisation of SA by integrating with the existing palm-plywood factories. Besides, biomass degradation and biodeterioration may occur during the storage of wet OPT over a prolonged period (Harun *et al.*, 2022). In reality, doable biomass projects involving OPT should occupy land closer to the source to minimise the cost of transportation due to high water content and raw material wastage.

Moreover, developing a viable and economical technology in SA production plus integrating the whole value chain, as depicted in *Figure 8*, helps reduce overall production costs and increase competitive edge over petroleum-based counterparts for a wider market. For oil palm biomass, the efficient use as well as selection and management of feedstock based on the biorefinery concept, focusing on multiple productions and high value addition, should be commercially implemented. The utilisation of feedstock as well as by-products gives other opportunities to improve the feasibility of the process. The biorefinery combines the material flows to reach a complete utilisation of the whole biomass components (García *et al.*, 2011). SA would be the main product. However, utilisation and market opportunities for the by-products and compounds from the waste stream should be evaluated. The inhibitors formed during pretreatment (*i.e.*, acetic acid) may be separated from the hydrolysate prior to fermentation, thereby improving the microbial growth and product yield, or may also be utilised as valuable chemicals. The undigested solid residue (containing lignin) generated from the process may be used as a source of energy to sustain the system.

Full exploitation of OPT from the oil palm industry for SA production is envisioned to benefit various sectors through new market creation, thus stimulating the country's economic growth. The resultant additional profits would be socio-economically generous to society as more than 220 000 plantation owners (~16%) in Malaysia are independent smallholders (Parveez *et al.*, 2021). Ultimately, this gears towards achieving sustainable oil palm plantation management by facilitating the removal and utilisation of felled OPT and making replantation feasibly more beneficial within the existing cultivation lands. Most importantly, this can address waste management systems and environmental issues, leading to a more responsive and dynamic industry.

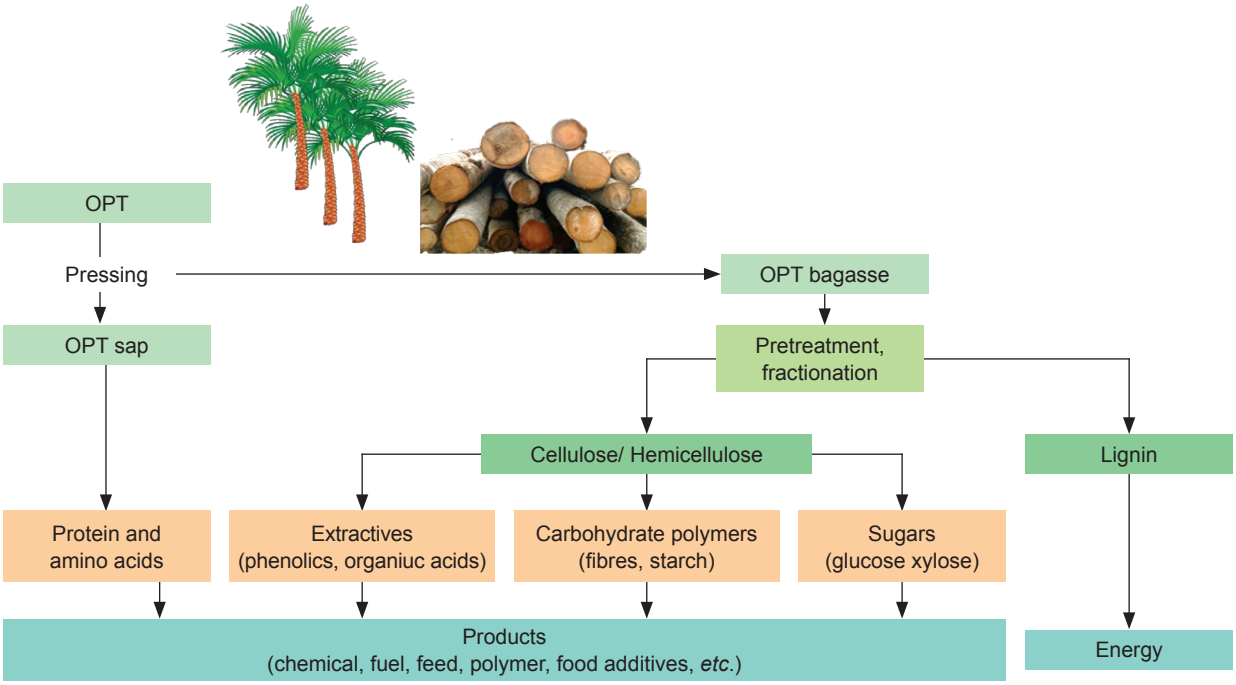


Figure 8. Essential steps towards biorefinery with multiple products utilising oil palm trunk (OPT).

CONCLUSION

Bio-based SA from inexpensive and renewable feedstock such as OPT biomass remains high potential as an alternative C4 building block to various other petroleum-derived counterparts via biotechnological routes. OPT comprises highly nutrient-rich sap and carbohydrate-dense bagasse that can be hydrolysed into fermentable sugars. In enhancing market competitiveness for the case of SA production from OPT, the selection of appropriate bioconversion steps such as inhibitor-free pretreatment, self-sustained enzymatic saccharification, and bacterium-specific fermentation is prudent. *A. succinogenes* performs greatly and has lots of potential but needs to be technologically simplified in terms of overall process and integration, to achieve economical SA production. This review provides useful insights and recommendations for advancing future biomass to chemical commodity development, SA from OPT in particular.

ACKNOWLEDGEMENT

The authors would like to thank the Director-General of MPOB for permission to publish this article.

REFERENCES

Adela, B N and Loh, S K (2015). Optimisation of fermentation conditions for bioethanol production from oil palm trunk sap by *Saccharomyces cerevisiae*. *Malays. J. Microbiol., 11*: 163-169.

Akhlisah, Z N; Yunus, R; Abidin, Z Z; Lim, B Y and Kania, D (2021). Pretreatment methods for effective conversion of oil palm biomass into sugars and high-value chemicals. *Biomass Bioenergy, 144*: 105901.

Akhtar, J; Hassan, N; Idris, A and Ngadiman, N H A (2020). Optimization of simultaneous saccharification and fermentation process conditions for the production of succinic acid from oil palm empty fruit bunches. *J. Wood Chem. Technol., 40*: 136-145.

Akhtar, J and Idris, A (2017). Oil palm empty fruit bunches a promising substrate for succinic acid production via simultaneous saccharification and fermentation. *Renew. Energy, 114*: 917-923.

Akhtar, J; Idris, A and Abd. Aziz, R (2014). Recent advances in production of succinic acid from lignocellulosic biomass. *Appl. Microbiol. Biotechnol., 98*: 987-1000.

Alcantara, J; Mondala, A; Hughey, L and Shields, S (2017). Direct succinic acid production from minimally pretreated biomass using sequential solid-state and slurry fermentation with mixed fungal cultures. *Fermentation, 3*: 1-10.

Alvira, P; Tomás-Pejó, E; Ballesteros, M and Negro, M J (2010). Pretreatment technologies for an efficient bioethanol production process based on enzymatic hydrolysis: A review. *Bioresour. Technol., 101*: 4851-4861.

Anwar, Z; Gulfraz, M and Irshad, M (2014). Agro-industrial lignocellulosic biomass a key to unlock the future bio-energy: A brief review. *J. Radiat. Res. Appl. Sci., 7*: 163-173.

Asif, M (2009). Sustainability of timber, wood and bamboo in construction. *Sustainability of Construction Materials* (Khatib, J M ed.). Woodhead Publishing Series in Civil and Structural Engineering. Woodhead Publishing, Sawston, UK. p. 31-54.

Bahmani, M; Schmidt, O; Fathi, L and Frühwald, A (2016). Environment-friendly short-term protection of palm wood against mould and rot fungi. *Wood Mater. Sci. Eng., 11*: 239-247.

Bajpai, P (2016). Structure of lignocellulosic biomass. *Pretreatment of Lignocellulosic Biomass for Biofuel Production* (Bajpai, P ed.). Springer Singapore, Singapore. p. 7-12.

Barisik, G; Isci, A; Kutlu, N; Bagder Elmaci, S and Akay, B (2016). Optimization of organic acid pretreatment of wheat straw. *Biotechnol. Prog., 32*: 1487-1493.

Beauprez, J J; De Mey, M and Soetaert, W K (2010). Microbial succinic acid production: Natural versus metabolic engineered producers. *Process Biochem., 45*: 1103-1114.

Bechthold, I; Bretz, K; Kabasci, S; Kopitzky, R and Springer, A (2008). Succinic acid: A new platform chemical for biobased polymers from renewable resources. *Chem. Eng. Technol., 31*: 647-654.

Bradfield, M F A; Mohagheghi, A; Salvachúa, D; Smith, H; Black, B A; Dowe, N; Beckham, G T and Nicol, W (2015). Continuous succinic acid production by *Actinobacillus succinogenes* on xylose-enriched hydrolysate. *Biotechnol. Biofuels, 8*: 1-17.

Bukhari, N A; Jahim, J M; Loh, S K; Bakar, N A and Luthfi, A A I (2019a). Response surface optimisation of enzymatically hydrolysed and dilute acid pretreated oil palm trunk bagasse for succinic acid production. *BioRes., 14*: 1679-1693.

Bukhari, N A; Jahim, J M; Loh, S K; Nasrin, A B; Harun, S and Abdul, P M (2020). Organic acid pretreatment of oil palm trunk biomass for succinic acid production. *Waste Biomass Valorization, 11*: 5549-5559.

Bukhari, N A; Loh, S K; Luthfi, A A I; Abdul, P M; Harun, S and Jahim, J M (2021a). Effect of neutralizing agents in the preparation of succinic acid from oil palm trunk. *IOP Conf. Ser. Mater. Sci. Eng., 1195*: 012032.

Bukhari, N A; Loh, S K; Luthfi, A A I; Abdul, P M and Jahim, J M (2022). Low cost nutrient-rich oil palm trunk bagasse hydrolysate for bio-succinic acid production by *Actinobacillus succinogenes*. *Prep. Biochem. Biotechnol., 52*: 950-960.

Bukhari, N A; Loh, S K; Luthfi, A A I; Abdul, P M; Nasrin, A B; Harun, S and Jahim, J M (2021b). Whole slurry saccharification of mild oxalic acid-pretreated oil palm trunk biomass improves succinic acid production. *Ind. Crops Prod., 171*: 113854.

Bukhari, N A; Loh, S K; Luthfi, A A I; Nasrin, A B; Abdul, P M; Harun, S and Jahim, J M (2021c). Oil palm trunk biomass pretreatment with oxalic acid and its effect on enzymatic digestibility and fermentability. *Materials Today: Proceedings*. Elsevier Ltd, Netherlands. p. 119-123.

Bukhari, N A; Loh, S K; Nasrin, A B; Luthfi, A A I; Harun, S; Abdul, P M and Jahim, J M (2019b). Compatibility of utilising nitrogen-rich oil palm trunk sap for succinic acid fermentation by *Actinobacillus succinogenes* 130Z. *Bioresour. Technol., 293*: 122085.

Cao, W; Wang, Y; Luo, J; Yin, J; Xing, J and Wan, Y (2018). Succinic acid biosynthesis from cane molasses under low pH by *Actinobacillus succinogenes* immobilized in luffa sponge matrices. *Bioresour. Technol., 268*: 45-51.

Cao, Y; Zhang, R; Sun, C; Cheng, T; Liu, Y and Xian, M (2013). Fermentative succinate production: An emerging technology to replace the traditional petrochemical processes. *Biomed Res. Int., 2013*: 723412.

Carvalho, M; Roca, C and Reis, M A M (2016). Improving succinic acid production by *Actinobacillus succinogenes* from raw industrial carob pods. *Bioresour. Technol., 218*: 491-497.

Castro, R C de A: Fonseca, B G; dos Santos, H T L; Ferreira, I S; Mussatto, S I and Roberto, I C (2017). Alkaline deacetylation as a strategy to improve sugars recovery and ethanol production from rice straw hemicellulose and cellulose. *Ind. Crops Prod., 106*: 65-73.

Chen, J; Yang, S; Alam, M A; Wang, Z; Zhang, J; Huang, S; Zhuang, W; Xu, C and Xu, J (2021). Novel biorefining method for succinic acid processed from sugarcane bagasse. *Bioresour. Technol., 324*: 124615.

Chen, P; Tao, S and Zheng, P (2016). Efficient and repeated production of succinic acid by turning sugarcane bagasse into sugar and support. *Bioresour. Technol., 211*: 406-413.

Cheng, K K; Wang, G Y; Zeng, J and Zhang, J A (2013). Improved succinate production by metabolic engineering. *Biomed Res. Int., 2013*: 538790.

Chimirri, F; Bosco, F; Ceccarelli, R; Venturello, A and Geobaldo, F (2010). Succinic acid and its derivatives: Fermentative production using sustainable industrial agro-food by-products and its applications in the food industry. *Ital. J. Food Sci., 22(2)*: 119-125.

Cok, B; Tsiropoulos, I; Roes, A L and Patel, M K (2014). Succinic acid production derived from carbohydrates: An energy and greenhouse gas assessment of a platform chemical toward a bio-based economy. *Biofuels, Bioprod. Biorefining, 8(1):* 12-29.

Corona-González, R I; Varela-Almanza, K M; Arriola-Guevara, E; Martínez-Gómez, Á de J; Pelayo-Ortiz, C and Toriz, G (2016). Bagasse hydrolyzates from *Agave tequilana* as substrates for succinic acid production by *Actinobacillus succinogenes* in batch and repeated batch reactor. *Bioresour. Technol., 205*: 15-23.

da Silva, A S A; Espinheira, R P; Teixeira, R S S; De Souza, M F; Ferreira-Leitão, V and Bon, E P S (2020). Constraints and advances in high-solids enzymatic hydrolysis of lignocellulosic biomass: A critical review. *Biotechnol. Biofuels, 13*: 1-28.

Dai, Z; Guo, F; Zhang, S; Zhang, W; Yang, Q; Dong, W; Jiang, M; Ma, J and Xin, F (2020). Bio-based succinic acid: An overview of strain development, substrate utilization, and downstream purification. *Biofuels, Bioprod. Biorefining, 14*: 965-985.

Dessie, W; Xin, F; Zhang, W; Jiang, Y; Wu, H; Ma, J and Jiang, M (2018). Opportunities, challenges, and future perspectives of succinic acid production by *Actinobacillus succinogenes*. *Appl. Microbiol. Biotechnol., 102*: 9893-9910.

Devarapalli, M and Atiyeh, H K (2015). A review of conversion processes for bioethanol production

with a focus on syngas fermentation. *Biofuel Res. J., 2*: 268-280.

Diaz, A B; Blandino, A and Caro, I (2018). Value added products from fermentation of sugars derived from agro-food residues. *Trends Food Sci. Technol., 71*: 52-64.

Dirkes, R; Neubauer, P R and Rabenhorst, J (2021). Pressed sap from oil palm (*Elaeis guineensis*) trunks: A revolutionary growth medium for the biotechnological industry? *Biofuels, Bioprod. Biorefining, 15*: 931-944.

Diyanilla, R; Hamidon, T S; Suryanegara, L and Hussin, M H (2020). Overview of pretreatment methods employed on oil palm biomass in producing value-added products: A review. *BioResources, 15*: 9935-09997.

Duff, S J B and Murray, W D (1996). Bioconversion of forest products industry waste cellulosics to fuel ethanol: A review. *Bioresour. Technol., 55*: 1-33.

Eom, I Y; Oh, Y H; Park, S J; Lee, S H and Yu, J H (2015a). Fermentative l-lactic acid production from pretreated whole slurry of oil palm trunk treated by hydrothermolysis and subsequent enzymatic hydrolysis. *Bioresour. Technol., 185*: 143-149.

Eom, I Y; Yu, J H; Jung, C D and Hong, K S (2015b). Efficient ethanol production from dried oil palm trunk treated by hydrothermolysis and subsequent enzymatic hydrolysis. *Biotechnol. Biofuels, 8*: 1-11.

Fisher, A B and Fong, S S (2014). Lignin biodegradation and industrial implications. *AIMS Bioeng., 1*: 92-112.

Galbe, M and Zacchi, G (2012). Pretreatment: The key to efficient utilization of lignocellulosic materials. *Biomass Bioenergy, 46*: 70-78.

García, V; Päkkilä, J; Ojamo, H; Muurinen, E and Keiski, R L (2011). Challenges in biobutanol production: How to improve the efficiency? *Renew. Sustain. Energy Rev., 15*: 964-980.

Guarnieri, M T; Chou, Y C; Salvachúa, D; Mohagheghi, A; St. John, P C; Peterson, D J; Bomble, Y J and Beckham, G T (2017). Metabolic engineering of *Actinobacillus succinogenes* provides insights into succinic acid biosynthesis. *Appl. Environ. Microbiol., 83(17)*: e00996.

Guettler, M V; Rumler, D and Jain, M K (1999). *Actinobacillus succinogenes* sp. nov., a novel succinic-acid-producing strain from the bovine rumen. *Int. J. Syst. Evol. Microbiol., 49*: 207-216.

Harun, S; Luthfi, A A I; Abdul, P M; Bukhari, N A and Jahim, J M (2022). Chapter 11 - Oil palm biomass zero-waste conversion to bio-succinic acid. *Value-chain of Biofuels* (Yusup, S and Rashidi, N A eds.). Elsevier Ltd., Netherlands. p. 249-275.

Hoffmann, C M and Kenter, C (2018). Yield potential of sugar beet - have we hit the ceiling? *Front. Plant Sci., 9*: 928.

Hoong, Y B; Loh, Y F; Nor Hafizah, A W; Paridah, M T and Jalaluddin, H (2012). Development of a new pilot scale production of high grade oil palm plywood: Effect of pressing pressure. *Mater. Des., 36*: 215-219.

Huffman, K M; Koves, T R; Hubal, M J; Abouassi, H; Beri, N; Bateman, L A; Stevens, R D; Ilkayeva, O R; Hoffman, E P; Muoio, D M and Kraus, W E (2014). Metabolite signatures of exercise training in human skeletal muscle relate to mitochondrial remodelling and cardiometabolic fitness. *Diabetologia, 57*: 2282-2295.

Ishak, H; Yoshida, H; Muda, N A; Ismail, M H S and Izhar, S (2019). Rapid processing of abandoned oil palm trunks into sugars and organic acids by sub-critical water. *Processes, 7(9)*: 593.

Jeong, S Y and Lee, J W (2016). Optimization of pretreatment condition for ethanol production from oxalic acid pretreated biomass by response surface methodology. *Ind. Crops Prod., 79*: 1-6.

Jiang, M; Chen, K; Liu, Z; Wei, P; Ying, H and Chang, H (2010). Succinic acid production by *Actinobacillus succinogenes* using spent brewer's yeast hydrolysate as a nitrogen source. *Appl. Biochem. Biotechnol., 160*: 244-254.

Juanssilfero, A B; Kahar, P; Amza, R L; Yopi; Sudesh, K; Ogino, C; Prasetya, B and Kondo, A (2019). Lipid production by *Lipomyces starkeyi* using sap squeezed from felled old oil palm trunks. *J. Biosci. Bioeng., 127*: 726-731.

Jung, Y H; Kim, I J; Kim, H K and Kim, K H (2014). Whole slurry fermentation of maleic acid-pretreated oil palm empty fruit bunches for ethanol production not necessitating a detoxification process. *Bioprocess Biosyst. Eng., 37*: 659-665.

Jung, Y H; Park, H M and Kim, K H (2015). Whole slurry saccharification and fermentation of maleic acid-pretreated rice straw for ethanol production. *Bioprocess Biosyst. Eng., 38*: 1639-1644.

Kamsani, N; Basri, S A; Mohamad, E and Aziz, S A (2018). Effects of surfactant on the enzymatic

degradation of oil palm empty fruit bunch (OPEFB). *Waste Biomass Valorization, 9*: 845-852.

Kamzolova, S V; Yusupova, A I; Dedyukhina, E G; Chistyakova, T I; Kozyreva, T M and Morgunov, I G (2009). Succinic acid synthesis by ethanol-grown yeasts. *Food Technol. Biotechnol., 47*: 144-152.

Kassim, M A; Meng, T K; Kamaludin, R; Hussain, A H and Bukhari, N A (2022). Chapter 9 - Bioprocessing of sustainable renewable biomass for bioethanol production. *Value-chain of Biofuels* (Yusup, S and Rashidi, N A eds.). Elsevier, Netherlands. p. 195-234.

Khairil Anwar, N A K; Hassan, N; Idris, A; Ramli, S and Malek, R A (2021). Large scale production of succinic acid by fermentation of sequential inorganic salt pretreated oil palm empty fruit bunch. *Biomass Bioenergy, 155*: 106307.

Komonkiat, I and Cheirsilp, B (2013). Felled oil palm trunk as a renewable source for biobutanol production by *Clostridium* spp. *Bioresour. Technol., 146C*: 200-207.

Kosugi, A; Tanaka, R; Magara, K; Murata, Y; Arai, T; Sulaiman, O; Hashim, R; Hamid, Z A A; Yahya, M K A; Yusof, M N M; Ibrahim, W A and Mori, Y (2010). Ethanol and lactic acid production using sap squeezed from old oil palm trunks felled for replanting. *J. Biosci. Bioeng., 110*: 322-325.

Kristensen, J B; Börjesson, J; Bruun, M H; Tjerneld, F and Jørgensen, H (2007). Use of surface active additives in enzymatic hydrolysis of wheat straw lignocellulose. *Enzyme Microb. Technol., 40*: 888-895.

Kubicek, C P and Kubicek, E M (2016). Enzymatic deconstruction of plant biomass by fungal enzymes. *Curr. Opin. Chem. Biol., 35*: 51-57.

Kuglarz, M and Grübel, K (2018). Integrated production of biofuels and succinic acid from biomass after thermochemical pretreatments. *Ecol. Chem. Eng., S 25(4)*: 521-536.

Kumar, R; Singh, S and Singh, O V (2008). Bioconversion of lignocellulosic biomass: biochemical and molecular perspectives. *J. Ind. Microbiol. Biotechnol., 35*: 377-391.

Kunasundari, B; Arai, T; Sudesh, K; Hashim, R; Sulaiman, O; Stalin, N J and Kosugi, A (2017). Detoxification of sap from felled oil palm trunks for the efficient production of lactic acid. *Appl. Biochem. Biotechnol., 183*: 412-425.

Lee, J S; Lin, C J; Lee, W C; Teng, H Y and Chuang, M H (2022). Production of succinic acid through the fermentation of *Actinobacillus succinogenes* on the hydrolysate of Napier grass. *Biotechnol. Biofuels Bioprod., 15*: 1-11.

Lee, J W and Jeffries, T W (2011). Efficiencies of acid catalysts in the hydrolysis of lignocellulosic biomass over a range of combined severity factors. *Bioresour. Technol., 102*: 5884-5890.

Lee, P; Lee, S; Hong, S and Chang, H (2002). Isolation and characterization of a new succinic acid-producing bacterium, *Mannheimia succiniciproducens* MBEL55E, from bovine rumen. *Appl. Microbiol. Biotechnol., 58*: 663-668.

Li, Q; Wu, H; Li, Z and Ye, Q (2016). Enhanced succinate production from glycerol by engineered *Escherichia coli* strains. *Bioresour. Technol., 218*: 217-223.

Lin, H; Bennett, G N and San, K Y (2005). Metabolic engineering of aerobic succinate production systems in *Escherichia coli* to improve process productivity and achieve the maximum theoretical succinate yield. *Metab. Eng., 7*: 116-127.

Lin, X; Lou, H; Qiu, X; Pang, Y and Yang, D (2017). Effect of sodium dodecyl sulfate and cetyltrimethylammonium bromide catanionic surfactant on the enzymatic hydrolysis of Avicel and corn stover. *Cellulose, 24*: 669-676.

Lloyd, T A and Wyman, C E (2005). Combined sugar yields for dilute sulfuric acid pretreatment of corn stover followed by enzymatic hydrolysis of the remaining solids. *Bioresour. Technol., 96*: 1967-1977.

Lo, E; Brabo-Catala, L; Dogaris, I; Ammar, E M and Philippidis, G P (2020). Biochemical conversion of sweet sorghum bagasse to succinic acid. *J. Biosci. Bioeng., 129*: 104-109.

Loh, S K (2017). The potential of the Malaysian oil palm biomass as a renewable energy source. *Energy Convers. Manag., 141*: 285-298.

Loh, S K; James, S; Ngatiman, M; Cheong, K Y; Choo, Y M and Lim, W S (2013). Enhancement of palm oil refinery waste - Spent bleaching earth (SBE) into bio organic fertilizer and their effects on crop biomass growth. *Ind. Crops Prod., 49*: 775-781.

Lokesh, B E; Hamid, Z A A; Arai, T; Kosugi, A; Murata, Y; Hashim, R; Sulaiman, O; Mori, Y and Sudesh, K (2012). Potential of oil palm trunk sap as a novel inexpensive renewable carbon feedstock for polyhydroxyalkanoate biosynthesis and as a bacterial growth medium. *Clean - Soil, Air, Water, 3*: 310-317.

Lokesh, K; Ladu, L and Summerton, L (2018). Bridging the gaps for a "circular" bioeconomy: Selection criteria, bio-based value chain and stakeholder mapping. *Sustain., 10(6)*: 1695.

Lu, J; Li, J; Gao, H; Zhou, D; Xu, H; Cong, Y; Zhang, W; Xin, F and Jiang, M (2021). Recent progress on bio-succinic acid production from lignocellulosic biomass. *World J. Microbiol. Biotechnol., 37*: 1-8.

Luthfi, A A I; Jahim, J M; Harun, S; Tan, J P; Manaf, S F A and Shah, S S M (2018). Kinetics of the bioproduction of succinic acid by *Actinobacillus succinogenes* from oil palm lignocellulosic hydrolysate in a bioreactor. *BioResources, 13*: 8279-8294.

Luthfi, A A I; Jahim, J M; Harun, S; Tan, J P and Mohammad, A W (2017a). Potential use of coconut shell activated carbon as an immobilisation carrier for high conversion of succinic acid from oil palm frond hydrolysate. *RSC Adv., 7*: 49480-49489.

Luthfi, A A I; Jahim, J M; Harun, S; Tan, J P and Mohammad, A W (2016). Biorefinery approach towards greener succinic acid production from oil palm frond bagasse. *Process Biochem., 51*: 1527-1537.

Luthfi, A A I; Manaf, S F A; Illias, R M; Harun, S; Mohammad, A W and Jahim, J M (2017b). Biotechnological route for sustainable succinate production utilizing oil palm frond and kenaf as potential carbon sources. *Appl. Microbiol. Biotechnol., 101*: 3055-3075.

Luthfi, A A I; Tan, J P; Isa, N F A M; Bukhari, N A; Shah, S S M; Mahmod, S S and Jahim, J M (2020). Multiple crystallization as a potential strategy for efficient recovery of succinic acid following fermentation with immobilized cells. *Bioprocess Biosyst. Eng., 43*: 1153-1169.

Maitan-Alfenas, G P; Visser, E M and Guimarães, V M (2015). Enzymatic hydrolysis of lignocellulosic biomass: Converting food waste in valuable products. *Curr. Opin. Food Sci., 1*: 440-449.

Mancini, E; Mansouri, S S; Gernaey, K V and Luo, J (2019). Technology from second generation feedstocks to innovative fermentation and downstream techniques for succinic acid production. *Crit. Rev. Environ. Sci. Technol., 50*: 1-45.

McKinlay, J B; Laivenieks, M; Schindler, B D; McKinlay, A A; Siddaramappa, S; Challacombe, J F; Lowry, S R; Clum, A; Lapidus, A L; Burkhart, K B; Harkins, V and Vieille, C (2010). A genomic perspective on the potential of *Actinobacillus succinogenes* for industrial succinate production. *BMC Genomics, 11*: 680.

McKinlay, J B; Zeikus, J G and Vieille, C (2005). Insights into *Actinobacillus succinogenes* fermentative metabolism in a chemically defined growth medium. *Appl. Environ. Microbiol., 71*: 6651-6656.

Mohd Zakria, R; Gimbun, J; Asras, M F F and Chua, G K (2017). Magnesium sulphate and ß-alanine enhanced the ability of *Kluyveromyces marxianus* producing bioethanol using oil palm trunk sap. *Biofuels, 8(5)*: 1-9.

Mokwatlo, S C; Nchabeleng, M E; Brink, H G and Nicol, W (2019). Impact of metabolite accumulation on the structure, viability and development of succinic acid-producing biofilms of *Actinobacillus succinogenes*. *Appl. Microbiol. Biotechnol., 105*: 6205-6512.

Monschein, M; Reisinger, C and Nidetzky, B (2014). Dissecting the effect of chemical additives on the enzymatic hydrolysis of pretreated wheat straw. *Bioresour. Technol., 169*: 713-722.

Murai, K; Uchida, R; Okubo, A and Kondo, R (2009). Characterization of the oil palm trunk as a material for bio-ethanol production. *J. Wood Sci. Soc., 55*: 346-355.

Murata, Y; Tanaka, R; Fujimoto, K; Kosugi, A; Arai, T; Togawa, E; Takano, T; Ibrahim, W A; Elham, P; Sulaiman, O; Hashim, R and Mori, Y (2013). Development of sap compressing systems from oil palm trunk. *Biomass Bioenergy, 51*: 8-16.

Naidu, Y; Siddiqui, Y and Idris, A S (2020). Comprehensive studies on optimization of ligno-hemicellulolytic enzymes by indigenous white rot hymenomycetes under solid-state cultivation using agro-industrial wastes. *J. Environ. Manage., 259*: 110056.

New, E K; Tnah, S K; Voon, K S; Yong, K J; Procentese, A; Yee Shak, K P; Subramonian, W; Cheng, C K and Wu, T Y (2022). The application of green solvent in a biorefinery using lignocellulosic biomass as a feedstock. *J. Environ. Manage., 307*: 114385.

Nghiem, N P; Kleff, S and Schwegmann, S (2017). Succinic acid: Technology development and commercialization. *Fermentation, 3*: 1-14.

Noor, M M (2003). Zero burning techniques in oil palm cultivation: An economic perspective. *Oil Palm Ind. Econ. J., 3*: 16-24.

Noparat, P; Prasertsan, P and O-Thong, S (2012). Potential for using enriched cultures and thermotolerant bacterial isolates for production of biohydrogen from oil palm sap and microbial community analysis. *Int. J. Hydrogen Energy, 37*: 16412-16420.

Noparat, P; Prasertsan, P; O-Thong, S and Pan, X (2017). Sulfite pretreatment to overcome recalcitrance of lignocellulose for enzymatic hydrolysis of oil palm trunk. *Energy Procedia, 138*: 1122-1127.

Noparat, P; Prasertsan, P; O-Thong, S and Pan, X (2015). Dilute acid pretreatment of oil palm trunk biomass at high temperature for enzymatic hydrolysis. *Energy Procedia, 79*: 924-929.

Nordin, K; Jamaludin, M A; Ahmad, M; Samsi, H W; Salleh, A H and Jalaludin, Z (2004). Minimizing the environmental burden of oil palm trunk residues through the development of laminated veneer lumber products. *Manag. Environ. Qual., 15*: 484-490.

Norhazimah, A H; Asmadiyana, M and Faizal, C K M (2013). Feasibility of acetone-butanol-ethanol (ABE) production from the fermentation of oil palm trunk juice. *Res. J. Chem. Environ., 17*: 66-69.

Ong, K L; Li, C; Li, X; Zhang, Y; Xu, J and Lin, C S K (2019). Co-fermentation of glucose and xylose from sugarcane bagasse into succinic acid by *Yarrowia lipolytica*. *Biochem. Eng. J., 148*: 108-115.

Palagina, I A (2017). Pro-/antioxidant reactions and nitrogen oxide metabolism under sub-chronic effect of succinic acid derivatives. *Ukr. Biochem. J., 89*: 22-33.

Parveez, G K A; Tarmizi, A H A; Sundram, S; Loh, S K; Ong-Abdullah, M; Palam, K D P; Salleh, K M; Ishak, S M and Idris, Z (2021). Oil palm economic performance in Malaysia and R&D progress in 2020. *J. Oil Palm Res., 33*: 181-214.

Patsalou, M; Menikea, K K; Makri, E; Vasquez, M I; Drouza, C and Koutinas, M (2017). Development of a citrus peel-based biorefinery strategy for the production of succinic acid. *J. Clean. Prod., 166*: 706-716.

Pereira, B; Miguel, J; Vilaça, P; Soares, S; Rocha, I and Carneiro, S (2018). Reconstruction of a genome-scale metabolic model for *Actinobacillus succinogenes* 130Z. *BMC Syst. Biol., 12*: 1-12.

Prabhu, A A; Ledesma-Amaro, R; Lin, C S K; Coulon, F; Thakur, V K and Kumar, V (2020). Bioproduction of succinic acid from xylose by engineered *Yarrowia lipolytica* without pH control. *Biotechnol. Biofuels, 13*: 1-15.

Pratiwi, W; Sugiharto, A and Sugesty, S (2018). The effect of pulping process variable and elemental chlorine free bleaching on the quality of oil palm trunk pulp. *J. Selulosa, 8*: 85-94.

Putri, D N; Sahlan, M; Montastruc, L; Meyer, M; Negny, S and Hermansyah, H (2020). Progress of fermentation methods for bio-succinic acid production using agro-industrial waste by *Actinobacillus succinogenes*. *Energy Reports, 6*: 234-239.

Rattanaporn, K; Tantayotai, P; Phusantisampan, T; Pornwongthong, P and Sriariyanun, M (2018). Organic acid pretreatment of oil palm trunk: Effect on enzymatic saccharification and ethanol production. *Bioprocess Biosyst. Eng., 41*: 467-477.

Raud, M; Tutt, M; Olt, J and Kikas, T (2016). Dependence of the hydrolysis efficiency on the lignin content in lignocellulosic material. *Int. J. Hydrogen Energy, 41*: 16338-16343.

Rivas-Cantu, R C; Jones, K D and Mills, P L (2013). A citrus waste-based biorefinery as a source of renewable energy: Technical advances and analysis of engineering challenges. *Waste Manag. Res., 31*: 413-420.

Sahu, S and Pramanik, K (2018). Evaluation and optimization of organic acid pretreatment of cotton gin waste for enzymatic hydrolysis and bioethanol production. *Appl. Biochem. Biotechnol., 186*: 1047-1060.

Salvachúa, D; Mohagheghi, A; Smith, H; Bradfield, M F A; Nicol, W; Black, B A; Biddy, M J; Dowe, N and Beckham, G T (2016). Succinic acid production on xylose-enriched biorefinery streams by *Actinobacillus succinogenes* in batch fermentation. *Biotechnol. Biofuels, 9*: 1-15.

Schindler, B D; Joshi, R V and Vieille, C (2014). Respiratory glycerol metabolism of *Actinobacillus succinogenes* 130Z for succinate production. *J. Ind. Microbiol. Biotechnol., 41*: 1339-1352.

Shahirah, M N N; Gimbun, J; Pang, S F; Zakria, R M; Cheng, C K; Chua, G K and Asras, M F F (2015). Influence of nutrient addition on the bioethanol yield from oil palm trunk sap fermented by *Saccharomyces cerevisiae*. *J. Ind. Eng. Chem., 23*: 213-217.

Shen, N; Qin, Y; Wang, Q; Liao, S; Zhu, J; Zhu, Q; Mi, H; Adhikari, B; Wei, Y and Huang, R (2015). Production of succinic acid from sugarcane molasses

supplemented with a mixture of corn steep liquor powder and peanut meal as nitrogen sources by *Actinobacillus succinogenes*. *Lett. Appl. Microbiol., 60*: 544-551.

Shen, N; Wang, Q; Zhu, J; Qin, Y; Liao, S; Li, Y; Zhu, Q; Jin, Y; Du, L and Huang, R (2016). Succinic acid production from duckweed (*Landoltia punctata*) hydrolysate by batch fermentation of *Actinobacillus succinogenes* GXAS137. *Bioresour. Technol., 211*: 307-312.

Shen, N; Zhang, H; Qin, Y; Wang, Q; Zhu, J; Li, Y; Jiang, M G and Huang, R (2018). Efficient production of succinic acid from duckweed *(Landoltia punctata*) hydrolysate by *Actinobacillus succinogenes* GXAS137. *Bioresour. Technol., 250*: 35-42.

Shuai, L; Yang, Q; Zhu, J Y; Lu, F C; Weimer, P J; Ralph, J and Pan, X J (2010). Comparative study of SPORL and dilute-acid pretreatments of spruce for cellulosic ethanol production. *Bioresour. Technol., 101*: 3106-3114.

Sivamani, S and Baskar, R (2018). Bioconversion of cassava stem to ethanol: Oxalic acid pretreatment and co-culture fermentation. *Biofuels, 9*: 559-566.

Song, H and Lee, S Y (2006). Production of succinic acid by bacterial fermentation. *Enzyme Microb. Technol., 39*: 352-361.

Sorokina, K N; Samoylova, Y V; Gromov, N V; Ogorodnikova, O L and Parmon, V N (2020). Production of biodiesel and succinic acid from the biomass of the microalga *Micractinium* sp. IC-44. *Bioresour. Technol., 317*: 124026.

Sriariyanun, M; Amnuaycheewa, P; Rodiahwati, W; Sanvarinda, P; Cheenkachorn, K and Tawai, A (2017). Effect of organic acid pretreatment on Napier grass (*Pennisetum purpureum*) straw biomass Conversion. *KMUTNB Int. J. Appl. Sci. Technol., 10(2):* 107-117.

Sun, Y and Cheng, J (2002). Hydrolysis of lignocellulosic materials for ethanol production: A review. *Bioresour. Technol., 83*: 1-11.

Taherzadeh, M J and Karimi, K (2007a). Enzyme-based hydrolysis processes for ethanol from lignocellulosic materials: A review. *BioResources, 2*: 707-738.

Taherzadeh, M J and Karimi, K (2007b). Acid-based hydrolysis processes for ethanol from lignocellulosic materials: A review. *BioResources, 2*: 472-499.

Tan, J P; Jahim, J M; Wu, T Y; Harun, S and Mumtaz, T (2016). Use of corn steep liquor as an economical nitrogen source for biosuccinic acid production by *Actinobacillus succinogenes*. *IOP Conf. Ser.: Earth Environ. Sci., 36:* 012058.

Tan, J P; Luthfi, A A I; Manaf, S F A; Wu, T Y and Jahim, J M (2018). Incorporation of CO_2 during the production of succinic acid from sustainable oil palm frond juice. *J. CO_2 Util., 26*: 595-601.

Tan, J P; Jahim, J M; Wu, T Y; Harun, S; Kim, B H and Mohammad, A W (2014). Insight into biomass as a renewable carbon source for the production of succinic acid and the factors affecting the metabolic flux toward higher succinate yield. *Ind. Eng. Chem. Res., 53*: 16123-16134.

Tang, P L; Abdul, P M; Engliman, N S and Hassan, O (2018). Effects of pretreatment and enzyme cocktail composition on the sugars production from oil palm empty fruit bunch fiber (OPEFBF). *Cellulose, 25*: 4677-4694.

Tareen, A K; Punsuvon, V and Parakulsuksatid, P (2020). Investigation of alkaline hydrogen peroxide pretreatment to enhance enzymatic hydrolysis and phenolic compounds of oil palm trunk. *Biotech, 10*: 179.

Tareen, A K; Punsuvon, V; Sultan, I N; Khan, M W and Parakulsuksatid, P (2021a). Cellulase addition and pre-hydrolysis effect of high solid fed-batch simultaneous saccharification and ethanol fermentation from a combined pretreated oil palm trunk. *ACS Omega, 6*: 26119-26129.

Tareen, A K; Sultan, I N; Songprom, K; Laemsak, N; Sirisansaneeyakul, S; Vanichsriratana, W and Parakulsuksatid, P (2021b). Two-step pretreatment of oil palm trunk for ethanol production by thermotolerent *Saccharomyces cerevisiae* SC90. *Bioresour. Technol., 320*: 124298.

Teugjas, H and Väljamäe, P (2013). Selecting β-glucosidases to support cellulases in cellulose saccharification. *Biotechnol. Biofuels, 6*: 1-13.

Thi, S and Lee, K M (2019). Comparison of deep eutectic solvents (DES) on pretreatment of oil palm empty fruit bunch (OPEFB): Cellulose digestibility, structural and morphology changes. *Bioresour. Technol., 282*: 525-529.

Uke, A; Nakazono-Nagaoka, E; Chuah, J A; Zain, N A A; Amir, H G; Sudesh, K; Abidin, N Z H A Z; Hashim, Z and Kosugi, A (2021). Effect of decomposing oil palm trunk fibers on plant growth

and soil microbial community composition. *J. Environ. Manage., 295*: 113050.

UNEP (2012). Converting waste oil palm trees into a resource. *United Nations Environment Programme*, Osaka, Japan. 200 pp.

Vallecilla-Yepez, L; Ramchandran, D; Long, D; Saha, R and Wilkins, M R (2021). Corn fiber as a biomass feedstock for production of succinic acid. *Bioresour. Technol. Reports, 16(9)*: 100868.

Valles, A; Álvarez-Hornos, J; Capilla, M; San-Valero, P and Gabaldón, C (2021). Fed-batch simultaneous saccharification and fermentation including *in-situ* recovery for enhanced butanol production from rice straw. *Bioresour. Technol., 342(20)*: 126020.

Van Der Werf, M J; Guettler, M V; Jain, M K and Zeikus, J G (1997). Environmental and physiological factors affecting the succinate product ratio during carbohydrate fermentation by *Actinobacillus* sp. 130Z. *Arch. Microbiol., 167*: 332-342.

Vávra, N (2009). The chemistry of amber - facts, findings and opinions. *Ann. des Naturhistorischen Museums Wien. Ser. A für Mineral. und Petrogr. Geol. und Paläontologie, Anthropol. und Prähistorie, 111*: 445-473.

VMR (2021). Global succinic acid market size by type (petro-based and bio-based), by end-user (industrial, coating, food & beverage, cosmetics, and pharmaceuticals), by geographic scope and forecast 2. 202 pp.

Vuoristo, K S; Mars, A E; Sanders, J P M; Eggink, G and Weusthuis, R A (2016). Metabolic engineering of TCA cycle for production of chemicals. *Trends Biotechnol., 34(3)*: 191-197.

Wang, G S; Pan, X J; Zhu, J Y; Gleisner, R and Rockwood, D (2009). Sulfite pretreatment to overcome recalcitrance of lignocellulose (SPORL) for robust enzymatic saccharification of hardwoods. *Biotechnol. Prog., 25*: 1086-1093.

Wang, Y; Kuo, S; Shu, M; Yu, J; Huang, S; Dai, A; Two, A; Gallo, R L and Huang, C M (2014). *Staphylococcus epidermidis* in the human skin microbiome mediates fermentation to inhibit the growth of *Propionibacterium acnes*: Implications of probiotics in acne vulgaris. *Appl. Microbiol. Biotechnol., 98*: 411-424.

Werpy, T and Petersen, G (2004). Top value added chemicals from biomass volume I, *National Renewable Energy Laboratory (NREL)*. 67 pp.

Xi, Y L; Chen, K Q; Dai, W Y; Ma, J F; Zhang, M; Jiang, M; Wei, P and Ouyang, P K (2013). Succinic acid production by *Actinobacillus succinogenes* NJ113 using corn steep liquor powder as nitrogen source. *Bioresour. Technol., 136*: 775-779.

Xiao, M; Yang, H; Xu, W; Ma, S; Lin, H; Zhu, H; Liu, L; Liu, Y; Yang, C; Xu, Y; Zhao, S; Ye, D; Xiong, Y and Guan, K L (2012). Inhibition of α-KG-dependent histone and DNA demethylases by fumarate and succinate that are accumulated in mutations of FH and SDH tumor suppressors. *Genes Dev., 26*: 1326-1338.

Yang, Q; Wu, M; Dai, Z; Xin, F; Zhou, J; Dong, W; Ma, J; Jiang, M and Zhang, W (2020). Comprehensive investigation of succinic acid production by *Actinobacillus succinogenes*: A promising native succinic acid producer. *Biofuels, Bioprod. Biorefining, 14*: 950-964.

Yong, K J; Wu, T Y; Lee, C B T L; Lee, Z J; Liu, Q; Jahim, J M; Zhou, Q and Zhang, L (2022). Furfural production from biomass residues: Current technologies, challenges and future prospects. *Biomass Bioenergy, 161*: 106458.

Zabed, H; Sahu, J N; Suely, A; Boyce, A N and Faruq, G (2017). Bioethanol production from renewable sources: Current perspectives and technological progress. *Renew. Sustain. Energy Rev., 71*: 475-501.

Zain, M M; Mohammad, A W; Harun, S; Fauzi, N A and Hairom, N H H (2018). Synergistic effects on process parameters to enhance enzymatic hydrolysis of alkaline oil palm fronds. *Ind. Crops Prod., 122*: 617-626.

Zhang, T; Kumar, R and Wyman, C E (2013). Sugar yields from dilute oxalic acid pretreatment of maple wood compared to those with other dilute acids and hot water. *Carbohydr. Polym., 92*: 334-344.

Zheng, P; Zhang, K; Yan, Q; Xu, Y and Sun, Z (2013). Enhanced succinic acid production by *Actinobacillus succinogenes* after genome shuffling. *J. Ind. Microbiol. Biotechnol., 40*: 831-840.

Zulkefli, S; Abdulmalek, E and Abdul Rahman, M B (2017). Pretreatment of oil palm trunk in deep eutectic solvent and optimization of enzymatic hydrolysis of pretreated oil palm trunk. *Renew. Energy, 107*: 36-41.

RESEARCH ARTICLES

Journal of Oil Palm Research Vol. 35 (4) December 2023 p. 582-595
DOI: https://doi.org/10.21894/jopr.2022.0054

PHENOTYPIC VARIABILITY OF *Elaeis oleifera* GERMPLASM REVEALED BY PRINCIPAL COMPONENT AND CLUSTER ANALYSES

ZULKIFLI YAAKUB[1]*; MARHALIL MARJUNI[1]; SUZANA MUSTAFFA[1]; WAN NOR SALMIAH TUN MOHD SALIM[1]; FATIN MOHD NASIR[1]; NORZIHA ABDULLAH[1]; MOHD DIN AMIRUDDIN[1]; RAJANAIDU NOOKIAH[2]; AHMAD KUSHAIRI DIN[3] and MEILINA ONG-ABDULLAH[1]

ABSTRACT

Despite the fact that large Elaeis oleifera *germplasm collections have been established and evaluated, little is known about the genetic diversity of its population. For this purpose, 572* E. oleifera *palms from eight germplasm collections together with one introgressed population* (Oleifera x Oleifera) *were evaluated from 17 sets of field data. The data were then subjected to principal component and cluster analyses. Correlation analysis among traits of* E. oleifera *showed a similar trend as* Elaeis guineensis*, and most of the characters displayed a wide range of variation. In the principal component analysis, the first four principal components (PC1-PC4) with eigenvalue of >1.0, accounted for 96.32% of the total variability, suggesting that* E. oleifera *accessions can be clearly differentiated using the traits studied. Cluster analysis showed that all accessions were clustered into two major groups (consisting of four sub-clusters), generally attributed to their geographical locations in Central and South America. The information obtained from this study aims to provide solutions for a more efficient and manageable approach towards conservation of the* E. oleifera *germplasm.*

Keywords: Central-South America, conservation, correlation analysis, genetic diversity, oil palm.

Received: 30 January 2022; **Accepted:** 28 July 2022; **Published online:** 6 September 2022.

INTRODUCTION

The genetic diversity of the oil palm species is being threatened by population growth, climate change, habitat loss and selection procedures in oil palm breeding programmes. These actions might impair the oil palm from genetic gains and withstand environmental threats. For that reason, a large accession of *Elaeis guineensis* from Africa and *Elaeis oleifera* from Latin America has been accumulated. Proper characterisation of these germplasm accessions has led to the identification of valuable traits for future oil palm improvements and optimisation of conservation strategies for its continued accessibility, given oil palm's long breeding cycle. As *E. oleifera* and *E. guineensis* may have diverged about 51 million years ago (Singh *et al*., 2013), the former is clearly rare compared to its African relative that is cultivated as the preferred commercial variety. *Elaeis oleifera* is found in Honduras, Nicaragua, Costa Rica, Panama, Colombia, Venezuela, Suriname, Ecuador, Brazil (Escobar, 1981; Meunier, 1975; Ooi *et al*., 1981; Rajanaidu, 1983) and Peru (de Blank, 1952; Escobar, 1981; Hardon and Turner, 1967; Meunier, 1975), where its distribution is patchy. They appear naturally in groves in open grasslands and riverine

[1] Malaysian Palm Oil Board,
6 Persiaran Institusi, Bandar Baru Bangi,
43000 Kajang, Selangor, Malaysia.

[2] 10-14-3 Danau Permai Condo,
Jalan 3/109F, Taman Danau Desa,
58100 Kuala Lumpur, Malaysia.

[3] No. 2, Jalan TH 1,
Tiara Heights, Salak Tinggi,
43900 Sepang, Selangor, Malaysia.

* *Corresponding author e-mail: zulkifly@mpob.gov.my*

areas and their distribution is associated with the migratory movement of indigenous Indians (Santos *et al*., 1986).

The potential genetic variability provided by the *E. oleifera* species is considered a promising resource for genetic improvement of the commercial oil palm *E. guineensis* species. Although not much commercially planted because of its very low yields, the oil palm breeders' interests in the *E. oleifera* species are its high content of unsaturated fatty acids (>60% oleic acid and >18% linoleic acid), low height increment (5-10 cm yr^{-1}) and tolerance to diseases such as bud rot and vascular wilt (Corley and Tinker, 2003; Rao *et al.,* 1989). The ability to transmit their traits has led to the production of interspecific hybrids with *E. guineensis* (Barcelos *et al.,* 2015). In addition, high carotene content and drought tolerance are other interesting characteristics of *E. oleifera*. The main drawback is that it is less productive than *E. guineensis* in terms of oil yield, with some degree of sterility precluding its extensive commercial exploitation (Rajanaidu *et al.*, 2017). As suggested by Choo and Yusof (1996), the possibility for *E. oleifera* to be commercialised is through the pharmaceutical industry and this would promote the development of planting materials with niche traits regardless of their yield performance. In general, *E. oleifera* palms within a population were found to be more uniform in comparison with the *E. guineensis* from West Africa. This observation was attributed to *E. oleifera* palms in South America being found in scattered areas which encouraged inbreeding that led to high levels of homozygosity (Rajanaidu, 1985). This was further supported by molecular marker information indicating *E. guineensis* as more heterozygous than *E. oleifera* (Zulkifli *et al.*, 2012).

Several expeditions to Central and South America to accumulate a series of *E. oleifera* collections for research purposes were initiated by breeders starting in 1982 (Kushairi *et al.*, 2017). A collection of 184 *E. oleifera* accessions are developed and maintained in the form of a field genebank as described by Rajanaidu *et al.* (2017). The collection aimed to capture the genetic variability of *E. oleifera* for utilisation in breeding programmes and as a long-term conservation. At present, *E. oleifera* genetic materials are maintained in the form of a field genebank which requires a large planting area and high maintenance cost. Despite these hurdles, genetic diversity studies are deemed essential for crop improvement and conservation in oil palm breeding programmes. Data collected from these field genebanks on a large number of palm traits provide breeders with the necessary information for maximum efficient selection for the said purpose.

Multivariate analysis has been developed to effectively handle a large amount of accumulated data for breeders to make more precise decisions (Rencher, 2002). Of all multivariate tools, principal component and clustering analyses are extensively used to classify germplasm materials, expose the variability of accessions and determine the genetic relationships among traits (Iqbal *et al.*, 2008). Principal component analysis (PCA) is a technique from applied linear algebra, a descriptive procedure for analysing relationships that may exist in a set of multivariate datasets. It is designed to identify the patterns of data by reducing the number of dimensions or variables (Ekezie, 2013). On the other hand, clustering is an exploratory data analysis tool for grouping accessions into several homogenous groups (Johnson and Wichern, 2007). Both methods have been extensively used to study genetic variability in crop germplasms including oil palm (Ahmad *et al.*, 2014; Li-Hammed *et al.*, 2015). The objectives of this study are to characterise the Malaysian Palm Oil Board (MPOB) *E. oleifera* germplasm collections using multivariate analysis and to identify the contributing characteristics to the overall variation in yield, bunch quality and vegetative traits. This has an important implication for the sampling strategy for field conservation while assuring a good range of diversity is maintained rather than random sampling.

MATERIALS AND METHODS

Plant Materials

Elaeis oleifera germplasms from eight countries in Latin America were obtained through bioprospection conducted in 1982, amounting to a total of 182 accessions. The palms were planted at the MPOB Research Station Kluang, Johor, Malaysia in an equilateral triangle design with a 9 m planting distance between palms. This study was carried out on 572 *E. oleifera* palms including one introgressed population [*Oleifera* (Suriname) x *Oleifera* (Brazil), (OxO)] from the germplasm collection (*Table 1*). The palms were planted either in a randomised complete block design (RCBD) or incomplete randomised design (ICRD).

Data Collection

A total of 17 field data was collected for each palm and classified into three groups; yield, bunch quality components and vegetative measurement. Bunch quality components and vegetative measurements were evaluated using the methods established by Blaak *et al*. (1963) and Breure and Powell (1988), respectively. For yield, three components were evaluated: mean fresh fruit bunch (MFFB), mean bunch number (MBNO) and mean average bunch weight (MABW). Meanwhile, nine parameters for

bunch components were measured: bunch weight (BWT), mean fruit weight (MFW), mesocarp to fruit (MTF), kernel to fruit (KTF), shell to fruit (STF), oil to dry mesocarp (OTDM), fruit to bunch (FTB), oil to bunch (OTB) and kernel to bunch (KTB). Five vegetative traits were also included: frond production (FP), petiole cross-section (PCS), rachis length (RL), leaf area index (LAI) and frond dry weight (FDW).

Statistical Analysis

Data were systematically extracted from the MPOB-Breeding Information System (MPOB-BIS) (Mohd Din *et al.*, 2012). Based on descriptive statistical analysis, the population mean, standard deviation and coefficient of variation (CV) for each trait were generated using Microsoft Excel version 14.0. PCA and cluster analysis were used to assess the level of diversity and to rank the contributions of the variables. Mean data were analysed for correlation and PCA using SAS version 9.4, after standardisation (mean=0, standard deviation=1). Based on the respective eigenvalues obtained, only a significant proportion of variance was explained by the first few principal components. The linear combinations with variance less than 1 (Eigenvalue < 1) were eliminated. In cluster analysis, Ward's hierarchical algorithm based on R-Square was used to construct the phylogenetic relationship.

TABLE 1. NUMBER OF SAMPLES REPRESENTING EACH *Elaeis oleifera* GERMPLASM

Region	Germplasm	No. of samples
Central America	Honduras (HND)	9
	Panama (PAN)	95
	Costa Rica (CRI)	94
South America	Suriname (SUR)	31
	Colombia (COL)	137
	Brazil (BRA)	21
	Ecuador (ECU)	158
	Peru (PER)	10
	Suriname x Brazil (OxO)	17
	Total	572

RESULTS AND DISCUSSION

Performance of *Elaeis oleifera* Germplasm

Evaluation of germplasm collections is the *sine qua non* of every breeding programme for crop improvement. There is a need for systematic evaluation to describe the collections and in the context of genetic resources, to unravel its various morphological, physiological and developmental characteristics including special features, such as dwarfness, compactness and disease resistance. These activities are required to aggregate useful genes and gene combinations into beneficial phenotypes and develop a foundation for selection for various breeding programmes. The distribution of variation for yield, bunch quality components and vegetative measurement for *E. oleifera* is given in *Table 2* and *3*. The ANOVA showed a highly significant (p<0.01) variation for all studied traits among the germplasms. A high range of variability was recorded for most traits with CV ranging from 5.95% to 78.88%. These results indicate sufficient variability exists for the traits under study, thus providing ample scope for characterisation and selection for future breeding programmes. MFFB yield and MBNO of *E. oleifera* from Central America were higher than the South American germplasms, ranging from 116.82-157.44 kg palm^{-1} yr^{-1} and 10.23-12.24 bunches palm^{-1} yr^{-1}, respectively. The OxO introgression progenies displayed the highest bunch weight, *i.e.*, MABW of 14.61 kg palm^{-1} yr^{-1}, followed by the Colombian and Central American *E. oleifera*.

For bunch quality components, all *E. oleifera* accessions recorded a high range of CV for BWT, OTB and KTB, implying that these traits have higher amounts of exploitable genetic variability among the attributes and therefore present a greater potential for these traits to be favoured for selection compared to others (Ndukauba *et al.*, 2015). Besides that, MTF was higher in the South American germplasm, which is in agreement with the mesocarp content of *E. oleifera* in the same region as reported by Rajanaidu *et al*. (2017). In contrast, KTF and STF were lower in the South American collections, except for Colombia. However, despite having higher MTF, OTDM in the South American *E. oleifera* was much lower compared to the ones in Central America. This suggests that increased fruit sets do not affect the OTDM ratio, concurring with previous observations by Haniff and Roslan (2002).

In terms of vegetative measurements, FP was high in *E. oleifera* accessions from Costa Rica, Honduras, Panama and Brazil with CV ranging from 7.82%-13.28%. Other traits such as PCS, RL and LAI were lowest in *E. oleifera* from Suriname, implying that this germplasm is unique in vegetative growth. The lower PCS and RL values contribute to the compactness of this palm (Zulkifli *et al.*, 2019). Thus, the Suriname *E. oleifera* can be considered an important genetic source for the development of compact palms for commercial planting, which allows more palms to be planted per hectare of land with a prolonged economic lifespan. As for FDW, the highest at approximately 45 kg was found in *E. oleifera* from Central America and Colombia with a CV above 20%.

In general, the Colombian germplasm showed similar characteristics as the Central American *E. oleifera,* which is not surprising as both locations are geographically bordering one another. With a few

exceptions, most of the traits in the OxO population also showed the same trend, which is expected to be the effect of heterosis. Traits, namely the FP, RL, MTF and STF recorded the lowest CV, suggesting that the Colombian germplasm possesses low exploitable genetic variability.

Correlation Analysis

The correlation coefficient, r, measures the degree (intensity / magnitude) and nature (direction) of association between characters. The correlation analysis of *E. oleifera*'s yield characters is showed in *Table 4*. MFFB was positively and highly correlated to MBNO (r=0.93) and MABW (r=0.83). This result is similar to the correlation trends reported by Lopes *et al*. (2012), whereby high positive correlation coefficient values for MFFB-MBNO (r=0.84) and MFBB-MABW (r=0.52) were observed in *E. oleifera* interspecific hybrids (*E. oleifera* x *E. guineensis*). Similarly, high correlation values between MFFB and MABW (r=0.96) as well as MBNO (r=0.95) were observed on an *E. oleifera* interspecific hybrid (Gomes Junior *et al.,* 2014). The magnitude of the correlation values for MFFB and MBNO is greater than that of MFFB and MABW, implying that MBNO has a greater influence on the total variation in MFFB as compared to MABW, a similar trend observed in *E. guineensis,* with moderate and positive correlation values for MFFB-MBNO (r=0.71) and MFFB-MABW (r=0.44) (Marhalil *et al.,* 2013). Therefore, selection for a high bunch number could suffice for the improvement of FFB yields in oil palm breeding programmes involving *E. oleifera*. In *E. guineensis* populations, high and moderate positive correlations between MFFB and MBNO were also observed by Okwuagwu *et al.* (2008) (r=0.86) and Okoye *et al.* (2009) (r=0.65). Correlation between MFFB and MABW in both studies showed positive but low correlation values of only 0.24 and 0.21, respectively.

Meanwhile, MBNO and MABW showed a positive correlation (r=0.59), in contrast to *E. guineensis* which normally is negatively correlated as reported in several studies (Gomes Junior *et al.,* 2014; Marhalil *et al.,* 2013; Okoye *et al.,* 2009; Okwuagwu *et al.,* 2008). This suggests that an increase in MABW is associated with a reduction in MBNO and *vice versa*. However, in *E. oleifera*, Lopes *et al.* (2012) reported a moderate positive correlation between these two components (r=0.42). This interesting result suggests that *E. oleifera* differs from *E. guineensis* in these traits. This may be due to the unique characteristics of *E. oleifera* bunches, which not only have moderate weight but also possess a high bunch number.

For bunch quality characters, the highest positive correlation was detected between KTF and STF (r=0.90), while the highest negative correlation was observed between MTF and STF (r=-0.99). KTF was highly and positively correlated to a few traits such as BWT, STF, OTDM and KTB but negatively correlated with MFW, MTF, FTB and OTB. As expected, MTF was negatively correlated to all bunch quality components except MFW, FTB and OTB. The positive correlation between FTB and OTB (r=0.44) suggests that more fruits are required to obtain a higher oil content. In general, the results indicate that an increase in OTB was associated with increases in MTF, MFW and FTB, but was also affected by the negative associations with KTF and STF. Selection of genotypes for low KTF would implicitly lead to palms with relatively low STF but high MTF.

The vegetative character PCS was positively and highly correlated with other vegetative characters such as RL (r=0.98), LAI (r=0.97) and FDW (r=0.97). In addition, the strong association of these traits with yield characters in this study was similar to previous observations by Rafii (1996) in *E. guineensis* and Mohd Din *et al.* (2000) in *E. oleifera*. Palms with higher LAI values will allow more light interception as LAI is related to photosynthesis and dry matter accumulation. Higher LAI is associated with increased yields due to a higher photosynthesis rate, which leads to better dry matter production (Rajanaidu *et al.,* 2011). Therefore, in selecting for yield, higher vegetative growth should be targeted as well as a greater proportion of the photosynthesised dry matter could be diverted to fruit bunches (Corley and Tinker, 2003).

Principal Component Analysis (PCA)

The partitioning of total variance into its components facilitates the use of oil palm germplasm as a genetic resource for crop improvement programmes. A well-defined relationship between traits through PCA helps know the traits contributing most to variation. The first four principal axes with Eigenvalues of >1.0 accounted for 96.32% of the total variation suggesting that the *E. oleifera* accessions can be clearly differentiated using these traits. The eigenvalue is often used to determine the number of major principal components and an eigenvalue of >1.0 has been the rule of thumb to select useful PCs with practical significance and therefore should be retained (Iezonni and Pritts, 1991). The contribution of each variable to the extracted principal components (PCs) is presented in *Table 5*. Eigenvalues associated with the first two principal components decreased drastically from 11.17 to 2.40. PC1 contributed 65.71% of the total variation in the data set whereas PC2 to PC4 explained the additional 14.12%, 9.99% and 6.50% variations, respectively. These results showed a higher

TABLE 2. THE MEAN AND DISTRIBUTION OF VARIATION FOR YIELD AND VEGETATIVE MEASUREMENT TRAITS IN *Elaeis oleifera* GERMPLASMS

Country	N	MFFB		MBNO		MABW		FP		PCS		RL		LAI		FDW	
		Mean	CV (%)	Mean	CV (%)	Mean	CV (%)	Mean	CV (%)	Mean	CV (%)	Mean	CV (%)	Mean	CV (%)	Mean	CV (%)
Suriname	31	8.69	68.52	4.46	37.91	1.94	61.61	19.16	8.95	1.96	21.54	1.25	8.88	0.43	20.6	7.81	16.03
Colombia	137	111.75	44.88	8.61	43.44	13.01	15.53	21.99	14.38	17.68	20.96	4.28	11.24	4.99	27.83	44.18	22.72
Costa Rica	94	116.82	44.58	10.23	42.20	11.62	19.29	23.82	13.28	16.79	17.81	4.16	14.06	5.10	24.94	45.97	21.89
Honduras	9	157.44	30.32	12.24	30.04	12.86	8.36	23.00	11.30	17.72	18.09	3.98	8.48	5.76	20.98	46.93	26.05
Panama	95	123.42	35.30	10.86	32.90	11.43	16.88	23.64	11.74	16.43	20.40	4.20	11.55	5.12	26.32	44.73	22.69
Brazil	21	38.55	65.30	6.64	61.86	6.10	24.77	23.05	7.82	5.07	20.68	1.99	10.60	1.19	34.39	16.71	17.28
OxO	17	81.45	40.14	5.65	41.54	14.61	14.67	22.53	9.82	15.64	15.22	3.72	12.78	4.10	19.44	40.68	16.19
Ecuador	158	24.26	45.68	4.66	37.89	5.12	21.60	18.83	10.19	10.54	20.41	3.35	10.23	2.68	23.62	24.21	20.44
Peru	10	12.53	76.10	1.54	69.62	7.58	26.85	17.10	9.33	13.42	15.68	3.79	9.86	3.03	16.36	27.03	16.99

Note: MFFB (kg palm^{-1} yr^{-1}) - mean fresh fruit bunch; MBNO (bunches palm^{-1} yr^{-1}) - mean bunch number; MABW (kg palm^{-1} yr^{-1}) - mean average bunch weight; FP (no.) - frond production; PCS (cm^2) - petiole cross section; RL (m) - rachis length; LAI - leaf area index; FDW (kg) - frond dry weight.

TABLE 3. THE MEAN AND DISTRIBUTION OF VARIATION FOR BUNCH QUALITY COMPONENT TRAITS IN *Elaeis oleifera* GERMPLASMS

Country	N	BWT		MFW		MTF		KTF		STF		OTDM		FTB		OTB		KTB	
		Mean	CV (%)	Mean	CV (%)	Mean	CV (%)	Mean	CV (%)	Mean	CV (%)	Mean	CV (%)	Mean	CV (%)	Mean	CV (%)	Mean	CV (%)
Suriname	31	3.18	78.88	3.41	18.56	48.95	8.04	7.17	27.38	43.88	6.90	27.77	9.72	51.91	13.19	3.28	24.82	3.40	40.09
Colombia	137	12.38	33.24	3.28	16.38	36.99	11.05	13.04	16.51	49.97	6.43	38.37	15.80	46.32	14.45	3.85	39.91	4.00	35.42
Costa Rica	94	10.57	41.03	3.81	18.83	36.72	10.52	12.53	17.32	50.74	6.07	40.30	13.93	51.33	13.98	4.84	40.57	3.73	43.65
Honduras	9	10.27	27.65	3.96	15.36	34.79	14.64	13.18	16.87	52.03	6.45	38.37	12.32	44.98	23.48	3.14	29.41	3.15	47.75
Panama	95	10.36	39.64	3.45	21.68	35.79	11.19	12.68	18.85	51.53	5.95	38.16	17.39	47.58	12.91	4.15	39.56	3.82	41.94
Brazil	21	11.03	41.86	10.72	29.53	47.32	9.68	9.94	16.49	42.74	8.72	40.43	12.45	50.40	21.28	5.49	32.64	3.79	28.65
OxO	17	14.47	26.74	3.87	14.67	36.77	11.56	12.09	13.75	51.14	6.46	36.04	22.55	53.72	13.13	3.56	58.61	4.55	24.45
Ecuador	158	6.47	31.16	11.78	17.64	62.13	6.01	6.69	20.86	31.18	9.38	23.85	13.41	55.14	13.56	4.24	35.58	2.81	36.44
Peru	10	6.82	26.21	11.73	26.64	55.86	10.15	6.16	30.99	37.98	11.84	30.12	19.86	59.29	19.80	5.16	39.13	2.97	33.22

Note: BWT (kg) - bunch weight; MFW (g) - mean fruit weight; MTF (%) - mesocarp to fruit; KTF (%) - kernel to fruit; STF (%) - shell to fruit; OTDM (%) - oil to dry mesocarp; FTB (%) - fruit to bunch; OTB (%) - oil to bunch; KTB (%) - kernel to bunch.

TABLE 4. THE CORRELATION COEFFICIENT ANALYSIS, R, OF *Elaeis oleifera* GERMPLASMS BETWEEN 17 TRAITS

	Correlation matrix																
	MFFB	**MBNO**	**MABW**	**BWT**	**MFW**	**MTF**	**KTF**	**STF**	**OTDM**	**FTB**	**OTB**	**KTB**	**FP**	**PCS**	**RL**	**LAI**	**FDW**
MFFB	1.0000																
MBNO	0.9302	1.0000															
MABW	0.8306	0.5937	1.0000														
BWT	0.6405	0.4768	0.8689	1.0000													
MFW	-0.664	-0.6329	-0.513	-0.3146	1.0000												
MTF	-0.8651	-0.7957	-0.7817	-0.6826	0.8499	1.0000											
KTF	0.9346	0.8737	0.8481	0.7989	-0.7198	-0.9453	1.0000										
STF	0.8121	0.7407	0.7334	0.6174	-0.8749	-0.9917	0.8956	1.0000									
OTDM	0.7244	0.7104	0.6709	0.7651	-0.4521	-0.8276	0.8519	0.7939	1.0000								
FTB	-0.7827	-0.8824	-0.43	-0.3913	0.6573	0.7418	-0.7925	-0.6987	-0.633	1.0000							
OTB	-0.3489	-0.2929	-0.2185	0.0321	0.6734	0.3728	-0.2832	-0.3958	0.158	0.439	1.0000						
KTB	0.3287	0.2327	0.5674	0.7611	-0.5508	-0.6694	0.6255	0.6668	0.6117	-0.2824	-0.1114	1.0000					
FP	0.7925	0.8549	0.6337	0.7308	-0.5792	-0.8404	0.9079	0.7885	0.8749	-0.7401	-0.0755	0.6211	1.0000				
PCS	0.7885	0.545	0.9027	0.6369	-0.3582	-0.5722	0.6748	0.516	0.4537	-0.3073	-0.152	0.2111	0.4084	1.0000			
RL	0.6847	0.4481	0.8193	0.5646	-0.2129	-0.4243	0.5549	0.3614	0.3549	-0.1888	-0.0209	0.1125	0.3038	0.9779	1.0000		
LAI	0.8977	0.7132	0.8913	0.6133	-0.4779	-0.6756	0.7719	0.6184	0.5284	-0.4805	-0.239	0.2011	0.5371	0.974	0.9295	1.0000	
FDW	0.8997	0.7089	0.9367	0.7053	-0.5032	-0.7251	0.8195	0.6672	0.5955	-0.4695	-0.204	0.3271	0.6065	0.9703	0.9189	0.9895	1.0000

Note: MFFB - mean fresh fruit bunch; MBNO - mean bunch number; MABW - mean average bunch weight; BWT - bunch weight; MFW - mean fruit weight; MTF - mesocarp to fruit; KTF - kernel to fruit; STF - shell to fruit; OTDM - oil to dry mesocarp; FTB - fruit to bunch; OTB - oil to bunch; KTB - kernel to bunch; FP - frond production; PCS - petiole cross section; RL - rachis length; LAI - leaf area index; FDW - frond dry weight.

TABLE 5. CONTRIBUTION OF EACH VARIABLE TO THE EXTRACTED FOUR PCs WITH RESPECTIVE EIGENVALUES AND PROPORTION OF TOTAL VARIABILITY

Field evaluation	Traits	PC1	PC2	PC3	PC4
Bunch yield	MFFB	0.287	0.039	-0.146	0.181
	MBNO	0.255	-0.105	-0.151	0.417
	MABW	0.271	0.201	0.073	-0.226
Bunch quality	BWT	0.235	0.081	0.380	-0.175
	MFW	-0.215	0.294	0.268	0.270
	MTF	-0.281	0.182	-0.006	0.082
	KTF	0.295	-0.084	0.050	0.050
	STF	0.268	-0.215	-0.010	-0.132
	OTDM	0.242	-0.117	0.349	0.224
	FTB	-0.218	0.275	0.187	-0.346
	OTB	-0.090	0.212	0.582	0.375
	KTB	0.171	-0.232	0.387	-0.488
Vegetative measurement	FP	0.253	-0.198	0.206	0.231
	PCS	0.233	0.392	-0.092	-0.083
	RL	0.200	0.469	-0.065	-0.040
	LAI	0.257	0.300	-0.159	0.034
	FDW	0.268	0.274	-0.073	-0.023
	Eigenvalue	11.171	2.400	1.698	1.105
	Variance (%)	65.71	14.12	9.99	6.50
	Cumulative (%)	65.71	79.83	89.82	96.32

Note: MFFB - mean fresh fruit bunch; MBNO - mean bunch number; MABW - mean average bunch weight; BWT - bunch weight; MFW - mean fruit weight; MTF - mesocarp to fruit; KTF - kernel to fruit; STF - shell to fruit; OTDM - oil to dry mesocarp; FTB - fruit to bunch; OTB - oil to bunch; KTB - kernel to bunch; FP - frond production; PCS - petiole cross section; RL - rachis length; LAI - leaf area index; FDW - frond dry weight.

percentage of variation contributed by the first two components compared to Camillo *et al.* (2014), who reported a total variability of 68.80% for the first two components of Brazil's *E. oleifera* germplasm. High phenotypic variability was observed on traits such as rachis length, height and fruit weight in *E. oleifera* (Rey *et al.*, 2004; Rios *et al.*, 2011). In *E. guineensis* however, a lower genetic variability (55.1%) was quantified for the first two components of yield and fatty acid traits (Li-Hammed *et al.*, 2016).

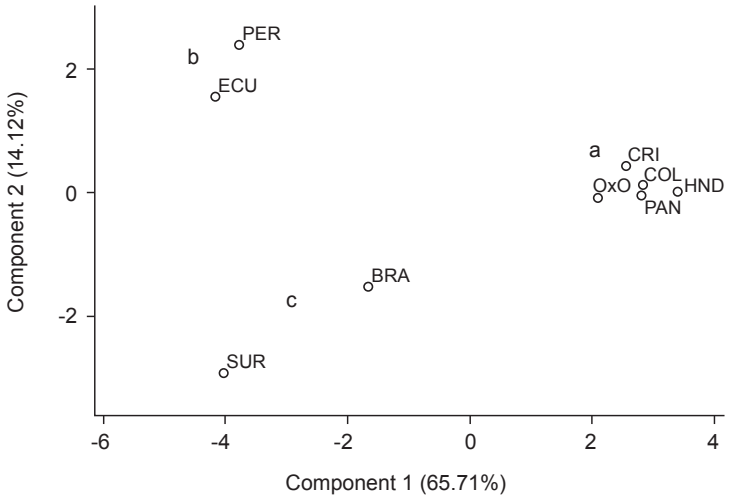
Variables with significant positive and negative impacts on each PC, especially PC1, are attributed mostly to diversity and are the primary source of variation beneficial for the selection of diverse genetic backgrounds (Denton and Nwangburuka, 2011). PC1 was mostly related to KTF (0.295), MFFB (0.287) and MABW (0.271). This PC exhibited positive effect for all variables except for MFW (-0.215), MTF (-0.281), FTB (-0.218) and OTB (-0.090). These characteristics play a vital role in differentiating the *E. oleifera* accessions and should be considered during selection in breeding programmes. For PC2, the largest positively significant component loadings were from RL (0.469), followed by PCS (0.392) and LAI (0.300) while the negatives were from KTB (-0.232), STF (-0.215) and FP (-0.198). The largest positive and highly significant coefficient in PC3 was observed in bunch quality components, *i.e.*, OTB (0.582), KTB (0.387) and BWT (0.380), and the least negative contributions were from LAI (-0.159), MBNO (-0.151) and MFFB (-0.146). PC4 was positively contributed by MBNO (0.417), OTB (0.375) and MFW (0.270), meanwhile negatively contributed by KTB (-0.488), FTB (-0.346) and MABW (-0.226). In general, vegetative characteristics and bunch quality components had a positive significant influence on PC2 and PC3, respectively. Meanwhile, most of the traits with high positive loading for PC1 and PC4 were mainly associated to yield and bunch quality components traits.

The relationship among the eight locations associated with MPOB *E. oleifera* and OxO populations was analysed from the score plot

between PC1 and PC2 (*Figure 1*). This provides a map of how the germplasms relate to each other. The germplasms from Central America, Colombia and OxO were closely connected and positively inclined towards PC1 as they performed well in the variables exhibiting the highest positive loading in PC1 such as MFFB (81.45-157.44 kg palm^{-1} yr^{-1}), MABW (11.43-14.61 kg palm^{-1} yr^{-1}) and FDW (40.68-46.93 kg). These populations were also positioned at the centre of PC2 due to being highest in vegetative traits such as RL (3.72-4.28 m), PCS (15.64-17.17 cm^2) and LAI (4.10-5.76).

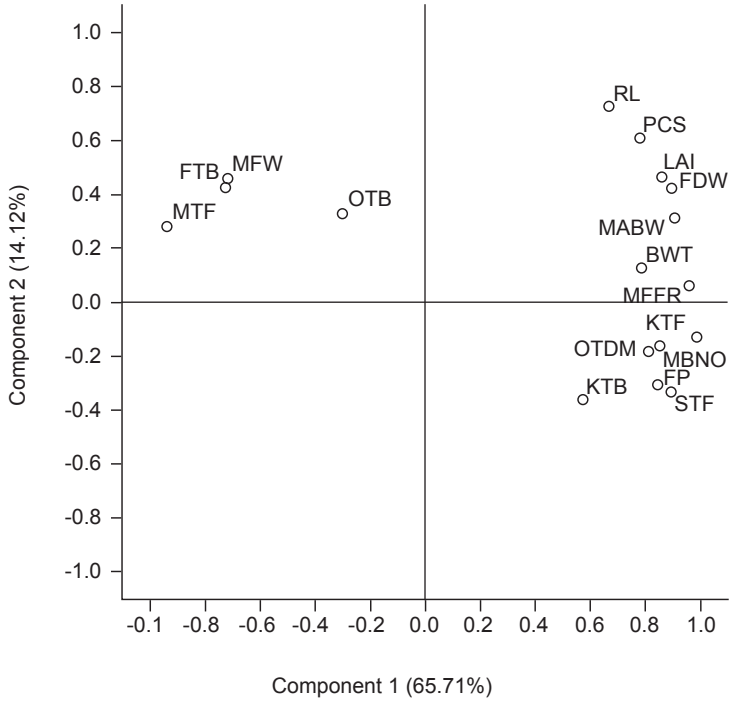
The Ecuador and Peru accessions were positioned together based on their high values in MFW, MTF, FTB while moderate in RL, PCS and LAI. Oil palm germplasm collected from Suriname and Brazil were negatively correlated with both PC1 and PC2. This is likely due to the poor performance of both germplasms in most variables such as FDW, MFFB, PCS and RL, in comparison to the other germplasms. Suriname oil palms have been observed to be vegetatively smaller and displayed low bunch production, resulting in low bunch yields compared to *E. oleifera* from other parts of the South American continent (Rao *et al.*, 1989). Field observations of Suriname germplasm exhibited unique physical characteristics among the *E. oleifera* accessions. Notably, OxO performance improved due to hybrid vigour contributed by Brazil and Suriname introgression. The superiority of OxO over both parents is indicated by the positive correlation of OxO to both PC1 and PC2 (*Figure 1*) which helps detect deviation from normality. Most of the traits exhibited by OxO improved, especially in yield and bunch quality components such as MFFB (81.45 kg palm^{-1} yr^{-1}), MABW (14.61 kg palm^{-1} yr^{-1}), BWT (14.47 kg), KTF (12.09%) and FTB (53.72%).

Biplot diagrams provide information to select genotypes that might have favourable combinations of traits that can be strategised in a breeding programme. Most of the variables grouped at quadrants 1 and 4 indicated that those variables were positively correlated to PC1, whilst FTB, OTB, MFW and MTF positioned at quadrant 2 were negatively correlated to PC1 but positively to PC2 (*Figure 2*). A PCA biplot was constructed to study the relationship between variables and to identify the best variables contributed by each germplasm (*Figure 3*). Variables with a small angle between them imply a positive and large correlation between them, indicating that an increase in one will increase in the other (Li-Hammed *et al.*, 2016). On the other hand, variables opposite to each other with large angles in between are negatively correlated. For instance, KTB is highly positively correlated with STF due to the small angle between them and is located in the same quadrant. However, they are negatively correlated to MFW and FTB. Therefore, oil palms from Ecuador and Peru have high FTB values but low KTB values. The Suriname oil palm is distinct as there is no interesting or unique variable associated with it. For other populations, most variables in yield parameters and bunch quality components such as MFFB, MBNO, BWT, FP, OTDM and KTF are good characters for selection in the breeding programme as they contribute positively to the primary component (PC1).



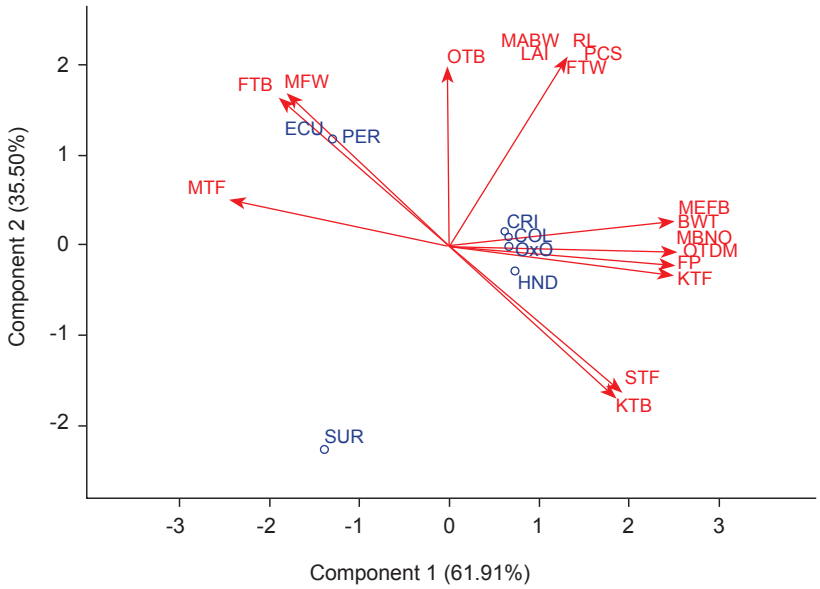
Note: (a) Costa Rica (CRI), Colombia (COL), Honduras (HND), Panama (PNM) and Suriname x Brazil (OxO) were positioned together and positively correlated toward both PC1 and PC2. (b) Peru (PER) and Ecuador (ECU) were negatively correlated to PC1 and positive toward PC2. (c) Brazil (BRA) and Suriname (SUR) were negatively correlated to PC1 and PC2.

Figure 1. PCA score plot of PC1 and PC2 among the eight locations associated to MPOB Elaeis oleifera *and OxO populations. Germplasms close to each other have similar field data performance profiles, whereas those far from each other are dissimilar.*



Note: Variables in quadrant 1; RL - rachis length; PCS - petiole cross-section; LAI - leaf area index; FDW- frond dry weight; MABW - mean average bunch weight; BWT - bunch weight and MFFB - mean fresh fruit bunch were positively correlated to both PC1 and PC2. Variables in quadrant 2; FTB - fruit to bunch; MFW - mean fruit weight; MTF - mesocarp to fruit and OTB - oil to bunch negatively correlated to PC1 but positively correlated towards PC2. KTF - kernel to fruit; OTDM - oil to dry mesocarp; MBNO - mean bunch number; FP - frond production; KTB - kernel to bunch and STF - shell to fruit together in quadrant 4 were positive to PC1 but negative to PC2.

Figure 2. Loadings plot showing the relationship of 17 variables on PC1 and PC2. Variables contributing similar information are correlated and grouped in the same quadrant.



Note: Germplasm from Peru (PER) and Ecuador (ECU) have a good character in fruit to bunch (FTB) and mean fruit weight (MFW). Brazil (BRA), Costa Rica (CRI), Colombia (COL), Honduras (HND), Panama (PAN) and Suriname x Brazil (OxO) were the best populations for mean fresh fruit bunch (MFFB), mean bunch number (MBNO), bunch weight (BWT), frond production (FP), oil to dry mesocarp (OTDM) and kernel to fruit (KTF). No interesting variable is associated with Suriname (SUR).

Figure 3. PCA Biplot of MPOB Elaeis oleifera *germplasms shows how strongly each variable influences the principal components.*

Cluster Analysis

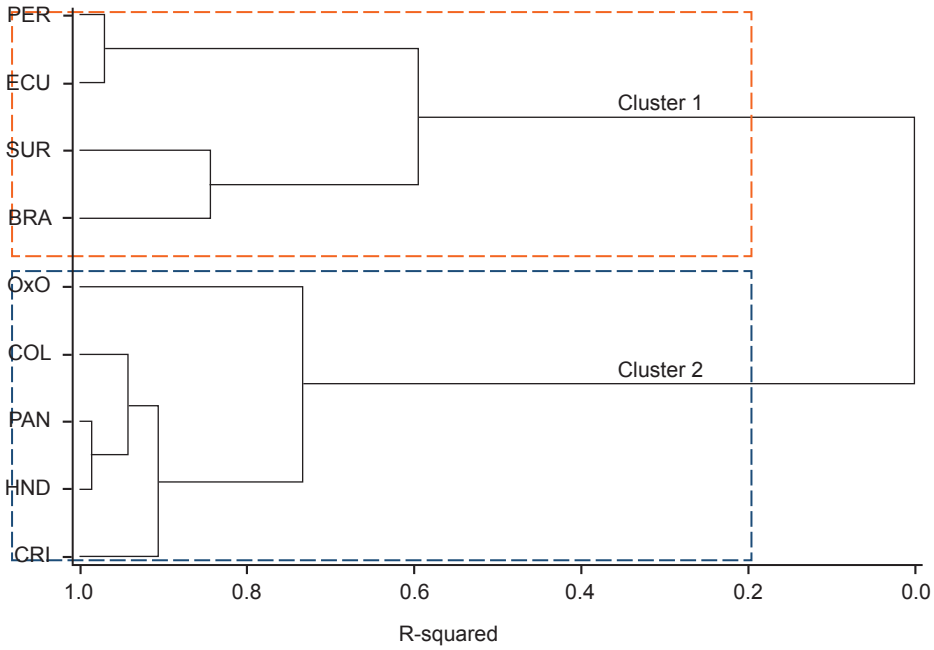
PCA is usually complemented with other analyses such as cluster analysis to provide a clear representation of the genetic diversity of the populations under study. The dendrogram (*Figure 4*) represents the hierarchical cluster analysis based on Ward's method, an approach commonly suggested for clustering quantitative variables (Siracli *et al.*, 2013). This method classifies the materials depending on the environment or correlation of the individuals as claimed by Granato *et al.* (2018). Two main clusters were observed, consisting of four sub-clusters. To envision the clustering pattern of *E. oleifera* germplasm, the mean value for each sub-cluster is presented in *Table 6*. Cluster 1 was divided into two sub-clusters in which Peru and Ecuador were coupled together in sub-cluster 1, while Brazil and Suriname formed another sub-cluster. MFW, MTF and OTB values for populations in Cluster 1, consisting of Peru, Ecuador, Suriname and Brazil, were greater than the populations in Cluster 2. However, the average MFW, MTF, FTB, OTB and RL values were slightly lower in the Brazil and Suriname populations, therefore comprising a different sub-cluster than Peru and Ecuador.

The second cluster (Cluster 2) comprised two sub-clusters, with OxO as a singleton and the second sub-cluster consisting of Colombia, Panama, Honduras and Costa Rica. These populations had higher mean values for MFFB, MBNO, MABW, BWT, KTF, STF, OTDM, PCS, LAI and FDW. In addition, the highest mean values of MABW, BWT and KTB but with lower values for other traits, possibly separated OxO from the other populations in Cluster 2. As mentioned earlier, the traits improvement in OxO resulted in a separate cluster from their original parents, Brazil and Suriname. This may be due to differences in gene combinations compared to both parents, resulting in hybrid vigour (Bingham, 1998). The results of the phylogenetic relationship also reflected the geographical origin of the populations. Populations in Costa Rica, Panama and Honduras tend to cluster together as they form part of Central America. Through sharing a border with Panama, it is not surprising that Colombia in South America is included in Cluster 2. High gene flow may have occurred between populations within countries where similar trends were also observed in *E. guineensis* (Zulkifli *et al.*, 2012) and Napirira bean (Fan and Beta, 2017).

It is a known fact that utilising and conserving germplasms involve proper consideration of developing genetic resources for varietal breeding programmes while avoiding loss of genetic diversity, respectively. Combining the results from correlation studies, principal component and cluster analyses provided knowledge on the patterns of genetic diversity, which are vital for developing proper breeding strategies for improvement and conservation. Crossing between morphologically distant populations, in this case between populations in Clusters 1 and 2, would theoretically result in a maximum degree of heterosis which could lead to improvement in certain traits of interest (Rahim *et al.*, 2010; Singh *et al.*, 2008). For conservation purposes, the focus should be directed towards germplasm with high variability to develop optimal sampling strategies and minimise any redundancies in the collection. Selection and conservation should also take into account unique populations such as Suriname, as this population may possess interesting genes for further exploitation.

The wealth of diversity in the *E. oleifera* populations in this study can be observed from the wide variability in traits such as MFFB, MBNO, LAI, BWT, FTB, OTB and KTB. However, their trait values are still incomparable to that of the commercial *E. guineensis* (Noh *et al.*, 2012). Although *E. oleifera* is not widely planted because of its very low yield, it has several interesting characteristics, such as compactness, which may be introgressed to improve *E. guineensis*. Compact palms generally demonstrate lower height increment, have shorter fronds (RL) and small petioles (PCS) (Barcelos *et al.*, 2015; Zulkifli *et al.*, 2020). All *E. oleifera* populations in this study showed lower RL and PCS mean values compared to the commercial *E. guineensis* (5.6 m and 29.0 cm^2, respectively) (Noh *et al.*, 2012). It would then be reasonable to cross populations with extreme mean values for both of these traits, *i.e.*, Suriname and Brazil, with commercial *E. guineensis* to derive compact offsprings. The correlation of both traits with other characters should be taken into account for the selection of parental palms in the breeding programme. Therefore, the high variability in *E. oleifera* accessions revealed through multivariate analyses would help breeders explore under-utilised genetic resources and guide future strategies for oil palm genetic improvement.

Although the Malaysian oil palm industry had significant success in generating new planting materials to gain a strong footing, the genetic variation of the planting materials was still considered narrow (Arasu and Rajanaidu, 1976; Rajanaidu *et al.*, 2000). The oil palm industry in Malaysia realised the risk of relying on a limited genetic base and recognised the necessity for an adequate genetic base for effective selection in breeding programmes. This realisation provided the impetus to systematically search for new oil palm genetic materials including *E. oleifera*. The exploitation of the *E. oleifera* germplasm materials in this study will provide potential new genes for incorporation into the existing breeding stock, as well as the flexibility of further developing planting materials including for niche markets. Information obtained by the characterisation of



Note: R-squared value measures the extent to which groups or clusters are different from each other. Germplasm was grouped in two major clusters. Cluster 1 (orange box) comprised germplasm from Peru (PER), Ecuador (ECU), Suriname (SUR) and Brazil (BRA). Cluster 2 (blue box) contained germplasm from Costa Rica (CRI), Honduras (HND), Panama (PAN), Colombia (COL) and Suriname x Brazil (OxO).

Figure 4. Cluster analysis of MPOB Elaeis oleifera *germplasms based on 17 variables.*

TABLE 6. WARD'S CLUSTER MEANS OF 17 TRAITS IN MPOB *Elaeis oleifera* GERMPLASM

Traits	Cluster 1 (Sub 1)	Cluster 1 (Sub 2)	Cluster 2 (Sub 1)	Cluster 2 (Sub 2)
MFFB	18.39	23.62	81.45	127.36
MBNO	3.10	5.55	5.65	10.48
MABW	6.35	4.02	14.61	12.23
BWT	6.64	7.10	14.47	10.90
MFW	11.73	7.06	3.87	3.63
MTF	59.00	47.91	36.77	36.07
KTF	6.43	8.55	12.09	12.86
STF	34.58	43.49	51.14	51.07
OTDM	26.99	34.10	36.04	38.80
FTB	57.22	51.16	53.72	47.55
OTB	4.70	4.38	3.56	3.99
KTB	2.89	3.60	4.55	3.64
FP	17.96	21.10	22.53	23.11
PCS	11.98	3.52	15.64	17.09
RL	3.57	1.62	3.72	4.15
LAI	2.85	0.81	4.10	5.24
FDW	25.62	12.26	40.68	45.20

Note: MFFB (kg palm^{-1} yr^{-1}) - mean fresh fruit bunch; MBNO (bunches palm^{-1} yr^{-1}) - mean bunch number; MABW (kg palm^{-1} yr^{-1}) - mean average bunch weight; BWT (kg) - bunch weight; MFW (g) - mean fruit weight; MTF (%) - mesocarp to fruit; KTF (%) - kernel to fruit; STF (%) - shell to fruit; OTDM (%) - oil to dry mesocarp; FTB (%) - fruit to bunch; OTB (%) - oil to bunch; KTB (%) - kernel to bunch; FP (no.) - frond production; PCS (cm^2) - petiole cross section; RL (m) - rachis length; LAI - leaf area index; FDW (kg) - frond dry weight.

these germplasms is useful as they open new avenues for crop improvement and have the potential for producing novel crop varieties. The ability to select palms for particular traits using new genetic resources would thus represent a major step forward in expediting oil palm breeding.

CONCLUSION

The richness of any germplasm collection is quantified in terms of the magnitude of the genetic variability of its accessions. It can be concluded from this study that multivariate analyses classified the *E. oleifera* germplasms generally based on their phenotypic characters. Most of the important traits of *E. oleifera* displayed a wide range of variation. Cluster analysis also grouped the *E. oleifera* germplasms into two distinct clusters, which were highly associated with their geographical locations in Central and South America. The optimum traits for measurement can be identified by focusing on variables that contribute most to the variation, to assist the selection of specific populations for regeneration purposes and selective breeding for oil palm improvement programmes. This phenotypic data will be integrated with molecular-based diversity patterns so that breeding and conservation strategies could be systematically formulated for *E. oleifera* populations.

ACKNOWLEDGEMENT

The authors would like to thank the Director-General of MPOB for permission to publish this article. The authors also would like to thank Ooi Siew Eng for editing and providing valuable comments on the manuscript.

REFERENCES

Ahmad, H F; Awar, S I; Aziz, O and Ali, M A (2014). Multivariate analysis of some metric traits in bread wheat (*Triticuma estivum* L.). *European J. Biotechnol. Biosci., 1*: 22-26.

Arasu, N T and Rajanaidu, N (1976). Oil palm genetic resources. *International Developments in Oil Palm* (Earp, D A and Newall, W eds.). International Society of Planters, Kuala Lumpur. p. 16-25.

Barcelos, E; Rios, S A; Cunha, R N V; Lopes, R; Motoike, S Y; Babiychuk, E; Skirycz, A and Kushnir, S (2015). Oil palm natural diversity and the potential for yield improvement. *Front. Plant Sci., 6*: 190. DOI: 10.3389/fpls.2015.00190.

Bingham, E T (1998). Role of chromosome blocks in heterosis and estimates of dominance and overdominance: Concept and breeding of heterosis in crop plant. *Crop Sci. Soc. Amer., 25*: 71-87. DOI: 10.2135/cssaspecpub25.c6.

Blaak, G; Sparnaaij, L D and Menendez, T J (1963). Breeding and inheritance in the oil palm (*Elaeis guineensis* Jacq.) II: Method of bunch quality analysis. *J. W. Afr. Inst. Oil Palm Res., 4*: 146-155.

Breure, C J and Powell, M S (1988). The one-shot method of establishing growth parameters in oil palm. *Proc. of the International Oil Palm Conferences - Agriculture*. PORIM, Bangi. p. 203-209.

Camillo, J; Braga, V C; de Abreu Mattos, J K; Lopes, R; da Cunha, R N V; Padilha, J and Scherwinski Pereira, J E (2014). Seed biometric parameters in oil palm accessions from a Brazilian germplasm. *Pesq. Agropec. Bras., 49*: 604-612. DOI: 10.1590/S0100-204X2014000800004.

Choo, Y M and Yusof, B (1996). PORIM Information Series. *Elaeis oleifera* palm for the pharmaceutical industry. PORIM, Bangi. TT 42.

Corley, R H V and Tinker, P B (2003). Care and maintenance of oil palms. *The Oil Palm.* 4th edition. Blackwell Science, Oxford. p. 287-326.

de Blank, S (1952). A reconnaissance of the American oil palm. *Trop. Agric. Trin., 29:* 90-101.

Denton, O A and Nwangburuka, C C (2011). Heritability, genetic advance and character association in six yield related characters of *Solanum anguivi*. *Asian J. Agric. Res., 5:* 201-207. DOI: 10.3923/ajar.2011.201.207.

Ekezie, D D (2013). Principal component analysis, an aid to interpretation data. A case study of oil palm (*Elaeis guineensis* Jacq.). *J Emerg. Trend Engine Appl. Sci., 4*: 237-241.

Escobar, R (1981). Preliminary results of the collection and evaluation of the American oil palm *Elaeis oleifera* (H.B.K.) Cortes in Costa Rica, Panama and Colombia. *The Oil Palm in Agriculture in the Eighties* (Pushparajah, E and Chew, P eds.). Incorporated Society of Planters, Kuala Lumpur. p. 17–20.

Fan, G and Beta, T (2017). Discrimination of geographical origin of Napirira bean (*Phaseolus vulgaris* L.) based on phenolic profiles and antioxidant activity. *J. Food Comp. Analy., 62*: 217-222. DOI: 10.1016/j.jfca.2017.07.001.

Gomes Junior, R A; de Lima Gurgel, F; de Azevedo Peixoto, L; Bhering, L L; Cunha, R N V; Ricardo, R; Pina, A J A and Veiga, A S (2014). Evaluation of interspecific hybrids of palm oil reveals great genetic variability and potential selection gain. *Ind. Crops Prod., 52*: 512-518. DOI: 10.1016/j.indcrop.2013.10.036.

Granato, D; Santos, J S; Escher, G B; Ferreira, B L and Maggio, R M (2018). Use of principal component analysis (PCA) and hierarchical cluster analysis (HCA) for multivariate association between bioactive compounds and functional properties in foods: A critical perspective. *Trends in Food Sci. Tech., 72*: 83-90. DOI: 10.1016/j.tifs.2017.12.006.

Haniff, H M and Roslan, M N M (2002). Fruit set and oil palm bunch components. *J. Oil Palm Res., 14*: 24-33.

Hardon, J J and Turner, P D (1967). Observations on natural pollination in commercial plantings of oil palm (*Elaeis guineensis*) in Malaya. *Experiment. Agri., 3:* 105-116. DOI: 10.1017/S0014479700021864.

Iezonni, A P and Pritts, M P (1991). Applications of principal component analysis to horticultural research. *Hortic. Sc., 26:* 334-338. DOI: 10.21273/HORTSCI.26.4.334.

Iqbal, Z; Arshad, M; Ashraf, M; Mahmood, T and Waheed, A (2008). Evaluation of soybean [*Glycine max* (L.) Merrill] germplasm for some important morphological traits using multivariate analysis. *Pak. J. Bot., 40*: 2323-2328.

Johnson, R A and Wichern, D W (2007). *Applied Multivariate Statistical Analysis*. 6th edition. Pearson, New Jersey. 455 pp.

Kushairi, A; Singh, R and Ong-Abdullah, M (2017). The oil palm industry in Malaysia: Thriving with transformative technologies. *J. Oil Palm Res., 29*: 431-439. DOI: 10.21894/jopr.2017.00017.

Li-Hammed, M A; Kushairi, A; Rajanaidu, N; Mohd Sukri, H; Che Wan Zanariah, C W N and Jalani, B S (2015). Multivariate analysis of vegetative and physiological traits in oil palm (*Elaeis guineensis* Jacq.) germplasm. *Expert Opin. Environ. Biol., 4*: 1-5. DOI: 10.4172/2325-9655.1000120.

Li-Hammed, M A; Kushairi, A; Rajanaidu, N; Mohd Sukri, H; Che Wan Zanariah, C W N and Jalani, B S (2016). Genetic variability for yield, yield components and fatty acid traits in oil palm (*Elaeis guineensis* Jacq.) germplasm using multivariate tools. *Intl. J. Agri. Forest Plant., 2*: 219-226.

Lopes, R; Cunha, R N V and Resende, M D V (2012). Bunch yield and genetic parameters of progenies between caiaué and African oil palm. *Pesqui. Agropecu. Bras., 47*: 1496-1503. DOI: 10.1590/S0100-204X2012001000012.

Marhalil, M; Rafii, M Y; Afizi, M M A; Arolu, I W; Noh, A; Mohd Din, A; Kushairi, A; Norziha, A; Rajanaidu, N and Latif, M A (2013). Genetic variability in yield and vegetative traits in elite germplasm of MPOB-Nigerian *dura* x AVROS *pisifera* progenies. *J. Food Agric. Environ., 11*: 515-519.

Meunier, J (1975). *Le palmier à huile américain* Elaeis melanococca. *Oléagineux., 30*: 51-61.

Mohd Din, A; Rajanaidu, N and Jalani, B S (2000). Performance of *Elaeis oleifera* from Panama, Costa Rica, Colombia and Honduras in Malaysia. *J. Oil Palm Res., 12*: 71-80.

Mohd Din, A; Rajanaidu, N; Kushairi, A; Marhalil, M and Zaharah, R (2012). MPOB Breeding Information System (MPOB-BIS). MPOB, Bangi. *MPOB Information Series,* 599.

Ndukauba, J; Nwofia, G E; Okocha, P I and Ene-Obon, E E (2015). Variability in Egusi-Melon genotypes (*Citrullus lanatus* [Thumb] Matsum and Nakai) in derived Savannah environment in South-Eastern Nigeria. *Int. J. Plant Res., 5*: 19-26. DOI: 10.5923/j.plant.20150501.04.

Noh, A; Rafii, M Y; Saleh, G; Kushairi, A and Latif, M A (2012). Genetic performance and general combining ability of oil palm Deli *dura* x AVROS *pisifera* tested on inland soils. *Sci. World J.,* 1-8. DOI: 10.1100/2012/792601.

Ooi, S; Barcelos, E; Muller, A and Nascimento, J (1981). Oil palm genetic resources- Native *E. oleifera* populations in Brazil offer promising sources. *Pesqui. Agropecu. Bras., 16*: 385-395.

Okoye, M; Okwuagwu, C and Uguru, M (2009). Population improvement for fresh fruit bunch yield and yield components in oil palm (*Elaeis guineensis* Jacq.). *Eurasian J. Sci. Res., 4*: 59-63.

Okwuagwu, C O; Okoye, M N; Okolo, E C; Ataga, C D and Uguru, M I (2008). Genetic variability of fresh fruit bunch yield in Deli *dura* x *tenera* breeding populations of oil palm (*Elaeis guineensis* Jacq.) in Nigeria. *J. Trop. Agri., 46*: 40-45.

Rafii, M Y (1996). *Genotype x environment interaction and stability analyses in 40 oil palm (*Elaeis guineensis *Jacq.) progenies over six locations*. PhD thesis. Universiti Kebangsaan Malaysia.

Rahim, M A; Mia, A A F; Mahmud, F; Zeba, N and Afrin, K S (2010). Genetic variability, character association and genetic divergence in mungbean (*Vigna radiata* L. Wilczek). *Plant Omic, J., 3*: 1-6. DOI: 10.3316/INFORMIT.982467342869605.

Rajanaidu, N (1983). Collection of oil palm (*Elaeis oleifera*) genetic material in Central and South America. *PORIM Bulletin*, p. 1-11.

Rajanaidu, N (1985). *Elaeis oleifera* collection in Central and South America. *Proc. of the International Workshop on Oil Palm Germplasm and Utilisation.* Selangor, Malaysia. p. 84-94.

Rajanaidu, N; Kushairi, A; Rafii, M; Mohd Din, A; Maizura, I and Jalani, B S (2000). Oil palm breeding and genetic resources. *Advances in Oil Palm Research Volume 1* (Basiron, Y; Jalani, and Chan, eds.). Malaysian Palm Oil Board (MPOB) Bangi, Selangor. p. 171-237.

Rajanaidu, N; Kushairi, A; Mohd Din, A; Marhalil, M; Fadila, A M and Isa, Z A (2011). Selection criteria (15-15-15) to develop sustainable oil palm planting materials. Paper presented at the International Seminar on Breeding for Sustainability in Oil Palm, Kuala Lumpur. 18 November 2011.

Rajanaidu, N; Kushairi, A and Mohd Din, A (2017). Utilisation of germplasm. *Monograph Oil Palm Genetic Resources*. MPOB, Bangi. 289 pp.

Rao, V; Chin, C W and Rajanaidu, N (1989). Biology and performance of Suriname *Elaeis oleifera* (H.B.K.) Cortes. *J. Oil Palm Res., 1*: 109-118.

Rencher, A C (2002). Methods of multivariate analysis. 2nd edition. *Wiley series in probability and mathematical statistics*. John Wiley and Sons., New York. 738 pp.

Rey, B L; Gomez, C P L; Ayala, D I M; Delgado A W and Rocha, S P J (2004). Colecciones genéticas de palma de aceite *Elaeis guineensis* (Jacq.) Y *Elaeis oleifera* (H.B.K.) de Cenipalma: Características de importancia para el sector palmicultor. *Revista Palmas., 25:* 39-48.

Rios, S D A; Cunha, R N V D; Lopes, R; Barcelos, E; Teixeira, P C; Lima, W A A D and Abreu, S C (2011). *Caracterização fenotípica e diversidade genética em subamostras de Caiaué* (Elaeis oleifera). *Unimontes Científica., 13*: 49-56.

Santos, d.M; Barcelos, E and Nascimento, J C (1986). Genetic resources of *E. oleifera* (H.B.K.) Cortes in the Brazilian Amazon. *Proc. of the International Workshop on Oil Palm Germplasm and Utilization*. PORIM, Kuala Lumpur. p. 95-101.

Singh, M; Kaur, K and Singh, B (2008). Cluster algorithm for genetic diversity. *World Academy of Sci. Eng. Tech., 18*: 453-457.

Singh, R; Low, E T L; Ooi, L C L; Meilina, O A; Ting, N C; Jayanthi, N; Rajanaidu, N; Mohd Din, A; Rozana, R; Mohamad Arif, M A; Chan, K L; Mohd Amin, H; Norazah, A; Lakey, N; Smith, S W; Budiman, M A; Hogan, M; Bacher, B; Van Brunt, A; Wang, C; Ordway, J M; Sambanthamurthi, R and Martienssen, R A (2013). The oil palm SHELL gene controls oil yield and encodes a homologue of SEEDSTICK. *Nature., 500*: 340-344. DOI: 10.1038/nature12356.

Siracli, S; Dogan, N and Dogan, I (2013). Comparison of hierarchical cluster analysis methods by cophenetic correlation. *J. Inequal App., 203*: 1-8. DOI: 10.1186/1029-242X-2013-203.

Zulkifli, Y; Maizura, I and Rajinder, S (2012). Genetic diversity study of *Elaeis guineensis* germplasm using EST-SSR. *J. Oil Palm Res., 24*: 1368-1377.

Zulkifli, Y; Maizura, I; Rajinder, S; Marhalil, M; Mohd Din, A and Ong-Abdullah, M (2019). An RFLP marker, CB75A, predicts for palmitic acid content across selected oil palm germplasm and interspecific-hybrids. *J. Oil Palm Res., 31*: 315-320. DOI: 10.21894/jopr.2018.0061.

Zulkifli, Y; Katialisa, K; Rajinder, S; Suzana, M; Marhalil, M; Ting, N C; Mohd Din, A; Leslie, L E T; Leslie, O C L; Kandha, S; Rajanaidu, N; Jansen, J and Meilina, O A (2020). An integrated linkage map of interspecific backcross 2 (BC2) populations reveals QTLs associated with fatty acid composition and vegetative parameters influencing compactness in oil palm. *BMC Plant Biol., 20*: 356. DOI: 10.1186/s12870-020-02563-5.

Journal of Oil Palm Research Vol. 35 (4) December 2023 p. 596-606
DOI: https://doi.org/10.21894/jopr.2022.0070

METABARCODING IN DIET ASSESSMENT OF ADULT PARASITOID SPECIES, *Dolichogenidea metesae* (HYMENOPTERA: BRACONIDAE) TOWARDS ITS CONSERVATION AND MANAGEMENT IN THE OIL PALM PLANTATION

FUAT SALBI[1,2]; AQILAH SAKINAH BADRULISHAM[1]; NUR AZURA ADAM[2]; IZFA RIZA HAZMI[1] and SALMAH YAAKOP[1]*

ABSTRACT

The abundance of parasitoids in the oil palm plantation is greatly influenced by the host and food availability. However, studies on the main diet or food sources of the adult parasitoid wasp, Dolichogenidea metesae *of the oil palm pest,* Metisa plana *is still lacking. This study investigated the diet of adult* D. metesae *sampled from Good Agricultural Practices (GAP) and non-GAP plantations through metagenomic analysis by using a* trnL *marker. A total of 761 145 food plant* trnL *sequences were generated from 12 samples of the parasitoids collected from four plantations. No significant differences (p=0.683) were observed for diversity (Shannon-Wiener index (H') of 0.12-1.22, p=0.68) among the total 62 OTU's of the food plant species when compared between the GAP and Non-GAP plantations. Polygonaceae was the most abundant plant family (59.95%), followed by Asteraceae (10.15%) and Acanthaceae (7.51%). The* Antigonon leptopus, Paraprenanthes oligolepis, Asystasiella neesiana *and wild banana* (Musa itinerans) *were among the most dominant plant species consumed by adult* D. metesae. *We recommend that these dominant food plant species for the* D. metesae *should be planted widely in the oil palm plantations to enhance the population abundance of* D. metesae *for successful Integrated Pest Management (IPM) practices.*

Keywords: DNA, food source, genetic, natural enemy, *trnL*.

Received: 20 December 2021; **Accepted:** 5 September 2022; **Published online:** 7 November 2022.

INTRODUCTION

Dolichogenidea metesae (Hymenoptera: Braconidae) is the predominant species of parasitoids that parasitises on a gregarious pest, *Metisa plana* (Psychidae: Lepidoptera) (Halim *et al*., 2017; 2019). As a primary parasitoid of the *M. plana*, *D. metesae* seeks to infest the third to sixth instar of the host insect, and this predilection has been utilised to become one of the most effective natural or biological control methods for major pests of agricultural crops under the Integrated Pest Management (IPM) in a sustainable ecosystem (Salmah *et al*., 2006). The longevity and fecundity of the parasitoids are influenced by the availability and type of their food sources (Liu and Ueno, 2012). Thus, the biological data on the *D. metesae,* especially on its diet, food source and consumption habits in the natural ecosystem would be invaluable for a better understanding of the intricate association between the parasitoids and their hosts, the pests, pollinators and other associates in the ecosystem (Fahimee *et al*., 2021).

The destruction of ground vegetation deprives food and shelter for adult parasitoids, therefore, suitable agricultural landscape and ecological infrastructure are important for the best habitat

[1] Centre for Insect Systematics, Department of Biological Science and Biotechnology, Faculty of Science and Technology, Universiti Kebangsaan Malaysia, 43600 Bangi, Selangor, Malaysia.

[2] Department of Plant Protection, Faculty Agriculture, Universiti Putra Malaysia, 43400 Serdang, Selangor, Malaysia.

* *Corresponding author e-mail: salmah78@ukm.edu.my*

management under the natural biological control system (Landis *et al*., 2000). Balmer *et al*. (2013) provided additional evidence regarding the importance of flowering weeds to the parasitoids by highlighting the effectiveness of flowering plants as intercropping plants or as companion plants that supply bountiful and nutritious resources for the natural enemies of the crop pests, including the parasitoids. Studies by Norman and Basri (2010) reported that *Asystasia gangetica*, a weed species that grew naturally in the oil palm plantations had influenced the population of the parasitoids. However, there is no evidence to prove the efficacy of all available food plants including the flowering weeds to supply their diet or to provide a host or conducive environment for the parasitoids.

The implementation of Good Agriculture Practice (GAP) has had a positive impact towards environmental sustainability in Malaysia (Tan *et al*., 2009) and in neighbouring countries such as Thailand and Indonesia (Apriani *et al*., 2020; Saswattecha *et al*., 2015). The Roundtable on Sustainable Palm Oil (RSPO), a global certification standard for sustainable palm oil, requires the implementation of GAP as part of the criteria in getting the certification (Morley, 2015). GAP principles emphasize on limiting the usage of chemical inputs and minimising the detrimental environmental impacts of farming operations through the implementation IPM (Norman *et al*., 2019). As a result, IPM practices such as planting beneficial plants and weed management are used in combating the oil palm pest, *M. plana* (Wood and Norman, 2019a). Failure to follow the GAP code of practice (CoP) had resulted in a high use of chemical pesticides, which had a very significant adverse impact on weed diversity (Aini *et al*., 2007). According to Möller *et al*. (2021), the abundance of parasitoids was higher in plots with a good ground cover compared to plots treated with herbicides. Wood and Norman (2019b) and Wood *et al*. (1974) also reported that the application of chemicals had consequently disrupted the natural enemies of *M. plana* in the plantation habitats.

Despite some previous successful studies demonstrating the relationship between flowering plants and parasitoids, *e.g*., *Cassia cobanenasis*, *Euphorbia heterophylla*, *Antigonon leptopus* and *Turnera subulata* (Siti Ramlah *et al*., 2005; Wood and Norman, 2019a), relatively very few studies had been undertaken to validate that these plants were consumed by the parasitoids. To our knowledge, there is no direct study investigating the various plant species foraged or consumed in the diet of adult *D. metesae*, the main parasitoid of *M. plana* in the oil palm plantation. Metabarcoding is now widely used in identifying insect diet. By using *trnL* marker, Fahimee *et al*. (2021) successfully revealed 262 plant species under 70 families foraged by stingless bee, *Heterotrigona itama*. This information benefits meliponiculture industry by recommending several food plant species to be planted such as *Momordica charantia*, *Melastoma* sp. and *Cucumis sativa*. According to Mallott *et al*. (2018), *trnL* yielded more sequences, higher resolution taxonomic identifications and identified a higher number of families in the diet of wild white-faced capuchins, *Cebus capucinus* compared to *rcbl*.

Therefore, based on the economic importance of *D. metesae* and *M. plana* in our oil palm industry (Basri *et al*., 1995; Halim *et al*., 2018), the main objective of this study was to identify the different food plant species consumed by adult *D. metesae* by conducting a metabarcoding analysis of the *D. metesae* diet using a *trnL* marker, thereby confirming the various species of plants foraged and utilised by *D. metesae* in the wild. The study also investigated how *D. metesae* diets differed between the GAP and non-GAP oil palm plantations. This information could facilitate towards a better understanding on the specific ecosystem components that could influence the introduction of *D. metesae* as an effective biological control of the main pests of oil palm as part of the IPM strategies.

MATERIALS AND METHODS

Sampling of *Dolichogenidea metesae*

Three *D. metesae* individuals (three replicates) were sampled from each plantation across Peninsular Malaysia, comprising two GAP plantations (certified with RSPO or MPOB CoGAP) and two non-GAP plantations, giving a total of 12 samples (n=12) from four sampling sites. The sampling sites were planted with specific beneficial plant species and had a history of *M. plana* infestation (*Table 1*). Samples of hymenopteran parasitoids were collected using a malaise trap and preserved in 90% ethanol for one year, from March 2020 to February 2021. All the specimens of *D. metesae* were collected and identified based on Norman *et al*. (2017) and Achterberg (1993), while only several individuals were used for the molecular analysis.

DNA Extraction

The DNA was extracted from the adults of *D. metesae* collected from four plantations with three biological replications representing each plantation. The DNA of 12 individuals of *D. metesae* were extracted from the whole body individually, using the NucleoSpin® DNA Insect protocol (Machery-Nagel, Germany) (Halim *et al*., 2018). Each sample was surface sterilised before molecular analysis was proceeded by submersing the insects in 70% ethanol and distilled water for 2-3 s for 3 times (Avanesyan, 2014; Cooper *et al*., 2016).

TABLE 1. LIST OF *Dolichogenidea metesae* SAMPLES USED FOR METABARCODING ANALYSIS

Sample code	Location	Grid	GAP status	Beneficial plant species
Plantation A	Peninsular Malaysia. Pahang: Gambang	3.623169771292426, 103.13824123987163	GAP	*Turnera* sp. *Cassia cobanensis*
Plantation B	Peninsular Malaysia. Perak: Slim River	3.6949601778100867, 101.48563129489453	GAP	*Antigonon leptopus*
Plantation C	Peninsular Malaysia. Pahang: Kuantan	3.673757257494192, 103.14538126430287	Non-GAP	*Antigonon leptopus* *Turnera* sp.
Plantation D	Peninsular Malaysia. Johor: Segamat	2.4408761993796264, 102.6866661993966	Non-GAP	*Antigonon leptopus* *Turnera* sp.

Library Preparation

Preparation of the library was conducted by using 2-step PCR. The first PCR was performed using locus-specific sequence primers (*trnL*) with overhang adapters: g-A49425-added overhang (5'-TCGTCGGCAGCGTCAGATGTGTATAAGAGACAG GG CAATCCTGAGCCAA-3') and h-B49466-added overhang (5'- GTCTCGTGGGCTCGGAGATGTGTATAAGAGACAGCCATTGAGTCTCTGCACCTATC-3'). A total of 25.00 μL was prepared for PCR amplification. The mixture consisted of 5.75 μL Q5® High Fidelity DNA Polymerase (New England BioLabs Inc.), 1.25 μL of each forward and reverse primer (10 μM), 15.75 μL of water, nuclease free and 1.00 μL of DNA template. A total of 5.00 μL of DNA template was used for the sample with concentration < 2.5 ng/μL. The amplification reactions were performed under the following protocol: initial denaturation of 95°C for 3 min, followed by 30 cycles of denaturation at 98°C for 30 s, annealing at 64°C for 30 s, extension at 72°C for 30 s and a final extension at 72°C for 5 min. The second PCR was conducted to attach dual indices to the amplicon PCR by using Illumina Nextera XT Index Kit v2 following manufacturer's protocols. Even though no qPCR was conducted, however the quality of the libraries was measured using Agilent Bioanalyzer 2100 System by Agilent DNA 1000 Kit and fluorometric quantification by Helixyte Green™ Quantifying Reagent. The libraries that passed the library QC were subsequently subjected to next-generation sequencing.

Next-Generation Sequencing

The libraries were normalised and pooled according to the protocol recommended by Illumina and then proceeded to sequencing by MiSeq platform using 150 paired-end. The next-generation sequencing was performed by Apical Scientific Sdn. Bhd. The raw data was then processed and analysed according to the bioinformatics analysis. All the read sequences were deposited in the Sequence Read Archive (SRA) of the NCBI (http://www.ncbi.nlm.nih.gov/sra) with the references number SRR20648567 (Plantation A R1), SRR20648580 (Plantation A R2), SRR20648647 (Plantation A R3), SRR20646195 (Plantation B R1), SRR20648581 (Plantation B R2), SRR20648441 (Plantation B R3), SRR20648771 (Plantation C R1), SRR20648869 (Plantation C R2), SRR20648867 (Plantation C R3), SRR20648625 (Plantation D R1), SRR20648622 (Plantation D R2) and SRR20648768 (Plantation D R3).

Bioinformatic Analysis

Sequence adaptors and low-quality reads were trimmed-off from paired-end reads using BBDuk from the BBTools package. After that, by using USEARCH v11.0.667, the forward and backward reads were merged. All sequences (sequenced on the MiSeq platform) with an average quality score of less than 150 bp or more than 600 bp were eliminated from downstream processing (Edgar, 2010). Following that, the reads were aligned with *trnL* sequences using the NCBI database. Operational taxonomic units (OTUs) were clustered with 97% similarity cut-off using UPARSE v11.0.66 (Edgar, 2013) and a single representative sequence from each OTU was picked at random. Pynast was used to construct a phylogenetic tree against NCBI database (Caporaso *et al*., 2010a) and QIIME V1.19.1 was used for taxonomic assignment of OTUs (Caporaso *et al*., 2010b). The rarefaction curve was plotted to determine the sufficiency of sequency depth by using R V3.6.2 (R Core Team, 2018). The heatmap was also created with R software to display the relative abundances of taxa (phyla) using different shades of colour, with darker colours representing greater values. Alpha diversity (Shannon-Wiener, Simpson, CHAO 1) with ANOVA showed pairwise analysis of variance between groups and its significance was annotated on the box plots with *p*-value set to 0.05. Other statistical analysis was also done in R V3.6.1. (R Core Team 2018).

RESULTS

A total of 761 145 plant *trnL* sequences were generated from 12 samples of *D. metesae*, ranging

from 47 893 to 73 893 (*Table 2*). Except for the Plantation C, all samples from Plantations A, B, and D had more than 60 000 reads, with Plantation A (R3) having the most reads (73 893), while Plantation C (R1) had the lowest reads (47 893). Overall, 62 OTU's were observed, with Plantation A (R1) recording the minimum OTU's (16) while Plantation C (R1) recorded the maximum of OTU's (29). The Shannon-Wiener and Simpson index indicated a higher diversity of OTU's from Plantation D (R2) (H' = 1.22, 1-D = 0.68) and the lowest from Plantation D (R3) (H' = 0.12, 1-D = 0.04). Chao 1 estimator abundance showed that Plantation C (R2) has the highest value (28.75) of OTU's, while conversely, Plantation A (R2) recorded the lowest value (11) (*Table 2*).

The rarefaction curves (*Figure 1*) indicate that all the samples are almost reaching asymptote, implying that sufficient sequencing depth has been achieved. The curve rises steeply at first, and then flattens out gradually at 35 000 sequences. The *D. metesae* sample taken from Plantation C (R2) had the most diverse food plant species, since the number of different species detected was higher than in all the other samples, while the *D. metesae* sample from Plantation A (R2), had the least diverse food plant species (*Figure 1*).

Overall, Polygonaceae (59.95%) was the most common family recorded (*Table 3*), followed by Asteraceae (21.65%) and Acanthaceae (7.51%), while Arecaceae, Campanulacea, Urticaceae and Phyllanthaceae were the least recorded, accounting for less than 1.00% of the total families observed. The heatmap (*Figure 2*) showed that Polygonaceae and Asteraceae were present in all the *D. metesae* samples. High abundance of Polygonaceae was recorded from the samples collected from Plantations B, C and D, while Asteraceae was recorded in high abundance in all samples collected from Plantation A only. Meanwhile, Acanthaceae was found mostly in the samples from Plantation D, while very little of Phyllanthaceae and Malvaceae were recorded and could only be found in one *D. metesae* sample, *i.e.,* from Plantation C (R2) (*Figure 2*).

As seen in the bar chart (*Figure 3*), *A. leptopus* (Polygonaceae) was the most dominant species of plant food recorded from Plantations B, C and D, accounting for more than half of the total plant species consumed by *D. metesae*. In contrast, *P. oligolepis* was the most dominant plant food recorded in the *D. metesae* samples collected from Plantation A, although it also occurred in all the other 12 samples. Likewise, Plantations A and D seemed to record a higher number of plant species (seven) compared to Plantations B and C, which recorded only four species among the dominant plant foods of *D. metesae*.

According to the Venn diagram (*Figure 4*), both GAP and non-GAP plantations shared 34 OTU's out of 62 OTU's. A Venn diagram is an illustration of the relationships between and among groups of samples with their own unique OTUs and those that share OTUs in common. Our study shows that alpha diversity metrics as given in the box plot (*Figure 5*) reveals no significant difference (Chao 1, $p = 0.23$; Simpson, $p = 0.45$; Shannon, $p = 0.68$) between the GAP and non-GAP plantations.

DISCUSSION

The metabarcoding analysis has been conducted to obtain the information on the diet of adult *D. metesae.* The results obtained from *D. metesae* samples collected from the GAP and non-GAP plantations are very significant and comparatively valuable in determining the diversity and abundance of *D. metesae* in oil palm plantations adopting different agricultural practices (Saswattecha *et al*., 2015).

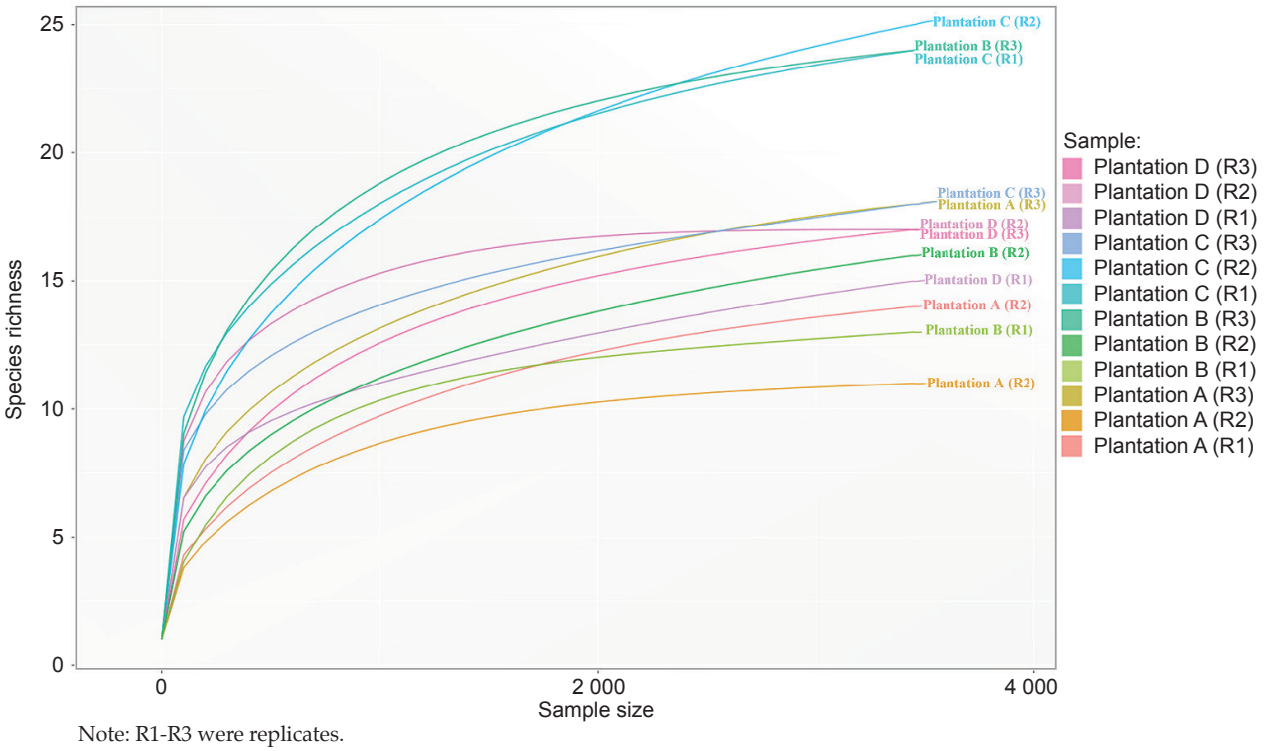
The rarefaction curve (*Figure 1*) indicates that the sequencing depth has almost reached asymptote, implying that the maximum number of OTU's have been collected in deriving at the conclusion in this study (Cayuela *et al*., 2015). The family Polygonaceae, belonging to the flowering plant group of angiosperms (Vandebroek *et al*., 2018), was recorded as the most abundant family (59.95%) found in the *D. metesae* diet, whereas several other families such as Asteraceae (21.65%), Acanthaceae (7.51%), Musaceae (6.29%) and Poaceae (2.47%) constitute the top five families consumed by the *D. metesae*. Both families, *i.e.,* Asteraceae and Acanthaceae are classified as weeds (Ali *et al*., 2021) and are abundantly found in the diet of *D. metesae*. Notably, the families Musaceae and Arecaceae (fruit plant species) also occurred in the *D. metesae* diet.

The five most abundant plant food species found in the *D. metesae* samples were *A. leptopus*, *P. oligolepis*, *A. neesiana*, *M. itinerans*, and *Cocos nucifera* (*Figure 3*). The *A. leptopus* was introduced into the oil palm plantations as a beneficial plant (Hariyadi and Syahlan, 2021) however, *P. oligolepis* and *A. neesiana* existed naturally as weeds in Malaysia (Shi *et al*., 2011). Both species *i.e., M. itinerans* and *C. nucifera* were naturally pollinated by animals such as the Long-tongued Fruit Bat (*Macroglossus sobrinus*), the nectar-feeding bird, Little Spiderhunter (*Arachnothera longirostris*) and the Indian Palm Squirrel, *Funambulus palmarum* (Chakravarthy and Thyagaraj, 2012; Liu *et al*., 2002). However, our own observations indicated that both species *i.e., M. itinerans* and *C. nucifera* were very sparse in all the four plantations. Additionally, the *C. nucifera* that belongs to the Palmae was not suggested to be planted in the plantation due to its potential to attract pest, Red Palm Weevil (RPW), *Rhyncophorus ferrugenius* (Aman-Zuki *et al*., 2021). According to Mathews *et al.* (2007) from a total of 333

TABLE 2. NUMBER OF OBSERVED OTU'S, ALPHA DIVERSITY INDICES FOR THE PLANT DNA FROM 12 SAMPLES OF *Dolichogenidea metesae*

Localities	Sample	Sequences		OTU's	Chao-1	Shannon-Wiener (H')	Simpson (1-D)	Evenness (E^HS)
		Before	After					
Plantation A	R1	458 2582	66 511	14	15.5	0.72	0.43	15.55
	R2	496 5272	66 931	11	11.0	0.70	0.49	11.29
	R3	593 4902	73 983	18	18.6	0.68	0.35	20.37
		Mean ± SD		14.33 ± 3.51a	15.03 ± 3.82b	0.70 ± 0.02a	0.42 ± 0.07a	15.74 ± 4.55a
Plantation B	R1	4 394 041	62 425	13	14.00	0.51	0.32	13.79
	R2	4 649 663	62 582	16	18.00	0.67	0.38	19.95
	R3	5 192 020	68 353	24	24.75	0.98	0.56	25.63
		Mean ± SD		17.67 ± 5.69a	18.92 ± 5.43a	0.72 ± 0.24a	0.42 ± 0.123a	19.79 ± 5.93a
Plantation C	R1	3 685 638	47 893	24	25.50	0.49	0.22	26.68
	R2	4 592 931	57 067	25	28.75	0.41	0.20	30.76
	R3	4 153 120	56 846	18	24.00	0.68	0.32	22.08
		Mean ± SD		22.33 ± 3.79a	26.08 ± 2.43a	0.52 ± 0.14a	0.24 ± 0.07a	26.51 ± 4.34a
Plantation D	R1	5 411 881	72 422	15	17.00	0.81	0.47	22.45
	R2	4 778 117	63 958	17	17.00	1.22	0.68	17.00
	R3	4 691 056	62 174	17	18.00	0.12	0.04	18.87
		Mean ± SD		16.33 ± 1.16a	17.33 ± 0.58a	0.72 ± 0.56a	0.40 ± 0.33a	19.44 ± 2.77a

Note: Mean ± SD value with a different letter indicates a significant difference (ANOVA, $p<0.05$).



Note: R1-R3 were replicates.

Figure 1. The rarefaction curve of trnL *gene sequence for 12 samples of* Dolichogenidea metesae.

plant species in 83 families collected in an oil palm plantation in Malaysia, 279 of them were angiosperms. The abundant flowers of the angiosperms would attract beneficial insects by providing nectar and sugar as a source of food and energy (Heimpel and Jervis, 2005; Tompkins *et al*., 2010). Our results have also proven that the angiosperm species serve as the main food source for *D. metesae* (Patt *et al*., 1997) providing for adult longevity and fecundity of the parasitoids (Olson *et al*., 2005).

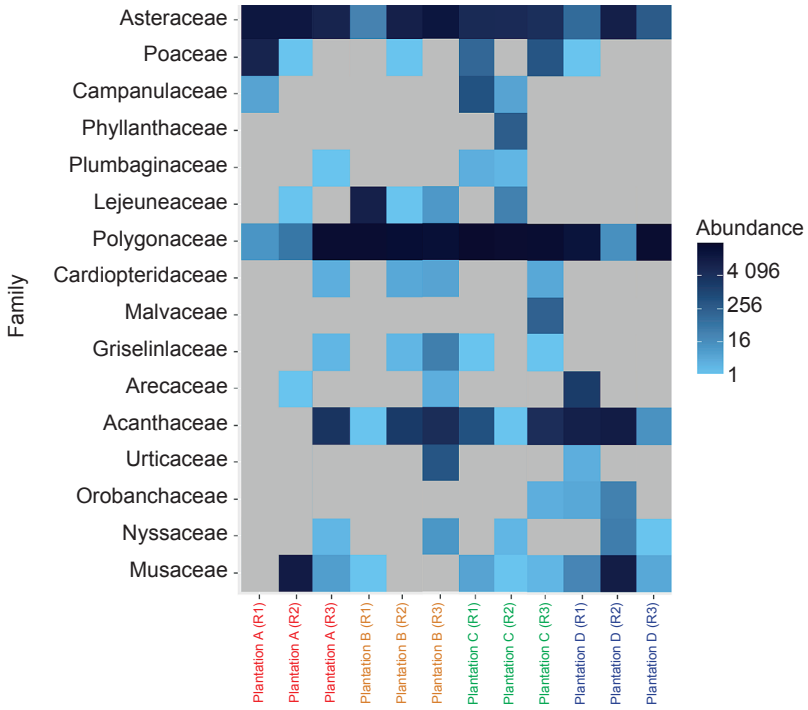


Figure 2. Heat analysis at the family level. The darker colour represents a correspondingly greater value of abundance.

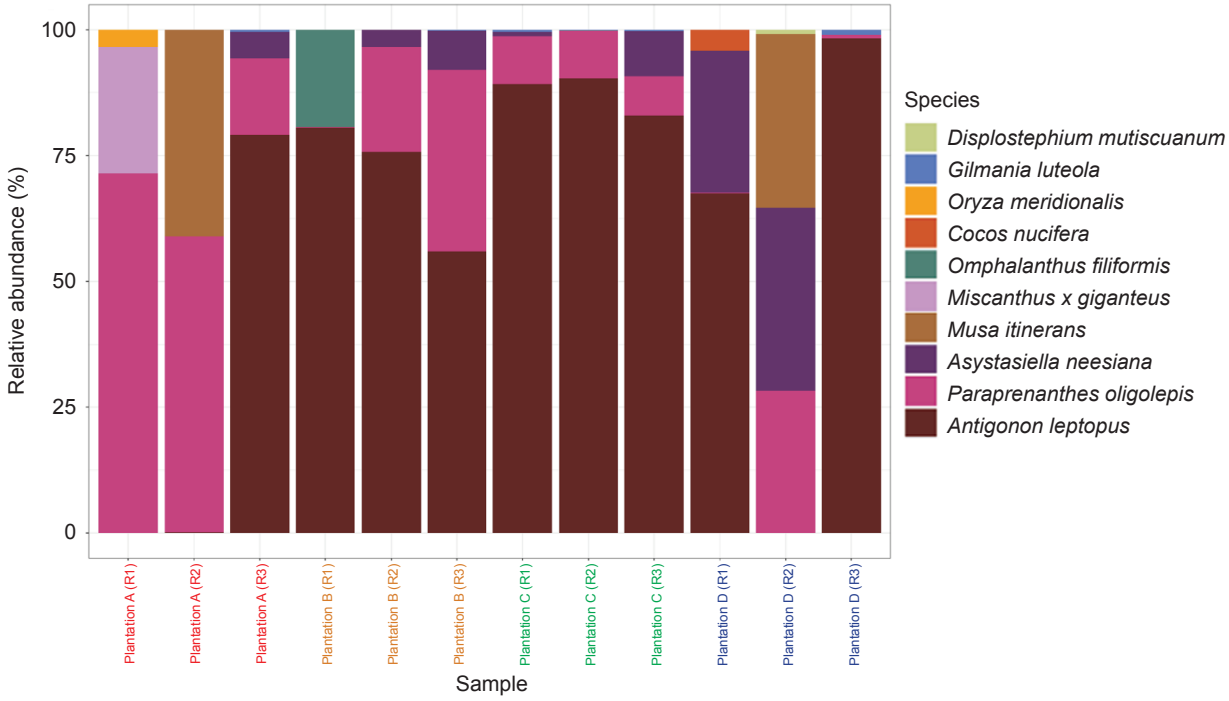


Figure 3. Relative abundancy bar chart at the species level. The ten most abundant food plant species recorded in all the 12 samples of Dolichogenidea metesae.

This study provides the first evidence that *A. leptopus* (Polygonaceae) is highly consumed by *D. metesae* as a source of diet (*Figure 3*). Yusdayati *et al*. (2014) reported that parasitoid wasps *Brachymeria carinata* and *D. metesae* could be found in higher abundance on the plant foods *C. cobanensis* and *Turnera* sp. compared to *A. leptopus*. However, our findings revealed that *D. metesae* consumed more *A. leptopus*, while there was no record of *C. cobanensis* and *Turnera* sp. in the diets despite their presence in the plantation. The use of metabarcoding here is novel since the protocol has not been used previously to confirm the diet of parasitoids. This information is important since nectar, pollen, and water are all necessary for the adult parasitoids to survive and flourish (Damien *et al*., 2020).

Although previous research works had shown that the common weed locally known as Chinese violet (*A. gangetica*: Achantaceae) could increase parasitoid diversity in the oil palm plantations

TABLE 3. RELATIVE ABUNDANCE OF THE TOP 10 FAMILIES OF PLANTS RECORDED IN THE 12 SAMPLES OF *Dolichogenidea metesae*

Family	Relative abundance (%)
Polygonaceae	59.95
Asteraceae	21.65
Acanthaceae	7.51
Musaceae	6.29
Poaceae	2.47
Lejeuneaceae	1.62
Arecaceae	0.35
Campanulaceae	0.07
Urticaceae	0.05
Phyllanthaceae	0.04

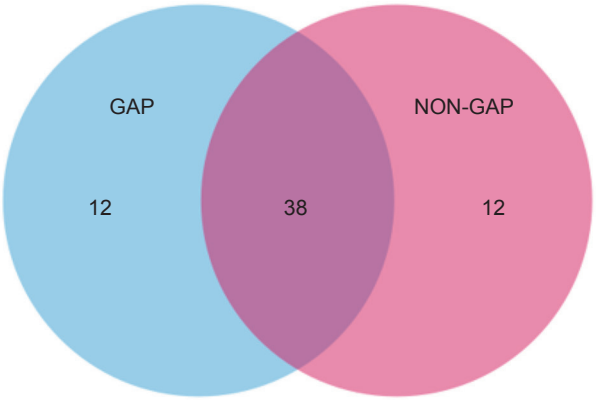


Figure 4. Comparison of the Venn diagrams between the GAP and non-GAP plantations.

(Norman and Basri, 2010; Tiong, 1982) our study data had shown that this weed species was not consumed or foraged by *D. metesae* despite its abundant presence in the sampling sites. In contrast, the weedy herbs *P. oligolepis* (Asteraceae) and *A. neesiana* (Acanthaceae) were detected in almost all *D. metesae* samples in this study (*Figure 3*). Based on literature information, the herbaceous species *P. oligolepis*, which is a synonym to *Melanoseris oligolepis* (Shi *et al*., 2011) and *A. neesiana*, which is a synonym to *Mackaya neesiana* (Wall.) (POWO, 2021), can both be found in Malaysia, although these two weedy species are not yet recorded so far in our oil palm plantations.

The differences in *D. metesae* diet shown in *Figure 2* could be due to food availability in the respective areas (Folgarait and Gilbert, 1999; Jervis *et al*., 1992). In an agroecosystem, two important resources (*i.e.*, host and food) for the parasitoids are rarely located within the same site, hence, the adult parasitoids must be able to fly regularly between the host site and the plant food site in order to reproduce successfully (Lewis *et al*., 1998). Furthermore, a study by Coudrain *et al*. (2014) found that the parasitoid species richness was higher in areas surrounding the forests than in isolated sites due to higher plant variability (richness) in the former. The importance of plant species such as *M. acuminata* and *C. nucifera*, in which the DNA of both have been detected as plant foods of *D. metesae* in this study cannot be overlooked, since both species can be planted as side crops or ornamentals in the oil palm plantations (Mathews *et al*., 2007). The intercropping strategy has been applied in many

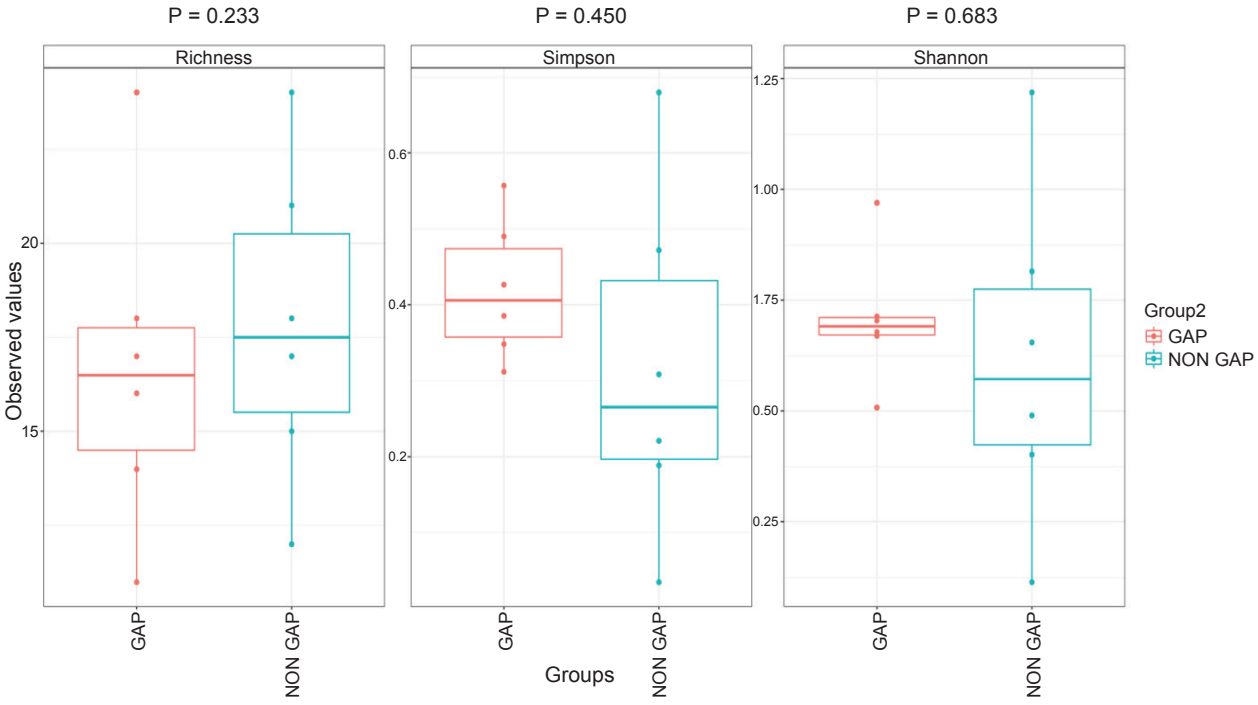


Figure 5. Comparison of the alpha diversity box plots between the GAP (Red) and non-GAP (Blue) plantations. The p-value threshold for significance is set to 0.05.

plantations for many purposes. One of it is to reduce or control the infestation of crop pests such as okra and legumes (Singh *et al*., 2017), pickerelweed and rice (Xiang *et al*., 2021) by increasing the population abundance and diversity of parasitoids (Amala and Shivalingaswamy, 2018; Devi *et al*., 2020), and the second objective is to provide two-in-one crop production (Nchanji *et al*., 2016; Rocha *et al*., 2020).

In this study, the molecular data and the mathematical analysis showed that there was no significant difference in plant diversity in the *D. metesae* diet between the GAP and non-GAP plantations (*Figure 5*), even though the agricultural practices differed significantly between the two in terms of chemical application (Saswattecha *et al*., 2015), which would have had very significant impacts on the diversity of weeds and the associated biota (Darras *et al*., 2019). This might be because in our study, the weed species commonly found in the oil palm plantations such as *A. gangetica*, *Clidemia hirta* and *Drymaria cordata* (Ali *et al*., 2021; Satriawan and Fuady, 2019) could not be traced or detected in the diet of *D. metesae* (*Figure 2*). However, *A. gangetica* had been documented in other studies as having an important role in the abundance of parasitoids other than *D. metesae* (Wood and Norman, 2019a). Although this study showed that there was no significant different in terms of plant species consumed by *D. metesae* in GAP and non-GAP plantations, Fuat *et al*. (2022) found that the parasitoid abundance was significantly higher in GAP plantations compared to non-GAP plantations.

CONCLUSION

This is the first study to use metabarcoding analysis in determining the plant communities consumed by the *D. metesae* as their food sources in the wild. Overall, the natural diet of *D. metesae* was dominated by the Coral vine or Bride's Tears (*A. leptopus*), a common creeper with abundant pink flowers and rich in nectar. Therefore, it is highly recommended that this beneficial plant should be planted in the oil palm plantations to attract more *D. metesae*, the dominant parasitoid species of *M. plana* as a control measure for bagworm infestation.

ACKNOWLEDGEMENT

The authors would like to express their gratitude to the Department of Crop Protection, Faculty of Agriculture, Universiti Putra Malaysia for enabling us to conduct some experiments in their laboratory. We wish to thank Maimon Abdullah for her useful comments and final editing of the manuscript. This project was funded by the research grants, code ZF-2019-005, GP-K013317-2021 and GP-K013317-2020.

REFERENCES

Achterbeg, C V (1993). Illustrated key to the subfamilies of the Braconidae (Hymenoptera: Ichneumonoidea). *Zool. Verh., 283*: 1-189.

Aini, K; Tan, Y A; Norman, K and Yeoh, C B (2007). Pesticide application in the oil palm plantation. *Oil Palm Bulletin*, *54*: 52-67.

Ali, N B M; Karim, M F A; Saharizan, N; Adnan, N S; Mazri, N H; Fikri, N; Amaludin, N and Zakaria, R (2021). Weeds diversity in oil palm plantation at Segamat, Johor. *IOP Conf. Ser. Earth Environ. Sci., 756(1)*: 012034. DOI: 10.1088/1755-1315/756/1/012034.

Amala, U and Shivalingaswamy, T M (2018). Effect of intercrops and border crops on the diversity of parasitoids and predators in agroecosystem. *Egypt. J. Biol. Pest Control, 28*: 1-4. DOI: 10.1186/s41938-017-0015-y.

Aman-Zuki, A; Ghazali, S Z; Badrulisham, A Z; Hazmi, I R; Nurul Wahida, O and Yaakop, O (2021). Proof on the divergence times of two sympatric species, *Rhynchophorus ferrugineus* and *R. vulneratus* (Coleoptera: Curculionidae) by molecular clock analysis. *J. Entomol. Res. Soc., 23(1)*: 11-26. DOI: 10.51963/jers.v23i1.1851.

Apriani, E; Kim, Y S; Fisher, L A and Baral, H (2020). Non-state certification of smallholders for sustainable palm oil in Sumatra, Indonesia. *Land Use Policy, 99*: 105112. DOI: 10.1016/j.landusepol.2020.105112.

Avanesyan, A (2014). Plant DNA detection from grasshopper guts: A step-by-step protocol, from tissue preparation to obtaining plant DNA sequences. *Appl. Plant Sci., 2(2)*: 1300082. DOI: 10.3732/apps.1300082.

Balmer, O; Pfiffner, L; Schied, J; Willareth, M; Leimgruber, A; Luka, H and Traugott, M (2013). Noncrop flowering plants restore top-down herbivore control in agricultural fields. *Ecol. Evol., 3(8)*: 2634-2646. DOI: 10.1002/ece3.658.

Basri, M W; Norman, K and Hamdan, A B (1995). Natural enemies of the bagworm, *Metisa plana* Walker (Lepidoptera: Psychidae) and their impact on host population regulation. *Crop Prot., 14(8)*: 637-645. DOI: 10.1016/0261-2194(95)00053-4.

Caporaso, J G; Bittinger, K; Bushman, F D; Desantis, T Z; Andersen, G L and Knight, R (2010a). PyNAST: A flexible tool for aligning sequences to a template alignment. *Bioinformatics, 26(2)*: 266-267. DOI: 10.1093/bioinformatics/btp636.

Caporaso, J G; Kuczynski, J; Stombaugh, J; Bittinger, K; Bushman, F D; Costello, E K; Fierer, N; Peña, A G; Goodrich, J K; Gordon, J I; Huttley, G A; Kelley, S T; Knight, D; Koenig, J E; Ley, R E; Lozupone, C A; Mcdonald, D; Muegge, B D; Pirrung, M; Reeder. J; Sevinsky, J R; Turnbaugh, P J; Walters, W A; Widmann, J; Yatsunenko, T; Zaneveld, J and Knight, R (2010b). QIIME allows analysis of high-throughput community sequencing data. *Nat. Methods, 7(5)*: 335-336. DOI: 10.1038/nmeth0510-335.

Cayuela, L; Gotelli, N J and Colwell, R K (2015). Ecological and biogeographic null hypotheses for comparing rarefaction curves. *Ecol. Monogr., 85(3)*: 437-455. DOI: 10.1890/14-1261.1.

Chakravarthy, A K and Thyagaraj, N E (2012). The palm squirrel in coconut plantations: Ecosystem services by therophily. *Mammalia, 76(2)*: 193-199. DOI: 10.1515/mammalia-2011-0073.

Cooper, W R; Horton, D R; Unruh, T R and Garczynski, S F (2016). Gut content analysis of a phloem-feeding insect, *Bactericera cockerelli* (Hemiptera: Triozidae). *Environ. Entomo., 45(4)*: 938-944. DOI: 10.1093/ee/nvw060.

Coudrain, V; Schüepp, C; Herzog, F; Albrecht, M and Entling, M (2014). Habitat amount modulates the effect of patch isolation on host-parasitoid interactions. *Front. Environ. Sci., 2*: 27. DOI: 10.3389/fenvs.2014.00027.

Damien, M; Llopis, S; Desneux, N; Van Baaren, J and Le Lann, C (2020). How does floral nectar quality affect life history strategies in parasitic wasps? *Entomol. Gen., 40(2)*: 147-156. DOI: 10.1127/entomologia/2020/0906.

Darras, K F A; Corre, M D; Formaglio, G; Tjoa, A; Potapov, A; Brambach, F; Sibhatu, K T; Grass, I; Rubiano, A A; Buchori, D; Drescher, J; Fardiansah, R; Hölscher, D; Irawan, B; Kneib, T; Krashevska, V; Krause, A; Kreft, H; Li, K; Maraun, M, Polle, A; Ryadin, A R; Rembold, K; Stiegler, C; Scheu, S; Tarigan, S; Valdés-Uribe, A; Yadi, S; Tscharntke, T and Veldkamp, E (2019). Reducing fertilizer and avoiding herbicides in oil palm plantations - Ecological and economic valuations. *Front. For. Glob. Change, 2*: 65. DOI: 10.3389/ffgc.2019.00065.

Devi, S; Ram, P and Rolania, K (2020). Effect of intercropping on the parasitoids, *Encarsia* spp. and *Trichogramma* spp. in cotton fields, India. *Egypt. J. Biol. Pest Control, 30(1)*: 71. DOI: 10.1186/s41938-020-00275-4.

Edgar, R C (2010). Search and clustering orders of magnitude faster than BLAST. *Bioinformatics, 26(19)*: 2460-2461. DOI: 10.1093/bioinformatics/btq461.

Edgar, R C (2013). UPARSE: Highly accurate OTU sequences from microbial amplicon reads. *Nat. Methods, 10(10)*: 996-998. DOI: 10.1038/nmeth.2604.

Fahimee, J; Badrulisham, A S; Zulidzham, M S; Reward, N F; Muzammil, N; Jajuli, R; Md-Zain, B M and Yaakop, S (2021). Metabarcoding in diet assessment of *Heterotrigona itama* based on *trnL* marker towards domestication program. *Insects, 12(3)*: 1-16. DOI: 10.3390/insects12030205.

Folgarait, P J and Gilbert, L E (1999). Phorid parasitoids affect foraging activity of *Solenopsis richteri* under different availability of food in Argentina. *Ecol. Entomol., 24(2)*: 163-173. DOI: 10.1046/j.1365-2311.1999.00180.x.

Fuat, S; Adam, N A; Hazmi, I R and Yaakop, S (2022). Interactions between *Metisa plana*, its hyperparasitoids and primary parasitoids from good agriculture practices (GAP) and non-gap oil palm plantations. *Community Ecol., 23*: 429-438. DOI: 10.1007/s42974-022-00092-9.

Halim, M; Aman-Zuki, A; Syarifah Zulaikha, S A; Muhaimin, A M D; Atikah, A R; Masri, M M M; Md-Zain, B M and Yaakop, S (2018). Exploring the abundance and DNA barcode information of eight parasitoid wasps species (Hymenoptera), the natural enemies of the important pest of oil palm, bagworm, *Metisa plana* (Lepidoptera: Psychidae) toward the biocontrol approach and it's application. *J. Asia. Pac. Entomol., 21(4)*: 1359-1365. DOI: 10.1016/j.aspen.2018.10.012.

Halim, M; Muhaimin, A M D; Syarifah Zulaikha, S A; Nor Atikah, A R; Masri, M M M and Yaakop, S (2017). Evaluation of infestation in parasitoids on *Metisa plana* Walker (Lepidoptera: Psychidae) in three oil palm plantations in Peninsular Malaysia. *Serangga, 22(2)*: 135-149.

Halim, M; Syarifah Zulaikha, S A; Muhaimin, A M D; Din, M and Yaakop, S (2019). The diversity and abundance of potential hymenopteran parasitoids assemblage associated with *Metisa plana* (Lepidoptera: Psychidae) in three infested oil palm plantations in Peninsular Malaysia. *AIP Conf Proc., 2111*: 060024. DOI: 10.1063/1.5111286.

Hariyadi and Syahlan, A (2021). The role of planting media and mulch in the growth of *Leptopus antigonon* as a beneficial plant on oil

palm plantation. *IOP Conference Series: Earth and Environmental Science, 694(1)*: 012029. DOI: 10.1088/1755-1315/694/1/012029.

Heimpel, G E and Jervis, M A (2005). Does floral nectar improve biological control by parasitoids? *Plant-Provided Food for Carnivorous Insects: A Protective Mutualism and its Applications* (Wäckers; van Rijn and Bruin eds.). Cambridge University Press, Cambridge, England. p. 267-304. DOI: 10.1017/CBO9780511542220.010.

Jervis, M A; Kidd, N A C and Walton, M (1992). A review of methods for determining dietary range in adult parasitoids. *Entomophaga, 37(4)*: 565-574. DOI: 10.1007/BF02372326.

Landis, D A; Wratten, S D and Gurr, G M (2000). Habitat management to conserve natural enemies of arthropod pests in agriculture. *Annu. Rev. Entomol., 45*: 175-201. DOI: 10.1146/annurev.ento.45.1.175.

Lewis, W J; Stapel, J O; Cortesero, A M and Takasu, K (1998). Understanding how parasitoids balance food and host needs: Importance to biological control. *Biol. Control, 11*: 175-183. DOI: 10.1006/bcon.1997.0588.

Liu, A Z; Li, D Z; Wang, H and Kress, W J (2002). Ornithophilous and Chiropterophilous pollination in *Musa itinerans* (Musaceae), a pioneer species in tropical rain forests of Yunnan, Southwestern China. *Biotropica, 34(2)*: 254-260. DOI: 10.1111/j.1744-7429.2002.tb00536.x.

Liu, H and Ueno, T (2012). The importance of food and host on the fecundity and longevity of a host-feeding parasitoid wasp. *J. Fac. Agr., Kyushu Univ., 57(1)*: 121-125. DOI: 10.5109/22058.

Mallott, E K; Garber, P A and Malhi, R S (2018). *trnL* outperforms *rbcL* as a DNA metabarcoding marker when compared with the observed plant component of the diet of wild white-faced capuchins (*Cebus capucinus*, Primates). *PLoS ONE, 13(6)*: e0199556. DOI: 10.1371/journal. pone. 0199556.

Mathews, J; Yong, K K and Nurulnahar, B E (2007). Preliminary investigation on biodiversity and its ecosystem in oil palm plantation. *Proc. PIPOC 2007 Int. Palm Oil Cong. Agri., Biotechnol. & Sustain., Vol. 2*: p. 1112-1158.

Möller, G; Keasar, T; Shapira, I; Möller, D; Ferrante, M and Segoli, M (2021). Effect of weed management on the parasitoid community in Mediterranean Vineyards. *Biology 10*: 7. DOI: 10.3390/biology 10010007.

Morley, D (2015). RSPO, the global standard for sustainable palm oil. *Agro. Food Ind. Hi Tech, 26(6)*: 29-30.

Nchanji, Y K; Nkongho, R N; Mala, W A and Levang, P (2016). Efficacy of oil palm intercropping by smallholders: Case study in South-West Cameroon. *Agroforest. Syst., 90*: 509-519. DOI: 10.1007/s10457-015-9873-z.

Norman, K and Basri, M W (2010). Interactions of the bagworm *Pteroma pendula* (Lepidoptera: Psycidae) and its natural enemies in an oil palm plantation in Perak. *J. Oil Palm Res., 22*: 758-764.

Norman, K; Basri, M W and Masijan, Z (2017). Handbook of common parasitoids and predators associated with bagworms and nettle caterpillars in oil palm plantations. MPOB, Bangi. 29 pp.

Norman, K; Idris, A S and Masri, M M M (2019). Prospects in sustainable control of oil palm pests and diseases through the enhancement of ecosystem services - the way forward. *J. Oil Palm Res., 31(3)*: 381-393. DOI: 10.21894/jopr.2019.0030.

Olson, D M; Takasu, K and Lewis, W J (2005). Food needs of adult parasitoids: Behavioral adaptations and consequences. *Plant-Provided Food for Carnivorous Insects: A Protective Mutualism and its Applications* (Wäckers; Van Rijn and Bruin eds.). Cambridge University Press, Cambridge. p. 137-147. DOI: 10.1017/CBO9780511542220.006.

Patt, J M; George, C H and James, H L (1997). Foraging success of parasitoid wasps on flowers: Interplay of insect morphology, floral architecture and searching behavior. *Entomol. Exp. Appl., 83*: 21-30.

POWO (Plants of the world online) (2021). *Mackaya neesiana* (Wall.) Das. http://www.plantsoftheworldonline.org/taxon/urn:lsid:ipni.org:names:52247-1, accessed on 21 July 2021.

R Core Team (2018). R: A language and environment for statistical computing. R Foundation for Statistical Computing, Vienna, Austria.

Rocha, R N C; Rodrigues, M D R L; Lopes, R; Cysne, A Q and Macedo, J L V D (2020). Production and cash flow of oil palm intercropping systems an Amazonian degraded area. *Nativa (Sinop), 8(1)*: 52-57. DOI: 10.31413/nativa.v8i1.8073.

Salmah, M; Idris, A B and Basri, M W (2006). Effect of host larval stages on development and oviposition behaviour of *Apanteles metesae* Nixon (Hymenoptera: Braconidae), a parasitoid of the oil

palm bagworm, *Metisa plana* Walker (Lepidoptera: Psychidae). *Malays. Appl. Biol., 35(2)*: 21-28.

Saswattecha, K; Kroeze, C; Jawjit, W and Hein, L (2015). Assessing the environmental impact of palm oil produced in Thailand. *J. Clean. Prod., 600*: 150-169. DOI: 10.1016/j.jclepro.2015.03.037.

Satriawan, H and Fuady, Z (2019). Short communication: Analysis of weed vegetation in immature and mature oil palm plantations. *Biodiversitas, 20(11)*: 3292-3298. DOI: 10.13057/biodiv/d201123.

Shi, Z; Chen, Y L; Chen, Y S; Lin, Y R; Liu, S W; Ge, X J; Gao, T G; Zhu, S X; Liu, Y; Yang, Q E; Humphries, C J; Raab-Straube, E von; Gilbert, M G; Nordenstam, B; Kilian, N; Brouillet, L; Illarionova, I D; Hind, D J N; Jeffrey, C; Bayer, R J; Kirschner, J; Greuter, W; Anderberg, A A; Semple, J C; Štěpánek, J; Freire, S E; Martins, L; Koyama, H; Kawahara, T; Vincent, L; Sukhorukov, A P; Mavrodiev, E V and Gottschlich, G (2011). Asteraceae (Compositae). *Flora of China* (Wu, Z Y; Raven, P H and Hong, D Y eds.). Science Press (Beijing) & Missouri Botanical Garden Press (St. Louis) Vol. 20-21. pp. 894.

Singh, A; Weisser, W W; Hanna, R; Houmgny, R and Zytynska, S E (2017). Reduce pests, enhance production: benefits of intercropping at high densities for okra farmers in Cameroon. *Pest Manag. Sci., 73(10)*: 2017-2027. DOI: 10.1002/ps.4636.

Siti Ramlah, A A; Wahid, M B; Najib, M and Masri, M M M (2005). Integrated pest management: Terakil-1, *Cassia cobanensis* and beneficial insects for controlling of bagworms infestation in Malaysia. *Proc. of the PIPOC 2005 International Palm Oil Congress - Technologies Breakthroughs and Commercialization the Way Forward*. MPOB, Bangi. p. 660-690.

Tan, K T; Lee, K T; Mohamed, A R and Bhatia, S (2009). Palm oil: Addressing issues and towards sustainable development. *Renew. Sust. Energ. Rev., 13(2)*: 420-427. DOI: 10.1016/j.rser.2007.10.001.

Tiong, A (1982). Oil palm pests in Sarawak and the use of natural enemies to control them. *Proc. of the International Conference on Plant Protection in the Tropics.* Malaysian Plant Protection Society, Kuala Lumpur. p. 363-372.

Tompkins, J M L; Wratten, S D and Wäckers, F L (2010). Nectar to improve parasitoid fitness in biological control: Does the sucrose:hexose ratio matter? *Basic Appl. Ecol., 11(3)*: 264-271. DOI: 10.1016/j.baae.2009.12.010.

Vandebroek, I; Picking, D; Aiken, S; Lewis, P A; Oberli, A; Mitchell, S and Boom, B (2018). A review of Coralilla (*Antigonon leptopus*): An invasive and popular urban bush medicine in Jamaica. *Econ. Bot., 72(2)*: 229-245. DOI: 10.1007/s12231-018-9415-5.

Wood, B J; Liau, S S and Knecht, J C X (1974). Trunk injection of systemic insecticides against the bagworm, *Metisa plana* (Lepidoptera: Pyralidae) on oil palm. *Oléagineux, 29(11)*: 499-505.

Wood, B J and Norman, K (2019a). A review of developments in integrated pest management (IPM) of bagworm (Lepidoptera: Psychidae) infestation in oil palms in Malaysia. *J. Oil Palm Res., 31(4)*: 529-539. DOI: 10.21894/jopr.2019.0047.

Wood, B J and Norman, K (2019b). Bagworm (Lepidoptera: Psychidae) infestation in the centennial of the Malaysian oil palm industry - A review of causes and control. *J. Oil Palm Res. 31(3)*: 364-380. DOI: 10.21894/jopr.2019.0032.

Xiang, H; Lan, N; Wang, F; Zhao, B; Wei, H and Zhang, J (2021). Reduced pests, improved grain quality and greater total income: Benefits of intercropping rice with *Pontederia cordata*. *J. Sci. Food Agric., 101(14)*: 5907-5917. DOI: 10.1002/jsfa.11243.

Yusdayati, R; Che Salmah, M D R; Ahmad, A H and Noor, H H (2014). Diversity and distribution of natural enemies (predators and parasitoids) of bagworms (Lepidoptera: Psychidae) on selected host plants in an oil palm plantation. *Planter, 90 (1055)*: 91-101.

Journal of Oil Palm Research Vol. 35 (4) December 2023 p. 607-615
DOI: https://doi.org/10.21894/jopr.2022.0074

DYNAMICS OF SUCROSE PHOSPHATE SYNTHASE AND FRUCTOSE BISPHOSPHATE SYNTHASE IN OIL PALMS FERTILISED WITH LOW NITROGEN [$(NH_2)_2CO$] DOSE WITH NPPT-NBPT COATING IN RED-YELLOW PODZOLIC SOIL

EKA TARWACA SUSILA PUTRA[1]*; BENITO HERU PURWANTO[2]; EKO HANUDIN[2] and TAUFAN ALAM[1]

ABSTRACT

One of the predominant deterrents of oil palm cultivation in Indonesia, especially in red-yellow podzolic soils, is nitrogen constraint, which is accelerated by heavy persistent rainfall and severe tropical temperature. This study was conducted with the objective to determine the effect of low-dose urea fertilisation with 0.12% N-(n-propyl) thiophosphoric triamide (NPPT) and N-(n-butyl) thiophosphoric triamide (NBPT) coating on the metabolic characters, the yield components, and the total yield of the oil palm. The field experiment was conducted for twelve months between November 2016 and November 2017 at the Seruyan Tengah Oil Palm Plantation, Seruyan Regency, Central Kalimantan Province, Indonesia. The experimental design utilised a single factor complete randomised block design with three blocks as repeatition. The applications consisted of the untreated one, without [$(NH_2)_2CO$], with 195 kg ha^{-1} [$(NH_2)_2CO$], 195 kg ha^{-1} [$(NH_2)_2CO$] + 0.12% NPPT and NBPT, 156 kg ha^{-1} [$(NH_2)_2CO$], and 156 kg ha^{-1} [$(NH_2)_2CO$] + 0.12% NPPT and NBPT. The results demonstrated that low-dose fertilisation of 156 kg ha^{-1} [$(NH_2)_2CO$] + 0.12% NPPT and NBPT elevated the N content of the leaf tissue, nitrate reductase activity (NRA), sucrose phosphate synthase (SPS), fructose biphosphate synthase (FBS), reducing sugar, sucrose, and invertase activity while reducing the dosage of [$(NH_2)_2CO$] by 20.00% in comparison to the high dose treatment of 195 kg ha^{-1} [$(NH_2)_2CO$].

Keywords: NBPT, NPPT, oil palm, red-yellow podzolic, urea fertiliser.

Received: 12 October 2021; **Accepted:** 8 September 2022; **Published online:** 21 November 2022.

INTRODUCTION

One of the principal plantation commodities that reinforces the Indonesian economy is palm oil (Ministry of Agriculture, 2019). Palm oil in Indonesia is predominantly cultivated in the areas that experience heavy and persistent rainfall throughout the year, without a firm dry month, and is spread over the Islands of Sumatra, Kalimantan, Sulawesi, and the West Papua region. Persistent rainfall along with soaring tropical temperature rapidly erodes the parent material, leaving the area covered with low-grade soil with poor nutrient content (Melisa *et al*., 2018; Ministry of Agriculture, 2019; Woittiez *et al*., 2017).

The dominant soil type found in the oil palm plantation area is the red-yellow podzolic (RYP) soil. It is characterised by the low nutrient and acidic cation content (Al^{2+}, Fe^{2+}, Mn^{2+}). Persistent rainfall throughout the year causes leaching of the alkaline cations and in turn accumulates the acidic cations in the soil (Putra *et al*., 2021; Rendana *et al*., 2016; Riyadi *et al*., 2020). The accumulation of acidic cations not only causes poisoning to the oil palm but also nutrients imbalance in the soil

[1] Department of Agronomy, Faculty of Agriculture, Universitas Gadjah Mada, 55281 Yogyakarta, Indonesia.

[2] Department of Soil, Faculty of Agriculture, Universitas Gadjah Mada, 55281 Yogyakarta, Indonesia.

* *Corresponding author e-mail: eka.tarwaca.s@ugm.ac.id*

leading to macronutrient deficiency of nitrogen (N), phosphorus (P), potassium (K), calcium (Ca), and magnesium (Mg) (Gafur and Putra, 2019; Nurwahyuni and Putra, 2021; Sari and Putra, 2019).

The primary macronutrient with reduced availability in the RYP soil is N. The N recurrently dissipates through several pathways such as evaporation in the form of NH_3, leaching as NO_3^-, and denitrifying to form N_2O and N_2, inhibiting its absorption efficiency at 45% and causing environmental pollution that proliferates N_2O, NH_3, and N_2 in the air and NO_3 accumulation in the water (Edy *et al*., 2020; Riyadi *et al*., 2020).

Efficient N uptake in the oil palm along with reduced priming of N fertiliser stabilises the production, thereby inducing a superior yield of the fresh fruit bunches (FFB) in comparison to the higher doses of fertiliser treatment. There are two main enzymes in the oil palm that influences the assimilation production capacity: Sucrose phosphate synthase (SPS) and fructose bisphosphate synthase (FBS). These two enzymes regulate the photosynthesis process in the dark reaction pathway (Anur *et al*., 2020; Bilska-Kos *et al*., 2020; Gesch *et al*., 2002).

One of the most used N fertilisers is urea [$(NH_2)_2CO$]. The loss of N in urea occurs through the evaporation of NH_4^+ to NH_3. Because of its chemical instability, it is prone to rapid decomposition and persistently releases NH_3. This occurs when urease activity in the soil is high and NH_4^+ is not rapidly absorbed by plants or is nitrified to nitrate (Rahman *et al*., 2019; Rasid *et al*., 2014; Sakata *et al*., 2015).

The efficiency of N uptake in RYP soil can be improved by inhibiting the urease activity in the soil (Alpandari *et al*., 2019; Liu *et al*., 2020; Zuki *et al*., 2020). Combining 75% N-(n-butyl) thiophosphate triamide (NBPT/$C_4H_{14}N_3PS$) with 25% N-(n-propyl) thiophosphate triamide (NPPT/$C_3H_{12}N_3PS$) was used at a dose of 0.12% (*w*/*w* to urea) has been hypothesised to impede the urease activity in the soil. The NBPT and NPPT compounds are proven to bind to the active site of urease, thereby inhibiting urea hydrolysis and minimising ammonia synthesis. This can reduce potential emissions and can lower production costs as well. Efficient application of N fertiliser, with approximately 100% absorption efficiency, has the potential to reduce almost half of the recommended dose while maintaining oil palm productivity at the same level (Dewi *et al*., 2018; Liu *et al*., 2020; Zanin *et al*., 2016).

This research is aimed to investigate the effect of low-dose $(NH_2)_2CO$ fertiliser with 0.12% NPPT and NBPT treatment on the SPS, FBS, and the yield capacity of the FFB of oil palm in the RYP soil. The results of this study will enable us to provide crucial information to the farmers, scientists and oil palm companies regarding the efficiency of using $(NH_2)_2CO$ fertiliser, especially on the RYP soil.

MATERIALS AND METHODS

Study Site

The field experiment was carried out for 12 months between November 2016 and November 2017 at the Seruyan Tengah Oil Palm Plantation, Seruyan Regency, Central Kalimantan Province, Indonesia. The experimental site consisted of RYP mineral soil. Oil palms of 10 years of maturity were selected for sampling because their productivity peaked at this age. Considering, that this research was focused on the implementation of the N fertilisers on oil palms, it was not applied at the study location for the last two years.

Experimental Design and Their Management

The experimental design utilised the randomised complete block design single factor with three blocks as the replicators. The study consisted of a total of five applications firstly the untreated one (without urea $(NH_2)_2CO$), then at 195 kg ha^{-1} of urea [$(NH_2)_2CO$], 195 kg ha^{-1} of urea [$(NH_2)_2CO$] + 0.12% NPPT and NBPT, 156 kg ha^{-1} of urea [$(NH_2)_2CO$], and 156 kg ha^{-1} of urea [$(NH_2)_2CO$] + 0.12% NPPT and NBPT.

The numbers sampled per treatment per block were five oil palm trees. A total of 45 oil palm trees were chosen for this analysis. The fertiliser P, K and Ca nutrients that were not treatments refer to the Indonesian Oil Palm Research Institute (2017). The fertiliser was spread in a circle slightly away from the base of the tree. Besides fertiliser application, other activities such as weed, pest and disease control were also carried out. The fertiliser dose of 227.50 kg ha^{-1} TSP, 292.50 kg ha^{-1} KCl, and 292.50 kg ha^{-1} dolomite. All the sampled trees received an equal dosage of P, K and Ca nutrients as well. The fertiliser application was carried out in November 2016.

Data Collection

In an order to record the metabolic indicators, the leaf sample of the oil palm was collected twice, that is three (February 2017) and five (April 2017) months after the fertiliser application. Leaf samples collected were mainly the leaflets located in the centre of the 17^{th} leaf midrib of each stand. The leaf samples were pruned evenly from the left and right sides of the midrib stalk. The metabolic indicators consisted of various parameters such as the N content of the leaf tissue (King *et al*., 1992), nitrate reductase activity (NRA) (Hartiko *et al*., 1982), SPS activity (Kohler *et al*., 1988), FBS activity (Harrison *et al*., 1998), invertase activity (Arai *et al*., 1991), total sugar content (Chow and Landhausser, 2004), reducing sugar content (Takahashi *et al*., 2018) and the sucrose content (Takahashi *et al*., 2018).

The oil palm yield was based on the weight of the FFB harvested from the research site during the 10 months between February and November 2017. The FFB yields of 10 months were then converted into various observation parameters such as the average number of FFB per tree per year, average weight per FFB, FFB productivity per hectare per year and the ratio of FFB productivity between each treatment to the FFB productivity of the untreated oil palms.

Data Analysis

The parameters observed are required to be normally distributed with homogeneity assumptions before the analysis of variance (ANOVA). The data that fulfilled the assumptions were analysed using the ANOVA ($p<0.05$) and continued with the LSD-Fisher test ($p<0.05$) as a post hoc test (Hinkelman and Kempthorne, 2008; Welham *et al*., 2015). The interaction pattern amongst the observed variables was determined with the partial least square structural equation modelling (PLS-SEM) and the stepwise regression analysis (Suryanto *et al*., 2020; 2022; Widyawan *et al*., 2020). The ANOVA and the stepwise regression analysis were carried out using SAS software version 9.4 for Windows with PROC GLM and REG (SAS Institute Inc, 2013). PLS-SEM was performed using SmartPLS 3 software (Smith *et al*., 1993; Suryanto *et al*., 2022).

RESULTS AND DISCUSSION

The Effects of NBPT and NPPT as Coating for [$(NH_2)_2CO$] on the Oil Palm

Nitrogen plays a key role in plant metabolism. It is the principal component of plant protein, enzymes, amino acids, and chlorophyll. However, it is also dynamic and mobile in both the soil and the plant tissues. In the case of oil palms, the dynamic nature of N in the soil heightens the risk of its deficiency, where it rapidly converts to an inaccessible form. Therefore, to strengthen the efficiency of the N fertiliser absorption, a potential need for technological innovation is critical (Liu *et al*., 2020; Zanin *et al*., 2016; Zuki *et al*., 2020). One of them is the urease activity inhibition technology, which delays the hydrolysis of [$(NH_2)_2CO$] by overlaying a mixture of 75% NBPT + 25% NPPT as a coating in the proportion of 0.12% by weight of the fertiliser.

The incorporation of 156 kg ha^{-1} [$(NH_2)_2CO$] + 0.12% NPPT and NBPT remarkably elevated the N content of the leaf tissue in comparison to the other treatments (*Table 1*). The N content of oil palm leaves with 156 kg ha^{-1} [$(NH_2)_2CO$] + 0.12% NPPT and NBPT application was equivalent to the oil palm treated with 195 kg ha^{-1} [$(NH_2)_2CO$] without the coating. However, oil palm primed with 195 kg ha^{-1} [$(NH_2)_2CO$] + 0.12% NPPT and NBPT recorded the highest leaf N content. These results illustrate the potential reduction in the dosage of [$(NH_2)_2CO$] from 195 to 156 kg ha^{-1} in the oil palm plantations, contingent to sustain the amount of leaf N at the same level.

The coating mixture consisting of 75% NBPT + 25% NPPT in the proportion of 0.12% by weight [$(NH_2)_2CO$] inhibited the rate of fertiliser hydrolysis by the urease enzyme that suppressed the loss of N due to volatile NH_3. Since the coating material impedes the urease activity significantly, the hydrolysis process of [$(NH_2)_2CO$] occurs at a slower rate and provides the right form of available N by the plant needs, thereby increasing the absorption rate and reducing the risk of N loss (Liu *et al*., 2020; Zanin *et al*., 2016; Zuki *et al*., 2020).

Application of 156 kg ha^{-1} [$(NH_2)_2CO$] + 0.12% NPPT and NBPT also considerably escalated the NRA in comparison to the oil palm that was left untreated and the one that was treated with 156 kg ha^{-1} [$(NH_2)_2CO$] without the coating. The value of NRA treated with 156 kg ha^{-1} [$(NH_2)_2CO$] + 0.12% NPPT and NBPT was also equivalent to the oil palm administered with 195 kg ha^{-1} [$(NH_2)_2CO$] without the coating. Meanwhile, oil palms covered with 195 kg ha^{-1} [$(NH_2)_2CO$] + 0.12% NPPT and NBPT had the highest leaf NRA. Based on the results, it can be concluded that reducing the dose of [$(NH_2)_2CO$] from 195 to 156 kg ha^{-1} in oil palm while sustaining the leaf NRA at the same level is attainable.

The results indicate that the presence of coating in the form of a combination of 75% NBPT + 25% NPPT in the proportion of 0.12% by weight of [$(NH_2)_2CO$] were significantly able to maintain the NRA at the same level between the low-dose coated and the high dose without the coating. This is in line with the requirements for the leaf N content of the oil palms. Oil palms could absorb N in two forms, namely NH_4^+ and NO_3^-. However, N uptake of oil palms in the form of NO_3^- is more dominant when compared to NH_4^+ (Liu *et al*., 2020; Zanin *et al*., 2016; Zuki *et al*., 2020).

Meanwhile, in crop tissues, the most functional form of N for metabolism is NH_4^+ instead of NO_3^-. Because the N availability in the tissues is more dominated by NO_3^-, a massive conversion of the N form from NO_3^- to NH_4^+ is required, to fulfil the NH_4^+ metabolic needs. The conversion process of NO_3^- to NH_4^+ occurs through the denitrification process. The NO_3^- is reduced to NH_4^+ by an electron donor derived from the nicotinamide adenine dinucleotide (NADH). The conversion of NO_3^- to NH_4^+ is assisted by the enzyme nitrate reductase, also known as NRA (Rahman *et al*., 2019; Rasid *et al*., 2014; Sakata *et al*., 2015).

The oil palms without [$(NH_2)_2CO$] have the lowest SPS and FBS activities. The [$(NH_2)_2CO$]

with a standard dose of 195 kg ha^{-1} considerably stimulated better SPS and FBS activities than the crops that were not applied with [$(NH_2)_2CO$] (*Table 1*). However, SPS and FBS capacities of oil palms incorporated with 195 kg ha^{-1} [$(NH_2)_2CO$] were the same as other crops primed at a lower dose of 156 kg ha^{-1} when [$(NH_2)_2CO$] was coated with 0.12% NPPT and NBPT. The treatment incorporating 156 kg ha^{-1} [$(NH_2)_2CO$] + 0.12% NBPT and NPPT also resulted in a noteworthy SPS and FBS capacity when compared to the oil palms treated with the same dose of [$(NH_2)_2CO$] without the coating. Meanwhile, the application of 195 kg ha^{-1} [$(NH_2)_2CO$] + 0.12% NPPT and NBPT resulted in the highest SPS and FBS activities in the oil palm.

The controlling factor of sucrose metabolism in the crop tissues is the sucrose biosynthesis-related protein. Two forms are categorised under the sucrose biosynthetic enzymes, namely SPS and FBS. The SPS enzyme plays a key role in catalysing the reaction to form sucrose-6-phosphate (S6P) from the substrate fructose-6-phosphate (F6P). Meanwhile, FBS contributes to the synthesis of F6P from the fructose-1.6-bisphosphate (FBP) substrate. These two enzymes are the key enzymes in the Calvin cycle, with carbohydrates as the final product (Anur *et al*., 2020; Bilska-Kos *et al*., 2020; Gesch *et al*., 2002).

The implementation of low-dose [$(NH_2)_2CO$] (156 kg ha^{-1}) triggered the SPS and FBS activities that were equivalent to the high doses (195 kg ha^{-1}) only if the application of low doses of [$(NH_2)_2CO$] were coated (*Table 1*). The coating materials were a combination of 75% NBPT and 25% NPPT, with a concentration of [$(NH_2)_2CO$] at only 0.12% by weight of the fertiliser. This was in line with the value of leaf N content and the leaf NRA which were also equivalent between oil palms treated with high doses (195 kg ha^{-1}) and the low doses (156 kg ha^{-1}) of [$(NH_2)_2CO$], provided that at the low doses, the materials were coated.

The adequacy of N at the same level, even when primed at a lower dose of [(NH2)2CO] (156 kg ha^{-1}), was caused by the increased nutrient uptake efficiency triggered by the presence of the coating materials. The N availability will trigger the Calvin cycle, thereby modulating the performance of the SPS and the FBS activities.

The prominent efficiency of the FBS can also be characterised by reducing sugar content, its by-product. Meanwhile, the performance of SPS can be characterised by the number of products available in the form of sucrose. Total sugar is a combination of sucrose and reduced sugar. This means that the total sugar is generated from the synergy between the FBS and the SPS (Anur *et al*., 2020; Bilska-Kos *et al*., 2020; Gesch *et al*., 2002).

The untreated oil palm had the lowest production capacity for reduced sugar, sucrose, and total sugar (*Table 1*). Priming the oil palm using [$(NH_2)_2CO$] at 195 kg ha^{-1} elevated the production capacity of reducing sugar, sucrose, and total sugar in comparison to the untreated ones. However, the production capacity of the reducing sugar, sucrose, and total sugar of oil palm applied with 195 kg ha^{-1} [$(NH_2)_2CO$] were the same as for the other plants treated with a lower dose of 156 kg ha^{-1} when [$(NH_2)_2CO$] was coated with 0.12 % NPPT and NBPT. Incorporation of 156 kg ha^{-1} [$(NH_2)_2CO$] + 0.12% NPPT and NBPT also resulted in a much better production capacity for reducing sugar, sucrose, and total sugar than oil palm manuring with [$(NH_2)_2CO$] at the same dose without the coating.

Meanwhile, the oil palm that was treated with 195 kg ha^{-1} [$(NH_2)_2CO$] + 0.12% NPPT and NBPT was able to produce the highest reducing sugar, sucrose, and total sugar. This is in line with the high capacity of the SPS and the FBS in the oil palm primed with a lower dose of [$(NH_2)_2CO$] (156 kg ha^{-1}) as long as the fertiliser was coated with NPPT and NBPT. The increased efficiency of the SPS and the FBS was the result of the maximum production capacity of the reducing sugar, sucrose, and total sugar.

Oil palm applied with 156 kg ha^{-1} [$(NH_2)_2CO$] + 0.12% NPPT and NBPT was able to produce sucrose equivalent to plants primed with 195 kg ha^{-1} [$(NH_2)_2CO$] without the coating and much higher than other crops that were left untreated or the ones applied with 156 kg ha^{-1} [$(NH_2)_2CO$] without the coating. The sucrose production capacity of this treatment was only inferior to the plants incorporated with 195 kg ha^{-1} [$(NH_2)_2CO$] + 0.12% NPPT and NBPT, which was indeed a much higher dose and also was evenly coated. The high sucrose production capacity at 156 kg ha^{-1} [$(NH_2)_2CO$] + 0.12% NPPT and NBPT enabled the plants to elevate the invertase enzyme activity. Invertase is an enzyme that converts sucrose into reducing sugars (Anur *et al*., 2020; Bilska-Kos *et al*., 2020; Gesch *et al*., 2002).

Invertase enzyme activity tends to accelerate if the cell contains an increased amount of sucrose substrate. Therefore, oil palm primed with 156 kg ha^{-1} [$(NH_2)_2CO$] + 0.12% NPPT and NBPT had invertase enzyme activity equivalent to 195 kg ha^{-1} [$(NH_2)_2CO$] treatment without the coating and much higher than the untreated one or the one with 156 kg ha^{-1} [$(NH_2)_2CO$] without the coating. This was related to the high sucrose production in the oil palm applied with 156 kg ha^{-1} $(NH_2)_2CO$ + 0.12% NPPT and NBPT. However, the invertase enzyme activity of the oil palm administered with 156 kg ha^{-1} [$(NH_2)_2CO$] + 0.12% NPPT and NBPT was reduced in comparison to the plants fertilised with 195 kg ha^{-1} [$(NH_2)_2CO$] + 0.12% NPPT and NBPT as the dose was far higher and both were coated evenly. In addition, the oil palm primed with 195 kg ha^{-1} [$(NH_2)_2CO$] + 0.12% NPPT and NBPT did produce significantly more sucrose when compared to 156 kg ha^{-1} [$(NH_2)_2CO$] + 0.12% NPPT and NBPT.

TABLE 1. THE EFFECTS OF NBPT-NPPT AS COATING FOR [$(NH_2)_2CO$] ON OIL PALM LEAF METABOLIC ACTIVITIES AT THREE MONTHS AFTER FERTILISER APPLICATION

Variables	[$(NH_2)_2CO$] fertiliser				
	Without	195 kg ha^{-1} of [$(NH_2)_2CO$]	195 kg ha^{-1} of [$(NH_2)_2CO$] + 0.12% NPPT and NBPT	156 kg ha^{-1} of [$(NH_2)_2CO$]	156 kg ha^{-1} of [$(NH_2)_2CO$] + 0.12% NPPT and NBPT
N content in the leaf tissue (%)	1.24^{d}	2.85^{b}	3.65^{a}	2.00^{c}	2.90^{b}
NRA (μm NO_2^- g^{-1} h^{-1})	2.32^{d}	3.44^{b}	4.00^{a}	2.84^{c}	3.50^{b}
SPS activity (μm sucrose mg^{-1} s^{-1})	3.22^{d}	5.46^{b}	7.20^{a}	4.21^{c}	5.78^{b}
FBS activity (μm fructose mg^{-1} s^{-1})	3.00^{d}	4.90^{b}	6.99^{a}	3.95^{c}	5.10^{b}
Reduction of sugar (%)	0.35^{c}	0.45^{b}	0.68^{a}	0.37^{c}	0.44^{b}
Sucrose (%)	3.00^{d}	4.54^{b}	5.64^{a}	3.68^{c}	4.62^{b}
Total sugar (%)	3.50^{d}	5.01^{b}	6.34^{a}	4.05^{c}	5.06^{b}
Invertase activity (mM fructose^{-1} mg s^{-1})	0.08^{c}	0.20^{b}	0.35^{a}	0.10^{c}	0.25^{b}

Note: Numbers in the same row with similar letters were not significantly different by the LSD-Fisher test (p<0.05).

Table 2 represents the metabolic characteristics of the oil palm five months after the fertiliser application. The trend of the leaf N content, NRA, SPS, FBS, reducing sugar content, sucrose, total sugar, and the invertase enzyme activity was in line with the characters as described in *Table 1*. All the characters in the two tables showed the same trend, whereas all the characters in the same treatment trended to be smaller than the variables as presented in *Table 1*. The oil palms are required to be treated with a fertiliser specifically at the same dose every six months due to which [$(NH_2)_2CO$] application was carried out a few rounds in a year (Gafur and Putra, 2019; Nurwahyuni and Putra, 2020; Sari and Putra, 2019).

In *Table 2*, oil palm administered with 156 kg ha^{-1} [$(NH_2)_2CO$] + 0.12% NBPT and NPPT sustained the leaf N levels, NRA, SPS, FBS, reducing sugar content, sucrose, total sugar, as well as the invertase enzyme activity, at an equivalent level in comparison to the plants manured with 195 kg ha^{-1} [$(NH_2)_2CO$] without coating, and for a much higher value than other plants that were not incorporated with 156 kg ha^{-1} [$(NH_2)_2CO$] without the coating. The capacity of the plants in this treatment was only inferior to the plants that were given fertiliser at 195 kg ha^{-1} [$(NH_2)_2CO$] + 0.12% NPPT and NBPT, which had a much higher dose, and both were evenly coated. This shows that NPPT and NBPT as the coating on [$(NH_2)_2CO$] could reduce the N loss and in turn, increasing the absorption efficiency. The elevated N absorption efficiency compensated for the N requirement of the oil palm due to the low dose of [$(NH_2)_2CO$] (156 kg ha^{-1}). At this dose, the adequacy of N remained equivalent to the administration of high doses (195 kg ha^{-1}), which is the standard dose for oil palm, but so far, it has been given without coating.

The FFB sampling was conducted to record the yield after three months of fertiliser application based on the presumption that the three months of fertiliser application would be sufficient to ensure that the FFB harvested was the tree's response to the applied fertiliser. Harvesting was carried out for a total of ten months. The FFB productions garnered for ten months were then converted into oil palm productivity per hectare per year (Melisa *et al*., 2018; Riyadi *et al*., 2020).

The average number of FFB per year per tree for the untreated [$(NH_2)_2CO$] treatment was only five FFB ha^{-1}, which is considerably low compared to the treated plants with the quantity of 156 kg ha^{-1} and 195 kg ha^{-1} [$(NH_2)_2CO$] (*Table 3*). Oil palm primed with 195 kg ha^{-1} [$(NH_2)_2CO$] also generated remarkably more FFB when compared to 156 kg ha^{-1} [$(NH_2)_2CO$]. However, decreasing the dose of [$(NH_2)_2CO$] from 195 kg ha^{-1} to 156 kg ha^{-1} sustained the average amount of FFB per tree per year equivalent to a higher dose considering the fertiliser was coated with 0.12% NPPT and NBPT. The treatment of 156 kg ha^{-1} [$(NH_2)_2CO$] + 0.12% NPPT and NBPT produced coequal amounts of FFB per stem per year in comparison to the application of 195 kg ha^{-1} [$(NH_2)_2CO$] + 0.12% NPPT and NBPT. This demonstrates that the incorporation of coatings in the form of NPPT and NBPT could substantially increase the efficiency of N uptake in the oil palm as well as indicate that even a lower dosage of the fertiliser at 156 kg ha^{-1} [$(NH_2)_2CO$] was sufficient to provide the optimal amount of FFB per tree.

TABLE 2. THE EFFECTS OF NBPT-NPPT AS COATING FOR [$(NH_2)_2CO$] ON OIL PALM LEAF METABOLIC ACTIVITIES AT SIX MONTHS AFTER FERTILISER APPLICATION

Variables	$(NH_2)_2CO$ fertiliser				
	Without	195 kg ha^{-1} of [$(NH_2)_2CO$]	195 kg ha^{-1} of [$(NH_2)_2CO$] + 0.12% NPPT and NBPT	156 kg ha^{-1} of [$(NH_2)_2CO$]	156 kg ha^{-1} of [$(NH_2)_2CO$] + 0.12% NPPT and NBPT
N content in the leaf tissue (%)	1.20^{d}	2.75^{b}	3.42^{a}	1.80^{c}	2.81^{b}
NRA (μm NO_2^- g^{-1} h^{-1})	2.12^{d}	3.00^{b}	4.10^{a}	2.72^{c}	3.20^{b}
SPS activity (μm sucrose mg^{-1} s^{-1})	3.01^{c}	5.16^{b}	6.25^{a}	3.46^{c}	5.19^{b}
FBS activity (μm fructose mg^{-1} s^{-1})	2.78^{d}	4.30^{b}	5.86^{a}	3.35^{c}	4.29^{b}
Reduction of sugar (%)	0.30^{c}	0.40^{b}	0.59^{a}	0.33^{c}	0.42^{b}
Sucrose (%)	2.71^{d}	4.44^{b}	5.54^{a}	3.26^{c}	4.36^{b}
Total sugar (%)	3.10^{d}	4.88^{b}	6.01^{a}	3.70^{c}	4.80^{b}
Invertase activity (mM fructose mg s^{-1})	0.10^{c}	0.25^{b}	0.42^{a}	0.14^{c}	0.26^{b}

Note: Numbers in the same row with similar letters were not significantly different by LSD-Fisher test (p<0.05).

TABLE 3. THE EFFECTS OF NBPT AND NPPT AS COATING FOR [$(NH_2)_2CO$] ON THE TOTAL YIELD AND ITS COMPONENTS

Variables	[$(NH_2)_2CO$] fertiliser				
	Without	195 kg ha^{-1} of [$(NH_2)_2CO$]	195 kg ha^{-1} of [$(NH_2)_2CO$] + 0.12% NPPT and NBPT	156 kg ha^{-1} of [$(NH_2)_2CO$]	156 kg ha^{-1} of [$(NH_2)_2CO$] + 0.12% NPPT and NBPT
Total number of FFB (trunk yr^{-1})	5.00^{c}	13.00^{ab}	15.00^{a}	10.00^{b}	13.00^{ab}
FFB weight average (kg)	10.50^{c}	20.10^{ab}	21.20^{a}	17.40^{b}	20.50^{ab}
Yields (tonnes ha^{-1} yr^{-1})	15.60^{c}	24.50^{ab}	26.00^{a}	18.40^{b}	25.00^{ab}
Yield each treatment per Yield without $(NH_2)_2CO$	1.00^{b}	1.57^{a}	1.67^{a}	1.12^{b}	1.60^{a}

Note: Numbers in the same row with similar letters were not significantly different by the LSD-Fisher test (p<0.05).

The average weight per FFB also had a trend in line with the average FFB per tree per year. Oil palm manured with 156 kg ha^{-1} [$(NH_2)_2CO$] + 0.12% NPPT and NBPT increased the average weight per FFB, in comparison to the untreated trees. Application of 156 kg ha^{-1} [$(NH_2)_2CO$] + 0.12% NPPT and NBPT was also able to produce FFB with the same average weight as the other trees that received higher doses of 195 kg ha^{-1} [$(NH_2)_2CO$] without or with 0.12% NPPT and NBPT coating when treated with 156 kg ha^{-1} [$(NH_2)_2CO$] as long as the fertiliser was coated using 0.12% NPPT and NBPT. Results indicated that the application of 195 kg ha^{-1} was not essential because even the coated one gives the same average weight per FFB as the low-dose treatment of 156 kg ha^{-1} [$(NH_2)_2CO$] + 0.12% NPPT and NBPT (Liu *et al*., 2020; Zanin *et al*., 2016; Zuki *et al*., 2020).

The oil palm productivity trend was in line with the indicators of the average number of FFB per tree per year and the average weight per FFB. Oil palm fertilised with 156 kg ha^{-1} [$(NH_2)_2CO$] + 0.12% NPPT and NBPT had much higher productivity than the untreated or the treated one with 156 kg ha^{-1} [$(NH_2)_2CO$] but without the coating. Treatment with a dose of 156 kg ha^{-1} [$(NH_2)_2CO$] + 0.12% NPPT and NBPT also generated a productivity equivalent to a higher dose of fertiliser, namely 195 kg ha^{-1} [$(NH_2)_2CO$] without the coating and 195 kg ha^{-1} [$(NH_2)_2CO$] + 0.12% NPPT and NBPT. This illustrated that the use of low doses of fertiliser along with the NPPT and NBPT coating [$(NH_2)_2CO$] (156 kg ha^{-1}) not only can elevate the efficiency of N absorption but also optimally fulfils the requirements of these elements (Alpandari *et al*., 2019; Dewi *et al*., 2018; Liu *et al*., 2020), coequally as growing N with the higher fertiliser dose (195 kg ha^{-1}). Thus, the productivity of oil palm at a dose of 156 kg ha^{-1} [$(NH_2)_2CO$] + 0.12% NPPT and NBPT was optimal and equivalent to the dose of 195 kg ha^{-1} [$(NH_2)_2CO$] without or with 0.12% NBPT and NPPT coating. The study concludes that the lower dose of fertiliser [$(NH_2)_2CO$] was ample for optimal productivity of the oil palm.

The productivity ratio of oil palm fertilised with 156 kg ha^{-1} [$(NH_2)_2CO$] + 0.12% NPPT and NBPT and the trees that were left untreated with [$(NH_2)_2CO$] was 1.60. This value was not significantly different from the fertiliser treatment ratio of 195 kg ha^{-1} [$(NH_2)_2CO$]

without or with 0.12% NPPT and NBPT coating, which had a ratio of 1.57 and 1.67, respectively (Anur *et al*., 2020; Bilska-Kos *et al*., 2020; Gesch *et al*., 2002).

The Relationship between the Metabolism Characters, the Yield Components and the Total Yield of Oil Palm

The results illustrated a notable interaction between the N metabolism and the sugar metabolism (p<0.000) and the yield component (p<0.000), while the total effect displayed that N metabolism had a considerable influence on the sugar metabolism (p<0.000), the yield component (p<0.000), and the total yield (p<0.000) (*Figure 1*). The conclusion of the stepwise regression analysis showed that the yield per hectare of oil palm (Y) was determined by the elevated level of N content in the leaf tissue with enhanced SPS activity and a reduction in the FBS. The regression equation was Y = 10.11 + 5.48 NC** – 3.44 FBS** + 2.78 SPS* (R^2 = 0.993**).

The tissue content, uptake and utilisation of N are correlated with the availability of sugar in the plants, which in turn is interlinked with the carbon assimilation that requires adequate N. The N deficiency leads to accumulation of the unstructured carbohydrates and changes the distribution of the assimilation between various plant organs (Geiger *et al*., 1999). In addition, the high N content influenced several reductions in the main sugar levels of the leaves (sorbitol, sucrose, glucose) which is interconnected to the assimilation competition due to rapid shoot growth. Furthermore, excessive use of N can reduce the carbohydrates, thereby increasing respiration, and consequently impacting the crop yield (Zhang *et al*., 2021).

CONCLUSION

The study illustrated that an increase in the nitrogen content of the leaf tissue of the oil palm with improved sucrose phosphate synthase (SPS) and a reduction in the fructose bisphosphate synthase (FBS), contributed to generating a comparatively higher yield per hectare of the oil palm. The results signified that the application of fertiliser even at a lower dose of 156 kg ha^{-1} [$(NH_2)_2CO$] + 0.12% NPPT and NBPT was capable of enhancing not only the N content of the leaf tissue, but also the NRA, SPS, FBS, reducing sugar, sucrose, and the invertase activity, while reducing the treatment rate of the same by 20% compared to the high dose at 195 kg ha^{-1} [$(NH_2)_2CO$] in the RYP soil.

ACKNOWLEDGEMENT

The research for this article was fully funded by BASF Company (2016-2017).

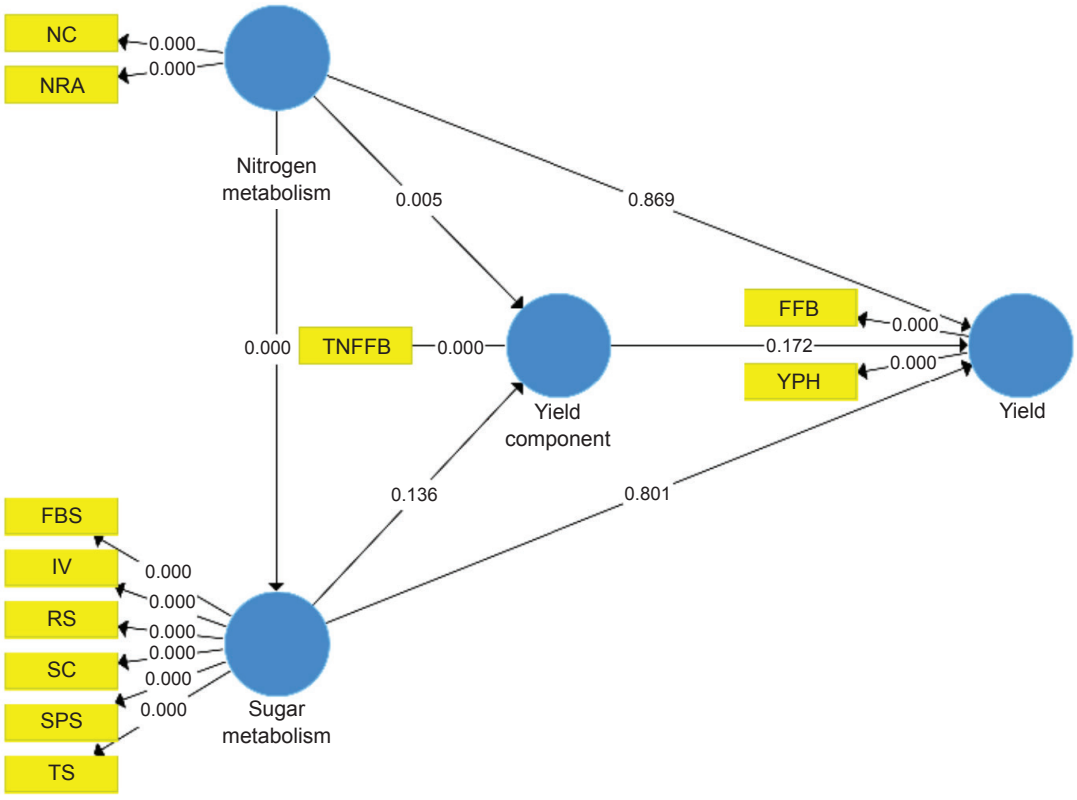


Figure 1. The relationship between the metabolism characters, the yield components and the total yield of oil palm.

REFERENCES

Alpandari, H; Putra, E T S and Wulandari, C (2019). Response of corn (*Zea mays*) growth and yield to urea fertilization techniques on vertisol in Playen, Gunungkidul. *Agric. Sci.*, *4*: 117-122.

Anur, R M; Mufithah, N; Sawitri, W D; Sakakibara, H and Sugiharto, B (2020). Overexpression of sucrose phosphate synthase enhanced sucrose content and biomass production in transgenic sugarcane. *Plants*, *9*: 200.

Arai, M; Mori, H and Imaseki, H (1991). Roles of sucrose 4-metabolizing enzymes in growth seedlings, purification of acid invertase from growing hipocotyls of mung bean seedlings. *Plant Cell Physiol.*, *32*: 1292-1298.

Chow, P S and Landhäusser, S M (2004). A method for routine measurements of total sugar and starch content in woody plant tissues. *Tree Physiol.*, *24*: 1129-1136.

Dewi, F C; Putra, E T S and Wulandari, C (2018). The effect of urease inhibitors coated urea on the growth, physiological activities and yield of maize (*Zea mays* L.) in inceptisol Jogonalan, Klaten. *IPAS*, *3*: 160-165.

Edy, N; Yelianti, U; Irawan, B; Polle, A and Pena, R (2020). Differences in root nitrogen uptake between tropical lowland rainforests and oil palm plantations. *Front. Plant Sci.*, *11*: 92.

Gafur, M A and Putra, E T S (2019). Effect of drought stress in physiological oil palm seedling (*Elaeis guineensis* Jacq.) using calcium application. *Asian J. Biol. Sci.*, *12*: 550-556.

Geiger, M; Haake, V; Ludewig, F; Sonnewald, U and Stitt, M (1999). The nitrate and ammonium nitrate supply have a major influence on the response of photosynthesis, carbon metabolism, nitrogen metabolism and growth to elevated carbon dioxide in tobacco. *Plant Cell Environ.*, *22*: 1177-1199.

Gesch, R W; Vu, J C V; Boote, K J; Junior, L H A and Bowes, G (2002). Sucrose-phosphate synthase activity in mature rice leaves following changes in growth CO_2 is unrelated to sucrose pool size. *New Phytol.*, *154*: 74-84.

Harrison, E P; Willingham, N M; Lloyd, J C and Raines, C A (1997). Reduced sedoheptulose-1,7-bisphosphatase levels in transgenic tobacco lead to decreased photosynthetic capacity and altered carbohydrate accumulation. *Planta*, *204*: 27-36.

Hartiko, H; Del Rosario, E J and Carlos, J T (1982). Leaf and root nitrate reductase activities of coconut (*Coconut nucifera* L.) cultivars and hybrids. *JIPI*, *3*: 227-235.

Hinkelman, K and Kempthorne, O (2008). *Design and Analysis of Experiments*. 2nd edition. John Wiley and Sons, USA. 688 pp.

Indonesian Oil Palm Research Institute (2017). *Optimum Fertilizer Dose to Maximize Productivity of Oil Palm Superior Progeny*. Indonesian Oil Palm Research Institute, Indonesia. 36 pp.

King, T V V; Clark, R N; Calvin, W M; Sherman, D M and Brown, R H (1992). Evidence for ammonium-bearing minerals on Ceres. *Science*, *255*: 1551-1553.

Kohler, E K J; Thom, M and Maretzki, A (1988). Activity of sucrose phosphate synthase in sugarcane leaves. *Phyto. Chemistry*, *27*: 1605-1608.

Bilska-Kos, A B; Mytych, J; Suski, S; Magoń, J; Ochodzki, P and Zebrowski, J (2020). Sucrose phosphate synthase (SPS), sucrose synthase (SUS) and their products in the leaves of *Miscanthus giganteus* and *Zea mays* at low temperature. *Planta*, *252*: 23.

Liu, G; Yang, Z; Du, J; He, A; Yang, H; Xue, G; Yu, C and Zhang, Y (2020). Adding NBPT to urea increases N use efficiency of maize and decreases the abundance of N-cycling soil microbes under reduced fertilizer-N rate on the North China Plain. *PLoS ONE*, *28*: 13.

Melisa, P; E T S and Hanudin, E (2018). Effects of urease inhibitor and nitrification inhibitor on the nitrogen losses, physiological activity and oil palm yield on red-yellow podzolic. *Agric. Sci.*, *3*: 127-134.

Ministry of Agriculture (2019). *Tree Crop Estate Statistics of Indonesia 2018-2019*. Directorate General of Estate Crops. Jakarta, Indonesia. 68 pp.

Nurwahyuni, E and Putra, E T S (2020). Calcium addition improving pectin level in oil palm seedlings (*Elaeis guineensis* Jacq.). *J. Penelitian Kelapa Sawit*, *28*: 168-179.

Nurwahyuni, E and Putra, E T S (2021). The role of calcium in drought stress response induced through antioxidant activity in oil palm (*Elaeis guineensis* Jacq.) seedlings. *Menara Perkebunan*, *89*: 51-61.

Putra, E T S; Purwanto, B H; Wulandari, C and Alam, T (2021). Metabolic activities of eight oil

palm progenies grown under aluminium toxicity. *Biodiversitas*, *22*: 3146-3155.

Rahman, N; Bruun, T B; Giller, K E; Magid, J; Ven, G W J and Neergaard, A (2019). Soil greenhouse gas emissions from inorganic fertilizers and recycled oil palm waste products from Indonesian oil palm plantations. *GCB Bioenergy*, *11*: 1056-1074.

Rasid, M N A; Chek, T C and Redzuan, A F (2014). Effectiveness of urea-coated fertilizer on young immature oil palm growth. *Adv. Agric. Technol.*, *1*: 56-59.

Rendana, M; Rahim, S A; Idris, W M R; Lihan, T and Rahman, Z A (2016). Mapping nutrient status in oil palm plantation using geographic information system. *Asian J. Agric. Res.*, *10*: 144-153.

Riyadi, A S; Putra, E T S and Hanudin, E (2020). The influence of urease and nitrification inhibitor on loss of N and oil palm harvest in peat. *IPAS, 5*: 110-116.

Sakata, R; Shimada, S; Arai, H; Yoshioka, N; Yoshioka, R; Aoki, H; Kimoto, N; Sakamoto, A; Melling, L and Inubushi, K (2015). Effect of soil types and nitrogen fertilizer on nitrous oxide and carbon dioxide emissions in oil palm plantations. *Soil Sci. Plant Nutr.*, *61*: 48-60.

Sari, N Y and Putra, E T S (2019). Contribution of calcium to changes leaf anatomy character of oil palm seedlings (*Elaeis guineensis* Jacq.) under drought stress. *Agric. Sci.*, *4*: 23-32.

SAS Institute (2013). *SAS System for Windows 9.4*. SAS Institute, Inc., North Carolina, USA.

Smith, J L; Halvorson, J J and Papendick, R I (1993). Using multiple variable indicator kriging for evaluating soil quality. *Soil Sci. Soc. Am. J.*, *57*: 743-749.

Suryanto, P; Faridah, E; Nurjanto, H H; Putra, E T S; Kastono, D; Handayani, S; Boy, R; Widyawan, M H and Alam, T (2022). Short-term effect of *in situ* biochar briquettes on nitrogen loss in hybrid rice grown in an agroforestry system for three years. *Agron.*, *12(3)*: 564.

Suryanto, P; Faridah, E; Triyogo, A; Kastono, D; Suwignyo, B; Nurmalasari, A I and Alam, T (2020). Designing of soil quality and climate assessment tool for sustainable production of signalgrass (*Brachiaria brizantha*) silvopasture system in mountain ecosystems. *Aust. J. Crop Sci.*, *14*: 614-621.

Takahashi, H; Xiaohua, Q; Shimamura, S; Yanagawa, A; Hiraga, S and Nakazono, M (2018). Sucrose supply from leaves is required for parenchymatous phellem formation in hypocotyl of soybean under waterlogged conditions. *Ann. Bot*, *121*: 723-732.

Welham, S J; Gezan, S A; Clark, S J and Mead, A (2015). *Statistical Methods in Biology: Design and Analysis of Experiments and Regression*. CEC Press, Boca Raton, USA. 602 pp.

Widyawan, M H; Hasanah, A; Sayekti, R R R S; Wulandari, R A; Alam, T; Taryono and Pramana, A A C (2020). Multivariate analysis unravel genetic diversity and relationship between agronomic traits, protein, and dietary fiber in yardlong bean (*Vigna unguiculata* subsp. *sesquipedalis* Verdc.). *Biodiversitas*, *21*: 5662-5671.

Woittiez, L S; van Wijk, M T; Slingerland, M; van Noordwijk, M and Giller, K E (2017). Yield gaps in oil palm: A quantitative review of contributing factors. *Eur. J. Agron.*, *83*: 57-77.

Zanin, L; Venuti, S; Tomasi, N; Zamboni, A; Francisco, R M D B; Varanini, Z and Pinton, R (2016). Short term treatment with the urease inhibitor N-(n-butyl) thiophosphoric triamide (NBPT) alters urea assimilation and modulates transcriptional profiles of genes involved in primary and secondary metabolism in maize seedlings. *Front. Plant Sci.*, *7*: 845.

Zhang, L; Sun, S; Liang, Y; Li, B; Ma, S; Wang, Z; Ma, B and Li, M (2021). Nitrogen levels regulate sugar metabolism and transport in the shoot tips of crabapple plants. *Front. Plant Sci.*, *12*: 626149.

Zuki, M M; Md. Jaafar, N; Sakimin, S Z and Yusop, M K (2020). N-(n-butyl) thiophosphoric triamide (NBPT)-coated urea (NCU) improved maize growth and nitrogen use efficiency (NUE) in highly weathered tropical soil. *Sustain.*, *12*: 8780.

Journal of Oil Palm Research Vol. 35 (4) December 2023 p. 616-625
DOI: https://doi.org/10.21894/jopr.2022.0079

GEOSTATISTICAL ASSESSMENT OF HEAVY METALS AND NUTRIENTS AVAILABILITY IN SOIL OF OIL PALM PLANTATION AFFECTED BY BAUXITE MINING

MAZIDAH ZULKIFLI[1]; NUR SHUHADA MUHAMAD TAJUDIN[1]*; MOHD FUAD MISKON[2]; FIKRIAH FAUDZI[2] and NURUL MAYZAITUL AZWA JAMALUDIN[3]

ABSTRACT

This study describes the contamination of heavy metals (Cu, Zn, Mn, Pb and Fe) and their effect on K, Ca and Mg availability in oil palm cultivated areas affected by bauxite mining activities using the combinations of geostatistic and geospatial analysis. A total of 64 soil samples were collected covering a total area of 420.21 ha by grid sampling technique. Spatial distributions of the heavy metals were determined using semivariogram and mapped using ArcGIS. The mean concentrations of Cu (138.94 ± 79.08 mg kg^{-1}), Zn (233.55 ± 79.16 mg kg^{-1}), Mn (847.88 ± 267.02) mg kg^{-1}) and Fe (249 703.71 ± 101 408.72 mg kg^{-1}) in this study were greater than the background values, the 95% 'Investigation Levels' determined for Malaysia soil and Dutch target values. Geoaccumulation index showed that the contamination was in the order of Fe> Cu>Pb>Zn> Mn. Semivariogram analysis of pH, Mn, Zn and Fe was aligned with the principal component analysis results, showing the contamination source originated from a similar identical source. In correlation to the nutrients, only $K_{ex.}$, was found to be affected by the contaminants. These results provide a useful basis for the related agencies in identifying hotspots for future rehabilitation programs.

Keywords: geoaccumulation index, geospatial, GIS, PCA.

Received: 27 December 2021; **Accepted:** 6 October 2022; **Published online:** 22 December 2022.

INTRODUCTION

The palm oil industry is a prominent contributor to Malaysia's economy. In 2020, oil palm planted area in Malaysia was approximately about 5.87 million hectares in Peninsular Malaysia covering about 2.74 million hectares, while Sabah and Sarawak were 1.54 million hectares and 1.55 million hectares, respectively (MPOC, 2020). After Johor, Pahang had the second-largest oil palm plantation (732 052 ha).

[1] Department of Plant Science, Kulliyyah of Science, International Islamic University of Malaysia (IIUM), 25200 Kuantan, Pahang, Malaysia.

[2] Department of Marine Science, Kulliyyah of Science, International Islamic University Malaysia (IIUM), 25200 Kuantan, Pahang, Malaysia.

[3] Laboratory of Climate-Smart Food Crop Production, Institute of Tropical Agriculture and Food Security, Universiti Putra Malaysia, 43400 Serdang, Selangor, Malaysia.

* *Corresponding author e-mail: nurshuhada@iium.edu.my*

In 2014, bauxite mining activities in Pahang received a lot of public attention. A total of 18 000 ha of land in Kuantan had been extensively used for bauxite mining purposes including the area of oil palm plantations. The mining operation has been reported to cause land subsidence, which destroyed the soil aggregation and caused environmental damages such as loss of topsoil and a decline in soil fertility due to erosion (Amanah and Yunanto, 2021; Prematuri *et al.*, 2020). During the mining process, about 20 m of soil surface was stripped to obtain bauxite ores, which caused the soil to lose its crucial topsoil layer. This inevitably resulted in the declining amount of organic layers in the soil, which is the integral site of nutrient storage and exchange. The loss of this layer will affect nutrient absorption and their availability to the crops, which ultimately results in declining yield production (Zhang *et al.*, 2020). Additionally, mining operations also alter soil chemical properties and pH values. Changes in pH will affect the availability of soil heavy metals

(HMs) and cause toxicity symptoms to the oil palm trees. Studies conducted by Kusin *et al.* (2016) reported that sediments affected by bauxite mining activities in Kuantan had a higher content of As in a few localities with a value of about 8 mg kg^{-1}, where the source of contamination was identified to be from the mining exploration that mobilised the As. Analysis of geoaccumulation index (I_{geo}) classified the As as slightly polluted in the study area. Other HMs were within the permissible values. However, slightly higher amounts of Mg, Na, Al, Fe, As and Pb was observed in the water bodies nearby. The study stated that anthropogenic sources such as fertilisers and chemical industry effluent could be the sources of the contamination. This can also be influenced by open-cast bauxite mining, which caused the soil surface to be eroded and carried to adjacent rivers.

Geostatistics and geographic information system (GIS) techniques have been widely employed to quantify the spatial distribution of soil properties to reduce uncertainties, minimising costs and to identify pollution sources, especially in areas of mined soil (Chen *et al.*, 2021; Kulikova *et al.*, 2019). It has additional advantages in research as its analysis includes the characteristics of space and time changes. Through these, researchers can effectively determine the relationship between HMs indicators and their potential sources of pollution (Shen *et al.*, 2021; Xu *et al.*, 2021; Zhang and Yang, 2017). Research related to HMs contamination in oil palm plantations impacted by bauxite mining is crucial. A visit to the study site revealed that the mined region was left abandoned without any rehabilitation efforts. Thus, preliminary data on soil quality is needed to assess the impact of bauxite mining on the surrounding oil palm plantation areas. The outcome of this study can be used for future rehabilitation and oil palm replanting program. With the aid of geospatial technologies, researchers are able to simplify the process of interpreting data in quantifying variability in the field. The aims of this research were: (a) to determine the contents of selected soil HMs, which are Cu, Zn, Mn, Pb and Fe in bauxite mining and oil palm cultivated area and their effect on selected macronutrient availability, (b) to evaluate the contamination of soil HMs (Cu, Zn, Mn, Pb and Fe) using multivariate statistical analysis and environmental index, and (c) to quantify and generate a spatial map of HMs (Cu, Zn, Mn, Pb and Fe) using geostatistical and geospatial analysis.

MATERIALS AND METHODS

Study Area

The study was conducted in Bukit Goh, Kuantan, Pahang, located between latitude 3°55′30″ to 3°55′0″ N and longitude 103°16′0″ to 103°17′0″ E, covering 420.21 ha (*Figure 1*). Bauxite mining and oil palm cultivation activities covered approximately 204.88 ha and 215.33 ha of the study area, respectively. The soil was categorised into Kuantan soil series, which is very fine, oxidic, isohyperthermic and brown Tipik Akrolemoks. The drainage was slightly excessive with deep soil profile (>2 m depth) and had a gently undulating terrain (4%-20% or 2-10° slopes) over quaternary basalts. The annual rainfall was about 2400 mm yr^{-1} with an average temperature of 28°C.

Soil Sampling and Analysis

Soil sampling was performed using systematic sampling technique based on a regular grid size of 300 x 300 m within the study area. A total of 64 soil samples were collected using a corer at depth of 0-20 cm. Each sampling position was recorded using global positioning system (GPS) (GPSMAP 64s, Garmin, USA).

Soil samples were air-dried, ground and subsequently sieved (<2.00 mm). Soil pH was determined using potassium chloride (KCl) with 1:2.5 ratio. Total organic carbon (TOC) was determined using Walkley-Black dichromate methods (Walkley Black, 1934). Soil exchangeable K, Ca and Mg were extracted using Mehlich 3 procedures (Mehlich, 1984), which is suitable for acidic soil type. Total content of Cu, Zn, Mn, Pb and Fe were digested using mixed acid with ratio of 3: 3.5: 3.5; HF: HNO_3: HCl and analysed by using inductively coupled plasma mass spectrometry (ICP-MS) (Elan 9000, Perkin Elmer, USA). For quality and precision assurance of the analysis, reference material (SRM 1694a) of National Institute of Standards and Technology (NIST) was used. The percentage of recovery for the metals studied ranged between 85% and 120%. Duplicate samples and blanks for each sample were performed to ensure the precision and accuracy of the analysis.

Statistical Analysis

All statistical analyses were performed using SPSS package version 26.0 and were tested using normality test of Shapiro-Wilk. As the data were of the compositional geological component, non-normal distribution data were logarithm transformed. The degree of soil variability in the study area, was evaluated through the coefficient of variation (CV) value. Ranking of the CV were categorised into three classes as in *Table 1* (Wilding, 1985).

Geostatistical Analysis Based on GIS

The HMs spatial interpolation was done using ArcGIS v.10.8. The normality of soil HMs concentrations in this study was assessed through the Kolmogorov-Smirnov (K-S) test and non-normal data were transformed using the log transformation

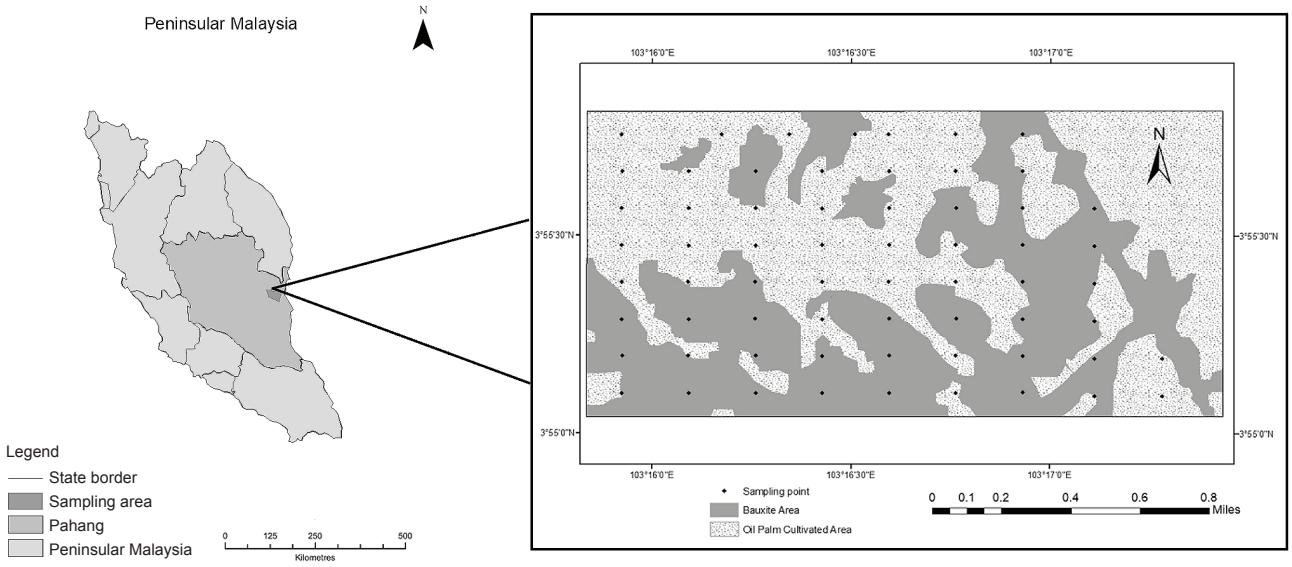


Figure 1. Location of study area in Kuantan, Pahang, Malaysia and the soil sampling points.

TABLE 1. RANGE OF COEFFICIENT OF VARIATION

CV (%)	Class
X < 15	Low variability
15 ≤ X ≤35	Moderate variability
X > 35	High variability

Source: Wilding (1985).

method. Experimental semivariogram was fitted using theoretical models; exponential, linear, spherical and gaussian models. A semivariogram is expressed using the regionalised variable theory and intrinsic hypotheses (Nielsen and Wendroth, 2003) as Equation (1):

$$\gamma(h) = \frac{1}{2N(h)} \sum_{i=I}^{N(h)} [Z(x_i) - Z(x_i + h)]^2 \quad (1)$$

where $Z(x_i)$ is the value of the variable Z at location of x_i, h the lag and N(h) the number of pairs of sample points separated by h. Theoretical semivariograms were used to fit the empirical semivariogram models to generate geostatistical parameters, such as structured variance (C_1), nugget variance (C_0), and sill variance ($C_0 + C_1$) and distance parameter (h). The fitted model was adopted based on high R^2 (> 50%) and low residual sum square (RSS) (Wang *et al.*, 2021). Ordinary kriging interpolation was employed after semivariogram models were constructed.

Geoaccumulation Index (I_{geo})

Geoaccumulation Index (I_{geo}) for HMs assessment was developed according to the world wide standard shale values (Muller, 1969). This index is denoted as Equation (2):

$$I_{geo} = log_2 \left[\frac{C_n}{1.5\, B_n} \right] \quad (2)$$

where C_n is the measured concentration of the element in soil, B_n is the value of geochemical background and the fix 1.5 value used to investigate natural changes in the level of a certain chemical in the environment and to identify extremely minor anthropogenic influences. Muller (1969) classified and described the Geoaccumulation Index (I_{geo}) into classes (*Table 2*).

RESULTS AND DISCUSSION

Statistical Analysis

Table 3 shows the descriptive statistics of soil pH and contents of selected HMs examined. The HMs in soil of the study areas were compared and referred to the natural background values published by Wedepohl (1995), Dutch target and intervention values for soil remediation (Dutch Target and Intervention Values, 2000), which has been widely used in HMs studies (Rudzi *et al.*, 2018) and the 95% 'Investigation Levels' determined for Malaysia soil (Zarcinas *et al.*, 2004).

The soil pH of the study area ranged between 3.65 to 4.82, indicating acidic conditions. This is similar to the pH of post mining soil reported by Prematuri *et al.* (2020), with value of 4.52 ± 0.09. Soil pH is one of the most important elements that controls cation mobility and governs HMs solubility in soil (Li *et al.*,

TABLE 2. I_{GEO} CLASSES

Class	Value	Soil quality
0	$I_{geo} \leq 0$	Uncontaminated
1	$0 \leq I_{geo} \leq 1$	Uncontaminated to moderately contaminated
2	$1 \leq I_{geo} \leq 2$	Moderately contaminated
3	$2 \leq I_{geo} \leq 3$	Moderately to heavily contaminated
4	$3 \leq I_{geo} \leq 4$	Heavily contaminated
5	$4 \leq I_{geo} \leq 5$	Heavily to extremely contaminated
6	$I_{geo} \geq 5$	Extremely contaminated

availability in the environment is influenced by anthropogenic activities, while CV less than 15% may only be occurred by the natural process such as geological and weathering factors. From the results, only soil pH showed a low variability (CV<15%), which indicated its changes within the study area were caused by natural factors such as climate, weathering process, topography and geological factors. While, Zn and Mn showed a moderate variability, with values of 33.63% and 31.49%, respectively, Cu, Pb and Fe showed a higher CV. This suggested that anthropogenic sources, such as

TABLE 3. SUMMARY STATISTICS OF SELECTED SOIL PROPERTIES AND HEAVY METALS CONTENT IN SOIL OF THE STUDY AREA (n=64)

Item	Range	Mean ± SD	CV (%)	Skewness	Kurtosis	Other studies references		
						a	b	c
pH	3.65 - 4.82	4.18 ± 0.28	6.59	0.02100	-0.91			
TOC	0 - 1.80	0.43 ± 0.33	76.19	1.63000	4.36			
Cu (mg kg^{-1})	22.86 - 315.37	138.94 ± 79.08	56.47	0.38000	-0.98	25.0	50	36
Zn (mg kg^{-1})	74.82 - 377.37	233.55 ± 79.16	33.63	-0.20000	-0.99	65.0	95	140
Mn (mg kg^{-1})	348.37 - 1425.11	847.88 ± 267.02	31.49	-0.00016	-0.32	716.0	n.a	n.a
Pb (mg kg^{-1})	17.60 - 171.06	57.58 ± 23.91	41.19	1.66000	6.87	14.8	65	85
Fe (mg kg^{-1})	23 459.12 – 446 985.00	249 703.71 ± 101 408.72	40.29	-0.25000	-0.66	43 200.0	n.a	n.a

Source: (a) Continental crust value (Wedepohl *et al.,* 1995), (b) The 95% 'Investigation Levels' determined for Malaysia soil (Zarcinas *et al.,* 2004), and (c) Dutch Target and Intervention Values for soil remediation (Dutch Target and Intervention Values, 2000).

2022). Lower value of soil pH in oil palm plantation is common due to the regular application of chemical and ammonium based fertiliser, high decomposition of organic materials, nutrients uptake by oil palm and other agricultural practices. Although oil palm is relatively tolerant to acidic soil, attention should be given as soil with low pH could result in unbalance nutrient and further could cause toxicity effect. At low soil pH, the availability of acidic cations such as Fe, Cu, Zn, Mn will be higher at the CEC site and this will supress the availability of K, Ca and Mg.

The content of Cu, Zn, Mn, Pb and Fe were greater than the background values (Wedepohl, 1995). This indicated that the soil of the bauxite mining and oil palm cultivated area could be possibly contaminated with Cu, Zn, Mn, Pb and Fe. However, in comparison to the Dutch target and intervention values for soil remediation and the 95% 'Investigation Levels' determined for Malaysia soil, the mean content of Pb obtained in this study was found to be lower. The content of Cu and Zn was two to three times higher than the Dutch target value and the 95% 'Investigation Levels' determined for Malaysia soil.

The coefficient of variation (CV) value aids in determining the HMs variability (*Table 1).* For HMs with CV greater than 35%, it is suggested that their mining and agricultural practises including the use of fertilisers, manures, pesticides, and the removal of the top soil layer could be the cause of Cu, Pb and Fe accumulation.

Analysis of Pearson Correlation

For analysis of Pearson correlation, the data were logarithm transformed and fitted to normality. The correlation analysis showed that Cu, Zn and Mn had a significant positive correlation with Fe at $p<0.01$ of 0.82, 0.63 and 0.75, respectively (*Table 4*) suggesting the possibility of their common origin. Abundant amount of this HMs might be bound together with Fe in the parent material of the soil as it is the major component of oxisols soil. The significant positive correlation between the HMs explained that the contamination of the HMs in the soil could be possibly from similar sources of contamination (Doabi *et al.,* 2019). The correlation coefficients between Cu-Zn, Cu-Mn, Cu-Fe, Zn-Mn, Zn-Fe and Mn-Fe were relatively larger than 0.5, explaining a strong correlation among the HMs, indicating a homologous sources of contamination (Wang *et al.*, 2021). However, Pb did not show any significant correlation with the HMs. It can be hypothesised that Pb could be primarily

TABLE 4. PEARSON'S CORRELATION COEEFICIENT OF THE SOIL HMs (n=64)

	Correlation matrix[a]						
	pH	TOC	Cu	Zn	Mn	Pb	Fe
pH	1.000	-.276	.236	.226	.149	.189	.207
TOC		1.000	-.166	-.189	-.214	-.185	-.162
Cu			1.000	**.849***	**.808***	.200	**.815***
Zn				1.000	**.754***	.462	**.627***
Mn					1.000	.263	**.745***
Pb						1.000	-.045
Fe							1.000

Note: Correlation is significant at the 0.01 level (2-tailed).

generated from lithogenic or other point sources of contamination.

Further analysis by using PCA found that two eigenvalues were obtained (F1 and F2), with a total variance of 68.29% (*Table 5*). The first factor (F1) had 49.80% of the total variance and was significantly loaded with Cu, Zn, Mn and Fe. Copper had the most significant loads with value of 0.94 followed by Fe, Mn and Zn. The same trend had been initially observed during the correlation analysis, where a significant relationship was found among Zn, Mn, Fe with Cu. Significant correlation obtained among F1 indicated their homologous origin, probably from anthropogenic sources, notably from the mining activities, long term agricultural practices, applications of chemical fertilisers and acceleration of soil geochemical weathering that could be caused by the long-term mining exposure. The second factor, F2, was dominated by pH and Pb, which accounts 18.50% of the total variance. The sources of contamination in the study area could be classified into two categories based on the results obtained.

TABLE 5. ROTATED COMPONENT MATRIX FOR THE SOIL HMs (n=64)

Element	Component	
	1	2
pH	0.194	**0.575**
TOC	-0.169	-0.169
Cu	**0.944**	0.091
Zn	**0.805**	0.365
Mn	**0.883**	0.154
Pb	-0.069	**0.788**
Fe	**0.920**	0.014
Eigenvalue	3.487	1.293
Variance contribution rate (%)	49.813	18.472
Cumulative variance contribution rate (%)	49.813	68.285

Geostatistic and Semivariogram Analysis

Semivariogram analysis showed that pH, Cu and Fe fit to the spherical model, while Mn and Pb fit to the exponential model (*Table 6*). Whereas Zn fits to the Gaussian model and lastly, TOC fits to the linear model. The nugget variance ranged from 1.00 x 10^{-5} to 0.19. The obtained values were less than 30% of the sill value, indicating good spatial continuity and minimal measurement errors (Paz-Gonzalez *et al.*, 2001).

Range value indicates the distance by which the HMs content change. The range obtained from the semivariogram analysis varied between 119 to 1262 m, with the lowest being in Pb followed by Zn, Mn, pH, Cu, Fe and TOC. The TOC had a longer effective range (1262 m) indicating that TOC had a better spatial structure and less variation caused by extrinsic factors. The soil range for pH, TOC, Cu and Fe exceeded the distance of 300 m between points. Nevertheless, Zn, Mn and Pb had range value less than 300 m, suggesting a closer sampling procedure should be done in future.

A quotient level of spatial distribution (X) in this sample was categorised into three different levels; < 25% resembles strong spatial dependence, 25%> X > 75% resembles moderate spatial dependence and X > 75% resembles weak spatial dependence (Cambardella *et al.*, 1994). Nugget to sill ratio indicates whether the geographical distribution of HMs is due to intrinsic or external reasons (Guan *et al.*, 2017). The soil pH, Mn, Zn, Pb and Fe were observed to have strong spatial autocorrelations indicating that natural factors were responsible for their distributions in the studied area. However, TOC and Cu showed a moderate spatial dependence reflecting their distributions could be from the mixed inputs of natural and anthropogenic sources. The semivariogram analysis revealed that Mn, Zn and Fe were grouped together in the same group as PCA, indicating identical contamination causes. However, pH, Pb and Cu had a contradictory results with the PCA. This could be due to the robust estimation of semivariogram, which is more extensive than PCA as it considers each data's coordinates (geographically). Semivariogram calculates and compares data points in all directions. Numerous internal factors such as pH, organic matter content, texture, redox state influenced the HMs dynamics in soil. These soil characteristics are thought to be a significant source of variation for HMs. Discussing about HMs distributions, the variation existed in the study area could be due to two soil-forming factors; the geological nature of the rock and topographic influences. In a small scale and stable natural landscape, such as in the study area, the parent material can be said to be homogenous, suggesting that topography could be the only source of variation. The studied area is characterised by a

TABLE 6. BEST FITTED SEMIVARIANCE MODELS AND THEIR PARAMETERS

Parameter	Nugget variance C_0	Structural sill (C_0+C)	Range A (m)	Nugget to sill ratio $C_0/(C_0+C)$ (%)	R^2	RSS	Model variogram model type
pH	1.0×10^{-5}	4.6×10^{-3}	613.00	**0.22**	0.95	3.145×10^{-7}	Spherical
TOC	0.0810	0.12	1262.91	**68.00**	0.52	6.08×10^{-4}	Linear
Cu	0.1900	0.45	903.00	**42.00**	0.98	5.43×10^{-4}	Spherical
Mn	0.0090	0.12	291.00	**7.50**	0.74	8.25×10^{-5}	Exponential
Zn	0.0120	0.15	167.00	**8.00**	0.87	2.21×10^{-4}	Gaussian
Pb	0.0085	0.16	119.00	**5.30**	0.77	2.70×10^{-5}	Exponential
Fe	0.0010	0.33	1 160.00	**0.30**	0.97	1.75×10^{-3}	Spherical

hilly topography with moderate slope. Irregular terrain and various activities conducted such as mining and long-term agricultural practices, may all be the factors in the circumstance, where soil is exposed to activities that are made by humans. Natural geochemical processes such as weathering can be accelerated through human anthropogenic activities by the changes and disturbance in soil chemical conditions such as pH, organic matter content and redox state. This will allow the stable mineral to become soluble and mobile in the environment. Therefore, we assume that in this study, soil forming factors, parent material, topography and human factors may influence the spatial variability of HMs.

Kriging Interpolation

The spatial distributions of pH, TOC, Cu, Zn, Mn, Pb and Fe are visualised in *Figures 2a - 2g*. The soil of the study area was classified as acidic, ranging from 3.60 to 4.82. Low soil pH in the study area is expected to cause adverse effect to the oil palm's growth and development. It also affect the availability of soil K, Ca and Mg as the cation exchange site will be dominated by the ion H^+. In addition, it will also increase the toxicity and mobility of HMs (Olafisoye *et al.*, 2020).

The distribution of TOC showed that organic carbon were found low throughout the studied region. This could be caused by the removal of the top soil layers for the mining purposes (Lee *et al.*, 2017). The lower TOC content indicates insufficient organic matter in the soil. Organic matter in soil is essential as it creates a good soil structure and promoted microbial activities. By enhancing the aggregate stability, the soil water infiltration, holding capacity and aeration will be improved. Contrasted to soil with poor porosity and high bulk density value, the growth of the crops such as oil palm will be impeded. In addition, poor soil water holding capacity and infiltration will also eventually cause mud floods to the plantation area and this will inevitably impede the oil palm growth and lead to a lower yield.

A total of 92.5% of the study area had elevated levels of Cu (*Figure 2c*). Only about 18.0% of area in *Figure 2c* showed a non-contaminated region, with Cu lower than 36 mg kg^{-1}. Most of agricultural soil contaminated by HMs were reported to be associated with the application of phosphate fertilisers (Wong *et al.*, 2017). Although the levels of trace elements in the fertilisers were within permissible limits, the accumulation of leached residues is still a worry. Copper-based fungicides and pesticides also are the main source of Cu contamination in agricultural soil (Apori *et al.*, 2018). Copper resides on the surface of plant tissues and can be washed off resulting to a higher Cu content in soil.

The distributions of Zn showed that almost 90.0% of the study area had Zn higher than 140 mg kg^{-1}. According to Ismail *et al.* (2018), Zn is naturally abundant in sedimentary rocks and this may be the reason for the higher distribution of Zn observed. The region with higher Zn level was in the area of bauxite mining rather than the oil palm cultivated area. This could be the consequence of the extensive mining operations that exposed the soil without cover crops. Once the land was left barren, the soil was exposed to an extensive weathering process. This leads to modification of soil chemical properties and resulted in availability of HMs to the environment.

Manganese was found higher at the northern and central part of the study area (*Figure 2e*). More than 70% of the study area had Mn higher than 716 mg kg^{-1}. Manganese is also a component of the silicate mineral structure and one of the most common and widely distributed metals in nature. It can be commonly found in the structure of rocks and soils (Ismail *et al.*, 2018). Nevertheless, the source of Mn might also be from the Mn-containing fertilisers used in the oil palm cultivation area. Low soil pH will intensify Mn toxicity and will cause necrotic lesion to the oil palm fronds and restrict nutrients availability.

Almost 100% of the study area (*Figure 2f*) had lower content of Pb compared to the Dutch target and intervention values for soil remediation. Sources of Pb in the soil was not known specifically.

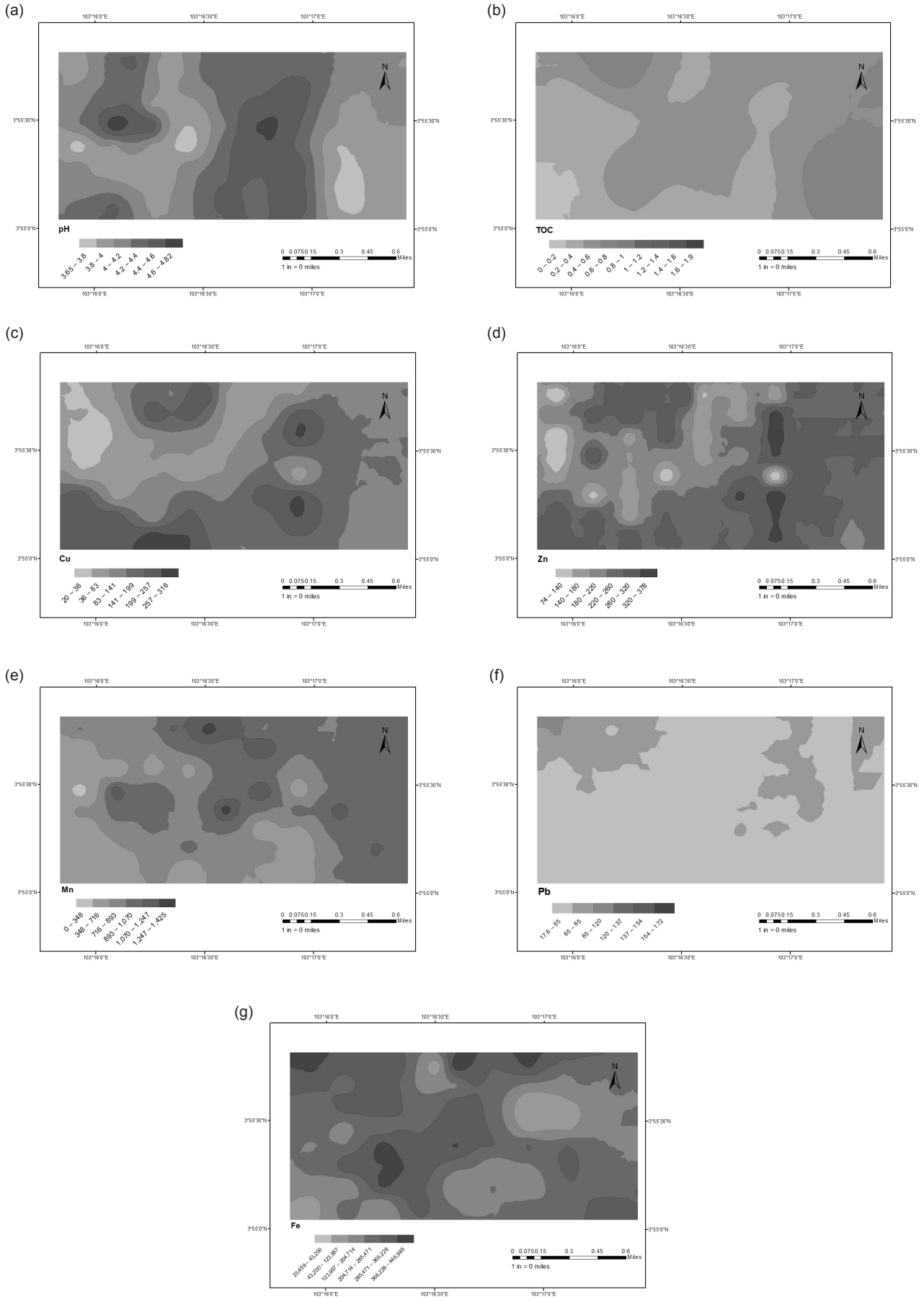


Figure 2. Spatial distribution of heavy metals in soil (a) pH, (b) TOC, (c) Cu, (d) Zn, (e) Mn, (f) Pb and (g) Fe.

However, its availability can be from the exhaust of automobiles, fertilisers and pesticides (Yang *et al.*, 2018).

A total of 100% of the study region had Fe greater than the background values. Soil of Kuantan series is composed of geothite (FeOOH) and hematite (Fe_2O_3), where the main component of their silicate mineral is the Fe element. Optimum amount of Fe in soil will enhance the nutrients uptakes by the plant. However, elevated level of Fe will cause toxicity effect and restrict the oil palm development (Nurmalasari *et al.*, 2016). Iron contamination has the ability to alter the plant's morphology, anatomy, and physiology. To reduce the toxicity occurrence, it is crucial to maintain the pH around neutral conditions and avoid pH lesser than 4.5.

The spatial distribution maps depict the study area with several zones of HMs concentration. With the aid of the map, nutrient site-specific management program and rehabilitation strategy can be developed. In addition, the contaminated area also can be measured quantitatively and this allows the government and related agencies to conduct a cost-effective analysis for a land restoration programme based on the identified area.

Macronutrients Availability

Oil palm yield and growth are significantly influenced by soil nutrients. *Table 7* shows the content of available nutrients; $K_{ex.}$, $Ca_{ex.}$ and $Mg_{ex.}$. The mean values of $K_{ex.}$ and $Mg_{ex.}$ were compared to the values suggested for oil palm published by Goh (1977). The mean of $K_{ex.}$ was slightly lower compared to $Ca_{ex.}$ and Mg_{ex}. This could be caused by the higher contents of $Ca_{ex.}$ and $Mg_{ex.}$ observed throughout the study area. Elevated level of $Ca_{ex.}$ and Mg_e reduced the possibility of $K_{ex.}$ being attached to the cation exchange site as Ca and Mg had a higher affinity attached to the CEC site.

The CV values for $K_{ex.}$, $Ca_{ex.}$ and $Mg_{ex.}$ were more than 35%, denoting high variability. This could be caused by the application of fertilisers especially in the oil palm cultivated area. Factors of uneven topography and human activities caused the cations to be easily leached and mobile throughout the study area.

The $K_{ex.}$, $Ca_{ex.}$ and $Mg_{ex.}$ shows a positive but low coefficient value with TOC (p<0.05) (*Table 8*). The $K_{ex.}$, which was found low showed a negative correlation with Cu, Zn, Mn, Pb and Fe. This could be the effect of higher Cu, Zn, Mn, and Fe dominating the soil's cation exchange site. It led to the lower availability of soil to retain K^+. In addition, K^+ in soil has lower affinity for cation adsorption relative to Ca^{2+} and Mg^{2+}, which might result in lower K^+ value in the soil.

Geoaccumulation Index (I_{geo})

Figure 3 displays the results of the I_{geo} in the study area. The contamination was in the order of Fe> Cu> Pb > Zn> Mn. The Mn was categorised as "uncontaminated" as the I_{geo} value was less than 0.

The Cu, Zn, Pb and Fe of the soil in the study region were categorised into moderately contaminated. Iron showed the highest I_{geo} value with an average of 1.77 ± 0.80. It showed a consistent trend as initially high Fe was observed compared to the reference value. However, although Pb showed a lower distribution throughout the region, the I_{geo} value was 1.26 ± 0.59 reflecting a moderate contamination within the region.

CONCLUSION

The mean concentrations of Cu, Zn, Mn and Fe in the study area were found greater than the background values, the 95% 'Investigation Levels' determined for Malaysia soil and Dutch target values. Analysis by I_{geo} showed that the contamination was in the order of Fe> Cu> Pb> Zn> Mn. Only $K_{ex.}$, was

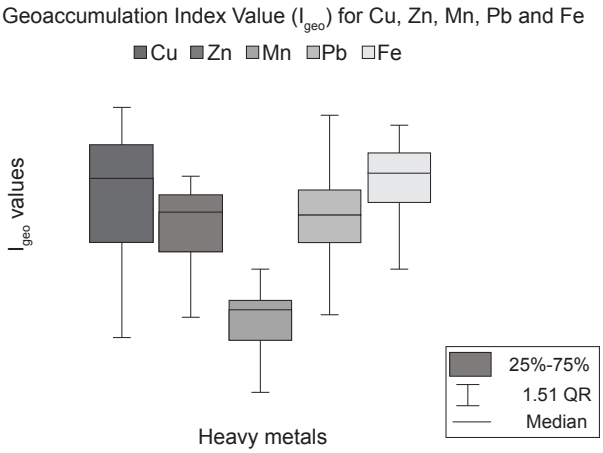


Figure 3. Boxplot of I_{geo} value for Cu, Zn, Mn, Pb and Fe with (n=64).

TABLE 7. DESCRIPTIVE STATISTICS OF SELECTED MACRONUTRIENTS IN SOIL OF THE STUDY AREA (n=64)

Nutrients	Mean ± STD (mg kg^{-1})	Range (mg kg^{-1})	Coefficient of variation (%)	Reference (Goh, 1977) (mg kg^{-1})		
				Very low	Low	Moderate
$K_{ex.}$	70.57 ± 45.49	0.55 - 190.37	64	<31.2	31.2 - 78.0	78.0 - 97.5
$Ca_{ex.}$	37.34 ± 41.57	0.00 - 149.26	110	n.a	n.a	
$Mg_{ex.}$	35.81 ± 18.72	3.05 - 139.75	52	<9.6	9.6 - 24.0	24.0 - 30.0

TABLE 8. PEARSON CORRELATION COEFFICIENTS OF HMS AND SELECTED MACRONUTRIENTS (n=64)

Nutrients	pH	TOC	Cu	Zn	Mn	Pb	Fe
K_{ex}	-0.08	0.19	-0.53	-0.44	-0.30	-0.02	-0.46
Ca_{ex}	-0.10	0.17	-0.45	-0.33	-0.34	0.06	-0.51
Mg_{ex}	-0.09	0.20	-0.47	-0.38	-0.39	0.05	-0.45

affected by the HMs contamination, while $Ca_{ex.}$ and $Mg_{ex.}$ showed a higher value and were not affected by the mining activities. The effectiveness of using multivariate statistical analysis and geostatistic in evaluating HMs concentration has been demonstrated in this study. It was identified that the availability of Mn, Zn, Cu, Fe and Pb in the study area could be from the natural component such as parent material and weathering processes. However, anthropogenic activities such as mining and agriculture practices had accelerated the HMs availability through soil properties changes and caused contamination. The geospatial mapping of HMs provides a good visualisation in determining hotspot areas of each HMs. In future, government and related agencies will be able to utilise the HMs variability map for soil rehabilitation program and implementing site specific fertilising scheme to enhance oil palm productivity.

ACKNOWLEDGEMENT

This research was funded by the MOHE under Fundamental Research Grant Scheme for Research Acculturation of Early Career Researchers (FRGS-RACER), IIUM (RACER/1/2019/WAB01/UIAM//1).

REFERENCES

Amanah, F and Yunanto, T (2021). Oil palm plantation in ex-coal mined site: A case study in East Kalimantan, Indonesia. *IOP Conf. Ser. Earth Environ. Sci., 918(1)*: 012049. DOI: 10.1088/1755-1315/918/1/012049.

Apori, O S; Hanyabui, E and Asiamah, Y J (2018). Remediation technology for copper contaminated soil: A review. *Asian Soil Res. J., 1(3)*: 1-7. DOI: 10.9734/ASRJ/2018/45322.

Cambardella, C A; Moorman, T B; Novak, J M; Parkin, T B; Karlen, D L; Turco, R F and Konopka, A E (1994). Field-scale variability of soil properties in Central Iowa soils. *Soil Sci. Soc. Am. J., 58(5)*: 1501-1511. DOI: 10.2136/sssaj1994.03615995005800050033x.

Chen, G; Yang, Y; Liu, X and Wang, M (2021). Spatial distribution characteristics of heavy metals in surface soil of Xilinguole coal mining area based on semivariogram. *ISPRS Int. J. Geo-Inf., 10*: 290. DOI: 10.3390/ijgi10050290.

Doabi, S A; Karami, M and Afyuni, M (2019). Heavy metal pollution assessment in agricultural soils of Kermanshah province, Iran. *Environ. Earth Sci., 78(3)*: 70. DOI: 10.1007/s10661-016-5225-3.

Dutch Target and Intervention Values (the New Dutch List) (2000). Annexes - circular on target values and intervention values for soil remediation. https://www.esdat.net/environmental%20standards/dutch/annexs_i2000dutch%20environmental%20standards.pdf, accessed on 16 August 2020.

Goh, K J (1977). Fertilizer recommendation systems for oil palm: Estimating the fertilizer rates. *Proc. of MOSTA Best Practices Workshops: Agronomy and Crop Management.* Malaysia. p. 235-268.

Guan, F Y; Xia, M P; Tang, X L and Fan, S H (2017). Spatial variability of soil nitrogen, phosphorus and potassium contents in Moso bamboo forests in Yong'an City, China. *Catena, 150*: 161-172. DOI: 10.1016/j.ecolind.2020.107285.

Ismail, S N S; Abidin, E Z; Praveena, S M; Rasdi, I; Mohamad, S and Ismail, W M I W (2018). Heavy metals in soil of the tropical climate bauxite mining area in Malaysia. *J. Phys. Sci., 29*: 7-14. DOI: 10.21315/jps2018.29.s3.2.

Kulikova, T; Hiller, E; Jurkovic, L; Filová, L; Šottník, P and Lacina, P (2019). Total mercury, chromium, nickel and other trace chemical element contents in soils at an old cinnabar mine site (Merník, Slovakia): Anthropogenic versus natural sources of soil contamination. *Environ. Monit. Assess., 191*: 263. DOI: 10.1007/s10661-019-7391-6.

Kusin, F M; Syazwan, M; Rahman, A and Madzin, Z (2016). The occurrence and potential ecological risk assessment of bauxite mine-impacted water and sediments in Kuantan, Pahang, Malaysia. *Environ. Sci. Pollut. Res., 24*: 1306-1321. DOI: 10.1007/s11356-016-7814-7.

Lee, K Y; Ho, L Y; Tan, K H; Tham, Y Y; Ling, S P; Qureshi, A M; Ponnudurai, T; Nordin, R and Cheah, J (2017). Environmental and occupational health impact of bauxite mining in Malaysia: A review. *Int. Med. J. Malays., 16(2)*: 137-150. DOI: 10.31436/imjm.v16i2.346.

Li, Q; Wang, Y; Li, Y; Li, L; Tang, M; Hu, W; Li, C and Ai, S (2022). Speciation of heavy metals in soils and their immobilization at microscale interfaces among diverse soil components. *Sci. Total Environ*., *825*: 153862. DOI: 10.1016/j.scitotenv.2022.153862.

MPOC (2020). Malaysian palm oil sector performance in 2020 and market opportunities. https://mpoc.org.my/malaysian-palm-oil-sector-performance-in-2020-and-market-opportunities/, accessed on 12 April 2022.

Mehlich, A (1984). Mehlich 3 soil test extractant: A modification of Mehlich 2 extractant, communications in soil science and plant analysis. *Commun. Soil Sci. Plant Anal., 15*: 1409-1416. DOI: 10.1080/00103628409367568.

Muller, G (1969). Index of geoaccumulation in sediments of the Rhine River. *Geo J., 2(1)*: 108-118.

Nielsen, D R and Wendroth, O (2003). Spatial and temporal statistics - sampling field soils and their vegetation. *GeoEcology Textbook*. Catena-Verlag. Reiskirchen Germany. 416 pp.

Nurmalasari, A I; Putra, E T S and Yudono, P (2016). Root morphology of eight hybrid oil palms under iron (Fe) toxicity. *Ilmu Pertanian (Agric. Sc.)*, *1(1)*: 13-18. DOI: 10.22146/ipas.11254.

Olafisoye, O B; Fatoki, O S; Oguntibeju, O O and Osibote, O A (2020). Accumulation and risk assessment of metals in palm oil cultivated on contaminated oil palm plantation soils. *Toxicol. Rep., 7*: 324-334. DOI: 10.1016/j.toxrep.2020.01.016.

Paz-Gonzalez, A; Taboada Castro, M T and Vieira, S R (2001). Geostatistical analysis of heavy metals in a one-hectare plot under natural vegetation in a serpentine area. *Can. J. Soil Sci., 81(4)*: 469-479. DOI: 10.4141/s00-095.

Prematuri, R; Turjaman, M; Sato, T and Tawaraya, K (2020). Post bauxite mining land soil characteristics and its effects on the growth of *Falcataria moluccana (Miq.)* Barneby & J. W. Grims and *Albizia saman* (Jacq.) Merr. *Appl. Environ. Soil Sc., 5:* 6764380.

Rudzi, S; Ho, Y and Kharni, A I (2018). Heavy metals contamination in paddy soil and water and associated dermal health risk among farmers. *Malaysian J. Med. Health Sci., 14(SP2)*: 2-10.

Shen, W; Hu, Y; Zhang, J; Zhao, F; Bian, P and Liu, Y (2021). Spatial distribution and human health risk assessment of soil heavy metals based on sequential Gaussian simulation and positive matrix factorization model: A case study in irrigation area of the Yellow River. *Ecotoxicol. Environ. Saf., 225*: 112752. DOI: 10.1016/j.ecoenv.2021.112752.

Walkley, A J and Black, I A (1934). Estimation of soil organic carbon by the chromic acid titration method. *Soil Sci., 37*: 29-38.

Wang, R; Zou, R; Liu, J; Liu, L and Hu, Y (2021). Spatial distribution of soil nutrients in farmland in a hilly region of the pearl river delta in China based on geostatistics and the inverse distance weighting method. *Agric. (Switz.), 11(1)*: 1-12. DOI: 10.3390/agriculture11010050.

Wedepohl, H K (1995). The composition of the continental crust. *Geochim. Cosmochim. Acta, 59(7)*: 1217-1232. DOI: 10.1016/0016-7037(95)00038-2.

Wilding, L P (1985). Soil spatial variability: Its documentation, accommodation and implications to soil surveys. *Soil spatial variability, workshop (Las Vegas NV 1984-11-30).* Pudoc, Wageningen, Netherlands. p. 166-194.

Wong, K W; Yap, C K; Nulit, R; Hamzah, M S; Chen, S K; Cheng, W H; Karami, A and Al-Shami, S A (2017). Effects of anthropogenic activities on the heavy metal levels in the clams and sediments in a tropical river. *Environ. Sci. Pollut. Res*., *24*: 116-134. DOI: 10.1007/s11356-016- 7951-z.

Xu, L; Zhao, Y; Wang, M and Jiang, Y (2021). Case study from Xuzhou area, Jiangsu, China. *Env. Pollut. Bioavail., 33(1)*: 326-333. DOI: 10.1080/26395940.2021.1987842.

Yang, Q; Li, Z; Lu, X; Duan, Q; Huang, L and Bi, J (2018). A review of soil heavy metal pollution from industrial and agricultural regions in China: Pollution and risk assessment. *Sci. Total Environ., 642(1)*: 690-700. DOI: 10.1016/j.scitotenv.2018.06.068.

Zarcinas, B A; Ishak, C F; McLaughlin, M J and Cozens, G (2004). Heavy metals in soils and crops in Southeast Asia. 1. Peninsular Malaysia. *Environ. Geochem. Health, 26(3)*: 343-357. DOI: 10.1007/s10653-005-4669-0.

Zhang, B and Yang, Y (2017). Spatiotemporal modeling and prediction of soil heavy metals based on spatiotemporal cokriging. *Sci. Rep., 7*: 16750. DOI: 10.1038/s41598-017-17018-5.

Zhang, H; Liu, W; Zhang, H; Fan, L and Ma, S (2019). Spatial distribution of soil organic matter in a coal mining subsidence area. *Acta Agric. Scand*., *70(2)*: 117-127. DOI: 10.1080/09064710.2019.1676916.

Journal of Oil Palm Research Vol. 35 (4) December 2023 p. 626-638
DOI: https://doi.org/10.21894/jopr.2022.0078

MOLECULAR SCREENING OF BASAL STEM ROT RESISTANCE GENES IN OIL PALM

MOHD AMIN AB-HALIM[1]; ROZANA ROSLI[1]; ENG TI LESLIE LOW[1]*; ZETI-AZURA MOHAMED-HUSSEIN[2] and RAJINDER SINGH[1]

ABSTRACT

Basal stem rot (BSR) is one of the main oil palm diseases that have led to tremendous losses in oil yields for almost a century. Having markers, especially those that are linked to resistance (R) genes could potentially alleviate this problem by providing the tools to select palms that are tolerant or resistant to the disease. This study aimed to develop oil palm genomic markers that can distinguish oil palm plants with different levels of resistance to BSR. We identified 144 homologous R genes in the oil palm genome based on the conserved domain structure of known R proteins. Six simple sequence repeat markers were identified and used to genotype 40 palms with different levels of resistance to BSR. The observed and effective number of alleles ranged from 2.00 to 7.00 and 1.57 to 4.30, respectively. The observed heterozygosity ranged from 0.13 to 0.67, with a mean of 0.46 while the expected heterozygosity ranged from 0.40 to 0.78, with a mean of 0.51. Analysis of genetic distances from the set of markers was able to differentiate susceptible and tolerant palm samples. These results may help in the early selection of durable BSR disease resistant oil palm cultivars.

Keywords: *Elaeis guineensis*, genetic distance, phylogenetic tree, R gene candidates, SSR.

Received: 14 October 2021; **Accepted:** 21 September 2022; **Published online:** 22 December 2022.

INTRODUCTION

Oil palm (*Elaeis guineensis*) is the most important commercial crop in Malaysia and Indonesia. The oil is suitable for the production of edible and non-edible oils, biodiesel, and nutritional and pharmaceutical products (Parveez *et al.*, 2021). The basal stem rot (BSR) disease, which was first described in 1915 in the Republic of Congo, West Africa (Wakefield, 1920), has caused significant losses to palm oil production as trees replanted on previously infected locations often die before reaching the optimum maturity age (Ariffin *et al.*, 2000). About 9.2% of Malaysian oil palm smallholders' replanted areas have been infected by the disease (Mohd Shukri *et al.*, 2020), and the *Ganoderma boninense* fungus was identified as the causal pathogen of the disease (Ho and Nawawi, 1985; Susanto *et al.*, 2005).

There are several methods used for early disease detection, from expert manual observation of basal stem decay and foliar symptoms (Turner and Gillbanks, 1974), isolation of the fungi using *Ganoderma* selective medium (GSM) (Ariffin and Idris, 1991) to remote sensing via spectroscopic image techniques using a sound sensor in GanoSken (Idris *et al.*, 2010), electrical resistance (ER) data (Nurnadiah *et al.*, 2014) and artificial neural networks (Ahmadi *et al.*, 2017). Nevertheless, no effective treatment or control for the BSR disease in oil palm is currently available (Naher *et al.*, 2015; Shamala *et al.*, 2008). The best practices in controlling the disease include field sanitation management, fungicidal treatment, and foliar supplement. But they require intensive labour especially to excavate stumps, followed by ploughing and rotavating the planting areas. A large-scale oil palm plantation requires a rapid and non-complex prevention system for the BSR

[1] Malaysian Palm Oil Board,
6 Persiaran Institusi, Bandar Baru Bangi,
43000 Kajang, Selangor, Malaysia.

[2] Department of Applied Physics,
Faculty of Science and Technology,
Universiti Kebangsaan Malaysia,
43600 UKM Bangi, Selangor, Malaysia.

[2] Centre for Bioinformatics Research,
Institute of System Biology (INBIOSIS),
Universiti Kebangsaan Malaysia,
43600 UKM Bangi, Selangor, Malaysia.

* *Corresponding author e-mail: lowengti@mpob.gov.my*

disease problem. Hence, developing planting materials with resistance to BSR caused by the fungus offers a long-term solution to control the disease (Hushiarian *et al*., 2013). Oil palm resistant to the fungal infection have not been found, but *G. boninense* inoculated oil palm progenies varied in disease severity (Idris *et al*., 2004). These results were used to classify samples to appropriate resistance levels.

In plants, genes that recognise invading pathogens and trigger the plant immune system are known as resistance (R) genes (Hammond-Kosack and Jones, 1997). Abundantly present in plant genomes, they are involved in pathogen interaction mechanisms that result in a signaling cascade to activate the plant's defence mechanism (Ellis and Dodd, 2003; Wanderley-Nogueira *et al.,* 2007). The 'zigzag' model by Jones and Dangl (2006) describes two approaches to the plant immune system. The first involves the transmembrane pattern recognition receptors (PRRs) which act as the first line of defence to arrest pathogen invasion in the extracellular space. These receptors include the Receptor-Like Protein (RLP) and Receptor-Like Kinase (RLK) classes of R genes (Sekhwal *et al.,* 2015). The second defence approach involves the Coiled-Coil (CC) or Toll/Interleukin Receptor (TIR)-Nucleotide-binding Site (NBS)-Leucine-Rich Repeat (LRR) and Kinase classes of R genes which interact with effector molecules from pathogens that successfully penetrate the cell wall (Song *et al.,* 1997). Successful recognition of effector molecules by R genes will trigger the host cell to activate the plant's defence mechanism. However, unrecognised interactions will most likely result in the host being susceptible to the disease. R genes, therefore, play an initial role in protection against pathogen invasion by detecting and initiating the plant's defense mechanisms against elicitor proteins (Ellis and Dodds, 2003).

The oil palm genome sequence was reported previously (Singh *et al.,* 2013), together with information on gene models for putative resistance genes. In this study, we used *GeneThresher*™ methylation filtered oil palm genomic sequence data, and a method for gene prediction and annotation that focuses on identifying resistance genes. The *GeneThresher*™ sequences are gene enriched sequences from the hypomethylated regions of the highly repetitive oil palm genome.

The purpose of this study was to develop a set of R genes associated genomic markers from the oil palm genome sequence. This set of markers were then used to genotype oil palm samples with different levels of resistance to the BSR disease. Clustering of the simple sequence repeat (SSR) profiles allowed identification of closely related samples and clustered profiles associated with BSR resistance levels.

MATERIALS AND METHODS

Plant Materials

Four hybrid crosses in MPOB Kluang Research Station, Johor that were previously classified based on their severity of foliar symptoms following *G. boninense* infection (Idris *et al.,* 2004) were used in this study. The most susceptible hybrid cross is the *dura* x *dura* (DxD) PK 2724 cross, with a death rate of 40% after *G. boninense* infection. The *dura* x *pisifera* (DxP) PK 2567 cross recorded the lowest death rate of 10%, and was thus designated as a partial resistant cross. Another DxP cross, PK2572, with a recorded death rate of 25% was classified as an intermediate group. The *tenera* x *tenera* (TxT) palms (PK 1708), with a death rate of 15%, were also classified as partial resistant palms.

Identification of Oil Palm Resistance Gene Candidates

A total of 139 120 *GeneThresher*™ genomic contigs (Low *et al.,* 2014) from the *E. guineensis* var. *pisifera* were used in this study. GenBank was mined for curated R gene information based on previous reports by Bendahmane *et al.* (1999), Dodds *et al.* (2001), Hammond-Kosack *et al.* (1997) and Martin *et al.* (2003). These protein sequences were then used as reference sequences to identify homologs in the *E. guineensis GeneThresher*™ genomic libraries using TBLASTN (Altschul *et al.,* 1990). The E-value cut-off used was 1^{e-20}, as described by Grzebelus
et al. (2007).

Protein prediction was carried out using a semi-Hidden Markov Model (HMM)-based Nucleic Acid Parser, SNAP (Korf 2004) and GeneSeqer software (Schlueter *et al.,* 2003). The prediction used oil palm and *Oryza sativa* HMM with default parameters. Oil palm R gene candidates (RGC) were compared to the NCBI non-redundant database using BLASTX for translation direction verification and BLASTP for homologous gene comparison. R genes were selected based on domains identified via comparisons to Pfam, PRINTS-S and Superfamily databases using InterProScan (Quevillon *et al.,* 2005) on both the curated R genes and oil palm RGC. The RGC with the same domain ID as the curated R gene domains were grouped into the same class. ClustalW (Thompson *et al.,* 1994) was then used to align RGC sequences, except for the 'Others' class. The alignment was used to build a phylogenetic tree using MEGA6 (Tamura *et al., 2013*).

To improve the identification and annotation of R genes in oil palm, this study utilised information from 43 R genes in 11 plant species, namely *Arabidopsis thaliana* (13), *Beta vulgaris* (1), *Capsicum chacoense* (1), *Hordeum vulgare* (3), *Lactuca sativa* (1),

Linum usitatissimum (3), *Lycopersicon esculentum* (11), *Nicotiana tabacum* (1), *O. sativa* (4), *Solanum acaule* (3) and *Zea mays* (2). The most highly represented class of R genes (~67%) is the NBS-LRR class. This class is divided into two sub-classes based on the 5'-terminal structure (Marone *et al.*, 2013). The Pfam IDs for the 43 R genes are listed in *Table 1*, with their respective predicted protein functions and gene classes.

Analysis of Amplified DNA from SSR Primers

The identification of SSR markers in the RGC sequences was carried out using MicroSAtellite (MiSA) version 2.02 (Thiel *et al.*, 2003) and primers were designed using Primer3 (Rozen and Skaletsky, 2000). The primer pairs were used to genotype 40 samples. DNA extraction and purification were carried out using 5 g of leaf samples according to Doyle and Doyle (1990). The DNA samples were labelled with [γ^{-33}P] dATP (Singh *et al.*, 2009). Polymerase chain reaction (PCR), followed by electrophoresis in 5% acrylamide gel were conducted (Billotte *et al.*, 2001; Singh *et al.*, 2009).

DNA bands were scored for the presence (1) or absence (0) of the amplified bands from each sample group. POPGENE software version 1.32 (Yeh and Boyle, 1997) was used to estimate the genetic distance (GD) between the samples. GD was calculated using the unweighted pair-group method with arithmetic averages (UPGMA) (Nei, 1978) and relationships between samples are shown in a dendrogram constructed using PHYLIP version 3.5c (Felsenstein, 1993).

RESULTS AND DISCUSSION

Identification of Oil Palm RGC

We identified 144 oil palm RGC from the *E. guineensis GeneThresher*™ genomic libraries using the 43 curated R genes as template, and classified them into six classes based on their domain arrangement (*Figure 1*). Each gene class denote the same domain ID as the curated R genes, enabling gene classification (*Table 2*). The *PTO* gene (Kinase class), responsible for the resistance of *L. esculentum* to the bacterial speck disease caused by the *Pseudomonas syringae* (Kim *et al.*, 2002; Martin *et al.*, 1993), forms the basis of the R gene Kinase Class. This gene encodes a single Pkinase (IPR000719) protein domain that encodes a Serine/Threonine Kinase (STK). *PTO* recognises *AVRPTOA*

TABLE 1. PROTEIN DOMAIN INFORMATION OF CURATED RESISTANCE GENES

Class	No. of known R genes from other crops	Domain ID	Domain name	Function
Kinase	1	IPR000719	Pkinase	ATP binding
CNL	19	IPR002182	NB-ARC	Signaling motif to bind and hydrolyse ATP
		IPR000767	DISEASERSIST	4-element fingerprint that provides a signature for disease resistance proteins
TNL	10	IPR002182	NB-ARC	Signaling motif to bind and hydrolyse ATP
		IPR000157	TIR	Involved in protein interaction and signal transductions
		IPR001611	LRR_1	Involved in protein-protein interaction
RLP	4	IPR013210	LRRNT_2	Involved in protein-protein interaction
RLK	1	IPR000719	Pkinase	ATP binding
		IPR013210	LRRNT_2	Involved in protein-protein interaction
		IPR001611	LRR_1	Involved in protein-protein interaction
Others	8	IPR001509	NAD-dependent epimerase/dehydratase	Involved in catalytic activity and coenzyme binding
		IPR002182	NB-ARC	Signaling motif to bind and hydrolyse ATP
		IPR016040	NADP-bd	NADP-binding domain
		IPR004326	Mlo	Trigger a cascade of events that result in plant cell death
		IPR006121	HMA	Involved in bacterial resistance to toxic metals, such as lead and cadmium
		IPR000719	Pkinase	ATP binding
		IPR003657	WRKY	Regulate various physiological programs that are unique to plants, including pathogen defence
		IPR011713	LRR_3	Involved in protein-protein interaction
		IPR000157	Toll/Interleukin receptor TIR domain	Involved in signal transductions

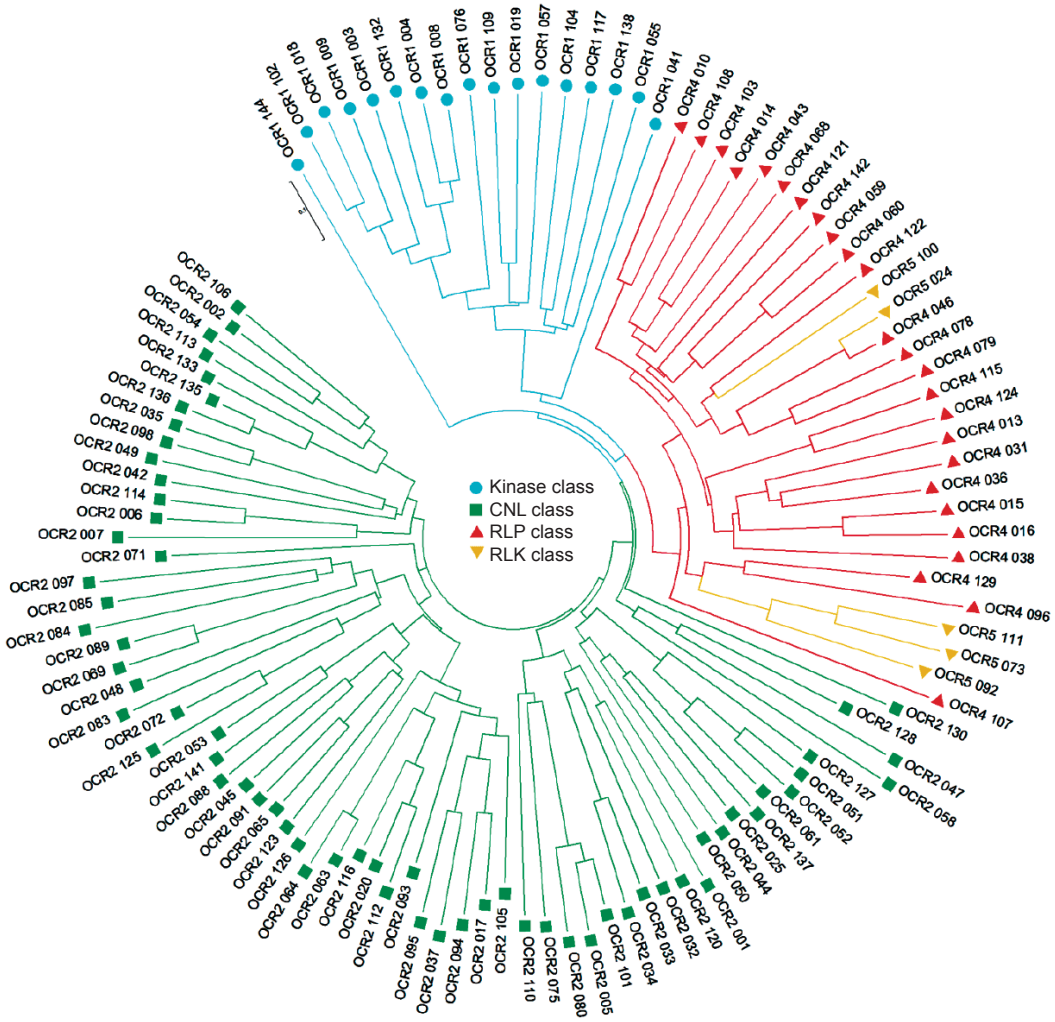


Figure 1. Phylogenetic analysis of the 144 oil palm RGCs identified from hypomethylated or gene-rich regions of the oil palm genome. Kinase, CNL, RLP and RLK classes are indicated in the legend at the centre of the image.

and *AVRPTOB* inside the host cell and halts the colonisation of *P. syringae* (Tang *et al.*, 1996). A total of 17 oil palm RGC were classified into the Kinase class, whereby these genes contain the Pkinase domain (IPR000719) which is similar to the *TaWAK6* genes associated with wheat resistance to leaf rust (Dmochowska-Boguta *et al.*, 2020). Most of the identified oil palm RGC are in the CNL class (65 candidate genes). We were unable to find candidate genes belonging to the TNL class. Analysis of gene models from seven monocot plants, namely *Musa acuminata*, *Setaria italica*, *Sorghum bicolor*, *Z. mays*, *O. sativa*, *Brachypodium distachyon* and *Phyllostachys heterocycle* also showed that the genomes do not have TNL genes, and it is likely that this class of genes were lost after the divergence of dicots and monocots (Shao *et al.*, 2016). Therefore, the TNL gene class may not exist in oil palm since oil palm is also a monocot. However, it is also possible that we could not identify these genes as the oil palm genome is not complete (Singh *et al.*, 2013).

Two important classes of R genes are RLK and RLP. Both contain LRR domains and a hydrophobic protein residue involved in protein-protein interaction (Jones and Jones, 1997). RLK genes also contain an additional Kinase domain. A total of 25 and five oil palm genes were identified as RLP and RLK genes respectively. These genes may be involved in the first stage of oil palm's defence mechanism. Plant defence mechanisms are represented as a four-phase zigzag model (Jones and Dangl, 2006). In phase 1, the pathogen-associated molecular pattern (PAMP) elicitors are recognised by RLK and RLP classes of R genes that contain extracellular domains to interact with these elicitors. These receptors mediate PAMP-triggered immunity (PTI) (Sekhwal *et al.*, 2015). In phase 2 of the infection, successful pathogens secrete effector molecules into the host cell to interfere with the PTI response, resulting in effector-triggered susceptibility. Phase 3 marks the beginning of the second stage of the defense mechanism in the plant immune system, triggered inside the host cell by the Kinase and CNL R gene classes. Once the effectors are recognised by these R genes, colonisation by the pathogen can be halted, usually via a hypersensitive cell death

TABLE 2. CLASSIFICATION OF OIL PALM RGC BASED ON PROTEIN DOMAIN AND BLASTP

Class	Contig	Domain ID	Domain name	Domain E-value	BlastP	Blast E-value
1	OCR1_003			1.90E-18	Pto-like serine/threonine kinase	8.00E-82
1	OCR1_004			1.40E-28	Pto-like serine/threonine kinase	4.00E-74
1	OCR1_008			4.40E-21	Pto	9.00E-79
1	OCR1_009			3.30E-37	Pto resistance protein candidate Tg-65	6.00E-77
1	OCR1_019			3.00E-44	Pto	1.00E-43
1	OCR1_041			8.60E-49	Pto-like protein	1.00E-67
1	OCR1_055			4.20E-34	Pto-like serine/threonine kinase	6.00E-04
1	OCR1_057	PF00069	Pkinase	8.10E-44	Pto-like serine/threonine kinase	1.00E-54
1	OCR1_076			1.60E-07	Pto-like serine/threonine kinase	1.00E-70
1	OCR1_102			1.20E-36	Pto kinase homologs	2.00E-116
1	OCR1_104			9.30E-57	Pto-like protein	2.00E-57
1	OCR1_109			7.80E-29	Putative Pto-like serine/threonine kinase	2.00E-18
1	OCR1_117			9.90E-57	Pto-like protein	4.00E-66
1	OCR1_132			3.10E-18	Pto-like serine/threonine kinase	8.00E-77
1	OCR1_138			3.60E-21	Pto	3.00E-30
1	OCR1_144			5.80E-29	Protein kinase family protein	1.00E-99
2	OCR2_080			2.30E-50	RPS5	1.00E-42
				1.50E-09		
2	OCR2_094			3.90E-36	Disease resistance protein RPS2	2.00E-40
				2.10E-18		
2	OCR2_097			1.70E-65	I2	9.00E-42
				4.10E-17		
2	OCR2_123			1.40E-59	Disease resistance protein RPS2	9.00E-36
				2.50E-07		
2	OCR2_063			1.50E-35	CC-NBS-LRR resistance protein	1.00E-36
				2.40E-10		
2	OCR2_064			7.50E-51	Late blight resistance protein Rpi-pta1	2.00E-67
				1.10E-14		
2	OCR2_128			3.00E-35	Disease resistance protein RPS2, putative	2.00E-77
				7.40E-06		
2	OCR2_098	PF00931 PR00364	NB-ARC Diseasersist	2.50E-23	Disease resistance protein RPM1, putative	4.00E-57
				7.00E-05		
2	OCR2_017			5.60E-58	Disease resistance protein RPS2	1.00E-41
				1.20E-09		
2	OCR2_020			1.80E-91	Disease resistance protein RPS2	2.00E-79
				1.10E-17		
2	OCR2_025			5.10E-55	Disease resistance protein RPS2	6.00E-61
				2.60E-11		
2	OCR2_033			1.40E-35	Disease resistance protein RPS2	8.00E-33
				2.30E-09		
2	OCR2_035			1.10E-20	Disease resistance protein RPM1	8.00E-30
				1.10E-05		
2	OCR2_037			1.70E-92	Disease resistance protein RPS2	9.00E-103
				3.80E-18		
2	OCR2_042			1.10E-34	Disease resistance protein RPP13	7.00E-48
				3.20E-06		

TABLE 2. CLASSIFICATION OF OIL PALM RGC BASED ON PROTEIN DOMAIN AND BLASTP (continued).

Class	Contig	Domain ID	Domain name	Domain E-value	BlastP	Blast E-value
2	OCR2_045			7.90E-81	Disease resistance protein RPS2	3.00E-52
				2.00E-15		
2	OCR2_048			3.50E-40	Disease resistance protein RPM1	2.00E-34
				7.90E-09		
2	OCR2_049			2.40E-27	Disease resistance protein RPM1	7.00E-58
				1.40E-05		
2	OCR2_050			9.80E-44	Disease resistance protein I2	7.00E-53
				2.60E-09		
2	OCR2_053			2.50E-73	Disease resistance protein RPS2	6.00E-52
				5.30E-18		
2	OCR2_061			2.80E-43	Disease resistance protein I2	2.00E-54
				9.20E-08		
2	OCR2_065			1.20E-48	Disease resistance protein RPS2	1.00E-47
				1.60E-07		
2	OCR2_069			3.00E-30	Disease resistance protein RPS2	2.00E-35
				5.50E-11		
2	OCR2_071			5.80E-46	Disease resistance protein RPM1	1.00E-54
				1.20E-10		
2	OCR2_072			3.70E-81	Disease resistance protein RPM1	7.00E-56
				8.90E-12		
2	OCR2_075			6.00E-17	RPS2	1.00E-66
				6.00E-17		
2	OCR2_083			1.40E-67	Disease resistance protein RPP8	2.00E-62
		PF00931 PR00364	NB-ARC Diseasersist	3.70E-16		
2	OCR2_084			9.00E-56	Disease resistance protein RPS2	5.00E-68
				3.10E-17		
2	OCR2_085			9.10E-60	Disease resistance protein RPS2	9.00E-71
				3.80E-17		
2	OCR2_088			8.90E-48	I2	1.00E-25
				1.30E-09		
2	OCR2_089			3.60E-56	Disease resistance protein RPS2	2.00E-61
				1.40E-15		
2	OCR2_091			1.40E-54	CC-NBS-LRR resistance protein	1.00E-55
				6.60E-09		
2	OCR2_093			2.30E-65	Disease resistance protein RPS2	4.00E-56
				1.30E-09		
2	OCR2_095			1.30E-82	Disease resistance protein RPS2	2.00E-83
				5.00E-17		
2	OCR2_101			1.70E-58	RPS5	2.00E-06
				8.70E-11		
2	OCR2_105			1.60E-81	Disease resistance protein RPS2	2.00E-96
				1.50E-17		
2	OCR2_110			1.70E-65	RPS2	9.00E-57
				5.30E-20		
2	OCR2_112			8.50E-38	CC-NBS-LRR resistance protein	3.00E-42
				4.80E-10		
2	OCR2_116			1.70E-36	CC-NBS-LRR resistance protein	1.00E-36
				4.40E-10		

TABLE 2. CLASSIFICATION OF OIL PALM RGC BASED ON PROTEIN DOMAIN AND BLASTP (continued).

Class	Contig	Domain ID	Domain name	Domain E-value	BlastP	Blast E-value
2	OCR2_125			9.50E-52	Disease resistance protein RPP13	1.00E-31
				5.00E-06		
2	OCR2_126			3.40E-43	Disease resistance protein RPS2	6.00E-39
		PF00931 PR00364	NB-ARC Diseasersist	1.10E-05		
2	OCR2_133			2.70E-41	Disease resistance protein RPM1	8.00E-86
				1.80E-05		
2	OCR2_136			1.60E-59	RPM1	3.00E-49
				5.60E-08		
4	OCR4_014			5.00E-12	Cf-2.2	3.00E-54
4	OCR4_043	PF08263	LRRNT_2	1.90E-13	Cf-2.1	4.00E-64
4	OCR4_096			2.50E-06	Cf-2.3	1.00E-40
4	OCR4_010			8.80E-03	Cf-2.3	1.00E-30
4	OCR4_015			2.50E-03	Cf-2.1	1.00E-25
4	OCR4_016			9.10E-04	Putative Cf2/Cf5	4.00E-28
4	OCR4_031			5.10E-03	Cf2/Cf5-like	1.00E-57
4	OCR4_036			2.50E-03	Cf2/Cf5-like	1.00E-122
4	OCR4_038			4.10E-04	Cf2/Cf5-like	2.00E-40
4	OCR4_013			1.30E-02	Putative Cf2/Cf5	1.00E-33
4	OCR4_046			1.60E-02	Cf-2.1 putative	3.00E-38
4	OCR4_059			3.40E-03	Cf-2.1	1.00E-68
4	OCR4_060			2.00E-04	Cf-2.2	4.00E-62
4	OCR4_068	PF00560	LRR_1	3.40E-03	Cf-2.1	2.00E-60
4	OCR4_078			2.10E-02	Cf-2.1	3.00E-55
4	OCR4_079			6.90E-04	Cf-2.1	1.00E-98
4	OCR4_103			1.60E-04	Cf-2.3	5. 00e-77
4	OCR4_107			1.30E-03	Putative Cf2/Cf5	2.00E-22
4	OCR4_108			4.40E-03	Cf-2.1	4.00E-73
4	OCR4_115			3.30E-03	Cf-2.2	5.00E-20
4	OCR4_121			6.60E-03	Cf-2.2	2.00E-67
4	OCR4_122			7.30E-03	Cf-2.1	9.00E-54
4	OCR4_124			4.40E-03	Cf-2.2	6.00E-31
4	OCR4_129			6.90E-04	Cf-2.3	2.00E-09
4	OCR4_142			4.50E-03	Cf-2.3	4.00E-68
5	OCR5_073			6.40E-51		4.00E-104
				3.70E-31		
				6.70E-02		
5	OCR5_092	SSF56112 PF00069 PF00560	Protein kinase-like Pkinase LRR_1	1.50E-53		0
				8.10E-35	Protein kinase Xa21	
				3.90E-01		
5	OCR5_024			2.50E-13		5.00E-121
				1.50E-04		
				1.30E-01		
6	OCR2_001			6.00E-30	RPS5	3.00E-39
6	OCR2_054			1.50E-22	Disease resistance protein RPM1	6.00E-62
6	OCR2_058	PF00931	NB-ARC	6.10E-45	Disease resistance protein RPH8A, putative	3.00E-58
6	OCR2_106			1.70E-36	Disease resistance protein RPM1	2.00E-54
6	OCR2_114			4.80E-64	Disease resistance protein RPP8	4.00E-53
6	OCR2_113			1.30E-41	Disease resistance protein RPM1	6.00E-48

TABLE 2. CLASSIFICATION OF OIL PALM RGC BASED ON PROTEIN DOMAIN AND BLASTP (continued).

Class	Contig	Domain ID	Domain name	Domain E-value	BlastP	Blast E-value
6	OCR2_002			6.90E-43	Disease resistance protein RPM1	9.00E-48
6	OCR2_120			2.70E-32	Putative RPS2	1.00E-47
6	OCR2_006			3.90E-52	Disease resistance protein RPP8	1.00E-46
6	OCR2_044			3.30E-31	Disease resistance protein RPS2	2.00E-40
6	OCR2_034			4.00E-27	Disease resistance protein RPS5	2.00E-36
6	OCR2_127			3.10E-33	Disease resistance protein RPM1	1.00E-34
6	OCR2_032	PF00931	NB-ARC	4.30E-17	RPS5	4.00E-27
6	OCR2_135			6.10E-22	Disease resistance protein RPM1	9.00E-24
6	OCR2_047			3.40E-27	Disease resistance protein RPS2	1.00E-23
6	OCR2_137			3.90E-14	Disease resistance protein RPS2	6.00E-23
6	OCR2_007			5.20E-31	Disease resistance protein Gpa2	2.00E-20
6	OCR2_141			1.00E-29	Disease resistance protein I-2	2.00E-17
6	OCR2_005			2.70E-22	Disease resistance protein RPS5	1.00E-13
6	OCR6_062			3.20E-25	Leucine-rich repeat transmembrane protein kinase	6.00E-96
6	OCR6_029			1.50E-32	Protein kinase Xa21	3.00E-79
6	OCR6_070			1.40E-37	Putative protein kinase Xa21	4.00E-78
6	OCR6_139			2.00E-53	Serine-threonine protein kinase	2.00E-74
6	OCR6_066			1.40E-54	Protein kinase family protein	9.00E-72
6	OCR6_087			6.10E-52	Putative rust resistance kinase Lr10	2.00E-71
6	OCR6_040			1.10E-48	Protein kinase-like resistance protein	1.00E-69
6	OCR6_021			2.10E-50	Resistance protein candidate	1.00E-68
6	OCR6_118			1.70E-50	Resistance protein candidate	3.00E-68
6	OCR6_099			9.10E-36	Putative protein kinase Xa21	8.00E-68
6	OCR6_056	PF00069 PF00069	Pkinase Pkinase	9.70E-41	Protein kinase-coding resistance protein	3.00E-67
6	OCR6_086			2.40E-41	Protein kinase-coding resistance protein	1.00E-62
6	OCR6_119			1.30E-23	Protein kinase family protein	2.00E-61
6	OCR6_030			2.10E-24	Protein kinase Xa21	1.00E-59
6	OCR6_027			1.20E-36	RFO1 (Resistance to *Fusarium Oxysporum* 1)	2.00E-49
6	OCR6_082			4.50E-26	Putative protein kinase Xa21	2.00E-48
6	OCR6_081			1.10E-17	Protein kinase-like resistance protein	8.00E-42
6	OCR6_074			5.80E-16	Putative protein kinase Xa21	2.00E-39
6	OCR6_143			1.60E-31	Bacterial blight resistance protein XA26	1.00E-37
6	OCR6_026			3.00E-44	Cf-2.2	5.00E-23
6	OCR6_011			3.20E-52	Protein kinase-like resistance protein	1.00E-12
6	OCR6_039			2.80E-32	Protein kinase-coding resistance protein	2.30E-02
6	OCR5_100				Protein kinase Xa21	2.00E-170
6	OCR6_134			2.00E-02	Disease resistance protein RPM1	7.00E-56
6	OCR6_012			9.00E-03	Rust resistance protein Rp1	4.00E-36
6	OCR6_077	PF00560	LRR_1	8.30E-03	Putative protein kinase Xa21	5.00E-33
6	OCR6_067			3.40E-03	Putative RPS2	6.00E-25
6	OCR2_130			3.20E-01	RPS2	3.00E-25
6	OCR2_051			5.30E-01	putative disease resistance RPP13-like protein 1-like	5.00E-21
6	OCR6_022	PF07014	Hs1pro-1_C	2.40E-71	Hs1pro-1	7.00E-43
6	OCR6_023			2.40E-56	Hs1pro-1	2.00E-26
6	OCR1_018	PF07714	Pkinase_Tyr	1.80E-33	Resistance gene homologs	5.00E-107
6	OCR6_140	SSF56112	Protein kinase-like	8.00E-14	Protein kinase-coding resistance protein	1.00E-11

TABLE 2. CLASSIFICATION OF OIL PALM RGC BASED ON PROTEIN DOMAIN AND BLASTP (continued).

Class	Contig	Domain ID	Domain name	Domain E-value	BlastP	Blast E-value
6	OCR6_131			7.90E-04	Leucine-rich repeat	0
6	OCR6_028	PF00560 PR00019 PF00069	LRR_1 LeuRichRpt Pkinase	1.30E-06 9.50E-40 7.90E-03 4.90E-06 2.50E-29	Protein kinase-coding resistance protein	6.00E-75
6	OCR2_052	PF00931	NB-ARC	2.00E-23	CC-NBS-LRR resistance protein	3.00E-57
6	OCR6_090	PF00560	LRR_1	2.30E-02	Hs1pro-1	3.00E-48
		PF07231	Hs1pro-1_N	1.00E-07		
		PF07014	Hs1pro-1_C	7.30E-40		
6	OCR5_111	SSF56112	Protein kinase-like	2.60E-01	Protein kinase Xa21	6.00E-16
		PF00069	Pkinase			

response. In phase 4, natural selection may result in pathogens that have gained new effectors. The selection process then favours host plants with new or different R genes that can neutralise the new effectors (Jones and Dangl, 2006). A total of 82 oil palm Kinase and CNL class RGC that are part of the second stage of plant defence mechanism were identified.

Identification of Polymorphic SSRs in Oil Palm RGC

A total of 32 out of the 144 oil palm RGC contain SSR motifs and 32 SSR primer pairs were thus designed. Ten SSR primer pairs that were able to produce amplified products with a Phred quality score of more than 20 were selected to screen 40 palms from the four populations. All primer pairs produced amplicons, of which six were polymorphic (*Table 3*) while four primer pairs, GC2.582.2, GC2.033.1, GC6.887_2 and GC2.033.2 showed monomorphic profiles.

An average of three alleles per locus were detected by the polymorphic SSR markers, with a total of 18 alleles in the progenies (*Table 4*). The highest number of alleles (Na) detected was with the GC6.651 marker, which was seven, and the minimum number of observed polymorphic alleles was two, which was the most common among the marker. The effective number of alleles (Ne) ranged from 1.568 to 4.300. The observed heterozygosity (Ho) and expected heterozygosity (He) ranged from 0.125 to 0.692 and 0.367 to 0.777, respectively. Markers are considered to be polymorphic if the heterozygosity score is more or equal to 0.1, and highly polymorphic if the value is more or equal to 0.7 (Romero *et al.*, 2019). The average Ho and He were 0.462 and 0.512 respectively, indicating that the markers were polymorphic. SSRs are widely used for marker-assisted selection (Lawson and Liqing 2006; Powell *et al.*, 1996; Robinson *et al.*, 2004) and have been applied as DNA markers to screen for RGC in rice (Fjellstrom *et al.*, 2006). Screening with additional markers can help verify the consistency of data obtained in this study.

The developed SSR markers did not include the oil palm RGC classes RLK and RLP. These two classes of R proteins are secreted into the extracellular environment and are not involved in the second stage of the plant defense mechanism.

Genetic Distance and Relationship of the Four Populations with Different BSR Resistance Levels

The amplification patterns of the SSR markers were used to calculate Nei's GD among the 40 oil palm samples with different resistance levels to BSR disease. The results showed that GD ranged from 0 to 0.372. A UPGMA dendrogram showed that the samples were grouped into four clusters (*Figure 2*). Cluster A comprises samples from the susceptible progeny (PK 2724) with a population death rate of 40% to BSR disease. Most (67%) of the intermediate resistant samples (PK 2572) with a population death rate of 25% are grouped into cluster B, which also contains four samples from population PK 2724. The clustering also showed that clusters A and B displayed the lowest genetic similarity coefficient, suggesting that they are closely related. This is in line with observations by Idris *et al*. (2004), where progeny PK 2724 is not significantly different in the severity of its foliar symptoms compared to PK 2572, but was distinctly different when compared to PK 2567 (population death rate of 10%) and PK 1708 (death rate of 15%). Cluster C comprise all of the partial resistance samples from population PK 2567, two samples from population PK 2724 and one sample from population PK 2572. All partial resistance samples from population PK 1708 were separated into a distinct cluster (cluster D). Both Cluster C and D could represent palms partially resistant to the disease.

TABLE 3. POLYMORPHIC SSR MARKERS IN OIL PALM RGC

No.	SSR name	Class	Candidate gene	SSR type	Motif	Size (nt)	Annealing temp. (°C)
1	GC1.365	Kinase	OCR1_057	p1	$(A)_{13}$	160-170	55
2	GC1.979	Kinase	OCR1_144	p3	$(GAG)_{6}$	120-130	51
3	GC2.582	CNL	OCR2_058	p3	$(GCA)_{5}$	270-280	51
4	GC6.398	Others	OCR6_027	p2	$(AT)_{8}$	140-150	51
5	GC6.887	Others	OCR2_114	p1	$(T)_{16}$	230-240	51
6	GC6.651	Others	OCR6_119	c	$(GT)_{10}(AT)_{19}$	250-260	55

TABLE 4. SUMMARY OF GENETIC VARIATIONS AND HETEROZYGOSITY STATISTICS FOR ALL LOCI

SSR name	Na	Ne	Ho	He
GC1.365	2	1.827	0.692	0.459
GC1.979	2	1.853	0.667	0.466
GC2.582	2	1.663	0.350	0.403
GC6.398	3	2.441	0.400	0.598
GC6.887	2	1.568	0.125	0.367
GC6.651	7	4.300	0.539	0.777

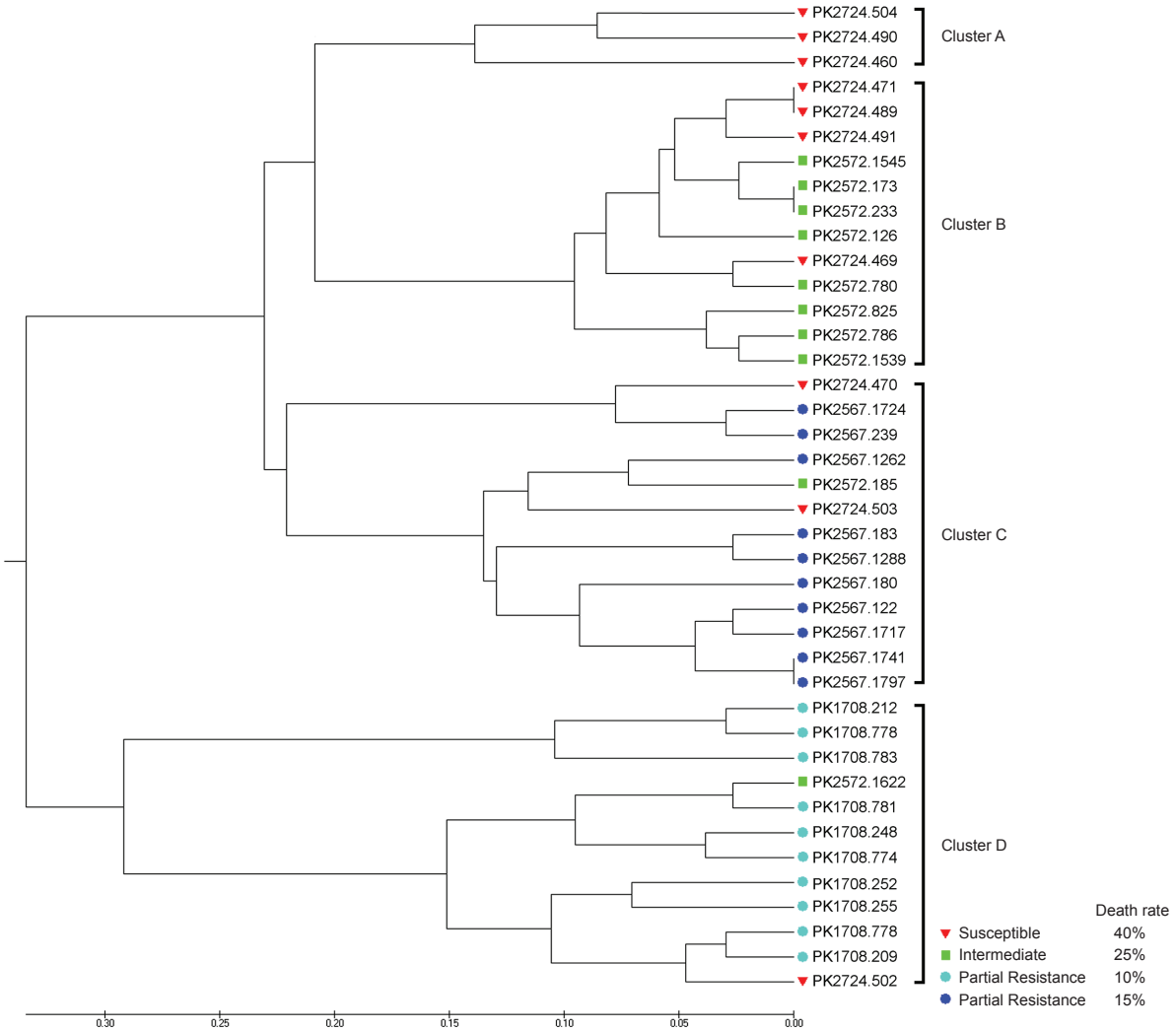


Figure 2. Dendrogram based on UPGMA analysis of 40 oil palm samples with different levels of resistance to Ganoderma boninense *infection.*

The dendrogram shows that the samples in each cluster are from the same population, with some exception that result in mixed samples from different populations. The relationship between sets of samples is shown in *Figure 3*. One of the reasons for the presence of mixed samples in a cluster is that populations will have some levels of spatial variation that can impact its resistance or susceptibility to diseases (Laine *et al.*, 2011). Palms could also be grouped into a cluster based on the similarity of their genetic backgrounds. Progeny PK 2724 originated from crosses of Deli (Elmina) palms while PK 2572 is from a Deli (Banting) x AVROS population. PK 2567 is a hybrid of Congo x Cameroon, and PK 1708 is from a Cameroon x Cameroon population (Idris *et al.*, 2004). The present set of markers were able to differentiate the partial resistant populations from the intermediate and susceptible populations. Using markers associated with resistance to BSR would be beneficial in breeding programs aimed at developing *G. boninense* resistant palms. Nevertheless, this study is limited in the number of samples tested, and needs to be extended to field trials to verify the findings.

CONCLUSION

Identification of resistance gene analogues in the oil palm genome enabled the development of SSR markers related to the BSR disease. These markers have the potential to predict and select oil palm progenies with a higher tolerance level to the disease before planting. Nevertheless, the evaluation of these potential markers needs to be expanded to study their effectiveness in more diverse populations.

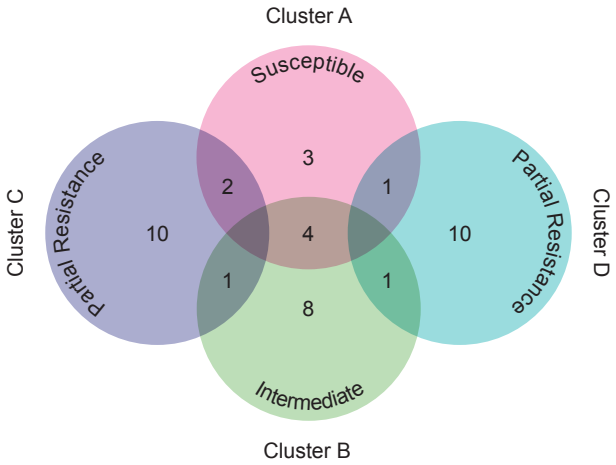


Figure 3. Frequency of oil palm samples with different levels of resistance to BSR disease sets according to UPGMA clusters. All of the partial resistance palm samples are unique and mixed samples are found in intermediate and susceptible sets.

ACKNOWLEDGEMENT

The authors would like to thank the Director-General of MPOB for permission to publish this article.

REFERENCES

Ahmadi, P; Muharam, F M; Khairulmazmi, A; Shattri and M and Idris, A S (2017). Early detection of *Ganoderma* basal stem rot of oil palms using artificial neural network spectral analysis. *Plant Dis., 101(6):* 1009-1016.

Altschul, S F; Gish, W; Miller, W; Myers, E W and Lipman, D J (1990). Basic local alignment search tool. *J. Mol. Boil., 215*: 403-410.

Ariffin, D and Idris, A S (1991). A selective medium for isolation of *Ganoderma* from diseased tissues. *Proc. of the 1991 International Palm Oil Conference, Progress, Prospects and Challenges Towards the 21st Century*. MPOB, Bangi. p. 517-519.

Ariffin, D; Idris, A S and Singh, G (2000). Status of *Ganoderma* in oil palm. *Ganoderma Diseases of Perennial Crops* (Flood, J; Bridge, P D and Holderness, M eds.). New York: Centre for Agricultural Bioscience International Publishing. p. 49-68.

Bendahmane, A; Kanyuka, K and Baulcombe, D C (1999). The *Rx* gene from potato controls separate virus resistance and cell death responses. *Plant Cell, 11*: 781-791.

Billotte, N; Risterucci, A M; Barcelos, E; Noyer, J L; Ambiard, P and Baurens, F C (2001). Development, characterisation, and across-taxa utility of oil palm (*Elaeis guineensis* Jacq.) microsatellite markers. *Genome, 44*: 413-425.

Dmochowska-Boguta, M; Kloc, Y; Zielezinski, A; Werecki, P; Nadolska-Orczyk, A; Karlowski, W M and Orczyk, W (2020). *TaWAK6* encoding wall-associated kinase is involved in wheat resistance to leaf rust similar to adult plant resistance. *PLoS ONE, 15(1)*: e0227713.

Dodds, P N; Lawrence, G J and ElliS, J G (2001). Six amino acid changes confined to the leucine-rich repeat β-strand/β-turn motif determine the difference between the *P* and *P2* rust resistance specificities in flax. *Plant Cell, 13*: 163-178.

Doyle, J J and Doyle, J L (1990). Isolation of plant DNA from fresh tissue. *Focus, 12(12)*: 13-15.

Ellis, J and Dodds, P (2003). Plant pathology: Monitoring a pathogen-targeted host protein. *Curr. Biol., 13*: 400-402.

Felsenstein, J (1993). PHYLIP (Phylogeny Inference Package) version 3.5c. Department of Genome Sciences, University of Washington, Seattle.

Fjellstrom, R; McClung, A M and Shank, A R (2006). SSR markers closely linked to the *Pi-z* locus are useful for selection of blast resistance in a broad array of rice germplasm. *Mol. Bred., 17*: 149-157.

Grzebelus, D; Lasota, S; Gambin, T; Kucherov, G and Gambin, A (2007). Diversity and structure of PIF/Harbinger-like elements in the genome of *Medicago truncatula*. *BMC Genomics, 8*: 409-422.

Hammond-Kosack, K E and Jones, J D G (1997). Plant disease resistance genes. *Annu. Rev. Physiol. Mol. Biol. Plants, 48*: 575-607.

Ho, Y W and Nawawi, A (1985). *Ganoderma boninense* pat. from basal stem rot of oil palm (*Elaeis guineensis*) in Peninsular Malaysia. *Pertanika, 8(3)*: 425-428.

Hushiarian, R; Yusof, N A and Dutse, S W (2013). Detection and control of *Ganoderma boninense*: Strategies and perspectives. *Springerplus 2*: 555.

Idris, A S; Kushairi, A; Ismail, S and Ariffin, D (2004). Selection for partial resistance in oil palm progenies to *Ganoderma* basal stem rot. *J. Oil Palm Res., 16(2)*: 12-18.

Idris, A S; Mazliham, M S; Loonis, P and Mohd Basri, W (2010). GanoSken for early detection of *Ganoderma* infection in oil palm. *MPOB Information Series No. 442*.

Jones, D A and Jones, J D G (1997). The role of leucine-rich repeat proteins in plant defences. *Adv. Bot. Res., 24*: 89-167.

Jones, J D G and Dangl, J L (2006). The plant immune system. *Nature, 444(16)*: 323- 329.

Kim, Y J; Lin, N C and Martin G B (2002). Two distinct *Pseudomonas* effector proteins interact with the *Pto* kinase and activate plant immunity. *Cell, 109(5)*: 589-598.

Korf, I (2004). Gene finding in novel genomes. *BMC Bioinform., 5*: 59.

Laine, A L; Burdon, J J; Dodds, P N and Thrall P H (2011). Spatial variation in disease resistance: From molecules to metapopulations. *J. Ecol., 99(1)*: 96-112.

Lawson, M J and Liqing, Z (2006). Distinct patterns of SSR distribution in the *Arabidopsis thaliana* and rice genomes. *Genome Biol., 7*: R14.

Low, E T L; Rosli, R; Jayanthi, N; Mohd Amin, A H; Azizi, N; Chan, K L; Maqbool, N J; Maclean, P; Brauning, R; Mcculloch, A; Morage, R; Ong-Abdullah, M and Singh, R (2014). Analyses of hypomethylated oil palm gene space. *PLoS ONE, 9(1)*: e86728.

Martin, G B; Bogdanove, A J and Sessa, G (2003). Understanding the functions of plant disease resistance proteins. *Annu. Rev. Plant Biol., 54*: 23-61.

Martin, G B; Brommonschenkel, S H; Chunwongse, J; Frary, A; Ganal, M W; Spivey, R; Wu, T; Earle, E D and Tanksley S D (1993). Map-based cloning of a protein kinase gene conferring disease resistance in tomato. *Science, 262(5138)*: 1432-1436.

Marone, D; Russo, M A; Laidò, G; De Leonardis, A M and Mastrangelo, A M (2013). Plant nucleotide binding site-leucine-rich repeat (NBS-LRR) genes: Active guardians in host defense responses. *Int. J. Mol. Sci., 24*: 7302-7326.

Mohd Shukri, I; Idris, A S; Rusli, M H; Izzuddin, M A; Norman, K; Khairuman, H and Zulkifli, A M (2020). Surveillance of *Ganoderma* disease in oil palm planted by participants of the smallholders replanting incentive scheme in Malaysia. *J. Oil Palm Res., 32(2)*: 237-244.

Naher, L; Siddiquee, S; Yusof, U K and Mondal, M M A (2015). Issues of *Ganoderma spp*. and basal stem rot disease management in oil palm. *Am. J. Agric. Res., 2(3)*: 103-107.

Nei, M (1978). Estimation of average heterozygosity and genetic distance from a small number of individuals. *Genetics, 89*: 583-590.

Nurnadiah, E; Aimrun, W; Amin, M S M and Idris, A S (2014). Preliminary study on detection of basal stem rot (BSR) disease at oil palm tree using electrical resistance. *Agric. Agric. Sci. Procedia, 2*: 90-94.

Parveez, G K A; Ahmad Tarmizi A H; Sundram S; Loh S K; Ong-Abdullah, M; Poo Palam, K D, Mohamed Salleh, K; Mohd Ishak, S and Idris, Z (2021). Oil palm economic performance in Malaysia and R&D progress in 2020. *J. Oil Palm Res., 33(2)*: 181-214.

Powell, W; Machray, G C and Provan, J (1996). Polymorphism revealed by simple sequence repeats. *Trends Plant Sci., 1(7)*: 215-222.

Quevillon, E; Silventoinen, V; Pillai, S; Harte, N; Mulder, N; Apweiler, R and Lopez, R (2005). InterProScan: protein domains identifier. *Nucleic Acids Res., 33*: 116-120.

Robinson, A J; Love, C G; Batley, J; Barker, G and Edwards, D (2004). Simple sequence repeat marker loci discovery using SSR primer. *Bioinformatics, 20(9)*: 1475-1476.

Romero, M; Mujica, A; Pineda, E; Ccamapaza, Y and Zavalla, N (2019). Genetic identity based on simple sequence repeat (SSR) markers for Quinoa (*Chenopodium quinoa* Willd.). *Cienc. Investig. Agrar., 46(2)*: 166-178.

Rozen, S and Skaletsky, H (2000). Primer3 on the WWW for general users and for biologist programmers. *Methods Mol. Biol., 132*: 365-86.

Schlueter, S D; Qunfeng, D and Brendel, V (2003). GeneSeqer@PlantGDB: Gene structure prediction in plant genomes. *Nucleic Acids Res., 31(13)*: 3597-3600.

Sekhwal, M K; Li, P; Lam, I; Wang, X; Cloutier, S and You, F M (2015). Disease resistance gene analogs (RGAs) in plants. *Int. J. Mol. Sci., 16*: 19248-19290.

Shamala, S; Faridah, A; Zainal Abidin, M A and Umi Kalsom, Y (2008). Efficacy of single and mixed treatments of *Trichoderma harzianum* as biocontrol agents of *Ganoderma* basal stem rot in oil palm. *J. Oil Palm Res., 20*: 470-483.

Shao, Z Q; Xue, J Y; Wu, P; Zhang, Y M; Wu, Y; Hang, Y Y; Wang, B and Chen, J Q (2016). Large-scale analyses of angiosperm nucleotide-binding site-leucine-rich repeat genes reveal three anciently diverged classes with distinct evolutionary patterns. *Plant Physiol., 170(4)*: 2095-2109.

Singh, R; Tan, S G; Panandam, J M; Rahimah, R A; Ooi, L C L; Low, E T L; Sharma, M; Jansen, J and Cheah, S C (2009). Mapping quantitative trait loci (QTLs) for fatty acid composition in an interspecific cross of oil palm. *BMC Plant Biol., 9*: 114.

Singh, R; Ong-Abdullah, M; Low, E T L; Mohammad Arif, A M; Rozana, R; Nookiah, R; Ooi, L C; Ooi, S; Chan, K; Mohd Amin, A H; Norazah, A; Nagappan, J; Bacher, B; Lakey, N; Smith, S W; He, D; Hogan, M; Budiman, M A; Lee, E K; Desalle, R; Kudrna, D; Goicoechea, J L; Wing, R A; Wilson, R K; Fulton, R S; Ordway, J M; Martienssen, R A and Sambanthamurthi, R (2013). Oil palm genome sequence reveals divergence of interfertile species in old and new worlds. *Nature, 500*: 335-339.

Song, W Y; Pi, L Y; Wang, G L; Gardner, J; Holsten, T and Ronald, P C (1997). Evolution of rice *Xa21* disease resistance gene family. *Plant Cell, 9*: 1279-1287.

Susanto, A; Sudharto, P S and Purba, R Y (2005). Enhancing biological control of basal stem rot disease (*Ganoderma boninense*) in oil palm plantations. *Mycopathologia, 159*: 153-157.

Tamura, K; Stecher, G; Peterson, D; Filipski, A and Kumar, S (2013). MEGA6: Molecular evolutionary genetics analysis version 6.0. *Mol. Biol. Evol., 30(12)*: 2725-2729.

Tang, X; Frederick, R D; Zhou, J; Halterman, D A; Jia, Y and Martin, G B (1996). Initiation of plant disease resistance by physical interaction of *AvrPto* and *Pto* Kinase. *Science, 274*: 2060-2063.

Thompson, J D; Higgins, D G and Gibson, T J (1994). CLUSTAL W: Improving the sensitivity of progressive multiple sequence. *Nucleic Acids Res., 22(22)*: 4673-4680.

Thiel, T; Michalek, W; Varshney, R K and Graner, A (2003). Exploiting EST databases for the development and characterization of gene-derived SSR-markers in barley (*Hordeum vulgare* L.). *Theor. Appl. Genet., 106*: 411-422.

Turner, P D and Gillbanks, R A (1974). *Oil Palm Cultivation and Management*. 2nd edition. The Incorporated Society of Planters, Kuala Lumpur. 672 pp.

Wakefield, E (1920). Diseases of the oil palm in West Africa. *Bull. Misc. Inform. (RBGK), 1920(9)*: 306-308.

Wanderley-Nogueira, A C; Soares-Cavalcanti, N M; Morais, D A L; Belarmino, L C; Barbosa-Silva, A and Benko-Iseppon, A M (2007). Abundance and diversity of resistance genes in the sugarcane transcriptome revealed by *in silico* analysis. *Genet. Mol. Res., 6(4)*: 866-889.

Yeh, F C and Boyle, T J B (1997). Population genetic analysis of co-dominant and dominant markers and quantitative traits. *Belg. J. Bot., 129*: 157-163.

Journal of Oil Palm Research Vol. 35 (4) December 2023 p. 639-652
DOI: https://doi.org/10.21894/jopr.2023.0011

THERMAL ANALYSIS AND NON-ISOTHERMAL THERMOGRAVIMETRIC KINETICS ANALYSIS USING COATS-REDFERN METHOD OF A TORREFIED EMPTY FRUIT BUNCHES

MOHAMAD AZRI SUKIRAN[1]*; PETER ADENIYI ALABA[2]; ABU BAKAR NASRIN[1]; ASTIMAR ABDUL AZIZ[1] and SOH KHEANG LOH[1]

ABSTRACT

Thermal and mechanistic behaviours of solid biofuel are essential for commercial exploitation. In this work, the suitability of torrefied EFB as a solid biofuel was evaluated by investigating its physicochemical characteristics, kinetics and reaction mechanism during pyrolysis. The pyrolysis behaviour of raw and torrefied EFB was predicted via thermogravimetric analysis, kinetic parameters via Coats-Redfern three pseudo-components model-fitting method and pyrolysis mechanism via Criado method with Z-master plot. The physicochemical properties of torrefied EFB improved significantly compared to raw EFB in terms of fuel properties such as carbon content (8%-41%), fixed carbon (79%-328%) and calorific value (7%-42%). The degradation rate of hemicellulose and cellulose of torrefied EFB increased when the torrefaction temperature increased from 225°C to 300°C, leading to lower char yield and overall activation energy to initiate the pyrolysis process. The model deduced that higher overall activation energy was exhibited by raw EFB (9.39 kJ/mol) than those of torrefied EFB ranging from 6.55-7.86 kJ/mol (300°C-225°C). Thermal degradation of hemicellulose from torrefied EFB dominated the process by about 74% compared to cellulose and lignin when torrefaction temperature increased from 225°C to 300°C. Torrefaction could convert the power law mechanism to nucleation and growth mechanism gradually, allowing for better EFB thermal decomposition as a whole.

Keywords: activation energy, empty fruit bunches, kinetic reaction mechanism, pyrolysis, torrefaction.

Received: 28 June 2022; **Accepted:** 8 January 2023; **Published online:** 9 March 2023.

INTRODUCTION

Every year, more than 100 million tonnes (wet basis) of oil palm biomass will be generated in the form of empty fruit bunches (EFB), palm kernel shells, mesocarp fibre, oil palm trunks and oil palm fronds. Of these, EFB is the most abundantly available, at the amount of ≈ 21.61 million tonnes (wet basis), from the processing of 96.09 million tonnes of fresh fruit bunches at 457 palm oil mills in 2020 (Parveez *et al.*, 2021). According to Chang (2014), EFB is generally 3.5 kg in mass and has a thickness of up to 130 mm and 300 mm in width and length. It usually encompasses a considerable amount of moisture, up to 70 wt.% due to sterilisation by steam during oil processing which is a natural way for fruit maturation (Loh, 2017; Sukiran *et al.*, 2020). Although EFB contains a substantially higher amount of holocellulosic components, 78 wt.% in total from cellulose and hemicellulose (Loh, 2017), which are

[1] Malaysian Palm Oil Board,
6 Persiaran Institusi, Bandar Baru Bangi,
43000 Kajang, Selangor, Malaysia.

[2] Department of Chemical Engineering,
Faculty of Engineering, University of Malaya,
50603 Kuala Lumpur, Malaysia.

* *Corresponding author e-mail: azri@mpob.gov.my*

more suitable for bioconversion compared to lignin (~20 wt.%), its high moisture and oxygen contents coupled with low energy density and calorific value (CV) have hindered the use of EFB as biofuel in its natural form. As EFB is not readily usable, it is therefore important to subject it to thermochemical pretreatment through pyrolysis, gasification and combustion before the biomass is turned into an easy-to-use biofuel.

Although pyrolysis is promising for biomass conversion into bio-oil, bio-char and combustible gas, it has several drawbacks. In the pyrolysis process, the bio-oil obtained exhibits some inferior properties: High water content and acidic value, poor volatility, low heating value and chemically unstable with the undesired aging problem. These characteristics hamper the direct and efficient utilisation of bio-oil as biofuel and fine chemicals. All the above-mentioned problems are caused by the low quality of biomass, hence pretreatment is necessary in order to improve the fuel properties (Abnisa and Alaba, 2021). Among the biomass pretreatment methods developed, torrefaction is an effective approach to reduce oxygen content and increase bulk density, *i.e.*, the key quality determinants of biomass feedstocks for pyrolysis.

Torrefaction is a thermochemical technique in biomass conversion at between 200°C and 300°C for 10-60 min in an inert atmosphere (Zhang *et al*., 2021). The chemical properties of biomass such as O/C and H/C ratios will improve due to the removal of hydroxyl and organic volatiles and the decomposition of hemicellulose during the torrefaction process. Thus, torrefied biomass is deemed to have superior properties similar to coal for the ease of handling, milling and transporting. The improvement made after the torrefaction process renders the torrefied biomass suitable to be used as a feedstock for the pyrolysis process. The resultant bio-oil will be associated with an increased fixed carbon content and reduced volatile matter. In addition, torrefaction prior to pyrolysis can subsequently increase the CV and decrease the acidity of bio-oil (Fleig *et al.*, 2021).

Thermogravimetric analysis (TGA) is the most common and simplest method of evaluating the kinetics of pyrolysis (Alaba *et al.*, 2020). TGA summarises the pyrolysis characteristics based on a kinetic model and shows the variation in activation energy. Many literatures can be found related to the pyrolysis kinetics of biomass using TGA (Kumar Mishra and Mohanty, 2021; Sharma and Sheth, 2018). For example, Müller-Hagedorn and Bockhorn (2007) studied the TGA behaviour of wheat and barley straw during pyrolysis. The formal kinetic parameters for the pyrolysis of the main components (hemicelluloses, lignin and cellulose) and their degradable amounts were modelled by assuming parallel, independent reactions. Damartzis *et al.* (2011) performed non-isothermal TGA behaviour of cardoon (*Cynara cardunculus*) stems and leaves. Three different kinetic models - the independent parallel reaction model, Kissinger-Akahira-Sunose (KAS) and Ozawa-Flynn-Wall (OFW) were evaluated for the kinetic parameters of the process. Meanwhile, Li *et al*. (2008) studied the thermal degradation kinetics of the main constituents of different parts of corn using two different three pseudo-component models.

On the other hand, several studies on the pyrolysis kinetics of oil palm biomass have been reported. Mohamed *et al.* (2018) modelled the kinetics of thermogravimetric catalytic pyrolysis of EFB with alumina using KAS and OFW. The presence of a catalyst increased the activation energy values of EFB pyrolysis. Soh *et al*. (2019) calculated pyrolysis kinetics parameters of oil palm biomass using Coats-Redfern integral method and Šesták-Berggren function to determine the activation energy and reaction mechanism. The activation energy of oil palm biomass pyrolysis during hemicellulose decomposition was found lower relative to the cellulose counterpart. Meanwhile, Kasim *et al.* (2018) applied the Coats-Redfern to model decomposition kinetics of raw and torrefied EFB to estimate the activation energy and pre-exponential factor. Both the kinetics parameters of torrefied EFB were higher than that for pyrolysis of EFB.

All these studies provide remarkable insights into understanding the fundamental reaction mechanisms and reaction kinetics of biomass pyrolysis, ranging from simple single-step kinetic model to a more complex reaction model. However, very few literature studies have examined the pyrolysis kinetics of torrefied biomass using multi pseudo-component (cellulose, hemicellulose and lignin) models (Brillard *et al.*, 2020; Singh *et al.*, 2019) Hence, there is a need for more in-depth understanding on thermal degradation of individual fibre component and also as a whole, for biofuel thermal conversion in particular. Therefore, this study aimed to fill this gap by investigating the thermal kinetics degradations of three pseudo-components of torrefied EFB by the Coats-Redfern method. The use of kinetic analysis to quantify the main lignocellulosic fractions allows for the inclusion of restrictions for a more precise quantification, while a physical interpretation can be added to the deconvolution process.

In this study, torrefaction of EFB commenced in a fixed bed reactor under nitrogen atmosphere at different temperatures (225°C, 250°C, 275°C and 300°C) for 30 min. TGA data of raw and torrefied EFB were used to predict the pyrolysis behaviour and estimate kinetic parameters using Coats-Redfern method with an assumption of three pseudo-components. In addition, the pyrolysis reaction mechanism of raw and torrefied EFB as predicted

using the Criado method with a Z-master plot, was new and not reported elsewhere for torrefied biomass pyrolysis. The approach used in this study offered a more reliable kinetics modelling, contributing to the design and simulation of torrefied biomass pyrolysis.

MATERIALS AND METHODS

Material Preparation

The raw material, EFB was collected from a palm oil mill located at Labu, Negeri Sembilan, Malaysia. The samples were milled to reduce their sizes and screened to obtain particle sizes within 0.1-1.0 mm. The resulting particles of EFB were dried at 103ºC for 24 hr until constant weight was achieved.

Torrefaction Experiment

The torrefaction of EFB was carried out in a vertical fixed bed reactor as the illustrated in *Figure 1*. The detailed procedure of torrefaction experiment has also been shown in our previous study (Sukiran *et al.*, 2021). A quartz reactor containing about 20 g of raw EFB was placed in the centre of furnace. After the equipment was assembled, nitrogen was used to exhaust the air inside the quartz reactor, and the gas was continuously introduced to maintain an inert environment. EFB samples were heated at a heating rate of 10°C/min until the desired torrefaction temperature namely 225°C, 250°C, 275°C and 300°C was reached, and maintained for 30 min of residence time. While vapour released from the process was condensed by a condenser and collected as a liquid product, a solid product (torrefied EFB) remaining inside the reactor was also collected. Both the products were weighed to obtain their mass yields based on Equation (1):

$$\text{Mass yield (wt.\%)} = \frac{\text{Mass of the desired product (liquid/solid)}}{\text{Mass of raw EFB}} \times 100\% \quad (1)$$

The gas yield was calculated by subtracting the mass yield (wt.%) of liquid and torrefied EFB from the total of 100%. The torrefaction experiment at each temperature was repeated three times to ensure experimental repeatability.

Characterisation of Raw and Torrefied EFB

The proximate analyses of raw and torrefied EFB were conducted to determine moisture content, volatile matter, fixed carbon and ash content according to ASTM D5142 (ASTM, 1998) using a thermogravimetric analyser (LECO TGA-701). LECO CHN 628 and LECO S 628 were used to determine carbon, hydrogen, nitrogen and sulphur contents according to ASTM D5373 (ASTM, 2014). Temperature and time of the combustion for CHN 628 ranged from 850°C to 950°C within 3 min, meanwhile combustion analysis for sulphur was set at 1350°C within 2 min. The oxygen content was determined from the difference between 100% and the total percentage of carbon, hydrogen, nitrogen and sulphur. The changes in the atomic composition of EFB were established using the Van Krevelen diagram. It was constructed using the molar ratio of

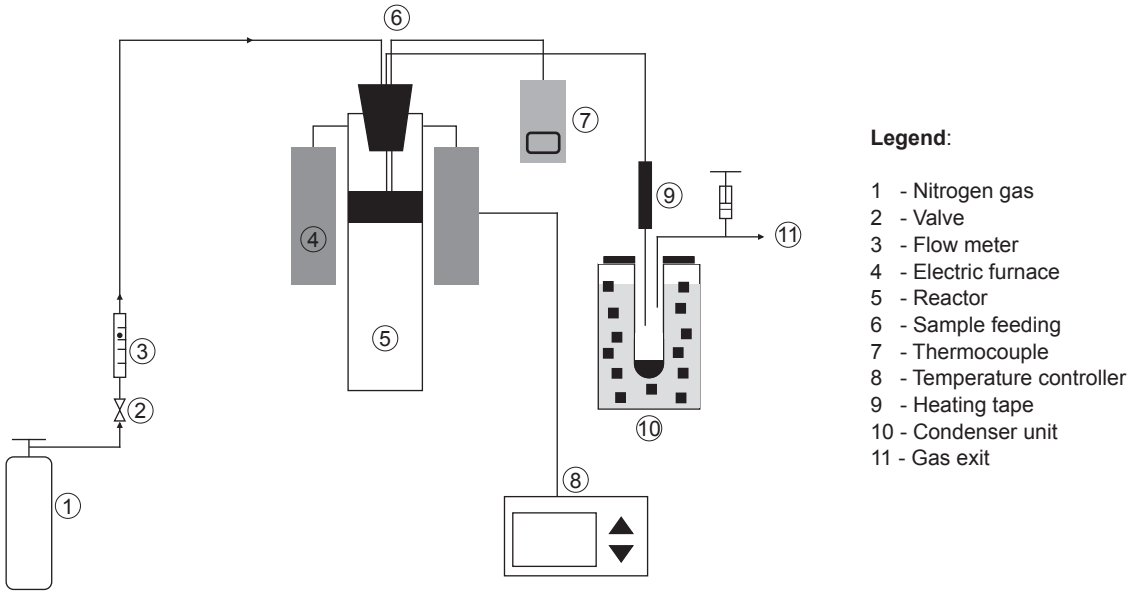


Figure 1. Schematic diagram of experimental setup for torrefaction of empty fruit bunches.

hydrogen: Carbon (hydrogen index) as the ordinate to the molar ratio of oxygen: Carbon (oxygen index) as the abscissa. The CV of raw and torrefied EFB were determined using a bomb calorimeter (LECO AC-600) according to ASTM D5865-07 (ASTM, 2019). The chemical compositions of the raw and torrefied EFB were analysed according to ASTM 1104-56 (ASTM, 1978a) and ASTM D1103-60 (ASTM, 1978b) for holocellulose and α-cellulose, respectively.

Briefly, a composite of cellulose and hemicellulose was extracted from raw and torrefied EFB using acidified sodium chlorite method. Approximately 24.0 g of sample was mixed with 960 mL distilled water and treated with 3.0 mL acetic acid and 9.0 g sodium chlorite at 70°C-80°C for 4 hr under continuous stirring. The mixture was then washed with hot water, filtered and dried at 105°C for 24 hr. Determination of holocellulose was carried out using dry weight method. A total of 12.0 g of dried holocellulose obtained was further dissolved in 240 mL of 17.5% (v/v) NaOH solution and stirred for 30 min. A total of 60 mL of NaOH solution was added into the mixture and allowed to mix to separate hemicellulose from the holocellulose and leaving α-cellulose. The insoluble α-cellulose was filtered and washed separately with 8.3% (v/v) NaOH solution followed by 10.0% (v/v) acetic acid. The α-cellulose was finally washed with hot water to a neutral pH and dried overnight at 80°C. The hemicellulose content was calculated as the difference in the weights of α-cellulose and holocellulose. The lignin content was determined using the gravimetric method according to TAPPI T222 om-11 (TAPPI, 2011). A 0.5 g sample was weighed into a 100 mL Erlenmeyer flask and stirred for 2 hr in 10 mL of cold 72.0% (v/v) H_2SO_4 solution. The mixture was transferred into a 500 mL beaker and boiled for 4 hr in 300 mL distilled water under continuous stirring. The mixture was filtered off using glass microfibre filter grade GF/B (Whatman) in porcelain crucible. The residue retained on the filter was washed with hot water until it was acid-free and allowed to dry at 105°C for 2 hr and weighed. Based on the obtained mass yield and CV of torrefied product, energy yield (E_y) was calculated as Equation (2):

$$E_y = \text{Mass yield of torrefied EFB} \times \left[\frac{\text{CV of torrefied EFB}}{\text{CV of raw EFB}}\right] \quad (2)$$

Pyrolysis Experiment

The thermogravimetric analyser (Perkin Elmer-Pyris 6) was used to determine pyrolysis of raw and torrefied EFB at different temperatures. In the experiment, an inert environment was created using high-purity nitrogen at 0.1 L/min using 10 mg of samples. The samples were heated from 30°C to 800°C at heating rates of 20°C/min. The gas atmosphere was high-purity nitrogen, and the gas flow rate was 0.2 L/min to ensure a pyrolysis reaction. Degradation of raw and torrefied EFB samples was determined from the thermogravimetric curves established via TGA based on ASTM E1131 (ASTM, 2020). Each experiment was replicated three times to ensure the reproducibility of the results. The temperature for calibration of TGA was accomplished using melting point standards to ensure accurate data collection. In addition, the data obtained were used for kinetics analysis.

Kinetics Analysis

Generally, the decomposition rate is given by Equation (3).

$$\frac{dx}{dt} = K(T) f(x)^2 \quad (3)$$

where x is the degree of conversion, T is temperature and t is time. The conversion rate $\frac{dx}{dt}$ for pyrolysis at constant heating rate, $\beta = \frac{dT}{dt}$, could be written as:

$$\frac{dx}{dt} = \beta\frac{dx}{dT} = K(T) f(x) \quad (4)$$

Also, the degree of advance, x is:

$$x = \frac{w_0 - w}{w_0 - w_f} \quad (5)$$

where w_0, w_f and w refer to mass of samples at the beginning, end and time, t, respectively. Since mass loss is temperature dependent, $K(T)$ is often modeled by Arrhenius Equation (Alaba *et al.*, 2016).

$$K(T) = A \exp\left(-\frac{E_A}{RT}\right) \quad (6)$$

where R is the gas constant (8.314 J mol^{-1} K^{-1}), A is the frequency factor, per min, E_A is the activation energy, kJ/mol and T is the absolute temperature, K. Combination of Equation (3) and (4) gives:

$$\beta\frac{dx}{dT} \; A \exp\left(-\frac{E_A}{RT}\right) f(x) \quad (7)$$

The kinetic models employed to analyse the thermogrametric data was Coats-Redfern model. The integral model developed by Coats and

Redfern suggests the correct order leading to the best straight-line plot. Therefore, Equation (7) becomes:

$$\ln\left(\frac{g(x)}{T^2}\right) = \ln\left(\frac{\mathrm{AR}}{\beta E_A}\right) - E_A/(RT) \quad (8)$$

Plotting $\ln(g(x)/T^2)$ versus $1/T$ results in a linear plot where the slope corresponds to $-E_A/R$ and the intercept gives $\ln(AR/\beta E_A)$. This gives the value of activation energy and Arrhenius constant/frequency factor. The overall conversion rate given by Equation (8) and overall activation energy (E_T) given by Equation (9) is the sum of the partial conversion rates and partial activation energy respectively, where Ci indicates the contribution factor of the volatile fraction produced from each component (hemicellulose, cellulose and lignin) in the following Equation (9) and (10):

$$\frac{d\alpha}{dt} = \sum_{i=1}^{3} C_i \frac{d\alpha_i}{dt} = C_1\frac{d\alpha_1}{dt} + C_2\frac{d\alpha_2}{dt} + C_3\frac{d\alpha_3}{dt} \quad (9)$$

$$E_T = \sum_{i=1}^{3} C_i E_i = C_1E_1 + C_2E_2 + C_3E_3 \quad (10)$$

Prediction of Reaction Model

The model for solid-state reaction during pyrolysis of torrefied EFB was investigated by Z-master plot associated with Criado method (Equation 11) (Criado, 1978).

$$\frac{Z(\alpha)}{Z(0.5)} = \frac{f(\alpha)\times g(\alpha)}{f(0.5)\times g(0.5)} = \left(\frac{T_\alpha}{T_{0.5}}\right)^2 \times \frac{(\mathrm{d}\alpha/dT)_\alpha}{(\mathrm{d}\alpha/dT)_{0.5}} \quad (11)$$

Equation (11) was employed to generate the master plots equivalent to various solid-state reaction mechanism. The term $[f(\alpha) \times g(\alpha)/f(0.5) \times g(0.5)]$ gives a theoretical curve, which signifies the characteristics of each reaction mechanism. On the other hand, the term $[(T_\alpha/T_{0.5})^2 \times ((\mathrm{d}\alpha/\mathrm{d}T)_\alpha/(\mathrm{d}\alpha/\mathrm{d}T)_{0.5})]$ is to be derived from a curve obtained from experimental values. The conversion value, α, is a value to define weight decomposition. The conversion rate is normally from 0 to 1.0. In most studies, the midpoint value (0.5) is used (Gogoi *et al.*, 2018; Luo *et al.*, 2021). The point $\alpha = 0.5$ is considered as the reference point, where the standard master plots of each considered kinetic mechanism intersect each other corresponding to value of $[Z(\alpha)/Z(0.5)] = 1$. The predominant reaction mechanism of the thermal degradation of solids can be deduced by comparison of the theoretical and experimental master plots.

RESULTS AND DISCUSSION

Product Distribution

Figure 2 shows EFB's torrefaction products distribution namely solid (torrefied EFB), liquid and gas at different temperatures for 30 min. As shown, the yields of torrefied EFB decreased with increasing torrefaction temperature, *i.e.*, between 40.50 wt.% - 90.30 wt.%. As torrefaction temperature increases, the yield of torrefied EFB decreases as the result of extensive decomposition of cellulose, hemicellulose and lignin present in EFB. According to Zhang and Zhang (2019), as temperature exceeds 200°C, volatile materials are released along with other components such as moisture, CO, CO_2 and some condensable matters such as acetic acid. Hence, higher amounts of these compounds were released at the employed higher temperature range in this study, therefore the mass of the torrefied EFB reduced and lower solid yield obtained at the end of the torrefaction process. At this rate, the colour of the torrefied EFB changed from dark brown to black as the temperature increased. Although high yield of torrefaction does not indicate that the EFB in the reactor is fully converted, several approaches can be used for quality checking. Visual observation of the physical appearance of raw biomass and their torrefied products, normally from light brown (raw EFB) to dark brown and then black, will be indicative of conversion status as the temperature and residence time increase. In addition, comparison of fuel properties (carbon content and CV) can also be accomplished to ensure full conversion of the materials. In this study, both high yield of torrefied product and good fuel properties are desirable. The trend of mass reduction of torrefied EFB was consistent with other studies concerning torrefaction of pigeon pea stalk and bamboo (Singh *et al.*, 2020a). Maximum reduction in mass yields of torrefied EFB was 40.50 wt.% at 300°C. Contrarily, the yields of liquid and gas products derived from torrefaction of EFB increased with torrefaction temperature. When the temperature increased from 225°C to 300°C, the mass yields of liquid and gas products increased from 3.00 wt.% to 21.27 wt.% and 6.70 wt.% to 38.20 wt.%, respectively. The maximum gas yield was attainable at 300°C, *i.e.*, 38.20 wt.%. At this temperature, secondary decomposition mainly occurred forming lots of condensable vapours.

Characterisation of Torrefied EFB

Figure 3 shows the volatile matter, moisture content, fixed carbon and ash content of torrefied EFB at different torrefaction temperatures. The results indicated that the fixed carbon and ash contents of torrefied EFB increased when

torrefaction temperature increased from 225ºC to 300ºC. The fixed carbon of torrefied EFB increased from 18.3 wt.% to 43.8 wt.%, about 79%-328% increment as compared to the raw EFB. Higher content of fixed carbon means that the torrefied product can produce more heat with a longer combustion time (Nudri *et al.*, 2020). Meanwhile, the ash contents increased from 3.1 wt.% to 11.9 wt.% with increasing torrefaction temperature. The breakdown of carbon-hydrogen bonds during torrefaction resulted in volatile losses and further concentrated the ash content in the torrefied EFB. In contrast, the volatile matter and moisture contents of torrefied EFB decreased when torrefaction temperature increased. The volatiles decreased from 75.8 wt.% to 42.5 wt.% when torrefaction temperature increased from 225ºC to 300ºC. Huge reduction in volatile matter was due to the catalytic effect of inorganic minerals present in the biomass (Almeida *et al.*, 2010). Low volatile matter in biomass indicates stable combustion since volatile matter is reactive, which causes spontaneous, unstable, incomplete combustion and emission of smoke when present in high quantity (Nudri *et al.*, 2020).

Elemental analysis of the raw and torrefied EFB at 225°C, 250°C, 275°C and 300°C is shown in *Table 1*. As the torrefaction temperature increased from 225ºC to 300ºC, the carbon content of torrefied EFB increased whereas the hydrogen and oxygen contents decreased. Similar trend for other torrefied biomasses has been reported previously (Chiou *et al.*, 2015). The carbon in the raw EFB amounted to 42.8 wt.%, which increased to 60.4 wt.% when it was torrefied at 300ºC. This was consistent with the increase in the fixed carbon as shown in *Figure 3*. Meanwhile, the oxygen and hydrogen contents decreased from 47.0 wt.% to 33.7 wt.% and 6.0 wt.% to 4.9 wt.%, respectively. Reduction of oxygen and hydrogen in the torrefied EFB was dominated by dehydration reaction in the form of water vapor and volatile compounds such as CO and CO_2. The sulphur content of torrefied EFB was in the range from 0.05 wt.%-0.06 wt.%.

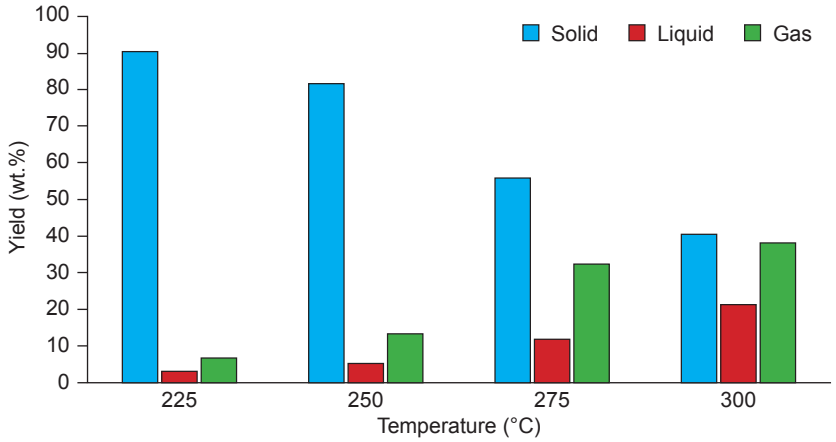


Figure 2. Torrefaction product distribution of empty fruit bunches at different temperatures.

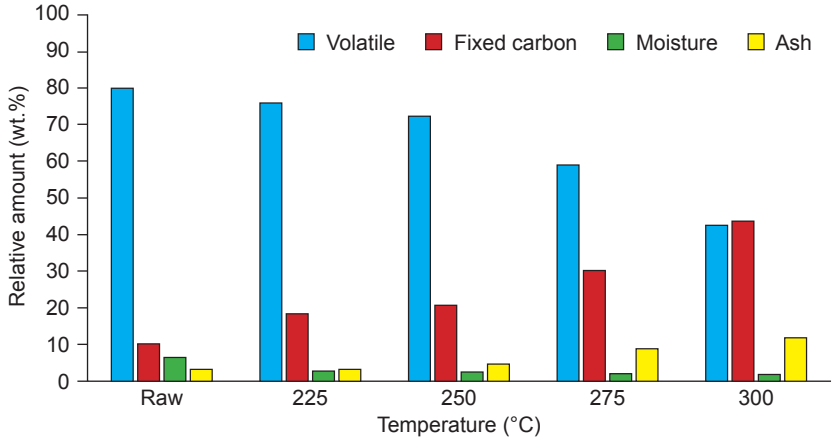


Figure 3. Proximate analysis of raw and torrefied empty fruit bunches at different temperatures.

Figure 4 shows the van Krevelen diagram for the raw and torrefied EFB at different temperatures. As can be seen, an increase in torrefaction temperature remarkably affected H/C and O/C atomic ratios. The H/C and O/C atomic ratios decreased from 1.70 and 0.89 (raw EFB) to 0.97 and 0.42 (torrefied EFB at 300°C), respectively. The decreases in the H/C and O/C ratios were mainly a result of the release of water and light volatile substances via dehydration, deoxygenation and dehydrogenation during torrefaction (Chen *et al.*, 2020). In addition, the atomic ratios of fossil-based coals such as lignite and bituminous were also illustrated in the same figure. As shown, the H/C and O/C atomic ratios of all the torrefied EFB were higher than those of lignite and bituminous; being that torrefied at 300°C the closest.

The CV of torrefied EFB was positively correlated with torrefaction temperatures, and vice versa for energy yield as listed in *Table 1*. The CV was in the range from 18.8 to 25.0 MJ/kg. This implies that the CV in the torrefied EFB increased by 7%-42% when compared to the raw EFB, due to the gradual increase of carbon content with torrefaction temperature. Similar trend of an increased CV for other torrefied biomasses has been reported previously (Wang *et al.*, 2018). Meanwhile, the trend of energy yield decreased significantly from 96.8% to 57.6% with increasing torrefaction temperature from 225°C to 300°C. Torrefied EFB with the least energy yield (57.6%) was generated at the most severe torrefaction conditions (300ºC), though with higher CV.

The chemical composition of the raw and torrefied EFB samples was determined to understand their conversion behaviour during torrefaction. *Figure 5* presents the chemical composition of the raw and torrefied EFB, namely, cellulose, hemicellulose and lignin. As shown in *Figure 5*, the cellulose content of raw EFB was higher than the hemicellulose and lignin contents. The high cellulose content in EFB is good for producing additional solid mass during the torrefaction process (Sukiran *et al.*, 2020). Not all celluloses are degraded to volatile products since the torrefaction process takes place at temperatures below 300°C, hence additional solid products are formed. Lignin is another component that is responsible for the major portion of the solid product in a thermal process. In *Figure 5*, the torrefaction process affected the lignocellulose components. As the temperature increases, the char yield decreases which could be associated with a higher degradation rate of hemicellulose, as indicated by the percentage of

TABLE 1. ULTIMATE ANALYSES, CALORIFIC VALUE AND ENERGY YIELD OF RAW AND TORREFIED EMPTY FRUIT BUNCHES AT DIFFERENT TEMPERATURES

Temperature (°C)	Ultimate analysis (wt.%)					CV (MJ/kg)	Energy yield (%)
	Carbon	Hydrogen	Nitrogen	Sulphur	Oxygen[a]		
Raw EFB	42.82	6.07	0.54	0.08	50.49	17.57	100
225	46.35	6.01	0.62	0.06	46.78	18.82	96.77
250	47.84	5.97	0.67	0.06	45.46	19.50	90.40
275	52.15	5.63	0.92	0.05	41.25	21.91	69.68
300	60.44	4.88	1.03	0.05	33.60	24.96	57.55

Note: [a]by difference.

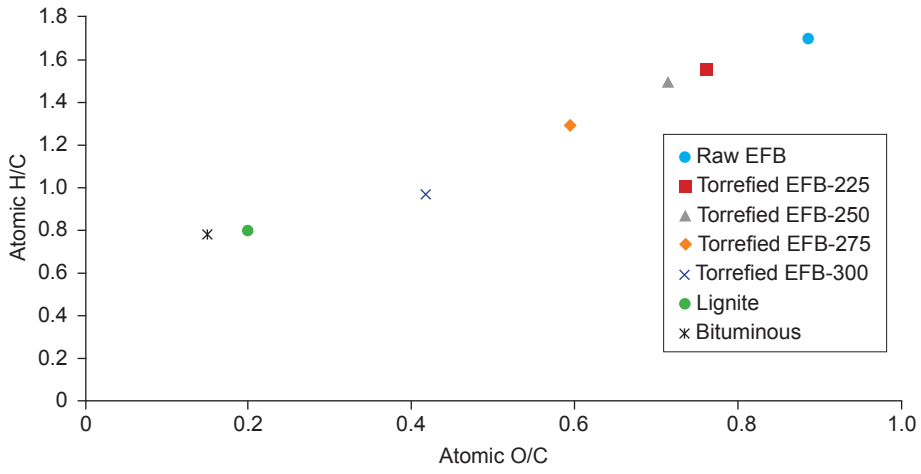


Figure 4. Van Krevelen plot of raw and torrefied empty fruit bunches (EFB) at various temperatures.

hemicellulose at different temperatures. Wang *et al.* (2017) obtained similar results during Norway spruce stem wood, stump and bark torrefaction. The hemicellulose content decreased significantly from 25.5% to 6.7% with increasing torrefaction temperature from 225°C to 300°C. After torrefaction at 275°C, more than half of the hemicellulose content in the EFB samples was degraded, while only a minor fraction occurring further at 300°C (6.7%). Decomposition of hemicellulose generated more CO_2, CO, water and oxygen-containing organic compounds during torrefaction (Chen *et al.*, 2018). The cellulose content of torrefied EFB decreased from 52.1% to 33.6% when the torrefaction temperature increased from 225°C to 300°C. Compared to hemicellulose content, the content of cellulose did not decrease evidently even at more severe torrefaction condition (300°C). At 225°C, the cellulose content was higher than that in the raw EFB. As severe degradation of hemicelluloses leads to a reduced mass, which further contributes to an increase of cellulose mass in totality of the EFB. The decomposed hemicellulose and cellulose further increased the lignin content of the torrefied EFB considerably with increasing torrefaction temperatures. The lignin content of torrefied EFB increased from 28.5% to 59.7%.

Thermogravimetric Analysis

The pyrolysis degradation behaviours of the raw and torrefied EFB at different temperatures and heating rate of 10°C/min are shown in *Figure 6a* and *6b*. The first stage was accompanied by elimination of water constituent and some light volatile compounds (Singh *et al.*, 2020b). As shown in *Figure 6a*, the peak value at the drying region (30°C and 150°C) became smaller and smaller when torrefaction temperature increased from 225°C to 300°C. This was expected as weight loss owing to moisture reduction for torrefied EFB was lesser than that of the raw biomass. Most water in the torrefied EFB samples had been removed as shown in *Figure 3*. For example, the weight loss of torrefied EFB at 250°C and 300°C were 8.1 wt.% and 10.0 wt.%, respectively as compared to the raw EFB, *i.e.*, 13.1 wt.%. The second stage was associated with devolatilisation process where major weight losses from EFB had occurred due to degradation of the hemicelluloses and celluloses. Such degradation took place between 200°C and 350°C, which was similar to our earlier finding (Sukiran *et al.*, 2017). As shown (*Figure 6a*), the shoulder on the lower temperature side during EFB torrefaction corresponded to thermal degradation of the extractives and also hemicellulose, which tend to decompose at much lower temperatures. Meanwhile, DTG curves (*Figure 6b*) show peaks of maximum degradation temperature for the EFB torrefied at 225°C, 250°C and 275°C. The peaks increased from 331°C to 337°C and to 344°C. The gradual increase in decomposition temperature of torrefied EFB might be due to total breakdown of hemicelluloses while retaining most of the celluloses and lignin. This phenomenon can be explained in *Figure 5*, where most hemicelluloses have been degraded along with a limited degradation of celluloses in the course of torrefaction. Thereafter, a continuous slight devolatilization occurred where lignin decomposition and char formation took place at temperature between 480°C and 700°C. As lignin is characterised by complex aromatic structure, its decomposition can only be accomplished with higher temperatures. Hence, the mass losses decreased slowly at this stage as shown in *Figure 6*. Besides, the inconsistency in thermal degradation of individual component of EFB contributed to deviation in residual char yield. The residual char yields after pyrolysis of the raw and torrefied EFB at 225°C, 250°C, 275°C and 300°C were 19.9%, 28.9%, 36.8%, 45.1% and 57.0%, respectively. The results correlated with the chemical compositions in *Figure 5*. The higher residual char yield in the torrefied EFB at higher pyrolysis temperature

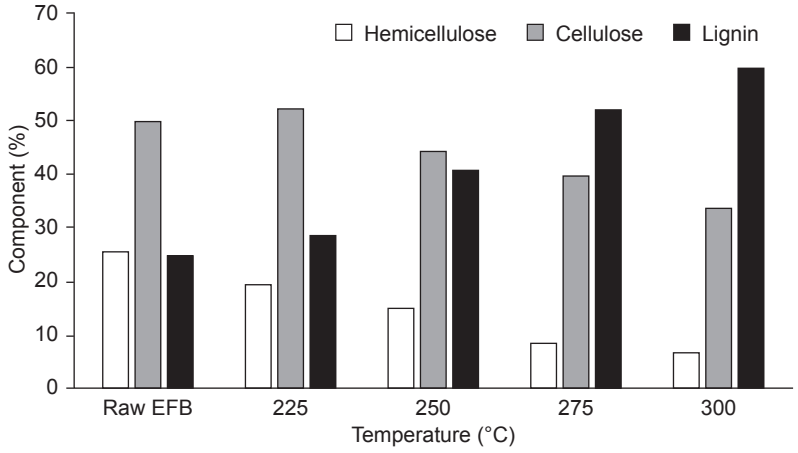


Figure 5. Chemical composition analysis of raw and torrefied empty fruit bunches at different temperatures.

was probably due to a larger mass of celluloses and lignin retained plus the cross-linkage reaction involved. At the end of the pyrolysis process, the mass rate curves exhibited small oscillations *(Figure 6b)* which corresponded to slow degradation of the lignin resided in torrefied EFB (Brillard *et al.*, 2020). Based on TGA and DTG (*Figure 6*), and chemical composition (*Figure 5*) analyses, the suitable torrefaction temperature to pre-treat EFB is 225°C-250°C, as for a more severe torrefaction condition a further loss of cellulose would significantly reduce bio-oil yield during pyrolysis.

Kinetics Analysis

Table 2 summarises the activation energy for individual hemicellulose, cellulose and lignin of the raw and EFB torrefied at different temperature (225°C, 250°C, 275°C and 300°C). In this study, the respective activation energy was calculated using Coats and Redfern method based on Equation (8). As the torrefaction temperature increased from 225ºC to 300ºC, the activation energy of hemicellulose, cellulose and lignin decreased as shown in *Table 2*. Similar trend has been reported previously for other torrefied biomasses (Singh *et al.*, 2019). The overall activation energy, E_T also showed a similar downward trend with increasing torrefaction temperature. However, these values are much lower than those of other studies (Tian *et al.*, 2020), thus indicating that torrefied EFB is a promising feedstock for pyrolysis process as the energy required to initiate the reaction is lower. The E_T of the raw EFB is 9.39 kJ/mol compared to those of torrefied EFB, in the range of 6.55-7.86 kJ/mol (300°C-225°C). These values are low, probably due to the different reaction models used and their corresponding kinetics parameters which are sensitive to individual fibre composition. This finding is supported by a similar study using EFB as feedstock employing the Coats-Redfern model (Surahmanto *et al.*, 2020), where the activation energy obtained is equally low (7.58-12.63 kJ/mol), especially at higher temperature range (347°C-535°C). As shown in *Table 2*, the activation energy of hemicellulose resided in the torrefied EFB ranged from 4.07 (300°C) to 5.65 kJ/mol (225°C), compared to that of 5.79 kJ/mol (raw hemicellulose in EFB). The fact that hemicellulose becomes unstable at around 230°C has caused reduction in activation energy. Meanwhile, the value of activation energy for cellulose decreased from 7.05 (raw cellulose in EFB) to 5.63 kJ/mol (300°C) during torrefaction. At this high torrefaction temperature, the thermal stability of cellulose decreased (Singh *et al.*, 2019).

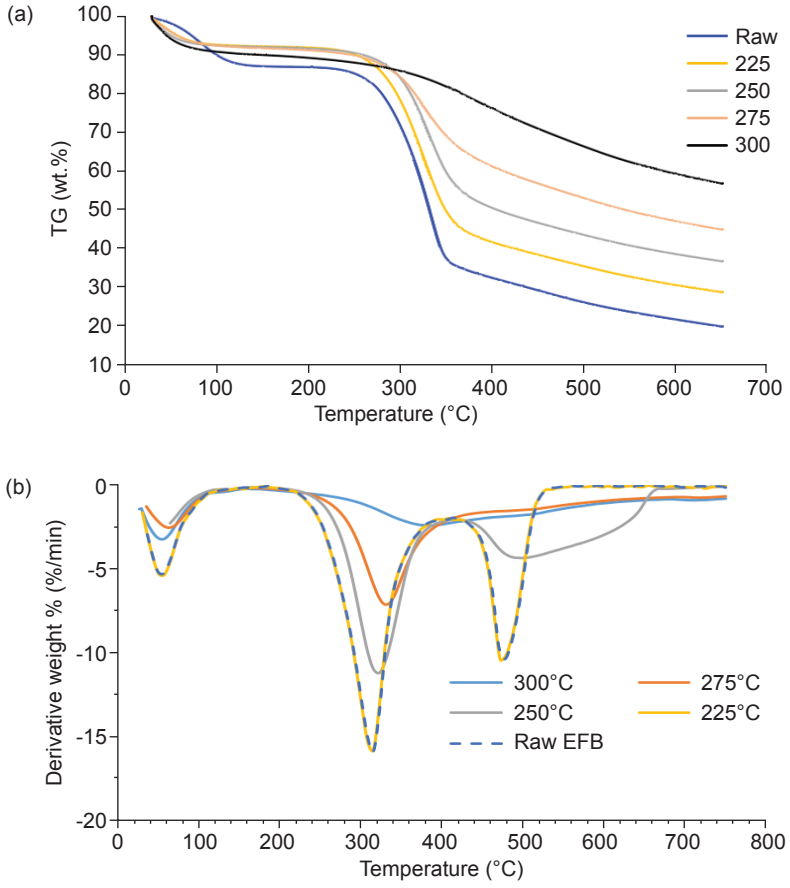


Figure 6. Experimental curves of (a) TGA and (b) DTG of raw and torrefied empty fruit bunches at different temperatures.

The activation energy of lignin decreased from 12.89 kJ/mol (225°C) to 10.02 kJ/mol (300°C) indicating a more severe decomposition rate of lignin at higher torrefaction temperature.

Linear correlation equations obtained by Coats and Redfern plot method are given in *Table 2*. From the equations, it is clear that the slope of hemicellulose decreased significantly for torrefied EFB at 275°C, while for cellulose and lignin at 300°C. Contribution factor of hemicellulose for torrefied EFB decreased from 0.32 to 0.12 when torrefaction temperature increased from 225°C to 300ºC, confirming the thermal degradation of hemicellulose during torrefaction. Meanwhile, the contribution factor of cellulose for torrefied EFB at 300°C decreased significantly from 0.42 (raw) to 0.25, indicating that only this torrefaction temperature can efficiently remove cellulose. Higher cellulose content of EFB torrefied at lower temperatures will potentially generate higher volatile matters, leading to an increase in pyrolysis oil yield. In contrast, the contribution factor for lignin increased exponentially towards the end of EFB torrefaction at 300ºC, suggesting that most hemicellulose and cellulose had remarkably decomposed and thus the torrefied EFB was rich in lignin (Singh *et al.*, 2019). This observation is also reflected in *Figure 5*, which shows mostly hemicellulose degradation along with limited content of degraded cellulose during torrefaction.

Prediction of Reaction Mechanism

Criado analysis was used to determine the reaction mechanism during pyrolysis of the raw and torrefied EFB at a different conversion level and heating rate of 10°C/min. *Figure 7* presents the plots for the raw and torrefied EFB at α of 0.1 to 0.9.

Reaction mechanism at lower conversion (α<0.5). *Table 3* represents the decomposition mechanisms of the raw and torrefied EFB at temperature 225°C-300°C (denoted by EFB_T-225, EFB_T-250, EFB_T-275 and EFB_T-300). For raw EFB at conversion less than 0.5, the closest match with the theoretical curve is associated with D4 mechanism which corresponds to three-dimensional diffusion (Ginstling-Broushtein equation). Torrefied EFB_T-225 and EFB_T-250 follow power law (P4) mechanism; EFB_T-275 follows power law (P4) mechanism and nucleation and growth mechanism (4^{th} order Avrami-Erofeev model); EFB_T-300 follows power law (P3 and P4) mechanism and nucleation and growth mechanisms (3^{rd} and 4^{th} order Avrami-Erofeev model). Diffusion is the rate-determining step for the raw EFB probably due to the higher volatile content as shown in *Figure 3*. The thickness of product layer around EFB increases with increasing level of conversion. The forming of product layer could hinder the transfer

TABLE 2. KINETIC PARAMETERS FOR THE PSEUDO-COMPONENTS OF RAW AND TORREFIED EMPTY FRUIT BUNCH USING COATS AND REDFERN

Kinetic parameters	Raw_EFB	EFB_T-225	EFB_T-250	EFB_T-275	EFB_T-300
E_H (kJ/mol)	5.79	5.65	5.31	4.97	4.07
A_H	8.80E-06	8.58E-06	8.48E-06	8.32E-06	8.11E-06
R^2	0.94	0.90	0.93	0.93	1.00
C_H	0.36	0.32	0.28	0.26	0.12
Linear correlation equation for hemicellulose (ln(g(x)/T2 vs 1/T)	y = 896.72x - 14.275	y = 850.48x - 14.504	y = 712.07x - 14.347	y = 638.74x - 14.213	y =597.65x - 14.101
E_C (kJ/mol)	7.05	7.33	6.98	6.05	5.63
A_C	9.72E-06	9.88E-06	9.70E-06	9.74E-06	9.15E-06
R^2	0.94	0.91	0.91	0.93	1.00
C_C	0.42	0.55	0.52	0.44	0.25
Linear correlation equation for cellulose (ln(g(x)/T2 vs 1/T)	y = 848.24x - 14.372	y = 839.92x - 14.365	y = 838.94x - 14.345	y = 727.65x - 14.217	y = 677.46x - 14.208
E_L (kJ/mol)	13.53	12.89	12.68	11.65	10.02
A_L	7.46E-06	6.82E-06	6.89E-06	7.20E-06	7.66E-06
R^2	0.98	1.00	1.00	1.00	0.99
C_L	0.33	0.17	0.20	0.31	0.62
Linear correlation equation for lignin (ln(g(x)/T2 vs 1/T)	y = 1386.9x - 15.129	y = 1583.6x - 15.297	y = 1524.9x - 15.314	y = 1401.4x - 15.175	y = 1205.6x - 14.962
Overall activation energy (ET), kJ/mol	8.39	7.86	7.74	7.49	6.55

Note: $y = \ln(g(x)/T^2)$ and $x = 1/T$; EFB_T-XXX = EFB torrefied at XXX°C; H - hemicellulose; C - cellulose; L - lignin.

of heat from the surrounding. Therefore, all the torrefied EFB (EFB_T-225, EFB_T-250, EFB_T-275 and EFB_T-300) were not controlled by diffusion, rather the very little volatile loss after torrefaction had changed the mechanism to power law.

Reaction mechanism at lower conversion (α>0.5). From 0.5 to 0.9, conversion of the raw and torrefied EFB occurs at higher degree with more complex reaction mechanism (*Table 3*). At conversion above 0.5, the raw biomass follows power law (P3 and P4) mechanism (Postawa *et al.*, 2022). This transition, from diffusion to power law mechanism was accomplished due to massive loss of volatile matter at conversion less than 0.5. In addition, to the power law (P3 and P4) torrefied EFB_T-225 could also experience 3rd order random nucleation (contracting volume, R3) with three nuclei on each particle, while EFB_T-250 could advance further into nucleation and growth pathway, A4 by Avrami-Erofeev model. Torrefied EFB_T-300 could also be described by Avrami-Erofeev models (A1, A3, and A4) for nucleation and growth mechanisms. At higher temperature, relatively higher conversion of biomass could occur due to an accelerated decomposition. Moreover, cleavage of some larger ordered cellulose into lower molecular mass chain could occur, which then facilitates the nucleation, growth and decomposition processes (Singh *et al.*, 2020b) .

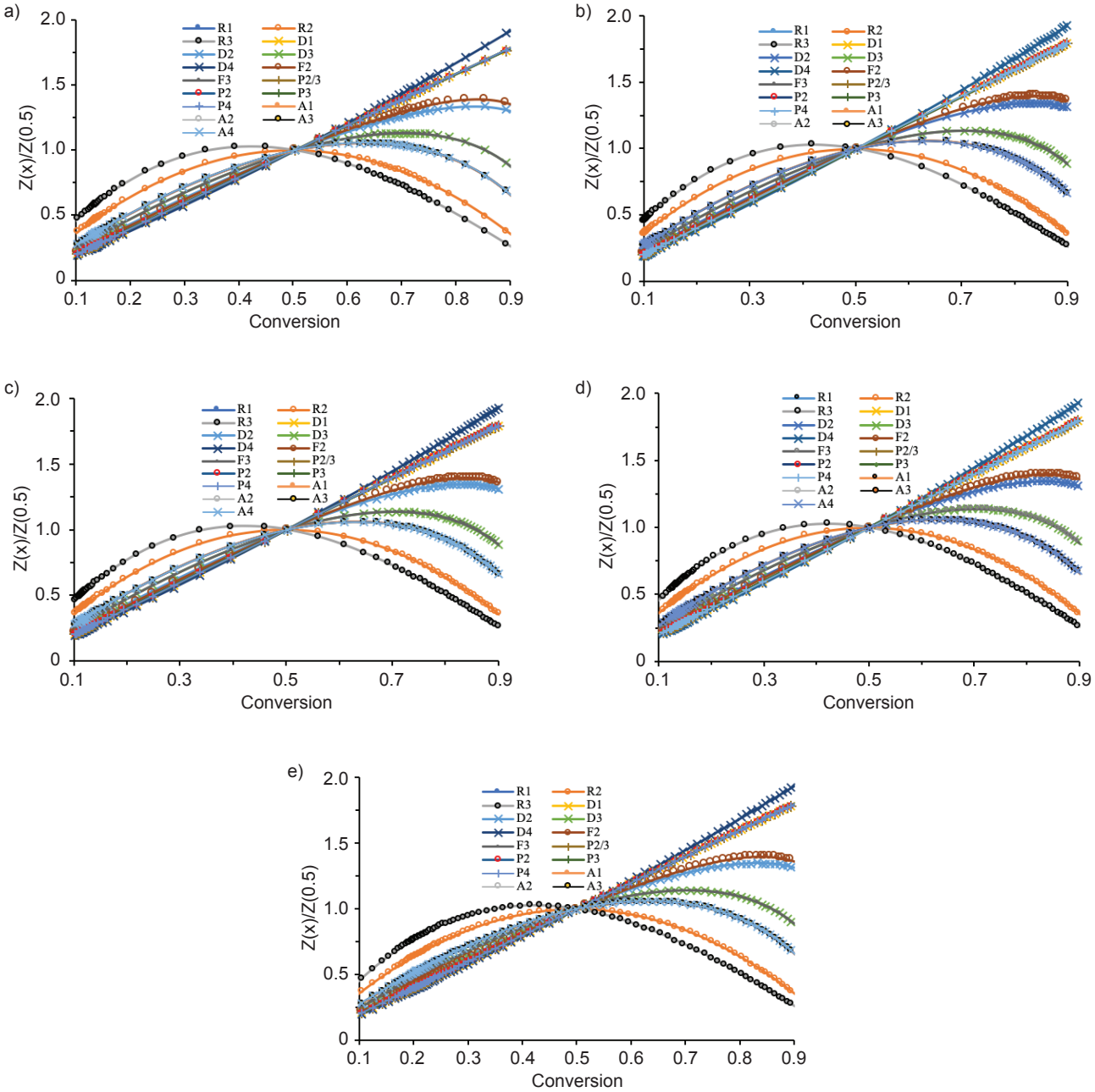


Figure 7. Theoretical and experimental plots for prediction of solid-state reaction mechanism using Criado method (Z-master plot). a) Raw_EFB, b) EFB_T-225, c) EFB-T250, d) EFB_T-275 and e) EFB_T-300.

TABLE 3. PREDICTED MODELS FOR RAW AND TORREFIED EMPTY FRUIT BUNCHES

Biomass	Solid state	
	Conversion less than 0.5	Conversion greater than 0.5
Raw EFB	Diffusion model D3(0.9994) D3 $f(\alpha) = 3/2(1-\alpha)^{2/3}[1-(1-\alpha)^{1/3}]^{-1}$ $g(\alpha) = [1-(1-\alpha)^{1/3}]^2$	Power Law models P3(0.9859), P4(0.9928) P3 $f(\alpha) = 3\alpha^{2/3}$, $g(\alpha) = \alpha^{1/3}$ P4 $f(\alpha) = 4\alpha^{3/4}$, $g(\alpha) = \alpha^{1/4}$
EFB_T-225	Power Law models P4(0.9487) P4 $f(\alpha) = 4\alpha^{3/4}$, $g(\alpha) = \alpha^{1/4}$	Power Law models P3(0.9667), P4(0.9807) P3 $f(\alpha) = 3\alpha^{2/3}$, $g(\alpha) = \alpha^{1/3}$ P4 $f(\alpha) = 4\alpha^{3/4}$, $g(\alpha) = \alpha^{1/4}$
EFB_T-250	Power Law models P4(0.9716) P4 $f(\alpha) = 4\alpha^{3/4}$, $g(\alpha) = \alpha^{1/4}$	Power Law models P3 (0.9762), P4 (0.9856) P3 $f(\alpha) = 3\alpha^{2/3}$, $g(\alpha) = \alpha^{1/3}$ P4 $f(\alpha) = 4\alpha^{3/4}$, $g(\alpha) = \alpha^{1/4}$ 3rd order random nucleation having three nucleus on individual particle R3 (0.9779) $f(\alpha) = (1-\alpha)^3$ $g(\alpha) = 1/2[(1-\alpha)^{-2}-1]$
EFB_T-275	P4(0.9735), P4 $f(\alpha) = 4\alpha^{3/4}$, $g(\alpha) = \alpha^{1/4}$ Avrami-Erofeev models, A4(0.9625) A4 $f(\alpha) = 4(1-\alpha)[-\ln(1-\alpha)]^{3/4}$ $g(\alpha) = [-\ln(1-\alpha)]^{1/4}$	P3(0.9716), P4(0.9716), P3 $f(\alpha) = 3\alpha^{2/3}$, $g(\alpha) = \alpha^{1/3}$ P4 $f(\alpha) = 4\alpha^{3/4}$, $g(\alpha) = \alpha^{1/4}$ Avrami-Erofeev models, A4(0.9894) A4 $f(\alpha) = 4(1-\alpha)[-\ln(1-\alpha)]^{3/4}$ $g(\alpha) = [-\ln(1-\alpha)]^{1/4}$
EFB_T-300	Power Law models P3 (0.9886), P4(0.9921), P3 $f(\alpha) = 3\alpha^{2/3}$, $g(\alpha) = \alpha^{1/3}$ P4 $f(\alpha) = 4\alpha^{3/4}$, $g(\alpha) = \alpha^{1/4}$ A3(0.9846), A4(0.9915) A3 $f(\alpha) = 3(1-\alpha)[-\ln(1-\alpha)]^{2/3}$ $g(\alpha) = [-\ln(1-\alpha)]^{1/3}$ A4 $f(\alpha) = 4(1-\alpha)[-\ln(1-\alpha)]^{3/4}$	Power Law models P3 (0.9871), P4(0.992), P3 $f(\alpha) = 3\alpha^{2/3}$, $g(\alpha) = \alpha^{1/3}$ P4 $f(\alpha) = 4\alpha^{3/4}$, $g(\alpha) = \alpha^{1/4}$ Avrami-Erofeev models, A1(0.9898), A3(0.9888), A4(0.9947) A1 $f(\alpha) = 1/2(1-\alpha)[-\ln(1-\alpha)]^{1/3}$ $g(\alpha) = [-\ln(1-\alpha)]^{2/3}$ A3 $f(\alpha) = 3(1-\alpha)[-\ln(1-\alpha)]^{2/3}$ $g(\alpha) = [-\ln(1-\alpha)]^{1/3}$ A4 $f(\alpha) = 4(1-\alpha)[-\ln(1-\alpha)]^{3/4}$ $g(\alpha) = [-\ln(1-\alpha)]^{1/4}$

Note: EFB_T-XXX = EFB torrefied at XXX°C.

CONCLUSION

In this study, torrefaction was performed on EFB before subjecting it to pyrolysis. Torrefaction was able to improve the physiochemical properties of raw EFB, and alter the chemical composition in such to be deemed desirable for pyrolysis with lower activation energy required. The fuel quality (volatile matter, H/C, O/C and CV) of the torrefied EFB had been greatly enhanced, while thermal stability decreased with temperature. The activation energy of hemicellulose, cellulose and lignin of the torrefied EFB decreased with increasing pyrolysis degradation temperature. The thermal degradation of torrefied individual component and the whole EFB was in the order of hemicellulose > cellulose > lignin, and EFB_T-300 > EFB_T-275 > EFB_T-250 > EFB_T-225 > raw EFB. These findings suggested that torrefied EFB could be a better solid fuel as torrefaction is able to convert the power law mechanism to nucleation and gradual growth mechanism, which eases decomposition during combustion. Overall, it can be concluded that torrefied EFB is a potential feedstock for bio-energy production.

ACKNOWLEDGEMENT

The authors would like to thank the Director-General of MPOB for permission to publish this article.

REFERENCES

Abnisa, F and Alaba, P A (2021). Recovery of liquid fuel from fossil-based solid wastes via pyrolysis technique: A review. *J. Environ. Chem. Eng.*, 106593.

Alaba, P A; Popoola, S I; Abnisal, F; Lee, C S; Ohunakin, O S; Adetiba, E; Akanle, M B; Patah, M F A; Atayero, A A and Daud, W M A W (2020). Thermal decomposition of rice husk: A comprehensive artificial intelligence predictive model. *J. Therm. Anal. Calorim., 140(4)*: 1811-1823.

Alaba, P A; Sani, Y M and Daud, W M A W (2016). A comparative study on thermal decomposition behavior of biodiesel samples produced from shea butter over micro- and mesoporous ZSM-5 zeolites

using different kinetic models. *J. Therm. Anal. Calorim.*, *126(2)*: 943-948.

Almeida, G; Brito, J and Perré, P (2010). Alterations in energy properties of eucalyptus wood and bark subjected to torrefaction: The potential of mass loss as a synthetic indicator. *Bioresour. Technol.*, *101(24)*: 9778-9784.

ASTM (1978a). Designation: D 1104-56. Method of test for holocellulose in wood. ASTM International, West Conshohocken.

ASTM (1978b). Designation: D 1103-60. Standard test method for α-cellulose. ASTM International, West Conshohocken.

ASTM (1998). Designation: D 5142. Standard test methods for proximate analysis of the analysis sample of coal and coke by instrumental procedures. ASTM International, West Conshohocken.

ASTM (2014). Designation: D 5373. Standard test methods for determination of carbon, hydrogen and nitrogen in analysis samples of coal and carbon in analysis samples of coal and coke. ASTM International, West Conshohocken.

ASTM (2019). Designation: D 5865. Standard test method for gross calorific value of coal and coke. ASTM International, West Conshohocken.

ASTM (2020). Designation: E 1131. Standard test method for compositional analysis by thermogravimetry. ASTM International, West Conshohocken.

Brillard, A; Trouvé, G; Maryandyshev, P; Kehrli, D; Lyubov, V and Brilhac, J F (2020). Analysis through thermogravimetric analyses of the impact of torrefaction processes performed under a non-oxidative atmosphere on hydrolysis lignin samples. *Fuel*, *260*: 116261.

Chang, S H (2014). An overview of empty fruit bunch from oil palm as feedstock for bio-oil production. *Biomass Bioenergy*, *62*: 174-181.

Chen, D; Chen, F; Cen, K; Cao, X; Zhang, J and Zhou, J (2020). Upgrading rice husk via oxidative torrefaction: Characterization of solid, liquid, gaseous products and a comparison with non-oxidative torrefaction. *Fuel*, *275*: 117936.

Chen, D; Gao, A; Ma, Z; Fei, D; Chang, Y and Shen, C (2018). In-depth study of rice husk torrefaction: Characterization of solid, liquid and gaseous products, oxygen migration and energy yield. *Bioresour. Technol.*, *253*: 148-153.

Chiou, B S; Valenzuela-Medina, D; Bilbao-Sainz, C; Klamczynski, A K; Avena-Bustillos, R J; Milczarek, R R; Du, W X; Glenn, G M and Orts, W J (2015). Torrefaction of pomaces and nut shells. *Bioresour. Technol.*, *177*: 58-65.

Criado, J M (1978). Kinetic analysis of DTG data from master curves. *Thermochimica Acta*, *24(1)*: 186-189.

Damartzis, T; Vamvuka, D; Sfakiotakis, S and Zabaniotou, A (2011). Thermal degradation studies and kinetic modeling of cardoon (*Cynara cardunculus*) pyrolysis using thermogravimetric analysis (TGA). *Bioresour. Technol.*, *102(10)*: 6230-6238.

Fleig, O P; Raymundo, L M; Trierweiler, L F and Trierweiler, J O (2021). Study of rice husk continuous torrefaction as a pretreatment for fast pyrolysis. *J. Anal. Appl. Pyrolysis*, *154*: 104994.

Gogoi, M; Konwar, K; Bhuyan, N; Borah, R C; Kalita, A C; Nath, H P and Saikia, N (2018). Assessments of pyrolysis kinetics and mechanisms of biomass residues using thermogravimetry. *Bioresour. Technol. Rep.*, *4*: 40-49.

Kasim, N N; Ismail, K; Mohamed, A R; Ishak, M A M; Ahmad, R; Nawawi, W I and Ismail, W (2018). Characteristic, thermochemical behaviors and kinetic of demineralized and torrefied empty fruit bunches (EFB). *Adv. Sci. Technol. Eng. Syst. J.*, *3(5)*: 365-373.

Kumar Mishra, R and Mohanty, K (2021). Kinetic analysis and pyrolysis behavior of low-value waste lignocellulosic biomass for its bioenergy potential using thermogravimetric analyzer. *Materials Science for Energy Technologies*, *4*: 136-147.

Li, Z; Zhao, W; Meng, B; Liu, C; Zhu, Q and Zhao, G (2008). Kinetic study of corn straw pyrolysis: Comparison of two different three-pseudocomponent models. *Bioresour. Technol.*, *99(16)*: 7616-7622.

Loh, S K (2017). The potential of the Malaysian oil palm biomass as a renewable energy source. *Energy Convers. Manag.*, *141*: 285-298.

Luo, L; Zhang, Z; Li, C; He, F; Zhang, X and Cai, J (2021). Insight into master plots method for kinetic analysis of lignocellulosic biomass pyrolysis. *Energy*, *233*: 121194.

Mohamed, A R; Li, N; Ahmad Sohaimi, K S; Iberahim, N I; Rohaizad, N M and Hamzah, R (2018). Kinetic parameters of non-isothermal thermogravimetric non-catalytic and catalytic pyrolysis of empty

fruit bunch with alumina by Kissinger and Ozawa methods. *IOP Conf. Ser.: Mater. Sci. Eng.*, *318*: 012019.

Müller-Hagedorn, M and Bockhorn, H (2007). Pyrolytic behaviour of different biomasses (angiosperms) (maize plants, straws, and wood) in low temperature pyrolysis. *J. Anal. Appl. Pyrolysis*, *79(1)*: 136-146.

Nudri, N A; Bachmann, R T; Ghani, W A W A K; Sum, D N K and Azni, A A (2020). Characterization of oil palm trunk biocoal and its suitability for solid fuel applications. *Biomass Convers. Biorefin.*, *10(1)*: 45-55.

Parveez, G K A; Tarmizi, A H A; Sundram, S; Loh, S K; Ong-Abdullah, M; Palam, K D P; Salleh, K M; Ishak, S M and Idris, Z (2021). Oil palm economic performance in Malaysia and R&D progress in 2020. *J. Oil Palm Res.*, *33(2)*: 181-214.

Postawa, K; Fałtynowicz, H; Szczygieł, J; Beran, E and Kułażyński, M (2022). Analyzing the kinetics of waste plant biomass pyrolysis via thermogravimetry modeling and semi-statistical methods. *Bioresour. Technol.*, *344*: 12618.

Sharma, R and Sheth, P N (2018). Multi reaction apparent kinetic scheme for the pyrolysis of large size biomass particles using macro-TGA. *Energy*, *151*: 1007-1017.

Singh, R K; Chakraborty, J P and Sarkar, A (2020a). Optimizing the torrefaction of pigeon pea stalk (*Cajanus cajan*) using response surface methodology (RSM) and characterization of solid, liquid and gaseous products. *Renew. Energ.*, *155*: 677-690.

Singh, R K; Sarkar, A and Chakraborty, J P (2019). Effect of torrefaction on the physicochemical properties of pigeon pea stalk (*Cajanus cajan*) and estimation of kinetic parameters. *Renew. Energ.*, *138*: 805-819.

Singh, S; Prasad Chakraborty, J and Kumar Mondal, M (2020b). Intrinsic kinetics, thermodynamic parameters and reaction mechanism of non-isothermal degradation of torrefied *Acacia nilotica* using isoconversional methods. *Fuel*, *259*: 116263.

Soh, M; Chew, J J; Liu, S and Sunarso, J (2019). Comprehensive kinetic study on the pyrolysis and combustion behaviours of five oil palm biomass by thermogravimetric-mass spectrometry (TG-MS) analyses. *BioEnergy Res.*, *12(2)*: 370-387.

Sukiran, M A; Abnisa, F; Syafiie, S; Wan Daud, W M A; Nasrin, A B; Abdul Aziz, A and Loh, S K (2020). Experimental and modelling study of the torrefaction of empty fruit bunches as a potential fuel for palm oil mill boilers. *Biomass Bioenergy*, *136*: 105530.

Sukiran, M A; Abnisa, F; Wan Daud, W M A; Abu Bakar, N and Loh, S K (2017). A review of torrefaction of oil palm solid wastes for biofuel production. *Energy Convers. Manag.*, *149*: 101-120.

Sukiran, M A; Wan Daud, W M A; Abnisa, F; Nasrin, A B; Abdul Aziz, A and Loh, S K (2021). A comprehensive study on torrefaction of empty fruit bunches: Characterization of solid, liquid and gas products. *Energy*, *230*: 120877.

Surahmanto, F; Saptoadi, H; Sulistyo, H and Rohmat, T A (2020). Investigation of the pyrolysis characteristics and kinetics of oil-palm solid waste by using Coats-Redfern method. *Energy Explor. Exploit.*, *38(1)*: 298-309.

TAPPI (2011). Designation: T222 om-11. Acid-insoluble lignin in wood and pulp. TAPPI Press, Atlanta, GA.

Tian, X; Dai, L; Wang, Y; Zeng, Z; Zhang, S; Jiang, L; Yang, X; Yue, L; Liu, Y and Ruan, R (2020). Influence of torrefaction pretreatment on corncobs: A study on fundamental characteristics, thermal behavior, and kinetic. *Bioresour. Technol.*, *297*: 122490.

Wang, L; Barta-Rajnai, E; Skreiberg, Ø; Khalil, R; Czégény, Z; Jakab, E; Barta, Z and Grønli, M (2018). Effect of torrefaction on physiochemical characteristics and grindability of stem wood, stump and bark. *Appl. Energy*, *227*: 137-148.

Wang, L; Barta-Rajnai, E; Skreiberg, Ø; Khalil, R; Czégény, Z; Jakab, E; Barta, Z and Grønli, M (2017). Impact of torrefaction on woody biomass properties. *Energy Procedia*, *105*: 1149-1154.

Zhang, J and Zhang, X (2019). The thermochemical conversion of biomass into biofuels. *Biomass, Biopolymer-Based Materials, and Bioenergy*. Elsevier. p. 327-368.

Zhang, R; Zhang, J; Guo, W; Wu, Z; Wang, Z and Yang, B (2021). Effect of torrefaction pretreatment on biomass chemical looping gasification (BCLG) characteristics: Gaseous products distribution and kinetic analysis. *Energy Conver. Manag.*, *237*: 114100.

Journal of Oil Palm Research Vol. 35 (4) December 2023 p. 653-667
DOI: https://doi.org/10.21894/jopr.2022.0075

STRUCTURAL DESIGN OF A PASSIVE WEARABLE EXOSKELETON TO ASSIST OIL PALM HARVESTING OPERATION

MUHAMMAD FUAD MOHAMAD[1]; SHARENCE NAI SOWAT[1,2]; HAZLINA SELAMAT[3]; AIZREENA AZAMAN[4] and HAZREEN H HARITH[1,2]*

ABSTRACT

Harvesting of oil palm fresh fruit bunches is still performed manually, involving extensive energy, awkward postures or repetitive motion, and often under strenuous conditions. Exoskeleton technologies are increasingly being explored for performance augmentation and ergonomics intervention in industrial settings. For challenging environments, like the oil palm plantation, the dynamic interactions between user, task and environment is non-trivial. Importantly, an exoskeleton should not impede a worker's movement and task performance throughout the period of wear. Intrinsically, designing an exoskeleton for oil palm harvesting entails that the dynamic interactions between the harvester, the pole, and surrounding objects is considered early in the design process. We adopted the systems approach to designing an upper limb exoskeleton to assist oil palm harvesters. The proposed design is a slimline passive exoskeleton that provides an assistive force through compression springs in the upper arm region. Structural analysis and a preliminary prototype evaluation were performed for design verification. The weakest component was the back plate. Nevertheless, permanent deformation would only occur when an equivalent of 26 kg load is applied to the exoskeleton arm. Future work includes optimising the design and elucidating its long-term effects on the harvester's efficiency and field productivity through biomechanical analysis and field tests.

Keywords: assistive technology, design, harvesting, human factors, oil palm.

Received: 20 April 2022**; Accepted:** 11 October 2022**; Published online:** 1 December 2022.

INTRODUCTION

The nature of agricultural field work is very dependent on local environmental factors, such as weather, crop type and farm or field layout. This leads to varying structures and characteristics of farm or field environments to suit the changing environmental conditions. Agricultural workers interact with and handle machines and tools of various sizes and shapes to match the characteristics of the crops and the environment. This unique characteristic of agricultural work is a challenge to comprehensive mechanisation and automation in the field (Marinoudi *et al.*, 2019; Sreeram and Nof, 2021; Vasconez *et al.*, 2019). Moreover, the dynamic interactions between the user, task and environment is especially critical for automation. Therefore, the synergistic relationship between human operators and machines will likely be a common view in the fields, especially for non-routine tasks and tasks performed by skilled workers (Marinoudi *et al.*, 2019).

In oil palm plantations, harvesting is performed by skilled workers who are adept at handling the cutting tool and manoeuvring through the

[1] Department of Biological and Agricultural Engineering, Faculty of Engineering, Universiti Putra Malaysia, 43400 UPM Serdang, Selangor, Malaysia.

[2] Smart Farming Technology Research Center, Faculty of Engineering, Universiti Putra Malaysia, 43400 UPM Serdang, Selangor, Malaysia.

[3] Centre for Artificial Intelligence & Robotics, Universiti Technology Malaysia, 81310 Johor Bahru, Johor, Malaysia.

[4] School of Biomedical Engineering and Health Sciences, Faculty of Engineering, Universiti Teknologi Malaysia, 81310 Johor Bahru, Johor, Malaysia.

* *Corresponding author e-mail: hazreen@upm.edu.my*

challenging plantation environment (Preethi *et al.*, 2016). The correlations between movements carried out during oil palm harvesting, its non-ergonomic nature, musculoskeletal problems and productivity have been well documented (Mohd Nawi *et al.*, 2014; Ng *et al.*, 2013; 2014). In fact, many manual agricultural tasks are typically performed in challenging and arduous conditions such as restricted space, unpredictable terrain and environment, and high cognitive load, leading to non-ergonomic working conditions for the workers and potentially musculoskeletal pains in the long run (Benos *et al.*, 2020a; 2020c; Castaneda *et al.*, 2020; Du *et al.*, 2022; Fathallah, 2010). Amongst these manual tasks, harvesting is postulated as one of the least mechanised tasks and one of the highest contributors toward musculoskeletal disorder (MSD), and this is similarly echoed in the oil palm industry (Benos *et al.*, 2020b). Ultimately, an optimal interaction between humans, machines and the working environment is pertinent to improve the ergonomics and productivity of manual harvesting or any manual field tasks.

Occupational exoskeletons are increasingly explored in the manufacturing and heavy industries, where manual tasks are still performed. An exoskeleton is a wearable device that augments, enables, assists, or enhances physical activity (Lowe *et al.*, 2019). Immediate positive effects of using occupational exoskeletons to assist manual operators in various industries are increasingly reported, mainly in terms of lower muscle activation in the assisted joints (Alabdulkarim *et al.*, 2019; Dahmen and Constantinescu, 2020; Iranzo *et al.*, 2020). For the oil palm harvesting industry specifically, exoskeletons could be a viable immediate solution for improving the worker's productivity while a fully mechanised system is being developed. Nevertheless, the design of the exoskeletons should consider the interactions between the user, the task and the working environment to increase their overall effectiveness in the field.

An Overview of Occupational Exoskeletons

There are multiple ways to categorise exoskeleton systems. They can be categorised based on the power source, *i.e.* active, passive or semi-active system, or mechanical structure, *i.e.* rigid or soft. Active systems contain electromechanical components and require external power sources for operation, while passive systems do not require an external power source. In terms of mechanical structure, rigid exoskeletons can deliver high assistive force to the body accurately, while soft exoskeletons sacrifice this aspect to allow more flexible motion (Xiloyannis *et al.*, 2019). More recently, semi-active systems, which use low-powered actuation units to modulate the amount of assistance provided by the assistive elements, have also been introduced such as by Grazi *et al.* (2020). Exoskeletons can also be categorised into lower, upper, and full-body systems. Lower body systems typically assist the waist and limbs below the waist, upper body systems assist limbs above the waist, while full-body systems assist both lower and upper bodies. Currently, many commercially available occupational exoskeletons are passive upper limb exoskeletons including ShoulderX (SuitX Emeryville, California, USA), EksoVest (EksoBionics, California, USA), PAEXO (Ottobock, Duderstadt, Germany) and AirFrame (Levitate Technologies, California, USA). A comprehensive review of occupational exoskeletons is available in Crea *et al.* (2021), De Bock *et al.* (2022), and Vries and Looze (2019).

Many occupational exoskeletons aim to improve the load-bearing capability of the assisted limbs or joints, and consequently the user's ergonomic condition. For example, the Chairless Chair (Noonee, Wendlingen, Germany) enables sitting without a chair by transferring the user's body weight to links that run in parallel with the thighs. For upper body exoskeletons, the load-bearing capability could be improved by distributing load to the larger muscles in the body. Upper body exoskeletons typically aim to assist arm raising or stabilising. An example is the Raku Vest (Kubota, Japan), an active system that aims to minimise the energy spent to stabilise the arm in specific positions. Finally, full-body exoskeletons have the advantage of assisting the upper limbs and transferring the load from the upper body directly to the ground. However, a full-body attachment can be cumbersome, partly due to multiple attachment points. Furthermore, bulky exoskeleton systems will interrupt the natural physical movement of the entire body, including causing imbalance (Kim *et al.*, 2018a; 2018b).

One of the first exoskeletons developed to assist agricultural tasks is an active full-body exoskeleton (Toyama and Yamamoto, 2010). The proposed system weighs 30 kg and has 10 joints with various control modes to match the user's movement during specific tasks, including radish harvesting, cucumber harvesting, and fruit tree pruning. An initial assessment of the prototype indicated problems in matching the motion of the system and the user at the shoulder and back, potentially caused by irregular movements by the users during harvesting.

Multiple studies have reported on the evaluation of passive exoskeletons for agricultural tasks, particularly in the last five years (Dewi and Komatsuzaki, 2018; Harith *et al.*, 2021; Thamsuwan *et al.*, 2020; Ulrey and Fathallah, 2013; Wang *et al.*, 2021). These studies evaluated either commercially available or prototype-staged exoskeletons. The overall results of these studies indicated some forms

of reduced demand on the assisted joints. However, many recommended observing exoskeleton usage onsite and over a longer duration, and/or modifying the designs for better user acceptance. Therefore, commercial exoskeletons may not be readily adopted in the field without further modification, particularly because many are designed for specific tasks and not for challenging environments (Mudie *et al.*, 2022). Moreover, field evaluation of exoskeletons in the agricultural field is currently too few (Thamsuwan *et al.*, 2020). A number of surveys also have highlighted the importance of aligning exoskeleton design with users, tasks and work environment for field adoption (Mudie *et al.*, 2022; Omoniyi *et al.*, 2020; Upasani *et al.*, 2019). Thus, considering the overall user's motion during usage and the working environment when designing the exoskeleton will reduce the mismatch between an exoskeleton's design and its application in the actual environment and encourage exoskeleton adoption in the industry (Mudie *et al.*, 2018).

Assistive Devices Design Considerations for Challenging Work Environment

Occupational exoskeletons are designed to improve the physical capability of the user in performing specific tasks. Interestingly, a recent study highlighted that exoskeletons designed for a specific task and not considering the operating environment prevent exoskeleton adoption in dismounted combatants (Mudie *et al.*, 2022). Agricultural operators similarly perform multiple tasks and handle different tools or machinery, typically in an unpredictable environment. In this setting, it is crucial that the exoskeleton or any assistive device is simple, easy to operate and does not restrict movement. Naturally, ease of use has been suggested as having a more important role in predicting the intention to use exoskeletons, compared to social influence and performance expectancy in a survey involving industrial workers (Elprama *et al.*, 2020). Moreover, wearing an exoskeleton will change an operator's body size, shape and inertia, and cause workers to modify their movements (Desbrosses *et al.*, 2021). Therefore, the technology should be adaptable and comfortable for the users throughout the duration of use.

In this study, we present the design of a passive upper limb exoskeleton for oil palm harvesting operators that was developed via the systems approach. For this approach, problem-solving focuses on systems taken as a whole, instead of their parts taken separately, as the interactions between parts cause dynamic changes in the system (Ackoff, 1971; Arnold and Wade, 2015; Monat and Gannon, 2018). In this study, the dynamic interactions between the user, the tasks, and the working environment was considered to establish the design criteria of the exoskeleton. The working environment is considered as the system, and the subcomponents are the harvester (and the movements performed), the pole, and surrounding objects including the uneven ground, the trees, hanging fronds, and other objects on the ground. The following sections describe the proposed design and the verification of its mechanical structure.

METHODOLOGY

The Oil Palm Plantation Environment

The dynamic interactions between the user, the device, the environment and the tasks should be considered in designing an assistive device to optimise its function in the actual operating environment (Mudie *et al.*, 2022; 2018). The oil palm plantation environment is characterised by dense canopies with hanging fronds from oil palm trees. The trees are now more commonly planted on hilly or undulating terrain. Other objects are also present on the ground, such as loose fruitlets, grass, weeds, and cut fronds. In short, a harvester must be aware of the surrounding while navigating through the plantation. *Figure 1* illustrates objects that could be present around the harvester during the operation. The presence of other objects in the harvester's surroundings and the plantation's uneven ground demand a slimline design without protruding components for ease of movement and safety. Additionally, since the pole extends below the waist and beyond the shoulder, both areas should be clear of any exoskeleton component to prevent interference with pole handling.

The Oil Palm Harvesting Tasks

Harvesting oil palm fresh fruit bunches (FFB) is a manual task that is physically demanding and ergonomically unfavourable (Nawi *et al.*, 2016; Ng *et al.*, 2013). Generally, harvesting comprises two main activities, cutting the fronds and FFB, and collecting the harvested FFB and loose fruits/fruitlets. These tasks may be performed by one operator, but a team of two operators is also widely practised. In this study, we focused on the cutting activity. A harvesting pole with a sickle is typically used for harvesting FFB from palms more than 3 m high. The weight and length of the pole increase with tree height, and the complexity of handling the pole increases with increasing pole length. The harvester's pole handling skills, pole structure, tree height and FFB locations are a few factors affecting efficiency.

For a harvester who performs cutting, the task involves two main movements, namely walking while handling the pole and cutting FFB and

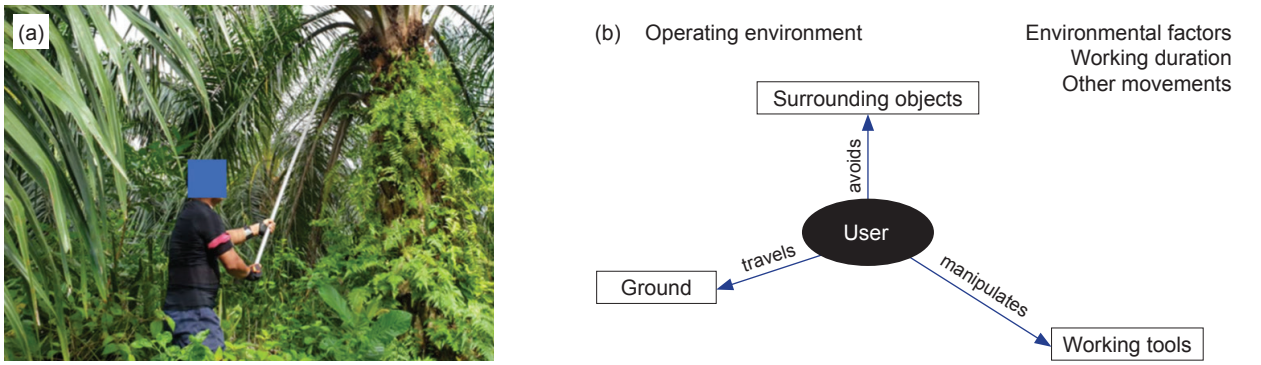


Figure 1. (a) An illustration of the work environment during oil palm harvesting. An operator is aiming the pole for the frond or bunch while hanging fronds are present in the surroundings and weeds are present on the ground and tree trunks. (b) A concept map highlighting the dynamic interactions between a harvester and multiple elements within the working environment.

fronds. The operator carries the pole most of the time throughout a shift. Walking while holding the pole mainly involves static holding with the arms positioned between the shoulder and the waist, while cutting involves frequent dynamic overhead movement. When harvesting trees that are more than 3 m high, the shoulder and the elbow move in extreme ranges of motion (Parras-Burgos *et al.*, 2020; Syuaib, 2015). The cutting movement, *i.e.* pushing and pulling of the pole has been postulated as the most fatiguing task, which has led to the development of a powered harvesting pole to reduce the intensity of pulling the pole (Jelani *et al.*, 2008). Our field observations of harvesting indicated that at least one side of the arm frequently moves in the region slightly above the shoulder and underneath the shoulder (Harith *et al.*, 2021). Similar descriptions of the cutting movement during oil palm harvesting have also been reported recently (Chan *et al.*, 2022; Tumit *et al.*, 2021). Additionally, the cutting movement, specifically pulling the pole, occurs very swiftly, *i.e.* over a fraction of a second (Chan *et al.*, 2022).

Ergonomics reports highlighted that the back, the shoulder and the neck had the most frequent complaints of pain in harvesters (Nawi *et al.*, 2016). Although harvesting is not limited to cutting tasks, biomechanical investigations on oil palm harvesting naturally focused on the cutting movement (Nawi *et al.*, 2016; Ng *et al.*, 2013). These investigations highlighted that the shoulder and/or the trunk are the main regions requiring assistance (Chan *et al.*, 2022; Harith *et al.*, 2021; Mohamaddan *et al.*, 2021; Tumit *et al.*, 2021). Nonetheless, the interpretation of these results is limited for exoskeleton design purposes because the exoskeleton will likely be worn throughout the harvesting operation during which movements are not limited to cutting. In this study, partial biomechanics analysis in terms of muscle activity for a complete harvesting operation was performed to enhance the interpretations of previous reports.

Muscle activity of selected shoulder muscles during harvesting. The human shoulder complex allows flexion/extension, internal/external rotation, and abduction/adduction of the upper limbs, and comprises four joints: Glenohumeral, acromioclavicular, sternoclavicular, and scapulothoracic joints. The elbow joint allows elbow extension and flexion. We observed the behaviour of two shoulders and two elbow muscles of three right-handed harvesters during harvesting (*Figure 2*). The muscle activity of the biceps, triceps, trapezius and deltoids was collected using electromyogram (EMG) sensors (Trigno Avanti, Delsys, MA, USA). The trapezius and deltoids were observed to mainly indicate shoulder motion, while the biceps and triceps were observed to mainly indicate elbow motion.



Figure 2. The position of four EMG sensors on four upper limb muscles based on SENIAM standards (1: Trapezius, 2: Deltoids, 3: Biceps, and 4: Triceps).

Three harvesters performed one cycle of harvesting comprising walking and holding the pole, followed by cutting one or two FFB on one tree. To detect EMG signals, dry electrodes were attached to the subjects throughout the experiment. Skin preparation was performed using alcohol

wipes to reduce electrode impedance with the skin. Eight electrodes were placed parallel to the muscle and away from other muscle groups according to the Surface Electromyography for the Non-Invasive Assessment of Muscles (SENIAM) recommendations. The EMG data were band-pass filtered and fully rectified by the international guidance; (10-500) Hz for surface electrodes, and denoised using wavelet transform (type DB6). The EMG averaged envelope was acquired using the moving averaging window method so that EMG levels can be compared. The peak root means square (RMS) of each muscle was averaged for three subjects to identify the strength of muscle activation during the harvesting cycle.

The data were analysed for two settings: (i) harvesting and walking, and (ii) harvesting only (excluding walking with a pole). This was done to observe the differences in muscle activity between a complete harvesting cycle (harvesting and walking) and cutting alone. All analyses were performed in EMGWorks (Delsys, MA, USA) software.

Design Criteria for an Oil Palm Harvesting Exoskeleton

Based on the description of the plantation environment and the dynamic interactions between the harvester, pole, task and environment, the proposed design criteria for the upper limb exoskeleton to assist harvesting are as follows:

i. A passive upper limb system
ii. Low-profile or slimline frame/structure
iii. Wearable standalone unit
iv. Minimal restriction on shoulder movements

A passive system was selected because an external power source may not be readily available outdoors. The dependency on power may increase the load carried by the user such as battery packs or chargers or may include complex components such as power sources and cables that may affect the user's safety. A rigid structure was selected for efficient force delivery and transfer. Nonetheless, the exoskeleton's frame should be slimline or low profile and light since the operators work on uneven ground, in restricted space and in an environment with hanging objects. The exoskeleton shall be worn like a backpack, attached to the body via harnesses. The assistive force is expected to be delivered in the upper arm region via compressive springs to assist the shoulder and elbow joints. To ensure ease of movement, kinematic misalignment at the shoulder shall be minimised and the assistive mechanism shall be easily turned on and off to free the harvester's arm when not handling the pole.

Minimal restriction on shoulder movements. A perfect match between the exoskeleton and a shoulder movement is difficult as the shoulder rotates and translates in multiple planes. We included three ways to minimise interruptions toward shoulder movements. They minimise kinematic misalignment, freeing the spaces beyond the shoulder joint and below the waist and lastly, include an on-body deactivation mechanism.

Kinematic misalignments between humans and the exoskeleton reduce the effectiveness of the system (Delgado *et al.*, 2020; Schiele and Van Der Helm, 2006). The techniques that have been used to reduce kinematic misalignment include: (1) increasing the number of joints on the exoskeleton, and (2) bypassing the user's shoulder joint altogether. Ekso Evo (Ekso Bionics, Richmond, USA) uses multiple joints that extend from the user's back and slightly below the shoulder to the upper arm, while ShoulderX (SuitX, Emeryville, USA) uses multiple rotational joints at the shoulder. These designs enable a more fluid shoulder motion compared to rigid links. However, increasing the number of joints may reduce load-transfer efficiency, increase the number of potential failure points, and lead to bulky design. Alternatively, Armor-man2 (Tilta, Burbank, USA) adopts a design that bypasses the shoulder joint altogether. Instead, the arm linkage directly connects the torso to the hand. However, this results in a high-profile design and extends further away from the body. This is unfavourable for the oil palm plantation environment because protruding parts are hazardous due to the presence of other objects in the surroundings and they will interrupt the harvester's movements. Therefore, both techniques to reduce kinematic alignment at the shoulder were adapted in the proposed design to produce a mechanism that allows uninterrupted shoulder movement.

It is also important that no component is placed above the shoulder and below the waist as the pole frequents both regions during the cutting movements. Since the pole is long, the presence of exoskeleton components may cause unnecessary worries for the harvester when manoeuvring the pole.

Agricultural workers commonly perform multiple tasks or handle various tools or machines (Upasani *et al.*, 2019). Harvesters work over long hours and will need to perform tasks other than harvesting. Therefore, an exoskeleton that could be turned on (assistance provided) and off (assistance not provided) without being taken off is very convenient and will potentially improve ease of use. For example, Armor-man2 (Tilta, Burbank, USA) and ExhaussWorker (Exhauss, France) allow

users to release their hands in the middle of a task to rest or perform other tasks and resume by securing their hands to the exoskeleton again. It is important to ensure that the arm is stowed securely as the unstowed linkage is hazardous and may interrupt movements in restricted space. Therefore, a mechanism to easily deactivate and securely stow the exoskeleton arms when users need to release their arms is included in the proposed design.

3D Model of the Proposed Design

The proposed design of the exoskeleton was built and analysed in CAD software, Autodesk® Inventor® 2018 (Autodesk, Inc., CA, USA). The overall dimensions of the exoskeleton frame followed the anthropometric data of Malaysian workers (Hassan *et al.*, 2015). Conceptually, the assist mechanism would be placed below the user's arm and above the waistline, and the assistive force would be provided through a compression spring. The on-body deactivation mechanism was incorporated into the design of the arm linkage and the assist mechanism.

Determining the spring specification. Next, the dynamic simulation environment in Inventor 2018 was utilised to determine the appropriate compression spring specifications to assist arm raising during pole handling. The stiffness of a spring varies with the spring wire diameter, the number of active coils and the mean coil diameter based on the selected material. The dynamic simulation was performed in multiple iterations to obtain four spring specifications, with a spring load between 4 to 15 kg (the expected weight of the pole is at least 7 kg). During the simulation, the spring's outer diameter, length and number of active coils were kept constant based on the size of the exoskeleton's arm dimensions, while only the wire diameter was varied.

Structural analysis of the proposed design. Once the spring specifications were obtained, structural analysis of the exoskeleton was performed using the stress analysis environment in the same software. The objective of this analysis was to ensure that the physical prototype is reasonably safe for testing using human participants. For this analysis, a 10 kg load was applied to the exoskeleton arm cuff, which was well beyond the targeted load (7 kg), and the best spring determined through the dynamic simulation was used for this analysis. The stresses, deformation and strain for each component were investigated. A safety factor of 5 was chosen as the minimum acceptable value. The definition of the safety factor adopted was based on the ratio of the maximum allowable stress to the equivalent stress (von-Mises), where a value larger than 1 indicates no permanent deformation on the structure. The frame of the proposed exoskeleton was modelled as a rigid frame with aluminium material properties. The shoulder and waist harnesses were modelled with nylon material properties. The boundary conditions were defined based on the range of motion designed for the exoskeleton.

Verification of the Assist Mechanism Design

Next, a set of four springs were fabricated based on the outcomes of the dynamic analyses for the design verification experiment. The experiment was carried out to determine the range of the assist/non-assist region as the physical prototype of the arm assembly rotates, and consequently, the most optimal spring to assist harvesting. The most suitable spring is one that can handle at least 6 kg of external load and an assist region between the waist and the shoulder. The arm was secured to a benchtop, and a digital force scale attached to the free end of the arm was pulled vertically downward (*Figure 3a* and *3b*). The displayed force at every 10° angle was recorded manually. The experiment was repeated three times.

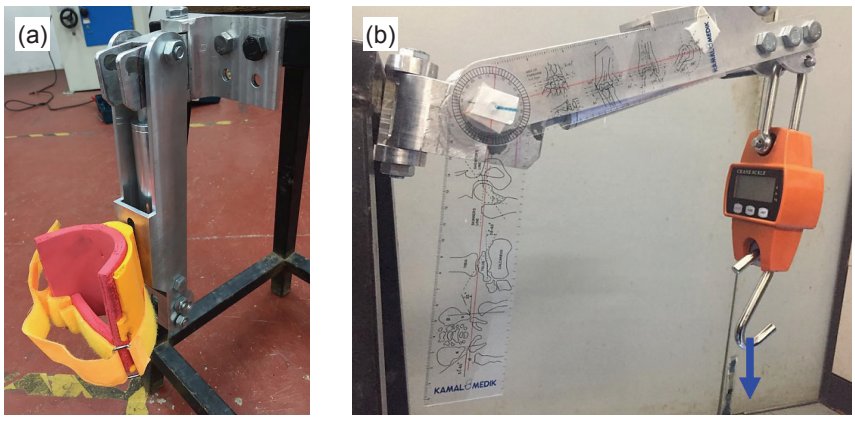


Figure 3. (a) The to-scale prototype of the arm linkage in stowed position secured to a benchtop. (b) The experimental setup to evaluate the range of motion of the arm linkage. The digital scale was pulled vertically downward as indicated by the blue arrow.

RESULTS AND DISCUSSION

The results are presented according to the order of the methods presented in the previous section, followed by a general discussion.

Muscle Activity for Selected Shoulder and Elbow Muscles During Harvesting

Harvesting the FFB involves two main movements, walking while handling the pole and cutting the frond and FFB. The average peak RMS of muscle activation for the observed muscles (deltoids and trapezius for the shoulder; triceps and biceps for the elbow) are shown in *Figure 4*. The average peak RMS pattern when comparing the left and right sides of each muscle is similar for harvesting and walking and harvesting alone, except for the trapezius. The trapezius is mainly used for scapular motion. For harvesting and walking, the peak RMS was highest in the left triceps, while for harvesting without walking, the peak RMS was highest in left deltoids and triceps. The level of activation was consistent for deltoids in both settings. Although triceps activation was high during walking and harvesting, its activation was almost halved during harvesting alone. Therefore, the assistive force was determined to be supplied from underneath the upper arm to benefit both the shoulder and elbow joints. We later learned that the immediate muscle activity in anterior deltoids and biceps indicated significant reduction when assisted by this exoskeleton during simulated pole raising and tugging (Harith *et al.*, 2021). Biceps brachii is responsible for elbow flexion, while anterior deltoids are responsible for shoulder flexion. Nevertheless, participants highlighted that the design should be optimised for better usability and acceptance.

CAD Model of the Proposed Exoskeleton

The conceptual design, the CAD model and the proof-of-concept prototype of the exoskeleton are shown in *Figure 5*. The proposed exoskeleton is designed to assist oil palm harvesting, without its structure and movement interrupting the user's movement during harvesting. An assistive force is supplied in the upper arm region through compressive springs. The exoskeleton has a slimline design, and its main components are the back plate, the shoulder and waist harnesses, the arm coupling links and the assist mechanism in the arm assembly (*Figure 5b*). The exoskeleton is designed to rotate in three axes and perform a one-dimensional relative translation to follow the shoulder's range of motion as close as possible.

For anthropometric fit, the width of the exoskeleton frame is set at 30 cm and adjustable by ± 10 cm in accordance with the biacromial breadth measurement. The exoskeleton frame length was determined by subtracting the hip height from the shoulder height, both measured from the ground. Based on this calculation, the frame length is set at 50 cm and adjustable by ± 10 cm. The length of the support mechanism is 40 cm from the arm linkage joint, following the elbow span. The arm cuff is pinned in a slot on the arm linkage with screws and bearings so that the cuff can translate and rotate (component 5 in *Figure 5b*).

Arm assembly. The arm assembly (component 4 in *Figure 5b*) moves with the user's arm and supplies assistive force through compression springs during movement. It houses the assist mechanism (illustrated in detail in *Figure 6a*). The arm assembly and the arm cuff are designed to work together in following the shoulder's motion and providing uninterrupted motion of the shoulder. To do so, the frame link (component 3 in *Figure 5b*) enables the assembly's rotation about the longitudinal/vertical and frontal axes. Additionally, the arm cuff is designed to rotate as it translates along a slot on the arm assembly, partly to minimise arm sliding within the cuff during motion. This movement configuration also aims to compensate for the length difference between the user's arm and the arm linkage, enabling smooth and comfortable movement.

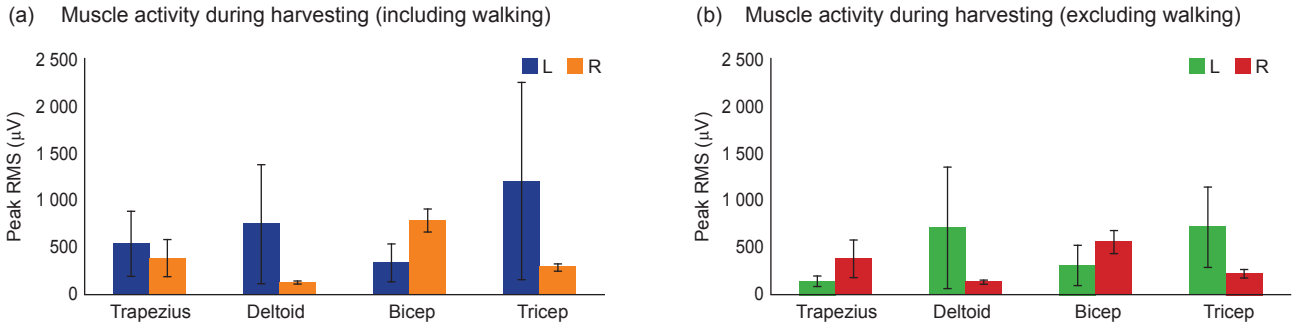


Figure 4. Average peak RMS of the EMG signal for all observed muscles during harvesting one oil palm tree (top: walking and harvesting, bottom: harvesting only). The results for harvesting only highlight the outcomes during the pushing and pulling of the pole for cutting.

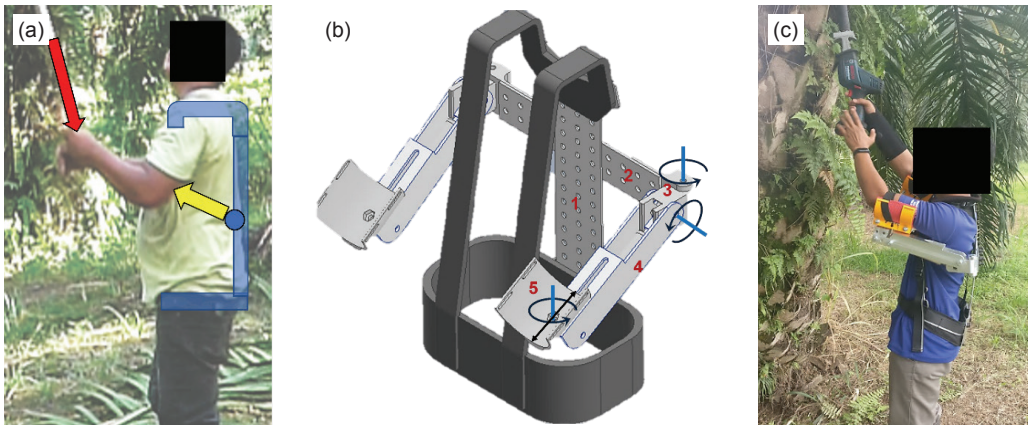


Figure 5. (a) The concept design of the exoskeleton. Thick blue lines represent the exoskeleton frame, which extends from the shoulder to the waist. The yellow arrow indicates the direction of the assistive force. The red arrow indicates the force from the pole. (b) Isometric view of the CAD model of the proposed design. The blue arrow is the axis of rotation at the joint and the black arrow is the type and the direction of movement of the component. The numbered components are [1] back plate, [2] top horizontal bar, [3] frame link, [4] arm assembly, and [5] arm cuff. (c) The physical proof-of-concept prototype is worn by a user.

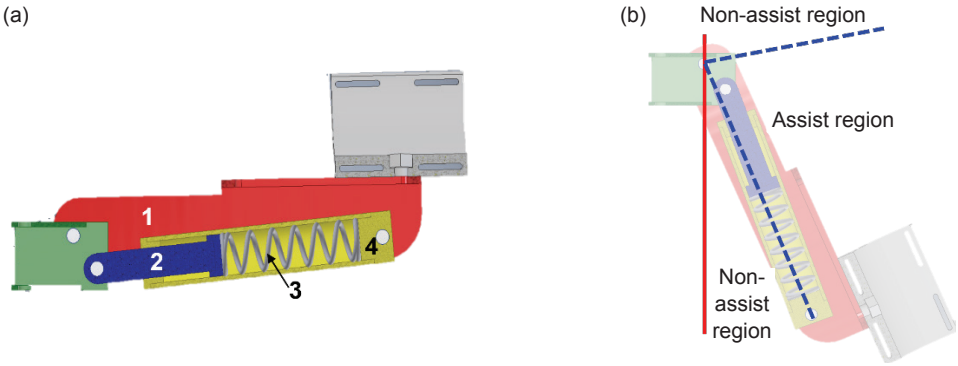


Figure 6. (a) A cross-sectional view of the arm assembly. The assist mechanism consists of [1] assembly frame, [2] guide shaft, [3] compression spring and [4] spring casing to prevent the shaft and spring from buckling. (b) The range of motion of the assembly (indicated by the red line) is limited by the shape of the frame link (green) and the configuration of the holes. The assembly moves between assist and two non-assist regions during motion.

The assist mechanism comprises an assembly frame, a guide shaft, a compression spring and a spring casing (*Figure 6a*). The assist mechanism is designed to move seamlessly between the assist and non-assist. Referring to (*Figure 6b*), when the assembly is loaded and begins to rotate downward, the guide shaft will push against the compression spring, shortening it and increasing its tension. When the maximum compression is reached, the spring returns to its original length and the assembly is now effectively in the non-assist region. This design allows uninterrupted arm movement when pushing/pulling the pole. On the other hand, if the assembly rotates upward from its unloaded/neutral position, the compression spring is already at its maximum length. Therefore, it does not provide any assistive force.

For on-body deactivation and safe stowing of the arm assembly, the assembly shall be lowered until it is in the non-assist region, where the spring returns to its original length and is unloaded. The absence of an assistive force that pushes up the arm assembly in this region allows it to be stowed safely for the user to free the arms for other tasks. The assist mechanism can be reactivated when the user raises the assembly into the assist region. The design on the exoskeleton also allows the unloaded/neutral position to be varied according to the user's anthropometry or preference, such as by changing the location of the arm assembly further up or down along the backplate, and spring specification by changing the spring (Tumit *et al.*, 2021).

Spring specification. Four spring specifications were selected based on the outcomes of the iterative dynamic analyses (*Table 1*). Only the wire diameter was varied in the simulations. Considering the design aim of this exoskeleton, Spring 3 is potentially the most optimal spring as it has a spring load of 6.0 kg (or a total of 12.0 kg for both sides). A verification experiment was performed to confirm this hypothesis.

Harvesting is a non-symmetric motion as the shape and dimension of the pole necessitate that one arm is positioned above the other when handling the pole. Therefore, the amount of assistance required

TABLE 1. THE SPECIFICATION OF FOUR COMPRESSION SPRINGS

Spring parameter	Spring 1	Spring 2	Spring 3	Spring 4
Outer diameter (mm)	26.0	26.0	26.0	26.0
Number of active coils	13.0	13.0	13.0	13.0
Wire diameter (mm)	3.5	4.0	4.5	5.0
Spring constant, *k* (N/mm)	10.0	18.3	31.4	51.4
Maximum spring load (kg)	3.7	5.8	6.7	13.6

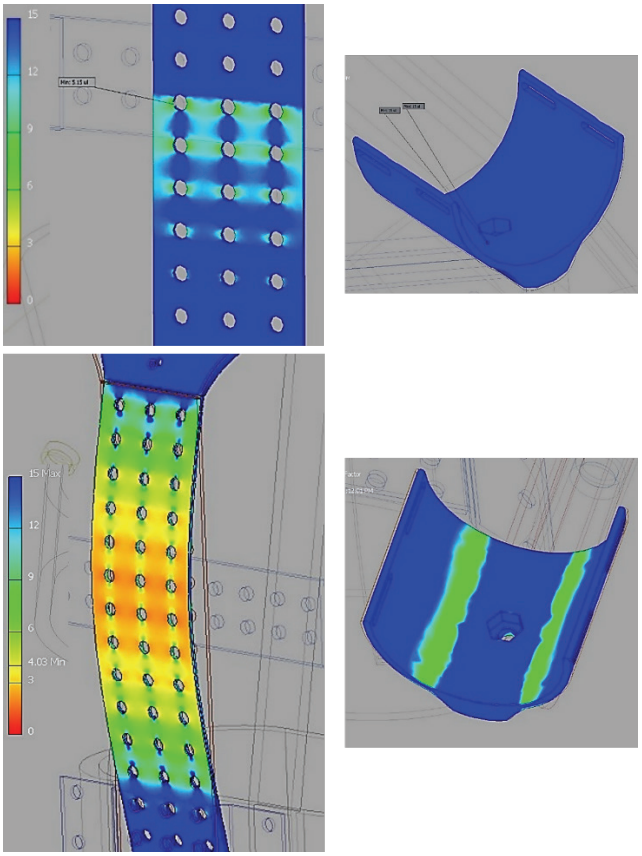


Figure 7. Two of the main exoskeleton components (left to right: back plate, arm cuff). Both were loaded with a 10.0 kg load (top row) and a 26.0 kg load (bottom row) on the arm support assembly. Legend indicates the safety factor (15, blue to 0, red). When loaded with 10 kg, the lowest safety factor (5.15) was found on the backplate in the green/aqua region. When loaded with a 26.0 kg load, permanent yield first occurred on the backplate in the red/orange region.

on each arm is likely different. Ideally, the spring specification should be customised according to the needs of each arm. This is also evident through the muscle activation results in *Figure 4*, which shows that the peak RMS for the left and right sides of each muscle were different.

Structural Analysis of the Proposed Design

Based on a safety factor of 5, the stress analysis results indicate that permanent deformation is not expected on the main components of the exoskeleton. The structural design verification of the exoskeleton is important prior to testing on human participants. Further optimisation of the design and usability is expected in future design iterations. Based on the structural analysis results, the back plate appears to be the weakest link in the design as it has the lowest safety factor, 5.15 [*Figure 7* (top row, left)] when the arm is loaded with 10.0 kg load, and it would be the first to deform permanently when a minimum of 26.0 kg load is applied on the arm [*Figure 7* (bottom row, left)]. A field analysis involving harvesters using the physical exoskeleton is required to verify if a load equivalent to 26.0 kg will be reached during its period of usage.

Verification of the Assist Mechanism Prototype

The profiles for Spring 1, Spring 2 and Spring 3 based on the design verification experiments are illustrated in *Figure 8a*. Spring 4 was excluded from

this experiment as it was found to be extremely stiff and unrealistic for actual usage. As seen from the profiles, the springs had slightly different unloaded/neutral positions, indicated by the largest angle for each curve. Generally, the neutral positions range between 20° to 40° from the horizontal axis. The peak assistive force and the range of assistive region also vary between springs. Spring 3 could handle the highest externally applied force (~61 N) and the widest assist region (~120°). Its assist region also lies between the waist and slightly above the shoulder. The peak force for Spring 3 is quite comparable to the spring load produced by the dynamic simulation (5.8 kg in *Table 1*). Therefore, it is postulated that Spring 3 is most suitable to assist harvesters.

As indicated in *Figure 8a*, for the current design, the spring specification influences the range of the assist region. This means that the spring can be changed to suit individual users and/or tree height. The expected weight of an aluminium pole to harvest trees less than 4.5 m high is 7.0 kg (3.2 m) for which Spring 2 or Spring 3 may be used (Jelani *et al.*, 2008). It is also highly likely that different springs can be used on each side as the range of motion and muscle activity of the joints differ between the dominant and supporting arm when aiming and cutting, which is also illustrated in *Figure 3* (Chan *et al.*, 2022; Harith *et al.*, 2021; Tumit *et al.*, 2021).

The variation in the assistive region between the springs can be attributed to the spring specifications and the design of the assist mechanism. The spring specification is represented by the value of the spring constant, k N/mm. Additionally, in the current design, the assist mechanism can be considered a three-link mechanism [*Figure 8(b)*]. The lengths of all links are constant. For this configuration, as the arm assembly rotates, the vertical force balance analysis occurs between the weight of the arm assembly, the downward force applied on the arm, and the vertical component of the spring force because the spring is always at an angle with respect to the assembly frame. The vertical component of the spring force can be calculated as k*ΔX*cosine θ, where k is the spring stiffness, ΔX is the change in spring length and θ is the angle between the assembly frame and the vertical axis. The value of k differs between springs and dictates the rate of shortening or lengthening of the spring according to an applied load. The compression spring will shorten when an external load is applied. Theoretically, softer springs need smaller force to start compressing in comparison to stiffer springs.

In this study, all springs had different k but the same unstretched length, and the length of all three links are constant (*Figure 8b*). Accordingly, given the same amount of external load, the ΔX and θ will vary between springs. This partly explains the variation in the neutral/unloaded position of the arm assembly illustrated in *Figure 8a*, which entails force balance between the weight of the arm assembly arm and the spring force. The neutral/unloaded position of Spring 1 (k = 10 N/mm) is closer to the body trunk as it is the softest spring (Spring 2, k = 18.3 N/mm and Spring 3, k = 31.4 N/mm). Next, when the arm assembly is pulled down, the force balance occurs between the weight of the arm assembly, the spring force and the downward pulling force. In this case, the pulling force, the spring constant, k and ΔX vary between springs and contributes toward the variation in the assist region illustrated in *Figure 8a*.

Design Limitations and Future Work

The exoskeleton design process commonly begins with considering the bodily area or joint requiring assistance when performing a task,

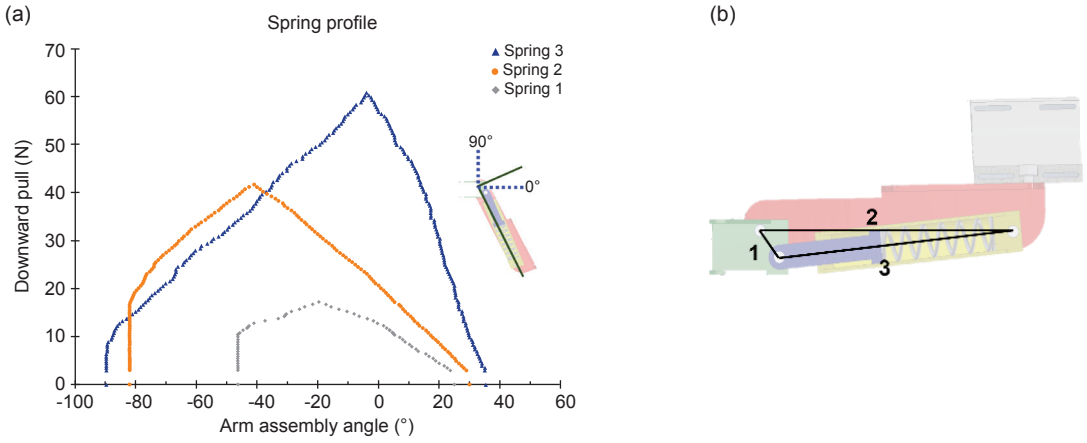


Figure 8. (a) The variation in the applied vertical force with the angle of the assistive arm assembly. Each curve corresponds to the three tested springs. The range of the assist region (between the two solid lines in the figure insert) is between the minimum and the maximum angle for each curve. 0° aligns with the horizontal axis and 90° aligns with the vertical axis. Spring 3 has the highest stiffness value and Spring 1 has the lowest stiffness value. (b) An illustration of the three links (numbered) for the assistive mechanism, which connects all of the components within the arm assembly.

followed by determining a potential assistive mechanism and then designing the mechanism and structure. This approach has not yet resulted in an exoskeleton that is optimally designed for a challenging environment and/or for an operation with varying tasks (Mudie *et al.*, 2022). Recent discussions on the need for systematic methods to introduce exoskeletons at workplace and the recommendation for using a user-centred design approach for designing exoskeleton also highlight the need for considering the work environment and the user-task-environment interaction when designing exoskeleton (Bornmann *et al.*, 2020; Dahmen *et al.*, 2018).

In this study, the systems approach was adopted to develop the design of the exoskeleton. This approach enable us to include the interactions between different elements interacting with the operators, including the tasks, the pole, and surrounding objects such as uneven ground, trees, hanging fronds, and objects on the ground, within its design criteria. Apart from the challenging oil plantation environment, the harvesting task itself is unique compared to the typical overhead task for which upper limb or shoulder exoskeletons are designed. Many upper limb exoskeletons aim to assist static overhead tasks by holding the arm for an extended duration. The harvesting of FFB involves dynamic and forceful pushing and pulling of the manual pole. Although forceful pulling can be reduced when using a motorised pole, carrying the pole and aiming it prior to cutting are still required. Hence, the proposed design is expected to still be applicable as the exoskeleton is intended for assisting the shoulder and elbow joints during harvesting. Furthermore, an on-body deactivation is included for the user's convenience and ease-of-use, in anticipation of the exoskeleton being worn throughout a long harvesting shift and that the user's movements are not limited to harvesting.

Design limitations. There are a few limitations in the current design. First, pole pushing and pulling is a bi-directional movement and is extremely frequent in harvesting. In this design, assistance is provided in one direction without interrupting the movement in the opposite direction. However, optimal assistance would be assisting in both directions. Therefore, alternative designs can be explored to assist in pushing and pulling, seamlessly.

Second, changes to the spring specification are limited to the spring casing and assembly frame dimensions, and the amount of assistive force is determined exclusively by the angle of the arm assembly. Future work on this design includes building passive mechanisms that can tune the assistive force to match the load experienced on each shoulder.

Current challenges in exoskeleton design. One of the key challenges in exoskeleton design is addressing the effects of complex and dynamic human-machine interactions on the user, the exoskeleton and the environment, especially over an extended duration (Howard *et al.*, 2020; Mudie *et al.*, 2022; 2018; Theurel *et al.*, 2018). Furthermore, industry players, including plantation owners and harvesters themselves, frequently inquire about the exoskeleton-wearing effects on workers' efficiency and field productivity. The answer to this question is not available, yet. Since the exoskeleton is constantly in physical contact with the user, it is important to elucidate the system's effects on the users, users' adaptation (physical and cognitive adaptation) to the system over time, and how these interactions translate into field and worker productivities. Common evaluation approaches on short-term effects include experiments involving human participants that are performed within relatively controlled environments, or simulations using complex modelling systems, such as seen in Hansen *et al.* (2018); Schmalz *et al.* (2019), and Theurel *et al.* (2018). Both approaches do not illustrate the real effects of exoskeleton wearing in the field. To date, reports on field effectiveness of exoskeletons are still limited, and when available, the assessment criteria varied, preventing one-to-one comparison.

Designing a functional and effective exoskeleton requires input and insights from multiple stakeholders and academic disciplines. Further work includes performing biomechanical investigation using computer simulations to better understand how and why users adapt to exoskeleton wearing when harvesting, modifying the structural design toward a leaner arm assembly and performing field tests involving experienced and non-experienced harvesters to elucidate the usability and reliability of the exoskeleton for harvesting operation and productivity. The outcomes of these tasks will be used to optimise the overall exoskeleton design so that it fits the user, the tasks, the operation, and the work environment appropriately.

CONCLUSION

Successful adoption of exoskeleton technology is partly contributed by the alignment between the design of the system, the tasks, the user's movements and the working environment, and the impact of the technology on workers' efficiency and field productivity. It is also easy to imagine that poor alignment between an exoskeleton design, users' needs and work environment will result in technology rejection altogether. In the proposed design, the working environment and the user's movement during harvesting were incorporated into

the design criteria via the systems approach. This aspect is largely missing in designing exoskeletons for challenging environment, partly contributing to poor applicability in the actual environment.

For this proposed design, the muscle activity during a complete harvesting task involving walking with a pole and cutting the FFB was observed to determine the targeted area requiring assistance. The exoskeleton is designed to assist harvesting task and minimise movement interruptions throughout the exoskeleton-wearing duration. Therefore, assistive force is provided in the upper arm region to benefit the shoulder and elbow joints, and no component is placed above the shoulder and below the waist that may interrupt pole movement. Moreover, an on-body deactivation mechanism is designed for the user's convenience, which allows users to release the arm without doffing the system by moving the arm linkage assembly into the lower non-assist region.

A detailed biomechanical investigation on the effects of the exoskeleton on the user's movements during field harvesting, and a comprehensive field assessment to determine the effects of exoskeleton usage on the harvester's efficiency and harvesting productivity are imperative to determine the overall impact of exoskeleton usage for harvesting. The need for technology to make harvesting more efficient is urgent. While full mechanised solutions are being developed, exoskeletons present an immediate alternative to enhance skilled harvesters. The exoskeleton design presented in this article is an initial attempt at exploring this alternative; further iterations and design concepts are inevitable. The combined outputs from biomechanical analysis and field tests should be synthesised for more accurate and faster exoskeleton development; that is an exoskeleton that can effectively assist harvesting, and enhance harvesters' performance and field productivity.

ACKNOWLEDGEMENT

The authors would like to thank Nur Syifa Fisal for her contribution during the arm linkage prototype experiment. This work was supported in parts by the Fundamental Research Grant Scheme (Ref. No: FRGS/1/2016/TK07/UPM/02/2, Vot: 5524897) from Malaysia Ministry of Higher Education, and Geran Putra-IPM (Vot: 9468200) from Universiti Putra Malaysia.

REFERENCES

Ackoff, R L (1971). Towards a system of systems concepts. *Manage. Sci.*, *17(11)*: 661-671. DOI: 10.1287/mnsc.17.11.661.

Alabdulkarim, S; Kim, S and Nussbaum, M A (2019). Effects of exoskeleton design and precision requirements on physical demands and quality in a simulated overhead drilling task. *Appl. Ergon.*, *80(August 2018)*: 136-145. DOI: 10.1016/j.apergo.2019.05.014.

Arnold, R D and Wade, J P (2015). A definition of systems thinking: A systems approach. *Procedia Comput. Sci.*, *44(C)*: 669-678. DOI: 10.1016/j.procs.2015.03.050.

Benos, L; Bechar, A and Bochtis, D (2020a). Safety and ergonomics in human-robot interactive agricultural operations. *Biosys. Eng.*, *200*: 55-72. DOI: 10.1016/j.biosystemseng.2020.09.009.

Benos, L; Tsaopoulos, D and Bochtis, D (2020b). A review on ergonomics in agriculture. Part I: Manual operations. *Appl. Sci. (Switzerland), 10(6)*: 1-21. MDPI AG. DOI: 10.3390/app10061905.

Benos, L; Tsaopoulos, D and Bochtis, D (2020c). A review on ergonomics in agriculture. Part II: Mechanized operations. *Appl. Sci., 10(10)*: 3484. DOI: 10.3390/app10103484.

Bornmann, J; Schirrmeister, B; Parth, T and Gonzalez-Vargas, J (2020). Comprehensive development, implementation and evaluation of industrial exoskeletons. *Curr. Dir. Biomed. Eng.*, *6(2*): 0-3. DOI: 10.1515/cdbme-2020-2001.

Castaneda, L; Baquero, W; Araujo, W; Isaza, A and Olaya, A F R (2020). Methods of ergonomic evaluation in upper limb: A review in agricultural manual work. *Health Sci. J.*, *14*(2): 1-14. DOI: 10.36648/1791-809X.14.2.711.

Chan, Y S; Teo, Y X; Gouwanda, D; Nurzaman, S G; Gopalai, A A and Thannirmalai, S (2022). Musculoskeletal modelling and simulation of oil palm fresh fruit bunch harvesting. *Sci. Rep.*, *12(1)*: 1-13. DOI: 10.1038/s41598-022-12088-6.

Crea, S; Beckerle, P; De Looze, M; De Pauw, K; Grazi, L; Kermavnar, T; Masood, J; O'Sullivan, L W; Pacifico, I; Rodriguez-Guerrero, C; Vitiello, N; Ristić-Durrant, D and Veneman, J (2021). Occupational exoskeletons: A roadmap toward large-scale adoption, methodology and challenges of bringing exoskeletons to workplaces. *Wearable Technologies*, *2*: E11. DOI: 10.1017/wtc.2021.11.

Dahmen, C and Constantinescu, C (2020). Methodology of employing exoskeleton technology in manufacturing by considering time-related and ergonomics influences. *Appl. Sci. (Switzerland)*, *10(5)*: 1-13. DOI: 10.3390/app10051591.

Dahmen, C; Wöllecke, F and Constantinescu, C (2018). Challenges and possible solutions for enhancing the workplaces of the future by integrating smart and adaptive exoskeletons. *Procedia CIRP*, *67*: 268-273. DOI: 10.1016/j.procir.2017.12.211.

De Bock, S; Ghillebert, J; Govaerts, R; Tassignon, B; Rodriguez-Guerrero, C; Crea, S; Veneman, J; Geeroms, J; Meeusen, R and De Pauw, K (2022). Benchmarking occupational exoskeletons: An evidence mapping systematic review. *Appl. Ergon.*, *98(January 2022)*: 103582. DOI: 10.1016/j.apergo.2021.103582.

Delgado, P; Alekhya, S; Majidirad, A; Hakansson, N A; Desai, J and Yihun, Y (2020). Shoulder kinematics assessment towards exoskeleton development. *Appl. Sci. (Switzerland)*, *10(18)*: 6336. DOI: 10.3390/APP10186336.

Desbrosses, K; Schwartz, M and Theurel, J (2021). Evaluation of two upper-limb exoskeletons during overhead work: Influence of exoskeleton design and load on muscular adaptations and balance regulation. *Eur. J. Appl. Physiol.*, *121(10)*: 2811-2823. DOI: 10.1007/s00421-021-04747-9.

Dewi, N S and Komatsuzaki, M (2018). On-body personal assist suit for commercial farming: Effect on heart rate, EMG, trunk movements, and user acceptance during digging. *Int. J. Ind. Ergon.*, *68*: 290-296. DOI: 10.1016/j.ergon.2018.08.013.

Du, Y; Baccaglini, L; Johnson, A; Puvvula, J and Rautiainen, R H (2022). Factors associated with musculoskeletal discomfort in farmers and ranchers in the US central states. *J. Agromedicine.*, *27(2)*: 232-244. DOI: 10.1080/1059924X.2021.1893880.

Elprama, S A; Vannieuwenhuyze, J T A; De Bock, S; Vanderborght, B; De Pauw, K; Meeusen, R and Jacobs, A (2020). Social processes: What determines industrial workers' intention to use exoskeletons? *Hum. Factors*, *62(3)*: 337-350. DOI: 10.1177/0018720819889534.

Fathallah, F A (2010). Musculoskeletal disorders in labour-intensive agriculture. *Appl. Ergon.*, *41(6)*: 738-743. DOI: 10.1016/j.apergo.2010.03.003.

Grazi, L; Trigili, E; Proface, G; Giovacchini, F; Crea, S and Vitiello, N (2020). Design and experimental evaluation of a semi-passive upper-limb exoskeleton for workers with motorized tuning of assistance. *IEEE Trans. Neural Syst. Rehabilitation Eng.*, *28(10)*: 2276-2285. DOI: 10.1109/TNSRE.2020.3014408.

Hansen, C; Gosselin, F; Ben Mansour, K; Devos, P and Marin, F (2018). Design-validation of a hand exoskeleton using musculoskeletal modeling. *Appl. Ergon.*, *68*: 283-288. DOI: 10.1016/j.apergo.2017.11.015.

Harith, H H; Mohd, M F and Nai Sowat, S (2021). A preliminary investigation on upper limb exoskeleton assistance for simulated agricultural tasks. *Appl. Ergon.*, *95(April)*: 103455. DOI: 10.1016/j.apergo.2021.103455.

Hassan, S N; Yusuff, R M; Zein, R M; Hussain, M R and Selvan, H K T (2015). Anthropometric data of Malaysian workers. *New Ergonomics Perspective - Selected Papers of the 10th Pan-Pacific Conference on Ergonomics*, *January*. p. 353-360. DOI: 10.1201/b17990-61.

Howard, J; Murashov, V V; Lowe, B D and Lu, M L (2020). Industrial exoskeletons: Need for intervention effectiveness research. *Am. J. Ind. Med.*, *63(3)*: 201-208. DOI: 10.1002/ajim.23080.

Iranzo, S; Piedrabuena, A; Iordanov, D; Martinez-Iranzo, U and Belda-Lois, J M (2020). Ergonomics assessment of passive upper-limb exoskeletons in an automotive assembly plant. *Appl. Ergon.*, *87(September)*: 103120. DOI: 10.1016/j.apergo.2020.103120.

Jelani, A R; Hitam, A; Jamak, J; Noor, M; Gono, Y and Ariffin, O (2008). Cantas ™ - A tool for the efficient harvesting of oil palm fresh fruit bunches. *J. Oil Palm Res.*, *20*: 548-558.

Kim, S; Nussbaum, M A; Mokhlespour Esfahani, M I; Alemi, M M; Alabdulkarim, S and Rashedi, E (2018a). Assessing the influence of a passive, upper extremity exoskeletal vest for tasks requiring arm elevation: Part I – "Expected" effects on discomfort, shoulder muscle activity, and work task performance. *Appl. Ergon.*, *70(September)*: 315-322. DOI: 10.1016/j.apergo.2018.02.025.

Kim, S; Nussbaum, M A; Mokhlespour Esfahani, M I; Alemi, M M; Jia, B and Rashedi, E (2018b). Assessing the influence of a passive, upper extremity exoskeletal vest for tasks requiring arm elevation: Part II – "Unexpected" effects on shoulder motion, balance, and spine loading. *Appl. Ergon.*, *70(March)*: 323-330. DOI: 10.1016/j.apergo.2018.02.024.

Lowe, B D; Billotte, W G and Peterson, D R (2019). ASTM F48 Formation and standards for industrial exoskeletons and exosuits. *IISE Trans. Occup. Ergon. Hum. Factors*, *7(3-4)*: 230-236. DOI: 10.1080/24725838.2019.1579769.

Marinoudi, V; Sørensen, C G; Pearson, S and Bochtis, D (2019). Robotics and labour in agriculture.

A context consideration. *Biosyst. Eng.*, *184*: 111-121. DOI: 10.1016/j.biosystemseng.2019.06.013.

Mohamaddan, S; Rahman, M A; Andrew Munot, M; Tanjong, S J; Deros, B M; Md Dawal, S Z and Case, K (2021). Investigation of oil palm harvesting tools design and technique on work-related musculoskeletal disorders of the upper body. *Int. J. Ind. Ergon.*, *86(October):* 103226. DOI: 10.1016/j.ergon.2021.103226.

Mohd Nawi, N S; Mad Deros, B and Nordin, N (2014). Barriers of adopting harvesting technology in Malaysian oil palm industry. *Aust. J. Basic Appl. Sci.*, *8(December)*: 198-200.

Monat, J P and Gannon, T F (2018). Applying systems thinking to engineering and design. *Syst.*, *6(3)*. DOI: 10.3390/systems6030034.

Mudie, K; Billing, D; Garofolini, A; Karakolis, T and LaFiandra, M (2022). The need for a paradigm shift in the development of military exoskeletons. *Eur. J. Sport Sci.*, *22(1)*: 35-42. DOI: 10.1080/17461391.2021.1923813.

Mudie, K L; Boynton, A C; Karakolis, T; O'Donovan, M P; Kanagaki, G B; Crowell, H P; Begg, R K; LaFiandra, M E and Billing, D C (2018). Consensus paper on testing and evaluation of military exoskeletons for the dismounted combatant. *J. Sci. Med. Sport*, *21(11)*: 1154-1161. DOI: 10.1016/j.jsams.2018.05.016.

Nawi, N S M; Deros, B M; Rahman, M N A; Sukadarin, E H and Nordin, N (2016). Malaysian oil palm workers are in pain: Hazards identification and ergonomics related problems. *Malays. J. Public Health Med.*, *16(May)*: 50-57.

Ng, Y G; Mohd Tamrin, S B; Md Yusoff, I S; Ippei, M and Hashim, Z (2013). Ergonomics observation: Harvesting tasks at oil palm plantation. *J. Occup. Health*, *55*: 405-414.

Ng, Y G; Mohd Tamrin, S B; Yik, W M; Mohd Yusoff, I S and Mori, I (2014). The prevalence of musculoskeletal disorder and association with productivity loss: A preliminary study among labour intensive manual harvesting activities in oil palm plantation. *Ind. Health*, *52*: 78-85.

Omoniyi, A; Trask, C; Milosavljevic, S and Thamsuwan, O (2020). Farmers' perceptions of exoskeleton use on farms: Finding the right tool for the work(er). *Int. J. Ind. Ergon.*, *80*(*April*): 103036. DOI: 10.1016/j.ergon.2020.103036.

Parras-Burgos, D; Gea-Martínez, A; Roca-Nieto, L; Fernández-Pacheco, D G and Cañavate, F J F (2020). Prototype system for measuring and analyzing movements of the upper limb for the detection of occupational hazards. *Sensors (Switzerland)*, *20(17)*: 1-17. DOI: 10.3390/s20174993.

Preethi, P; Singh, T V; Ramajayam, D and Prasad, M V (2016). Pole harvesting-A skillful operation in oil palm fresh fruit bunch (FFB) harvest. *J. Plant. Crops*, *46(3)*: 204-209. DOI: 10.25081/jpc.2018.v46.i3.2016.

Schiele, A and Van Der Helm, F C T (2006). Kinematic design to improve ergonomics in human machine interaction. *IEEE Trans. Neural Syst. Rehabil. Eng.*, *14(4)*: 456-469. DOI: 10.1109/TNSRE.2006.881565.

Schmalz, T; Schändlinger, J; Schuler, M; Bornmann, J; Schirrmeister, B; Kannenberg, A and Ernst, M (2019). Biomechanical and metabolic effectiveness of an industrial exoskeleton for overhead work. *Int. J. Environ. Res. Public Health*, *16(23)*: 4792. DOI: 10.3390/ijerph16234792.

Sreeram, M and Nof, S Y (2021). Human-in-the-loop: Role in cyber physical agricultural systems. *Int. J. Comput. Commun. Control*, *16(2)*: 1-19. DOI: 10.15837/ijccc.2021.2.4166.

Syuaib, M F (2015). Ergonomic of the manual harvesting tasks of oil-palm plantation in Indonesia based on anthropometric, postures and work motions analyses. *Int. Agric. Eng. J.*, *17(3)*: 248-262.

Thamsuwan, O; Milosavljevic, S; Srinivasan, D and Trask, C (2020). Potential exoskeleton uses for reducing low back muscular activity during farm tasks. *Am. J. Ind. Med.*, *63(11)*: 1017-1028. p. 1-12. DOI: 10.1002/ajim.23180.

Theurel, J; Desbrosses, K; Roux, T and Savescu, A (2018). Physiological consequences of using an upper limb exoskeleton during manual handling tasks. *Appl. Ergon.*, *67*: 211-217. DOI: 10.1016/j.apergo.2017.10.008.

Toyama, S and Yamamoto, G (2010). Wearable agrirobot. *J. Vibroeng.*, *12(3)*: 287-291.

Tumit, N P; Rambely, A S and Deros, B M (2021). The effects of age and initial shoulder posture on the upper limb range of harvesting movements among oil palm harvesters. *Appl. Sci.(Switzerland)*, *11(21)*: 10280. DOI: 10.3390/app112110280.

Ulrey, B L and Fathallah, F A (2013). Effect of a personal weight transfer device on muscle

activities and joint flexions in the stooped posture. *J. Electromyogr. Kinesiol.*, *23(1)*: 195-205. DOI: 10.1016/j.jelekin.2012.08.014.

Upasani, S; Franco, R; Niewolny, K and Srinivasan, D (2019). The potential for exoskeletons to improve health and safety in agriculture - Perspectives from service providers. *IISE Trans. Occup. Ergon. Hum. Factors*, *7*(*3-4*): 222-229. DOI: 10.1080/24725838.2019.1575930.

Vasconez, J P; Kantor, G A and Auat Cheein, F A (2019). Human-robot interaction in agriculture: A survey and current challenges. *Biosyst. Eng.*, *179*: 35-48. DOI: 10.1016/j.biosystemseng.2018.12.005.

Vries, A De and Looze, M De (2019). The effect of arm support exoskeletons in realistic work activities: A review study. *J. Ergon.*, *9(4)*: 1-9. DOI: 10.35248/2165-7556.19.9.255.

Wang, H M; Le, D K L and Lin, W C (2021). Evaluation of a passive upper-limb exoskeleton applied to assist farming activities in fruit orchards. *Appl. Sci. (Switzerland)*, *11(2)*: 1-14. DOI: 10.3390/app11020757.

Xiloyannis, M; Chiaradia, D; Frisoli, A and Masia, L (2019). Physiological and kinematic effects of a soft exosuit on arm movements. *J. Neuroeng. Rehabilitation*, *16(1)*: 1-15. DOI: 10.1186/s12984-019-0495-y.

Journal of Oil Palm Research Vol. 35 (4) December 2023 p. 668-681
DOI: https://doi.org/10.21894/jopr.2023.0005

OPTIMISATION OF FAME PRODUCTION FROM WASTE COOKING PALM OIL WITH KOH CATALYST SUPPORTED ON PALM KERNEL SHELLS ASH (PKSA) USING RESPONSE SURFACE METHODOLOGY (RSM)

HUSSANAI SUKKATHANYAWAT[1] and KITTISAK WICHIANWAT[1]*

ABSTRACT

Fatty acid methyl ester (FAME) was produced from waste cooking palm oil (WCPO) using KOH catalyst supported on palm kernel shells ash (PKSA). Response surface methodology (RSM) based on Box Behnken design (BBD) was used to design the experiment and analyse three parameters: Catalyst amount, KOH loading and methanol to oil molar ratio. The result found that the catalyst activity depended on basicity of the catalysts. The statistical model predicted that the highest yield of 96.73% was achieved with an optimised parameter of 15 wt.% catalyst amount, 20 wt.% of KOH loading and 11.39:1 methanol to oil ratio at the temperature of 65°C. Experiments performed at the predicted condition yield of 92.74% suggest that the RSM is an accurate method for biodiesel production. The Gas Chromatography Mass Spectrometry (GC-MS) was used to identify the chemical composition of biodiesel. The catalyst reusability test verified that the synthesised catalyst could be reused up to 3 times. The results demonstrated that waste cooking palm oil can be completely transformed into methyl ester. This study indicates that KOH supported on palm kernel shell ash is an effective catalyst for the conversion of waste cooking palm oil to biodiesel.

Keywords: biodiesel, palm kernel shells ash, RSM, waste cooking palm oil.

Received: 27 April 2022**; Accepted:** 31 October 2022**; Published online:** 8 February 2023.

INTRODUCTION

Renewable sources of energy have become a more attractive alternative due to global warming and environmental concerns. Worldwide population growth at a rapid rate increases the global energy consumption from petroleum sources and resulting in the increase of the greenhouse gases emissions which are mainly responsible for global warming and has impact on human health (Basumatary *et al.,* 2021). The alternative energy technologies can overcome the much-exploited use of fossils fuel. Among the various possible alternatives, biodiesel has been seen as tremendous potential for growth for a long time ago. In this regard, biodiesel from vegetable oil is an environmental-friendly fuel due to non-toxic, renewable, biodegradable, less sulphur and greenhouse gases emissions (Sharma *et al.,* 2020).

Biodiesel is derived from the transesterification of triglycerides present in vegetable oil or animal fat and alcohol with the presence of a catalyst (Sharma *et al.,* 2020). Appropriate selection of feedstock for biodiesel production is one of the crucial factors for reducing the cost of biodiesel feedstock. The use of low-price oil such as waste cooking oil will considerably reduce the cost of the final product (Putra *et al.,* 2018). This is because of the low cost of waste cooking oil (WCO), which is 2-3 times less than virgin vegetable oil.

[1] Faculty of Science Energy and Environment, King Mongkut's University of Technology North Bangkok, Rayong Campus, Thailand.

* *Corresponding author e-mail*: *kittisak.w@sciee.kmutnb.ac.th*

Bio or green catalyst is a type of catalyst derived from natural source as biomass. The advancement in the agricultural sector provides tons of waste and by-products daily and hence a potential low-cost precursor of green catalysts (Arumugam and Sankaranarayanan, 2020). The total amount of waste from oil palm plantations is approximately 13.71 million tonnes, comprising fibre, palm shells, empty fresh fruit bunches and palm oil trunks (Malithong *et al.*, 2017). Currently, the wastes are either disposed of as landfills or used in a boiler to generate electricity. For instance, palm kernel shells (PKS) do not decompose easily and require furnace modifications if there are to be used in boilers in place of firewood or fuel oil. Direct use of PKS in boiler in their raw form produces a large amount of smoke and insufficient energy (Bazargan *et al.*, 2015).

The current research goal is to produce the catalyst from agricultural biomass such as palm kernel shell, which will therefore reduce costs and improves overall efficiency. The present study aimed to improve the activity of palm kernel shells as a catalyst by impregnation method to increase the basicity through the addition of base metal onto the surface of the catalyst (Oko and Kurniawan, 2019).

Therefore, transesterification parameters were optimised using response surface methodology (RSM) based on the Box-Behnken design to establish the best condition for biodiesel production (Singh *et al.*, 2018). Dwivedi and Sharma (2015) use the Box-Behnken design to optimise Pongamia biodiesel yield of 98.4% with a methanol molar ratio of 11.06:1, 1.43 wt.% of KOH catalyst, at a reaction temperature of 56.6°C and 81.43 min of time. Latchubugata *et al.* (2018) have reported optimisation of reaction parameter at 6 wt.% calcium oxide (CaO) catalyst and methanol molar ratio of 15:1 at a reaction temperature of 65.0°C in 4 hr reaction time using Box-Behnken design, the experimentally obtained yield of biodiesel was 93.50%. Marwaha *et al.* (2019) used Box-Behnken response surface design to maximise biodiesel yield at 97.98% from *Terminalia bellerica* oil with a methanol molar ratio of 9:1, 2.25 wt.% calcium oxide (CaO) catalyst from waste eggshells and reaction temperature of 62.5°C.

The present work attempted to develop a low-cost support base catalyst using KOH impregnated onto PKS for the transesterification of Waste Cooking Palm Oil (WCPO) for biodiesel production. The influence of catalyst basicity, methanol-to-oil molar ratio and catalyst weight percent were investigated using response surface methodology (RSM) combined with a Box-Behnken design. Furthermore, the physicochemical properties of the produced biodiesel are compared with the standard requirements of Thailand.

MATERIALS AND METHODS

Material

The WCPO was collected at a cafeteria nearby King Mongkut's University of Technology, North Bangkok (Rayong Campus). The oil was filtered to remove impurities and heated to 100°C to remove moisture. To prevent oxidation, the WCPO was stored in a container with a tight seal. After that, the WCPO's acid value, iodine value, moisture and volatile matter content, and saponification value were determined.

Palm kernel shells ash (PKSA) was donated by an Indorama Petrochem (PTA) thermal power plant in the city of Rayong. The PKSA was crushed in a mortar before being sieved to a mesh size of 250 μm. To eliminate moisture and impurities, the sieved PKSA was heated in an oven at 120°C for 12 hr.

PKSA Multi-element Characterisation

In Teflon tubes, 5 g PKSA was digested with 9 mL of 65% nitric acid, 3 mL of hydrofluoric acid, and 2 mL of 37% hydrochloric acid. A microwave-heated pressure digestion apparatus was used to digest the solution (Berghof Speedwave 4). The digestion conditions used were as follows: The temperature was ramped to 210°C with a heating rate of 5°C/min at 80% power, followed by a dwell time of 30 min. After digestion, about 10% boric acid was added to a mixture to re-dissolve the insoluble fluoride compounds. Once again, the solution was transported to a microwave-heated pressure digestion system. The temperature was ramped up to 190°C using a heating rate of 5°C/min, and held for 10 min at that temperature. After that, the solution was transferred to 25 mL volumetric flasks, filled with MilliQ water to the correct volume, and stored in a refrigerator at 4°C for MP-AES analysis.

The Agilent MP-AES was utilised to determine the concentration of residual Si, Al, Fe, Ca, Mg, and K in the digested solutions. The calibration curve was linear, and quantification was based on a five-point standard calibration curve (2.0, 4.0, 6.0, 8.0 and 10.0 mg/L). For every determination, both the standard and the sample were scanned three times. The metal determination wavelengths were as follows: Si (251 nm), Al (396 nm), Fe (259 nm), Ca (393 nm), Mg (285 nm), and K (766 nm). *Figure 1* depicts the graphical representation of the standard calibration curve for each metal. The R^2 values from the standard were Si 0.9991, Al 0.9998, Fe 0.9983, Ca 0.9956, Mg 0.9979 and K 0.9976. The results demonstrated that all determination coefficients (R^2) were within the acceptable values.

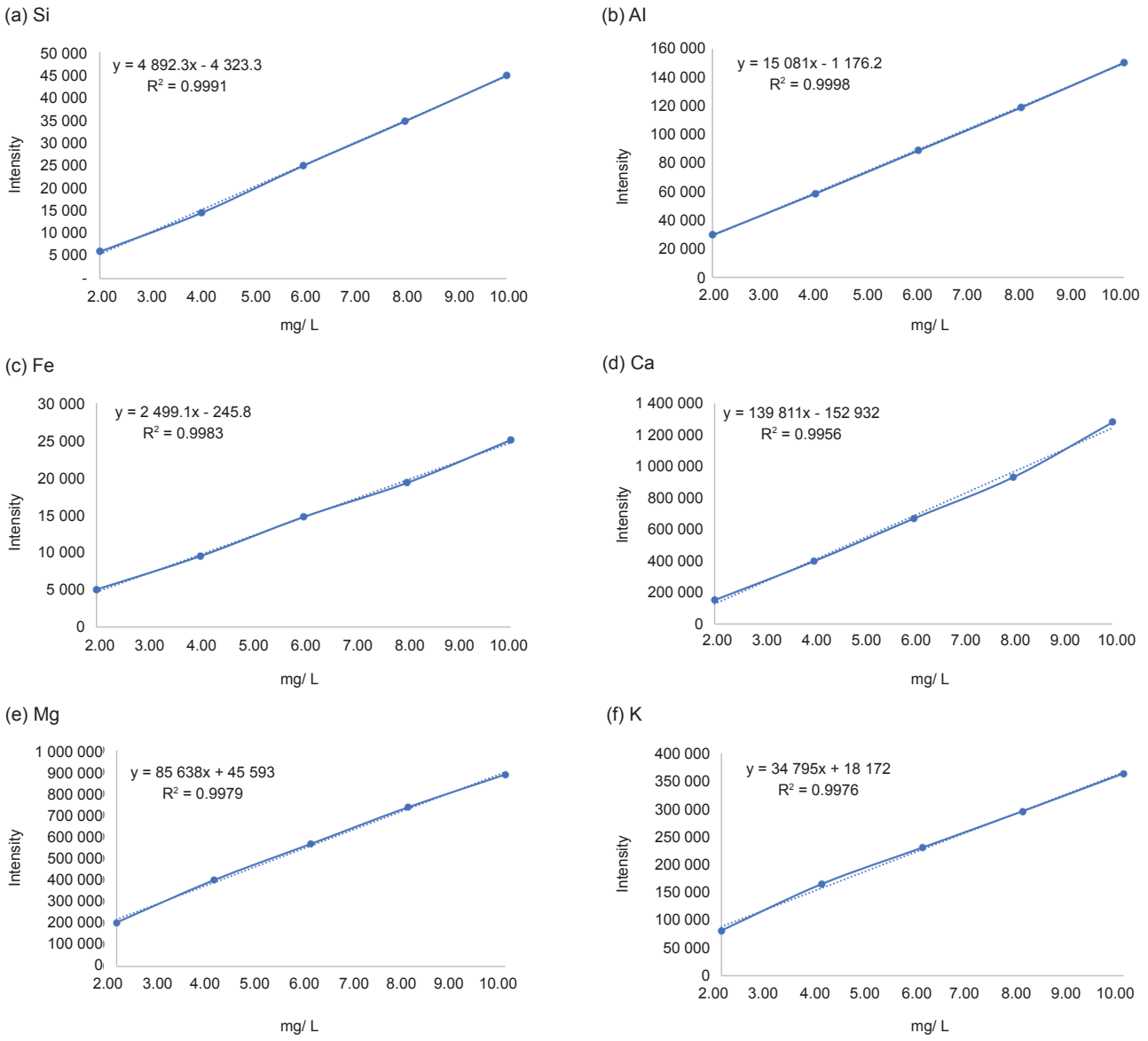


Figure 1. Calibration curve for (a) Si, (b) Al, (c) Fe, (d) Ca, (e) Mg and (f) K using MP-AES.

Catalyst Preparation

The KOH-supported PKSA catalysts were synthesised using the incipient wetness impregnation method. Potassium hydroxide solution was introduced dropwise to PKSA at various weight percentages (10%, 15% and 20%) and agitated for 12 hr. The KOH/PKSA mixture was heated in an oven at 110°C for 6 hr, after that the dried catalysts were calcined at 600°C for 6 hr. The calcined catalyst was then placed in a desiccator.

Catalyst Characterisation

The synthesised catalysts were characterised using various techniques. By using the Hammett indicator method, the basicity of the KOH/PKSA catalyst was investigated. This method is used to indicate the catalyst's basic strength (Leung and Gua, 2006). Typically, 0.05 g of catalysts were mixed with 5 mL of methanol and 3 drops of Hammett indicator and allowed to equilibrate for 2 hr. The catalyst's alkaline abnormality was indicated by a colour change. Thermogravimetric analysis (TGA, TA Instruments Q50) was used to obtain volatile components by monitoring the weight change of PKSA from room temperature to 800°C at a heating rate of 10°C/min under a flow of nitrogen. The Brunauer-Emmett-Teller (BET) and Barrett-Joyner-Halenda (BJH) techniques were used to calculate the specific surface area and pore volume of the catalyst which uses nitrogen adsorption. Before the experiment, the sample was outgassed under vacuum for 4 hr at 150°C to remove moisture from the catalyst surface.

WCPO Characterisation

To characterise the properties of WCPO, the standard method was used. The moisture content, acid value, and iodine value of the used palm cooking oil were all measured. The acid valve and FFA concentration were determined by titrating against 0.025 M KOH and phenolphthalein as an indicator. A moisture analyser was used to determine the moisture content (Mettler Toledo model HC103). The iodine value was determined by volumetric titration; 0.2 g of WCPO was mixed with 15 mL of cyclohexane and 25 mL of Wijs reagent, and the mixture was shaken for 5 min and placed in the dark for 30 min. The mixture was then added with 20 mL of 10% KI and 50 mL of boiled distilled water. Following that, the mixture was titrated with 0.1 $Na_2S_2O_3.5H_2O$ using starch as an indicator to determine the endpoint.

Experimental for Transesterification Reaction

The transesterification reaction for WCPO was performed at atmospheric pressure in a 250 mL three-necked, flat-bottom flask equipped with a reflux condenser and magnetic stirrer. The reaction flask was placed on a hotplate stirrer. About 50 g of WCPO was heated to 65°C in the reaction flask. Following that, methanol and PKSA catalyst were added to the process. The mixture was then maintained at 65°C for 60 min while being constantly stirred. After the reaction was complete, the mixture was transferred to a separation funnel and allowed to settle for 12 hr before separating the top layer (biodiesel) from the bottom layer (glycerol and solid catalyst). The biodiesel was evaporated at a temperature of 110°C to remove moisture and methanol. A Fourier transform infrared spectrum (FTIR) equipped with a diamond attenuated total reflectance (ATR) was utilised to measure the FAME content of the sample.

Box-Behnken Design of Experiment

Response surface methodology (RSM) based on Box-Behnken design was used to optimise the biodiesel conversion parameters using Minitab software. The three independent variables used in this study were ash catalysts dosage (amount of catalyst (wt.%): 5% to 15%), KOH concentration on the supported catalyst (%K: 10% to 20%), and methanol to oil molar ratio (M/O: 6 to 12 molar ratio) (*Table 1*). FAME yield (Y) was chosen as the dependent variable. The reaction time was set to 60 min and the temperature was set to 65°C. The significance of the components and their interaction was determined using analysis of variance (ANOVA) with a confidence level of 95% (P<0.05).

TABLE 1. LEVEL OF THE INDEPENDENT VARIABLES IN THE BOX-BEHNKEN DESIGNS (BBD)

Independent variables	Code	Level		
		-1	0	-1
PKSA	Catalyst (wt.%)	5	10	15
KOH concentration	%K	10	15	20
Methanol to oil molar ratio	M/O	6	9	12

Biodiesel Characterisation

The produced biodiesel was evaluated by functional groups and methyl esters profile analyses. Thirteen calibration solutions of biodiesel standard (Biodiesel standard donated by a biodiesel factory from the Suksomboon group located in Chonburi, Thailand) were prepared with varying concentrations of WCPO, ranging from 0% to 100%. A Fourier transform infrared spectrum (FTIR) equipped with a diamond attenuated total reflectance (ATR) was used to characterise the functional groups of standard and produce biodiesel. FTIR spectra were collected from 4000 to 400 cm^{-1} with a 4 cm^{-1} resolution and 32 scans.

A 100 mg sample was placed in a 10 mL volumetric flask and diluted to the desired volume with toluene. A gas chromatography-mass spectrometer (Agilent 7890B GC and Agilent 5977B MSD) with an HP5MS capillary column was used to analyse the prepared sample. Helium was used as the carrier gas, and the injector and detector temperatures were set to 250°C. The temperature program started at 60°C and was held for 2 min then increased to 200°C at a rate of 10°C/min and finally to 240°C at a rate of 5°C/min and held constant for 7 min.

Catalyst Regeneration and Reusability

After each reaction, the used catalyst was filtered. The catalyst was successfully treated in two steps. In the first step, the used catalyst was rinsed in n-hexane and sonication for 30 min, then dried at 110°C overnight. In the second step, the catalyst was rinsed in methanol and sonication for 30 min, then dried at 110°C overnight. The recovered catalyst was used for another transesterification process.

RESULTS AND DISCUSSION

Properties of WCPO

The results of WCPO's characterisation are shown in *Table 2*. The initial FFA value of WCPO was 0.34%. The result was below the optimal threshold limit of FFA 1 wt.%, which indicates that the WCPO could be directly converted into biodiesel with an alkali base catalyst. The moisture and volatile

content of WCPO was 1 wt.%; therefore, the oil must be heated to eliminate the moisture and volatile impurities before transesterification to prevent a saponification reaction. The iodine value of WCPO was 58.23 per 100 g of oil. It is a measure of the degree of unsaturation of WCPO and will indicate the stability of the raw material. The result of iodine value was within the suitable range for conversion into biodiesel.

TABLE 2. PROPERTY OF WCPO

Property	Unit	Value
Free fatty acid	%	0.34
Iodine value	g I_2/100 g oil	58.23
Moisture and volatile matter	wt.%	1.00

Elemental Composition of PKSA

The elemental composition of PKSA is summarised in *Table 3*. The major elements found in 100 g of PKSA were Si (30.00 wt.%), Al (3.33 wt.%), Fe (0.67 wt.%), Ca (13.33 wt.%), Mg (3.33 wt.%), and K (1.33 wt.%). Metal concentrations found in PKSA decrease in the following order: Si > Ca > Al = Mg > K > Fe. Si ion in PKSA was 30.00 wt.% in form of SiO_2, equal to 63.37 wt.%. Thus, SiO_2 is suitable for catalyst support.

TABLE 3. ELEMENTAL COMPOSITION OF PKSA

	Composition (%)					
PKSA	Si	Al	Fe	Ca	Mg	K
	30.00	3.33	0.67	13.33	3.33	1.33

Basicity of Catalyst

The Hammett indicator method was used to estimate the basicity of the catalyst. The titration was accomplished in presence of Methyl red (H _ 5.1), Neutral red (H _ 6.8), Bromothymol blue (H _ 7.0) and Phenolphthalein (H _ 9.7). *Table 4* shows the strength of distribution and total basicity of the catalyst. The alkalinity of PKSA was found to be in the range of 6.8 < H _< 7.0, indicating that the support has a low-basicity. The overall basicity of the catalyst gradually increases in the range of 7.0 < H _ < 9.7 after being loaded with KOH from 10 to 20 wt.%. The basic strength of the catalyst increases in the order of PKSA < 10%K/PKSA = 15%K/PKSA < 20%K/PKSA respectively.

Thermogravimetric Analysis

TGA was used to investigate the PKSA's degradation patterns. *Figure 2* depicts the profile of PKSA's decomposition in the atmosphere. According to the TGA curve, there was a 99.62% weight loss between 100°C and 230°C due to the elimination of adsorbed moisture from the material. The significant loss of 97.63% and 96.70% in the range of 336°C to 568°C due to the decomposition of organic matters such as hemicellulose, cellulose and lignin (Abdullah *et al*., 2021). The mass loss stage at 600°C to 800°C may possibly be due to the decomposition of residual products of CO_2, CO and tar which originated from the decomposition of residue lignin (Abdullah *et al*., 2021; Ashok *et al*., 2015; Yashim *et al*., 2016).

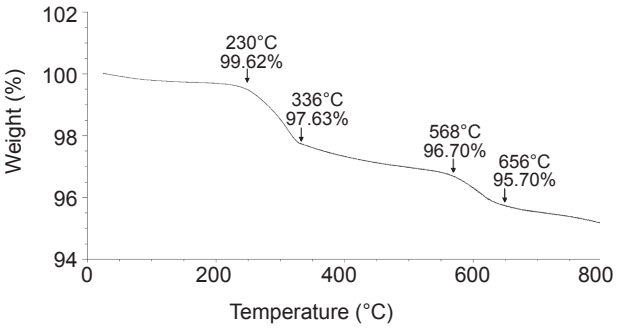


Figure 2. TGA profile.

BET Surface Area

BET surface of PKSA was observed to be 4.99 m^2/g. Pore size adsorption average pore width was obtained at 12.27 nm. Single pore adsorption total pore volume was obtained at 0.02 cm^3/g. The result shows that surface area of PKSA was less, the activity of PKSA catalyst needs to be improve by adding basicity site as KOH onto the surface of PKSA. However, after impregnation of KOH at 10 wt.%, 15 wt.% and 20 wt.% the result of BET surface area was observed as non-porous material with very low

TABLE 4. LIST OF HAMMETT INDICATORS USED FOR SURFACE ACIDITY MEASUREMENT

Indicator	Color		H _	Color			
	Acidic	Basic		PKSA	10%K/ PKSA	15%K/ PKSA	20%K/ PKSA
Methyl red	Red	Yellow	5.1	Yellow	Yellow	Yellow	Yellow
Neutral red	Yellow	Red	6.8	Red	Red	Red	Red
Bromothymol blue	Yellow	Blue	7.0	Blue	Blue	Blue	Blue
Phenolphthalein	Colorless	Pink	9.7	Colorless	Light pink	Light pink	Pink

surface area for all impregnation catalysts. A similar behaviour has been reported for potassium and TiO_2 when calcined at high temperature. Salinas *et al*. (2012) found that using a high loading of potassium and a high calcination temperature resulted in the lower BET surface area of potassium supported TiO_2 catalysts. The BET areas of the catalyst calcinated at 300°C, 500°C and 700°C were 18, 19 and 2 m^2/g, respectively. In addition, Soetaredjo *et al*. (2011) have reported that the BET surface area of the bentonite catalyst decreased with KOH loading. During the impregnation, the KOH molecules filled the catalyst's available pores, resulting in a decrease in the catalyst's surface area. This suggests that the KOH molecules present on the surface of the pores were probably converted to K_2O during calcination. As a result, after loading with KOH, the pore structure of mesoporous material changes to a nonporous structure. The activity of the K/PKSA catalyst was investigated using RSM to determine the optimal reaction.

Quantitative Analysis of Biodiesels by ATR-FTIR

FTIR analysis of thirteen calibration solutions of biodiesel standard with different levels of biodiesel in WCPO is presented in *Figure 3*. The overlaid peak at 1435 cm^{-1} band corresponds to the asymmetric stretching of $-CH_3$ present in the biodiesel spectrum and absent in the WCPO spectrum (Soria-Figueroa *et al.*, 2019). The calibration curve for the FAME concentration was made by measuring the peak at 1435 cm^{-1}. According to the data, a linear calibration model was created. The method was used to predict the concentration of biodiesel and unreacted starting WCPO, or reaction intermediates (*e.g*., mono-, di-, and triglycerides).

For qualitative analysis, The FTIR spectra of biodiesel standard and biodiesel standard blends with WCPO were compared. The biodiesel yield was calculated using the relation shown in Equation (1).

$$\text{Yield (\%)} = \frac{\text{(Weight of biodiesel produced)} \times \text{(\%FAME from FTIR)}}{\text{Weight of waste cooking oil}} \times 100 \quad (1)$$

Optimisation of Methyl Ester using Response Surface Methodology

The relationship between FAME yield and three independent variables were analysed with RSM based on Box-Behnken design. Three variables affected such percentage of catalyst [Catalyst (wt.%)], percentage of potassium on surface of catalyst (%K) and methanol/oil ratio (M/O ratio) were studied. The fifteen experiments conducted are presented in *Table 5*. The methyl ester yield is the response variable which depended on the different variation in the three parameters. The validity of the significant model is verified by a low *p*-value ($p < 0.05$). Regression analysis of the biodiesel yield prediction was employed to fit full second-degree polynomial model, including linear, quadratic, and interaction at 5% level of significance except for %K*%K, Catalyst (wt.%)*%K and %K*M/O ratio as shown in *Table 6*. Meanwhile, a *p*-value of lack of fit greater than 0.05 indicates that when compared to error, lack of fit was found to be insignificant (Arumugam and Sankaranarayanan, 2020).

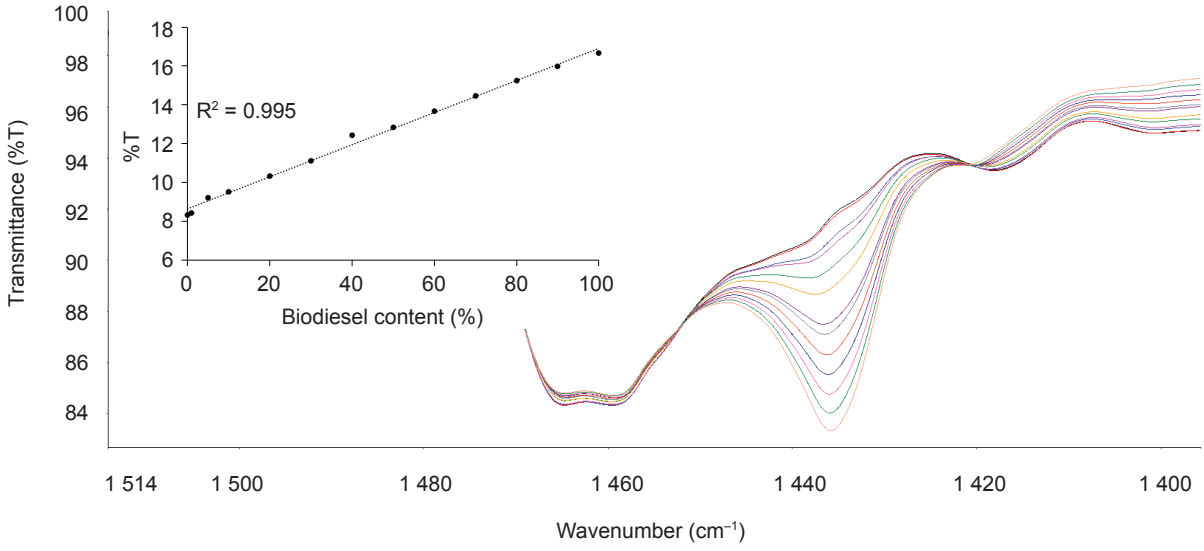


Figure 3. Infrared spectra for different percentages of biodiesel blend with WCPO.

TABLE 5. BIODIESEL YIELD RESPONSES OF BBD

Runs	Catalyst (wt.%)	%K	M/O	Biodiesel yield
1	5	10	9	9.55
2	15	10	9	43.48
3	5	20	9	65.21
4	15	20	9	84.58
5	5	15	6	34.92
6	15	15	6	2.18
7	5	15	12	2.94
8	15	15	12	80.97
9	10	10	6	3.87
10	10	20	6	49.42
11	10	10	12	38.14
12	10	20	12	72.45
13	10	15	9	69.85
14	10	15	9	65.42
15	10	15	9	67.38

TABLE 6. ANOVA STATISTICS FOR RESPONSE SURFACE QUADRATIC MODEL OF BIODIESEL YIELDS

Source	Sum of squares	df	Mean square	F-value	*p*-value	Remarks
Model	12 195.9	9	1 355.10	100.63	0.000	Significant
Linear	6 469.1	3	2 156.38	160.13	0.000	Significant
Catalyst (wt.%)	1 215.1	1	1 215.05	90.23	0.000	Significant
%K	3 899.3	1	3 899.29	289.55	0.000	Significant
M/O	1 354.8	1	1 354.81	100.60	0.000	Significant
Square	2 527.1	3	858.38	63.74	0.000	Significant
Catalyst (wt.%)2	701.2	1	701.18	52.07	0.001	Significant
%K2	34.7	1	34.74	2.58	0.169	
M/O2	2 042.2	1	2 042.22	181.65	0.000	Significant
2-Way interaction	3 151.6	3	1 050.54	78.01	0.000	Significant
Catalyst (wt.%) * %K	53.1	1	53.06	3.94	0.104	
Catalyst (wt.%) * %M/O	3 067.0	1	3 067.01	227.75	0.000	Significant
%K * M/O	31.6	1	31.56	2.34	0.000	Significant
Error	67.3	5	13.47			
Lack of fit	57.3	3	19.16	3.89	0.000	
Pure error	9.8	2	4.92			
Total	12 263.3	14				

R^2 = 0.9945, adj = 0.9846, pred = 0.9232.

The regression coefficient (R^2) indicates and measures the goodness and accuracy of fit for regression models. The R^2 value determined was 99.45%. R^2 adjusted and R^2 predicted shows a close correlation among predicted and observed values. The R^2 adjusted was determined as 98.46% and R^2 predicted was determined as 92.32% indicating that a model's accuracy is high. Regression equation for FAME yield (%) obtained by regression analysis as Equation (2).

$$\% \text{ Yield} = -237.7 - 0.94 \text{ Catalyst (wt.\%)} + 11.24 \text{ \%K} + 35.72 \text{ M/O ratio} - 0.5512 \text{ Catalyst (wt.\%)}^* \text{Catalyst (wt.\%)} - 0.1227 \text{ \%K}^*\text{\%K} - 2.613 \text{ M/O ratio}^*\text{M/O ratio} - 0.1457 \text{ Catalyst (wt.\%)}^*\text{\%K} + 1.846 \text{ Catalyst (wt.\%)}^*\text{M/O ratio} - 0.187 \text{ \%K}^*\text{M/O ratio} \quad (2)$$

The distribution of residuals was analysed to evaluate the adequacy of the model. The residuals plots were straight lines as shown in *Figure 4a* indicated that the residuals follow a normal distribution (Körbahti and Rauf, 2008; Noshadi *et al.*, 2012). *Figures 4b, 4d* shows the value of the residual random pattern, which suggests that the model is consistent with the experimental data with no error recorded (Hasni *et al.*, 2017). The histogram of the residual was shown in *Figure 4c*. The following histogram of residuals suggests that the residuals (and hence the error terms) are normally distributed.

Surface and contour plots illustrated in *Figure 5* depict the effect of independent parameter variables on the percent yield of biodiesel. It was observed that the parameter variables influence the processing of biodiesel. The effect of the interaction of Catalyst (wt.%) and %K on biodiesel yield was demonstrated in *Figure 5a and 5d*. The biodiesel yield of over 80% can be obtained at 12 wt.% of Catalyst and 18%K this could be attributed to the fact that at high alkalinity of the catalyst increases the rate of reaction. When the number of catalysts is increased, the reaction species also increased, thereby shifting the reaction forward, hence increase yields of biodiesel. It indicates that both %K and Catalyst (wt.%) has a positive effect on biodiesel yield. It has been shown that catalyst weight present increase over 13% shows a decrement in biodiesel yield. *Figure 5b, 5e* show the effect of Catalyst (wt.%) and M/O ratio on the yield of biodiesel. The yield of biodiesel increases to over 80% at Catalyst (wt.%) and M/O ratio to about 13% and 11 molar ratio respectively. It has been observed that biodiesel yield decreases when Catalyst (wt.%) was beyond 13 wt.%, substantiating the previous results. The surface plots and contour plots of *Figure 5c, 5f* show combined effect of %K and M/O ratio on biodiesel yield respectively. The result shows that increasing both variables increase the yield of biodiesel. The biodiesel yield increases over 80% were observed at 18%K and 10:1 molar of M/O ratio, the biodiesel yield declined beyond the M/O ratio (10:1) this could be attributed that the excess methanol deactivated the catalyst activity thereby reducing its effectiveness (Ezekannagha *et al.*, 2017).

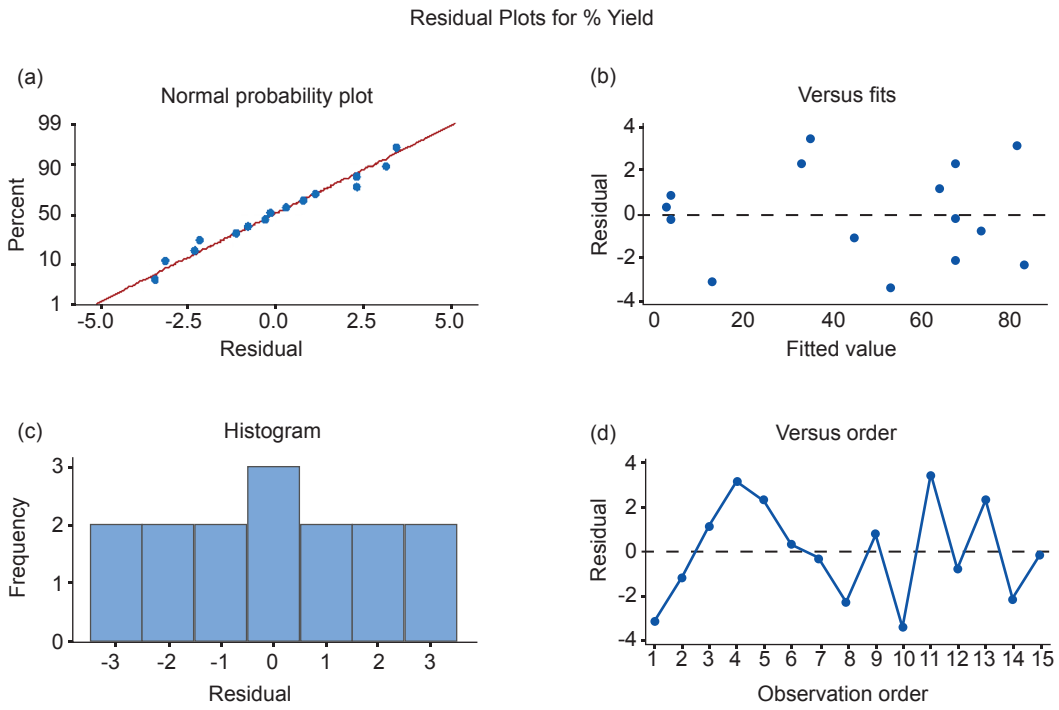


Figure 4. Residual plots for biodiesel yield.

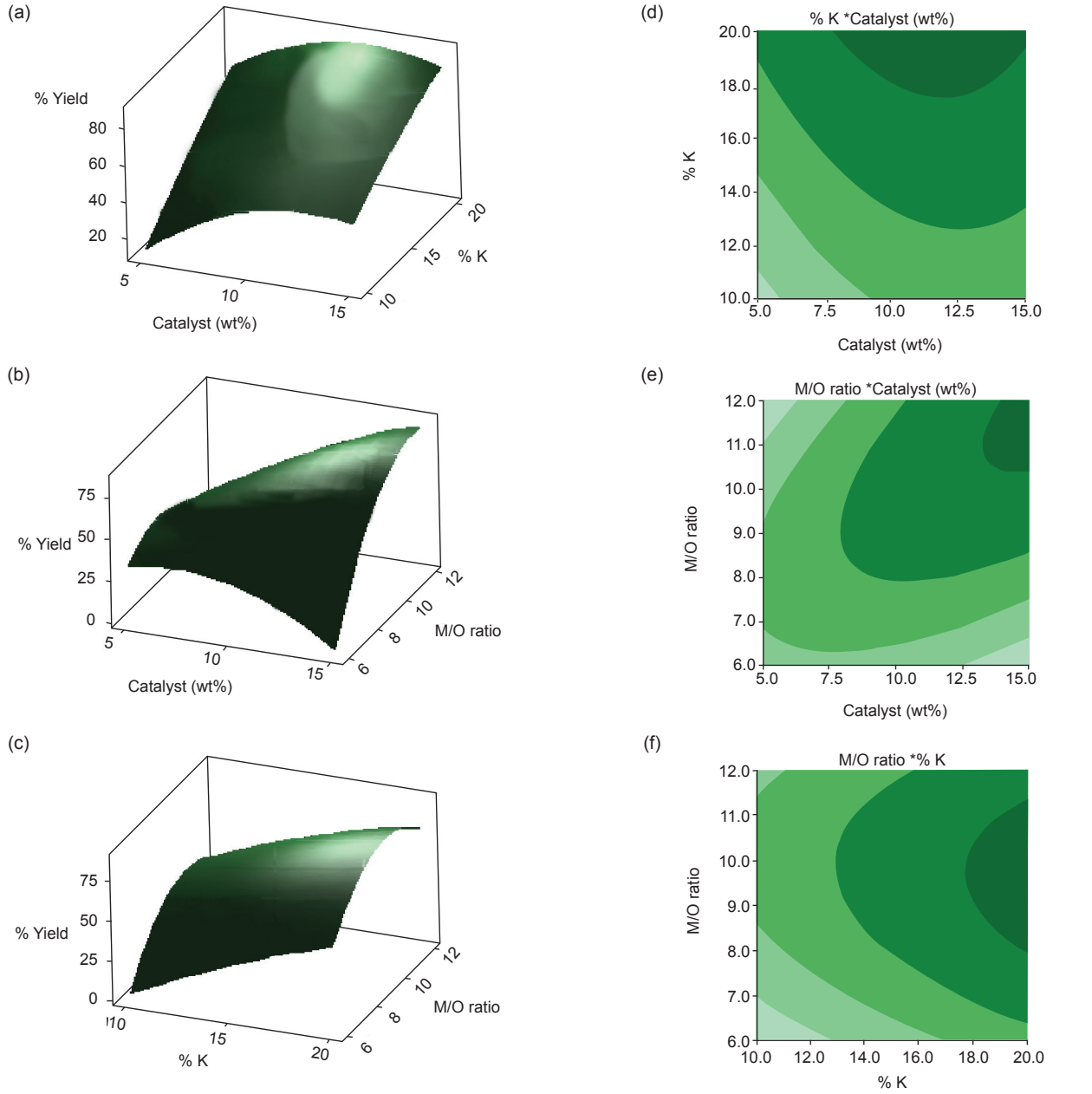


Figure 5. Contour and 3D surface.

The optimisation parameter of individual responses was 15% Catalyst (wt.%), 20% K and 11.39 M/O with the highest biodiesel yield of 96.73%. The experimental verification yielded a maximum of 92.74%, which corresponded well with the value obtained from the regression model.

Physicochemical Properties of FAME Derived from WCPO

The physicochemical properties of biodiesel were measured and compared with the fuel reference standard of Thailand. From the results, the fuel properties of the synthesised biodiesel met the established standard. The properties such as kinematic viscosity, density, acid value, flash point and moisture content of the synthesised biodiesel were measured and listed in *Table 7*.

TABLE 7. PHYSICOCHEMICAL PROPERTIES OF BIODIESEL PRODUCED FROM WCPO WITH PKSA CATALYST

Properties	Unit	Biodiesel from WCPO	Biodiesel standard
Viscosity	mm^2/s	4.77	3.5 – 5.0
Acid value	mg KOH/g	0.27	< 0.5
Cloud point	°C	7.00	-
Pour point	°C	6.00	-
Flash point	°C	166.00	> 120.0
Iodine value	g I_2/100 g oil	56.00	< 120.0

The chemical composition of biodiesel was determined by using GC-MS analysis and the mass percent of fatty acid methyl ester is presented in *Table 8*. From the table, it was observed that biodiesel primarily contained methyl myristate (0.44 wt.%), methyl palmitoleate (4.43 wt.%), methyl palmitate (22.49 wt.%), methyl linoleate (20.50 wt.%), methyl oleate (41.33 wt.%), methyl elaidate (2.88 wt.%), methyl stearate (7.24 wt.%) and methyl eicosenoate (0.69 wt.%). *Figure 6* shows the fatty acid methyl ester chromatogram of biodiesel produced from WCPO.

TABLE 8. BIODIESEL COMPOSITION DETERMINED BY GAS CHROMATOGRAPHY – MASS SPECTROMETRY

RT (min)	Compound	Content (%)
15.77	Methyl myristate	0.44
17.83	Methyl palmitoleate	4.43
18.08	Methyl palmitate	22.49
20.28	Methyl linoleate	20.50
20.38	Methyl oleate	41.33
20.43	Methyl elaidate	2.88
20.68	Methyl stearate	7.24
23.14	Methyl eicosenoate	0.69
Total		100

Comparison Studies

The activity of the 20%K/PKSA was compared with previous reports as presented in *Table 9*. The effects of reaction temperature, reaction time, methanol to oil molar ratio, percentage yields, and catalyst recyclability are compared. The maximum biodiesel yield provided by the 20%K/PKSA under optimum conditions was 92.74%. It was discovered that the 20%K/PKSA catalyst has a comparable catalytic activity to the catalyst previously reported in the literature as stated in *Table 9*. In several studies, biodiesel production using various biomass base catalysts report higher percentage yields with longer reaction time and higher reaction temperature than 20%K/PKSA. It demonstrates that the 20%K/PKSA catalyst was more active than the catalysts used in this investigation.

Catalyst Regeneration and Reusability

Figure 7 shows the effect of the recycling process on the production of biodiesel. For the third successive cycle performed under the optimal conditions, the biodiesel yields were 92.74%, 73.55% and 52.23%, respectively. Subsequently, the catalytic activity of the catalyst continued to

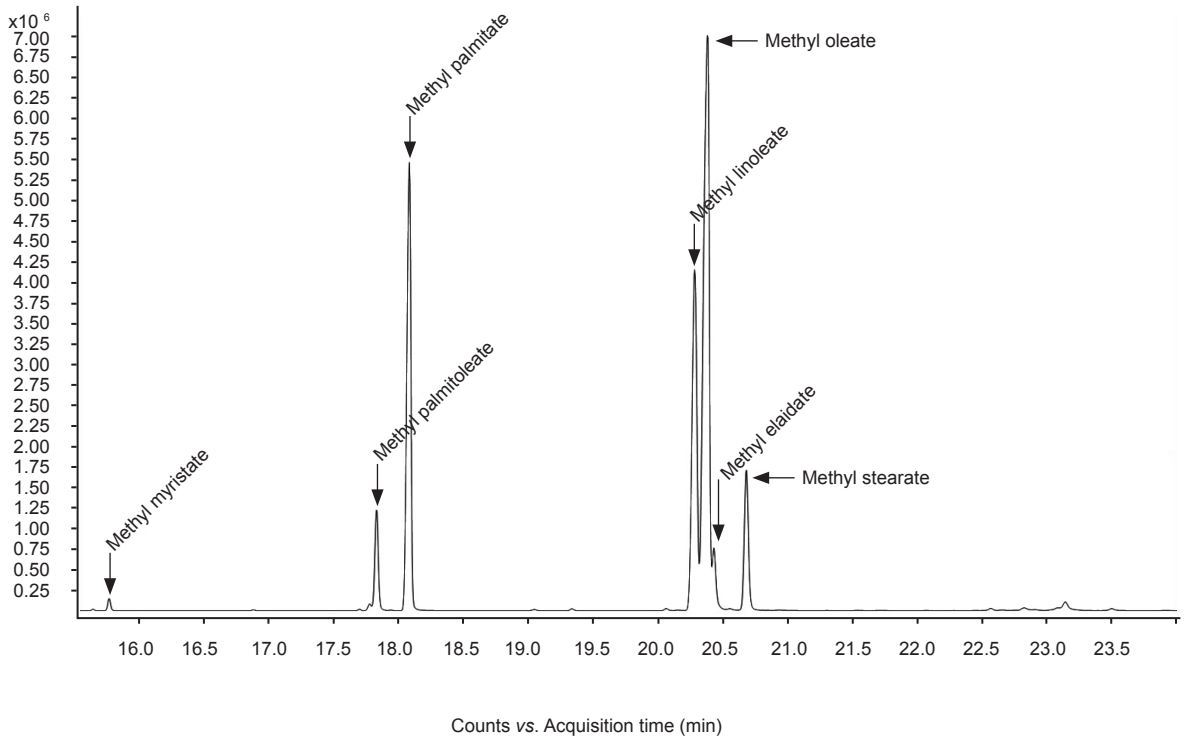


Figure 6. Chromatogram biodiesel production from WCPO.

TABLE 9. THE COMPARISON OF BIODIESEL PRODUCTION USING ASH AS HETEROGENEOUS CATALYSIS REPORTED IN THE LITERATURE WITH THE PRESENT WORK

Catalyst	Temp. (°C)	Time (min)	Molar ratio	Yield (%)	Ref.
ZnO/Coal fly ash	140.0	180.00	12:1	83.17	Yusuff *et al*., 2021
CaO/Wheat ran ash	54.6	144.21	12:1	93.60	Gouran *et al*., 2021
CaO/SiO_2/Rice husk biochar	65.0	180.00	9:1	93.40	Zhao *et al*., 2018
KOH/bentonite	60.0	180.00	6:1	90.70	Soetaredjo *et al*., 2011
KOH/palm shell activated carbon	64.1	60.00	24:1	97.72	Baroutian *et al*., 2010
K_2CO_3-CuO/PKSAC	70.0	120.00	12:1	95.36	Abdullah *et al*., 2021
Sugarcane leaf ash catalyst	64.0	180.00	19:1	97.00	Arumugam and Sankaranarayanan, 2020
$CaO/CaCO_3$/palm oil mill boiler ashes	60.0	180.00	12:1	94.48	Ho *et al*., 2012
20%K/PKSA	65.0	60.00	11.39:1	92.74	Present study

decrease. The reduction in biodiesel yield could be due to triglyceride poisoning of the active sites. To determine the cause of deactivation, used catalysts were analysed using FTIR techniques. *Figure 8* depicts the FTIR spectra of fresh 20%K/PKSA, 20%K/PKSA used after the third cycle with WCPO addition. In comparison to the spectrum of a fresh catalyst, the spectrum of a used catalyst after three cycles indicates an additional band between 3000 to 2800 cm^{-1} and a region at 1743 cm^{-1}. These additional spectra correspond to the vibrations of adsorbed species and are comparable to the WCPO spectra's bands. The additional function groups on the reused catalyst were 2923 and 2852 cm^{-1} (-C-H of methylene group) and 1743 cm^{-1} (C=O stretch of lipid and fatty acid), confirmed the triglyceride blockage on active sites and hence negatively affect the catalytic active sites (Yusuff *et al*., 2021). The results indicate that the washing process using n-hexane and methanol is unable to completely remove the triglyceride accumulation from the surface of the catalyst.

However, the decline in the activity of the catalyst could be due to the leaching of the active phase to the methanol phase. According to Ghasemi *et al*. (2014), the loss of catalyst activity could be attributed to the leaching of potassium content as K_2O to the methanol phase. The leached and dissolved of K_2O in the methanol would react as a homogeneous catalyst. As a result, the process advantages of heterogeneous catalysts are reduced. Other than that, another study reported by Alonso *et al*. (2007) confirmed that the leaching of the active phase to the methanol phase, the potassium content of $K/\gamma\text{-}Al_2O_3$ was measured by ICP-AES in the fresh catalyst and after the reaction. The results confirmed that the K/Al ratio remaining in the catalyst decreased by 40% in the second run and 75% in the fourth run. These results demonstrate that the decrease in catalyst activity between catalytic runs was due to the leaching of active species to the methanol phase. In addition, the leached of K_2O was also observed by Saba *et al*. (2016). The XRF results obtained for the spent 35KOH/ZSM5 catalyst showed that 3.8% of the K_2O active phase was leached after 1st run and 9.4% after the 4th run in the experiment. These results explain how a yield of FAME decreases as the number of runs increases.

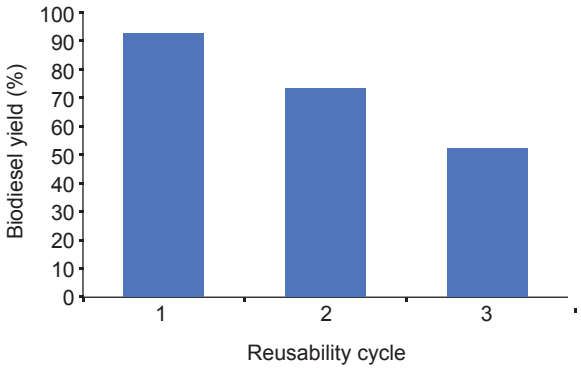


Figure 7. Effect of reusability of 20%K/PKSA on WCPO transesterification at optimal conditions (at 65°C, 60 min reaction time, 15% PKSA, 20% K and 11.39 M/O).

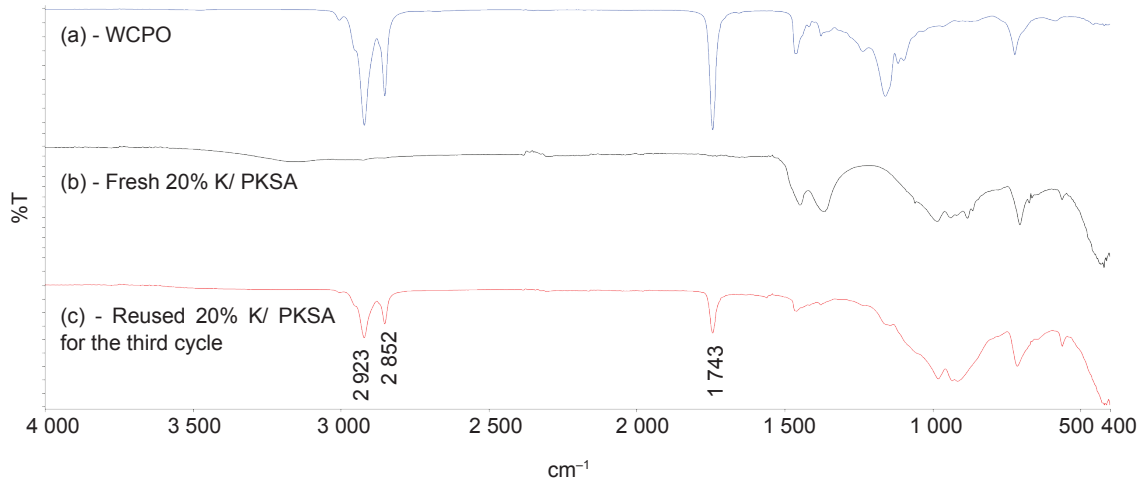


Figure 8. FTIR spectra of (a) WCPO, (b) Fresh 20%K/PKSA catalyst and (c) Reused 20%K/PKSA catalyst for the third cycle.

In this study, the 20%K/PKSA catalyst demonstrated greater stability and reusability for the transesterification process than the eco-friendly catalysts previously reported. For example, when a CaO-fly ash catalyst was used to produce biodiesel from crude palm oil, the yield decreased from 79.76% to 38.93% after the third cycle (Ho *et al*., 2014). In addition, Olutoye *et al*. (2016) produced biodiesel from used cooking oil and reported that the yield decreased from 83.38% to 21.50% after the third cycle of reuse of the montmorillonite K10-supported BaO catalyst. Yusuff *et al*. (2019) demonstrated that an eggshell-supported alumina catalyst could be reused four times with the product yield decreasing from 77.56% to 18.92%.

CONCLUSION

The study demonstrated that the modified palm kernel shells ash (PKSA) with KOH can produce the WCPO biodiesel by using the response surface methodology on Box-Behnken design. The highest biodiesel yield of 92.74% was obtained at the optimum reaction conditions of 15.00% Catalyst (wt.%), 20% K, and 11.39 M/O at 65°C reaction temperature for 60 min. Analysis of variance showed a high coefficient of determination $R^2 = 0.9945$ and Adj-$R^2 = 0.9846$. This demonstrated that response surface methodology with Box-Behnken design can be an effective method to optimise the process parameter for biodiesel production. Furthermore, the prepared catalyst demonstrated a remarkable reusability profile up to the third cycle with a 52.23% biodiesel yield. The physicochemical properties of synthesised biodiesel properties meet with the established standard in Thailand. This study revealed that modified PKSA with KOH is an eco-friendly catalyst with the capability for cost-effective applications for biodiesel production. Biodiesel from WCPO could be used as an alternative diesel fuel that can be considered as renewable energy and environmental recycling process of waste oil after frying.

ACKNOWLEDGEMENT

This research was funded by King Mongkut's University of Technology North Bangkok. Contract no. KMUTNB-64-DRIVE-21. The authors would like to thank the Scientific Instrument and Analytical Testing Center (SIATC), Faculty of Science, Energy and Environment, King Mongkut's University of Technology North Bangkok (KMUTNB), Rayong campus, for analytical support.

REFERENCES

Abdullah, R F; Rashid, U; Ibrahim, M L; Hazmi, B; Alharthi, F A and Nehdi, I A (2021). Bifunctional nano-catalyst produced from palm kernel shell via hydrothermal-assisted carbonization for biodiesel production from waste cooking oil. *Renew. Sustain. Energy Rev.*, *137*: 110638. DOI: 10.1016/j.rser.2020.110638.

Alonso, D M; Mariscal, R; Moreno-Tost, R; Poves, M Z and Granados, M L (2007). Potassium leaching during triglyceride transesterification using K/γ-Al_2O_3 catalysts. *Catal. Commun.*, *8(12)*: 2074-2080. DOI: 10.1016/j.catcom.2007.04.003.

Arumugam, A and Sankaranarayanan, P (2020). Biodiesel production and parameter optimization:

An approach to utilize residual ash from sugarcane leaf, a novel heterogeneous catalyst, from *Calophyllum inophyllum* oil. *Renew. Energy*, *153*: 1272-1282. DOI: 10.1016/j.renene.2020.02.101.

Ashok, A; Kumar, A; Bhosale, R R; Saleh, M A H and Van den Broeke, L J (2015). Cellulose assisted combustion synthesis of porous Cu–Ni nanopowders. *RSC Advances*, *5(36)*: 28703-28712. DOI: 10.1039/c5ra03103f.

Baroutian, S; Aroua, M K; Raman, A A A and Sulaiman, N M N (2010). Potassium hydroxide catalyst supported on palm shell activated carbon for transesterification of palm oil. *Fuel Process. Technol.*, *91(11)*: 1378-1385. DOI: 10.1016/j.fuproc.2010.05.009.

Basumatary, S; Nath, B; Das, B; Kalita, P and Basumatary, B (2021). Utilization of renewable and sustainable basic heterogeneous catalyst from *Heteropanax fragrans* (Kesseru) for effective synthesis of biodiesel from *Jatropha curcas* oil. *Fuel*, *286*: 119357. DOI: 10.1016/j.fuel.2020.119357.

Bazargan, A; Kostić, M D; Stamenković, O S; Veljković, V B and McKay, G (2015). A calcium oxide-based catalyst derived from palm kernel shell gasification residues for biodiesel production. *Fuel*, *150*: 519-525. DOI: 10.1016/j.fuel.2015.02.046.

Dwivedi, G and Sharma, M P (2015). Application of Box–Behnken design in optimization of biodiesel yield from Pongamia oil and its stability analysis. *Fuel*, *145*: 256-262. DOI: 10.1016/j.fuel.2014.12.063.

Ezekannagha, C B; Ude, C N and Onukwuli, O D (2017). Optimization of the methanolysis of lard oil in the production of biodiesel with response surface methodology. *Egypt. J. Pet., 26(4)*: 1001-1011. DOI: 10.1016/j.ejpe.2016.12.004.

Ghasemi, M and Molaei Dehkordi, A (2014). Transesterification of waste cooking oil to biodiesel using KOH/γ-Al_2O_3 catalyst in a new two-impinging-jets reactor. *Ind. Eng. Chem. Res.*, *53(31)*: 12238-12248. DOI: 10.1021/ie403408r.

Gouran, A; Aghel, B and Nasirmanesh, F (2021). Biodiesel production from waste cooking oil using wheat bran ash as a sustainable biomass. *Fuel*, *295*: 120542. DOI: 10.1016/j.fuel.2021.120542.

Hasni, K; Ilham, Z; Dharma, S and Varman, M (2017). Optimization of biodiesel production from *Brucea javanica* seeds oil as novel non-edible feedstock using response surface methodology. *Energy Convers. Manag.*, *149*: 392-400. DOI: 10.1016/j.enconman.2017.07.037.

Ho, W W S; Ng, H K and Gan, S (2012). Development and characterisation of novel heterogeneous palm oil mill boiler ash-based catalysts for biodiesel production. *Bioresour. Technol.*, *125*: 158-164. DOI: 10.1016/j.biortech.2012.08.099.

Ho, W W S; Ng, H K; Gan, S and Tan, S H (2014). Evaluation of palm oil mill fly ash supported calcium oxide as a heterogeneous base catalyst in biodiesel synthesis from crude palm oil. *Energy Convers. Manag.*, *88*: 1167-1178. DOI: 10.1016/j.enconman.2014.03.061.

Körbahti, B K and Rauf, M A (2008). Response surface methodology (RSM) analysis photoinduced decoloration of toludine blue. *J. Chem. Eng., 136(1)*: 25-30. DOI: 10.1016/j.cej.2007.03.007.

Latchubugata, C S; Kondapaneni, R V; Patluri, K K; Virendra, U and Vedantam, S (2018). Kinetics and optimization studies using Response Surface Methodology in biodiesel production using heterogeneous catalyst. *Chem. Eng. Res. Des.*, *135*: 129-139. DOI: 10.1016/j.cherd.2018.05.022.

Leung, D Y C and Guo, Y (2006). Transesterification of neat and used frying oil: Optimization for biodiesel production. *Fuel Process. Technol.*, *87(10)*: 883-890. DOI: 10.1016/j.fuproc.2006.06.003.

Malithong, A; Piputsitee, C; Sarobol, E and Sriroth, K (2017). Zero waste management to increase efficiency in palm oil production and processing for food security in Thailand. *Walailak J. Sci. Tech. (WJST), 14(7)*: 589-596.

Marwaha, A; Rosha, P; Mohapatra, S K; Mahla, S K and Dhir, A (2019). Biodiesel production from *Terminalia bellerica* using eggshell-based green catalyst: An optimization study with response surface methodology. *Energy Rep.*, *5*: 1580-1588. DOI: 10.1016/j.egyr.2019.10.022.

Noshadi, I; Amin, N A S and Parnas, R S (2012). Continuous production of biodiesel from waste cooking oil in a reactive distillation column catalyzed by solid heteropolyacid: Optimization using response surface methodology (RSM). *Fuel, 94*: 156-164. DOI: 10.1016/j.fuel.2011.10.018.

Oko, S and Kurniawan, A (2019). Modification of CaO catalyst with impregnation method using KOH in biodiesel synthesis from waste cooking oil. *Logic: Jurnal Rancang Bangun dan Teknologi, 19(2)*: 62-67. DOI: 10.31940/logic.v19i2.1318.

Olutoye, M A; Wong, S W; Chin, L H; Amani, H; Asif, M and Hameed, B H (2016). Synthesis of fatty acid methyl esters via the transesterification of waste

cooking oil by methanol with a barium-modified montmorillonite K10 catalyst. *Renew. Energy*, *86*: 392-398. DOI: 10.1016/j.renene.2015.08.016.

Putra, M D; Irawan, C; Ristianingsih, Y and Nata, I F (2018). A cleaner process for biodiesel production from waste cooking oil using waste materials as a heterogeneous catalyst and its kinetic study. *J. Clean. Prod., 195*: 1249-1258. DOI: 10.1016/j.jclepro.2018.06.010.

Saba, T; Estephane, J; El Khoury, B; El Khoury, M; Khazma, M; El Zakhem, H and Aouad, S (2016). Biodiesel production from refined sunflower vegetable oil over KOH/ZSM5 catalysts. *Renew. Energy*, *90*: 301-306. DOI: 10.1016/j.renene.2016.01.009.

Salinas, D; Araya, P and Guerrero, S (2012). Study of potassium-supported TiO_2 catalysts for the production of biodiesel. *Appl. Catal. B: Environ.*, *117*: 260-267. DOI: 10.1016/j.apcatb.2012.01.016.

Sharma, A; Kodgire, P and Kachhwaha, S S (2020). Investigation of ultrasound-assisted KOH and CaO catalyzed transesterification for biodiesel production from waste cotton-seed cooking oil: Process optimization and conversion rate evaluation. *J. Clean. Prod., 259*: 120982. DOI: 10.1016/j.jclepro.2020.120982.

Singh, V; Belova, L; Singh, B and Sharma, Y C (2018). Biodiesel production using a novel heterogeneous catalyst, magnesium zirconate ($Mg_2Zr_5O_{12}$): Process optimization through response surface methodology (RSM). *Energy Convers. Manag., 174*: 198-207. DOI: 10.1016/j.enconman.2018.08.029.

Soetaredjo, F E; Ayucitra, A; Ismadji, S and Maukar, A L (2011). KOH/bentonite catalysts for transesterification of palm oil to biodiesel. *Appl. Clay Sci., 53(2)*: 341-346. DOI: 10.1016/j.clay.2010.12.018.

Soria-Figueroa, E; Mena-Cervantes, V Y; García-Solares, M; Hernández-Altamirano, R and Vazquez-Arenas, J (2020). Statistical optimization of biodiesel production from waste cooking oil using CaO as catalyst in a Robinson-Mahoney type reactor. *Fuel*, *282*: 118853. DOI: 10.1016/j.fuel.2020.118853.

Yashim, M M; Razali, N; Saadon, N and Rahman, N A (2016). Effect of activation temperature on properties of activated carbon prepared from oil palm kernel shell (OPKS). *ARPN J. Eng. Appl. Sci., 11(10)*: 6389-6392.

Yusuff, A S and Popoola, L T (2019). Optimization of biodiesel production from waste frying oil over alumina supported chicken eggshell catalyst using experimental design tool. *Acta Polytechnica*, *59(1)*: 88-97. DOI: 10.14311/AP.2019.59.0088.

Yusuff, A S; Bhonsle, A K; Trivedi, J; Bangwal, D P; Singh, L P and Atray, N (2021). Synthesis and characterization of coal fly ash supported zinc oxide catalyst for biodiesel production using used cooking oil as feed. *Renew. Energy*, *170*: 302-314. DOI: 10.1016/j.renene.2021.01.101.

Zhao, C; Yang, L; Xing, S; Luo, W; Wang, Z and Lv, P (2018). Biodiesel production by a highly effective renewable catalyst from pyrolytic rice husk. *J. Clean. Prod.*, *199*: 772-780. DOI: 10.1016/j.jclepro.2018.07.242.

Journal of Oil Palm Research Vol. 35 (4) December 2023 p. 682-693
DOI: https://doi.org/10.21894/jopr.2023.0001

ECONOMICAL STUDY OF BIO-BASED POLYBUTYLENE SUCCINATE PRODUCTION FROM OIL PALM BIOMASS

ROHANI ARPA[1]; ABDULLAH AMRU INDERA LUTHFI[1,2]*; NURUL ADELA BUKHARI[3]; JIAN PING TAN[4]; SAFA SENAN MAHMOD[2] and MUHAMMAD ZULHAZIMAN MAT SALLEH[1,2]

ABSTRACT

This work demonstrates the economic feasibility of the production of bio-polybutylene succinate (bio-PBS) with 99.69% purity. Based on an extensive literature review, bio-succinic acid (bio-SA) was produced via fermentation from oil palm fronds (OPF), which was then purified via vacuum filtration, evaporated, crystallised and dried to attain 99.27% purity. The purified bio-SA was then hydrogenated to produce 1,4-butanediol (BDO), prior to polymerisation with bio-SA to produce bio-PBS via esterification. The mass balance analysis performed with SuperPro Designer® showed a negligible error. The proposed design gained profit in a short period of time based on 24.14% internal rate of return (IRR), 6.33 years dynamic payback period (DPP) and RM3366.31 million net present value (NPV). Direct comparison between simulation data and manual calculations showed <25.00% difference, which proved the dependability of the simulation results. Sensitivity analysis predicted that an increment in either bio-PBS's production rate or bio-PBS and by-products pricing can increase the value of NPV and IRR. However, the increment in raw material price and fixed capital investment (C_{FCI}) can lower their values. Collectively, the results highlighted the feasibility of this process on a large scale as it has the potential to generate revenues, ultimately resulting in a sustainable bioplastic industry for packaging applications.

Keywords: bio-polybutylene succinate, economic analysis, oil palm fronds, SuperPro Designer®.

Date received: 27 July 2022**; Date accepted:** 7 November 2022**; Publish online:** 18 January 2023.

INTRODUCTION

For more than half a century, plastics have been widely used in practically all commercial products, most notably in packaging via petrochemical processes (Ncube *et al.*, 2021). Among the advantages of plastic packaging are its lightweight, strength, flexibility and low cost (Gerassimidou *et al.*, 2021). Accordingly, the world produced an estimated 6.3 billion tonnes of plastic waste, with only 9% being recycled and more than 80% being deposited in landfills or natural environments (Liang *et al.*, 2021). Such conventional plastic contains potentially harmful components such as phthalates, polyfluorinated compounds, bisphenol-A (BPA), brominated flame retardants, and antimony trioxide. The strong chemical bonds on the plastics make them nearly impossible to be completely decomposed in the natural environment (Rafiqah *et al.*, 2021).

As a country that is heading towards championing the sustainable development goals (SDGs), especially SDGs 13 (climate action), 14 (life below water) and 15 (life on land), Malaysia has been lauded for making good progress in minimising plastic waste in the country. Bioplastics

[1] Department of Chemical and Process Engineering, Faculty of Engineering and Built Environment, Universiti Kebangsaan Malaysia, 43600 Bangi, Selangor, Malaysia.

[2] Research Centre for Sustainable Process Technology (CESPRO), Faculty of Engineering and Built Environment, Universiti Kebangsaan Malaysia, 43600 Bangi, Selangor, Malaysia.

[3] Malaysian Palm Oil Board, 6 Persiaran Institusi, Bandar Baru Bangi, 43000 Kajang, Selangor, Malaysia.

[4] School of Energy and Chemical Engineering, Xiamen University Malaysia, Jalan Sunsuria, Bandar Sunsuria, 43900 Sepang, Selangor, Malaysia.

* *Corresponding author e-mail: amru@ukm.edu.my*

were introduced in place of traditional plastics to reduce dependency on limited petroleum resources and associated environmental impacts (Siracusa *et al.*, 2020). Bioplastics are a type of polymer that is derived from biological material, wherein microorganisms such as bacteria, fungi, actinomycetes, and others can degrade them in a short period of time. Bio-polybutylene succinate (bio-PBS) is one of the biodegradable bioplastics that can be produced from agro-industrial biomass, such as oil palm biomass, to minimise environmental pollution (Ioannidou *et al.*, 2022).

Currently, the oil palm (*Elaeis guineensis* Jacq.) generates one of the most abundant biomass sources in Malaysia, particularly the oil palm fronds (OPF) (Onoja *et al.*, 2019). *Figure 1* illustrates the OPF biomass comprising the juice (*i.e.*, liquid fraction) and bagasse (*i.e.*, solid fraction obtains after mechanical pressing). OPF is a major component of the oil palm waste generated by fresh fruit bunch (FFB) pruning, which amounted to ca. 1.5 million tonnes in 2010 and ca. 21.0 million tonnes in 2014 (Mohamad *et al.*, 2020). OPF is the main carbohydrate used in the production of bio-succinic acid (bio-SA) and its application focused more on zero waste technology (Luthfi *et al.*, 2017; Tan *et al.*, 2016).

Given the richness in carbohydrate content, OPF is recommended to be used as raw material for bio-SA production, which serves as a monomer unit in bio-PBS. The first step of bio-SA production is mechanical pre-treatment, such as grinding and crushing, which would reduce the size and moisture content of the OPF (Luthfi *et al.*, 2017; Tu *et al.*, 2019). Pre-treatment is a critical step in the biochemical conversion pathway, which can account for up to ca. 20% of the total cost of the overall process (Amin *et al.*, 2017; Luthfi *et al.*, 2017). Acid hydrolysis is commonly used as pre-treatment to recover pentose from biomass hemicellulose while preserving cellulose and lignin (Bukhari *et al.*, 2021). Thereafter, the recovered sugars can be used in the fermentations to produce bio-SA using *Actinobacillus succinogenes* 130Z as succinate-producing microorganisms (Luthfi *et al.*, 2017; Tu *et al.*, 2019). This bio-SA alongside other carboxylate byproducts were in the form of liquid broth during the fermentation stage.

Purification of fermentation broth is required to achieve bio-SA with 99.00% purity for efficient bio-PBS synthesis (Dai *et al.*, 2020). Evidence in literature suggested that carboxylic acids such as formic and acetic acids could be eliminated by evaporation and distillation, depending on the boiling point of the compound (Law *et al.*, 2019; Omwene *et al.*, 2021). While vacuum distillation for 12 hr at 60°C could eliminate both formic acid and acetic acid, bio-SA with 99.18% purity could be achieved by evaporation before undergoing crystallisation (Li *et al.*, 2010; Thuy *et al.*, 2017). Following that, hydrochloric acid (HCl) or sulphuric acid (H_2SO_4) was used to adjust the pH of the fermentation broth from 6.0-7.0 to 2.0. This is because SA has only 3.00% solubility, whereas formic acid and acetic acid are still soluble in water at 4°C and pH 2.0 (Law *et al.*, *2019*; Li *et al.*, 2010). Then, hydrogenation of bio-SA with γ-butyrolactone (GBL), an intermediate product, could result in the production of 1,4-Butanediol (BDO) and tetrahydrofuran (THF) using ruthenium (Ru) and rhenium (Re) as catalysts. THF is a high-performance solvent while GBL is an essential intermediate chemical in pyrrolidone derivatives manufacturing (Baidya *et al.*, 2019; Di *et al.*, 2015). PBS, on the other hand, is a versatile semi-crystalline polymer, which makes it popular in a variety of industries (Rafiqah *et al.*, 2021).

Generally, the synthesis of PBS involving bio-SA is divided into two steps: esterification and polycondensation (Rafiqah *et al.*, 2021). The esterification of bio-SA with BDO involved the use of excess diol and diacid to produce PBS oligomer while removing water. The PBS

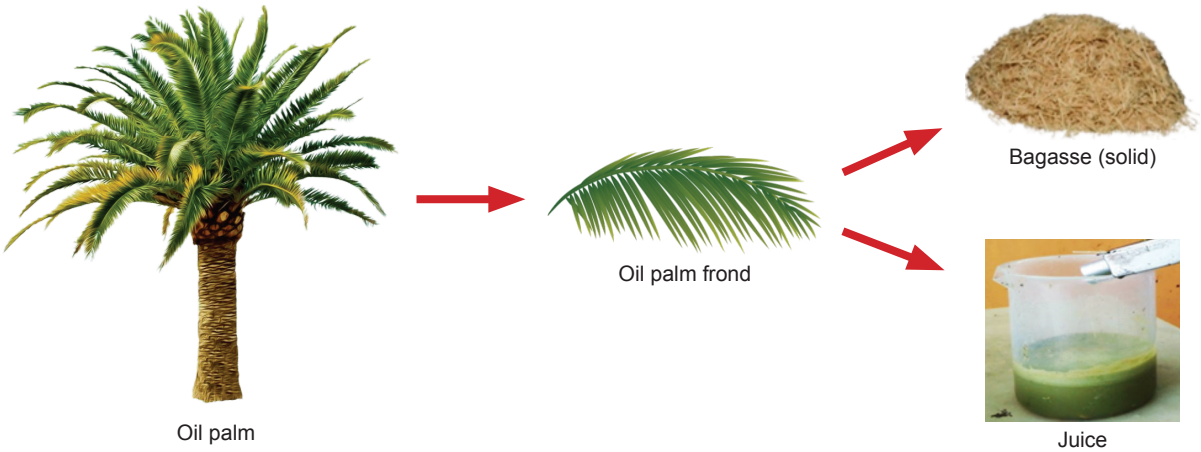


Figure 1. Illustration of oil palm fronds biomass.

oligomers will then be transesterified under vacuum using various catalysts, such as stannous octoate ($SnOct_2$), antimony (III) trioxide (Sb_2O_3), and titanium (IV) butoxide ($Ti(OBu)_4$) to produce high molar mass PBS (Ferreira *et al.*, 2015). The vacuum should be sufficient to remove water and BDO during polycondensation. This method can improve mechanical properties, heat resistance and thermoplastic processes simultaneously (Luthfi *et al.*, 2017; Rafiqah *et al.*, 2021; Tu *et al.*, 2019).

Many studies reported the use of bio-PBS as a composite matrix for multifold applications, including agriculture, packaging, medicine and textiles, given its excellent mechanical properties, high flexibility, melting processing efficiency and biodegradable permeability (Luthfi *et al.*, 2017; Rafiqah *et al.*, 2020; 2021). Thus, bio-PBS is suitable to be used for packaging and provides interesting features such as rigid, robust and exhibits excellent adhesiveness. Processing of bio-PBS is quite simple and can be carried out either by extrusion, thermal formation, or injection moulding (Thurber *et al.*, 2020).

Currently, there is lack of studies dealing with OPF and its possible valorisation into bio-PBS, mostly pointing to OPF as a potential source for biofuels, eco-products, succinic acid production, or livestock feed (Luthfi *et al.*, 2017). There is yet a study on large-scale production of bio-PBS, particularly, using biomass as raw material. Various simulation software, such as DWSIM, SuperPro Designer®, Aspen Plus®, and HYSIS, have been used to demonstrate the chemical operating units used in each processes (SimulateLive.com 2017). SuperPro Designer® software was used in this study to demonstrate the operation of chemical units used in bio-PBS production as it has an extensive database, covering special units of chemical operations. It has also been used in various industries, including pharmaceuticals and biotechnology. Besides that, SuperPro Designer® software can be used for process optimisation, project economic analysis, pollution reduction and control, as well as utility and manpower management (Mabrouki *et al.*, 2015).

Lastly, the data collated from the simulation can be used for economic assessment. The economic analysis can be used to determine the economic efficiency of the bio-PBS manufacturing process, including the profit and whether the whole process is feasible (Turton *et al.*, 2018). Profitability analysis can also be used to determine the rate of return on investment (ROI), dynamic payback period (DPP), internal rate of return (IRR) and net present value (NPV). Besides that, sensitivity analysis was performed to determine parameters that had the most significant influence on the project's performance (Mahmod *et al.*, 2021).

To our best knowledge, the present paper is the first effort that aims to identify the technical and economic feasibility of the production of bio-PBS from OPF. Identifying the best process for producing bio-PBS from bio-SA through extensive literature review is one of the main requirements in simulating large-scale production of bio-PBS. *Figure 2* illustrates the overall research idea of this work. The process simulation to produce bio-PBS was then performed using SuperPro Designer® software, which includes the input and output structure, mass balance analysis and process flow diagram. Lastly, an economic feasibility study on bio-PBS production was performed, including the cost of manufacturing (COM), profitability analysis, comparison of calculations versus simulation data and sensitivity analysis.

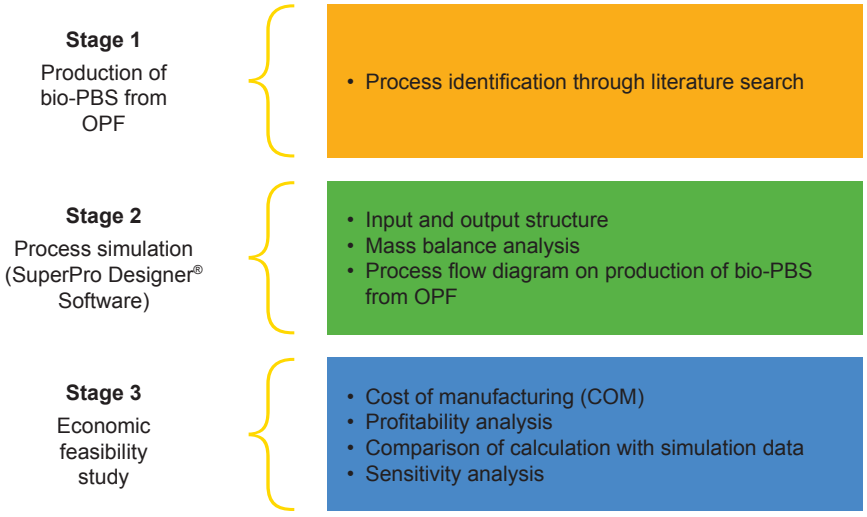


Figure 2. Overall research idea (objective) of this work.

MATERIALS AND METHODS

Raw Materials and Process Description

The information about the process design for the production of bio-SA from OPF was collected from a previous study by Tan *et al.* (2016). OPF (52% glucose, 37% sucrose, 8% fructose, and 3% arabinose) was used as the main carbon source. Size and moisture content of the OPF was reduced through grinding. Then, the ground OPF is acid hydrolysed with 26% H_2SO_4. The sugars in the OPF were then fermented using wild-type *A. succinogenes* 130Z, a succinate-producing microorganism. The conditions for fermentation were 37°C, pH 6.8, 200 rpm and 0.50 vvm carbon dioxide (CO_2). Unreacted CO_2 was recycled into a bioreactor to reduce emissions to the environment.

According to previous studies from Law *et al.* (2019); Li *et al.* (2010); Thuy *et al.* (2017), purification includes several steps of filtration, evaporation, crystallisation and drying of bio-SA. Fermentation broths were purified and evaporated to remove compounds that may affect the purity of the bio-SA. Then, HCl was used to reduce the pH of the fermentation broth before crystallisation to produce bio-SA with at least 99% purity. Lastly, drying was carried out to remove excess volatile compounds and to increase the purity of bio-SA.

Optimal hydrogenation conditions, such as high pressures (45-80 bar) and temperatures (180°C-250°C), were used to produce BDO from bio-SA. Ru-Rutile was chosen as catalyst in hydrogenation due to its high selectivity over BDO (Baidya *et al.*, 2019; Di *et al.*, 2015). Bio-SA and BDO were then esterified to produce bio-PBS and water. $Ti(OBu)_4$ was chosen as catalyst for this process because of its ability to increase the average molecular weight (M_w) of bio-PBS by 33% (Ferreira *et al.*, 2015). The stoichiometric equation for hydrogenation and esterification can be seen in Equation (1) and (2), respectively.

$$C_4H_6O_4\,(s) = 1.31C_4H_{10}O_2\,(l) \quad (1)$$

$$C_4H_6O_4\,(s) + C_4H_{10}O_2\,(l) = (C_8H_{12}O_4)_n\,(s) + 2H_2O\,(l) \quad (2)$$

Process Flow in the Production of Bio-polybutylene Succinate

The process flow diagram for this study, represented in *Figure 3*, was constructed to aid the next step, which was to simulate the mass balance of bio-PBS production from OPF using SuperPro Designer® software (Intelligen, Australia). In this study, OPF was used as raw material and was pre-treated with hydrothermal-assisted acid hydrolysis using H_2SO_4. The sugars in OPF were then fermented with ammonia and CO_2 to produce bio-SA, formic acid, acetic acid, biomass, and water. Next, the fermentation broth was vacuum filtered to remove the biomass. The volatile by-products such as water, acetic acid, and formic acid were then eliminated from fermentation broths through evaporation. The pH of the fermentation broth was then adjusted with HCl prior to the crystallisation process. After that, the fermentation broth was dried to remove extra water and produce bio-SA crystals. Some bio-SA crystals were hydrogenated to produce BDO, while other bio-SA crystals were esterified with BDO to produce the end product (bio-PBS) and water.

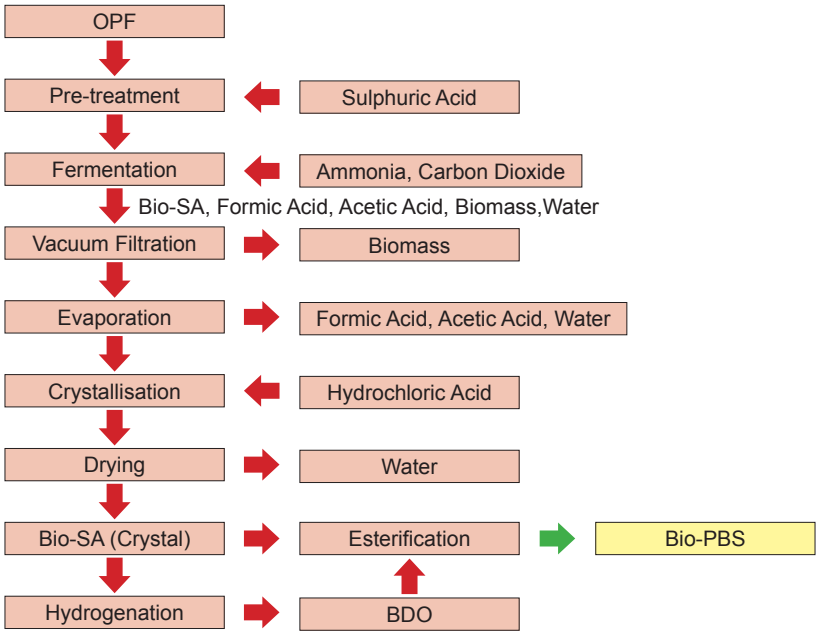


Figure 3. Process flow diagram of bio-PBS production.

Economic Analysis

The use of PBS worldwide registered a CAGR of 38.9% between 2014 to 2020, given its potential in packaging application as well as increasing demand in bioplastics (Tan *et al.*, 2017). Based on Data Bridge Market Research (2020), market for PBS is expected to reach 155.89 ktons by 2027. Thus, the global demand for bio-PBS in 2020 was estimated to be 146 ktons, with only 87 ktons supplied. The market vacancy in Asia-Pasific (APAC) region is around 41 ktons to overcome 59 ktons of shortage. In this research, the bio-PBS production capacity is 5129.46 kg hr^{-1} with the plant operating for 330 days in a year. Some major assumptions were made including a project life of 12 years. Furthermore, the plant start-up and working capital (C_{WC}) were assumed at the end of year 2. Then, 10.0% for start-up cost and 50.0% for investment in year 1 and 2 were assumed from fixed capital investment (C_{FCI}). Besides, the taxation rate is estimated to be 40.0%. Lastly, the depreciation method is based on a 5-year MACR plant life. These assumptions were then used to construct a profitability analysis for the production of bio-PBS from OPF.

C_{TCI} in Equation (3) is the amount of investment required in the construction of a plant where C_{FCI} is the sum of a project's direct and indirect costs. C_{WC}, on the other hand, accounted 20% of C_{FCI} (Bonem, 2018; Turton *et al.*, 2018).

$$C_{TCI} = C_{FCI} + C_{WC} \quad (3)$$

The cost of manufacturing (COM) is the total direct manufacturing cost (DMC), fixed manufacturing cost (FMC) and general expenditure (GE). The simplified expressions to calculate COM and manufacturing costs without depreciation (COM_d) were shown in Equation (4) and (5). Where, C_{RM}, C_{WT}, C_{UL} and C_{OL} are the costs for raw materials, wastewater treatment, utilities and labour, respectively (Turton *et al.*, 2018).

$$COM = 0.28C_{FCI} + 2.73C_{OL} + 1.23(C_{UT} + C_{WT} + C_{RM}) \quad (4)$$

$$COM_d = 0.18C_{FCI} + 2.73C_{OL} + 1.23(C_{UT} + C_{WT} + C_{RM}) \quad (5)$$

Depreciation is classified as four categories: Straight line (SL), double declining balance (DDB), sum of years depreciation (SOYD) and unit of production (UOP). The most recent depreciation method used in the United States is the modified accelerated cost recovery system (MACRS), as shown in Equation (6) and (7) (Investopedia, 2021).

$$d_k^{DDB} = \tfrac{2}{5}\left[100 - \textstyle\sum_{j=0}^{k-1} d_j^{DDB}\right] \quad (6)$$

$$d_k^{SL} = \frac{(Capital\ without\ deppreciation)}{(Excess\ deppreciation\ time)} \quad (7)$$

Payback period (PBP) and ROI are determined in non-discounted cash flow. PBP is the amount of time required to recover C_{FCI}, with shorter PBP value preferred. ROI, in Equation (8), is the ratio of net income to investment. High ROI value indicates high return on investment from the cost of the process (Bonem, 2018; Mahmod *et al.* 2021; Turton *et al.*, 2018). DPP, NPV and IRR are determined in discounted cash flows. NPV, as shown in Equation (9), is used to evaluate investment profitability, whereas IRR is the value obtained when NPV becomes zero (Bonem, 2018; Turton *et al.*, 2018).

$$ROI = \frac{(Average\ annual\ net\ profit)}{Fixedcapitalinvestment(C_{FCI})} - \frac{1}{n} \quad (8)$$

$$NPV = \frac{\sum_{k=1}^{N} NCF_k}{(1+i)^k} \quad (9)$$

Sensitivity analysis was also performed to predict the uncertainties caused by laboratory-scale parameters and some of the assumptions made during the simulation process (Mahmod *et al.*, 2021). In this study, sensitivity analysis was used to identify the parameters that most influenced the study's performance, with 10% variation in baseline case values.

RESULTS AND DISCUSSION

Production of Bio-polybutylene Succinate

According to Tan *et al.* (2016), the main raw material used in the production of bio-PBS is 19 286.45 kg hr^{-1} of OPF, which composed of 75% solid biomass and 25% juice. The OPF biomass was acid hydrolysed in acid hydrolysis reactor (P-4/R-101) at 82% conversion using H_2SO_4 at 100°C and 1.01 bar (*Figure 4*). At the same time, OPF juice is sterilised in heat steriliser (P-2/ST-101) to prevent contamination of the sugar (Tan *et al.*, 2016). The sugars in the OPF are then fermented in bioreactor (P-6/FR-101) with CO_2, ammonia, and *A. succinogenes* 130Z to produce bio-SA, formic acid, acetic acid, biomass, and water at 95% conversion. This fermentation process takes place at 37°C and 1.01 bar.

The fermentation broth was then vacuum filtered in rotary vacuum filtration (P-7/RVF-102) to remove 98.00% of the biomass, solids suspended in the OPF juice, and excess foreign matter from the acid hydrolysis. Thereafter, the fermentation broth was evaporated in evaporator (P-8/EV-101) to remove 80.00% of the formic acid, acetic acid and water. The pH of the fermentation broth was then adjusted from 6.8 to 2.0 with HCl before going through crystallisation in crystalliser

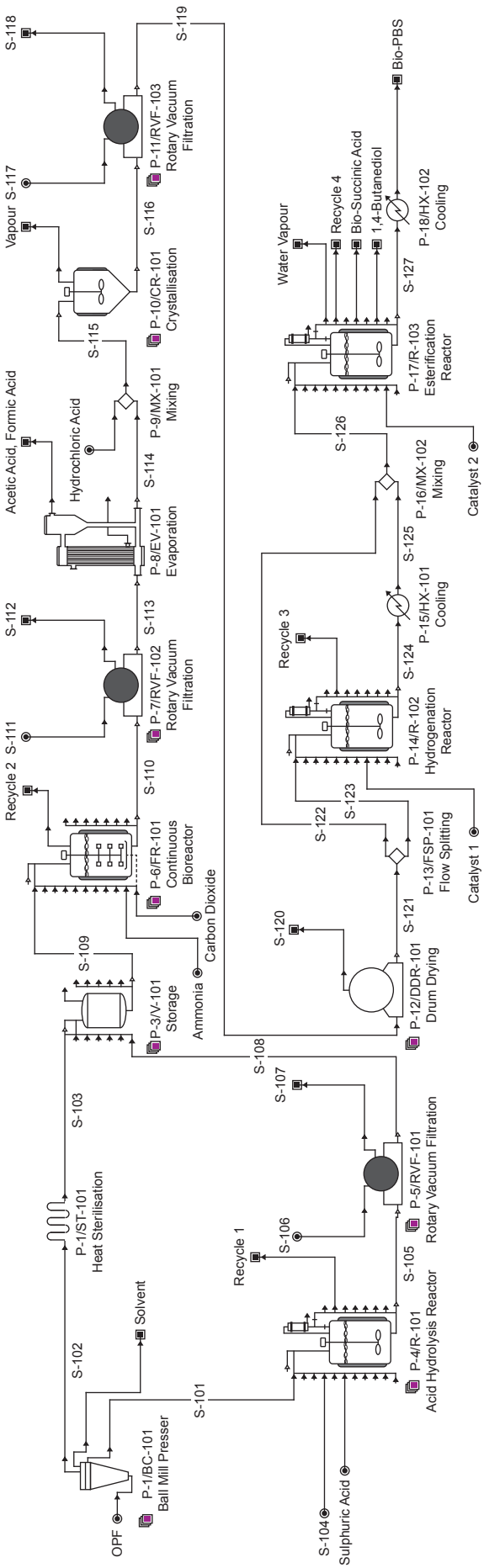


Figure 4. Process flow diagram on production of bio-PBS from OPF using SuperPro Designer® software.

(P-10/CR-101) to increase the purity of bio-SA. Lastly, drying in drum dryer (P-12/DDR-101) was performed to remove any remaining volatile compounds, resulting in bio-SA with 99.27% purity (Law *et al.*, 2019; Li *et al.*, 2010; Thuy *et al.*, 2017).

The bio-SA crystals were then separated into two streams, where one was to be hydrogenated in hydrogenation reactor (P-14/R-102) with Ru-Rutile catalyst to produce BDO with 56% selectivity. The hydrogenation process was carried out at 235.70°C and 60.93 bar (Brzezinska *et al.*, 2020). Lastly, bio-SA crystals and BDO in 1.00:0.74 ratio were esterified in esterification reactor (P-17/R-103) with $Ti(OBu)_4$ catalyst to produce bio-PBS and water with 90% conversion. This esterification process takes place at 170°C and 1.01 bar (Ferreira *et al.*, 2015; Rafiqah *et al.*, 2021).

The annual production of bio-PBS is 40 624.32 tonnes with 99.69% purity. The ratio of OPF to bio-PBS in this study was 1.00:0.27. Low selectivity of bio-SA hydrogenation to BDO led to low yield of bio-PBS from OPF. *Table 1* shows the most common types of catalysts used in SA hydrogenation process. A more in-depth study on the bio-SA hydrogenation can be carried out with the selection of catalysts capable of producing bio-SA with high conversion. According to Luthfi *et al.* (2016), autohydrolysis with sodium hydroxide (NaOH-AH) as pre-treatment prior to enzymatic hydrolysis can yield 33.1 g SA (without formate) and 35.7 g SA (with formate) from 100 g OPF dry biomass. Thus, the yield of bio-PBS production from OPF could be increased by using enzymatic hydrolysis instead of acid hydrolysis.

TABLE 1. CATALYST IN HYDROGENATION OF BIO-SA

Catalyst	Selectivity (%)		
	BDO	GBL	THF
Ruthenium- Rutile (Ru-Rutile)[a]	58.0	40.0	2.0
Ruthenium-P25[a]	5.0	93.0	2.0
Ruthenium-P90[a]	38.0	51.0	11.0
Ruthenium-Anatase-P[a]	29.0	58.0	13.0
Rhenium/Carbon-5%[b]	8.4	41.8	44.5

Source: Brzezinska *et al.*, 2020[a]; Di *et al.*, 2015[b].

Process Simulation on Production of Bio-polybutylene Succinate

Figure 5 illustrates the input and output structure constructed to determine the materials used in the production of bio-PBS from OPF. The mass balance was manually calculated in this study.

According to the input-output mass balance for continuous process in steady state (Turton *et al.*, 2018), the differences between total input and output were 0.17 kg hr^{-1}. The percentage of error for the overall process is 3.35 x 10^{-5} %.

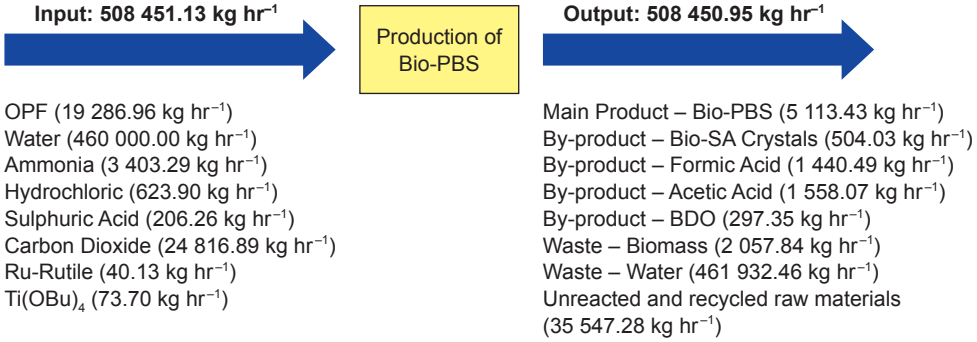


Figure 5. Input and output structure.

Economic Analysis

C_{TCI} was determined by calculating the total cost of equipment (C_{PE}), which is RM189.98 million, as shown in *Table 2*.

The equipment sizing in this study was determined by the SuperPro Designer® software. Thereafter, the direct and indirect costs were calculated, as illustrated in *Table 3*.

The values of C_{FCI} and C_{WC} calculated were RM736.93 million and RM147.39 million, respectively. Using the values obtained, the C_{TCI} value was then calculated to be RM884.32 million. The equation for profit margin calculation is shown in Equation (10), whereby the profit margin obtained was RM1163.51 million (Turton *et al.*, 2018). The value of R in this study was RM2538 million (India Mart, 2021; Molbase, 2021; Tan *et al.*, 2017). COM and COM_d values were calculated to be RM2134.21 million and RM2060.52 million, respectively.

$$\text{Profit Margin} = \sum \text{Revenues} - \sum \text{Cost of Raw Materials} \quad (10)$$

The discounted cash flows for discount rates of 0.00%, 7.00%, 10.00%, 20.00% and 25.00% are shown in *Figure 6*. The IRR value was obtained when NPV equals zero, which was 24.14% in this study. The minimum acceptable rate of return (MARR) is a value that depends on the process and risk level. The MARR in this study was determined to be 16.00% (Tan *et al.*, 2016). This is because integrated process technologies with developed market such as purification, hydrogenation, and esterification were included in this study. Equation (11) was used to determine the reference value of PBP_{ref} at 3.68 years.

$$PBP_{ref} = \frac{0.85}{(MARR + \frac{0.85}{n})} \quad (11)$$

Table 4 summarises the profitability analysis conducted in this study, with DPP value of 6.33 years. To summarise, this study is profitable and worthwhile as the net profit is greater than total capital investment and requires less time to achieve revenue and profits. Manual calculations were compared to the SuperPro simulation considering eight aspects: C_{PE}, equipment installation, C_{TCI}, R, ROI, PBP, NPV at 7% discount rate, and IRR (*Table 5*). Significant differences were observed in C_{PE} and equipment installation since local manufacturing costs are significantly lower than SuperPro software's default settings. The differences also influenced the C_{TCI}, contributing to 53% difference. However, other profitability matrices, such as R, ROI, PBP, NPV and IRR, showed a difference of less than 25%.

Sensitivity Analysis

The sensitivity analysis was conducted with 10% variation in baseline values to identify the parameters (rate of bio-PBS production, price of by-products, bio-PBS, and raw materials, and C_{FCI}) that had the greatest influence on the study's performance. The values and variations of NPV and IRR were analysed in this study as shown in *Figures 7* and *8*.

A positive NPV value indicated that the project is profitable. The value of NPV increased with the increase in bio-PBS production rate, by-product price, and bio-PBS price. In contrast, the value of NPV decreased with the increase in raw material's price and C_{FCI}. Variation in the price of by-products had less impact on NPV due to its lower price, RM22.30 kg^{-1}, compared to RM60.00 kg^{-1} bio-PBS. The minimum value of NPV was obtained with -10% variation in the price of bio-PBS, resulting in RM965.43 million NPV. The +10% variation in the production rate of bio-PBS had greatest impact on the maximum NPV value of RM4266.05 million (*Figure 7*).

High value IRR over MARR, which is 16%, indicated that the project is profitable. According to the findings, the IRR value increased with the increase in the value of bio-PBS production rate, as well as the price of by-products and bio-PBS. The increase in raw material price and C_{FCI}, on the

TABLE 2. TOTAL COST OF EQUIPMENT

Equipment	Capacity	Price at 2021 (RM in million)
Ball mill presser	1 696.84 L hr^{-1}	12.67
Heat sterilisation	5 020.98 L hr^{-1}	0.48
Storage	48 165.43 L	3.64
Acid hydrolysis reactor	36 721.77 L	39.08
Rotary vacuum filtration	76.97 m^2	9.06
Continuous bioreactor	237 156.14 L	18.40
Rotary vacuum filtration	75.30 m^2	11.60
Evaporator	418.23 m^2	4.15
Crystalliser	29 569.04 L	6.00
Rotary vacuum filtration	72.04 m^2	4.80
Drum drying	19.87 m^2	44.09
Hydrogenation reactor	4 350.68 L	2.77
Cooler	10.00 m^2	0.11
Esterification reactor	6 591.36 L	3.04
Cooler	10.00 m^2	0.11
Others	-	30.00

TABLE 3. DIRECT AND INDIRECT COST

Details	% of C_{PE}	% of C_{DPE}
Direct cost (RM)		
Total purchased equipment, C_{PE}	100.00	
Delivered purchased equipment, C_{DPE}	10.00	
Equipment installation	60.00	
Piping system installation	20.00	
Instrumentation and control system		26.00
Electrical system		15.00
Building	50.00	
Yard improvements	10.00	
Land[a]	RM30.00 million (Land Pajam Industrial Land)	
Service facilities (Installed)	55.00	
Indirect cost (RM)		
Design and engineering	20.00	
Contractor' fee	6.00	
Legal expenses	5.00	
Construction expenses	17.00	
Contingencies Allowance	15.00	

Source: [a] - Propertyguru (2021).

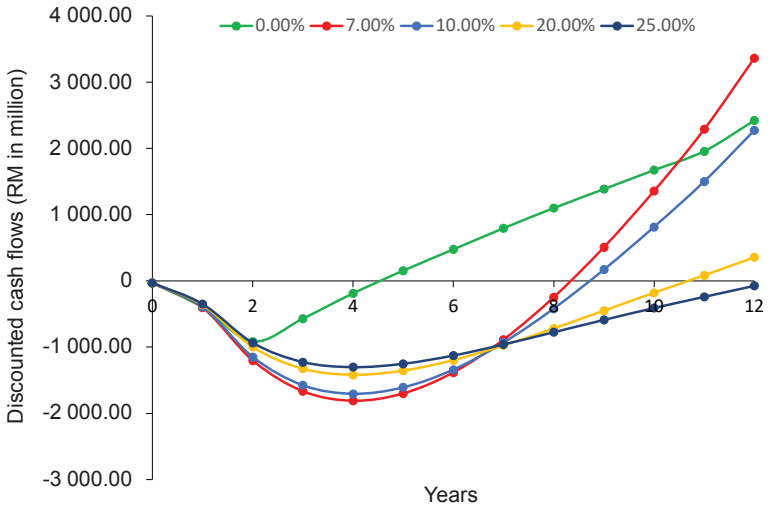


Figure 6. Summary on discounted cash flows.

TABLE 4. SUMMARY ON PROFITABILITY ANALYSIS

In this study		Summary
ROI (32.88%)	MARR (16%)	ROI>MARR
PBP (2.55 yr)	PBP_{ref} (3.68 yr)	PBP<PBP_{ref}
NPV (RM3366.31 million)	Positive value	Positive value
IRR (24.14%)	MARR (16%)	IRR>MARR
R (RM2538.11 million)	Positive value	Positive value

TABLE 5. COMPARISON MANUAL CALCULATION WITH SUPERPRO

Details	Manual	SuperPro Software	Differences (%)
C_{PE} (RM in million)	189.98	288.27	34
Equipment installation (RM in million)	113.99	127.78	10
C_{TCI} (RM in million)	884.32	1 918.10	53
R (RM in million)	2 538.11	2 160.28	17
ROI (%)	32.88	42.59	22
PBP (yr)	2.55	2.35	8
NPV (RM in million) at discounted rate 7%	3 366.31	3 971.96	15
IRR (%)	24.14	32.58	25

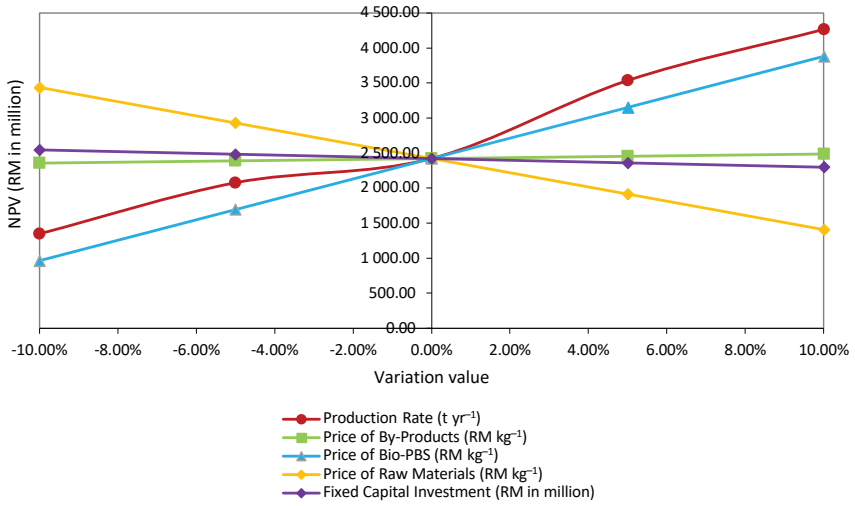


Figure 7. Sensitivity analysis on NPV.

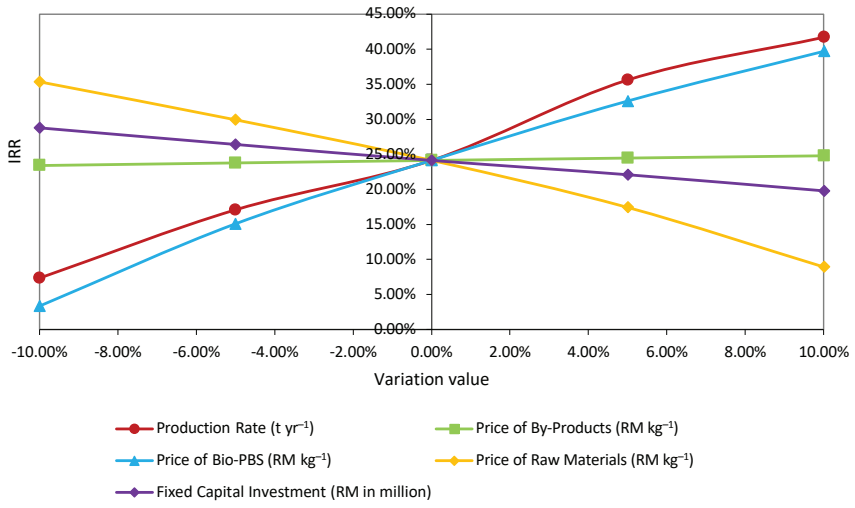


Figure 8. Sensitivity analysis on IRR.

TABLE 6. COMPARISON WITH PREVIOUS STUDIES

Raw materials	Production rate (ktons yr^{-1})	Selling price (RM kg^{-1})	DPP (yr)	References
Glucose	58.63	12.62	7.00	Ioannidou *et al.*, 2022
Corn stover	58.63	13.51	9.00	Ioannidou *et al.*, 2022
Sugar beet pulp	58.63	5.78	6.00	Ioannidou *et al.*, 2022
Sugarcane	24.32	30.12	n.a	Ratshoshi *et al.*, 2021
OPF	40.62	60.00	6.33	This study

other hand, resulted in a decrease in IRR value. These findings are comparable to the sensitivity analysis of NPV. The price parameter of bio-PBS has a minimum IRR of 3.34% with -10% variation. The production rate parameter of bio-PBS, on the other hand, had maximum IRR value of 41.70% with +10% variation (*Figure 8*).

Comparison of economic analysis with previous studies in terms of raw materials, production rate (ktons yr^{-1}), selling price (RM kg^{-1}), and DPP (yr) are shown in *Table 6*. Ioannidou *et al.* (2022) and Ratshoshi *et al.* (2021) produced 58.63 ktons yr^{-1} and 24.32 ktons yr^{-1} of bio-PBS, respectively, while only 40.62 ktons yr^{-1} bio-PBS was produced in this study. The selling price of bio-PBS also showed significant differences, as the value of the selling price is the minimum price from the research conducted by Ioannidou *et al.* (2022) and Ratshoshi *et al.* (2021). This is due to the differences in the process used to produce bio-PBS which led to different effect on the yields of bio-SA and BDO.

According to Ioannidou *et al.* (2022), the fermentation process for producing bio-SA from various raw materials such as glucose, corn stover, and sugar beet pulp involved different process conditions with different succinate-producing microorganism. Purification includes centrifugation adsorption with activated carbon, cation-exchange resin, evaporation, crystallisation and drying to achieve bio-SA with 99.5% purity. Ratshoshi *et al.* (2021), on the other hand, used dilute acid pre-treatment and enzymatic hydrolysis before fermentation of sugarcane to produce bio-SA. The purification of bio-SA, in this case, includes extraction, evaporation, crystallisation and drying to achieve 99.9% purity. Both researchers produced BDO from sugars via fermentation by using an *E. coli* strain. The selling prices of bio-PBS produced from glucose, corn stover, sugar beet pulp and sugarcane were therefore RM12.62 kg^{-1}, RM13.51 kg^{-1}, RM5.78 kg^{-1} and RM30.12 kg^{-1} respectively. This study, on the other hand, focused on hydrogenation process to produce BDO from bio-SA. Low selectivity of BDO (56.00%) resulted in low yield of bio-PBS (Baidya *et al.*, 2019; Brzezinska *et al.*, 2020). Therefore, further study should be conducted on the use of catalysts to achieve high BDO yield.

A similarity between previous reports and this study is that the same catalyst ($Ti(OBu)_4$) was used to produce bio-PBS. Thus, to compensate for the low yield of bio-PBS as a result of low yield from BDO processing, the selling price for bio-PBS should be at least RM60.00 kg^{-1} to generate profit. With bio-PBS as main product in this process, the value of DPP is 6.33 years as OPF as raw material compared to glucose (7 years), corn stover (9 years) and sugar beet pulp (6 years). It can be concluded that this process has reasonable economic feasibility for scaling up by using OPF as raw materials for bio-PBS production.

CONCLUSION

This study provided evidence to the potential of OPF as one of the most promising raw materials in the production of bio-PBS. Based on an extensive literature review, acid hydrolysis of OPF was followed by fermentation with CO_2, ammonia, and *A. succinogenes* 130Z to produce bio-SA, formic acid, acetic acid, biomass, and water. Vacuum filtration, evaporation, crystallisation, and drying were then used to purify the bio-SA to 99.27% purity. Hydrogenation of bio-SA with Ru-Rutile catalyst yielded BDO with 56.00% selectivity. Lastly, bio-SA crystals and BDO are esterified with $Ti(OBu)_4$ catalyst at 1.00:0.74 ratio to yield 90.00% conversion of bio-PBS and water. In terms of profitability, values of ROI and IRR values were higher than MARR (16.00%) while PBP value was lower than the PBP_{ref} (3.68 years) which showed that this project can be profitable in a short period of time. The positive NPV and R values further strengthened the process's economic feasibility, demonstrated that it can be done on a large scale and generating profits in less than 10 years.

ACKNOWLEDGEMENT

The authors acknowledge the profound financial support from the Ministry of Science, Technology and Innovation, Malaysia through Technology Development Fund 1 (TeD 1) (TDF05211384). We also thank the financial assistance from Universiti Kebangsaan Malaysia's Young Lecturers Incentive Grant (GGPM-2021-005).

REFERENCES

Amin, F R; Khalid, H; Zhang, H; Rahman, S; Zhang, R; Liu, G and Chen, C (2017). Pretreatment methods of lignocellulosic biomass for anaerobic digestion. *AMB Express, 7*: 1-12.

Baidya, P K; Sarkar, U; Villa, R and Sadhukhan, S (2019). Liquid-phase hydrogenation of bio-refined succinic acid to 1,4-butanediol using bimetallic catalysts. *BMC Chem. Eng., 1*: 1-12.

Bonem, J M (2018). Chemical projects scale up: How to go from laboratory to commercial. *Project evaluation using CAPEX and OPEX inputs*. Elsevier. p. 107-123.

Brzezinska, M; Niemeier, J; Louven, Y; Keller, N; Palkovits, R and Ruppert, A M (2020). TiO_2 supported Ru catalysts for the hydrogenation of succinic acid: Influence of the support. *Catal. Sci. Technol., 10*: 6860-6869.

Bukhari, N A; Loh, S K; Luthfi, A A I; Abdul, P M; Nasrin, A B; Harun, S and Jahim, J M (2021). Whole slurry saccharification of mild oxalic acid-pretreated oil palm trunk biomass improves succinic acid production. *Ind. Crops Prod., 171*: 113854.

Dai, Z; Guo, F; Zhang, S; Zhang, W; Yang, Q; Dong, W; Jiang, M; Ma, J and Xin, F (2020). Bio-based succinic acid: An overview of strain development, substrate utilization and downstream purification. *Biofuel Bioprod. Biorefin., 14*: 965-985.

Data Bridge Market Research (2020). Global polybutylene succinate (PBS) market – Industry trends and forecast to 2027. https://www.databridgemarketresearch.com/reports/global-polybutylene-succinate-pbs-market, accessed on 13 October 2021.

Di, X; Shao, Z; Li, C; Li, W and Liang, C (2015). Hydrogenation of succinic acid over supported rhenium catalysts prepared by the microwave-assisted thermolytic method. *Catal. Sci. Technol., 5*: 2441-2448.

Ferreira, L P; Moreira, A N; Pinto, J C and de Souza Jr, F G (2015). Synthesis of poly (butylene succinate) using metal catalysts. *Polym. Eng. Sci., 55*: 1889-1896.

Gerassimidou, S; Martin, O V; Chapman, S P; Hahladakis, J N and Iacovidou, E (2021). Development of an integrated sustainability matrix to depict challenges and trade-offs of introducing bio-based plastics in the food packaging value chain. *J. Clean. Prod., 286*: 125378.

India Mart (2021). Price of Formic Acid. https://www.indiamart.com/productdetail/formic-acid, accessed on 21 October 2021.

Investopedia (2021). Modified Accelerated Cost Recovery System (MACRS). https://www.investopedia.com/terms/m/macrs.asp, accessed on 15 October 2021.

Ioannidou, S M; Ladakis, D; Moutousidi, E; Dheskali, E; Kookos, I K; Câmara-Salim, I; Moreira, M T and Koutinas, A (2022). Techno-economic risk assessment, life cycle analysis and life cycle costing for poly(butylene succinate) and poly(lactic acid) production using renewable resources. *Sci. Total Environ., 806*: 1-13.

Law, J Y; Mohammad, A W; Tee, Z K; Zaman, N K; Jahim, J M; Santanaraj, J and Sajab, M S (2019). Recovery of succinic acid from fermentation broth by forward osmosis-assisted crystallization process. *J. Memb. Sci., 583*: 139-151.

Li, Q; Wang, D; Wu, Y; Li, W; Zhang, Y; Xing; J and Su, Z (2010). One step recovery of succinic acid from fermentation broths by crystallization. *Sep. Purif. Technol., 72*: 294-300.

Liang, Y; Tan, Q; Song, Q and Li, J (2021). An analysis of the plastic waste trade and management in Asia. *Waste Manag., 119*: 242-253.

Luthfi, A A I; Md Jahim, J; Harun, S; Tan, J P and Mohammad, A W (2016). Biorefinery approach towards greener succinic acid production from oil palm frond bagasse. *Process Biochem., 51*: 1527-1537.

Luthfi, A A I; Manaf, S F A; Illias, R M; Harun, S; Mohammad, A W and Jahim, J M (2017). Biotechnological route for sustainable succinate production utilizing oil palm frond and kenaf as potential carbon sources. *Appl. Microbiol. Biotechnol., 101*: 3055-3075.

Mabrouki, J; Abbassi, M A; Guedri, K; Omri, A and Jeguirim, M (2015). Simulation of biofuel production via fast pyrolysis of palm oil residues. *Fuel, 159*: 819-827.

Mahmod, S S; Jahim, J M; Abdul, P M; Luthfi, A A I and Takriff, M S (2021). Techno-economic analysis of two-stage anaerobic system for biohydrogen and biomethane production from palm oil mill effluent. *J. Environ. Chem. Eng., 9*: 105679.

Mohamad, N; Abd-Talib, N and Kelly Yong, T L (2020). Furfural production from oil palm frond (OPF) under subcritical ethanol conditions. *Mater. Today Proc., 31*: 116-121.

Molbase (2021). Price of acetic acid. https://www.molbase.com/cas/search?search_type=text&keyword=acetic+acid, accessed on 16 October 2021.

Ncube, L K; Ude, A U; Ogunmuyiwa, E N; Zulkifli, R and Beas, I N (2021). An overview of plasticwaste generation and management in food packaging industries. *Recycling, 6*: 12.

Omwene, P I; Sarihan, Z B O; Karagunduz, A and Keskinler, B (2021). Bio-based succinic acid recovery by ion exchange resins integrated with nanofiltration/reverse osmosis preceded crystallization. *Food Bioprod. Process., 129*: 1-9.

Onoja, E; Chandren, S; Abdul Razak, F I; Mahat, N A and Wahab, R A (2019). Oil palm (*Elaeis guineensis*) biomass in Malaysia: The present and future prospects. *Waste Biomass Valori., 10*: 2099-2117.

Propertyguru (2021). Price of Land Pajam Industrial Land, Negeri Sembilan. https://www.propertyguru.com.my/bm/hartanah-komersial/nilai-pajam-mantin-industrial-land-1-acres-rm100-psf-dijual-oleh-gary-khoo-29587458, accessed on 15 November 2021.

Rafiqah, S A; Khalina, A; Harmaen, A S; Zaman, K; Isma, T; Liu, Q; Ilyas, R A and Hao Lee, C (2020). Characterization study of empty fruit bunch (EFB) fibres reinforcement in poly(butylene) succinate (PBS)/starch/glycerol composite sheet. *Polymers, 12*: 1571.

Rafiqah, S A; Khalina, A; Harmaen, A S; Tawakkal, I A; Zaman, K; Asim, M; Nurrazi, M N and Lee, C H (2021). A review on properties and application of bio-based poly(butylene succinate). *Polymers, 13*: 1436.

Ratshoshi, B K; Farzad, S and Görgens, J F (2021). Techno-economic assessment of polylactic acid and polybutylene succinate production in an integrated sugarcane biorefinery. *Biofuel Bioprod. Biorefin., 15*: 1871-1887.

SimulateLive.com (2017). Complete List of Process Simulators (Part 1/2). http://www.simulatelive.com/product-reviews/simulation/complete-list-of-process-simulators-part-1-2, accessed on 16 October 2021.

Siracusa, V and Blanco, I (2020). Bio-polyethylene (Bio-PE), Bio-polypropylene (Bio-PP) and Bio-poly(ethylene terephthalate) (Bio-PET): Recent developments in bio-based polymers analogous to petroleum-derived ones for packaging and engineering applications. *Polymers, 12*: 1641.

Tan, J P; Jahim, J M; Harun, S; Wu, T Y and Mumtaz, T (2016). Utilization of oil palm fronds as a sustainable carbon source in biorefineries. *Int. J. Hydrog. Energy, 41*: 4896-4906.

Tan, J P; Jahim, J M; Harun, S and Wu, T Y (2017). Overview of the potential of bio-succinic acid production from oil palm fronds. *J. Phys. Sci., 28*: 53-72.

Thurber, H and Curtzwiler, G W (2020). Suitability of poly(butylene succinate) as a coating for paperboard convenience food packaging. *Int. J. Biobased Plast., 2*: 1-12.

Thuy, N T H and Boontawan, A (2017). Production of very-high purity succinic acid from fermentation broth using microfiltration and nanofiltration-assisted crystallization. *J. Memb. Sci., 524*: 470-481.

Tu, W C and Hallett, J P (2019). Recent advances in the pretreatment of lignocellulosic biomass. *Curr. Opin. Green Sustain. Chem., 20*: 11-17.

Turton, R; Shaeiwitz, J A; Bhattacharyya, D and Whiting, W B (2018). Analysis, synthesis and design of chemical processes. Pearson Education. 5th edition. p. 204-717.

Journal of Oil Palm Research Vol. 35 (4) December 2023 p. 694-712
DOI: https://doi.org/10.21894/jopr.2022.0055

CHARACTERISTICS OF SUNFLOWER WAX, CARNAUBA WAX AND BEESWAX IN PALM SUPEROLEIN BLENDED OIL

NORAZURA AILA MOHD HASSIM[1]*; SIVARUBY KANAGARATNAM[1]; SAW MEI HUEY[1]; NUR HAQIM ISMAIL[1]; RAFIDAH ABD. HAMID[1]; MUHAMMAD HANIF MISKANDAR[1] and NOOR-SOFFALINA SOFIAN-SENG[2]

ABSTRACT

The aim of the study was to analyse the effect of different percentages (0.0%-3.5%) of sunflower wax (SFW), carnauba wax (CW) and beeswax (BW) in 1:1 (v:v) palm superolein (POOo) and sunflower oil blend (SFO). Selected physicochemical analyses, namely fatty acid composition, crystal structure and shear viscosity were conducted for oleogel or oil system with wax (OSW) selection to be used in a product that is spreadable at low temperature (5°C-10°C) and phase separation does not occur at high temperature (40°C-45°C). Mono-unsaturated and poly-unsaturated as well as saturated fatty acids of all OSW were significantly different (p<0.05). Crystals in OSW with SFW showed needle-like structure and fibrous, while OSW with CW was observed to be spherulitic and OSW with BW was needle-like in shape at 10°C, 25°C, 40°C and 45°C. OSW with 3.5% SFW and 3.5% CW showed dense packing at 45°C; hence, it had the potential to prevent phase separation in the end product at high temperatures. The shear viscosity of all OSW at all temperatures was below 2.0 Pa.s, in which SFW showed the highest value at 5°C, although the value was low. Therefore, based on the experimental parameters, 3.5% CW can be implied as the best structuring agent, followed by 3.5% SFW.

Keywords: crystal structure, fatty acid composition, high and low temperature, shear viscosity.

Received: 28 April 2022; **Accepted:** 3 August 2022; **Published online:** 6 September 2022.

INTRODUCTION

Lipid is the main ingredient used in various types of food products. It imparts texture, aroma, taste and makes food more appealing (Pehlivanoğlu *et al.*, 2018). Most food products that have high lipid content also contain solid fats. These solid fats consist of *trans* fatty acids and/or saturated fatty acids that might have a negative impact on health (de Souza *et al*., 2015; Wassell *et al*., 2010). Therefore, one of the reasons for the utilisation of oleogelation (a gelling agent that traps liquid vegetable oils to form three-dimensional (3D) network system) is due to scientific evidence, which showed that *trans* fatty acids produced from partial hydrogenation are detrimental to health. The partial hydrogenation method uses liquid vegetable oil by converting liquid oil into a solid form with the desired hardness. As *trans* fatty acids are harmful to health, the GRAS status (generally recognised as safe) for *trans* fatty acids was revoked by the Food and Drug Administration (FDA), the United States on 16 June 2015. The use of *trans* fatty acids in food products was fully banned in the United States starting June 2018 (FDA, 2018).

Oleogelation is also proposed to replace the use of saturated fatty acids to improve the nutritional properties of food products as it only utilises unsaturated fatty acids and gels. This oleogelation

[1] Malaysian Palm Oil Board,
6 Persiaran Institusi, Bandar Baru Bangi,
43000 Kajang, Selangor, Malaysia.

[2] Department of Food Sciences,
Faculty of Science and Technology,
Universiti Kebangsaan Malaysia,
43600 UKM, Bangi, Selangor, Malaysia.

* *Corresponding author e-mail: azuraaila@mpob.gov.my*

method does not change the saturation level of fatty acids found in food products (Öğütcü and Yilmaz, 2014). The use of unsaturated fatty acids without gel is technically challenging, especially in the structuring of food products. For example, liquid vegetable oils that contain many unsaturated fatty acids give unsatisfactory performance when used for cake-making and related purposes due to their low viscosity (Kim *et al.*, 2017).

To replace these *trans* and saturated fatty acids, the oleogelation method that uses gels to produce oleogel was reported to physically replace the function and texture of solid fats by trapping liquid vegetable oils in their network structure (Daniel and Rajasekharan, 2003; Hwang *et al.,* 2012; Singh *et al.,* 2017). The oleogel produced has solid/gel-like properties (Co and Marangoni, 2012). Nevertheless, this type of oleogel will still have a high content of unsaturated fatty acids and low saturated fatty acids. Furthermore, the oleogel does not contain water, possesses viscoelasticity and can undergo a process of thermal reversal (Gallego *et al.,* 2013; Hughes *et al.,* 2009).

The incorporation of oleogel into various products has made oleogelation an important structuring method that was widely researched and applied over the past two decades (Co and Marangoni, 2012; Zetzl and Marangoni, 2014). For example, the cosmetics and pharmaceutical industries have used this oleogelation method for a long time to produce a desirable stable product by using liquid organic solvents such as benzene and hexane (Balasubramaniam *et al.*, 2014; Kumar and Katare, 2005; Vintiloiu and Lerouex, 2008). The term organogelation is usually used for organic solvents, while the term oleogelation is used when this organic solvent is replaced with liquid vegetable oil. The mechanism of oleogelation depends on various factors, amongst which are the composition of a gel material and its interaction with the lipid phase. The most commonly used method for liquid vegetable oil structuring is the addition of a gel material (one or more ingredients) directly into the liquid vegetable oil. One of the gel ingredients is food-grade wax. Wax is commonly used in small quantities to produce oleogel (Doan *et al.,* 2018; Hughes *et al.,* 2009; Patel *et al.*, 2013; Sánchez *et al.,* 2011; Stortz *et al.,* 2012). Waxes are categorised as non-lipid monomeric liners. In addition to waxes, other gel materials that can be used are polymeric coatings (ethyl cellulose), and lipid monomeric coatings (fatty acids, phospholipids, monoglycerides and ceramides) and non-lipid monomeric coatings (sorbitol and γ-oryzanol phytosterols other than wax) (Rogers *et al.*, 2014).

This article will discuss the fatty acid composition (FAC), crystal structure and shear viscosity of blended oleogel or oil system with wax (OSW), containing 50% of palm superolein (POOo) and 50% of sunflower oil (SFO) with various percentages of sunflower wax (SFW), carnauba wax (CW) and beeswax (BW) to obtain OSW that can be spreadable at low temperature (5°C-10°C), but the oleogel will not experience phase separation at high temperature (40°C-45°C). This characteristic has not yet been researched or published. The rationale for the selection of 50% of POOo and 50% of SFO base oil was discussed in the paper by Norazura *et al*. (2021). In this article, the term OSW will be used to replace oleogel.

MATERIALS AND METHODS

Material

POOo (IV 62) was bought from Mewah Oils Sdn. Bhd., while sunflower oil (SFO) (Naturel brand) was from a local supermarket in Selangor. SFW was bought from Hufaqa Sepakat Enterprise, Selangor, Malaysia. Meanwhile CW and BW were from Anizz Legacy Resources, Selangor, Malaysia.

Method

Preparation of OSW. As shown in *Table 1*, three types of waxes, namely SFW, CW and BW at different percentages (0.0%-3.5%) were blended with 1:1 (v:v) palm superolein and sunflower oil. Then, OSW was heated to 90°C and stirred to dilute the waxes.

TABLE 1. EXPERIMENTAL DESIGN OF OIL SYSTEM WITH SUNFLOWER WAX, CARNAUBA WAX AND BEESWAX

Oil	Type of wax	Percentage of wax
Superolein and sunflower wax (1:1)	Sunflower wax (SFW)	0.0%
		0.5%
		1.0%
		1.5%
		2.0%
		2.5%
		3.0%
		3.5%
	Carnauba wax (CB)	0.0%
		0.5%
		1.0%
		1.5%
		2.0%
		2.5%
		3.0%
		3.5%
	Beeswax (BW)	0.0%
		0.5%
		1.0%
		1.5%
		2.0%
		2.5%
		3.0%
		3.5%

***Fatty acid composition* (FAC)**. FAC of oil system with wax was analysed according to MPOB Test Method (MPOB, 2005) based on fatty acid methyl esters (FAME) by using gas chromatography. Then, samples of 0.1 g were weighed and dissolved in hexane (1.8 mL). The solution of sample was mixed by using a vortex mixer. Sodium methoxide solution (100 µL) was added to the samples, followed by water. Mixing was performed in between each process. The sample solution was left for 1 hr to separate. The clear supernatant was transferred into another vial with added sodium sulphate anhydrous. It was kept for 15 min before a complete clear supernatant of 1.5 mL was injected into GC (Agilent Technologies, Model 7890B) that has a flame ionisation detector (FID). The column was set at 185°C while the injector and detector temperatures were set at 230°C. Helium gas (carrier) with a flow rate of 1 mL/min was used. Identification of peaks was done by comparing retention times with FAME standards and quantified by using the peak area normalisation method.

Crystal structure. The crystal microstructure of OSW was determined by using a polarised light microscope (PLM) as described by Chai *et al.* (2018) with slight modification. A Leica DMLP polarised light microscope (Wetzlar, Germany) equipped with a Linkam THMS 600 temperature controller stage and a JVC 3-CCD colour video camera was used. The sample was first heated to 90°C for at least 60 min to erase crystal memory. A small droplet (about 15 µL) of the melted sample was placed on a glass slide and covered with a glass slip. The sample was measured at 10°C, 25°C, 40°C and 45°C. The temperature was thermostatically controlled by a Linkam TP 94 multiramp temperature programmer and LNP automatic cooling system (Linkam, Tadworth, Surrey, United Kingdom). Liquid nitrogen was used as the coolant. The Photomicrograph of the crystal was taken at 10× magnification.

Rheology (shear viscosity). Shear viscosity of OSW was measured by using modular advanced rheometer (Haake, Mars). OSW (17 g) were placed in a cylindrical cup (diameter of 27.206 mm) with rotor (diameter of 25.082 mm). Sample was tested at temperature of 5°C, 10°C, 25°C, 40°C and 45°C. Prior to this, the OSW was stored at 5°C, 10°C, 25°C, 40°C and 45°C for 24 hr. The shear viscosity was measured at 100, 200, 300, 400 and 500/s.

Statistical analysis. Results were analysed with Minitab Version 16.0 (Pennsylvania, United States) by using one-way ANOVA. Significance differences ($p \leq 0.05$) amongst the samples were analysed by using Tukey's post-hoc test. All tests were carried out in triplicate.

RESULTS AND DISCUSSION

The Effect of Waxes on FAC of OSW

FAC of POOo and SFO as well as oil system containing 50.00% POOo and 50.00% SFO with 0.00%-3.50% SFW, CW and BW, were shown in *Table 2*. POOo contained 58.46% unsaturated fatty acids (USAFA, combination of monounsaturated and polyunsaturated fatty acids) and 41.54% of saturated fatty acids (SAFA). Meanwhile SFO had 91.24% of USAFA and 8.76% of SAFA. POOo was high in oleic acid (45.09%) and palmitic acid (36.01%), while SFO was high in linoleic acid (55.96%) and oleic acid (34.68%). FAC of POOo at the range of 45.26%-46.26% of oleic acid and 34.9%-36.13% of palmitic acid were reported by Abdel-Razek *et al.* (2017), Ng *et al.* (2014) and Romano *et al.* (2012).

An oil system containing 50.00% POOo and 50.00% SFO without wax had 73.75% of USAFA and 26.25% of SAFA. The oil system without wax was also high in oleic, linoleic and palmitic acids. The oil demonstrated increment in USAFA and decrement in SAFA as compared to 100% POOo. The OSW with SFW, CW and BW at all percentages had a similar FAC trend, in which they were high in oleic, linoleic and palmitic acids. Within OSW with SFW, oleic acid of 2.50% SFW and 3.50% SFW were significantly different ($p<0.05$) from other experimental percentages (0.50%, 1.00%, 1.50%, 2.00% and 3.00%) while for OSW with CW and BW, 3.50% of wax was significantly different ($p<0.05$) from other experimental percentages (0.50%, 1.00%, 1.50%, 2.00%, 2.50% and 3.00%) within their own system. For linoleic acid, OSW with 3.00% SFW had significantly different values ($p<0.05$) as compared to other experimental percentages (0.50%, 1.00%, 1.50%, 2.00%, 2.50% and 3.50%) while for OSW with CW and BW, 3.50% of wax was significantly different ($p<0.05$) from other experimental percentages (0.50%, 1.00%, 1.50%, 2.00%, 2.50% and 3.00%) within their own system. For palmitic acid, OSW with 2.00% and 3.00% SFW, OSW with 3.00% and 3.50% CW and OSW with 3.50% BW had significantly different values ($p<0.05$) within their own systems. Although FAC values of the waxes were significantly different ($p<0.05$), their range was small, and thus, their saturation level was comparable due to not much difference observed for the overall composition range of their respective FAC. OSW with SFW at all percentage levels had oleic acid in the range of 37.44%-41.51%, CW in the range of 35.53%-37.28% and BW in the range of 36.46%-39.65%. Linoleic acid of OSW with SFW, CW and BW of all experimental percentages (0.50%-3.50%) was in the range of 32.84%-36.30%, 35.00%-39.91% and 34.69%-36.79%, respectively. This was in line with the findings

by Jang *et al*. (2015) which showed quite a similar FAC value for all fatty acids when 3.00% and 6.00% of candelilla wax were added to canola oil as compared to the FAC value of 100.00% canola oil. Notwithstanding this, the fatty acid values of OSW were quite close to the value of the oil system without wax.

USAFA of OSW ranged from 74.88%-76.02% for SFW, 74.75%-75.94% for CW and 75.39%-76.10% for BW. SAFA of OSW with SFW, CW and BW were in the range of 23.93%-26.33%, 24.02%-26.39% and 23.41%-27.41%, respectively. OSW of all waxes was statistically significant in terms of MONO, POLY and SAFA. However, no trend was observed with different percentages of wax as the values of USAFA and SAFA did not vary much, and thus, would not affect the saturation level.

The Effect of Waxes on Crystal Structure of OSW

Crystal structure of OSW with SFW, CW and BW at 0.5%-3.5% for 10°C, 25°C, 40°C and 45°C are shown in *Figures 1, 2* and *3*. Crystal structure at 5°C could not be determined in the reaction of OSW with SFW, CW and BW for 0.5%-3.5% due to water condensation. Theoretically, there will be no crystal for the oil system without wax at 10°C and above as both of the oil used were liquid oil. Moreover, more than 70.0% of their FAC was USAFA. Crystal in OSW with SFW showed needle-like structure and fibrous similar to the findings by Patel *et al.* (2014). The fibrous morphology of the system reflected the high content of wax esters in SFW, which was a major component that contributed to the good gelation (Blake *et al*., 2014). The network of SFW crystals experienced significant changes when the percentage of SFW was increased from 0.5% to 3.5% for all experimental temperatures. At 10°C, OSW with SFW showed a denser structure when the wax percentage was increased from 0.5% to 3.5%, and this could affect the end product which required good spreadability at that temperature. At 25°C, a similar result as at 10°C was observed when the wax percentage increased. However, the packing was less dense than at 10°C. This trend was similar to the results by Sandoval *et al.* (2020), which had 2.0%, 3.5% and 5.0% of SFW at room temperature. At 40°C and 45°C, crystals in the OSW with SFW were still dense except for 0.5% and 1.0% SFW as well as 0.5%, 1.0% and 1.5% SFW, respectively. There was an increase in birefringence at a high concentration of SFW and crystals were observed to be aggregated. The high percentage of SFW in the emulsion may produce nucleation of crystal and domination of crystal growth, which resulted in finer crystals (Sandoval *et al*., 2020). Due to the morphology and arrangement of the SFW network, an increase in hardness might be found in OSW which had a higher percentage of SFW, especially at 10°C. In addition, 3.5% SFW showed dense packing. It was interesting to observe that 2.5%, 3.0% and 3.5% SFW were still in dense packing at 45°C; hence, could better retain the base oil from oiling out. Notwithstanding this, OSW with 2.0%-3.5% SFW was observed to be dense in packing and could affect the end product which required good spreadability at that temperature.

The crystal structure of OSW with CW was observed to be spherulitic. A similar finding was reported by Öğütcü and Yılmaz (2015) with 7.0% and 10.0% addition of CW to hazelnut oil. This was also supported by Dassanayake *et al.* (2009) for CW in olive oil. The crystal structure of OSW with CW at 10°C was almost evenly spread for all wax percentages. Finer crystals were observed at a low percentage of CW. At 3.5% CW, agglomeration of crystals was observed. At 25°C, OSW with 3.5% CW was observed to have denser packing compared to other wax percentages. At 3.0% CW, the crystal structures were coarse. OSW with 0.5% and 1.0% CW was liquefied with very minor crystals present at 25°C. At 40°C and 45°C, the crystal structure became denser when it reached 3.0% CW, which was similar to the trend of OSW with CW at 25°C. However, the crystals became coarser and lumpy at 3.5% CW at 40°C and 45°C. Crystal in OSW of 2.5% CW at 45°C was more homogenised than 3.0% CW at similar temperatures. OSW with 3.0% and 3.5% CW were observed to be less dense as compared to SFW at similar percentages at 45°C, and thus, oiling out might occur more (in volume) compared to 3.5% SFW. However, wax structure, especially for OSW with 3.5% CW, was observed to trap base oil, and thus, might hinder the base oil from excessive oiling out. OSW with 3.5% CW also showed dense packing but lesser than OSW with 3.5% SFW at 10°C; hence, it was anticipated to be more spreadable as compared to OSW with 3.5% SFW but with a coarser texture.

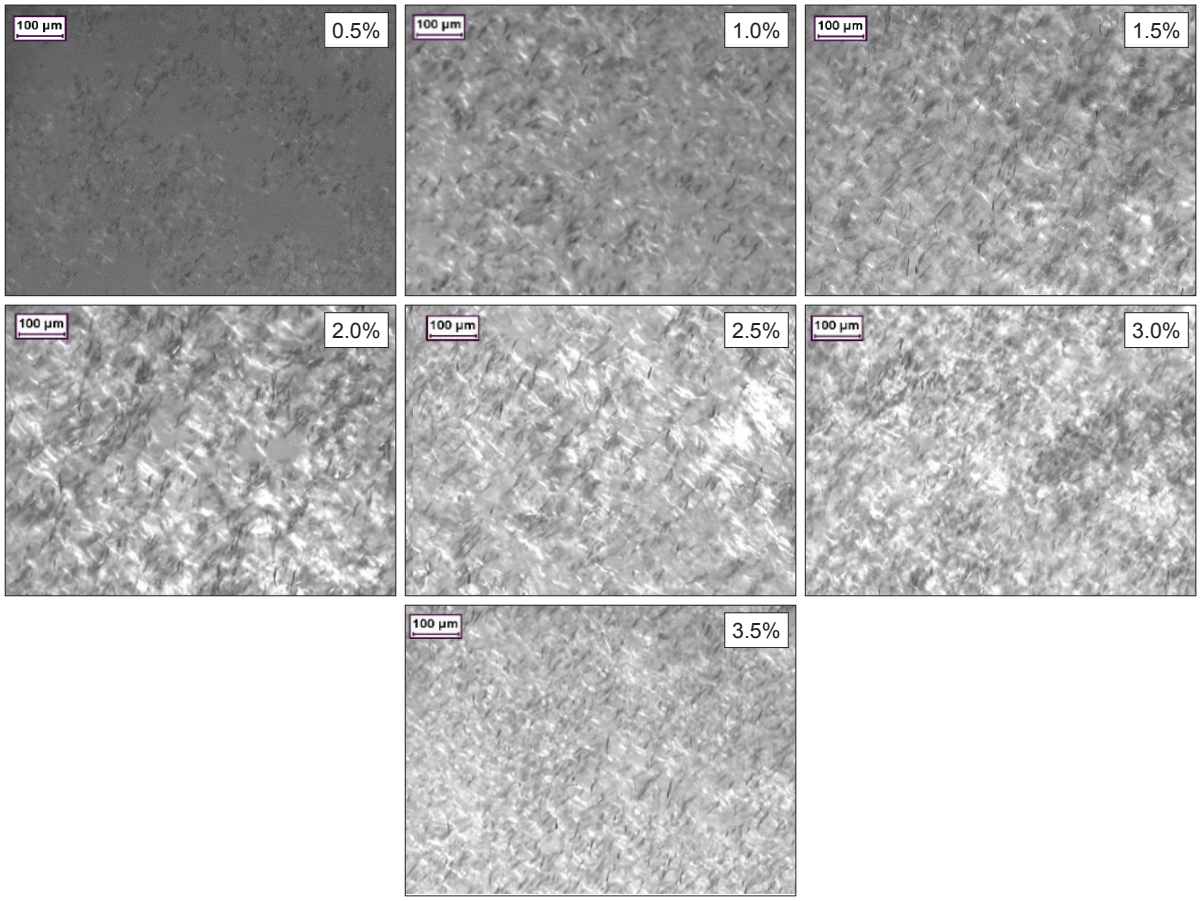
The crystal structure of OSW with BW at all percentages and experimental temperatures was needle-like in shape, which was similarly reported by Moghtadaei *et al.* (2018) and Martin *et al.* (2016). At 10°C, 25°C, 40°C and 45°C, less crystal was observed for OSW at 0.5%-1.5%. OSW with a higher percentage of wax yielded a denser system but was influenced by temperature. However, for 3.5% BW at 40°C, the crystal became clumpy. Notwithstanding this, this denser crystal system was similar to the finding by Martin *et al.* (2017) who observed a denser packing for 2.0%-8.0% BW in high oleic sunflower oil. The densest crystal was observed at 3.5% BW at 10°C. In view that the crystal structure of OSW with 3.5% BW was very loose in packing at 45°C, the OSW might oil out more and faster than 3.5% SFW and 3.5% CW.

TABLE 2. FATTY ACID COMPOSITION OF OIL SYSTEM (50% PALM SUPEROLEIN & 50% SUNFLOWER OIL) WITHOUT AND WITH SUNFLOWER WAX, CARNUBA WAX AND BEESWAX AT VARIOUS PERCENTAGE

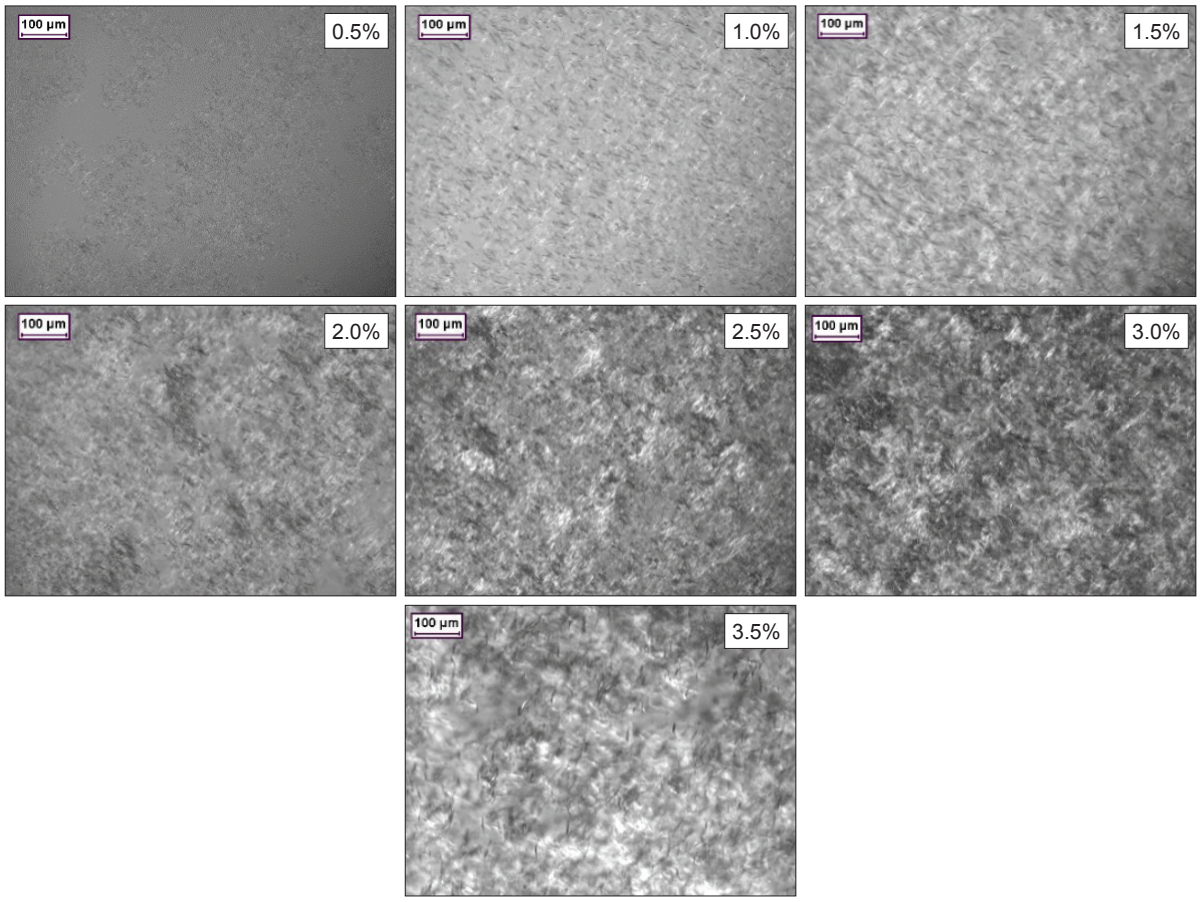
Sample	12:0	14:0	16:0	16:1	18:0	18:1	18:2	18:3	20:0	20:1	OTHERS	MONO	POLY	SAT.
POOo 100%	0.44±0.02^{a}	1.08±0.00^{a}	36.01±0.21^{a}	0.32±0.05^{a}	3.76±0.06^{d}	45.09±0.31^{a}	12.69±0.30^{m}	0.36±0.12^{efg}	0.24±0.07^{efg}	N/D	0.24±0.00^{a}	45.41±0.28^{a}	13.05±0.38^{h}	41.54±0.10^{a}
SFO 100%	N/D	0.07±0.01^{e}	5.55±0.20^{i}	N/D	3.06±0.04^{f}	34.68±0.33^{m}	55.96±0.10^{a}	0.60±0.01^{cdefg}	0.10±0.00^{cdefg}	N/D	0.00±0.00^{a}	34.68±0.04^{l}	56.56±0.26^{a}	8.76±0.22^{l}
SFW 0.0%	0.17±0.01^{bcd}	0.59±0.02^{b}	21.45±0.08^{bc}	0.22±0.02^{b}	3.83±0.07^{cd}	39.88±0.11^{ef}	33.40±0.05^{kl}	0.26±0.08^{efg}	0.22±0.08^{efg}	N/D	0.00±0.00^{a}	40.10±0.13^{cde}	33.65±0.06^{g}	26.25±0.12^{c}
SFW 0.5%	0.17±0.03^{bcd}	0.54±0.02^{bcd}	21.39±0.05^{bcd}	N/D	2.00±0.01^{h}	41.48±0.19^{c}	33.42±0.08^{kl}	0.88±0.15^{bcd}	0.12±0.11^{bcd}	N/D	0.00±0.01^{a}	41.48±0.19^{b}	34.30±0.21^{g}	24.22±0.09^{ghij}
SFW 1.0%	0.16±0.01^{bcd}	0.53±0.20^{cd}	21.12±0.07^{cd}	N/D	2.90±0.07^{fg}	40.63±0.00^{c}	34.38±0.05^{jl}	0.14±0.01^{fg}	0.11±0.01^{fg}	N/D	0.04±0.03^{a}	40.63±0.00^{c}	34.52±0.04^{g}	24.81±0.07^{def}
SFW 1.5%	0.19±0.00^{bcd}	0.55±0.01^{bcd}	21.25±0.02^{bcd}	N/D	2.99±0.02^{fg}	40.52±0.04^{cd}	34.25±0.06^{jk}	0.11±0.01^{g}	0.14±0.04^{g}	N/D	0.00±0.00^{a}	40.52±0.04^{cd}	34.36±0.07^{g}	25.12±0.04^{de}
SFW 2.0%	0.22±0.02^{bcd}	0.57±0.03^{bc}	20.35±0.10^{efg}	N/D	2.94±0.03^{fg}	39.95±0.20^{de}	35.49±0.43^{efgh}	0.36±0.10^{efg}	0.10±0.06^{efg}	N/D	0.01±0.02^{a}	39.95±0.20^{de}	35.86±0.32^{f}	24.19±0.12^{ghij}
SFW 2.5%	0.23±0.01^{bcd}	0.55±0.00^{bcd}	21.56±0.06^{b}	N/D	2.05±0.00^{h}	41.51±0.01^{b}	32.84±0.00^{l}	0.96±0.01^{abc}	0.26±0.01^{abc}	N/D	0.04±0.05^{a}	41.51±0.01^{b}	33.80±0.01^{g}	24.65±0.05^{efg}
SFW 3.0%	0.25±0.08^{bc}	0.53±0.02^{cd}	20.15±0.13^{efg}	N/D	2.90±0.03^{fg}	39.27±0.12^{fgh}	36.30±0.13^{de}	0.45±0.05^{defg}	0.10±0.02^{defg}	N/D	0.05±0.08^{a}	39.27±0.12^{fg}	36.75±0.18^{def}	23.93±0.02^{jk}
SFW 3.5%	0.13±0.00^{d}	0.54±0.01^{bcd}	21.30±0.07^{bcd}	N/D	4.09±0.01^{b}	37.44±0.05^{i}	35.04±0.10^{ghij}	1.19±0.19^{ab}	0.27±0.01^{ab}	N/D	0.00±0.00^{a}	37.44±0.05^{h}	36.23±0.11^{ef}	26.33±0.06^{c}
CW 0.0%	0.17±0.01^{bcd}	0.59±0.02^{b}	21.45±0.08^{bc}	0.22±0.02^{b}	3.83±0.07^{cd}	39.88±0.11^{ef}	33.40±0.05^{kl}	0.26±0.08^{efg}	0.22±0.08^{efg}	N/D	0.00±0.00^{a}	40.10±0.13^{cde}	33.65±0.06^{g}	26.25±0.12^{c}
CW 0.5%	0.14±0.01^{cd}	0.53±0.01^{bcd}	20.37±0.02^{efg}	N/D	2.80±0.19^{g}	35.98±0.1^{jkl}	39.66±0.30^{b}	0.30±0.17^{efg}	0.17±0.03^{efg}	N/D	0.04±0.07^{a}	35.98±0.09^{ijk}	39.96±0.13^{b}	24.02±0.10^{ij}
CW 1.0%	0.16±0.02^{bcd}	0.53±0.01^{cd}	20.39±0.07^{ef}	N/D	2.92±0.06^{fg}	35.58±0.33^{l}	39.39±0.31^{b}	0.62±0.13^{cdef}	0.33±0.05^{cdef}	N/D	0.09±0.08^{a}	35.58±0.33^{k}	40.01±0.41^{b}	24.33±0.19^{fghij}
CW 1.5%	0.18±0.01^{bcd}	0.53±0.02^{cd}	20.39±0.17^{ef}	N/D	2.89±0.03^{fg}	35.76±0.20^{l}	39.77±0.55^{b}	0.37±0.17^{efg}	0.11±0.04^{efg}	N/D	0.00±0.00^{a}	35.76±0.17^{k}	40.14±0.39^{b}	24.10±0.23^{hij}
CW 2.0%	0.18±0.01^{bcd}	0.53±0.02^{bcd}	20.38±0.11^{efg}	N/D	2.89±0.02^{fg}	35.53±0.20^{l}	39.91±0.08^{b}	0.50±0.20^{cdefg}	0.06±0.01^{cdefg}	N/D	0.02±0.03^{a}	35.53±0.16^{k}	40.41±0.28^{b}	24.05±0.10^{ij}
CW 2.5%	0.18±0.06^{bcd}	0.53±0.00^{cd}	20.45±0.06^{e}	N/D	2.95±0.02^{fg}	35.83±0.00^{kl}	39.35±0.01^{b}	0.51±0.16^{cdefg}	0.20±0.12^{cdefg}	N/D	0.00±0.01^{a}	35.83±0.03^{jk}	39.86±0.18^{b}	24.30±0.15^{fghij}
CW 3.0%	0.26±0.13^{b}	0.54±0.03^{bcd}	21.37±0.12^{bcd}	N/D	2.95±0.00^{fg}	36.60±0.10^{j}	38.02±0.53^{c}	0.12±0.01^{g}	0.08±0.02^{g}	N/D	0.05±0.09^{a}	36.60±0.15^{i}	38.14±0.53^{c}	25.20±0.31^{d}
CW 3.5%	0.13±0.00^{d}	0.57±0.00^{bc}	21.32±0.03^{bcd}	N/D	4.08±0.06^{bc}	37.28±0.13^{i}	35.00±0.32^{ghij}	1.18±0.07^{ab}	0.28±0.05^{ab}	0.12±0.02^{a}	0.02±0.04^{a}	37.41±0.11^{h}	36.18±0.24^{ef}	26.39±0.12^{c}
BW 0.0%	0.17±0.01^{bcd}	0.59±0.02^{b}	21.45±0.08^{bc}	0.22±0.02^{b}	3.83±0.07^{cd}	39.88±0.11^{ef}	33.40±0.05^{kl}	0.26±0.08^{efg}	0.22±0.08^{efg}	N/D	0.00±0.00^{a}	40.10±0.13^{cde}	33.65±0.06^{g}	26.25±0.12^{c}
BW 0.5%	0.15±0.01^{bcd}	0.51±0.01^{d}	19.63±0.13^{h}	N/D	2.98±0.10^{fg}	39.10±0.16^{gh}	36.73±0.20^{d}	0.65±0.06^{cde}	0.13±0.05^{cde}	N/D	0.11±0.10^{a}	39.10±0.16^{fg}	37.36±0.25^{cd}	23.41±0.04^{k}
BW 1.0%	0.15±0.01^{cd}	0.52±0.01^{cd}	20.01±0.04^{fgh}	N/D	3.08±0.10^{f}	39.07±0.30^{gh}	36.79±0.10^{d}	0.25±0.14^{efg}	0.06±0.02^{efg}	N/D	0.08±0.10^{a}	39.07±0.27^{fg}	37.04±0.21^{de}	23.82±0.05^{jk}
BW 1.5%	0.15±0.02^{bcd}	0.52±0.01^{cd}	19.97±0.35^{gh}	N/D	3.35±0.06^{e}	39.65±0.49^{efg}	35.76±0.50^{efg}	0.48±0.32^{cdefg}	0.12±0.02^{cdefg}	N/D	0.01±0.01^{a}	39.65±0.49^{ef}	36.24±0.82^{ef}	24.11±0.34^{hij}
BW 2.0%	0.16±0.00^{bcd}	0.53±0.01^{bcd}	20.27±0.00^{efg}	N/D	3.59±0.09^{de}	39.60±0.18^{efg}	35.23±0.10^{fghi}	0.54±0.10^{cdefg}	0.08±0.02^{cdefg}	N/D	0.00±0.00^{a}	36.60±0.18^{ef}	35.77±0.25^{f}	24.63±0.06^{efgh}
BW 2.5%	0.16±0.01^{bcd}	0.52±0.01^{cd}	20.18±0.15^{efg}	N/D	3.61±0.12^{de}	39.08±0.19^{gh}	36.15±0.50^{def}	0.23±0.05^{efg}	0.08±0.02^{efg}	N/D	0.00±0.00^{a}	39.08±0.19^{fg}	36.38±0.42^{def}	24.54±0.24^{fghi}
BW 3.0%	0.15±0.01^{bcd}	0.52±0.00^{cd}	19.98±0.15^{fgh}	N/D	3.73±0.07^{d}	38.82±0.21^{h}	36.05±0.46^{def}	0.53±0.02^{cdefg}	0.22±0.06^{cdefg}	N/D	0.00±0.00^{a}	38.82±0.21^{g}	36.58±0.48^{def}	24.60±0.26^{efgh}
BW 3.5%	0.13±0.01^{d}	0.59±0.06^{b}	20.98±0.18^{d}	N/D	5.29±0.23^{a}	36.46±0.32^{jk}	34.69±0.42^{hij}	1.43±0.45^{a}	0.42±0.26^{a}	N/D	0.00±0.00^{a}	36.46±0.32^{ij}	36.13±0.11^{ef}	27.41±0.31^{b}

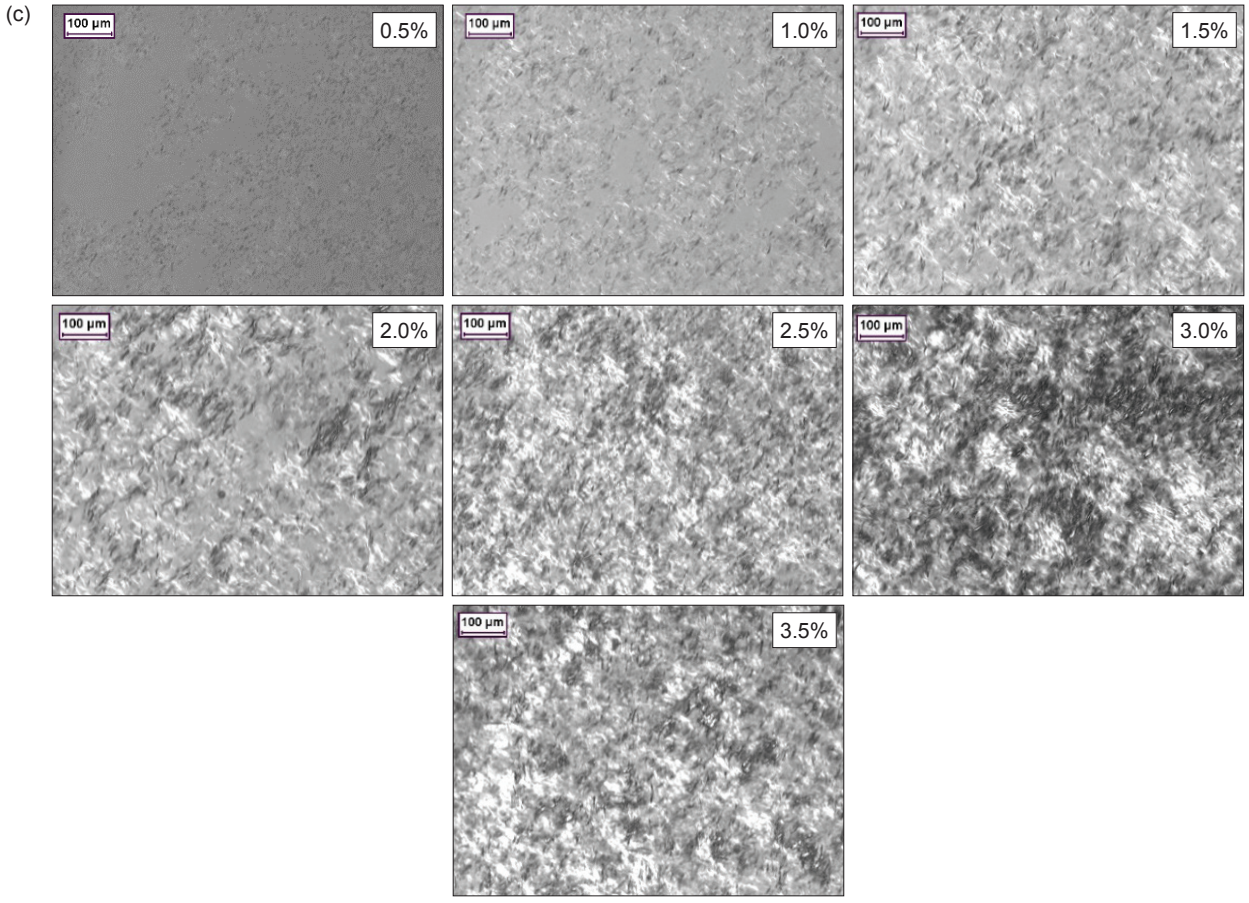
Note: Means within each column bearing different superscript letters are significantly different (p<0.05).
N/D - not detected; POOo - palm superolein; SFO - sunflower oil; 12:0 - lauric acid; 14:0 - myristic acid; 16:0 - palmitic acid; 16:1 - palmitoleic acid; 18:0 - stearic acid; 18:1 - oleic acid; 18:2 - linoleic acid; 18:3 - linolenic acid; 20:0 - arachidic acid; 20:1 - eicosenoic acid; MONO - monounsaturated fatty acid; POLY - polyunsaturated fatty acid; SAT. - saturated fatty acid.

(a)


100 µm
0.5%
100 µm
1.0%
100 µm
1.5%
100 µm
2.0%
100 µm
2.5%
100 µm
3.0%
100 µm
3.5%

(b)


100 µm
0.5%
100 µm
1.0%
100 µm
1.5%
100 µm
2.0%
100 µm
2.5%
100 µm
3.0%
100 µm
3.5%



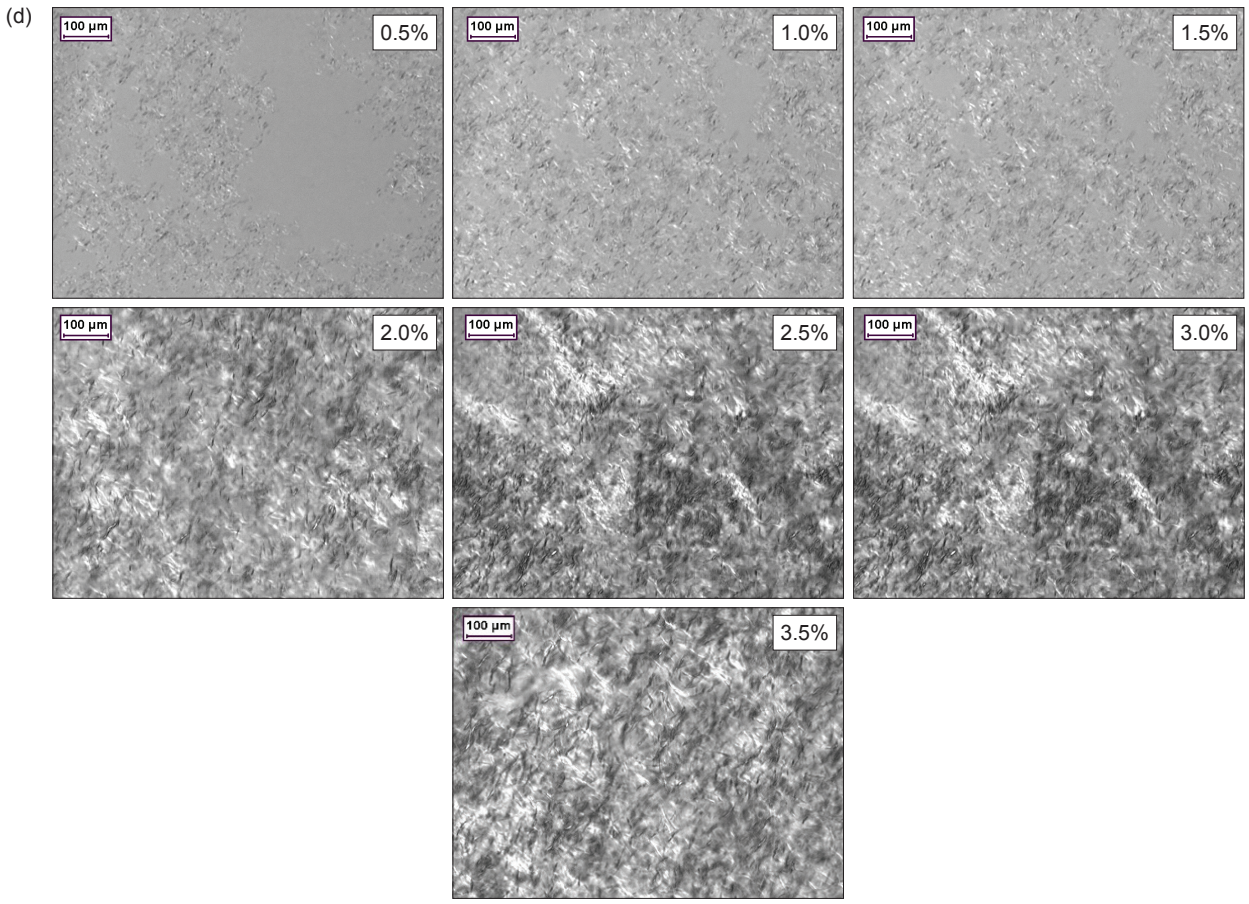
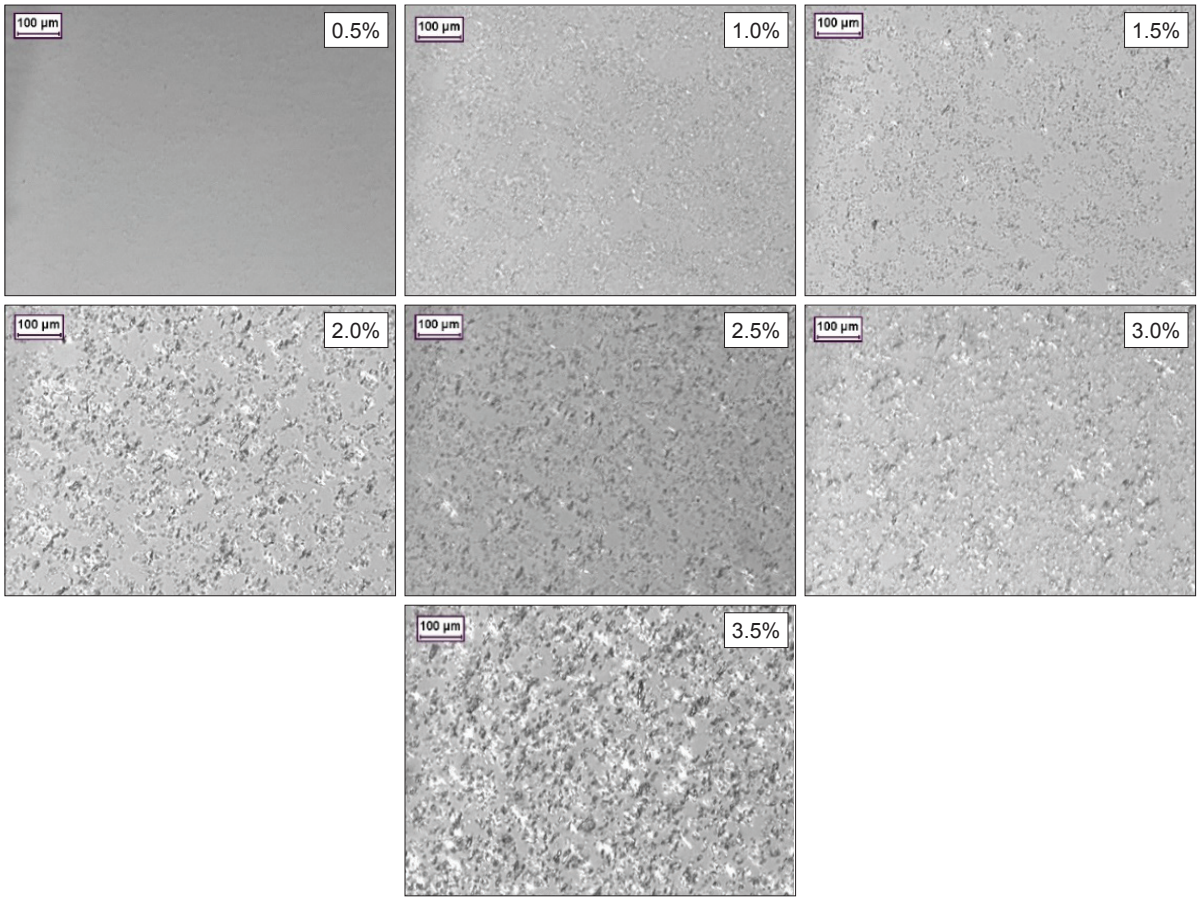
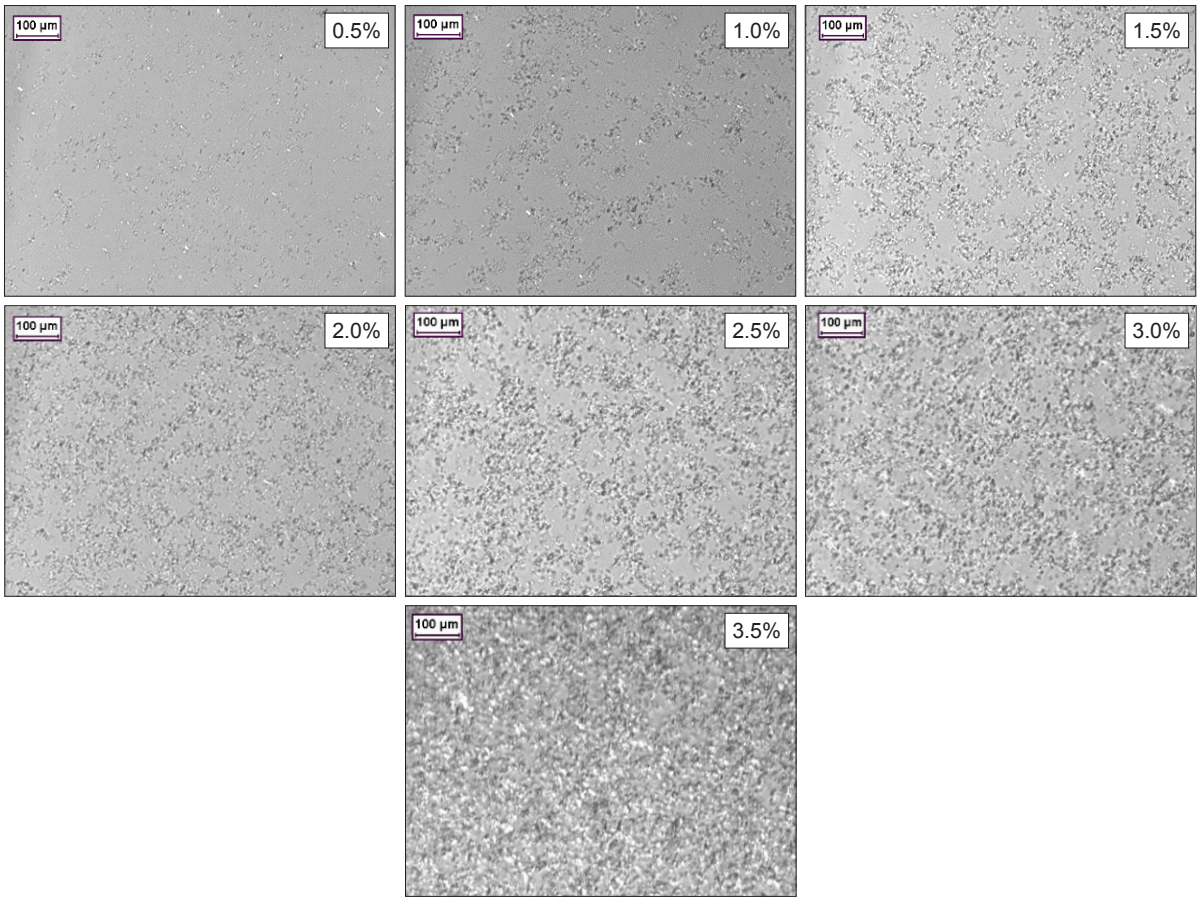


Figure 1. Polarised light micrographs (10x lens) of oil system with 0.5%-3.5% sunflower wax at (a) 10°C, (b) 25°C, (c) 40°C and (d) 45°C.

(a)


100 µm
0.5%
100 µm
1.0%
100 µm
1.5%
100 µm
2.0%
100 µm
2.5%
100 µm
3.0%
100 µm
3.5%

(b)


100 µm
0.5%
100 µm
1.0%
100 µm
1.5%
100 µm
2.0%
100 µm
2.5%
100 µm
3.0%
100 µm
3.5%

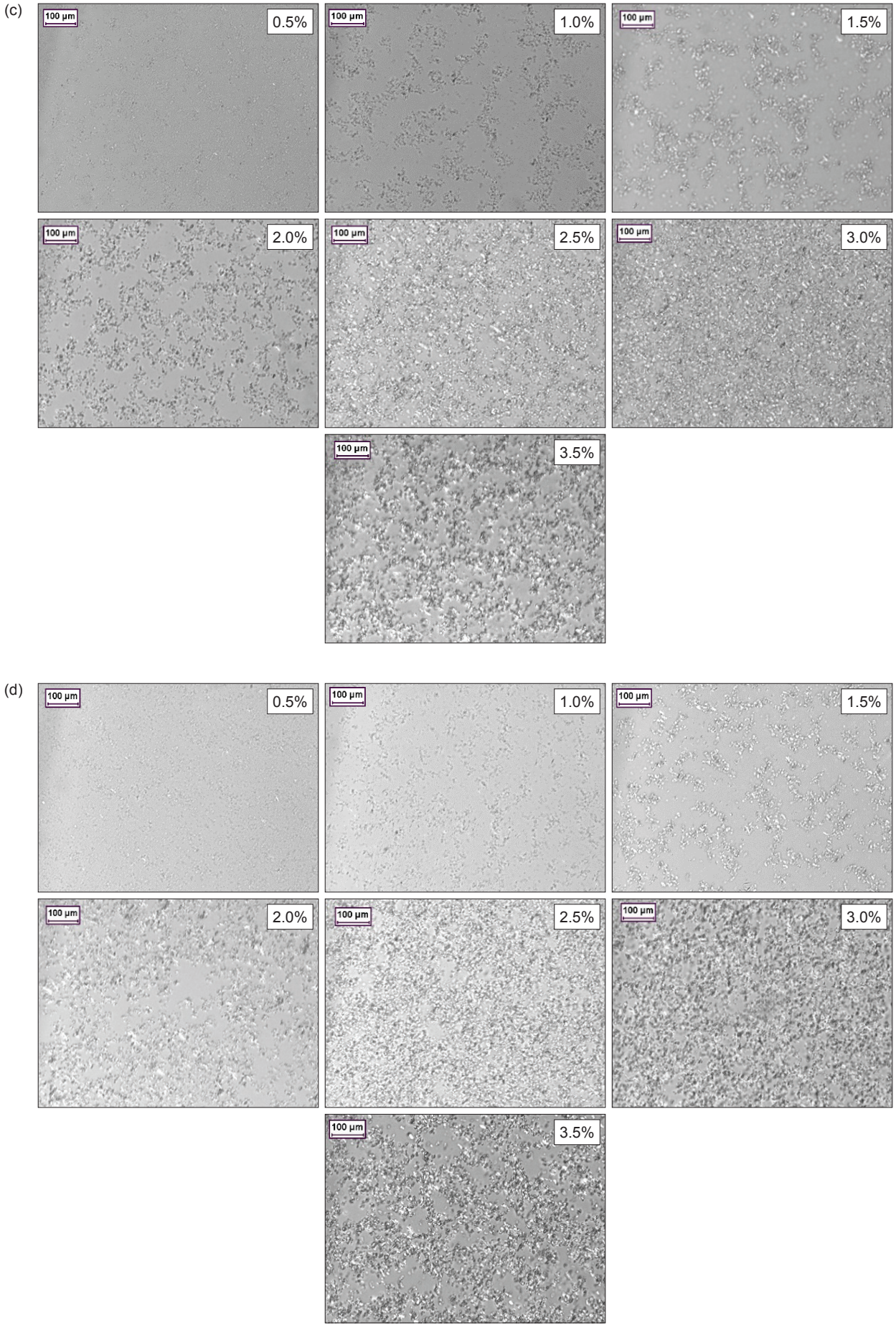
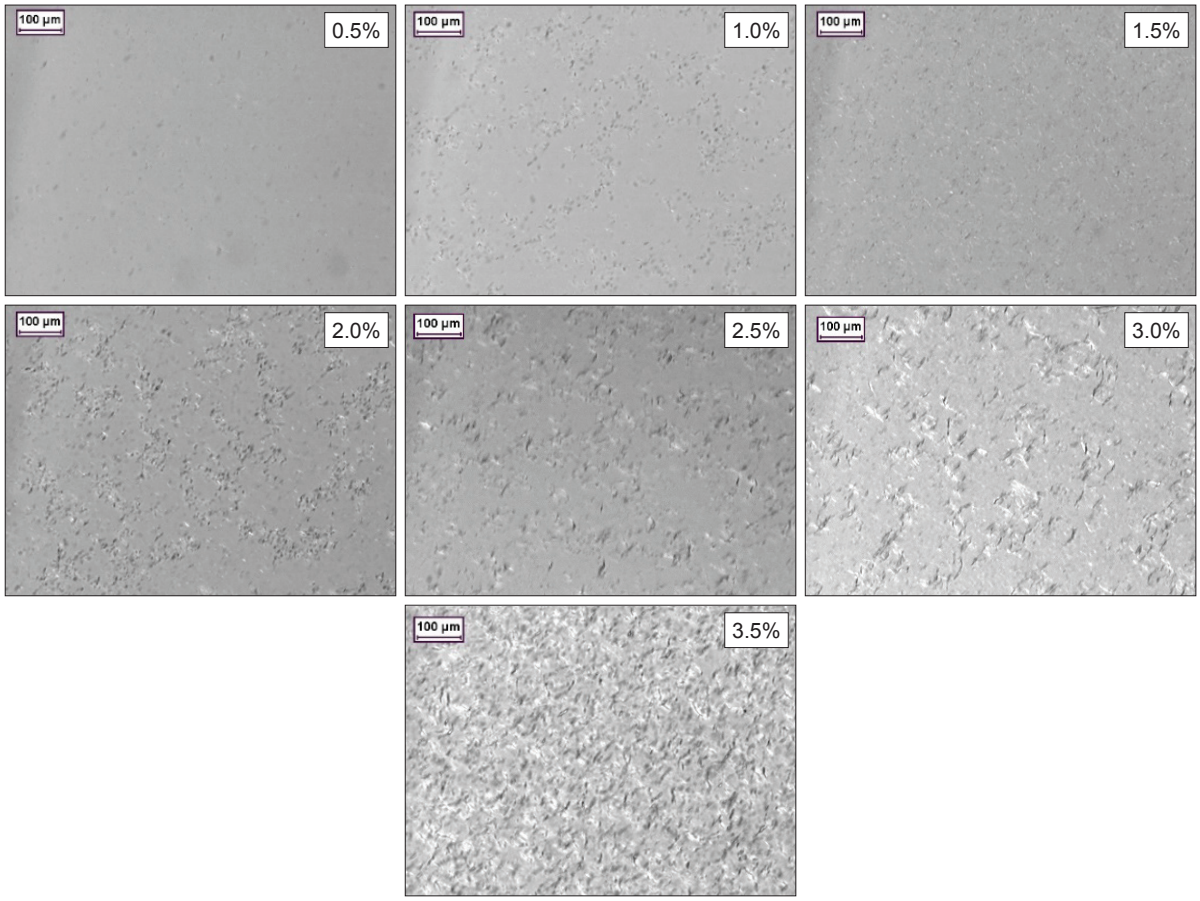
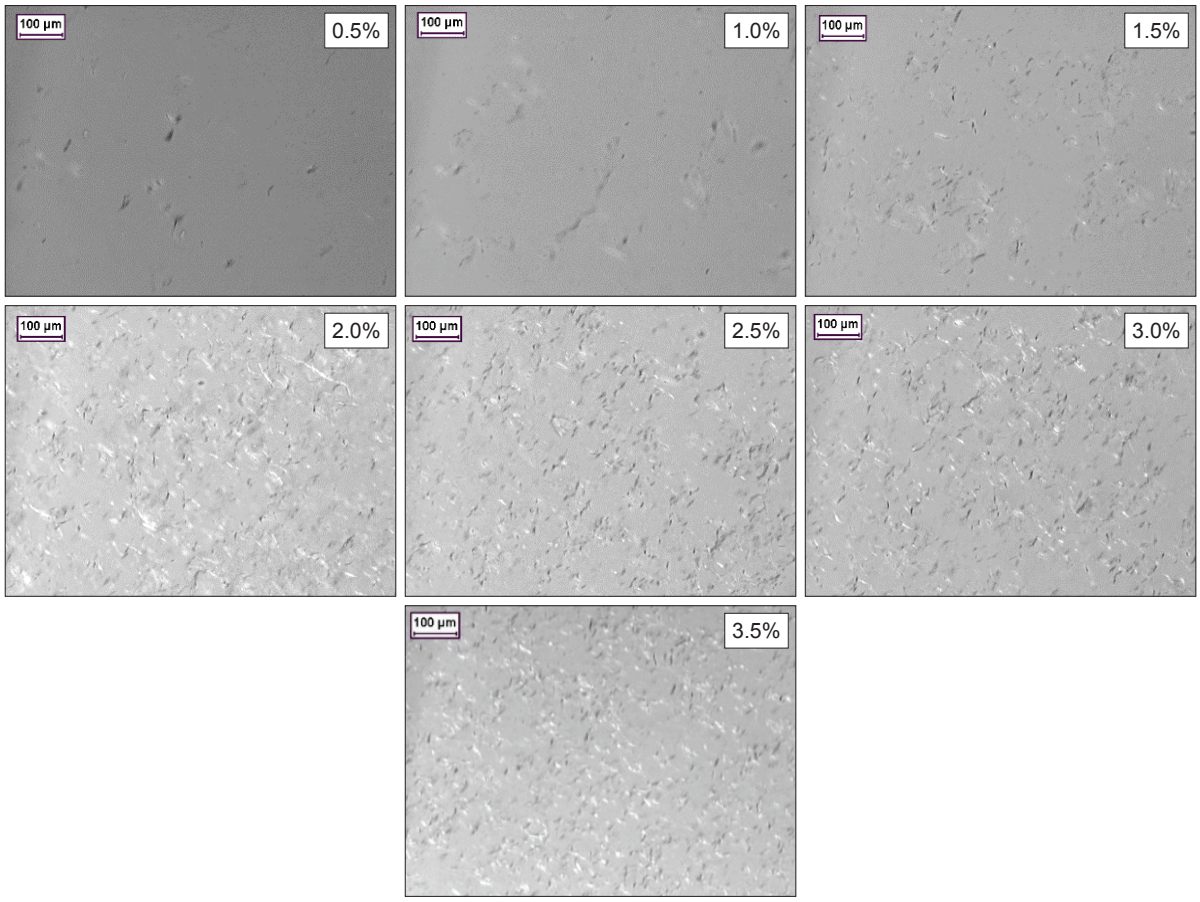


Figure 2. Polarised light micrographs (10x lens) of oil system with 0.5%-3.5% carnauba wax at (a) 10°C, (b) 25°C, (c) 40°C and (d) 45°C.

(a)


100 µm
0.5%
100 µm
1.0%
100 µm
1.5%
100 µm
2.0%
100 µm
2.5%
100 µm
3.0%
100 µm
3.5%

(b)


100 µm
0.5%
100 µm
1.0%
100 µm
1.5%
100 µm
2.0%
100 µm
2.5%
100 µm
3.0%
100 µm
3.5%

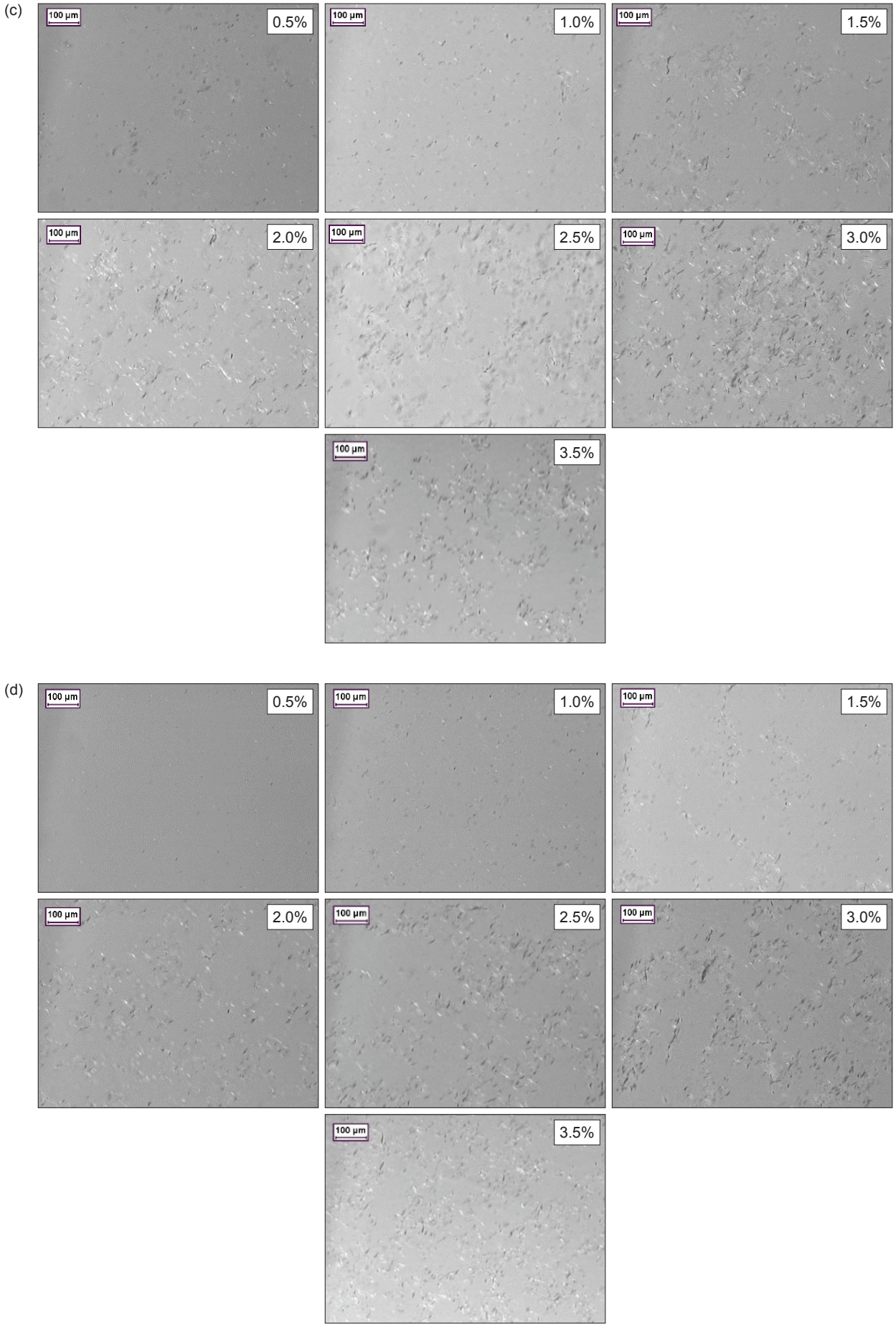


Figure 3. Polarised light micrographs (10x lens) of oil system with 0.5%-3.5% beeswax at (a) 10°C, (b) 25°C, (c) 40°C and (d) 45°C.

The Effect of Waxes on Shear Viscosity of OSW

Shear viscosity of OSW with SFW, CW and BW at 0.5%-3.5% for 10°C, 25°C, 40°C and 45°C is shown in *Figure 4*, *5* and *6*. At 5°C, shear viscosity of OSW with SFW was increased with increasing percentage of wax and all were statistically different (p<0.05). This OSW with SFW showed that non-Newtonian and shear thinning behaviour for all oil percentages as shear viscosity was decreased with increasing shear rate as wax thickened the oil system, except for 0.0% SFW. It was expected to observe that OSW with 3.0% SFW and 3.5% SFW produced the highest shear viscosity while the OSW with 0.5% SFW produced the lowest shear viscosity at 5°C at all experimental shear rates. Nevertheless, all shear viscosity of OSW with SFW was below 2.00 Pa.s. The shear viscosity was considered very low, and thus, should not affect spreadability. One of the commercial vegetable fats for confectionery spread was found to be 1.97 Pa.s for the shear rate at 100/s and about 6.00 Pa.s for the shear rate at 500/s at 30°C (Hadnađev *et al*., 2011). According to Mazzanti *et al.* (2003), a low shear rate during cooling promoted the alignment of the gelator (10°C prior to the crystallisation onset temperature) during nucleation. However, the nuclei alignment and nucleation rate might change due to the high shear rate, which resulted in alteration of crystal in terms of size, distribution and population. This will consequently alter the strength of the gel (Blake and Marangoni, 2015; Da Pieve *et al.*, 2010; Doan *et al.*, 2018). At 10°C and 25°C, similar non-Newtonian and shear thinning behaviour were observed for OSW with 1.0%-3.5% SFW. However, the shear viscosity values were smaller than that observed at 5°C, especially at 100/s of shear rate with values of less than 1.30 Pa.s and 0.80 Pa.s, respectively. During shearing, heat and mass transfer occurred due to molecular collision which shattered the interaction between gelator, and thus damaged the linkage of crystals and altered the crystal size (Chopin-Doroteo *et al*., 2011). A higher shear rate produced more heat and higher mass transfer occurred; hence, there was occurrence of shear thinning. Shear viscosity of OSW with 0.5% SFW at 10°C and 25°C were observed to have Newtonian behaviour. At 40°C and 45°C, the shear viscosity values were small, especially at the shear rates of 300/s and 400/s. At shear rate of 100/s, the shear viscosity for 40°C and 45°C were 0.48 Pa.s and 0.39 Pa.s, respectively for OSW with 3.5% SFW. OSW with 0.5% and 1.0% SFW were observed to have Newtonian behaviour while other systems showed non-Newtonian behaviour.

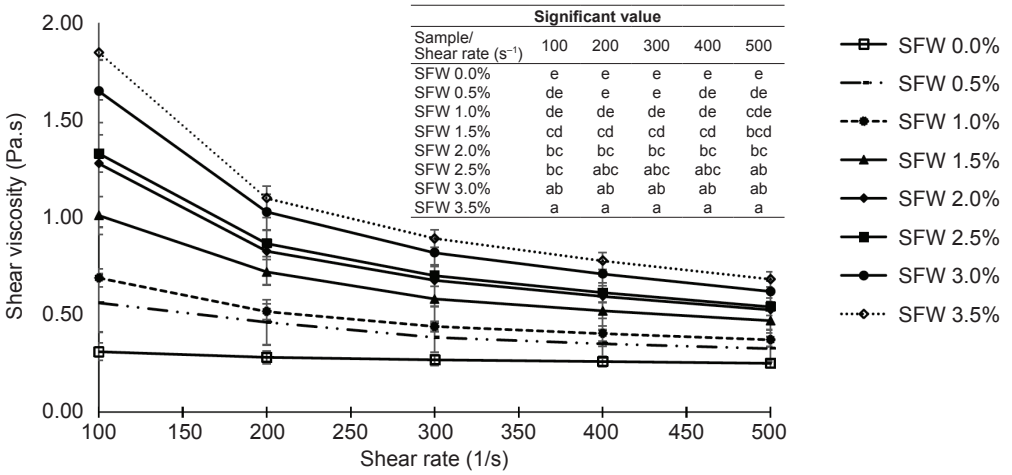
Shear viscosity values of OSW with CW at 5°C were small although they were significantly different (p<0.05). OSW with 0.5%-1.5% CW at 5°C showed Newtonian behaviour while others showed non-Newtonian and shear thinning behaviour. Shear viscosity values of OSW with 3.5% CW at 100/s shear rate were 0.60 Pa.s and was well below the shear viscosity of OSW with 3.5% SFW. Therefore, spreadability at low temperature was possible. At 10°C, OSW with CW was comparable to 5°C. However, only OSW with 0.5% and 1.0% CW were observed to be Newtonian. At 25°C, 40°C and 45°C, the shear viscosity values were quite alike, with small shear viscosity for all percentages with less than 0.10 Pa.s.

At 5°C, shear viscosity of OSW with all percentages of BW were low although they were significantly different (p<0.05). Newtonian behaviour was observed for shear rate of 200/s - 500/s at 5°C. OSW with 3.5% BW was observed to have shear viscosity of less than 0.50 Pa.s for shear rate of 100/s; hence, will be the easiest to spread at low temperature for a spreadable product as compared to 3.5% SFW and 3.5% CW. At 10°C, 0.5% BW was observed to have Newtonian behaviour while other percentages showed non-Newtonian behaviour. Shear viscosity of OSW at 25°C, 40°C and 45°C were comparable for all percentages, except for 0.5%-1.5% BW with values of below 0.20 Pa.s. 0.5%-1.5% BW had shear viscosity of near 0 Pa.s for all shear rates.

CONCLUSION

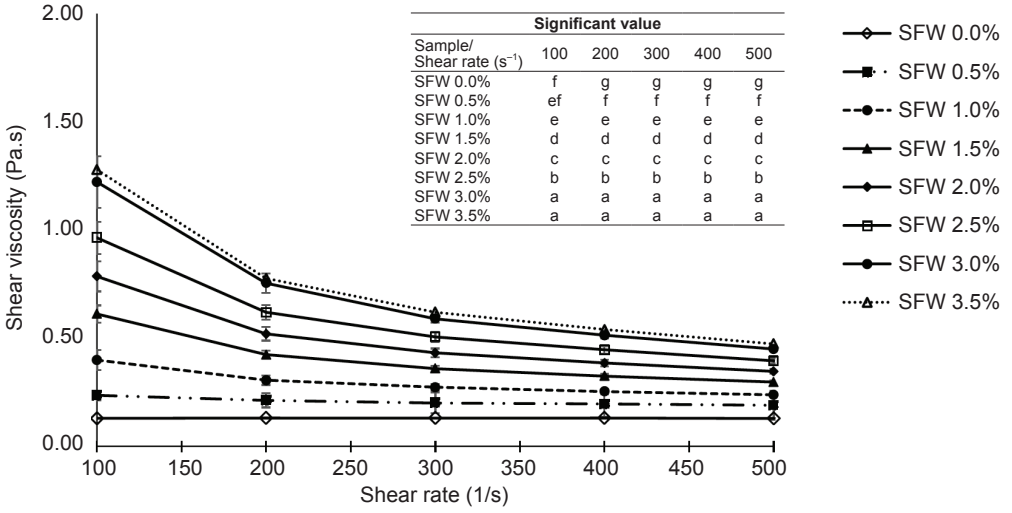
FAC for all OSW was significantly different (p<0.05) although the FAC values were not much different from one another, indicating no major impact on saturation level for wax addition in base oil. In view of this, selection of any percentage of OSW might not affect the saturation level of the end product. Notwithstanding this, further selection of OSW was based on crystal structure and shear viscosity. Crystal structure of 3.5% waxes at 10°C showed that OSW with SFW was denser than CW followed by BW. OSW with 3.5% SFW might have difficulty in spreadability at low temperature (10°C). At 40°C and 45°C, crystal structures of OSW with 3.5% SFW were denser as compared to OSW of 3.5% CW and BW. Therefore, OSW with 3.5% SFW might potentially hinder the phase separation. In terms of shear viscosity at 5°C, OSW with 3.5% SFW had the highest value, followed by OSW with 3.5% CW and 3.5% BW. This demonstrated that OSW with 3.5% SFW was difficult to spread, which aligned with the finding of the crystal structure at low temperatures. At 40°C and 45°C, OSW with 3.5% SFW exhibited a higher shear viscosity value as compared to OSW with 3.5% CW and 3.5% BW. To choose a suitable OSW for the end product which requires spreadability at low temperature (5°C-10°C) and to minimise oil separation at high temperature (40°C-45°C), OSW with 3.5% CW might be the optimal choice.

(a)



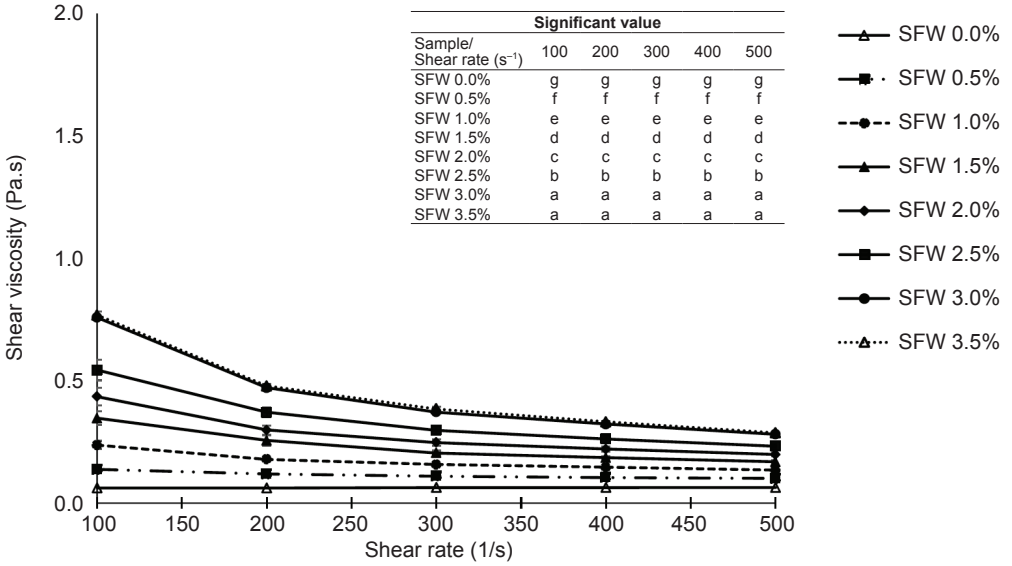
Significant value					
Sample/ Shear rate (s^{-1})	100	200	300	400	500
SFW 0.0%	e	e	e	e	e
SFW 0.5%	de	e	e	de	de
SFW 1.0%	de	de	de	de	cde
SFW 1.5%	cd	cd	cd	cd	bcd
SFW 2.0%	bc	bc	bc	bc	bc
SFW 2.5%	bc	abc	abc	abc	ab
SFW 3.0%	ab	ab	ab	ab	ab
SFW 3.5%	a	a	a	a	a

(b)



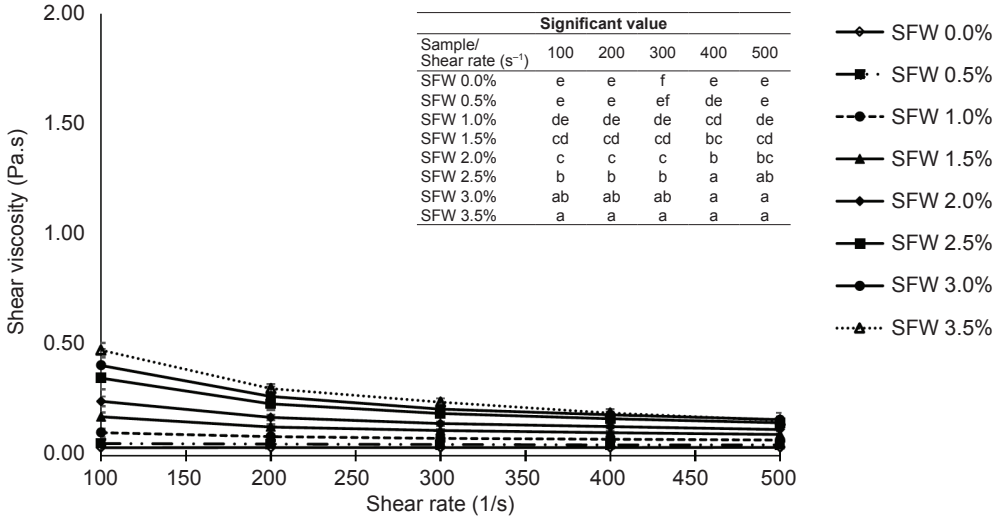
Significant value					
Sample/ Shear rate (s^{-1})	100	200	300	400	500
SFW 0.0%	f	g	g	g	g
SFW 0.5%	ef	f	f	f	f
SFW 1.0%	e	e	e	e	e
SFW 1.5%	d	d	d	d	d
SFW 2.0%	c	c	c	c	c
SFW 2.5%	b	b	b	b	b
SFW 3.0%	a	a	a	a	a
SFW 3.5%	a	a	a	a	a

(c)



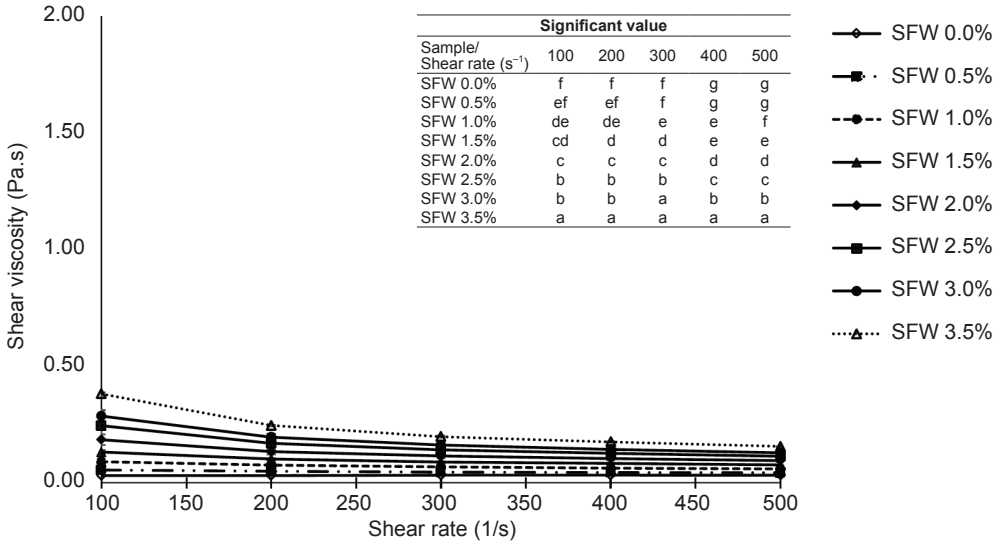
Significant value					
Sample/ Shear rate (s^{-1})	100	200	300	400	500
SFW 0.0%	g	g	g	g	g
SFW 0.5%	f	f	f	f	f
SFW 1.0%	e	e	e	e	e
SFW 1.5%	d	d	d	d	d
SFW 2.0%	c	c	c	c	c
SFW 2.5%	b	b	b	b	b
SFW 3.0%	a	a	a	a	a
SFW 3.5%	a	a	a	a	a

(d)



Sample/ Shear rate (s^{-1})	Significant value				
	100	200	300	400	500
SFW 0.0%	e	e	f	e	e
SFW 0.5%	e	e	ef	de	e
SFW 1.0%	de	de	de	cd	de
SFW 1.5%	cd	cd	cd	bc	cd
SFW 2.0%	c	c	c	b	bc
SFW 2.5%	b	b	b	a	ab
SFW 3.0%	ab	ab	ab	a	a
SFW 3.5%	a	a	a	a	a

(e)

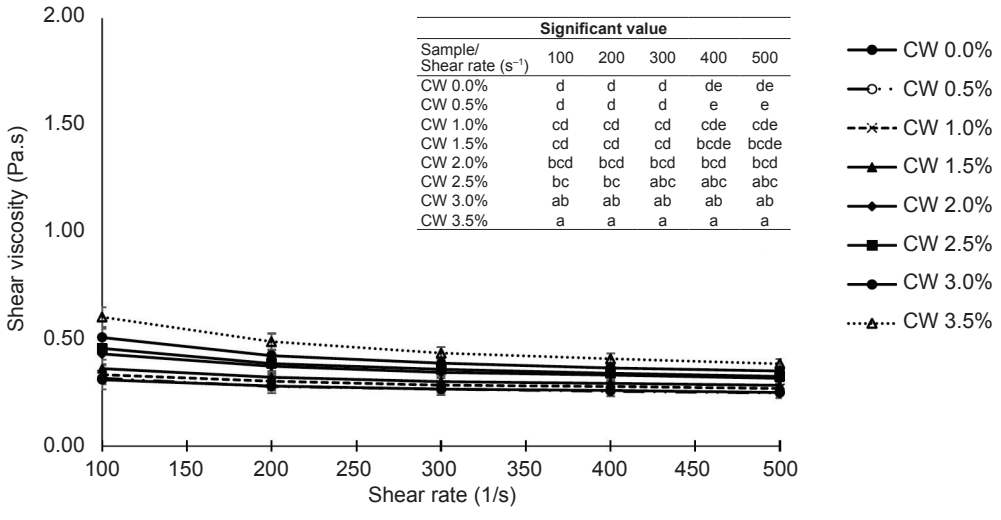


Sample/ Shear rate (s^{-1})	Significant value				
	100	200	300	400	500
SFW 0.0%	f	f	f	g	g
SFW 0.5%	ef	ef	f	g	g
SFW 1.0%	de	de	e	e	f
SFW 1.5%	cd	d	d	e	e
SFW 2.0%	c	c	c	d	d
SFW 2.5%	b	b	b	c	c
SFW 3.0%	b	b	a	b	b
SFW 3.5%	a	a	a	a	a

Note: Different small letters within each column in the table are significantly different (p<0.05).

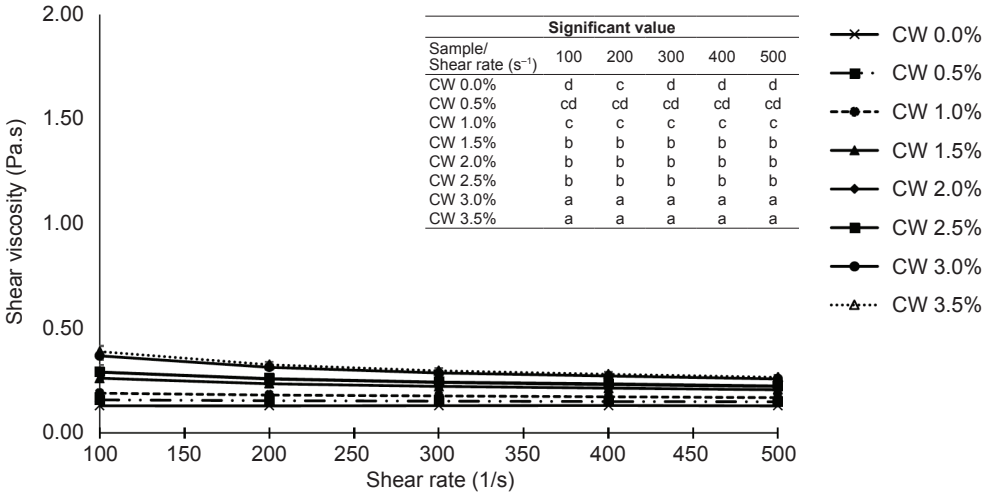
Figure 4. Shear viscosity at different shear rates of oil system with various percentages of sunflower wax (SFW) at (a) 5°C (b) 10°C (c) 25°C (d) 40°C and (e) 45°C.

(a)



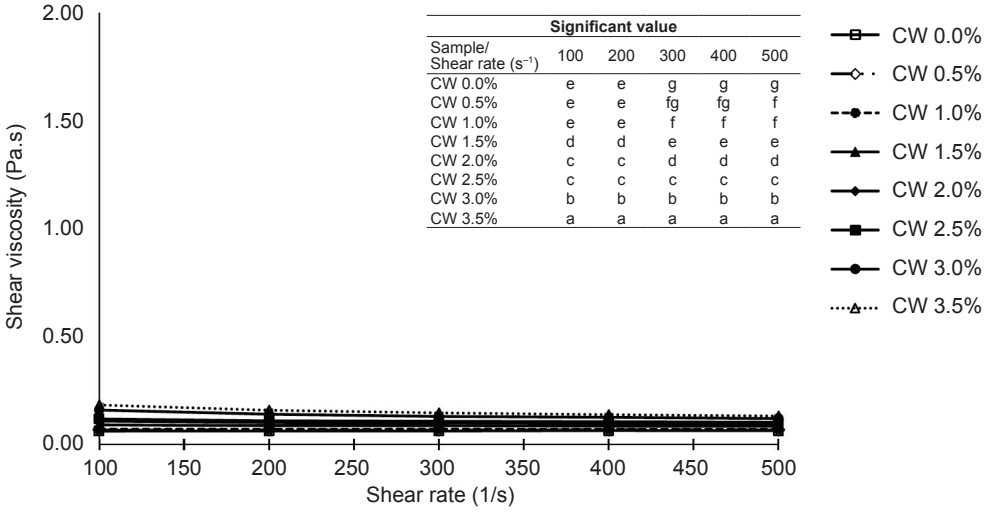
Sample/ Shear rate (s^{-1})	Significant value				
	100	200	300	400	500
CW 0.0%	d	d	d	de	de
CW 0.5%	d	d	d	e	e
CW 1.0%	cd	cd	cd	cde	cde
CW 1.5%	cd	cd	cd	bcde	bcde
CW 2.0%	bcd	bcd	bcd	bcd	bcd
CW 2.5%	bc	bc	abc	abc	abc
CW 3.0%	ab	ab	ab	ab	ab
CW 3.5%	a	a	a	a	a

(b)



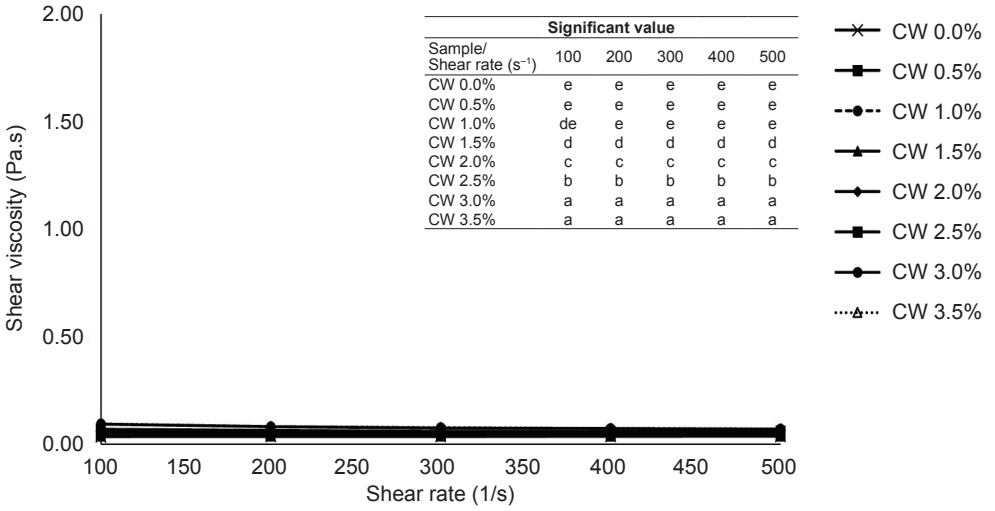
Significant value					
Sample/ Shear rate (s^{-1})	100	200	300	400	500
CW 0.0%	d	c	d	d	d
CW 0.5%	cd	cd	cd	cd	cd
CW 1.0%	c	c	c	c	c
CW 1.5%	b	b	b	b	b
CW 2.0%	b	b	b	b	b
CW 2.5%	b	b	b	b	b
CW 3.0%	a	a	a	a	a
CW 3.5%	a	a	a	a	a

(c)

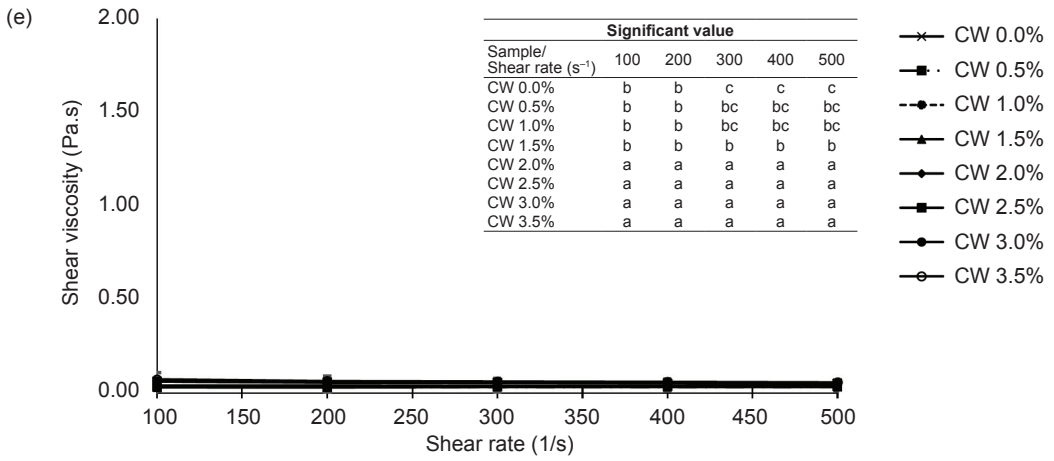


Significant value					
Sample/ Shear rate (s^{-1})	100	200	300	400	500
CW 0.0%	e	e	g	g	g
CW 0.5%	e	e	fg	fg	f
CW 1.0%	e	e	f	f	f
CW 1.5%	d	d	e	e	e
CW 2.0%	c	c	d	d	d
CW 2.5%	c	c	c	c	c
CW 3.0%	b	b	b	b	b
CW 3.5%	a	a	a	a	a

(d)



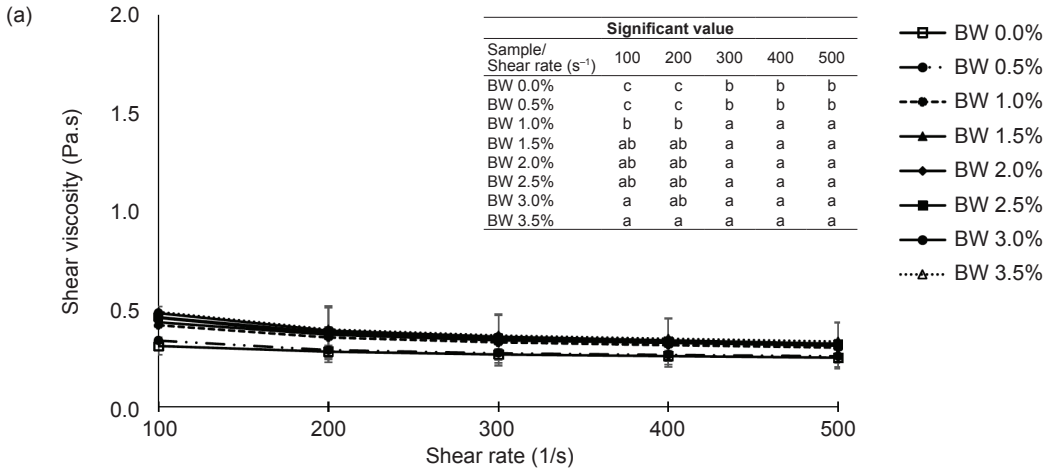
Significant value					
Sample/ Shear rate (s^{-1})	100	200	300	400	500
CW 0.0%	e	e	e	e	e
CW 0.5%	e	e	e	e	e
CW 1.0%	de	e	e	e	e
CW 1.5%	d	d	d	d	d
CW 2.0%	c	c	c	c	c
CW 2.5%	b	b	b	b	b
CW 3.0%	a	a	a	a	a
CW 3.5%	a	a	a	a	a



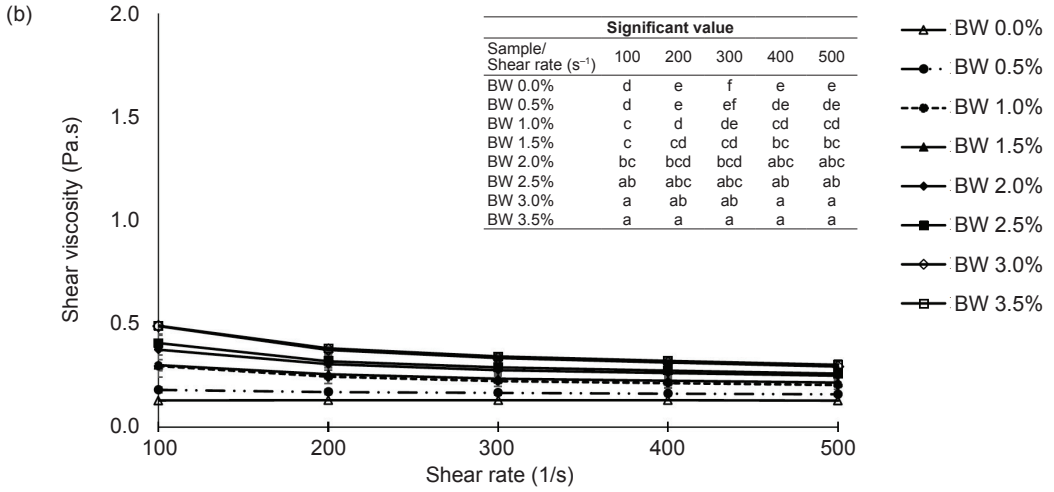
Significant value					
Sample/ Shear rate (s^{-1})	100	200	300	400	500
CW 0.0%	b	b	c	c	c
CW 0.5%	b	b	bc	bc	bc
CW 1.0%	b	b	bc	bc	bc
CW 1.5%	b	b	b	b	b
CW 2.0%	a	a	a	a	a
CW 2.5%	a	a	a	a	a
CW 3.0%	a	a	a	a	a
CW 3.5%	a	a	a	a	a

Note: Different small letters within each column in the table are significantly different (p<0.05).

Figure 5. Shear viscosity at different shear rate of oil system with various percentages of carnauba wax (CW) at (a) 5°C (b) 10°C (c) 25°C (d) 40°C and (e) 45°C.

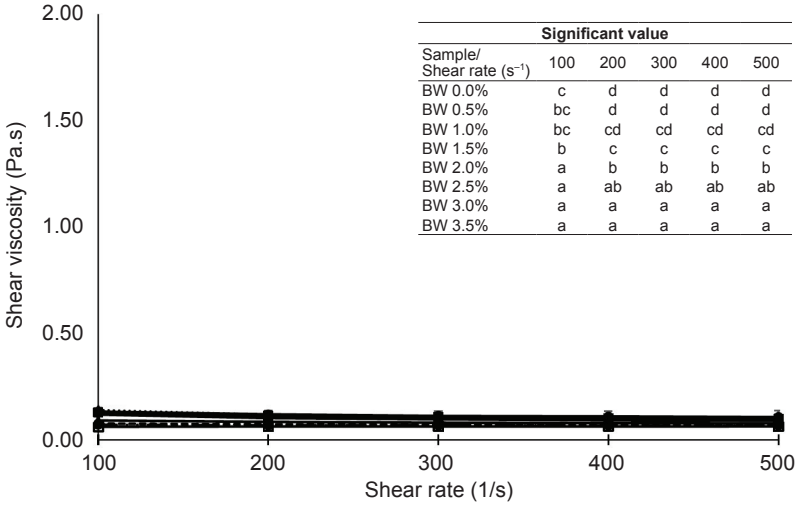


Significant value					
Sample/ Shear rate (s^{-1})	100	200	300	400	500
BW 0.0%	c	c	b	b	b
BW 0.5%	c	c	b	b	b
BW 1.0%	b	b	a	a	a
BW 1.5%	ab	ab	a	a	a
BW 2.0%	ab	ab	a	a	a
BW 2.5%	ab	ab	a	a	a
BW 3.0%	a	ab	a	a	a
BW 3.5%	a	a	a	a	a



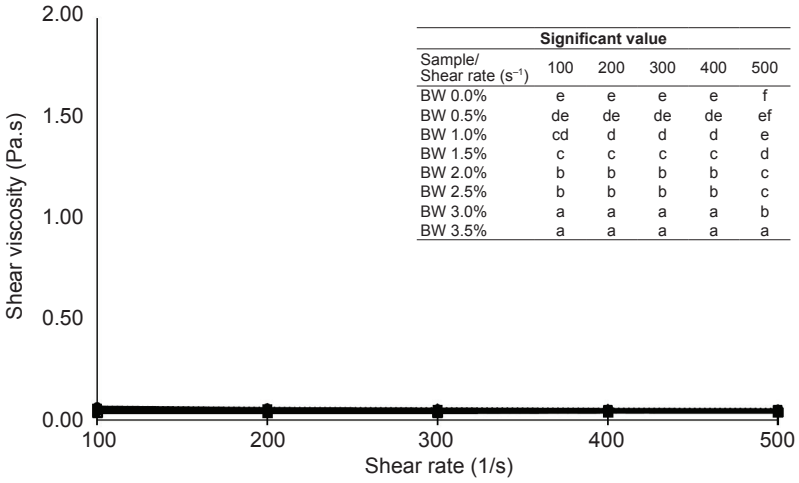
Significant value					
Sample/ Shear rate (s^{-1})	100	200	300	400	500
BW 0.0%	d	e	f	e	e
BW 0.5%	d	e	ef	de	de
BW 1.0%	c	d	de	cd	cd
BW 1.5%	c	cd	cd	bc	bc
BW 2.0%	bc	bcd	bcd	abc	abc
BW 2.5%	ab	abc	abc	ab	ab
BW 3.0%	a	ab	ab	a	a
BW 3.5%	a	a	a	a	a

(c)



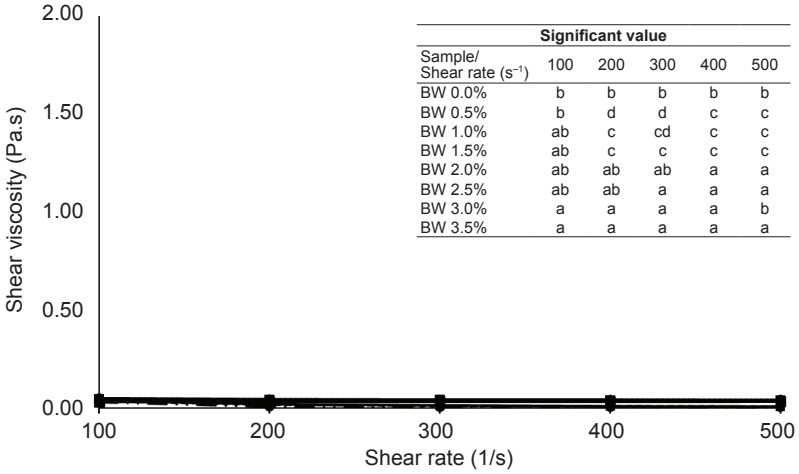
Significant value					
Sample/ Shear rate (s^{-1})	100	200	300	400	500
BW 0.0%	c	d	d	d	d
BW 0.5%	bc	d	d	d	d
BW 1.0%	bc	cd	cd	cd	cd
BW 1.5%	b	c	c	c	c
BW 2.0%	a	b	b	b	b
BW 2.5%	a	ab	ab	ab	ab
BW 3.0%	a	a	a	a	a
BW 3.5%	a	a	a	a	a

(d)



Significant value					
Sample/ Shear rate (s^{-1})	100	200	300	400	500
BW 0.0%	e	e	e	e	f
BW 0.5%	de	de	de	de	ef
BW 1.0%	cd	d	d	d	e
BW 1.5%	c	c	c	c	d
BW 2.0%	b	b	b	b	c
BW 2.5%	b	b	b	b	c
BW 3.0%	a	a	a	a	b
BW 3.5%	a	a	a	a	a

(e)



Significant value					
Sample/ Shear rate (s^{-1})	100	200	300	400	500
BW 0.0%	b	b	b	b	b
BW 0.5%	b	d	d	c	c
BW 1.0%	ab	c	cd	c	c
BW 1.5%	ab	c	c	c	c
BW 2.0%	ab	ab	ab	a	a
BW 2.5%	ab	ab	a	a	a
BW 3.0%	a	a	a	a	b
BW 3.5%	a	a	a	a	a

Note: Different small letters within each column in the table are significantly different (p<0.05).

Figure 6. Shear viscosity at different shear rates of the oil system with various percentages of beeswax (BW) at (a) 5°C (b) 10°C (c) 25°C (d) 40°C and (e) 45°C.

ACKNOWLEDGEMENT

The authors would like to thank the Director-General of MPOB for his permission to publish the article.

REFERENCES

Abdel-Razek, A G; Hassanein, M M M; Rudzinska, M and El-Mallah, M H (2017). Role of minor constituents and balanced fatty acids in upgrading the low stability of cooking oils blended with palm super olein. *Asian J. Sci. Res., 10*: 150-159.

Balasubramaniam, R; Damodar, G and Sughir, A (2012). Oleogel: A promising base for transdermal formulations. *Asian J. Pharm., 6:* 1-10.

Blake, A I and Marangoni, A G (2015). The effect of shear on the microstructure and oil binding capacity of wax crystal networks. *Food Biophys., 10*: 403-415.

Blake, A I; Co, E D and Marangoni, A G (2014). Structure and physical properties of plant wax crystal networks and their relationship to oil binding capacity. *JAOCS, 91*: 885-903.

Chai, X H; Meng, Z; Cao, P R; Liang, X Y; Piatko, M; Campbell, S; Koon Lo, S and Liu, Y F (2018). Influence of indigenous minor components on fat crystal network of fully hydrogenated palm kernel oil and fully hydrogenated coconut oil. *Food Chem., 255*: 49-57.

Chopin-Doroteo, M; Morales-Rueda, J A; Dibildox-Alvarado, E; Charó-Alonso, M A; de la Peña-Gil, A and Toro-Vazquez, J F (2011). The effect of shearing in the thermomechanical properties of candelilla wax and candelilla wax-tripalmitin organogels. *Food Biophys., 6*: 359-376.

Co, E D and Marangoni, A G (2012). Organogels: An alternative edible oil-structuring method. *JAOCS, 89*: 749-780.

Da Pieve, S; Calligaris, S; Nicoli, M C and Marangoni, A G (2010). Shear nanostructuring of monoglyceride organogels. *Food Biophys., 5*: 211-217.

Daniel, J and Rajasekharan, R (2003). Organogelation of plant oils and hydrocarbons by long-chain saturated FA, fatty alcohols, wax esters, and dicarboxylic acids. *JAOCS, 80*: 417-421.

Dassanayake, L S K; Kodali, D R; Ueno, S and Sato, K (2009). Physical properties of rice bran wax in bulk and organogels. *JAOCS, 86*: 1163-1173.

De Souza, R J; Mente, A; Maroleanu, A; Cozma, A I; Ha, V; Kishibe, T; Uleryk, E; Budylowski, P; Schünemann, H; Beyene, J and Anand, S S (2015). Intake of saturated and trans unsaturated fatty acids and risk of all cause mortality, cardiovascular disease, and type 2 diabetes: Systematic review and meta-analysis of observational studies. *BMJ (Online), 351*: 1-16.

Doan, C D; Tavernier, I; Okuro, P K and Dewettinck, K (2018). Internal and external factors affecting the crystallization, gelation and applicability of wax-based oleogels in food industry. *Innov. Food Sci. Emerg. Technol., 45*: 42-52.

FDA (2018). Final determination regarding partially hydrogenated oils (removing *trans* fat). https://www.fda.gov/food/food-additives-petitions/final-determination regarding-partially-hydrogenated-oils-removing-trans-fat, accessed on 20 April 2020.

Gallego, R; Arteaga, J F; Valencia, C and Franco, J M (2013). Rheology and thermal degradation of isocyanate-functionalized methyl cellulose-based oleogels. *Carbohydr. Polym., 98*: 152-160.

Hadnađev, M; Hadnađev, T D; Torbica, A; Dokić, L; Pajin, B and Krstonošić, V (2011). Rheological properties of maltodextrin based fat-reduced confectionery spread systems. *Procedia Food Sci., 1*: 62-67.

Hughes, N E; Marangoni, A G; Wright, A J; Rogers, M A and Rush, J W E (2009). Potential food applications of edible oil organogels. *Trends Food Sci. Technol., 20*: 470-480.

Hwang, H S; Kim, S; Singh, M; Winkler-Moser, J K and Liu, S X (2012). Organogel formation of soybean oil with waxes. *JAOCS, 89*: 639-647.

Jang, A; Bae, W; Hwang, H-S; Lee, H G and Lee, S (2015). Evaluation of canola oil oleogels with candelilla wax as an alternative to shortening in baked goods. *Food Chem., 187*: 525-529.

Kim, J Y; Lim, J; Lee, J H; Hwang, H S and Lee, S (2017). Utilization of oleogels as a replacement for solid fat in aerated baked goods: Physicochemical, rheological, and tomographic characterization. *J. Food Sci., 8*: 445-452.

Kumar, R and Katare, O P (2005). Lecithin organogels as a potential phospholipid-structured system for topical drug delivery: A review. *AAPS J., 6*: 298-310.

Martins, A J; Cerqueira, M A; Cunha, R L and Vicente, A A (2017). Fortified beeswax oleogels:

Effect of β-carotene on the gel structure and oxidative stability. *Food Funct., 8*: 4241-4250.

Martins, A J; Cerqueira, M A; Fasolin, L H; Cunha, R L and Vicente, A A (2016). Beeswax organogels: Influence of gelator concentration and oil type in the gelation process. *Food Res. Int., 84*: 170-179.

Mazzanti, G; Guthrie, S E; Sirota, E B; Marangoni, A G and Idziak, S H (2003). Orientation and phase transitions of fat crystals under shear. *Crys. Growth Des., 3*: 721-725.

Moghtadaei, M; Soltanizadeh, N and Goli, S A H (2018). Production of sesame oil oleogels based on beeswax and application as partial substitutes of animal fat in beef burger. *Food Res. Int., 108*: 368-377.

MPOB (2005). Methods of test for palm oil and palm oil products. *MPOB Test Method.* MPOB, Bangi.

Ng, S P; Lai, O M; Abas, F; Lim, H K; Beh, B K; Ling, T C and Tan, C P (2014). Compositional and thermal characteristics of palm olein-based diacylglycerol in blends with palm super olein. *Food Res. Int., 55*: 62-69.

Norazura Aila, M H; Sivaruby, K; Nur Haqim, I; Noor Lida, H M D; Wan Rosnani, A I and Noor Soffalina, S S (2021). Palm-based chocolate spread for wide range temperature applications using sunflower wax, carnauba wax and bees wax. *J. Oil Palm Res.* DOI: 10.21894/jopr.2021.0051.

Öğütcü, M and Yilmaz, E (2014). Oleogels of virgin olive oil with carnauba wax and monoglyceride as spreadable products. *Grasas y Aceites, 65*: e040.

Öğütcü, M and Yılmaz, E (2015). Characterization of hazelnut oil oleogels prepared with sunflower and carnauba waxes. *Int. J. Food Prop., 18*: 1741-1755.

Patel, A R; Rajarethinem, P S; Grędowska, A; Turhan, O; Lesaffer, A; De Vos, W H; Van de Walle, D and Dewettinck, K (2014). Edible applications of shellac oleogels: Spreads, chocolate paste and cakes. *Food Funct., 5*: 645-652.

Patel, A R; Schatteman, D; De Vos, W H; Lesaffer, A and Dewettinck, K (2013). Preparation and rheological characterization of shellac oleogels and oleogel-based emulsions. *J. Colloid Interface Sci., 411*: 114-121.

Pehlivanoğlu, H; Demirci, M; Toker, O S; Konar, N; Karasu, S and Sagdic, O (2018). Oleogels, a promising structured oil for decreasing saturated fatty acid concentrations: Production and food-based applications. *Crit. Rev. Food Sci. Nutr., 58*: 1330-1341.

Romano, R; Giordano, A; Vitiello, S; Grottaglie, L L and Musso, S S (2012). Comparison of the frying performance of olive oil and palm superolein. *J. Food Sci., 77*: 519-531.

Rogers, M A; Strober, T; Bot, A; Toro Vazquez, J F; Stortz, T and Marangoni, A G (2014). Edible oleogels in molecular gastronomy. *Int. J. Gastron. Food Sci., 2*: 22-31.

Sánchez, R; Stringari, G B; Franco, J M; Valencia, C and Gallegos, C (2011). Use of chitin, chitosan and acylated derivatives as thickener agents of vegetable oils for bio-lubricant applications. *Carbohydr. Polym., 85*: 705-714.

Sandoval, J M; Carelli, A; Palla, C and Baümler, E (2020). Preparation and characterization of oleogel emulsions: A comparative study between the use of recovered and commercial sunflower waxes as structuring agent. *J. Food Sci., 85*: 2866-2878.

Singh, A; Auzanneau, F I and Rogers, M A (2017). Advances in edible oleogel technologies - A decade in review. *Food Res. Int., 97*: 307-317.

Stortz, T A; Zetzl, A K; Barbut, S; Cattaruzza, A and Marangoni, A G (2012). Edible oleogels in food products to help maximize health benefits and improve nutritional profiles. *Lipid Technol., 24*: 151-154.

Vintiloiu, A and Leroux, J C (2008). Organogels and their use in drug delivery - A review. *J. Control. Release, 125*: 179-192.

Wassell, P; Bonwick, G; Smith, C J; Almiron-Roig, E and Young, N W G (2010). Towards a multidisciplinary approach to structuring in reduced saturated fat-based systems - A review. *Int. J Food Sci., 45*: 642-655.

Zetzl, A K and Marangoni, A G (2014). Structured emulsions and edible oleogels as solutions to trans fat. *Trans Fats Replacement Solutions*. AOCS Press. p. 215-243.

Journal of Oil Palm Research Vol. 35 (4) December 2023 p. 713-724
DOI: https://doi.org/10.21894/jopr.2023.0020

LINEAR KINETICS MODELLING AND THERMODYNAMICS STUDY OF SUPERCRITICAL CO_2-DERIVED OIL EXTRACTS FROM PALM FRUIT MESOCARP

USMAN BELLO[1]; NURUL AINI AMRAN[1,2]*; SHAFIRAH SAMSURI[1,2] and MUHAMMAD SYAFIQ HAZWAN RUSLAN[3]

ABSTRACT

Supercritical fluid extraction (SFE) is a green processing technique that employed the use of carbon dioxide (CO_2) as an extractant in place of organic or inorganic solvents. In this study, SFE was used to recover oil from the milled palm fruit peels as a sustainable feedstock. The process was carried out at five different temperatures of 40°C-80°C, varied extraction time of 30-150 min, a fixed pressure of 25 MPa, a flow rate of 5 mL min^{-1}, and a co-solvent ratio of 5.00% vol. The result shows that an optimum extract yield of 3.95% was recovered at the maximum temperature (80°C) after 150 min. The experimentally obtained data were subjected to kinetic analysis using Elovich's, Hyperbolic and Pseudo second-order models. Models' suitability to the data fitness was tested using seven error functions, in which Elovich's was found to be the best-fitted model, succeeded by the Hyperbolic and then Pseudo second-order. Also, the result of statistical analysis using ANOVA, indicates that temperature has more impact on improving the rate of extract recovery than extraction time. Finally, the thermodynamic studies revealed that an irreversible and endothermically forward reaction was observed considering the values of the entropy change (ΔS) = 0.138 J mol^{-1} K^{-1}, enthalpy change (ΔH) = 53.50 K J mol^{-1}, and Gibbs' free energy, (ΔG) = -6.04 K J mol^{-1} respectively.

Keywords: kinetics, oil extracts, supercritical fluid extraction, thermodynamics study.

Received: 18 October 2022; **Accepted:** 22 February 2023; **Published online:** 3 May 2023.

INTRODUCTION

The palm fruit is noteworthy for its high concentration of various bioactive compounds, particularly carotenoids, which can be used as dietary supplements, antioxidants and other health-value promoting compounds (Aini *et al*., 2022). In Malaysia, the expansion of palm oil plantations and processing has been intensified, particularly in the forested areas of Borneo, Sumatra, and the Malay Peninsula, due to the significant economic importance of palm oil as a source of revenue through exports (Anuar *et al*., 2021; Meijaard *et al*., 2020). Palm oil is widely used to meet the global annual demand of 40% of vegetable oil for food, as well as in a variety of industrial processes, including pharmaceuticals, body care products and biofuel production (Mohajershojaei *et al*., 2015). However, the push towards finding suitable extraction techniques that are environmentally friendly, less time-consuming and economically viable, led to the transition from the use of conventional to non-conventional extraction techniques. Part of the reasons for this includes the relatively poor success recorded in the recovery of bioactive compounds

[1] Chemical Engineering Department, Universiti Teknologi PETRONAS, 32610 Seri Iskandar, Perak, Malaysia.

[2] HICoE - Centre for Biofuel and Biochemical Research (CBBR), Universiti Teknologi PETRONAS, 32610 Seri Iskandar, Perak, Malaysia.

[3] School of Chemical Engineering, College of Engineering, Universiti Teknologi MARA, 40450 Shah Alam, Selangor, Malaysia.

* *Corresponding author e-mail: nurul.amran@utp.edu.my*

from extracts derived using conventional extraction methods, coupled with high temperature and energy demand for the process (Chai *et al*., 2020).

The growing objections coming from chemical industries on the risk associated with hazardous solvents for extraction using conventional techniques have led to the increased popularity of non-conventional methods (Rodrigues *et al*., 2020). One such method is SFE, which is favoured for being a clean and green process that is non-polluting and toxic-free (Rodrigues *et al*., 2020). This has made SFE a promising extraction technique as it eliminates the drawbacks of conventional methods, such as long processing time, expensive solvents, high temperature, and high energy consumption (Miękus *et al*., 2019). Furthermore, the non-polar nature of the solvent used in SFE (CO_2) prevents oxidation, which can negatively impact the stability and potency of extracts obtained through traditional methods (Garcia-Mendoza *et al*., 2015). Additionally, the environmental-friendly nature of the extractant (CO_2) makes the SFE process more sustainable (Mohammad *et al*., 2007; Valdivia-Rivera *et al*., 2021). The solubilisation and mass transfer reaction of carotenoids from milled palm fruit peel to liquid extract is influenced by the similarity in polarity between the analyte and the extracting solvent (CO_2) (Mohammad *et al*., 2019).

The mechanism of the SFE process involves cooling the CO_2 in the reservoir to 0°C to enable it to be transferred into the reactor as a liquid. A polar modifier is added to increase the polarity of polar extractable compounds. Subsequently, the liquid CO_2 is then pumped into the extraction vessel which is kept at a temperature above its critical temperature (Chai *et al*., 2020). The pumping rate affects the fluid flow rate, and the pressure valve regulates the pressure. Thereafter, extracts are collected by releasing the collection pressure to atmospheric pressure (Miękus *et al*., 2019). However, the factors such as CO_2 flow rate, temperature, pressure and co-solvent ratio, are known to affect the extraction efficiency (Ruslan *et al*., 2018). On top of that, an increase in flow rate and temperature enhances diffusion rate and facilitates mass transfer reaction, thereby rupturing the plant cell wall and subsequent withdrawal of the bioactive compounds (Chanioti *et al*., 2021). Thus, an increase in pressure is proportional to the increase in yield theoretically, due to the growing solubility ratio, fluid density, solvating power of the Sc-CO_2, and increased solubility of the solute compounds (Yang *et al*., 2015).

Several kinetic models have been examined in studying the mass transfer reaction involving SFE in the literature (Patidar *et al*., 2022; Vélez-Erazo *et al*., 2021). However, a report on kinetic modelling of palm fruit extract derived from SFE using Elovich's, Hyperbolic and Pseudo second-order models are lacking to date. Kinetic modelling is crucial in engineering processes, as it helps understand the extraction mechanism and scale up the process for industrial use. This study aims to determine the suitability of these models in predicting mass transfer coefficients and identify the best-fit kinetic model for the extraction process. Effective modeling offers a deeper insight into the relationship between mass transfer reaction and solubility mechanism, leading to improved process design, reduced energy loss, and cost savings. The prediction of models' accuracy in fitting the experimental data was evaluated using seven statistical error functions (RMS, SEE, ARE%, SSE, HYBRID%, MPSED%, SD, and R^2). ANOVA was used to examine the impact of extraction time and temperature on extract rate and Tukey's *post hoc* HSD was used to compare the means. Additionally, the thermodynamic parameters ΔG, ΔH and ΔS of the extraction process were analysed.

EXPERIMENTAL

Supercritical Fluid Extraction (SFE)

Milled palm fruit peels were extracted using SFE according to a procedure reported by Ruslan *et al*. (2018). As presented in *Figure 1*, the 2D schematic assembled SFE setup comprises the solvent reservoir (CO_2 supply tank) supplying liquid chilled CO_2 (0°C) via conducting pipe to the extraction vessel inside the oven. The pumping rate normally controls the flow rate while pressure drop is controlled by the automated back pressure regulator, ABPR (Jasco, BP-2080 Plus). Extraction conditions for the significant SFE parameters used were a pressure of 25 MPa, a flow rate of 5 mL min^{-1}, and a co-solvent ratio of 5% vol. A 5 g of the milled palm fruit peel sample was loaded into the extraction vessel (Jasco, EV-3-50-2), and the time was noted after the first released pressure purge from the ABPR was completed. Subsequently, the oil extract was collected in an amber glass bottle immersed in an ice bath for 30, 60, 90, 120 and 150 min. Finally, the collected extracts were diluted with 2.0 mL of n-hexane and stored in a refrigerator at 4°C for HPLC analysis. Consequently, percentage yields recovered extracts were determined using Equation (1).

$$X_0\,(\%) = \frac{\text{Weight of extract obtained}}{\text{Weight of milled sample used}} \times 100 \quad (1)$$

Kinetic Studies

In this work, Elovich's, Hyperbolic, and Pseudo second-order models were explored in studying the kinetics of SFE for the recovered palm fruit extracts.

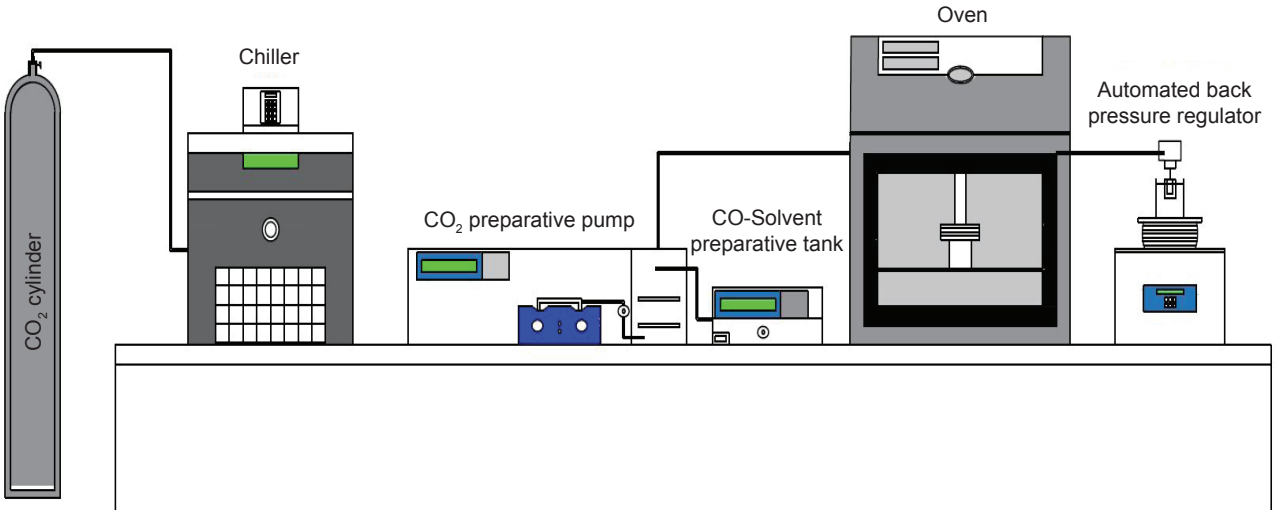


Figure 1. A schematic 2D diagram of SFE assembled setup.

TABLE 1. MODELS' DESCRIPTION FOR THE NON-LINEAR, LINEAR AND SLOPE-INTERCEPT FORMS

Kinetic models	Non-linear forms	Linear forms	Plots	Slopes	Intercepts
Elovich's model	$\frac{d\bar{q}}{dt} = \beta x + exp\,(-a\bar{q})$	$q = E_0 + E_1 \ln t$	q *vs* ln *t*	E_1	E_0
Hyperbolic model	$q = \frac{C_1 t}{1 + C_2 t}$	$\frac{1}{q} = \frac{1}{C_1} \times \frac{1}{t} + \frac{C_2}{C_1}$	$\frac{1}{q}$ *vs* $\frac{1}{t}$	$1/C_1$	C_2/C_1
Pseudo second-order model	$q = \frac{Cs^2Kt}{1 + CsKt}$	$\frac{t}{Cs} = \frac{1}{KCs^2} + \frac{1}{Cs} t$	$\frac{t}{Cs}$ *vs* *t*	$1/C_s$	$\frac{1}{KCs^2}$

Note: C_1, C_2 - concentrations of extraction rate at the beginning and maximum extraction yield respectively; *Cs* - extraction capacity (g L^{-1}); *K* - extraction rate constant (L g^{-1} min^{-1}); E_0, E_1 - Elovich's parameters; *q* - extraction yield; *t* - time (min).

Table 1 presents the various expressions for the linear and non-linear forms of the study models, as well as their plots, slopes, and intercepts.

Elovich's model. This model established that an increment in the extraction yield is proportionally linked to a reduction in the extraction rate. As shown in the linear expression of this model (Equation 2), a plot of $\bar{q}$ against ln *t* gives the slope and intercepts as E_1 and E_0 respectively.

$$\bar{q} = E_0 + E_1 \ln t \tag{2}$$

Hyperbolic model. Using the linear form of this model is presented in Equation (3), a plot of 1/q against 1/t accounts for $1/C_1$ and C_2/C_1 as slope and intercept respectively.

$$\frac{1}{q} = \frac{1}{C_1} \times \frac{1}{t} + \frac{C_2}{C_1} \tag{3}$$

where the extraction yield is represented by $\bar{q}$, C_1 and C_2 are the initial rate and final extraction yield; and *t* is the extraction time.

Pseudo second-order model. Equation (4) represents the linear form of this model. From that, a plot of t/Cs against *t*, is plausible, with 1/Cs and $1/KCs^2$ as slope and intercept respectively.

$$\frac{t}{Ct} = \frac{1}{KCs^2} + \frac{1}{Cs} t \tag{4}$$

where *Cs* represent the extraction capacity, *Ct* is the fraction of extract yield after time *t* and *K* stands for the extraction rate constant.

Error Analysis

Seven error functions were utilised as statistical methods to determine the accuracy of the studied models in fitting the experimental data. This selection of variables was based on previous similar studies conducted by Riahi *et al*. (2017). Equations (5)-(12) were employed to calculate these error parameters.

$$R^2 = \frac{\sum_{N=1}^{N} (\bar{q}_{exp} + \bar{q}_{cal})^2}{\sum_{N=1}^{N} (\bar{q}_{exp} - \bar{q}_{cal})^2} \tag{5}$$

$$RMS = \sqrt{\frac{1}{N}\sum_{i=1}^{N}\left(\frac{\bar{q}_{exp} - \bar{q}_{cal}}{\bar{q}_{exp}}\right)^2} \quad (6)$$

$$SEE = \sqrt{\frac{\sum(x\text{-}y)^2}{dt}} \quad (7)$$

$$ARE\ \% = \frac{100}{N} \times \sum\left[\frac{|\bar{q}_{exp} - \bar{q}_{cal}|}{\bar{q}_{exp}}\right] \quad (8)$$

$$SSE = \sum(\bar{q}_{exp} - \bar{q}_{cal})^2 \quad (9)$$

$$HYBRID\ \% = \frac{1}{N-P}\sum\left[\frac{\bar{q}_{exp} - \bar{q}_{cal}}{\bar{q}_{exp}}\right]100 \quad (10)$$

$$MPSED\ \% = \sqrt{\frac{\sum\left[\frac{\bar{q}_{exp} - \bar{q}_{cal}}{\bar{q}_{exp}}\right]^2}{N-P}} \times 100 \quad (11)$$

$$SD = \sqrt{\frac{1}{N-1}\sum_{i=1}^{N}\left(\left|\frac{\bar{q}_{exp\,(i)} - \bar{q}_{cal\,(i)}}{\bar{q}_{exp\,(i)}}\right| - ARRE\right)^2} \quad (12)$$

Thermodynamic Parameters

Variables such as ΔG, ΔH and ΔS were calculated and interpreted using Equations (13)-(17). For the other parameters, R represents the molar gas constant (8.314 J mol^{-1} K^{-1}), and T is the equilibrium temperature (Kelvin).

$$\Delta G = -RT ln\ K \quad (13)$$

$$ln\ K = \frac{\Delta G}{-RT} \quad (14)$$

$$ln\ K = -\frac{\Delta H}{RT} + \frac{\Delta S}{R} \quad (15)$$

$$ln\ K = -\frac{\Delta G}{RT} = \frac{-\Delta H}{RT} + \frac{\Delta S}{R} \quad (16)$$

$$\Delta G = \Delta H + T\Delta S \quad (17)$$

Statistical Analysis

The impact of temperature and extraction time on the rate of extract recovery was analysed using SPSS (Version 21) and determined based on F-values and *P*-values. ANOVA was used to compare the statistical difference between and within groups, and Tukey's post hoc HSD was used to calculate the minimum difference between group means.

RESULTS AND DISCUSSION

Extract Yield

This study found that extract yields were recovered at temperatures ranging from 40°C-80°C and extraction times from 30-150 min as shown in *Table 2*. The initial rate of extract recovery was low at all temperatures, but higher recoveries were seen with longer extraction time (150 min) across all temperatures. The highest and lowest yields were recovered at 40°C, 30 min, and 80°C, 150 min, at 2.61% and 3.95% respectively, indicating a positive relationship between increased time, temperature and extract recovery rate. Kinetically, a forward reaction is driving the recovery rate as yields increase linearly with rising temperature and increasing extraction time. This trend was previously reported by Mgoma *et al*. (2021) in their study of avocado oil extraction using the Soxhlet method. At the initial extraction (30 min), there was a 0.21% difference in yield between 40°C and 80°C, but a significantly higher difference of 0.74% was seen at the final extraction time of 150 min, implying that prolonging the extraction time leads to higher extract recovery. This observation was supported by the work of Baldino *et al*. (2018) and Mohammad and Arami, (2009), who found that longer extraction time leads to greater solubility and higher extract recovery due to increased interaction between the analyte and the extractive solvent (CO_2).

The rate and yield of palm oil extraction increase with temperature as shown in *Figure 2*. A 0.60% difference in yield was observed at the lowest temperature (40°C) between the initial (30 min) and final extraction time (150 min). At the optimum temperature (80°C) during the same time range, a 1.13% difference was obtained. The higher yields at higher temperatures are due to improved solute mass transfer, as supported by the theory of SFE (Mahmoodi *et al*., 2010; Souza *et al*., 2019). The extract yield of 2.61%-3.95% obtained in this work is considerably higher as per extract recovered from non-polar compounds using SCO_2 extraction (Bello *et al*., 2021; Silva *et al*., 2016). Perhaps, this must be connected to the greater molecular interactions between the polar compounds present in the palm fruit peel extracts (carotenoids) and the non-polar SCO_2, which utterly dissolves the compounds due to the similarity law of like dissolve-like since the carotenoids are non-polar (Garcia-Mendoza *et al*., 2015).

TABLE 2. RESULTS OF THE RECOVERED EXTRACTS AT DIFFERENT TEMPERATURES OVER TIME

	Temperature (°C)				
Time (min)	**40**	**50**	**60**	**70**	**80**
30	2.61	2.65	2.68	2.71	2.82
60	2.72	2.78	2.85	3.00	3.18
90	2.90	3.15	3.41	3.57	3.63
120	3.15	3.41	3.68	3.76	3.82
150	3.21	3.50	3.75	3.84	3.95

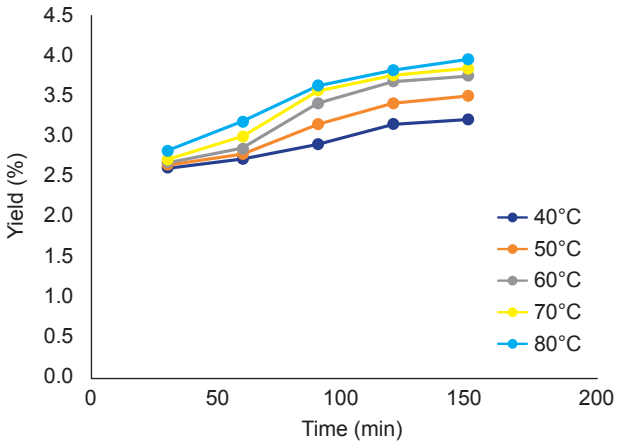


Figure 2. Impact of extraction time and temperature on the recovered oil extract yield.

Kinetic Analysis and Extent of the Models' Fitness

Table 3 presents the model's parameters and the various error estimates calculated using Equations (2)-(12). For the initial and equilibrium oil adsorbed concentrations (E_0 and E_1) of Elovich's model, E_0 decreases as the temperature increases while an increase over temperature rise was seen across the E_1 values except for a sharp decrease at maximum temperature (80°C). Similarly, there is a relative increase in the value of R^2, with the maximum (0.982) obtained at the highest temperature. This suggests that the model supported forward reaction considering the yield increment over temperature rise (Bello *et al*., 2023; Mahmoodi, 2014). However, the calculated R^2, C_1 and C_2 values of the Hyperbolic model show an irregular pattern, such that C_1 and C_2 decrease upon an increase in temperature except at the maximum temperature. This implies that the extraction rate at the initial and final stages of the process are not the same according to the model. For the pseudo-second-order model, the values for the extraction capacity, *Cs* increases as the temperature rises. This confirms that higher temperature resulted in greater extraction capacity due to improving solute mass transfer into the plant matrices. This observation was in close agreement with the findings reported by Gadkari and Balaramanl, (2017). Unlikely, the extraction rate constant, *K* values show an indefinite pattern across the temperatures. Therefore, the higher *K* value (0.0211) obtained at the lowest temperature (40°C), reflects that higher density and diffusion rate at low temperatures resulted in a higher extraction rate (Mahmoodi *et al*., 2019).

TABLE 3. MODELS' PARAMETERS AND ERROR ANALYSIS VALUES FOR THE STUDIED MODELS'

Temperature (°C)	**40**	**50**	**60**	**70**	**80**
Elovich's Model					
E_0	1.2230	0.6260	0.0720	0.0500	0.2830
E_1	0.3880	0.5670	0.7340	0.7630	0.7330
R^2	0.9110	0.9220	0.9190	0.9530	0.9820
RMS	0.0244	0.0332	0.0428	0.0310	0.0176
SEE	0.0282	0.0382	0.0505	0.0393	0.0231
ARE %	0.1029	0.0620	0.1010	0.0713	0.0405
SSE	0.0238	0.0438	0.0765	0.0462	0.0159
HYBRID %	0.1715	0.1034	0.1684	0.1189	0.0675
MPSED %	3.1516	4.2852	5.5238	4.0058	2.2729
SD	0.0021	0.0019	0.0030	0.0021	0.0008
Hyperbolic Model					
C_1 (min^{-1})	0.3897	0.2952	0.2455	0.2395	0.2635
C_2 (min^{-1})	0.1189	0.0812	0.0611	0.0570	0.0617
R^2	0.8000	0.8200	0.8370	0.9080	0.9460
RMS	0.0362	0.0470	0.0561	0.0418	0.0297
SEE	0.0423	0.0565	0.0687	0.0530	0.0400
ARE %	0.2112	0.0155	0.0475	0.0394	0.0195
SSE	0.0536	0.0958	0.1416	0.0843	0.0479
HYBRID %	0.3521	0.0259	0.0791	0.0656	0.0325
MPSED %	4.6422	6.0329	7.2187	5.3946	3.8283
SD	0.0063	0.0005	0.0014	0.0012	0.0006
Pseudo 2nd Order Model					
k ($L\ g^{-1}\ min^{-1}$)	0.0211	0.0133	0.0096	0.0101	0.0110
C_s ($g\ L^{-1}$)	3.4722	3.9216	4.3478	4.4248	4.4643
R^2	0.9950	0.9930	0.9900	0.9940	0.9970
RMS	0.0465	0.0549	0.0606	0.0444	0.0336
SEE	0.0509	0.0610	0.0687	0.0523	0.0408
ARE %	0.5170	0.3814	0.2251	0.1723	0.2806
SSE	0.0777	0.1117	0.1416	0.0822	0.0500
HYBRID %	0.8616	0.6357	0.3751	0.2871	0.4677
MPSED %	6.0014	7.0882	7.8239	5.7350	4.3375
SD	0.0103	0.0076	0.0045	0.0034	0.0056

Models Degree of Comparable Fitness

Figure 3a, *3b* and *3c* show the histograms for the degree of the comparable fitness of the tested models to the experimentally derived data of oil extract. The highest calculated yield of 3.96% and 3.17% was obtained by Elovich's model at 80°C and 40°C respectively after 150 min of extraction (*Figure 3a*). Also, at an initial extraction time of 30 min, the same model gave an extract yield of 2.78% and 2.54% at similar temperatures. Comparatively, at the initial extraction (30 min), it was observed that the difference between the model's calculated and the experimentally obtained yield at 80°C and 40°C are 0.04 (<5%) and 0.07 (>5%) respectively. However, at the final extraction time (150 min), the least difference was observed at 80°C and 40°C, corresponding to 0.01 (1%) and 0.04 (<5%) respectively. These insignificant differences obtained at the boundary temperatures over time indicate the suitability of this model in fitting the experimental data. Moreover, the correctness of the model was further attested by considering the higher average R^2 value of 0.9374 (close to unity) presented by the model (Riahi *et al*., 2017). For the Hyperbolic model (*Figure 3b*), the calculated model's yields were 3.86% and 3.10% after 150 min of extraction at 80°C and 40°C respectively. However, at the initial extraction time (30 min), the model's calculated yield was 2.77% and 2.56% obtained at 80°C and 40°C. The difference between the model calculated and the experimentally obtained yield at the two boundary temperatures (80°C and 40°C) are 0.09 (>5%) and 0.11 (>10%), at the extraction time of 150 min and 30 min respectively.

Unlike the other two models, a significant difference was observed between the experimental data obtained, and the calculated yield presented by the pseudo-second model (*Figure 3c*). However, at the initial time (30 min), a difference of 0.16 (>15%) and 0.22 (>20%) were recorded at the 80°C and 40°C respectively. On the other hand, a much lower difference of 0.02 and 0.03 (<5%) were recorded at 80°C and 40°C respectively after 150 min. Therefore, this wide variance indicates the non-suitability of this model in fitting the experimental data. Consequently, the results of the comparative analysis between the models' calculated and the experimental yields, aligned with that of the kinetic analysis of the error functions. Hence, Elovich's is the most suitable model that best fitted the experimental data owing to its lower error values and least significant difference between the model's calculated and experimental extract yield. This was followed by Hyperbolic and then Pseudo second order respectively.

As shown in *Table 4*, the average values of the statistical error functions, Elovich's model had the lowest average values of the calculated error functions. This was followed by Hyperbolic and then Pseudo 2nd order. However, the highest average R^2 values 0.9938, 0.9374 and 0.8622 were presented by Pseudo second order, Elovich's, and Hyperbolic respectively. This shows that Elovich's is the most suitable model that best fitted the kinetics data since it gave the lowest average values of the tested error parameters. This was followed by Hyperbolic and then Pseudo second order model as shown in *Table 4*. This kinetic pathway was similar to that reported by Bello *et al*. (2023), on the oil extraction and kinetics of banana peel.

Thermodynamic Analysis

The effect of heat energy changes otherwise called the thermodynamic effects associated with the extraction process was studied and the values of the relevant thermodynamic parameters are presented in *Table 5*. Equations (13) and (15), were used in determining the values of the various thermodynamic parameters namely ΔG, ΔH and ΔS. A plot of *ln* K against 1/T (*Figure 4*), produced a straight-line graph that accounts for the changes in enthalpy and entropy, ΔH and ΔS respectively. According to the results, a value of 53.50 K J mol^{-1} was obtained for ΔH. This positive value implies that the process releases heat to the surroundings (endothermic reaction), hence less energy is required to extract the oil from the milled palm fruit sample. Amarante *et al*. (2014) and Riahi *et al*. (2017) reported similar observations in the past following an oil extraction from castor cake and date palm fibres respectively. From the slope and intercept of the thermodynamic plot (*Figure 4*), a value of 0.138 J mol^{-1}K^{-1} was obtained for the ΔS. This positive ΔS value suggests that the extraction of the palm fruit peels reported in this work is a forward reaction. Perhaps, this is justified considering the symmetrical increase in the rate of extract recovery over temperature rise. Furthermore, the values for the ΔG calculated at both temperatures were negative (*Table 5*), indicating that the extraction proceeds independently without energy input from the external source, as such energy is released (Nasrollahi *et al*., 2018).

One-way ANOVA for the Effect of Temperature and Time on the Yield

Table 6 displays the results of ANOVA on the impact of temperature and extraction time on extract yield. The ANOVA found an increase in extract yield with temperature and time, leading to the rejection of the null hypothesis since

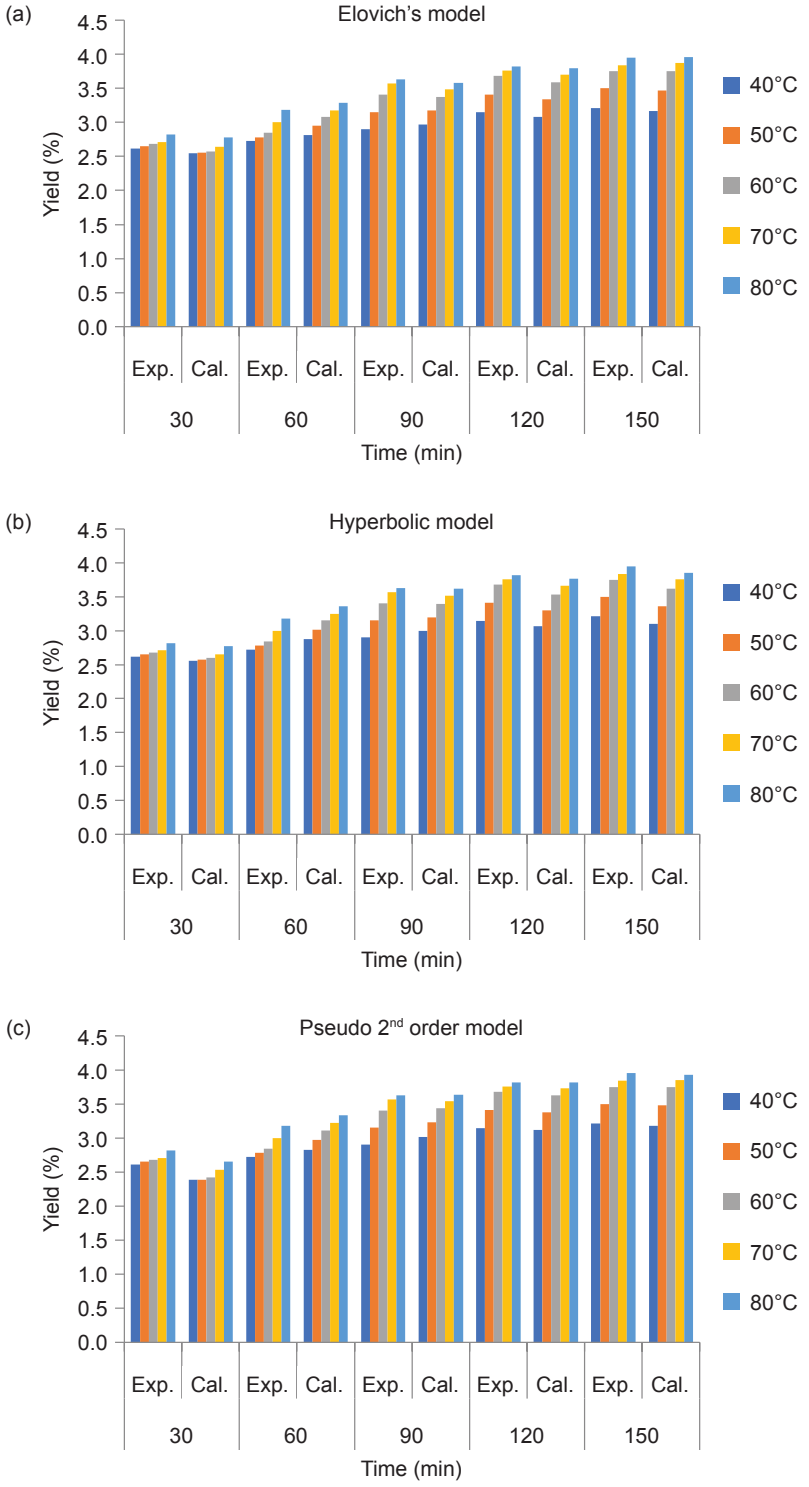


Figure 3. Comparative evaluation of the experimental and models calculated palm fruit extracts for (a) Elovich's, (b) Hyperbolic, and (c) Pseudo 2nd order at different temperatures.

TABLE 4. CALCULATED AVERAGE VALUES OF THE STUDIED ERROR FUNCTIONS

Models	RMS	SEE	ARE	SSE	HYBRID	MPSED	SD
Elovich's	**0.0298**	**0.0359**	0.0755	**0.0412**	0.1259	**3.8479**	**0.0019**
Hyperbolic	0.0422	0.0521	**0.0666**	0.0846	**0.1110**	5.4233	0.0020
Pseudo 2nd order	0.0480	0.0547	0.3153	0.0926	0.5254	6.1972	0.0063

Note: The lowest error values are in bold.

TABLE 5. THERMODYNAMIC PARAMETER FOR PALM FRUIT PEELS EXTRACTION

(K)	K	ΔH KJ mol^{-1}	ΔS KJ mol^{-1}	ΔG KJ mol^{-1}
313	7.86×10^{1}			-11.36
323	2.53×10^{0}			-8.67
333	9.02×10^{0}	53.50	0.138	-6.09
343	8.22×10^{0}			-6.01
353	7.84×10^{0}			-6.04

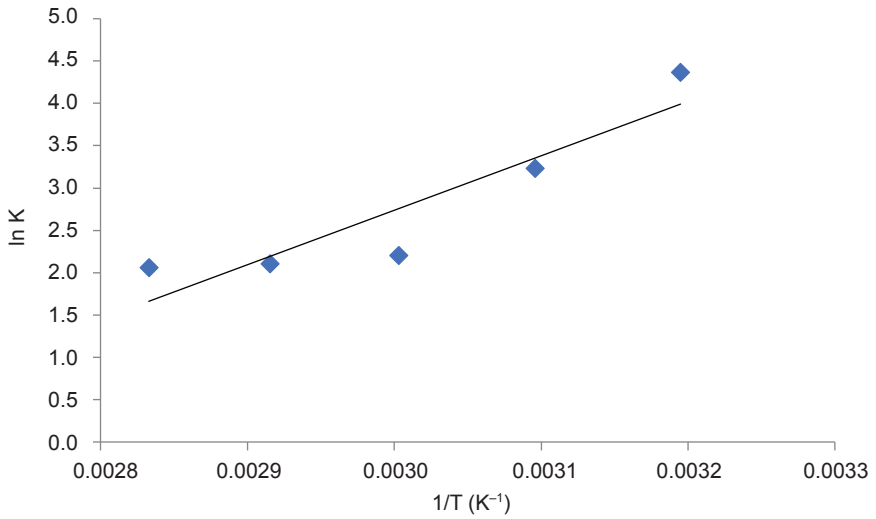


Figure 4. Plot of ln K against 1/T for palm fruit peels.

TABLE 6. ANOVA RESULT FOR THE EFFECT OF THE PROCESS PARAMETERS ON EXTRACT YIELD

Effect of temperature	Sum of squares	DF	Mean squares	F-values	*P*-values	Percentage contribution
Between groups	28.93	4	14.46	91.97	0.000	76.8
Within groups	2.75	25	0.10			
Total	31.68	29				
Effect of extraction time						
Between groups	3.61	4	0.2278	27.78	0.044	23.1
Within groups	1.20	25	0.0874			
Total	4.81	29				

both parameters had *P*-values less than 0.05, indicating statistical differences. To determine significant changes, Tukey's post hoc HSD analysis was performed, as shown in *Tables 7* and *8* for temperature and time respectively, revealing significant differences between performance means. The mean differences marked with an asterisk ($p<0.05$) were considered significant, while those without ($p\geq0.05$) were not. A similar trend was reported by Bello *et al*. (2023) in their study on banana peel extraction. The relative significance of the parameters was also evaluated at 95% confidence using F-values and *P*-values. Hence, the ANOVA results showed that temperature had a higher impact on the rate of extract recovery with an F-value of 91.97, compared to extraction time which had an F-value of 27.78. This means that temperature contributed 76.8% while extraction time contributed 23.1% to the rate of extract recovery. The results suggest that a higher temperature and shorter extraction time resulted in greater extract yield, as it improves solubility, mass transfer and diffusion (Senthilkumar *et al*., 2019). These findings are in line with the data presented in *Table 2*, which shows that higher temperatures result in increased extract recovery.

TABLE 7. EFFECT OF TEMPERATURE ON % YIELD ANALYSED USING TUKEY HSD

Temp. (I)	Temp. (I)	Mean diff (I-J)	Std. error	Sig.	95% confidence level	
					Lower bound	Upper bound
40°C	50°C	2.1920*	0.0882	0.000	2.0109	3.3731
	60°C	1.9080	0.0882	0.101	1.7269	2.0891
	70°C	-2.1920*	0.0882	0.003	-2.3731	-2.0109
	80°C	-0.2840	0.0882	0.052	-1.0199	1.5099
50°C	40°C	-1.9080*	0.0882	0.012	-3.7399	-0.7899
	60°C	0.2840	0.0882	0.050	-1.9099	0.6199
	70°C	2.2320*	0.0882	0.000	-1.9832	0.5466
	80°C	1.9900*	0.0882	0.001	0.7899	1.7399
60°C	40°C	-0.2420*	0.0882	0.000	-1.4349	1.0949
	50°C	-0.0933	0.0882	0.092	0.3660	1.1799
	70°C	-0.2033*	0.0882	0.011	-1.4766	-0.0699
	80°C	-0.3816*	0.0882	0.000	-1.6549	0.8916
70°C	40°C	0.0933*	0.0882	0.000	-1.70116	0.8449
	50°C	-0.1100*	0.0882	0.000	-1.1799	1.3666
	60°C	-0.0460*	0.0882	0.001	-1.9604	0.5170
	80°C	0.2500	0.0882	0.086	2.0787	0.3987
80°C	40°C	-0.8400	0.0882	0.061	-2.1654	0.3120
	50°C	0.9267*	0.0882	0.000	-0.5170	1.9604
	60°C	0.7217*	0.0882	0.000	0.9370	1.5404
	70°C	0.3016*	0.0882	0.000	1.4437	1.0337

Note: *The mean difference is significant at the 0.05 level.

TABLE 8. EFFECT OF TIME ON % YIELD ANALYSED USING TUKEY HSD

Time. (I)	Time. (I)	Mean diff (I-J)	Std. error	Sig.	95% confidence level	
					Lower bound	Upper bound
30 (min)	60 (min)	0.2050	0.6014	0.736	-1.3570	1.1204
	90 (min)	0.8400	0.6014	0.175	-1.4437	1.0337
	120 (min)	0.4200*	0.6014	0.003	-0.3897	2.0787
	150 (min)	0.1183	0.6014	0.846	-0.8187	1.6587
60 (min)	30 (min)	0.2450	0.6014	0.693	-3.7399	-0.7899
	90 (min)	-0.4750	0.6014	0.447	-1.9099	0.6199
	120 (min)	0.6450*	0.6014	0.000	-1.9832	0.5466
	150 (min)	0.7183	0.6014	0.304	-1.9099	0.6199
90 (min)	30 (min)	0.2450	0.6014	0.253	-1.9832	0.5466
	60 (min)	-0.4750*	0.6014	0.001	-0.5448	1.9849
	120 (min)	0.7200	0.6014	0.110	-0.7899	1.7399
	150 (min)	0.1700	0.6014	0.071	-1.4349	1.0949
120 (min)	30 (min)	0.6450	0.6014	0.160	-1.70116	0.8449
	60 (min)	0.1700*	0.6014	0.004	-1.1799	1.3666
	90 (min)	-0.0460*	0.6014	0.000	-1.9604	0.5170
	150 (min)	-0.7333	0.6014	0.086	2.0787	0.3987
150 (min)	30 (min)	0.9633	0.6014	0.129	-0.3016	2.2282
	60 (min)	0.7183*	0.6014	0.002	-0.5466	1.9832
	90 (min)	0.2433	0.6014	0.695	-1.0216	1.5082
	120 (min)	0.0733	0.6014	0.906	-1.1916	1.3382

Note: *The mean difference is significant at the 0.05 level.

CONCLUSION

This work reported the utilisation of a green extraction technique (SFE) to recover liquid extract from palm fruit peels, yielding 3.95% at the highest temperature with a prolonged extraction time. The increase in yield with rising temperature is due to increased diffusivity and solubilisation of the analyte from the plant matrix. The results of the kinetic analysis indicate that the Elovich model is the most suitable for the experimental data due to its lower error values and closest agreement with the experimental data. The Hyperbolic and Pseudo second order models were also evaluated. The significance of extraction time and temperature in improving the rate of extract recovery was confirmed by the ANOVA and Tukey's *post hoc* HSD analysis. Finally, the thermodynamic analysis showed that the extraction process was spontaneous, and that heat is released considering positive values and negative values.

ACKNOWLEDGEMENT

The financial support offered by the HICOE, Centre for Biofuel and Biochemical Research (CBBR), and Yayasan Universiti Teknologi Petronas (Cost Centre of 015MA0-052 and 015LC0-438) is gratefully acknowledged. The support from the Chemical Engineering Department, UTP, and the Centre Graduate Studies, CGS, through the HICoE award to CBBR is duly acknowledged.

REFERENCES

Aini, N; Bello, U; Sya, M and Ruslan, H (2022). The role of antioxidants in improving biodiesel's oxidative stability, poor cold flow properties, and the effects of the duo on engine performance: A review. *Heliyon, 8(7)*: e09846. DOI: 10.1016/j.heliyon.2022.e09846.

Amarante, R C A; Oliveira, P M; Schwantes, F K and Morón-Villarreyes, J A (2014). Oil extraction from castor cake using ethanol: Kinetics and thermodynamics. *Ind. Eng. Chem. Res.*, *53(16)*: 6824-6829. DOI: 10.1021/ie500508n.

Anuar, M A M; Amran, N A and Ruslan, M S H (2021). Optimization of progressive freezing for residual oil recovery from a palm oil-water mixture (POME Model). *ACS Omega*, *6(4)*: 2707-2716. DOI: 10.1021/acsomega.0c04897.

Baldino, L; Della Porta, G; Osseo, L S; Reverchon, E and Adami, R (2018). Concentrated oleuropein powder from olive leaves using alcoholic extraction and supercritical CO_2-assisted extraction. *J. Supercrit. Fluids*, *133(June 2017)*: 65-69. DOI: 10.1016/j.supflu.2017.09.026.

Bello, U; Aini, N and Samsuri, S (2023). Kinetics, thermodynamic studies, and parametric effects of supercritical CO_2 extraction of banana peel wastes. *Sustain. Chem. Pharm.*, *31(December 2022)*: 100912. DOI: 10.1016/j.scp.2022.100912.

Bello, U; Udofia, L; Ibitowa, O A; Abdullahi, A M; Sulaiman, I and Yahuza, K M (2021). Renewable energy transition: A panacea to the ravaging effects of climate change in Nigeria. *J. Geosci. Environ. Prot.*, *09(12)*: 151-167. DOI: 10.4236/gep.2021.912010.

Chai, Y H; Yusup, S; Ruslan, M S H and Chin, B L F (2020). Supercritical fluid extraction and solubilization of *Carica papaya* Linn. leave in a ternary system with CO_2 + ethanol solvents. *Chem. Eng. Res. Des.*, *156*: 31-42. DOI: 10.1016/j.cherd.2020.01.025.

Chanioti, S; Katsouli, M and Tzia, C (2021). Novel processes for the extraction of phenolic compounds from olive pomace and their protection by encapsulation. *Molecules*, *26(6)*: 56-65. DOI: 10.3390/molecules26061781.

da Silva, R P F F; Rocha-Santos, T A P and Duarte, A C (2016). Supercritical fluid extraction of bioactive compounds. *TrAC - Trends in Analytical Chemistry*, *76*: 40-51. DOI: 10.1016/j.trac.2015.11.013.

Gadkari, P V and Balaramanl, M (2017). Mass transfer and kinetic modelling of supercritical CO_2 extraction of fresh tea leaves (*Camellia sinensis* L.). *Braz. J. Chem. Eng.*, *34(3)*: 799-810. DOI: 10.1590/0104-6632.20170343s20150545.

Garcia-Mendoza, M P; Paula, J T; Paviani, L C; Cabral, F A and Martinez-Correa, H A (2015). Extracts from mango peel by-product obtained by supercritical CO_2 and pressurized solvent processes. *LWT*, *62(1)*: 131-137. DOI: 10.1016/j.lwt.2015.01.026.

Mahmoodi, N M (2014). Synthesis of magnetic carbon nanotube and photocatalytic dye degradation ability. *Environ Monit Assess (December)*. DOI: 10.1007/s10661-014-3805-7.

Mahmoodi, N M; Hayati, B; Arami, M and Mazaheri, F (2010). Single and binary system dye removal from colored textile wastewater by a dendrimer as a polymeric nanoarchitecture: Equilibrium and kinetics. *J. Chem. Eng. Data*, *78*: 4660-4668.

Mahmoodi, N M; Taghizadeh, A and Taghizadeh, M (2019). Surface modified montmorillonite with cationic surfactants: Preparation, characterization, and dye adsorption from aqueous solution. *J. Environ. Chem. Eng.*, *7(4)*: 103243. DOI: 10.1016/j.jece.2019.103243.

Meijaard, E; Brooks, T M; Carlson, K M; Slade, E M; Garcia-Ulloa, J; Gaveau, D L A; Lee, J S H; Santika, T; Juffe-Bignoli, D; Struebig, M J; Wich, S A; Ancrenaz, M; Koh, L P; Zamira, N; Abrams, J F; Prins, H H T; Sendashonga, C N; Murdiyarso, D; Furumo, P R and Sheil, D (2020). The environmental impacts of palm oil in context. *Nature Plants*, *6(12)*: 1418-1426. DOI: 10.1038/s41477-020-00813-w.

Mgoma, S T; Basitere, M and Mshayisa, V V (2021). Kinetics and thermodynamics of oil extraction from South Africa hass avocados using hexane as a solvent. *S. Afr. J. Chem. Eng.*, *37*: 244-251. DOI: 10.1016/j.sajce.2021.06.007.

Miękus, N; Iqbal, A; Marszałek, K; Puchalski, C and Świergiel, A (2019). Green chemistry extractions of carotenoids from *daucus carota* L.-Supercritical carbon dioxide and enzyme-assisted methods. *Molecules*, *24(23)*: 1-20. DOI: 10.3390/molecules24234339.

Mohajershojaei, K; Mahmoodi, N M and Khosravi, A (2015). Immobilization of laccase enzyme onto titania nanoparticle and decolorization of dyes from single and binary systems. *Biotechnol. Bioprocess Eng.*, *20(1)*: 109-116. DOI: 10.1007/s12257-014-0196-0.

Mohammad, N and Arami, M (2009). Numerical finite volume modeling of dye decolorization using immobilized titania nano-photocatalysis. *J. Chem. Eng.*, *146(2)*: 189-193. DOI: 10.1016/j.cej.2008.05.036.

Mohammad, N; Arami, M and Yousefi, N (2007). Nanophotocatalysis using immobilized titanium dioxide nanoparticle. Degradation and mineralization of water containing organic pollutant: A case study of Butachlor. *Mater. Res. Bull.*, *42*: 797-806. DOI: 10.1016/j.materresbull.2006.08.031.

Mohammad, N; Oveisi, M; Bakhtiari, M; Hayati, B; Akbar, A; Bagheri, A and Rahimi, S (2019). Environmentally friendly ultrasound-assisted synthesis of magnetic zeolitic imidazolate framework - Graphene oxide nanocomposites and pollutant removal from water. *J. Mole. Liq.*, *282*: 115-130. DOI: 10.1016/j.molliq.2019.02.139.

Nasrollahi, N; Aber, S; Vatanpour, V and Mohammad, N (2018). The effect of amine functionalization of CuO and ZnO nanoparticles used as additives on the morphology and the permeation properties of polyethersulfone ultrafiltration nanocomposite membranes. *Composites Part B*, *154(September)*: 388-409. DOI: 10.1016/j.compositesb.2018.09.027.

Patidar, K; Singathia, A; Vashishtha, M; Kumar Sangal, V and Upadhyaya, S (2022). Investigation of kinetic and thermodynamic parameters approaches to non-isothermal pyrolysis of mustard stalk using model-free and master plots methods. *Mater. Sci. Energy Technol.*, *5*: 6-14. DOI: 10.1016/j.mset.2021.11.001.

Riahi, K; Chaabane, S and Thayer, B Ben. (2017). A kinetic modeling study of phosphate adsorption onto *Phoenix dactylifera* L. date palm fibers in batch mode. *J. Saudi Chem. Soc.*, *21*: S143-S152. DOI: 10.1016/j.jscs.2013.11.007.

Rodrigues, J S; do Valle, C P; Uchoa, A F J; Ramos, D M; da Ponte, F A F; Rios, M A de S; de Queiroz Malveira, J and Pontes Silva Ricardo, N M (2020). Comparative study of synthetic and natural antioxidants on the oxidative stability of biodiesel from Tilapia oil. *Renew. Energ.*, *156(13)*: 1100-1106. DOI: 10.1016/j.renene.2020.04.153.

Ruslan, M S H; Idham, Z; Nian Yian, L; Ahmad Zaini, M A and Che Yunus, M A (2018). Effect of operating conditions on catechin extraction from betel nuts using supercritical CO_2-methanol extraction. *Sep. Sci. Technol. (Philadelphia)*, *53(4)*: 662-670. DOI: 10.1080/01496395.2017.1406947.

Senthilkumar, C; Krishnaraj, C; Sivakumar, P and Sircar, A (2019). Statistical optimization and kinetic study on biodiesel production from a potential non-edible bio-oil of wild radish. *Chem. Eng. Commun.*, *206(7)*: 909-918. DOI: 10.1080/00986445.2018.1538973.

Souza, M E A O; Mezzomo, N; Correa, L C; Lima, M S; Azevêdo, L C and Ferreira, S R S (2019). Recovery of antioxidant compounds from mango peel by green extraction processes. *Int. Food Res. J.*, *26(2)*: 1845-1859.

Valdivia-Rivera, S; Herrera-Pool, I E; Ayora-Talavera, T; Lizardi-Jiménez, M A; García-Cruz, U; Cuevas-Bernardino, J C; Cervantes-Uc, J M and Pacheco, N (2021). Kinetic, thermodynamic, physicochemical, and economical characterization of pectin from Mangifera indica L. cv. Haden residues. *Foods*, *10*(9). DOI: 10.3390/foods10092093.

Vélez-Erazo, E M; Pasquel-Reátegui, J L; Dorronsoro-Guerrero, O H and Martínez-Correa, H A (2021). Phenolics and carotenoids recovery from agroindustrial mango waste using microwave-assisted extraction: Extraction and modeling. *J. Food Process Eng.*, *44(9)*. DOI: 10.1111/jfpe.13774.

Yang, G; Zhao, Y; Feng, N; Zhang, Y; Liu, Y and Dang, B (2015). Improved dissolution and bioavailability of silymarin delivered by a solid dispersion prepared using supercritical fluids. *Asian J. Pharm. Sci.*, *10(3)*: 194-202. DOI: 10.1016/j.ajps.2014.12.001.

Journal of Oil Palm Research Vol. 35 (4) December 2023 p. 725-737
DOI: https://doi.org/10.21894/jopr.2022.0064

SYNTHESIS AND PHYSICOCHEMICAL PROPERTIES OF ESTOLIDE ESTER AND AMIDE MADE FROM USED COOKING OIL AS BIO-LUBRICANT

SENG SOI HOONG[1]*; MOHD ZAN ARNIZA[1]; NEK MAT DIN NIK SITI MARIAM[1]; ABU HASSAN NOOR ARMYLISAS[1]; SOOK WAH TANG[1]; TUAN ISMAIL TUAN NOOR MAZNEE[1] and SHOOT KIAN YEONG[1]

ABSTRACT

Palm-based used cooking oil (UCO) is an inexpensive material that could be used as a bio-lubricant. However, its use as a bio-lubricant is limited by its inferior cold flow and oxidation stability properties. This study shows an approach to make bio-lubricant base oil from UCO that displayed good cold flow and oxidation stability. UCO was saponified and hydrolysed to yield a mixture of fatty acids, which was subsequently reacted with hydrogen peroxide and acetic acid to generate an estolide mixture with hydroxyl and carboxylic acid groups. The hydroxyl groups of the estolide mixture were end-capped with lauric acid, while its carboxylic acid groups were converted to either ester or amide functionality with 2-ethylhexanol and dibutylamine, respectively. Physicochemical properties evaluation revealed that the saturated branched structure of estolide ester and amide contributed to improved pour point (-12°C) and better oxidation stability up to 200°C as compared to UCO. Additionally, the estolide ester and amide exhibited a better viscosity index and pour point than a commercial mineral oil lubricant. The estolide ester can be classified as ISO VG 68 base oil, while the estolide amide displayed a higher viscosity grade (ISO VG 150) due to the presence of dibutylamide moiety.

Keywords: esterification, kinematic viscosity, oxidation stability, palm oil, pour point.

Received: 30 March 2022; **Accepted:** 29 August 2022; **Published online:** 3 October 2022.

INTRODUCTION

The global consumption of oils and fats in 2021 was estimated to be about 209 million tonnes and palm oil was the most consumed oil at about 73 million tonnes, in which 90% of palm oil was consumed as food while the remaining 10% was used for non-food purposes (Shahbandeh, 2022). One of the many ways to consume palm oil is to use it as frying oil for food preparation (Parveez *et al*., 2021), but after a certain duration, the frying oil is unfit for that purpose and will be discarded as used cooking oil (UCO). A study estimated that 26% of globally consumed oils could end up as UCO, which could amount to 54 million tonnes based on 208 million tonnes of consumed oils in 2020 (Orjuela and Clark, 2020).

In consideration of the massive amount of UCO, proper disposal of UCO is crucial for many countries as a large portion of UCO was deliberately released into the environment, which creates many ecological problems (Ahmed and Hossain, 2020). Therefore, it is important to find uses for UCO to resolve problems associated with the disposal of UCO. Additionally, the use of UCO to make other products also conform to the principles of circular economy, which is gaining wider acceptance than the conventional linear economy (Orjuela and Clark, 2020).

Many scientists have evaluated UCO as feedstock to produce various products such as biodiesel (Milano *et al*., 2022), surfactants and bio-lubricant (Orjuela and Clark, 2020). Among these potential applications, bio-lubricant is a value-added product that represents the circular economy and the idea of generating wealth from waste. Furthermore, the relatively inexpensive UCO could help to mitigate the issue of high material costs associated with bio-lubricant, which is a

[1] Malaysian Palm Oil Board,
6 Persiaran Institusi, Bandar Baru Bangi,
43000 Kajang, Selangor, Malaysia.

* *Corresponding author e-mail: sengsoi@mpob.gov.my*

major barrier to market acceptance of bio-lubricant (Zhang *et al*., 2020).

The properties of a bio-lubricant made from UCO are very dependent on the fatty acid composition of UCO and the chemical process employed to modify the UCO. Specifically, UCO with high content of saturated fatty acids such as palmitic acid will generate bio-lubricant with undesirable cold flow properties but satisfactory oxidation stability (Heikal *et al*., 2017). Conversely, bio-lubricant made with UCO that is rich in unsaturated fatty acids will exhibit good cold flow properties but inferior oxidation stability due to the presence of the alkene group (Li and Wang, 2015).

Hence, chemical modification conducted on UCO is designed to overcome drawbacks related to its chemical structure. One of the most common methods employed to modify UCO is transesterification with trimethylolpropane, which converts UCO to polyol esters that enhance the cold flow properties of resultant polyol esters. For example, Wang *et al*. (2014) reported a process that converted a UCO rich in oleic acid to trimethylolpropane esters, which displayed similar cold flow properties in comparison with ISO VG32 mineral oil-based lubricant. Nevertheless, the prepared polyol esters have alkene groups that are susceptible to oxidation degradation, which will reduce the service life of the resultant lubricants. Hence, it will be advantageous to prepare bio-lubricant from UCO that has a minimal alkene group.

A prominent method to convert vegetable oils into bio-lubricants with minimal alkene group is through the formation of estolide (Isbell, 2011; Salimon *et al*., 2012). Generally, estolide is prepared from unsaturated fatty acids such as oleic acid through a reaction with strong acids. Cermak *et al*. (2015) reported that a mixture of saturated fatty acids and oleic acid was converted to estolide in the presence of perchloric acid. Subsequently, the prepared estolide was reacted with a branched alcohol that yielded estolide ester, which showed excellent cold flow properties and acceptable oxidation stability. Nonetheless, the use of perchloric acid poses safety hazards to the community because it is known to form an explosive mixture in addition to its corrosive nature and should be substituted with a less hazardous material whenever possible (Schilt, 1979).

Alternatively, we have recently reported a synthetic method to make polyhydroxy estolide (PE) from oleic acid through a reaction with hydrogen peroxide and acetic acid, which is relatively safer in comparison with the perchloric acid method (Hoong *et al*., 2021). Then, the prepared PE was further converted to yield estolide ester and amide, which exhibited properties comparable to commercial samples in terms of pour point, oxidation stability, viscosity index and anti-wear (Hoong *et al*., 2020). Additionally, the estolide ester and amide were found to be readily biodegradable, which indicated that the prepared estolide ester and amide have good potential to be used as environment-friendly lubricant base oils (Hoong *et al*., 2020). These positive results encourage further evaluation of this method on cheaper feedstocks such as palm-based UCO.

To the best of the author's knowledge, palm-based UCO has not been evaluated as feedstock for making estolide ester, albeit it is abundantly available. This could be due to the high content of saturated fatty acids in palm-based UCO that would contribute to inferior cold flow properties of the resultant lubricant, and hence discourage the evaluation of palm-based UCO as feedstock. Nonetheless, it will be advantageous to produce a bio-lubricant from palm-based UCO that exhibits properties comparable to commercial lubricants. Therefore, this article reports the synthesis of PE from palm-based UCO through reaction with hydrogen peroxide and acetic acid. Subsequently, the prepared PE was converted to estolide ester and amide which exhibited properties comparable to commercial lubricant. The results of this article will help to establish a safe and feasible method to produce bio-lubricant from palm-based UCO.

MATERIALS AND METHODS

Materials

Used cooking oil was obtained from a local restaurant located in Kajang, Selangor, Malaysia. Fresh cooking oil (Alif brand, Sime Darby Oils Trading Sdn. Bhd.) was purchased from a local grocery store. Sodium hydroxide (98%), phosphoric acid (85%), hydrogen peroxide (50% in H_2O), acetic acid glacial (99%), lauric acid (98%), dibutylamine (99%) and 2-ethylhexanol (99%) were purchased from Sigma Aldrich (St Louis, MO, USA). All acquired chemicals were used without further purification unless otherwise stated.

Characterisation Methods

All measurements were performed in triplicate and data were reported as the mean ± standard deviation. Gas chromatography (GC) analysis was conducted using Agilent 7890B GC System equipped with Agilent J&W HP-88 (60 m x 0.25 mm x 0.2 μm) capillary column and flame ionisation detector. Fatty acid methyl esters were prepared from UCO according to AOCS's official method Ce 2-66 (AOCS, 2009). Temperature programme used for the GC analysis: oven temperature, 150°C; initial temperature, 150°C; heating rate at 3°C min^{-1}; final temperature, 210°C; injector temperature, 250°C and

detector temperature, 250°C. Helium was supplied at a rate of 0.8 mL min^{-1}. Fatty acid methyl esters solution (1 µL) was injected into the GC system.

FTIR spectra were recorded on a Perkin-Elmer Spectrum100 FTIR spectrometer. Samples were analysed as a thin film over a diamond attenuated total reflectance (ATR) top plate. Spectra were recorded in a range of 650-4000 cm^{-1} and the average value of eight scans at 4 cm^{-1} resolution was recorded for each sample.

Proton (^{1}H) and carbon (^{13}C) nuclear magnetic resonance (NMR) spectra were acquired on JOEL JNM-ECZ600R at 600 MHz and 150 MHz, respectively at 25°C. Samples were dissolved in deuterated NMR solvents with approximately 10% w/v solution. Chemical shifts were referenced to internal standard tetramethylsilane (TMS).

Gel permeation chromatography (GPC) was performed with a Polymer Laboratories PL-GPC 50 Plus equipped with a combined detector of differential refractive index (DRI)/viscometer. The sample (2 mg mL^{-1}) was dissolved in tetrahydrofuran (THF) and was analysed using a set of Phenogel columns that measure molecular weight in the range of 10^{2}-10^{6} Da. The sample was eluted in THF at a flow rate of 1 mL min^{-1}. The GPC was calibrated using polystyrene standards with a range from 162 to 1 x 10^{5} Da.

Wet chemical analysis was performed in accordance with the AOCS official methods (AOCS, 2009): Acid value (AV), Te 1a-64; hydroxyl value (OHV), Cd 13-60; iodine value (IV), Cd 1d-92; saponification value (Sap V), Cd 3-25; oxirane oxygen content (OOC), Cd 9-57.

Kinematic viscosity measurements were carried out in accordance with ASTM D445 standard method at 40°C and 100°C using calibrated Ubbellohde viscometer tubes and a Normalab NVB Classic viscosity bath with a constant temperature. The viscosity index was calculated in accordance with the standard method ASTM D2270-93.

Pour point and cloud point measurements were conducted in accordance with standard methods ASTM D97 and ASTM D2500, respectively. Measurements were carried out using a Normalab CPP Classic test cabinet with integrated cooling.

The oxidation onset temperature (OOT) analysis was conducted in accordance with the standard method ASTM E2009 using a DSC Q20P thermal analyser equipped with a Tzero pressure DSC cell acquired from TA Instruments.

The anti-wear properties of samples were evaluated in accordance with the ASTM 4172 (Four-ball method). The test was carried out using a four-ball tester TR-30L made by DUCOM Instrument, India. The test balls with product code RB-12.7/G20W were acquired from SKF Malaysia Sdn. Bhd.

Saponification of Used Cooking Oil (UCO) and Hydrolysis of Soap

Suspended particles in UCO were removed by filtration through a normal sieve. The filtered UCO (1200 g) was poured into a 10 L reactor equipped with a motor stirrer. The UCO was heated to 80°C and sodium hydroxide solution (3 M, 2000 mL) was added to the UCO. The mixture was stirred vigorously (300 rpm) and heated at 80°C. After 4 hr of reaction, phosphoric acid solution (4 M, 2000 mL) was added, and the reaction was continued for another 2 hr. Next, the reaction mixture was left to separate into two layers. The aqueous layer was discarded, and the organic layer was washed twice with deionised water (1500 mL). Thereafter, the organic layer was dried over anhydrous $MgSO_4$ to yield a mixture of fatty acids (1021 g, 95% yield).

Synthesis of Estolide Mixture from UCO-based Fatty Acids Mixture

The fatty acids mixture prepared from UCO (500 g) and acetic acid glacial (66 g) were charged into a 2 L reactor equipped with a motor stirrer. The reaction mixture was heated to 80°C and then hydrogen peroxide (190 mL) was added dropwise. The reaction mixture was stirred vigorously (300 rpm) and heated at 80°C for 8 hr. Thereafter, the reaction mixture was left to separate into two layers and the aqueous layer was discarded. The organic layer was washed twice with deionised water (250 mL). The organic layer was then dried over anhydrous $MgSO_4$ to yield a solid labelled as estolide mixture (491 g, 95% yield).

Synthesis of Lauric Acid-capped Estolide (LaE)

Estolide mixture (450 g, 0.955 mole of OH, OHV = 119 mg KOH g^{-1}) and lauric acid (68 g, 0.34 mole) were charged into a reaction flask equipped with a magnetic stirrer and distillation apparatus. The reaction mixture was stirred and heated at 200°C for 8 hr. Subsequently, the product was diluted with ethyl acetate (400 mL) after it was cooled to room temperature and was dried over anhydrous $MgSO_4$. The solvent was removed to yield a viscous yellowish liquid labelled as lauric acid-capped estolide (485 g, 97% yield).

Synthesis of 2-ethylhexyl Ester of Lauric Acid-capped Estolide (2EHLaE)

Lauric acid-capped estolide (200 g, 0.32 mole of CO_2H, AV= 89 mg KOH g^{-1}) and 2-ethylhexanol (2EH) (90 g, 0.69 mole) were charged into a reaction flask equipped with a magnetic stirrer and Dean-Stark apparatus. The mixture was stirred and heated to 200°C for 10 hr. Thereafter, excess

2-ethylhexanol was removed from the product by vacuum distillation. Then, the product was diluted with ethyl acetate (200 mL) and dried over anhydrous $MgSO_4$. The solvent was removed to yield a viscous yellowish liquid labelled as 2-ethylhexyl ester of lauric acid-capped estolide (229 g, 97% yield).

Synthesis of Dibutylamide of Lauric Acid-capped Estolide (DBALaE)

Lauric acid-capped estolide (200 g, 0.32 mole of CO_2H, AV= 89 mg KOH g^{-1}) and dibutylamine (DBA) (83 g, 0.64 mole) were charged into a reaction flask equipped with a magnetic stirrer and Dean-Stark apparatus. The mixture was stirred and heated to 200°C for 16 hr. Subsequently, excess dibutylamine was removed from the product by vacuum distillation. Thereafter, the product was diluted with ethyl acetate (200 mL) and dried over anhydrous $MgSO_4$. The solvent was removed to yield a viscous yellowish liquid labelled as dibutylamide of lauric acid-capped estolide (225 g, 95% yield).

RESULTS AND DISCUSSION

Characterisation of Used Cooking Oil

The palm-based UCO was analysed using gas chromatography to determine its fatty acid composition (FAC) and it was also subjected to wet chemistry analyses to ascertain a few properties. The properties of UCO are listed in *Table 1* together with local fresh cooking oil for comparison purposes. Fresh cooking oil is a refined, bleached and deodorised palm olein (RBDPOo), which is a typical cooking oil used in Malaysia for food preparation that would eventually end up as UCO.

Referring to *Table 1*, the acid value (AV) of UCO (5.82 mg KOH g^{-1}) was significantly higher than AV of fresh cooking oil (0.17 mg KOH g^{-1}) due to the hydrolysis of palm olein's triglycerides molecules that occurred during the food frying process, which generated free fatty acids that contributed to the observed high AV of UCO (Lam *et al*., 2010). The AV of UCO would vary depending on the duration the cooking oil is used as a medium for the food frying process and the type of food preparation. A typical range of AV of palm olein-based UCO would be between 2 to 21 mg KOH g^{-1} as reported in the literature (Cheah *et al*., 2016; Loh *et al*., 2006).

The iodine value (IV) analysis quantifies the amount of alkene group in vegetable oil, in which a higher IV denotes a higher amount of alkene group in the vegetable oil. Results from *Table 1* show that the IV of UCO was slightly lower than fresh cooking oil due to oxidation of the alkene group by molecular oxygen during the food frying process (Kulkarni and Dalai, 2006). Nevertheless, the IV of UCO was found acceptable as feedstock for making estolide because it had an adequate amount of alkene group that can be modified to generate estolide.

TABLE 1. PROPERTIES OF FRESH COOKING OIL AND USED COOKING OIL

Analysis	Unit	Fresh cooking oil	Used cooking oil
Acid value	mg KOH g^{-1}	0.17 ± 0.05	5.82 ± 0.05
Iodine value	g I_2 100 g^{-1}	58.90 ± 0.40	54.60 ± 0.30
Moisture content	wt%	0.05 ± 0.01	0.30 ± 0.03
Saponification value	mg KOH g^{-1}	195.20 ± 0.90	203.00 ± 1.20
Fatty Acid Composition			
Lauric acid, C12:0	wt%	0.20 ± 0.01	0.20 ± 0.01
Myristic acid, C14:0	wt%	0.90 ± 0.02	1.00 ± 0.03
Palmitic acid, C16:0	wt%	36.30 ± 0.40	37.30 ± 0.40
Palmitoleic acid, C16:1	wt%	0.20 ± 0.01	0.20 ± 0.01
Margaric acid, C17:0	wt%	ND*	0.4 ± 0.05
Stearic acid, C18:0	wt%	5.70 ± 0.20	6.20 ± 0.30
Oleic acid, C18:1	wt%	44.80 ± 0.50	43.90 ± 0.60
Linoleic acid, C18:2	wt%	11.10 ± 0.30	10.20 ± 0.30
Linolenic acid, C18:3	wt%	0.20 ± 0.02	0.10 ± 0.01
Arachidic acid, C20:0	wt%	0.30 ± 0.01	0.30 ± 0.02
Eicosenoic acid, C20:1	wt%	0.20 ± 0.02	0.10 ± 0.01
Behenic acid, C22:0	wt%	0.10 ± 0.01	0.10 ± 0.02

Note: *ND - not detected.

The FAC analysis revealed that the food frying process had increased the amount of saturated fatty acid in UCO at the expense of unsaturated fatty acids such as oleic acid due to oxidation reaction on alkene groups of cooking oil that resulted in conversion to a saturated moiety. Additionally, the FAC analysis also detected a small amount of margaric acid in UCO, which did not originate from RBDPOo but most likely originated from animal fat introduced into UCO during the food frying process. Nonetheless, the small amount of margaric acid has an insignificant impact on the performance of the targeted bio-lubricant. Overall, the results of analyses conducted on UCO suggested that the palm-based UCO is suitable to be used as feedstock to produce estolide.

Preparation of UCO-based Fatty Acids Mixture

The UCO was saponified with excess sodium hydroxide solution to yield soap and glycerol. Subsequently, the soap was hydrolysed with phosphoric acid to generate a mixture of fatty acids. Results of the analyses showed that the mixture of fatty acids had an IV (54 g I_2 100 g^{-1}) like UCO and an AV of 202 mg KOH g^{-1}. Additionally, the mixture of fatty acids had a similar FAC in comparison with UCO, which indicated that the saponification of UCO and hydrolysis of soap did not change the FAC of UCO as expected.

The subsequent synthesis of estolide from the UCO-based fatty acids mixture is dependent on the alkene groups of the fatty acids mixture as chemical modification will occur on the alkene group and eventually affects the physicochemical properties of the resultant bio-lubricant. The FAC analysis revealed that the fatty acids mixture had about 54% of unsaturated fatty acids, in which oleic and linoleic acid were the major components. The level of unsaturated fatty acids found in the fatty acid mixture is considered sufficient to provide an adequate amount of alkene group for making estolide.

Synthesis of Estolide Mixture from UCO-based Fatty Acids Mixture

The prepared UCO-based fatty acids mixture was reacted with a relatively safe oxidant namely hydrogen peroxide (H_2O_2) and acetic acid to yield an estolide mixture, as shown in *Figure 1*. During the reaction, H_2O_2 reacted with acetic acid, which converted it into a peroxy acid. The generated peroxy acid eventually reacted with alkene groups of fatty acids mixture and transformed the alkene group into an epoxide group. Subsequently, the epoxide groups of epoxidised fatty acids mixture were ring-opened by nucleophiles presence in the reaction mixture, namely the carboxylic acid group of fatty acids and acetic acid along with water molecule.

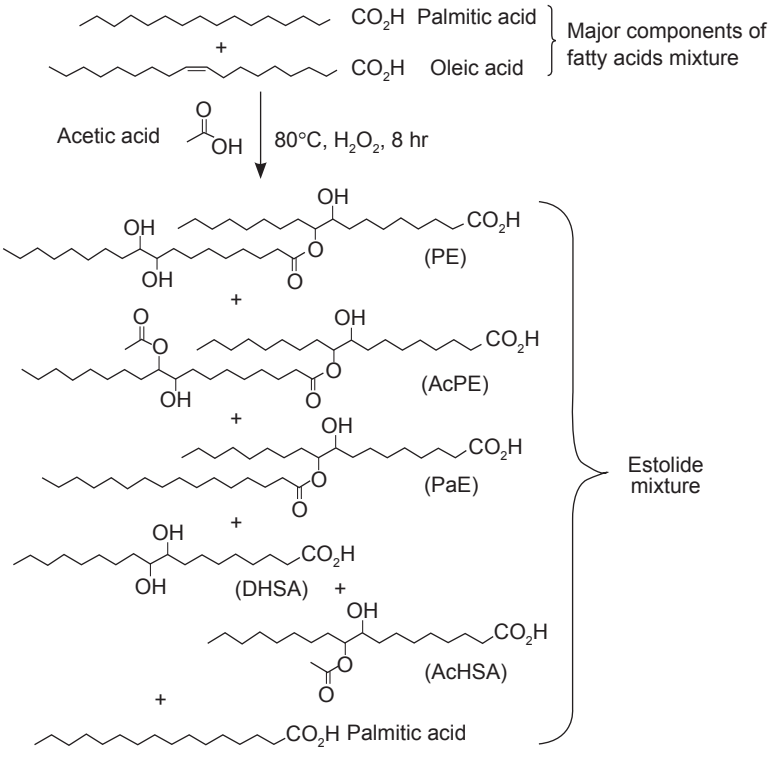


Figure 1. Synthesis of estolide mixture from UCO-based fatty acids mixture.

As a result, the epoxidation and epoxide ring-opening reactions performed on fatty acids mixture yielded a blend of compounds collectively known as estolide mixture, which comprised polyhydroxy estolide (PE), acetylated polyhydroxy estolide (AcPE), palmitic acid-capped estolide (PaE), 9,10-dihydroxystearic acid (DHSA), acetylated hydroxystearic acid (AcHSA) and unreacted saturated fatty acids such as palmitic acid.

Palmitic acid is one of the nucleophiles that can ring-open the epoxide group, which produced the compound PaE. Likewise, AcHSA and DHSA were generated from epoxide ring-opening by acetic acid and water, respectively. Meanwhile, the same epoxide ring-opening reaction with oleic acid yielded estolide with alkene group that can be further epoxidised and subsequently ring-opened with either acetic acid or water to yield AcPE and PE, respectively.

The progress of the reaction was monitored through oxirane oxygen content (OOC) analysis as shown in *Figure* 2. The OOC values increased in the first 3 hr of the reaction to a maximum of 0.81% and then gradually reduced to below 0.20% as the reaction progressed further. The OOC data suggested that epoxidation and epoxide ring-opening reactions occurred concurrently, in which the newly formed epoxide group was rapidly ring-opened by nucleophiles and this prohibited the OOC value from reaching the maximum theoretical value of 3.37%.

The conversion of the alkene group can be measured by using IV analysis, which revealed a conversion of 96% was achieved as the IV of fatty acid mixtures was reduced from an initial value of 54 g I_2 100 g^{-1} to less than 2 g I_2 100 g^{-1}. Additionally, the AV of the fatty acids mixture was reduced from 202 mg KOH g^{-1} to 152 mg KOH g^{-1}, which suggested that carboxylic acid groups of the fatty acids mixture were involved in the epoxide ring-opening reaction that resulted in the formation of estolide with hydroxyl functionality.

This idea is supported by ^{1}H NMR analysis of the estolide mixture as shown in *Figure 3a*, which exhibited a peak at 4.80 ppm that correlated with the methine proton linked to an ester group. Further analysis with ^{1}H-^{1}H COSY NMR showed that the methine proton peak at 4.80 ppm correlated with another methine proton of a hydroxyl group detected at 3.56 ppm, which indicated that the hydroxyl group was adjacent to the ester group due to epoxide ring-opening by a carboxylic acid group of fatty acid that formed the ester linkage of estolide's molecular structure. The GPC analysis (*Figure 4a*) revealed that the estolide mixture contained about 60% of estolides, which included PE, AcPE and PaE, with an average molecular weight of 950 Da. The other 40% of the estolide mixture comprised monomeric compounds AcHSA, DHSA and unreacted fatty acids, with an average molecular weight of 370 Da. Overall, the average molecular weight of the estolide mixture was about 740 Da.

Synthesis of LaE

Salimon *et al*. (2011) disclosed that lubricant base oils without a hydroxyl group achieved higher oxidation stability than those with a hydroxyl group.

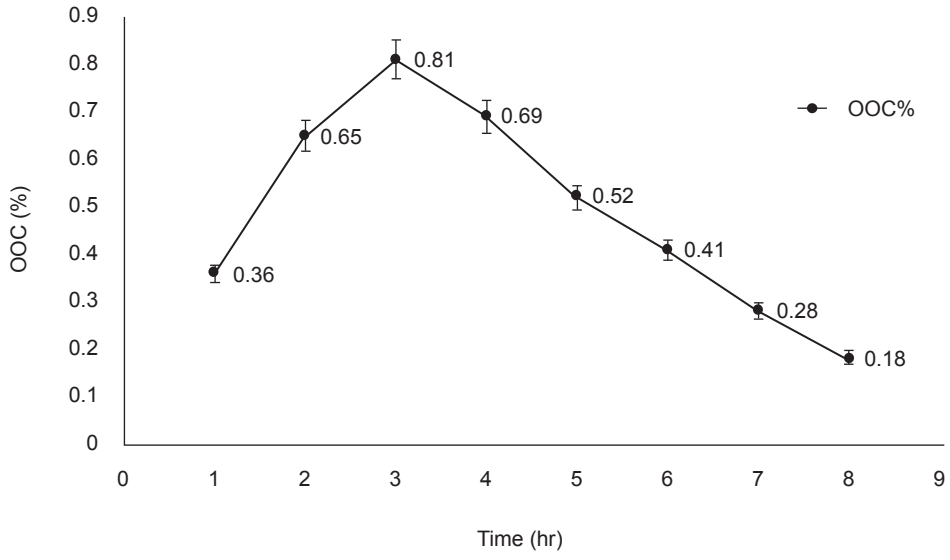


Figure 2. Oxirane oxygen content (OOC) of reaction mixture against time.

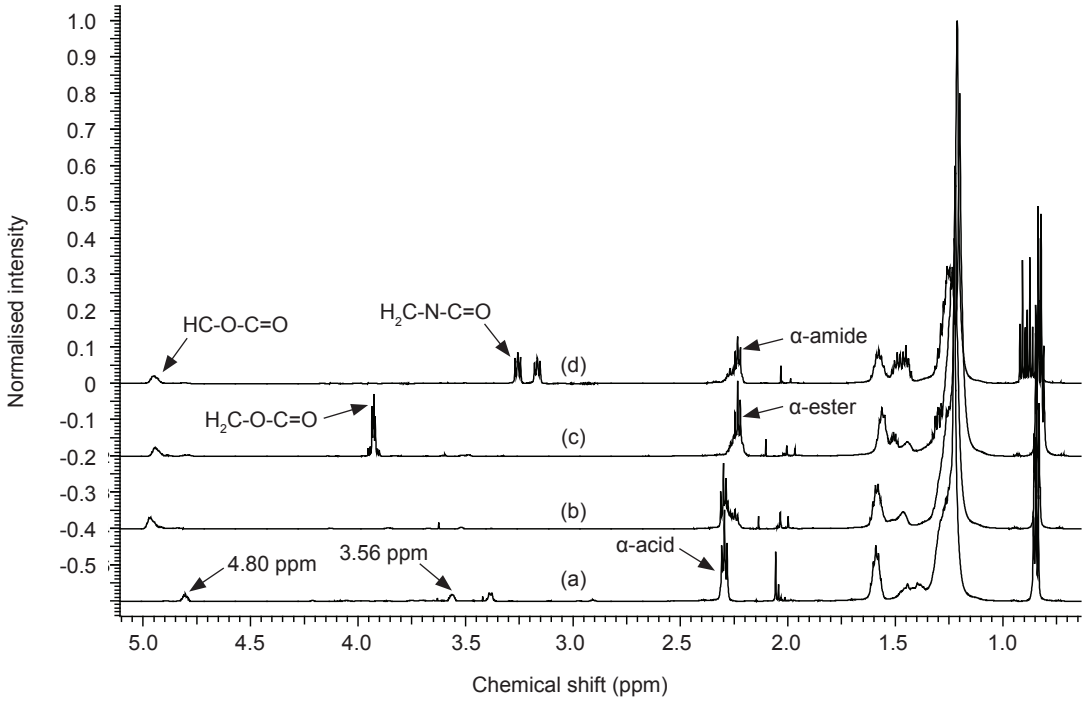


Figure 3. [1]H NMR spectrum of (a) estolide mixture, (b) lauric acid-capped estolide (LaE), (c) estolide ester (2EHLaE) and (d) estolide amide (DBALaE).

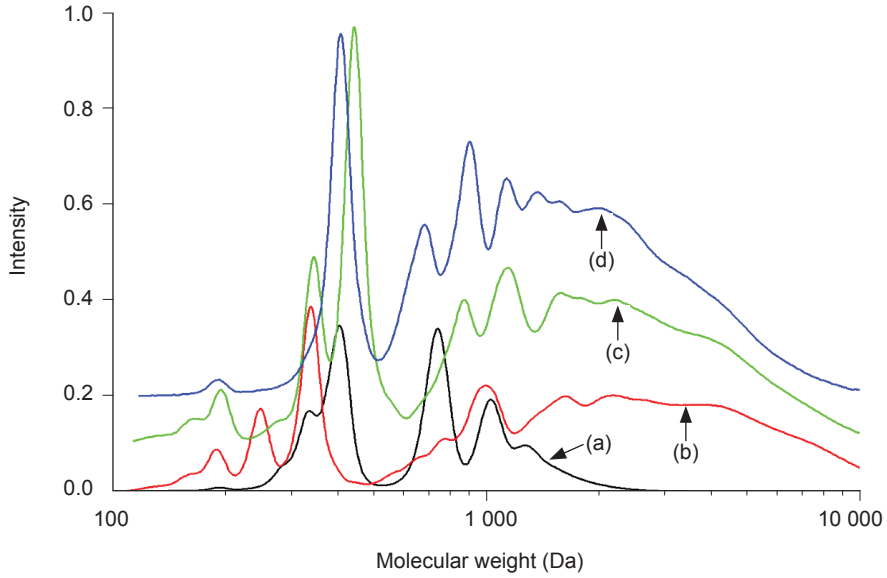


Figure 4. GPC chromatogram of (a) estolide mixture, (b) lauric acid-capped estolide (LaE), (c) estolide ester (2EHLaE) and (d) estolide amide (DBALaE).

Hence, the estolide mixture was self-esterified in combination with lauric acid (*Figure* 5) to transform hydroxyl groups of the estolide mixture into ester groups to attain better oxidation stability. The selection of lauric acid to end-cap the hydroxyl group was based on a study reported by Isbell (2011), which revealed that lubricant base oils made with lauric acid exhibited good cold flow properties and oxidation stability.

The amount of lauric acid used in the reaction varied from 15% to 30% (w/w) based on the amount of estolide mixture. Hydroxyl value (OHV) analysis was performed on the product and revealed that the reaction conducted with 15% of lauric acid was sufficient to convert all hydroxyl groups to ester functionality as indicated by OHV of the LaE, which was below 5 mg KOH g^{-1}. When the same reaction was conducted with

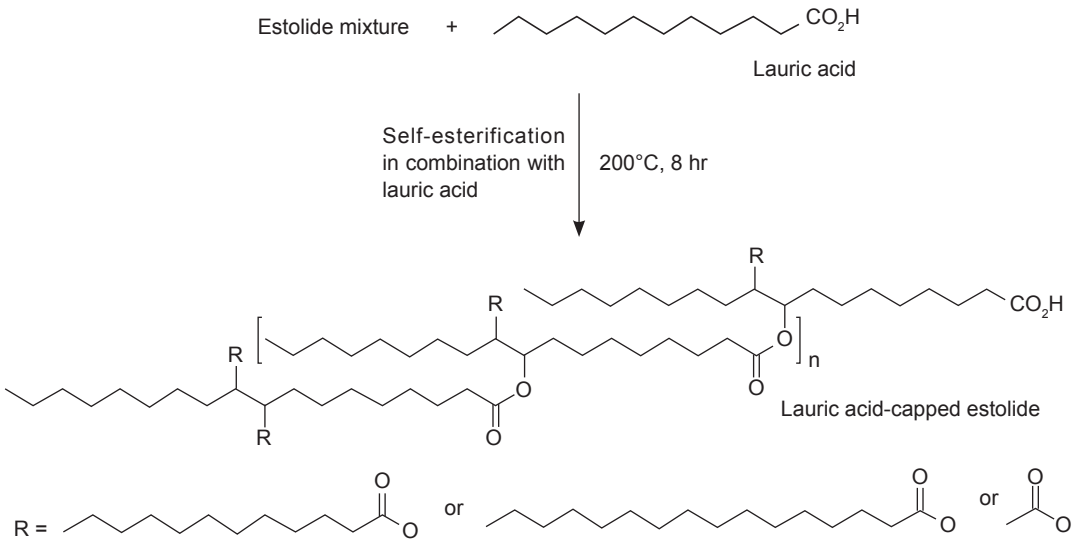


Figure 5. Synthesis of lauric acid-capped estolide (LaE).

30% lauric acid, the product displayed a layer of solid sedimentation upon storage, which suggested that 30% lauric acid was excessive for the reaction.

The conversion of the hydroxyl group of estolide mixture to the ester group was confirmed by ^{1}H NMR analysis. Referring to *Figure 3a*, the two peaks that represented hydroxyl groups of estolide mixture at 3.56 ppm and 3.33 ppm were not observed in the ^{1}H NMR spectrum of LaE (*Figure 3b*), which indicated that all hydroxyl groups of estolide mixture were converted to ester functionality. Moreover, a new peak was observed at 4.95 ppm in the ^{1}H NMR spectrum of LaE (*Figure 3b*), which correlated with a methine proton attached to the newly formed ester group. Additionally, the methylene proton peak of α-ester was observed at 2.25 ppm and all these ^{1}H NMR data proved the formation of LaE.

Moreover, the self-esterification of the estolide mixture in combination with lauric acid not only managed to end-cap all the hydroxy groups of the estolide mixture but also increased the molecular weight of LaE through the formation of ester linkages between fatty acid molecules. The GPC analysis showed that the average molecular weight of LaE (*Figure 4b*) was about 1900 Da, which was more than twice the average molecular weight of the estolide mixture (*Figure 4a*) and the oligomeric content of LaE was about 80%, which consisted of dimer, trimer and higher oligomers of LaE, while the remaining 20% comprised unreacted monomeric fatty acids. Additionally, the GPC chromatogram of LaE (*Figure 4b*) also revealed that the oligomers of LaE exhibited a broad molecular weight distribution in the range of 500 Da to 10 000 Da due to the self-esterification of the estolide mixture. It is noteworthy to mention that the presence of lauric acid and other saturated fatty acids in the reaction mixture prohibited the formation of cross-linked (gel) product, which would have formed in the self-esterification of estolide mixture without lauric acid and other saturated fatty acids as end-capping fatty acid to limit the degree of polymerisation.

Synthesis of 2EHLaE and DBALaE

Literature (Beran, 2010) reported that ester-based bio-lubricants typically have AV lower than 1 mg KOH g^{-1} to achieve good hydrolytic stability. Therefore, carboxylic acid groups of prepared LaE were converted to ester groups through reaction with 2-ethylhexanol (2EH) as it was reported by Sammaiah *et al*. (2016) to impart good cold flow and oxidation stability. Hence, the prepared LaE was reacted with an excess amount of 2EH as shown in *Figure 6* to generate a 2EHLaE. The reaction was considered completed when the AV of the product was below 1 mg KOH g^{-1}.

Alternatively, the carboxylic acid groups of LaE can be converted to amide bond, which is known to have better hydrolysis resistance in comparison with the ester group (Lee *et al*., 2002). Thus, LaE was reacted with excess dibutylamine (DBA) to yield estolide amide with AV below 1 mg KOH g^{-1} labelled as DBALaE (*Figure 6*). Dibutylamine was chosen because it is a biodegradable and relatively low-cost secondary amine (Kalla *et al*., 2014), which will form a tertiary amide with a branched structure that would impart good cold flow properties.

The ^{1}H NMR spectrum of 2EHLaE (*Figure 3c*) showed a peak at 2.25 ppm that correlated with methylene protons adjacent to an ester group (α-ester), while methylene protons adjacent to a carboxylic acid group (α-acid) were not detected at 2.3 ppm, which indicated that all the carboxylic acid groups of LaE were completely transformed to ester functionality. Additionally, the spectrum also exhibited another peak at 3.93 ppm, which represented the methylene protons of 2EH moiety adjacent to the ester group, which proved the conversion of the carboxylic acid group to the ester group by 2EH.

As for estolide amide DBALaE, ^{1}H NMR analysis (*Figure 3d*) showed two peaks at 3.26 and 3.17 ppm, which corresponded with the methylene group of dibutylamine moiety adjacent to the amide bond. The ^{1}H NMR spectrum of DBALaE also showed that methylene protons adjacent to the amide group (α-amide) were detected at 2.23 ppm, while the methylene protons adjacent to the carboxylic acid (α-acid) were not detected. These results strongly suggested that all the carboxylic acid groups of LaE were converted to amide groups.

Furthermore, the GPC analysis revealed that the average molecular weight of 2EHLaE and DBALaE was slightly increased to 2000 Da (*Figure 4c* and *4d*) in comparison with LaE due to the addition of 2EH and DBA moiety, respectively. The GPC analysis also showed that 2EHLaE and DBALaE exhibited similar chromatogram patterns in comparison with LaE. In addition, the oligomeric composition of 2EHLaE and DBALaE was about 80%, which was similar to LaE. This indicated that the esterification and amidation reactions did not alter the oligomeric composition of the reactant and eventually produced oligomers of 2EHLaE and DBALaE with molecular weights between 600 Da to 10 000 Da. On the other hand, the remaining 20% of 2EHLaE and DBALaE mainly consisted of monomeric 2-ethylhexyl ester and dibutyl amide of fatty acids, respectively.

Evaluation of 2EHLaE and DBALaE as Lubricant Base Oil

The prepared 2EHLaE and DBALaE were subjected to a typical evaluation of lubricant properties as shown in *Table 2*. The properties of estolide ester and amide were compared with palm-based trimethylolpropane triesters (TMPTE) synthesised from palm oil and trimethylolpropane (Nurazira *et al*., 2019) as well as a commercial mineral oil-based lubricant (HLP68), which serve as a benchmark for commercially acceptable properties of a lubricant. Additionally, a triglycerides-based estolide that was prepared from palm olein (Derawi and Salimon, 2013) is also included in *Table 2* for comparison of lubricant properties with 2EHLaE and DBALaE. The triglyceride-based estolide (labelled as DOPO) was prepared from palm olein through several reaction steps namely epoxidation, epoxide ring-opening with water and finally esterification with oleic acid.

One of the important attributes of a lubricant is its viscosity, which directly affects its lubrication performance at operational temperature. Hence,

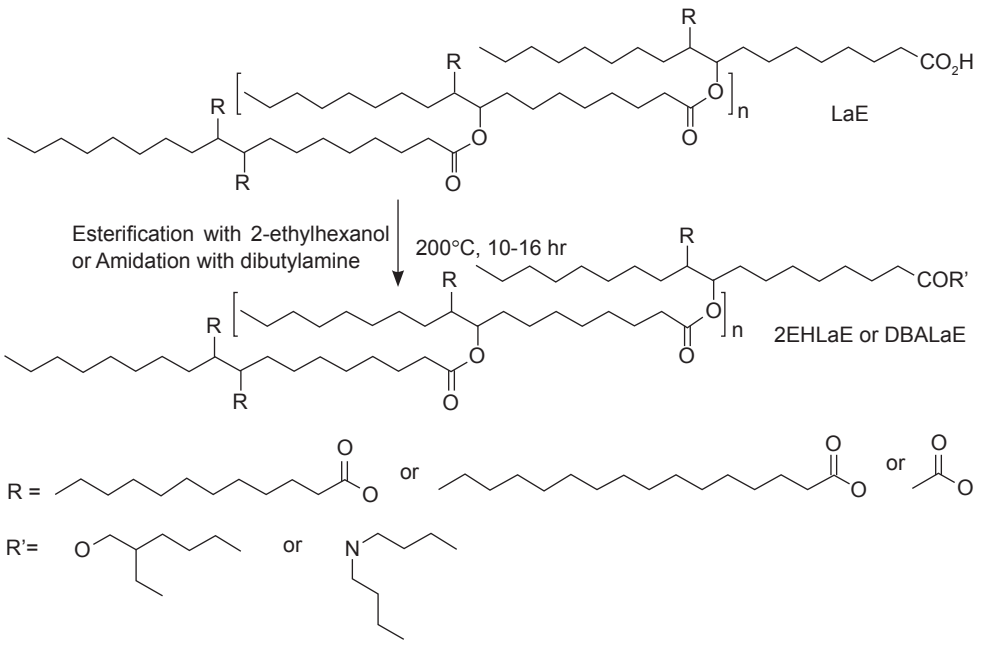


Figure 6. Synthesis of lauric acid-capped estolide ester (2EHLaE) and estolide amide (DBALaE).

TABLE 2. PHYSICOCHEMICAL PROPERTIES OF 2EHLAE, DBALAE, TMPTE, DOPO AND HLP68

Sample	KV		VI	PP (°C)	OOT (°C)	WSD (mm)
	40°C, cSt	100°C, cSt				
2EHLaE	63.1 ± 0.1	11.8 ± 0.1	190	-12.0 ± 0.0	199.8 ± 0.2	0.58 ± 0.06
DBALaE	136.2 ± 0.2	20.3 ± 0.1	169	-12.0 ± 0.0	200.3 ± 0.2	0.56 ± 0.05
TMPTE[a]	61.8	14.0	236	9.0	183.0	ND
DOPO[b]	417.5	45.4	166	-5.0	155.8	ND
HLP68[c]	68.2 ± 0.2	8.8 ± 0.1	107	-6.0 ± 0.0	199.2 ± 0.1	0.60 ± 0.05

Note: KV - kinematic viscosity; VI - viscosity index; PP - pour point; OOT - oxidation onset temperature; WSD - four-ball wear scar diameter, ND - not determined.

Source: [a]Nurazira *et al*. (2019).
[b]Derawi and Salimon (2013).
[c]Commercial mineral oil-based lubricant.

the kinematic viscosity of a lubricant is typically measured at 40°C and 100°C to ascertain the viscosity profile of a lubricant. Consequently, lubricants are classified according to their kinematic viscosity measured at 40°C, which is known as ISO viscosity grade (ISO VG) classification. Referring to *Table 2*, the kinematic viscosities of 2EHLaE, TMPTE and HLP68 can be classified as ISO VG 68 lubricant, which is suitable to be used as a base oil for hydraulic fluid, gear oil and compressor oil.

In contrast, DBALaE exhibited significant higher kinematic viscosity at 40°C (136 cSt) than its ester counterpart and is classified under ISO VG 150. The substitution of ester bond with tertiary amide bond contributed to the higher kinematic viscosity due to branched dibutylamine moiety that increased intermolecular chain entanglement as well as the higher polarity of the amide bond, which led to the observed increment of kinematic viscosity. Based on its kinematic viscosity, DBALaE can be used as a base oil for gear oil that requires higher viscosity for better prevention of friction and wear. For the same reason of intermolecular chain entanglement, the reported triglycerides-based estolide (DOPO) exhibited even higher kinematic viscosities at 40°C (417 cSt) due to its triglycerides molecular structure and the use of oleic acid as an end-capping fatty acid.

Viscosity index (VI) is another important feature of a lubricant, in which a high VI number suggests that the viscosity of the lubricant is less affected by changes in temperature and *vice versa*. In accordance with the commercial standard, a good lubricant will exhibit a VI value above 100. Both prepared 2EHLaE and DBALaE can be considered good lubricants in terms of VI as they displayed VI values of 190 and 169, respectively, which were significantly higher than the commercial sample HLP68. Both TMPTE and DOPO also showed good VI numbers above 100 as bio-lubricants are known to have good VI attributes (Cecilia *et al*., 2020).

Another important aspect of a lubricant is the cold flow characteristic which can be determined by measuring the pour point of the lubricant. The pour point is described as the lowest temperature at which the lubricant ceases to flow, which signifies the lower limit of the lubricant operational temperature. The high pour point of palm oil-based lubricants is a major hindrance that limits their market acceptance in countries with cold climates and chemical modification of palm oil is required to achieve an acceptable pour point (Erhan *et al*., 2006).

Referring to *Table 2*, the commercial lubricant HLP68 exhibited a pour point of -6°C, which represented the acceptable pour point in the lubricant market. Conversely, the TMPTE made from palm oil can only achieve a pour point of 9°C due to the molecular structure of TMPTE and the high content of saturated fatty acids in TMPTE that originated from palm oil. In comparison, both synthesised 2EHLaE and DBALaE exhibited a pour point of -12°C, which was significantly better than TMPTE and HLP68. The substantial improvement in pour point shown by 2EHLaE and DBALaE can be attributed to the branched structure of 2EHLaE and DBALaE that hindered molecules from packing albeit having a similarly high content of saturated fatty acids as compared to TMPTE. In contrast, the DOPO can only achieve a pour point of -5°C due to its triglycerides molecular structure even though it has estolide moieties, which significantly improved its pour point in comparison with starting material palm olein.

The oxidation stability of a lubricant at a high operating temperature is another important quality that can be measured using the pressure differential scanning calorimetry (PDSC) method. A lubricant with good oxidation stability will show a high oxidation onset temperature (OOT) and *vice versa*. Palm oil-based lubricants have lower oxidation stability due to inherent alkene groups that are susceptible to oxidation degradation. Therefore,

the palm-based TMPTE and DOPO that contained significant alkene groups exhibited OOT of 183°C and 156°C, respectively, which were inferior to both 2EHLaE and DBALaE that showed a higher OOT of 200°C due to the conversion of alkene groups to oxidation stable functional groups as seen in the synthesis of 2EHLaE and DBALaE. Furthermore, both 2EHLaE and DBALaE displayed similar oxidation stability as compared to commercial sample HLP68.

One of the main functions of lubricant is to minimise friction between two surfaces in close contact by the formation of a lubricating layer that prevents wear. Generally, a lubricant with excellent anti-wear quality will display a small wear scar diameter when evaluated in accordance with ASTM 4172 standard method. Referring to *Table 2*, both synthesised samples 2EHLaE and DBALaE exhibited slightly smaller wear scar diameters (0.58 mm and 0.56 mm, respectively) in comparison with commercial mineral oil (0.60 mm), which suggested that the anti-wear properties of 2EHLaE and DBALaE were comparable to the commercial product.

One of the main advantages of bio-lubricant is its inherent good biodegradability, which ensures the lubricant product is environment-friendly. On top of that, most bio-lubricants are made from renewable resources, which contribute to sustainable product development. Specifically, an earlier study on the biodegradability of estolide ester and amide (Hoong *et al*., 2020), reported that 2-ethylhexyl ester of estolide and dibutyl amide of estolide were readily biodegradable. Hence, the prepared 2EHLaE and DBALaE of this study should have the same biodegradability performance as those estolide ester and amide reported in the literature since they have the same molecular structures albeit different fatty acid compositions, which ensure the environmental-friendly feature of the prepared 2EHLaE and DBALaE.

CONCLUSION

Analyses conducted on palm-based UCO showed that it had higher free fatty acid, moisture and saturated fatty acids content as compared to fresh cooking oil (RBDPOo). Nonetheless, the UCO was found to have an adequate amount of unsaturated fatty acids that enable it to be used as feedstock to produce estolide ester and amide.

In the process of making estolide ester and amide, the UCO was converted to a mixture of fatty acids, which was then reacted with acetic acid and hydrogen peroxide to yield an estolide mixture with hydroxyl and carboxylic acid groups. Subsequently, the hydroxyl groups of the estolide mixture were end-capped with fatty acids while its carboxylic acid groups were converted to either ester or amide functionalities, which eventually afforded 2EHLaE)and DBALaE with a saturated branched structure.

Physicochemical properties evaluation revealed that the saturated branched structure of 2EHLaE and DBALaE contributed to better cold flow properties and enhanced oxidation stability in comparison with starting material UCO. Overall, this study demonstrated that the drawbacks of palm-based UCO lubricants such as inferior cold flow and oxidation stability properties can be improved through chemical modification performed on UCO that generated 2EHLaE and DBALaE, which displayed lubricant properties comparable with commercial lubricants. Additionally, the prepared 2EHLaE and DBALaE should exhibit good biodegradability, which ensures their suitability as an environment-friendly bio-lubricant.

ACKNOWLEDGEMENT

The authors would like to thank the Director-General of MPOB for permission to publish this article. We would like to thank the following personnel for analyses conducted on samples: Selasiah Abdullah, Ahmad Lutfi Md Yusof, Sapiah Hashim, Bahriah Bilal, Makmor Abd. Wahab, Norizan Ali, Mohd Zambri Yusof and Mohd Taib Samsudin.

REFERENCES

Ahmed, R B and Hossain, K (2020). Waste cooking oil as an asphalt rejuvenator: A state-of-the-art review. *Constr. Build. Mater.*, *230*: 116985.

American Oil Chemists' Society (AOCS), 2009. Acid value Te 1a-64; hydroxyl value Cd 13-60; iodine value Cd 1d-92; saponification value Cd 3-25; oxirane oxygen content Cd 9-57: Preparation of methyl esters of fatty acids Ce 2-66. *Official Methods and Recommended Practices of the American Oil Chemists' Society*. 6th edition. AOCS Press, Champaign, USA. 1200 pp.

Beran, E (2010). Effect of chemical structure on the hydrolytic stability of lubricating base oils. *Tribol. Int.*, *43*: 2372-2377.

Cecilia, J A; Plata, D B; Saboya, R M A; Luna, F M T; Cavalcante, C L and Castellon, E R (2020). An overview of the biolubricant production process: Challenges and future perspectives. *Processes*, *8*: 257.

Cermak, S C; Bredsguard, J W; Roth, K L; Thompson, T; Feken, K A; Isbell, T A and Murray, R E (2015).

Synthesis and physical properties of new coco-oleic estolide branched esters. *Ind. Crops Prod.*, *74*: 171-177.

Cheah, K W; Yusup, S; Chuah, L F and Bokhari, A (2016). Physico-chemical studies of locally sourced non-edible oil: Prospective feedstock for renewable diesel production in Malaysia. *Procedia Eng.*, *148*: 451-458.

Derawi, D and Salimon, J (2013). Palm olein based biolubricant basestocks: Synthesis, characterization, tribological and rheological analysis. *Malaysian J. Anal. Sci.*, *17*: 153-163.

Erhan, S Z; Sharma, B K and Perez, J M (2006). Oxidation and low temperature stability of vegetable oil-based lubricants. *Ind. Crops Prod.*, *24*: 292-299.

Heikal, E K; Elmelawy, M S; Khalil, S A and Elbasuny, N M (2017). Manufacturing of environment friendly biolubricants from vegetable oils. *Egypt. J. Pet.*, *26*: 53-59.

Hoong, S S; Arniza, M Z; Mariam, N M D N S; Armylisas, A H N; Ishak, S A; Ismail, T N M T and Yeong, S K (2020). Synthesis of estolide ester and amide from acetylated polyhydroxy estolide for lubricant base oil. *Eur. J. Lipid Sci. Technol.*, *122*: 2000098.

Hoong, S S; Arniza, M Z; Mariam, N M D N S; Armylisas, A H N; Tang, S W; Ismail, T N M T and Yeong, S K (2021). Synthesis and physicochemical properties of new estolide esters as potential biolubricant base oil. *J. Oil Palm Res.*, *34*: 152-166.

Isbell, T (2011). Chemistry and physical properties of estolides. *Grasas Y Aceites*, *62*: 8-20.

Kalla, R M N; Choi, J S; Yoo, J W; Byeon, S J; Heo, M S and Kim, I (2014). Synthesis of 2-amino-3-cyano-4*H*-chromen-4-ylphosphonates and their anticancer properties. *Eur. J. Med. Chem.*, *76*: 61-66.

Kulkarni, M G and Dalai, A K (2006). Waste cooking oil – an economical source for biodiesel: A review. *Indian Chem. Eng.*, *45*: 2901-2913.

Lam, M K; Lee, K T and Mohamed, A R (2010). Homogeneous, heterogeneous and enzymatic catalysis for transesterification of high free fatty acid oil (waste cooking oil) to biodiesel: A review. *Biotechnol. Adv.*, *28*: 500-518.

Lee, S Y; Park, J W; Yoo, Y T and Im, S S (2002). Hydrolytic degradation behaviour and microstructural changes of poly(ester-co-amide)s. *Polym. Degrad. Stab., 78*: 63-71.

Li, W M and Wang, X B (2015). Bio-lubricants derived from waste cooking oil with improved oxidation stability and low-temperature properties. *J. Oleo Sci.*, *64*: 367-374.

Loh, S K; Choo, Y M; Cheng, S F and Ma, A G (2006). Recovery and conversion of palm olein-derived used frying oil to methyl esters for biodiesel. *J. Oil Palm Res.*, *18*: 247-252.

Milano, J; Shamsuddin, A H; Silitonga, A S; Sebayang, A H; Siregar, M A; Masjuki, H H; Pulungan, M A; Chia, S R and Zamri, M F M A (2022). Tribological study on the biodiesel produced from waste cooking oil, waste cooking oil blend with *Calophyllum inophyllum* and its diesel blends on lubricant oil. *Energy Rep.*, *8*: 1578-1590.

Nurazira, M N; Derawi, D and Salimon, J (2019). Esterification and evaluation of palm oil as biolubricant base stock. *Malays. J. Chem.*, *21*: 28-35.

Orjuela, A and Clark, J (2020). Green chemicals from used cooking oils: Trends, challenges, and opportunities. *Curr. Opin. Green Sustain. Chem., 26*: 100369.

Parveez, G K A; Tarmizi, A H A; Sundram, S; Loh, S K; Ong-Abdullah, M; Palam, K D P; Salleh, K M; Ishak, S M and Idris, Z (2021). Oil palm economic performance in Malaysia and R&D progress in 2020. *J. Oil Palm Res.*, *33*: 181-214.

Salimon, J; Salih, N and Yousif, E (2011). Chemically modified biolubricant basestocks from epoxidized oleic acid: Improved low temperature properties and oxidative stability. *J. Saudi Chem. Soc.*, *15*: 195-201.

Salimon, J; Salih, N and Yousif, E (2012). Biolubricant basestocks from chemically modified ricinoleic acid. *J. King Saud Univ. Sci.*, *24*: 11-17.

Sammaiah, A; Padmaja, K V and Prasad, R B N (2016). Synthesis and physical properties of novel estolides from dicarboxylic acids and methyl ricinoleate. *Eur. J. Lipid Sci. Technol.*, *118*: 486-494.

Schilt, A A (1979). *Perchloric Acid and Perchlorate*. The G. Frederick Smith Chemical Company, Columbus, Ohio, USA. p. 153.

Shahbandeh, M (2022). Vegetable oils: Global consumption 2013/14 to 2021/2022, by oil type. https://www.statista.com/statistics/263937/vegetable-oils-global-consumption/, accessed on 6 March 2022.

Wang, E P; Ma, X; Tang, S Z; Wang, Y; Wiley, W W and Reaney, M J T (2014). Synthesis and oxidative stability of trimethylolpropane fatty acid triester as a biolubricant base oil from waste cooking oil. *Biomass Bioenergy*, *66*: 371-378.

Zhang, W; Ji, H R; Song, Y L; Ma, S; Xiong, W; Chen, C J; Chen, B Q and Zhang, X (2020). Green preparation of branched biolubricant by chemically modifying waste cooking oil with lipase and ionic liquid. *J. Clean. Prod.*, *274*: 122918.

SHORT COMMUNICATION

Journal of Oil Palm Research Vol. 35 (4) December 2023 p. 738-746
DOI: https://doi.org/10.21894/jopr.2023.0021

CHEMICAL PROFILING OF PALM OIL AND OTHER SELECTED PLANT OILS BY PROTON NUCLEAR MAGNETIC RESONANCE COMBINED WITH CHEMOMETRICS

NOOR IDAYU TAHIR[1]*; ASIAH NABIHAN ISHAK[2]; TEH SOEK SIN[1]; ABRIZAH OTHMAN[1] and UMI SALAMAH RAMLI[1]

ABSTRACT

Nuclear magnetic resonance (NMR) spectroscopy is an important and universal tool for chemical profiling. Combined with chemometrics for statistical interpretation and visualisation, the technique has gained recognition as an efficient method for assessing the quality and safety of vegetable oils. Nevertheless, its application in palm oil traceability is scarce. In this investigation, different origins, types and preparations of palm oils, olive oils, virgin coconut oils (VCO) and seed oils from sesame, black caraway, argan, corn, peanut and sunflower were examined for their chemical attributes using proton (^1H) NMR. The analysis used milligrams quantity of samples and was proven to be rapid with minimal sample preparation and analysis time. The statistical components of the multivariate model generated from the dataset were significant and highlighted the characterisation of the specimens into groups of palm, olive, virgin coconut and seed oils based on the presence and abundance of various types of proton signals. Different packaging and blends of commercial palm cooking oils exhibited similar proton profiles while the lab-prepared palm oil is closely linked to VCO. The work contributes to the development of authentication and traceability analytical methods for palm oil and will be expanded into a predictive platform with a larger dataset.

Keywords: chemical signatures, NMR spectroscopy, oil purity and stability, proton signals, vegetable oil.

Received: 12 July 2022**; Accepted:** 31 January 2023**; Published online:** 18 May 2023.

INTRODUCTION

The oils of plant origin especially palm oil are largely used in the food-based application and oleochemicals (Parveez *et al*., 2021). In addition to being a renewable resource, each plant oil has its unique chemical, physical and nutritional properties, *i.e*., oils with high amounts of saturated fatty acids such as palm and coconut oils are well suited for frying due to their thermal stability (Mitrea *et al*., 2022), extra virgin olive oil (EVOO) and sesame oils show better oxidative stability due to their natural antioxidants (Hashempour-Baltork *et al*., 2016; Kittipongpittaya *et al*., 2020), while black caraway seed (*Nigella sativa*) oil contains fat-soluble bioactives which enriched and improved the stability of sunflower oil as a blend (Kiralan *et al*., 2017). Several plant oils of high value, *e.g*., EVOO are targets for adulteration with less expensive sunflower and corn oils, while some oils are purposely blended to achieve desirable criteria such as canola with palm oil to enhance ω-3 (omega) fatty acid (Hashempour-Baltork *et al*., 2016; Hong *et al*., 2017).

NMR spectroscopy is one of the reliable and widely used analytical tools to evaluate the purity and stability of edible oils (Almoselhy *et al*., 2014; Ravaglia *et al*., 2019) and to monitor oil compositional and oxidative changes (Alonso-Salces *et al*., 2021). Although it offers a high potential in detecting the chemical variability within food systems with

[1] Malaysian Palm Oil Board,
6 Persiaran Institusi, Bandar Baru Bangi,
43000 Kajang, Selangor, Malaysia.

[2] Department of Plant Science, Kulliyyah of Science,
International Islamic University Malaysia (IIUM),
Bandar Indera Mahkota, 25200 Kuantan, Pahang, Malaysia.

* *Corresponding author e-mail: idayu@mpob.gov.my*

minimal analysis time and sample preparation compared to gas chromatography that requires derivatisation, the technique is still underutilised mainly due to its high acquisition cost and the lack of instrument and data handling expertise by food scientists (Hatzakis, 2019). To facilitate the discovery of distinguishable chemical attributes from spectral patterns obtained from analytical instruments such as the NMR, a data analysis technique termed 'chemometrics' that links chemical information to interpretive models is required (Bressanello *et al*., 2018). Chemometrics determines the features that are statistically different between sample classes (Rankin *et al*., 2014) and enables characterisation and interpretation of the data output (Ishak *et al*., 2021). The future of edible oil traceability and geographical authentication relies on the evolving chemometrics tool that can harmonise the output from diverse analytical platforms into a fingerprint database (Tahir *et al*., 2022).

Although widely used in the assessment of botanical sources for other vegetable oils especially olive (Ingallina *et al*., 2019; Ravaglia *et al*., 2019), the utilisation of combined NMR spectroscopy and chemometrics approach in determining the origin and traceability of palm oil is still scarce as reviewed by Ramli *et al.* (2020). Only recently, the method of NMR and chemometrics was applied to monitor the thermostability of palm oil as reported by Pinto *et al.* (2021). In view of this, palm oils of different processing, packaging and blend were subjected to NMR spectroscopy and chemometrics along with selected commercial vegetable oils to gain insights into their chemical signatures and discover their distinct characteristics. This work demonstrates the capacity of the employed method for palm oil traceability and authentication efforts, and the data serves as a groundwork for obtaining baseline information to detect the genuineness of edible plant oils, especially palm oil.

MATERIALS AND METHODS

Oil Samples

Palm oil samples from three ripe (20 to 22 weeks after anthesis) *tenera* oil palm fresh fruit bunches (FFB) sourced from MPOB planting trials in Johor, Terengganu and Teluk Intan were manually prepared in the lab. The FFBs were chopped into spikelets and placed into stainless steel round wire baskets of a Hirayama HICLAVE HVE-50 autoclave (Hirayama Manufacturing Corp., Japan) and sterilised at 100°C for 60 min. The sterilised fruitlets were detached and fitted into a container for a mechanical screw-pressing machine. The resulting liquid mixture was allowed to stand in an oven at 50°C to separate the oil from water, sludge and debris. The oil was collected and filtered through anhydrous sodium sulphate (ChemAR System, Classic Chemicals Sdn. Bhd., Malaysia) until the crystals were not clumped together indicating moisture traces have been removed. The oil was labelled as lab-prepared crude palm oil (LCPO1, 2 and 3).

A total of 35 commercial plant oil samples from bottled and pouch-packed palm cooking oils, red palm oils, olive and extra virgin olive, virgin coconut, corn, sunflower, peanut, sesame, argan and black caraway seed oils were obtained from various commercial sources. All the commercial samples had their country of origin or manufacturing listed in accordance with the information stated on their packaging and manufacturer's website. The argan tree is naturally endemic to Morocco and a few other countries with dryland such as Algeria and Tunisia (Gharby and Charrouf, 2022), therefore it is suggested that Brand 1 argan oil (sample Argan1) was processed in the manufacturing country but originated from a different location such as Morocco. More than three replicates were analysed for the palm oil commercial samples due to their availability in the local grocery stores. The countries of origin or production of the samples are indicated in *Table 1*.

Proton (^{1}H) NMR Spectroscopy Analysis

The oil sample chemical profiles were determined using a JNM-ECZ600R/S1 600 MHz NMR spectrometer (JEOL, Japan). 50 mg of oil was dissolved in 1.0 mL of deuterated chloroform ($CDCl_3$) (Merck KGaA, Germany) and transferred into standard 5 mm NMR tubes (Norell Inc., USA) for direct measurement. The one-dimensional proton spectra were acquired at a frequency of 600.1723 MHz at 14.09637 Tesla (T) magnetic field strength, with the observation nucleus (x_domain) set as 'proton', 5 ppm observation centre frequency (x_offset) and 15 ppm observation range (x_sweep). The pulse width used for the measurement (x_pulse) was 3.15 μs at a pulse angle of 45°, while the pulse delay time (relaxation_delay) was 5 s for rapid and routine 1D ^{1}H experiment.

Data Analysis

The Delta NMR Processing and Control Software v6.0 (JEOL Resonance Inc., Japan) was used to view, process and annotate the raw spectral data in terms of peak intensity and chemical shifts (δ), expressed in parts per million (ppm) relative to tetramethylsilane (TMS, $\delta = 0.00$). The intensity and shift information were tabulated into a comma separated values (.csv) format file using the Delta v6.0 'Chemometrics' function with baseline correction and tolerance referencing at 0.2 ppm and bucket integration width of 0.02 ppm. Chemometric analysis was performed

TABLE 1. PLANT OIL SAMPLES AND THEIR SOURCES

	Oil specimen	Analysis label	Origin/production
1	Crude palm oil from fresh fruit bunch plantation 1	LCPO1	MPOB laboratory preparation
2	Crude palm oil from fresh fruit bunch plantation 2	LCPO2	MPOB laboratory preparation
3	Crude palm oil from fresh fruit bunch plantation 3	LCPO3	MPOB laboratory preparation
4	Extra virgin olive oil Brand 1	EVOO1	Commercial, Tunisia
5	Extra virgin olive oil Brand 2	EVOO2	Commercial, Spain
6	Extra virgin olive oil Brand 3	EVOO3	Commercial, Italy
7	Olive oil Brand 1	OO1	Commercial, Spain
8	Olive oil Brand 2	OO2	Commercial, Spain
9	Olive oil Brand 3	OO3	Commercial, Italy
10	Virgin coconut oil Brand 1	VCO1	Commercial, Malaysia
11	Virgin coconut oil Brand 2	VCO2	Commercial, Turkey
12	Virgin coconut oil Brand 3	VCO3	Commercial, Malaysia
13	Pouch packed palm cooking oil Brand 1	Pouch1	Commercial, Malaysia
14	Pouch Brand 2	Pouch2	Commercial, Malaysia
15	Pouch Brand 3	Pouch3	Commercial, Malaysia
16	Bottled palm cooking oil Brand 1	BPO1	Commercial, Malaysia
17	Bottled palm cooking oil Brand 2	BPO2	Commercial, Malaysia
18	Bottled palm cooking oil Brand 3	BPO3	Commercial, Malaysia
19	Bottled palm cooking oil Brand 4	BPO4	Commercial, Malaysia
20	Bottled palm cooking oil Brand 5	BPO5	Commercial, Malaysia
21	Bottled palm cooking oil with unknown blend % of peanut and sesame oil Brand 1	BPOM1	Commercial, Malaysia
22	Bottled palm cooking oil with unknown blend % of peanut and sesame oil Brand 2	BPOM2	Commercial, Malaysia
23	Bottled palm cooking oil with unknown blend % of peanut and sesame oil Brand 3	BPOM3	Commercial, Malaysia
24	Bottled palm cooking oil with unknown blend % of peanut and sesame oil Brand 4	BPOM4	Commercial, Malaysia
25	Red palm oil Brand 1	RPO1	Commercial, Malaysia
26	Red palm oil Brand 2	RPO2	Commercial, Malaysia
27	Corn cooking oil Brand 1	Corn1	Commercial, Malaysia
28	Corn cooking oil Brand 2	Corn2	Commercial, Malaysia
29	Sunflower cooking oil	Sunflower	Commercial, Malaysia
30	Sesame oil Brand 1	Sesame1	Commercial, Malaysia
31	Sesame oil Brand 2	Sesame2	Commercial, Malaysia
32	Sesame oil Brand 3	Sesame3	Commercial, Malaysia
33	Argan seed oil Brand 1	Argan1	Commercial, Turkey
34	Argan seed oil Brand 2	Argan2	Commercial, Morocco
35	Peanut oil	Peanut	Commercial, Italy
36	Black caraway seed oil Brand 1	BC1	Commercial, Egypt
37	Black caraway seed oil Brand 2	BC2	Commercial, Malaysia
38	Black caraway seed oil Brand 3	BC3	Commercial, Turkey

using the online public MetaboAnalyst Version 5.0 (https://www.metaboanalyst.ca) with a coefficient of determination calculated via leave-one-out cross-validation (LOOCV) (Lee *et al*., 2018). Preprocessing of the data includes normalisation by sum and Pareto scaling (mean-centered and divided by the square root of the standard deviation of each variable) and permutation tests by 'between' and 'within' classes separation distance (B/W). The hierarchical clustering heatmap was constructed using analysis of variance (ANOVA), Minkowski distance measure and average clustering. The diagnostic statistics to

evaluate the performance of the machine learning algorithms for the multivariate analysis is based on Q2 and R2 values (R2 > Q2, and, the difference between R2 and Q2 < 0.2) as outlined by Kiralj and Ferreira (2009).

RESULTS AND DISCUSSION

The resulting multivariate model constructed from the ^{1}H NMR profiles showed excellent statistical components with an accuracy of 0.81579, R2 (goodness of fit) value of 0.90322 and Q2 (the predictive ability of the model) of 0.83894. The permutation test revealed its significance under possible rearrangements of the observed data points (*Table* 2). The probability of attaining a result at least as extreme as the test statistic with a true null hypothesis (exchangeable sample classes) is expressed in *p*-value. Lower *p*-values indicate that the features are not interchangeable and that the original classification is relevant with respect to the data (Knijnenburg *et al*., 2009).

The principal component analysis (PCA) scores plot (*Figure 1*) of the ^{1}H NMR data showed clear groupings of the oil samples respective to their classes. The accompanying biplot displayed the chemical shifts that contributed to the greatest distribution of the samples shown in the scores plot. VCO samples were set apart from the other oils on the upper segment of the plots followed by the LCPO proton profiles which were scored in between the VCO and the commercial palm oil specimens based on their higher abundance of 1.26 and 1.27 ppm proton signals corresponding to the methylene protons of fatty acid chains (-$(CH_2)_n$-) (Di Pietro *et al*., 2020). The scores of RPO and refined palm oils (cooking palm oils either sold in bottles or pouches, labelled as BPOs, BPOMs and Pouches) were plotted on a lower segment next to the olive oils with higher abundance of 1.24 and 1.27 ppm signals also for fatty acid chain methylene protons [-$(CH_2)_n$-], and 0.87 ppm signal for acyl chain methyl protons (-CH_3).

RPO1 score was observed separately from another red palm oil specimen RPO2 towards the seed oil group. Higher proton peak abundances were found at shift 0.93-0.96 ppm in RPO1 proton spectra compared to the other palm oil samples (*Figure* 2) indicating the notable presence of linolenic acid (Alexandri *et al*., 2017), possibly due to its blend with another type of plant oil. RPO1 is a commercial blend of red palm and canola (rapeseed) oils, which supports this claim.

Linolenic acid is an octadecatrienoic, polyunsaturated fatty acid occurring in plant oils as either or both the α-linolenic (ALA), an omega-3 (ω-3/n-3) and the γ-linolenic (GLA), an ω-6 (n-6). It is found in a significant amount of at least 7.8%-9.9% in soybean and rapeseed oils (Dubois *et al*., 2007) (*Table 3*).

TABLE 2. PERMUTATION TEST STATISTICS

Permutation numbers	Empirical *p*-value
20	$p < 0.05$
100	$p < 0.01$
1 000	$p < 0.001$
2 000	$p < 0.0005$

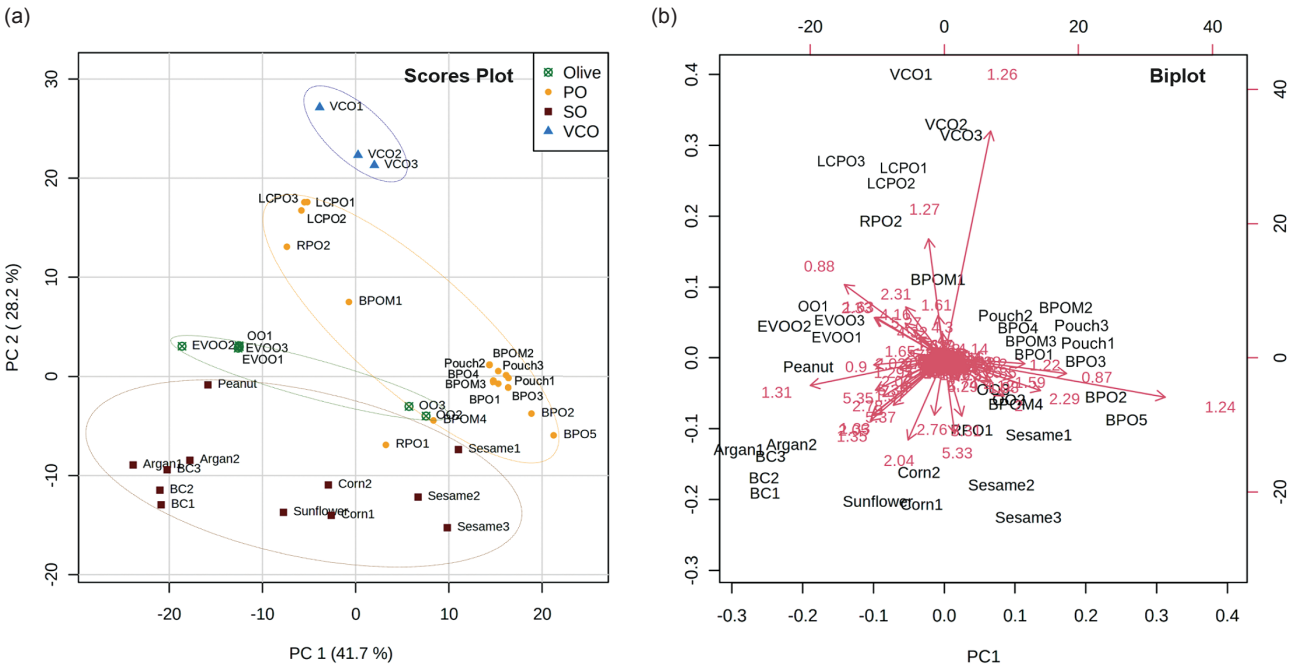


Figure 1. PCA scores plot (a) and biplot (b) of plant oils ^{1}H NMR data. Classes of oils: Olive and extra virgin olive oils (Olive); palm oil (PO); seed oils (SO) and virgin coconut oil (VCO).

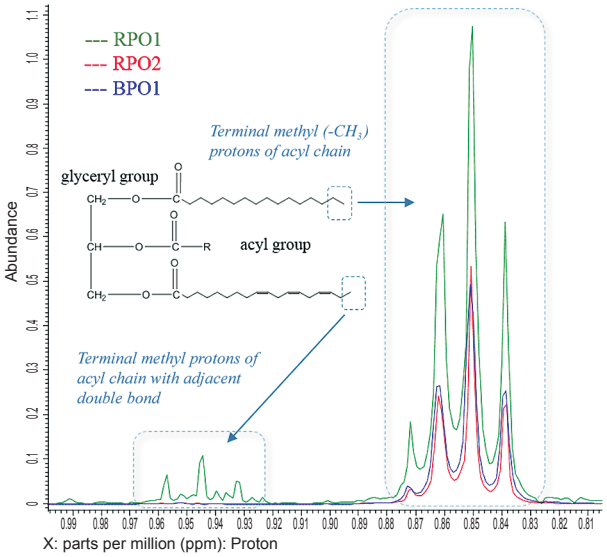


Figure 2. Traces of proton signals at shift 0.93-0.96 ppm in RPO1 proton spectra compared to RPO2 and BPO1 denoting the terminal methyl (-CH_3) group of linolenic acid.

TABLE 3. PERCENTAGE OF LINOLENIC ACID (18:3) CONTENT IN COMMERCIAL PLANT OILS

Oils	%	
	α (18:3 n-3)	γ (18:3 n-6)
Hemp seed oil	19.7	2.8
Rapeseed	9.9	0.0
Soybean	7.8	0.0
Black caraway	2.4	0.0
Argan	1.4	0.0
Corn	1.0	0.0
Olive	0.6	0.0
Sunflower	0.5	0.0
Sesame	0.4	0.0
Peanut	0.4	0.0
Palm	0.3	0.0
Coconut	0.1	0.0

Source: Dubois *et al.* (2007).

The abundance of the proton signal for the terminal methyl (-CH_3) group of linolenic acid which appears as a triplet after 0.9 ppm as shown in *Figure 2* was averaged and plotted into a column chart according to their respective species of black caraway, argan, corn, sunflower, sesame, peanut and coconut; the processing of EVOO and OO, and packaging of pouch-packed, bottled and lab-prepared crude palm oil (*Figure 3*). RPO1 showed the highest abundance of the triplet signal compared to the other oil specimens most likely attributed to its canola (rapeseed) oil blend.

The scores for EVOO and OO were observed in the middle segment of the PCA plots next to the seed oils with a higher abundance of various chemical shifts of 0.88 ppm (acyl chain methyl protons), 1.63 ppm (methylene protons in relation to the carbonyl group, HOCO-CH_2-CH_2-), and also 2.31 and 2.33 ppm (methylene protons in relation to the carbonyl group, HOCO-CH_2-). Overall, the seed oils were grouped by the abundance of 5.33 and 5.35 ppm for proton signals of unsaturated acyl chain (Ün and Ok, 2018) and 2.05 and 2.78 ppm for the linoleic acid diallylic protons (Ingallina *et al.*, 2019). The seed oils of peanut, argan and black caraway showed higher signals of 1.31, 1.33 and 1.35 ppm for fatty acid chain methylene protons compared to the other specimens of olives, palm and coconut oils. The different abundances and shifts of several acyl chain methylene protons in the range of 1.20 to 1.3 ppm suggest different types of fatty acid chain composition for the respective samples, as postulated by Di Pietro *et al.* (2020).

The commercial palm cooking oil proton profiles showed a compact clustering for their PCA scores except for BPOM1, suggesting no significant differences between the samples despite their different packaging (bottle or pouch) and the addition of peanut and sesame oil as aroma enhancers. This result coincides with a recent assessment of commercial palm-based cooking oils sold in plastic pouches and polyethylene terephthalate (PET) bottles using gas and liquid chromatography by Hassim *et al.* (2021). A separate PCA scores plot and hierarchical clustering dendrogram for the palm cooking oils (*Figure 4*) demonstrated that apart from samples BPOM1 and BPOM4, the proton profiles of palm cooking oils of all packaging and blends are intermixed together.

A more detailed distribution of the proton profiles for all the oil specimens can be observed in a heatmap in *Figure 5* which lists the top 50 significant ^{1}H NMR signals differentiating the olive, palm, seed and coconut oils (designated as class) ranked by ANOVA. A close inspection of the heatmap revealed that the seed oils contained a higher abundance of aromatic hydrocarbons, olefins and phenolic components at region 5.00 ppm downfield (Alonso-Salces *et al.*, 2021). However, the proton signals that grouped the seed oils in the PCA were not from the downfield region as the aromatic proton signals were very low except for 5.33 and 5.35 ppm for the olefin. A magnification onto the 6.00-7.00 ppm and 3.00-4.00 ppm regions of the sesame oil ^{1}H NMR spectra to the thousandth (x1000) (*Figure 6*) as previously analysed by Schripsema (2019) and Jin *et al.* (2017) discovered the proton signals for sesamolin and sesamin lignans in very low abundance in comparison to the other proton signals. No significant signal was detected after magnification of the lignan peak regions across all the BPOM samples. However, blended cooking

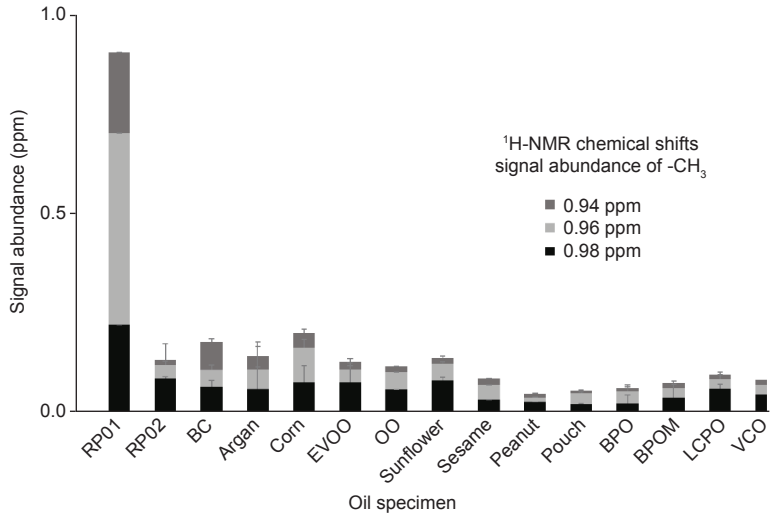


Figure 3. Average abundance of linolenic acid terminal methyl (-CH_3) group proton signals in the investigated oil specimens compared to RPO1 and RPO2.

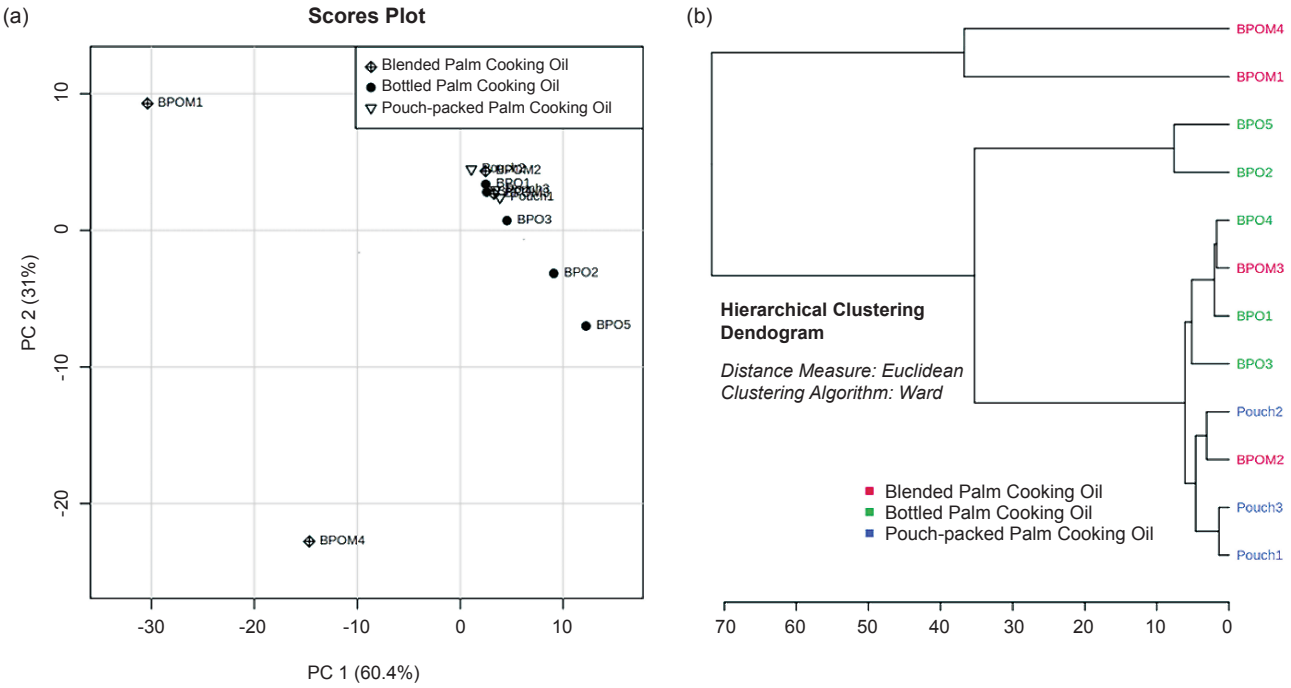


Figure 4. (a) PCA scores plot and (b) hierarchical clustering dendrogram of palm cooking oil proton NMR profiles.

oil sample BPOM4 showed similarities to the seed oil profiles in the downfield region probably due to the trace background signals from sesame and/or peanut oil. Upfield proton signal abundances at 1.35 and 2.11 ppm shifts were also detected higher for BPOM4 at levels similar to those of the peanut oil sample, suggesting comparable protons of methyl and unsaturated acyl chain (-CH_2-CH=CH).

The proton signals at 3.4 ppm observed in the seed oil and olive samples were previously reported as water presence probably due to several factors such as absorption of water during processing, *e.g.*, cooling and preservation, storage environment and hydrolytic rancidity (Cai *et al.*, 2019). It is also interesting to note that from the heatmap, the black caraway seed, olive oil, and sesame showed slight individual distinctiveness in their proton profiles while the EVOO and VCO oil samples were similarly grouped although sourced from different origins or countries.

CONCLUSION

This work demonstrates the rapid and efficient approach of ^{1}H NMR spectroscopy combined with chemometrics as a tool for the characterisation of plant oils. The different types and origins of palm oils, extra virgin and refined olive oils, virgin coconut oils, corn oils and seed oils (sesame, black caraway,

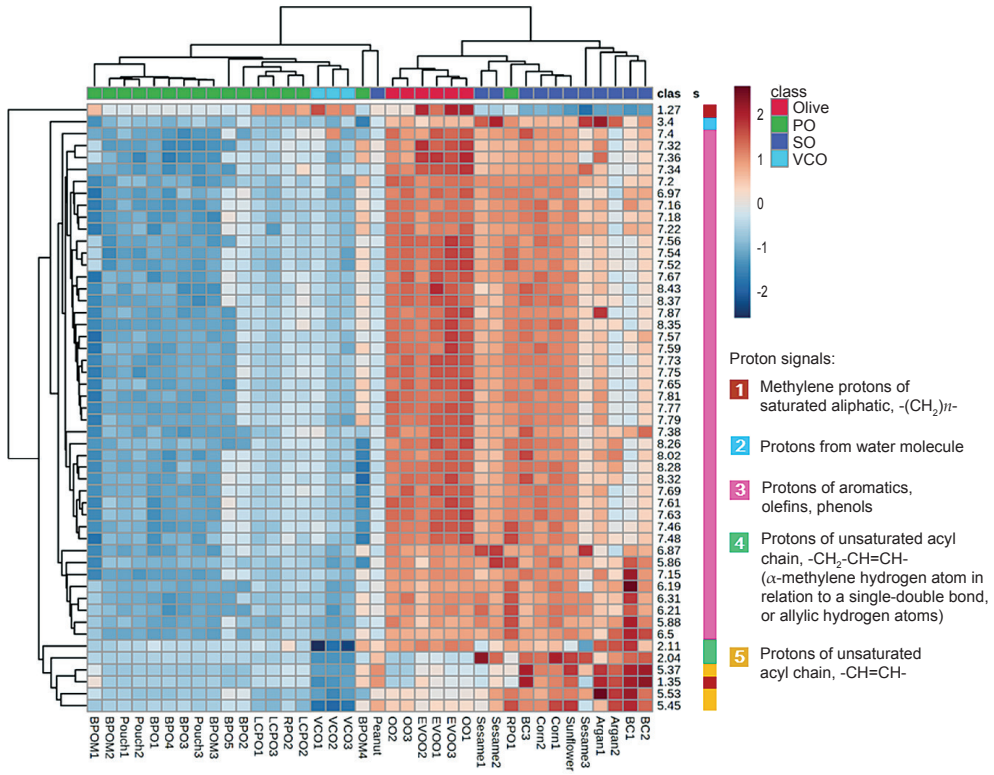


Figure 5. Heatmap of the top 50 significant plant oils proton NMR signals. Each cell corresponds to the signal abundance value from low (blue) to high (red). The signals are described according to their categories (1-5). Classes of oils: Olive and extra virgin olive oils (Olive); palm oil (PO); seed oils (SO) and virgin coconut oil (VCO).

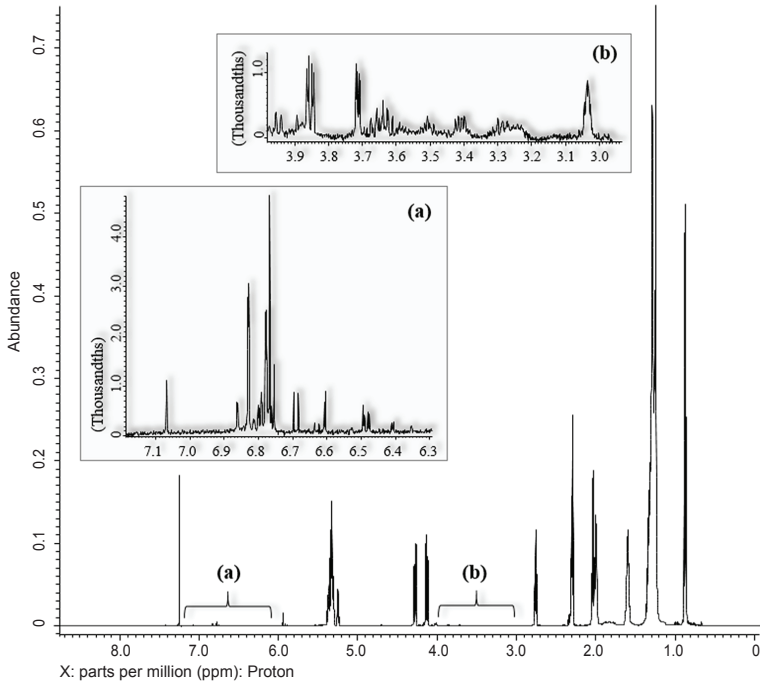


Figure 6. Magnification of the sesame oil NMR spectra to the thousandth (x1000) onto (a) 6-7 ppm and (b) 3-4 ppm proton chemical shift regions of lignans.

argan, peanut, sunflower) can be distinguished based on the similarities and differences of their proton signal abundances which correspond to their methylene (-$(CH_2)_n$-), methyl (-CH_3), unsaturated acyl chain, aromatic hydrocarbons, olefins and phenolic chemical components. The analysis requires no prior separation or treatment and the resulting spectral raw data can be processed into a statistically sound and reliable chemometric dataset to obtain maximum information. These findings can be further utilised in establishing edible oil ^{1}H NMR fingerprints for authentication and traceability purposes.

ACKNOWLEDGEMENT

The authors thank the Director-General of MPOB for the permission to publish this article. Special appreciation goes to Ms. Nik Farhana Nadiah Nik Mustapha of Boustead Life Sciences Research Sdn. Bhd. for the Turkey and Egypt commercial oil samples, Mr. Mohamad Faiz Abdullah of PROMET Lab, Mdm. Norizah Halim and Mr. Mohamed Noor Petrus of Product Development and Advisory Services for their technical assistance.

REFERENCES

Alexandri, E; Ahmed, R; Siddiqui, H; Choudhary, M I; Tsiafoulis, C G and Gerothanassis, I P (2017). High resolution NMR spectroscopy as a structural and analytical tool for unsaturated lipids in solution. *Molecules, 22(10)*: 1663.

Almoselhy, R I M; Allam, M H; El-Kalyoubi, M H and El-Sharkawy, A A (2014). ^{1}H NMR spectral analysis as a new aspect to evaluate the stability of some edible oils. *Ann. Agric. Sci., 59(2)*: 201-206.

Alonso-Salces, R M; Gallo, B; Collado, M I; Sasía-Arriba, A; Viacava, G E; García-González, D L; Toschi, T G; Servili, M and Berrueta, L Á (2021). ^{1}H–NMR fingerprinting and supervised pattern recognition to evaluate the stability of virgin olive oil during storage. *Food Control, 123*: 107831.

Bressanello, D; Liberto, E; Cordero, C; Sgorbini, B; Rubiolo, P; Pellegrino, G; Ruosi, M R and Bicchi, C (2018). Chemometric modelling of coffee sensory notes through their chemical signatures: Potential and limits in defining an analytical tool for quality control. *J. Agric. Food Chem., 66(27)*: 7096-7109.

Cai, S; Zhang, Y; Xia, F; Shen, G and Feng, J (2019). An expert system based on ^{1}H NMR spectroscopy for quality evaluation and adulteration identification of edible oils. *J. Food Compost. Anal., 84*: 103316.

Di Pietro, M E; Mannu, A and Mele, A (2020). NMR determination of free fatty acids in vegetable oils. *Processes, 8*: 410.

Dubois, V; Breton, S; Linder, M; Fanni, J and Parmentier, M (2007). Fatty acid profiles of 80 vegetable oils with regard to their nutritional potential. *Eur. J. Lipid Sci. Technol., 109(7)*: 710-732.

Gharby, S and Charrouf, Z (2022). Argan oil: Chemical composition, extraction process, and quality control. *Front. Nutr., 8*: 804587.

Hashempour-Baltork, F; Torbati, M; Azadmard-Damirchi, S and Savage, G P (2016). Vegetable oil blending: A review of physicochemical, nutritional and health effects. *Trends Food Sci. Technol., 57*: 52-58.

Hassim, N A M; Ismail, N H; Kanagaratnam, S; Isa, W R A and Dian, N L H M (2021). Quality of commercial palm-based cooking oil packed in plastic pouch and polyethylene terephthalate (PET) bottle. *J. Oil Palm Res., 33(3)*: 493-513.

Hatzakis, E (2019). Nuclear magnetic resonance (NMR) spectroscopy in food science: A comprehensive review. *Compr. Rev. Food Sci. Food Saf., 18(1)*: 189-220.

Hong, E; Lee, S Y; Jeong, J Y; Park, J M; Kim, B H; Kwon, K and Chun, H S (2017). Modern analytical methods for the detection of food fraud and adulteration by food category. *J. Sci. Food Agric., 97(12)*: 3877-3896.

Ingallina, C; Cerreto, A; Mannina, L; Circi, S; Vista, S; Capitani, D; Spano, M; Sobolev, A P and Marini, F (2019). Extra virgin olive oils from nine Italian regions: An ^{1}H NMR-Chemometric characterization. *Metabolites, 9(4)*: 65.

Ishak, N A; Tahir, N I; Mohd Sa'id, S N; Kathiresan, G; Abrizah, O and Ramli, U S (2021). Comparative analysis of statistical tools for oil palm phytochemical research. *Heliyon, 7(2)*: e06048.

Jin, G; Kim, J; Lee, Y; Kim, J; Akoh, C C; Chun, H S; Ahn, S and Kim, B H (2017). A nuclear magnetic resonance spectroscopy approach to discriminate the geographic origin of roasted Asian sesame oils. *J. Oleo Sci., 66(4)*: 337-344.

Kiralan, M; Ulaş, M; Özaydin, A; Özdemïr, N; Ozkan, G; Bayrak, A and Ramadan, M F (2017). Blends of cold pressed black cumin oil and sunflower oil with improved stability: A study based on changes in the levels of volatiles, tocopherols and thymoquinone during accelerated oxidation conditions. *J. Food Biochem., 41*: e12272.

Kiralj, R and Ferreira, M M C (2009). Basic validation procedures for regression models in QSAR and QSPR studies: Theory and application. *J. Braz. Chem. Soc., 20(4)*: 770-787.

Kittipongpittaya, K; Panya, A; Prasomsri, T and Sueaphet, P (2020). Tropical oil blending and their effects on nutritional content and physicochemical properties during deep fat frying. *J. Nutr. Sci. Vitaminol., 66*: S206-S214.

Knijnenburg, T A; Wessels, L F; Reinders, M J and Shmulevich, I (2009). Fewer permutations, more accurate P-values. *Bioinformatics*, *25(12)*: i161-i168.

Lee, L C; Liong, C and Jemain, A A (2018). Partial least squares-discriminant analysis (PLS-DA) for classification of high-dimensional (HD) data: A review of contemporary practice strategies and knowledge gaps. *Analyst*, *143*: 3526-3539.

Mitrea, L; Teleky, B; Leopold, L; Nemes, S; Plamada, D; Dulf, F V; Pop, I and Vodnar, D C (2022). The physicochemical properties of five vegetable oils exposed at high temperature for a short-time-interval. *J. Food Compost. Anal.*, *106*: 104305.

Parveez, G K A; Tarmizi, A H A; Sundram, S; Loh, S K; Ong-Abdullah, M; Kosheela Devi, P P; Kamalrudin, M S; Sheilyza, M I and Zainab, I (2021). Oil palm economic performance in Malaysia and R&D progress in 2020. *J. Oil Palm Res.*, *33(2)*: 181-214.

Pinto, V S; dos Anjos, M M; Pinto, N S and Lião, L M (2021). Analysis of thermal degradation of Brazilian palm oil by quantitative ^{1}H NMR and chemometrics. *Food Control, 130*: 108406.

Ramli, U S; Tahir, N I; Rozali, N L; Othman, A; Muhammad, N H; Muhammad, S A; Tarmizi, A H A; Hashim, N; Sambanthamurthi, R; Singh, R; Manaf, M A A and Parveez, G K A (2020). Sustainable palm oil – The role of screening and advanced analytical techniques for geographical traceability and authenticity verification. *Molecules*, *25(12)*: 2927.

Rankin, N J; Preiss, D; Welsh, P; Burgess, K E; Nelson, S M; Lawlor, D A and Sattar, N (2014). The emergence of proton nuclear magnetic resonance metabolomics in the cardiovascular arena as viewed from a clinical perspective. *Atherosclerosis*, *237(1)*: 287-300.

Ravaglia, L M; Pizzotti, A B C and Alcantara, G B (2019). NMR-based and chemometric approaches applicable to adulteration studies for assessment of the botanical origin of edible oils. *J. Food Sci. Technol.*, *56*: 507-511.

Schripsema, J (2019). Similarity and differential NMR spectroscopy in metabolomics: Application to the analysis of vegetable oils with ^{1}H and ^{13}C NMR. *Metabolomics, 15(3)*: 39.

Tahir, H E; Arslan, M; Komla Mahunu, G; Adam Mariod, A; Hashim, S B H; Xiaobo, Z; Jiyong, S; El-Seedi, H R and Musa, T H (2022). The use of analytical techniques coupled with chemometrics for tracing the geographical origin of oils: A systematic review (2013-2020). *Food Chem.*, *366*: 130633.

Ün, İ and Ok, S (2018). Analysis of olive oil for authentication and shelf life determination. *J. Food Sci. Technol.*, *55(7)*: 2476-2487.

JOURNAL OF OIL PALM RESEARCH

GUIDE FOR AUTHORS

(for more details, kindly surf http://jopr.mpob.gov.my)

Type of Articles

1. **Regular Article**
   Full-length original empirical investigations, consisting of introduction, materials and methods, results and discussion, conclusions. Original work must provide references and an explanation on research findings that contain new and significant findings. Conclusion should be brief and focus on the research output, should not be in point form. These papers should not exceed 6000 words of text (including tables, figures and references) and generally not more than a total of 10 figures and tables. After peer-review, the article word count limit can be extended to a maximum of 8000 words to better address the reviewers' and editors' comments. Any additional figures or tables can be included in the supplementary data. Please note that papers submitted to JOPR will be sent back to authors because of poor figure resolution or exceeding the number of figures permitted.

2. **Short Communication**
   Significant new information to readers of the Journal in a short but complete form. Preferably not exceeding 3000 words (including tables, figures and references), and is intended for rapid publication. They are not intended for publishing preliminary results or to be a reduced version of regular article.

3. **Review Article**
   Critical evaluation of materials about current research that have already been published by organising, integrating, and evaluating previously published materials. Re-analyses as meta-analysis and systemic reviews are encouraged. Review articles provide systemic overview, evaluation and interpretation of research in a given field. They should not exceed 12 000 words (excluding references only) and should contain no more than a total of 20 figures and tables. Any additional figures or tables can be included in the supplementary data. Please note that papers submitted to JOPR will be sent back to authors because of poor figure resolution or exceeding the number of figures permitted. The same information should not be repeated in a figure and a table.

Language

Please write your text in good English (only British English is accepted). We do not accept American English or a mixture of these.

JOPR's Template

JOPR's template, which is a standard format that facilitates the manuscript writing and copyediting process. This template is created to provide a detail and clear house style of JOPR. The template is drafted according to JOPR's house style, but in standard word version format. When writing a paper, authors need to format their papers to fit into the journal's house style. To make this easier, Word templates are available for many of other established journals, ready for them to download and apply to their research paper format. It is crucial for author to write a research paper while considering formatting. Each journal has its own guidelines for formatting; hence, the template defines how an article will look when it is published online or in print.

JOPR's Aims & Scope

This is established to provide a detail and clear aims and scope for author reference. Authors should declare in the cover letter how the research fits the aims and scope of JOPR.

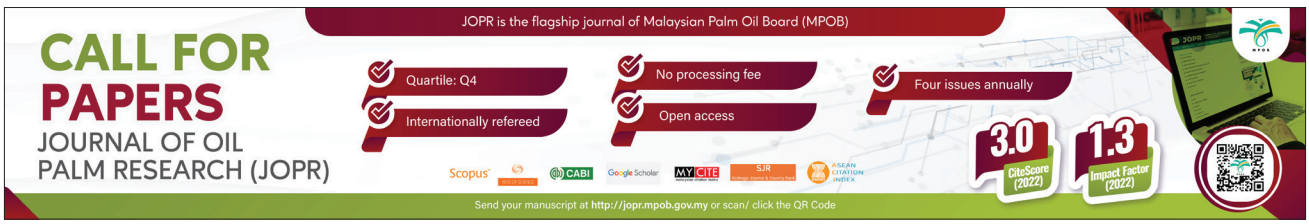
JOPR's House Style

A detail listing of JOPR's house style for authors and a checklist to facilitate the copyediting process and standardise the copyediting process. The JOPR's house style remains the same and is drafted into a detail version for author's reference.

Manuscript Submission

- Manuscripts should be submitted via: https://www2.cloud.editorialmanager.com/jopres/
- JOPR does not permit dual submission, publication and/or any archive platform (preprint) in violation of journal ethical practices.

For more details and to download the JOPR's House Style and Template, kindly surf http://jopr.mpob.gov.my



Contents of the Coming Issue
Journal of Oil Palm Research
Vol. 36 (1) March 2024*

- The Environmental and Health Sustainability Challenges of Malaysian Palm Oil in the European Union
  Lakhsmy Naidu; Ravichandran Moorthy and Mohd Ikbal Mohd Huda

- *In Vitro* Studies on Palm Phytonutrients: A Nutrigenomic Review
  Maisarah Ab Fatah and Voon Phooi Tee

- Initial Characterisation of Metarhizium anisopliae CPMa1502 for the Development of a Biopesticide Against the Oil Palm Fruit Scraper Demotispa neivai (Coleoptera: Chrysomelidae)
  Ginna Quiroga-Cubides; Felipe Borrero-Echeverry; Ana Maria Jimenez; Luis Guillermo Montes-Bazurto; Alex Bustillo Pardey; Martha I. Gomez and Paola E. Cuartas-Otalora

- Solketal Levulinate Ester as Potential Fuel Additive for Palm Biodiesel
  NMD Nik Siti Mariam; Seng Soi Hoong; Tuan Noor Maznee, T I, Mohd Zan Arniza and Rahimi M Yusop

- Comparative Studies on Cure Characteristics and Mechanical Properties of Oil Palm Biomass Filled Natural Rubber Composites
  M. T. Nur 'Aisyah Ar-Raudhoh; M. F. Muhamad Haziq; Z. A. Zafirah; M. Siti Nur Liyana and Z. Nahrul Hayawin

- Molecular Approaches in Assessing the Soil Microbial Diversity of Malaysian Oil Palm Plantations: A Review
  Zahidah Ayob; Nor Azizah Kusai; Nur Maisarah Jantan and Law Mei Ching

Note: * Subject to change.